YUKON
EXPLORATION
& GEOLOGY

2010

YUKON
GEOLOGICAL SURVEY

Yukon
Energy, Mines and Resources

YUKON
EXPLORATION
& GEOLOGY
2010

Front cover photograph: Mike Burke (YGS) and Bill Wengzynowski (ATAC Resources) view drill core at the recently-discovered Osiris showing. Photo by Carolyn Relf.

PREFACE

Yukon Exploration and Geology (YEG) continues to be the main publication of the Yukon Geological Survey (Energy, Mines and Resources, Yukon government). This is the 33rd volume of the series. We have moved to digital only distribution of YEG. Individual YEG papers, with colour images, can be downloaded from our website. The Yukon Exploration and Geology Overview continues to be available in print and digital formats.

YEG 2010 contains up-to-date information on mining and mineral exploration activity, studies by industry, and results of recent geological field studies. Information in this volume comes from prospectors, exploration and government geologists, mining companies and students who are willing to contribute to public geoscience for the benefit of the scientific community, general public, and mineral and petroleum industries of Yukon. Their efforts are appreciated.

YEG co-editors Leyla Weston and Carolyn Relf are thanked for their assistance this year. Appreciation is also extended to Yukon Geological Survey (YGS) staff that helped edit earlier versions of manuscripts, before they even crossed our path; this year we thank Joyia Chakungal, Venessa Bennett, Tammy Allen, Maurice Colpron, Kristen Kennedy and Don Murphy.

Sherry Tyrner of the Queen's Printer ensured that the printing process went smoothly.

This year's Yukon Exploration and Geology is dedicated to the administrative, financial and GIS staff that work in survey, exploration, or mining offices. At one time or another you have made my life easier.

We welcome any input or suggestions that you may have to improve future YEG publications. Please contact me at (867) 667-8519, or by e-mail at karen.macfarlane@gov.yk.ca.

Karen MacFarlane

JIM DODGE
IN MEMORIUM

Jim Dodge died in Whitehorse on August 21, 2010, about 3 month shy of his 90th birthday. A familiar face to Yukon explorationists and residents, he is remembered for his easy smile and positive disposition, his genuine interest in others, and a keen sense of individuality and independence. He was known to many as someone with a sharp inquisitive mind, and an appreciation for beauty, kindness and friendship.

Jim had a full and colourful life and loved to tell stories: he would talk about his first job in a mine in Alaska; of landing in Hiroshima as a lieutenant-colonel with the US military in 1945 to help with reconstruction of the Japanese economy (the silence, he said, was eerie); of evading his military bodyguards in Japan to hop on a train to go skiing in the Japanese Alps; of meeting his future wife Elizabeth and bringing her on these skiing adventures; of he and his pregnant wife hearing the Rhodesian lions roar outside their trailer (he closed the screen window; she, matter-of-factly said: "I don't think this is going to help"); of bear encounters in Yukon... He also loved to hear stories. When I met Jim, he was already an elderly man who had an amazing capacity to be open to the experience of others, and reflect on them with kindness and wisdom.

Returning from Japan, Jim went to Germany to study African ore deposits. He subsequently worked with the Atomic Energy Commission in the US, but eventually formally protested the effects of their testing on humans. With Elizabeth, he operated a uranium mine in Utah, before going with her to Africa to look for emeralds. They had two children, Michael and Sarah, who helped him on the standard drill he was using in the MacPass district. In Yukon, Jim prospected for gold, zinc, jade and emeralds, but will be remembered for the development of the Tea barite deposit and the subsequent lawsuit that cost him all his personal assets. He prospected for rare earth elements before they became a hot commodity. His latest wish was to investigate the occurrence of diamonds in non-craton rocks of Australia. He maintained an interest in current developments in the mining business and the exploration scene in Yukon through the final months of his life.

At 80 years old Jim hiked the Chilkoot trail, and in that same decade also taught himself to use a personal computer and the internet. Jim made friends wherever he went. Following the death of his wife, his annual migration cycle was to arrive in Yukon in the spring, spend the summer engaged in solitary prospecting ventures, then fly to New Zealand for our winter months. He eventually settled in the town of Glenorchy, NZ, where, like in Whitehorse, he made a circle of good friends that welcomed him into their family life. He took an interest in a 2nd World War- era scheelite battery (mill) and single-handedly started a renovation effort that eventually mobilized the community, brought government funding and historical designation to the site, and led to an appearance on NZ TV.

Jim was an educated man with a varied geological career in which he witnessed many significant moments in Canadian mining history. I remember him as a proud, kind, independent man that taught me the grace of acceptance. He initially resisted the loss of independence caused by aging, but he persevered, never showing self-pity and always looking forward. He gracefully accepted help and friendship, and his friendship was the treasure offered in return. We will miss him very much.

Danièle Héon

Yukon Geological Survey staff: (front row, left to right) Laurie Fahr, Olwyn Bruce, Lara Lewis, Tammy Allen, Carolyn Relf, Karen MacFarlane, Tara Genier and Joyia Chakungal; (middle row, left to right) Jeff Bond, Sarah Laxton, Mike Burke, Bailey Staffen, Aubrey Sicotte, Kristen Kennedy, Sue Roy, Danièle Héon, Venessa Bennett, Lee Pigage, Tiffani Fraser; (back row, left to right) Bill LeBarge , Maurice Colpron, Steve Israel, Robert Deklerk, Charlie Roots, Don Murphy, Panya Lipovsky and Ed Long.
Missing from photo: Grant Lowey, Karen Pelletier.

TABLE OF CONTENTS

Preliminary results from a diamond drill hole study to assess shale gas potential of Devonian strata, Eagle Plain, Yukon

Tammy L. Allen[1] and Tiffani A. Fraser[2]
Yukon Geological Survey

Larry S. Lane
Geological Survey of Canada

ABSTRACT

An evaluation of hydrocarbon resource potential in Eagle Plain is one aspect of the Yukon Sedimentary Basins Project, a five-year (2008-2013), collaborative Geo-Mapping for Energy and Minerals (GEM) Program of the Geological Survey of Canada (GSC), in partnership with the territorial governments and universities. As part of this project, Yukon Geological Survey (YGS) and Northern Cross (Yukon) Limited (NCY) are collaborating with the GSC to assess shale gas potential of Devonian shale at Eagle Plain.

Diamond drill core was retrieved from mineral exploration properties to evaluate shale gas potential of Devonian shale of Road River Group and Canol and Imperial formations. Diamond drill core from four holes, located on the Rich property east of Eagle Plain Hotel, were examined and sampled. The core was systematically sampled and analysed by Rock-Eval pyrolysis, optical microscopy, X-ray diffraction (XRD) mineralogy, and palynology.

The results indicate that the succession is thermally overmature with respect to hydrocarbon generation. Due to the high levels of thermal maturity, the Rock-Eval data are unreliable. However, high amounts of residual organic carbon suggest that the Canol Formation has the potential to be an important source rock in the region, under favourable burial conditions. The very high level of thermal maturity of the strata also resulted in very few identifiable Palynomorphs; however, Canol and Imperial formation samples yielded dates of Middle to Late Devonian and Frasnian to Famennian, respectively. XRD analyses indicate Canol Formation shale is highly siliceous whereas Road River Group shale and silty shale of the Imperial Formation are less siliceous and exhibit a more varied lithology. This study suggests that the Canol Formation is more prospective for shale gas than strata of the Imperial Formation or Road River Group.

[1]*tammy.allen@gov.yk.ca*
[2]*tiffani.fraser@gov.yk.ca*

INTRODUCTION

Eagle Plain basin is an underdeveloped prospective hydrocarbon exploration area in north Yukon that is only broadly understood. Minimal hydrocarbon exploration has been conducted in the region since the height of exploration in the 1950s through the 1970s.

A large part of Eagle Plain Devonian stratigraphy underlies thick Cretaceous sedimentary cover. Continuously exposed outcrop is rare. Dempster Highway roadcuts and borrow pits provide discontinuous exposure of Cretaceous and Paleozoic strata. Drainages along the western flank of the Richardson Mountains provide limited exposures, though they are not always accessible due to the small valley sizes, abundant tree cover, and local fluvial and lacustrine deposits.

Previously, Late Devonian shales were sampled along the highway, in river cutbanks, and in petroleum exploration wells; samples were subjected to Rock-Eval pyrolysis (Link *et al.*, 1989; Snowdon, 1988, 1990). Recently, more outcrop samples from the neighbouring Peel Plateau and Plain were analysed using Rock-Eval (Gal *et al.*, 2007; Allen and Fraser, 2008; Allen *et al.*, 2008; Allen, 2010). Surface samples collected and analysed in the past have demonstrated source rock potential but the effects of surface weathering, permafrost and associated fracturing and mineral oxidation common to surface samples may have compromised the accuracy of analytical data. Additional limitations are related to the distance between in-situ exposures areally and vertically, so variations in the petroleum source characteristics are not readily quantifiable.

Exploration activities in the region conducted by Archer, Cathro and Associates (1981) Ltd. during 2007-08, on behalf of a mineral industry client, resulted in Devonian strata being cored continuously over an interval up to 565 m, providing composite stratigraphic sections that include uppermost Road River Group, Canol and Imperial formations (Dumala, 2007; Gregory, 2008). Examining and analysing this drill core can greatly improve our understanding of these stratigraphic units including their lithology, contact relationships, sedimentary structures, and regional variations. The core also provides an opportunity to analyse fresh intact samples, which will significantly reduce analytical problems associated with surface weathering. The full exploration drilling program extended over a distance of 170 km in an approximate north-south direction. Core extracted from this mineral exploration program was donated to the Yukon Geological Survey, Geological Survey of Canada and Northern Cross Yukon. This report focuses on preliminary results from the Rich property where the thickest composite section was recovered.

Results enhance our understanding of both conventional and unconventional petroleum potential in the region and will be integrated in future petroleum resource assessments of Eagle Plain.

STUDY AREA

Eagle Plain basin lies between 65°N and 67°N latitudes and 136°W and 140°W longitudes, bound to the east by the Richardson Mountains, to the northeast by the Keele Range, and south and west by the Ogilvie Mountains (Taiga and Nahoni ranges, respectively; Fig. 1). North to south, the region is approximately 170 km long, and extends approximately 80 km east to west, covering an area of 20 600 km^2. Traversing the southeast corner of the basin is Yukon Highway 5, known as the Dempster Highway. The Eagle Plains Hotel and government maintenance camp are situated in the southeastern portion of the basin, at kilometre 369 of the highway.

The diamond drilling program, from which the core for this study originates, was conducted on the Rich property, located on NTS map sheet 116I/08 at latitude 66°19'N and longitude 136°14'W (Fig. 2). The property is 23 km east of Eagle Plains Hotel, along the western flank of the southern Richardson anticlinorium. Access to the property is via helicopter from the Hotel.

GEOLOGICAL SETTING

PHYSIOGRAPHIC AND TECTONIC SETTING

The Eagle Plain basin exploration region, as identified by the Yukon Oil and Gas Resources Branch (Oil and Gas Resources, 2010) roughly corresponds to the limit of Cretaceous cover (Fig. 1), and includes the Eagle Lowland and part of the southern Richardson Mountains physiographic regions of Matthews (1986).

Eagle Plain basin includes the Eagle fold belt and minor parts of the western Richardson anticlinorium and northern Taiga-Nahoni fold belt of D.K. Norris (1997; Fig. 3). The Eagle fold belt is characterized by a thick Cretaceous sediment cover, and symmetrical and open folds trending almost north, up to 120 km long.
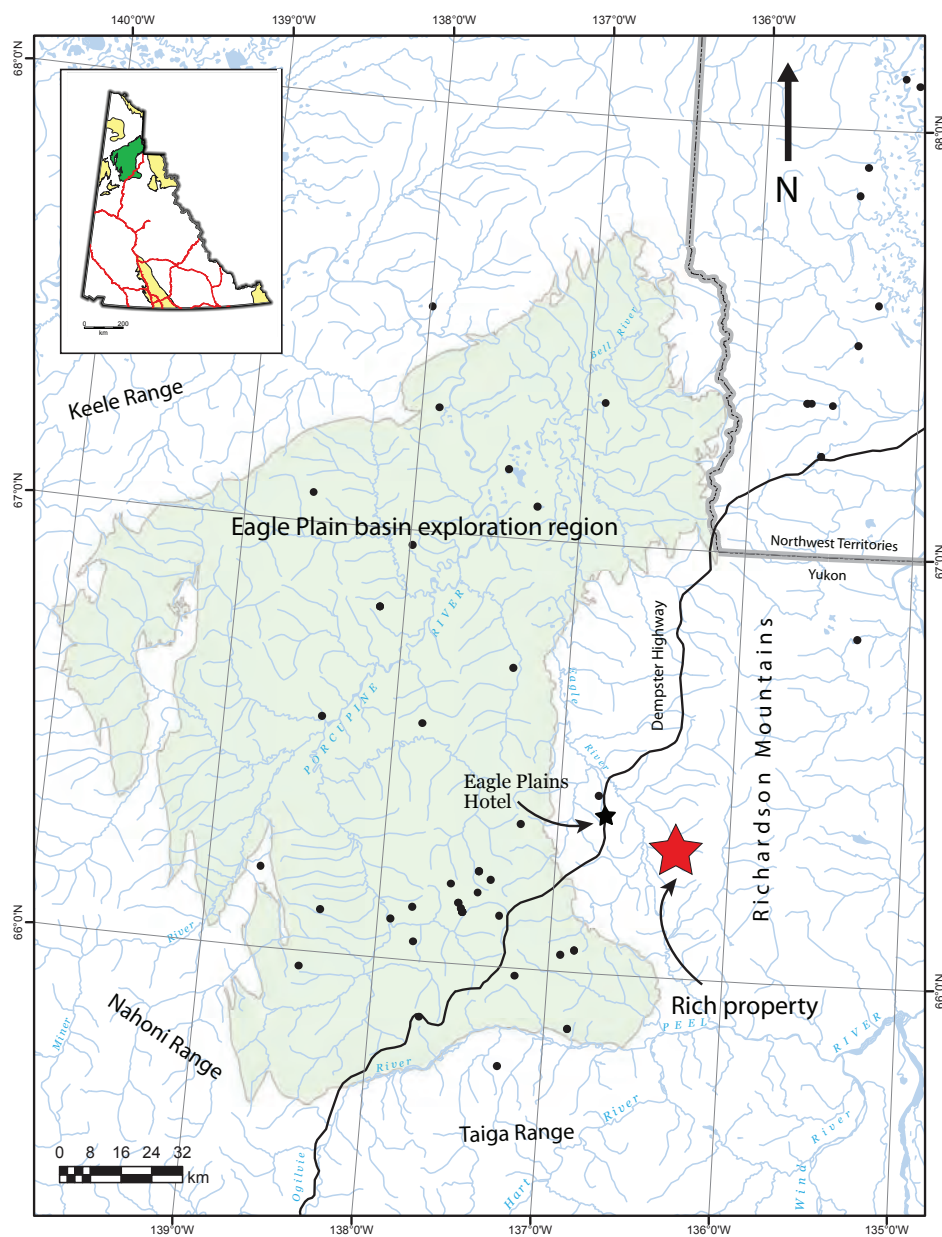
Figure 1. *Map of Eagle Plain basin exploration region and the location of the Rich Property. Black dots represent oil and gas exploration well locations. Inset map of Yukon Territory with Eagle Plain exploration region in green and other oil and gas regions in yellow.*

STRATIGRAPHY

Eagle Plain basin is underlain by an easterly tapering wedge of Phanerozoic sedimentary rock, locally up to 6 km-thick, that overlies Proterozoic strata (Osadetz *et al.*, 2005). The wedge consists of a Paleozoic succession unconformably overlain by a Mesozoic succession. Paleozoic strata generally include Cambrian to Middle Devonian carbonate platform strata deposited on the Yukon Stable Block in the west and associated basinal strata deposited in the Richardson trough to the east (Morrow, 1999; Fig. 3); Middle Devonian to Carboniferous siliciclastic rocks, including distal orogenic foredeep deposits; and mixed-carbonate siliciclastic deposits from Carboniferous to Permian time (Pugh 1983; Morrow, 1999). Mesozoic strata comprise locally preserved Jurassic and Early Cretaceous siliciclastic sediments overlain by widespread Albian shelf deposits up to 1500 m thick; and up to 2 km of Late Cretaceous foreland basin sediments (Dixon, 1992).

In Late Carboniferous and Early Permian time, development of the northeast-trending Ancestral Aklavik Arch (Morrow, 1999; Fig. 3) across the northern margin of the Yukon Stable Block removed a significant section of Carboniferous and uppermost Devonian strata in the central and northern areas of the basin (Dixon, 1998). Jurassic rocks and several Early Cretaceous units are preserved locally, especially on the northern and southern margins of the basin. Each remnant is separated by an unconformity, documenting successive cycles of marine inundation and subaerial exposures during this interval (Dixon, 1992).

This study concerns Middle Devonian to Carboniferous stratigraphy including the uppermost Road River

The Rich property, the location of this study, occupies part of the western limb of the north to northwest-trending Richardson anticlinorium, defining the southern Richardson Mountains. Rocks exposed in the anticlinorium are predominantly Cambrian to Devonian in age. At the Rich property, Road River Group, Canol and Imperial formations are exposed at surface (Figs. 2 and 3).
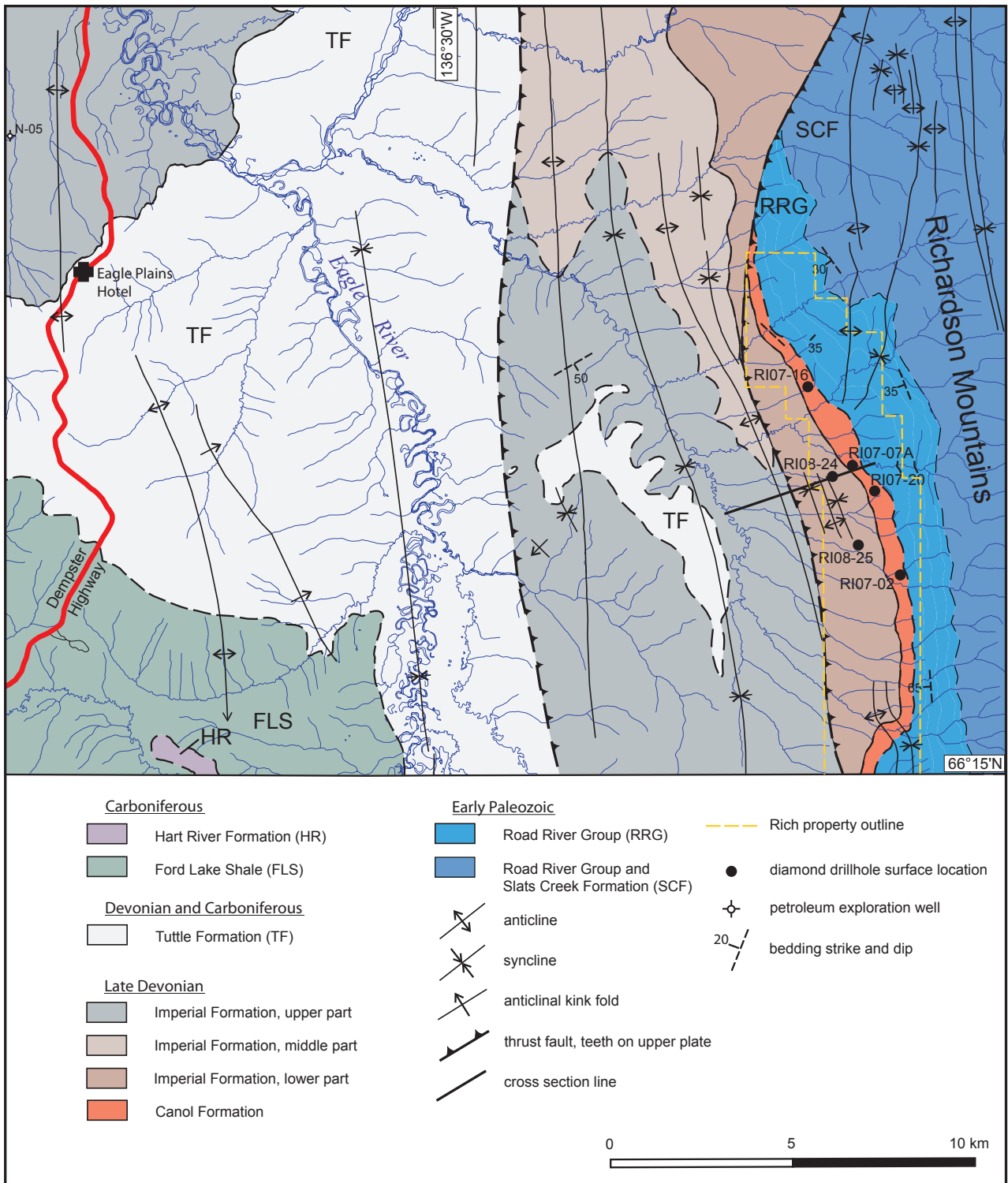
Figure 2. *Geological map of part of Mount Raymond (NTS 116I08), showing locations of the Rich property diamond drill holes from which core was recovered, in relation to the local stratigraphy and structure, as well as the Dempster Highway and Eagle Plains Hotel.*
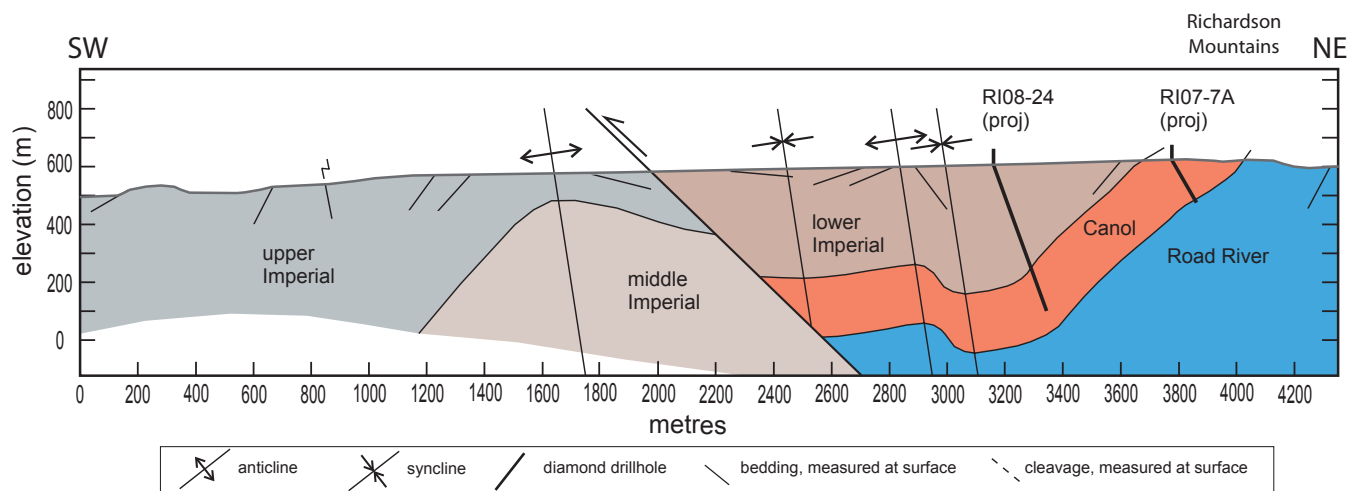
Figure 3. *Local structural cross section through the Rich property showing diamond drill holes RI07-7A (oriented -60° toward 070°) and RI08-24 (oriented -70° toward 090°) projected into the line of section.*

Group and Canol and Imperial formations. A stratigraphic column for the Silurian to Carboniferous is shown in Fig. 4, displaying the relationship and ages of the Road River Group, Canol and Imperial formations. Sedimentation in the study region was affected in the Middle Devonian by the Richardson trough and adjacent (present day west) Yukon Stable Block, and during the Late Devonian and Early Carboniferous by the Ellesmerian orogeny, which resulted in the deposition of a thick package of siliciclastic strata forming a progradational clastic wedge derived from a northern source (Pugh, 1983; Braman and Hills, 1992).

The Road River Group, originally defined by Jackson and Lenz (1962) and elevated to group status by Fritz (1985), was deposited in Late Cambrian to Middle Devonian time in the Richardson trough and on most of the Yukon Stable Block (Morrow, 1999). The upper part of the Road River Group, and that section of stratigraphy that relates to this study, includes the Upper Silurian and Lower to Middle Devonian Vittrekwa unit of Cecile *et al.* (1982). In outcrop, this unit is generally a graptolitic, black shale and shaly limestone, although the upper 50 m, and the stratigraphy pertinent to this study, is white weathering, siliceous shale, and chert. Road River Group strata are thickest, almost 3000 m, in the Richardson trough, however on the Yukon Stable Block it is less than that (Morrow, 1999). The nature of the contact of the Canol Formation with the Road River Group is contentious. Earlier work refers to a significant unconformity there, however more recent work favours the interpretation of the Canol as a condensed section possibly initiated by rapid sea level rise in Givetian time (Pugh, 1983; Morrow, 1999).
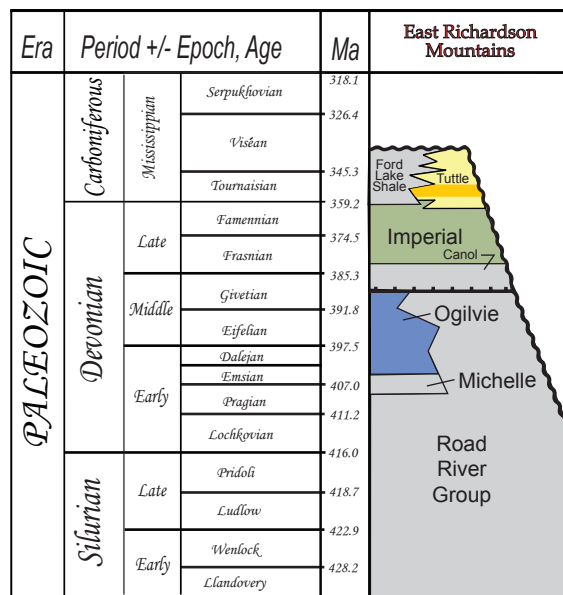
Figure 4. *Stratigraphic column of Silurian to Carboniferous geology of the Richardson Mountains (modified from Morrow, 1999).*

The Middle to Upper Devonian (late Givetian and early Frasnian) Canol Formation (Bassett, 1961) is a grey to black, siliceous thin-bedded, fissile and predominantly non-calcareous shale (Bassett, 1961; Norris, 1985). In the Eagle Plain basin, it ranges in thickness from approximately 4 to 80 m (based on well intersections; Fraser and Hogue, 2007). It is highly organic and is considered a hydrocarbon source rock in the region. In the Richardson Mountains, the Imperial Formation (A.W. Norris, 1997) conformably overlies the Canol Formation.

The Upper Devonian Imperial Formation, originally defined by Link (1921) and formalized by Hume and Link (1945), is a thick package of siliciclastic strata representing shelf, slope and basin deposits derived from the Ellesmerian orogeny (Pugh, 1983; Braman and Hills, 1992). In the western Richardson Mountains, the Imperial Formation consists of three lithologically different units: a lower rusty weathering, siliceous siltstone and shale with minor sandstone; a middle unit dominated by siliceous siltstone, turbiditic sandstone and shale; and an upper portion of light grey weathering, laminated shale and siltstone with thin orange weathering pyritic sandstone beds. The lower portion has been dated in this region as Frasnian to Famennian (Table 3; Braman and Hills, 1992; Dolby, 2010). In the subsurface of Eagle Plain, the Imperial Formation attains a maximum thickness of 1229 m in well intersections, and is overlain, depending on location, either conformably by the Ford Lake Shale or Tuttle Formation or unconformably by Permian or Cretaceous strata (Fraser and Hogue, 2007). Figure 3 displays a cross section of the geology through the Rich property, showing the projected localities of two of the drill holes examined in this study.

STRUCTURE

The Richardson Mountains and Eagle foldbelt comprise local elements of the northern Yukon fold complex that forms a 500 km-long deformed belt extending northward from the Ogilvie Mountains in the south to the Beaufort Sea in the north, and includes the structural salient of the northeastern Brooks Range. The latest Cretaceous and Tertiary deformation that produced this upland complex occurred in multiple pulses (Lane and Dietrich, 1995), with most of the shortening, uplift and cooling occurring in Paleocene to middle Eocene time, based on seismic stratigraphy, biostratigraphy and apatite fission track cooling ages (Lane, 1998). By Late Miocene time the regional tectonic setting had altered to produce broadly northward-directed displacements accommodated by right-

lateral strike slip on faults in the Richardson Mountains and east-west trending folds in the offshore Beaufort Foldbelt (Lane and Dietrich, 1995; Mazzotti *et al.,* 2008).

PREVIOUS WORK

The majority of petroleum exploration wells in Eagle Plain were drilled in the 1960s and 1970s, where the Canol Formation, a principal petroleum source rock, is between 2000 and 3000 m deep. Drilling occurred where underlying lower Paleozoic carbonate was interpreted as a prospective conventional hydrocarbon objective, resulting in only eight of 34 wells intersecting the Canol Formation. The depth to the top of the Canol Formation ranges from 761.4 m below kelly bushing (KB) in borehole North Cathedral YT B-62 to 2775 m below KB in Alder YT C-33. The Canol Formation, ranges in thickness from 3.7 to 79 m, based on log responses interpreted in Eagle Plain exploration wells; the Imperial Formation, intersected in 13 wells, is up to 1228.6 m thick (Fraser and Hogue, 2007). However, no wells preserve a complete section of the Imperial Formation. In contrast, the Canol Formation typically varies between 150 and 250 m thick in outcrop along the western flank of the Richardson anticlinorium. Interpretations of limited seismic data from eastern Eagle Plain indicate preserved thickness for the Imperial Formation of up to 3000 m (*e.g.*, Lane, 1996, Fig. 9), but thinning westward, bevelled beneath the sub-Mesozoic unconformity.

The Canol Formation is considered to be the source rock in the Norman Wells oil field of Northwest Territories (Snowdon *et al.*, 1987). Other documented potential Paleozoic petroleum source rocks in Eagle Plain and Peel Plateau include shale of the Road River Group, Bluefish Member of the Hare Indian Formation, Imperial, Tuttle, Hart River, and Blackie formations and Ford Lake Shale (Link, 1988; D.K. Norris, 1997; Morrow, 1999; Allen and Fraser, 2008; Gal *et al.*, 2009). Recently, Rock-Eval and Oil Show Analyzer results obtained from core and well cutting samples were published for selected Eagle Plain wells (Lane *et al.*, 2010), five of which intersected both the Imperial and Canol formations.

Principal petroleum targets in the Eagle Plain basin include the Permian Jungle Creek Formation, Carboniferous Canoe River and Chance Sandstone members of the Hart River Formation (Osadetz *et al.*, 2005). In some wells, cores were cut in the Carboniferous and shallower Permian sections but few core intervals were cut in shale of the

Upper Devonian Imperial or Canol formations during oil and gas exploration in Eagle Plain. Canol Formation core exists for two wells, ranging from 30 cm to 2.74 m thick, while Imperial Formation core exists for five Eagle Plain wells, ranging in thickness from 30 cm to 8.23 m. All core collected from these oil and gas exploration wells are stored at the GSC Core Repository in Calgary, Alberta.

In 2007 and 2008, at the eastern margin of the Eagle Plain basin, a mineral exploration company undertook a diamond drilling program targeting a stratabound nickel-molybdenum (NiMo) occurrence within the Canol Formation. Individual holes penetrated the lowermost Imperial Formation, Canol Formation, and uppermost Road River Group, recovering continuous core up to 565 m long. BTW (42 mm), NQ (47.6 mm), and HQ (63.5 mm) core from this exploration program were used in our analytical study.

METHODS

FIELD WORK

During September 2009, Yukon government and Northern Cross (Yukon) Limited personnel retrieved approximately 1400 m of the core drilled in 2007 and 2008 along the eastern margin of the Eagle Plain basin. This core program by Archer Cathro and Associates (1981) Limited was part of mineral assessment work performed on behalf of their client Southampton Ventures Inc. on the Rich property, an assemblage of mineral claims staked in 2006 by Archer, Cathro. The core was slung by helicopter to Eagle Plains Hotel and then transported by truck to the Geological Survey of Canada, Calgary office, for sample collection and analyses, including age determination, shale gas and petroleum source rock potential. Core salvaged from the sites were selected in order to collect a representative suite of continuous core along the 170 km-long north-

south trend of Canol and Imperial formations, preserved at relatively shallow depth parallel to the structural uplift of the Richardson Mountains, allowing for both regional and local variation determination. Results presented here include six separate diamond drill holes all of which are from the Rich property (RI07-02, RI07-07A, RI07-16, RI07-20, RI08-24, and RI08-25). Location information for these holes is provided on Figure 2 and in Table 1.

ANALYTICAL WORK

Preliminary analytical work conducted on the core includes Rock-Eval/TOC, shale mineralogical and palynological determinations. All analyses were undertaken by GSC Calgary. Methods and results are presented here.

i) ROCK EVAL/TOC

Core samples from the Road River Group, Canol and Imperial formations were analysed for source rock determination using a Rock-Eval 6 Turbo pyrolysis apparatus in the Organic Geochemistry Laboratory of the Geological Survey of Canada, Calgary. These analyses provide information on organic matter quantity and quality, thermal maturity, and hydrocarbon potential. The sample spacing in the wells was typically every 10-18 m. As with all samples, the Rock-Eval/TOC samples were selected at a constant spacing measured perpendicular to local bedding, with minor adjustments to ensure suitable lithologies were sampled, and with selective additional sampling near contacts. A bitumen sample was also included in the sample set.

ii) SHALE MINERALOGY

XRD is a common method used to determine the mineral composition of shale, which is important in determining a formation's brittleness or 'fracability'

Table 1. *Summary of diamond drill holes used in this study.*

Diamond Drill Hole	Location (NAD83, Zone 8W))		Total Hole Depth (m)	Top - Canol (m)	Top - Road River (m)	Core Size	Azimuth	Dip
	Easting	Northing						
RI07-02	445508	7353769	176.79			BTW	090º	-50
RI07-07A	444283	7356805	170.69	24.83	158.67	BTW	070º	-60
RI07-16	443054	7359059	121.92	16.02	91.91	BTW	060º	-75
RI07-20	444880	7356092	189.28	51.30		BTW	060º	-75
RI08-24	443753	7356495	565.71	370		HQ and NQ	090º	-70
RI08-25	444390	7354600	343.50			HQ and NQ	090º	-70

(mechanically-induced fracture development). Sampling for semi-quantitative XRD analyses was carried out on shale samples from the Road River Group, Canol and Imperial formations at a typical spacing of 25 m measured perpendicular to bedding, with some additional samples collected in the vicinity of contacts. The XRD analyses were run on a Philips PW1700 powder diffraction system with cobalt x-ray source. All analyses were run on powder mounted samples, and executed by the PANalytical X'Pert Quantify software. Mineral determination was processed by PANalytical's X'pert Highscore program, and the quantification of minerals within samples was calculated from their mineral peak intensities (or peak area). Whole rock results are semi-quantitative and are expressed in mineral ratio percent. Total quartz (including chert), total carbonate, and total clay percentages were summed and recalculated out of 100% based on the XRD analyses, and plotted as ternary diagrams (Fig. 6).

iii) PALYNOLOGY

In addition to the organic geochemistry and mineralogy, additional samples were processed for biostratigraphy (palynology) at approximately 50 m intervals, measured perpendicular to local bedding. Thirteen core samples from the 66.9-565 m interval of diamond drill holeRI08-24 were analysed for palynology, spanning the Canol and Imperial formations. The Road River Group was not sampled for palynology.

PRELIMINARY RESULTS

i) ROCK EVAL/TOC

Table 2 summarizes the Rock-Eval/TOC results. Guidelines for interpreting these data are provided in several publications (Espitalié *et al.*, 1985; Peters, 1986; Lafargue *et al.*, 1998). In interpreting the results, it should be noted that Rock-Eval/TOC parameters have significance only above threshold S1, S2 and TOC values, otherwise all parameters have questionable meaning.

The Rock-Eval derived T_{max} values for all samples range between 271°C and 610°C. Of note are S1 and S2 yields approaching zero which indicate that all the available hydrocarbons have been produced (overmature) and that the T_{max} values are unreliable (Peters, 1986). These T_{max} values correspond to vitrinite Ro (random) values between 2.0 and 3.1% (Tissot and Welte, 1984). S2 pyrolysis yields of less than 0.2 mg HC/g rock render meaningless other hydrocarbon indicators such as Hydrogen Index (HI).

Nonetheless, TOC values in the Road River Group and Canol Formation are typically higher than those reported for the Imperial Formation. TOC values for the Road River Group and Canol Formation range from 0.31 to 7.31 wt%, but typically fall in the 2-5% range; whereas TOC values in the Imperial are typically below 1% and therefore suggest poor source rock potential (Fig. 5).

The high residual TOC values for the Road River Group and Canol Formation samples indicate that the initial TOC values were originally much higher. For Type II organic matter, hydrocarbon utilizes roughly half of the initial TOC (Tissot and Welte, 1984). Using this rule of thumb, the initial TOC of the Road River and Canol Formation in this area was typically in the 5-10% range, locally approaching 15%. These findings document that these units were excellent source rocks in the past, consistent with what is already well known for the formation beneath the Interior Platform to the southeast, where the Canol is identified as the principal source unit for the Norman Wells oil.

ii) MINERALOGY RESULTS

Each of the units studied has a distinct mineralogical composition (Fig. 6). XRD results suggest that shale in the Canol Formation is highly siliceous, typically exceeding 95% quartz, whereas the silty shale of the Imperial Formation shows a more varied lithology with up to 17% clay minerals (phyllosilicates) and less than 6% carbonate. Road River Group strata also have a more varied lithology, but are less clay-rich than the Imperial Formation with up to 36% carbonate. Two carbonate-rich samples from the Imperial Formation including one dolomite-rich sample (45% carbonate) and one siderite concretion (55% carbonate) are also presented in Figure 6. Results of XRD analyses are listed in Table 4. Caution should be used with these results as the amount of quartz tends to be overestimated and clay underestimated in many shale samples using standard XRD techniques (Spencer *et al.*, 2010).

Determination of shale mineralogy can be used as a first approximation in determining whether shale is 'fracable', however, other shale characteristics such as fabric may be even more important than mineralogy in determining the mechanical and flow properties of shale (Spencer *et al.*, 2010). This study assessed only the mineralogy of the shale sampled, with the premise that 'fracable' shale contains higher proportions of brittle minerals such as quartz, and lesser proportions of more ductile minerals such as phyllosilicates. An initial observation is that shales of the

Table 2. *Summary of Rock-Eval/TOC data from six diamond drill holes. Parameters measured and derived from Rock-Eval pyrolysis include TOC = total organic carbon as percent weight of whole rock; S1 = mg hydrocarbons/g rock; S2 = mg hydrocarbons/g rock; S3 = mg CO2/g rock; PI = Production Index (S1/S1+S2); HI = Hydrogen Index (100x(S2/TOC)); OI = Oxygen Index (100x(S3/TOC)); Tmax = maximum temperature (°C) at top of S2 peak. Note where S2 values are less than 0.2 mg HC/g rock, the PI and Tmax values are unreliable. Bitumen sample is highlighted.*

Sample	GSC Curation #	Downhole Depth (m)	Formation	S1	S2	PI	S3	Tmax	TOC	HI	OI
R107-02-1	C-491561	105.60	Road River	0.01	**0.10**	0.10	0.24	608	**6.06**	2	4
R107-02-2	C-491562	90.00	Road River	0.01	**0.07**	0.17	0.24	428	**2.40**	3	10
R107-02-3	C-491563	75.80	Road River	0.02	**0.10**	0.16	0.35	343	**2.68**	4	13
R107-02-4	C-491564	58.70	Road River	0.02	**0.12**	0.15	0.21	534	**3.43**	3	6
R107-02-5	C-491565	44.70	Road River	0.02	**0.08**	0.19	0.78	606	**2.53**	3	31
R107-02-6	C-491566	34.00	Road River	0.02	**0.08**	0.19	0.43	607	**2.27**	4	19
R107-07A-1	C-491515	166.50	Road River	0.01	**0.02**	0.25	0.10	316	**2.44**	1	4
R107-07A-2	C-491516	140.21	Canol	0.01	**0.05**	0.12	0.08	610	**3.73**	1	2
R107-07A-3	C-491517	127.50	Canol	0.01	**0.04**	0.23	0.09	611	**3.60**	1	3
R107-07A-4	C-491518	114.80	Canol	0.01	**0.03**	0.21	0.07	357	**2.43**	1	3
R107-07A-5	C-491519	102.30	Canol	0.00	**0.01**	0.26	0.07	343	**2.42**	0	3
R107-07A-6	C-491520	91.00	Canol	0.00	**0.02**	0.20	0.09	611	**3.61**	1	2
R107-07A-7	C-491521	78.10	Canol	0.01	**0.02**	0.20	0.15	340	**4.71**	0	3
R107-07A-10	C-491524	63.20	Canol	0.00	**0.02**	0.19	0.10	513	**5.65**	0	2
R107-07A-11	C-491525	50.60	Canol	0.01	**0.03**	0.19	0.13	421	**3.66**	1	4
R107-07A-12	C-491526	37.80	Canol	0.01	**0.02**	0.26	0.18	389	**5.12**	0	4
R107-16-1	C-491554	121.92	Road River	0.01	**0.04**	0.19	0.14	607	**1.57**	3	9
R107-16-2	C-491555	103.10	Road River	0.02	**0.03**	0.32	0.17	607	**1.60**	2	11
R107-16-3	C-491556	86.00	Canol	0.01	**0.02**	0.29	0.11	606	**2.53**	1	4
R107-16-4	C-491557	72.90	Canol	0.01	**0.05**	0.16	0.10	606	**3.51**	1	3
R107-16-5	C-491558	58.50	Canol	0.01	**0.04**	0.20	0.13	607	**4.83**	1	3
R107-16-6	C-491559	42.00	Canol	0.01	**0.05**	0.19	0.13	606	**3.76**	1	3
R107-16-7	C-491560	25.50	Canol	0.01	**0.04**	0.20	0.09	522	**2.11**	2	4
R107-20-1	C-491567	185.93	Canol?	0.02	**0.07**	0.21	0.23	604	**2.92**	2	8
R107-20-2	C-491568	169.26	Canol?	0.02	**0.08**	0.23	0.21	606	**1.74**	5	12
R107-20-3	C-491569	152.59	Canol	0.04	**0.10**	0.29	0.30	607	**3.64**	3	8
R107-20-4	C-491570	135.92	Canol	0.02	**0.11**	0.13	0.24	606	**3.32**	3	7
R107-20-5	C-491571	119.25	Canol	0.01	**0.04**	0.14	0.11	607	**3.72**	1	3
R107-20-6	C-491572	102.58	Canol	0.01	**0.03**	0.18	0.20	607	**3.60**	1	6
R107-20-7	C-491573	85.91	Canol	0.00	**0.02**	0.16	0.12	489	**2.40**	1	5
R108-24-1	C-486467	565.00	Canol	0.01	**0.03**	0.17	0.04	420	**1.64**	2	2
R108-24-3	C-486469	546.50	Canol	0.01	**0.06**	0.13	0.47	606	**2.69**	2	17
R108-24-4	C-486470	531.30	Canol	0.01	**0.02**	0.17	0.11	608	**7.31**	0	2
R108-24-5	C-486471	521.30	Canol	0.01	**0.04**	0.16	0.27	371	**4.61**	1	6
R108-24-6	C-486472	511.70	Canol	0.01	**0.04**	0.17	0.49	383	**3.69**	1	13
R108-24-7	C-486473	507.70	Canol	0.01	**0.03**	0.16	0.06	386	**4.17**	1	1
R108-24-8	C-486474	494.50	Canol	0.00	**0.00**	0.28	0.17	541	**5.01**	0	3
R108-24-9	C-486475	483.25	Canol	0.00	**0.04**	0.08	0.15	609	**0.31**	13	48
R108-24-10	C-486476	477.50	Canol	0.01	**0.03**	0.17	0.04	357	**2.81**	1	1
R108-24-12	C-486479	458.80	Canol	0.00	**0.02**	0.10	0.00	609	**3.08**	1	0
R108-24-13	C-486480	441.00	Canol	0.01	**0.05**	0.12	0.00	446	**3.42**	1	0
R108-24-14	C-486481	425.00	Canol	0.01	**0.03**	0.15	0.00	606	**2.76**	1	0
R108-24-15	C-486482	408.75	Canol	0.01	**0.04**	0.13	0.11	394	**2.61**	2	4
R108-24-16	C-486483	401.70	Canol	0.01	**0.03**	0.17	0.25	609	**6.45**	0	4
R108-24-17	C-486484	393.00	Canol	0.01	**0.03**	0.16	0.06	610	**3.42**	1	2
R108-24-18	C-486485	384.30	Canol	0.00	**0.02**	0.15	0.21	609	**3.70**	1	6

Table 2 continued

| Sample	GSC Curation #	Downhole Depth (m)	Formation	S1	S2	PI	S3	Tmax	TOC	HI	OI
R108-24-19	C-486486	376.20	Canol	0.01	**0.04**	0.15	0.11	608	**2.69**	1	4
R108-24-20	C-486487	366.80	Imperial?	0.01	**0.03**	0.13	0.00	537	**1.12**	3	0
R108-24-21	C-486488	360.00	Imperial	0.00	**0.03**	0.10	0.34	568	**0.72**	4	47
R108-24-22	C-486489	345.70	Imperial	0.00	**0.03**	0.12	0.01	359	**0.83**	4	1
R108-24-23	C-486490	330.85	Imperial	0.00	**0.03**	0.10	0.09	609	**0.91**	3	10
R108-24-24	C-486491	316.00	Imperial	0.00	**0.03**	0.09	0.12	608	**0.94**	3	13
R108-24-26	C-486493	302.80	Imperial	0.01	**0.03**	0.13	0.09	609	**0.89**	3	10
R108-24-27	C-486494	287.30	Imperial	0.00	**0.03**	0.11	0.00	607	**0.76**	4	0
R108-24-28	C-486495	273.20	Imperial	0.00	**0.02**	0.10	0.06	607	**0.79**	3	8
R108-24-29	C-486496	258.90	Imperial	0.01	**0.06**	0.10	0.21	499	**0.73**	8	29
R108-24-30	C-486497	244.10	Imperial	0.00	**0.02**	0.10	0.07	605	**0.88**	2	8
R108-24-31	*C-486498*	*236.20*	*Imperial*	*0.09*	***3.04***	*0.03*	*0.94*	*608*	***97.96***	*3*	*1*
R108-24-33	C-486500	230.00	Imperial	0.00	**0.03**	0.11	0.06	609	**0.85**	4	7
R108-24-34	C-491501	214.30	Imperial	0.00	**0.03**	0.12	0.04	609	**0.76**	4	5
R108-24-36	C-491503	199.00	Imperial	0.01	**0.03**	0.17	0.18	385	**3.09**	1	6
R108-24-37	C-491504	184.50	Imperial	0.01	**0.04**	0.12	0.33	609	**0.83**	5	40
R108-24-38	C-491505	170.50	Imperial	0.00	**0.03**	0.10	0.06	608	**0.79**	4	8
R108-24-39	C-491506	155.00	Imperial	0.00	**0.02**	0.11	0.09	609	**0.77**	3	12
R108-24-40	C-491507	141.50	Imperial	0.01	**0.03**	0.15	0.01	607	**0.79**	4	1
R108-24-41	C-491508	129.60	Imperial	0.01	**0.18**	0.04	0.10	436	**0.81**	22	12
R108-24-42	C-491509	111.40	Imperial	0.01	**0.05**	0.22	0.05	334	**0.87**	6	6
R108-24-43	C-491510	96.32	Imperial	0.00	**0.03**	0.14	0.05	609	**0.82**	4	6
R108-24-44	C-491511	86.20	Imperial	0.01	**0.04**	0.17	0.00	601	**1.21**	3	0
R108-24-45	C-491512	66.90	Imperial	0.00	**0.03**	0.13	0.00	609	**0.79**	4	0
R108-24-46	C-491513	52.00	Imperial	0.00	**0.02**	0.15	0.03	610	**0.66**	3	5
R108-24-47	C-491514	39.30	Imperial	0.00	**0.01**	0.15	0.11	609	**0.73**	1	15
R108-25-1	C-491574	343.51	Imperial	0.01	**0.04**	0.23	0.09	605	**0.76**	5	12
R108-25-2	C-491575	329.10	Imperial	0.02	**0.04**	0.35	0.10	292	**0.82**	5	12
R108-25-3	C-491576	314.70	Imperial	0.01	**0.04**	0.15	0.06	606	**0.71**	6	8
R108-25-4	C-491577	300.60	Imperial	0.01	**0.03**	0.26	0.08	607	**0.90**	3	9
R108-25-5	C-491578	286.50	Imperial	0.02	**0.04**	0.33	0.08	607	**0.80**	5	10
R108-25-7	C-491580	271.00	Imperial	0.01	**0.05**	0.21	0.11	607	**2.13**	2	5
R108-25-8	C-491581	255.70	Imperial	0.01	**0.04**	0.26	0.07	605	**0.71**	6	10
R108-25-9	C-491582	240.40	Imperial	0.02	**0.04**	0.35	0.09	605	**0.78**	5	12
R108-25-10	C-491583	225.10	Imperial	0.01	**0.03**	0.25	0.14	422	**0.85**	4	16
R108-25-11	C-491584	209.70	Imperial	0.01	**0.02**	0.27	0.09	607	**0.76**	3	12
R108-25-12	C-491585	194.40	Imperial	0.01	**0.04**	0.17	0.08	606	**2.16**	2	4
R108-25-13	C-491586	179.10	Imperial	0.01	**0.04**	0.23	0.12	434	**0.76**	5	16
R108-25-14	C-491587	163.80	Imperial	0.01	**0.03**	0.14	0.06	607	**0.76**	4	8
R108-25-15	C-491588	148.50	Imperial	0.01	**0.06**	0.15	0.16	607	**0.74**	8	22
R108-25-16	C-491589	134.50	Imperial	0.02	**0.03**	0.37	0.11	473	**0.74**	4	15
R108-25-17	C-491590	120.50	Imperial	0.01	**0.05**	0.21	0.11	605	**0.75**	7	15
R108-25-18	C-491591	105.50	Imperial	0.11	**0.08**	0.59	0.10	334	**0.71**	11	14
R108-25-19	C-491592	91.50	Imperial	0.06	**0.09**	0.41	0.14	271	**0.72**	12	19
R108-25-20	C-491593	77.50	Imperial	0.01	**0.02**	0.43	0.16	607	**0.57**	4	28
R108-25-21	C-491594	63.50	Imperial	0.01	**0.02**	0.23	0.08	606	**0.60**	3	13
R108-25-22	C-491595	49.50	Imperial	0.01	**0.03**	0.30	0.06	607	**0.67**	4	9
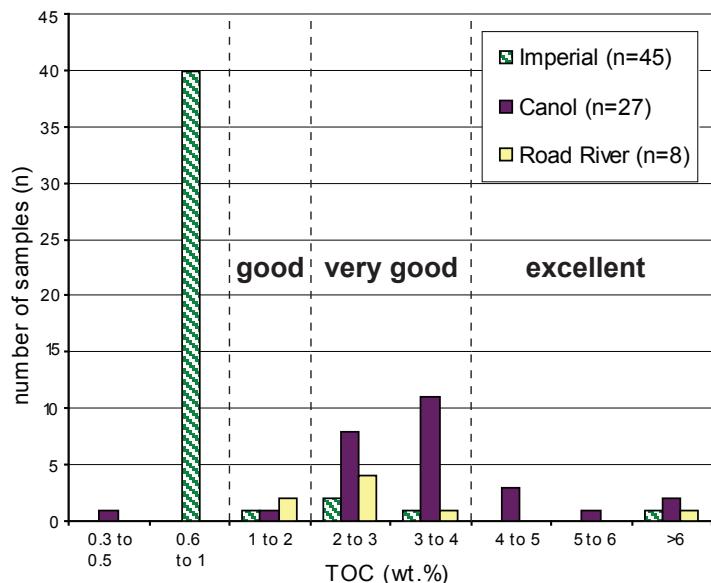
Figure 5. *Histogram summarizing total organic carbon (TOC), expressed in weight percent (wt%), from samples collected during this study of the Road River Group, Canol and Imperial formations. The TOC categories (good to excellent) correspond with source rock generative potential (Peters, 1986). See Table 2 for corresponding dataset.*

Figure 6. *Ternary diagram displaying the relative mineralogical composition of Road River Group, Canol and Imperial formations shale. The square represents the iron carbonate concretion sample; the star represents a dolomite-rich sample from the Imperial Formation. The corresponding data are in Table 4.*

Canol Formation have the best prospects for fracability when compared to the Imperial Formation and Road River Group. Enhancing this study with thin section examination utilizing a scanning electron microscope (SEM) would provide a more comprehensive understanding of the mechanical properties of the shale.

iii) PALYNOLOGY

Due to very high thermal maturities throughout the section, very few palynomorphs could be identified from the Canol and Imperial formations. Spores were abundant in some samples, however most of them are opaque and unidentifiable (Dolby, 2010). Palynomorphs and chitinozoa fragments suggest the Canol Formation is Middle to Late Devonian in age. Spores identified in Imperial strata are characteristic of undifferentiated Frasian to mid Famennian species (Dolby, 2010). Results are summarized in Table 3.

SUMMARY AND DISCUSSION

Retrieval of diamond drill core from the Road River Group, Imperial and Canol formations on the western flank of the Richardson Mountains has provided an opportunity to

examine relatively 'fresh' rock for the purpose of assessing shale gas potential in the region.

The Canol Formation sampled in the Rich property diamond drill holes is highly siliceous, organic-rich, and contains Middle to Late Devonian palynomorphs. The overlying lowermost Imperial Formation is siltier, less organic-rich, and less siliceous than the Canol, and is dated as Frasnian to mid Famennian in age based on palynology. Road River Group shale is organic-rich and the least siliceous of all strata examined. The thermal maturity of all strata studied is very high, with corresponding vitrinite reflectance values in the range of 2-3%. Thermal maturity data indicate that the hydrocarbon generative potential of these rocks has been exhausted and the remaining organic carbon is inert.

The influence of Laramide orogenesis and associated heat flow along the western margin of the Richardson uplift is likely greater than occurs in the more stable setting of the Eagle Plain basin further to the west, where thermal maturities have been established as much lower or even immature for hydrocarbon generation. Somewhere between these extremes, shale gas potential seems likely to be present. Previous studies of Canol and Imperial strata have indicated that the thermal maturity is less extreme

Table 3. *Summary of palynological data from diamond drill hole RI08-24 for the Canol and Imperial formations. Dolby (2010) completed the identifications and assignments.*

Sample ID	GSC Curation #	Unit	Downhole Depth (m)	Probable ages based on palynology
RI08-24-1	C486467	Canol	565.00	Middle Devonian (chitinozoans)
RI08-24-8	C486474	Canol	494.50	Middle Devonian (chitinozoans)
RI08-24-16	C486483	Canol ?	401.70	Middle to Late Devonian undifferentiated
RI08-24-18	C486485	Canol ?	384.30	Middle to Late Devonian undifferentiated
RI08-24-19	C486486	Canol ?	376.20	Middle to Late Devonian undifferentiated
RI08-24-20	C486487	Imperial	366.80	Late Devonian - Frasnian to mid Famennian
RI08-24-21	C486488	Imperial	360.00	Late Devonian - Frasnian to mid Famennian
RI08-24-26	C486493	Imperial	302.80	Late Devonian - Frasnian to mid Famennian
RI08-24-30	C486497	Imperial	244.10	Late Devonian - Frasnian to mid Famennian
RI08-24-37	C491504	Imperial	184.50	Late Devonian - Frasnian to mid Famennian
RI08-24-41	C491508	Imperial	129.60	Late Devonian - Frasnian to mid Famennian
RI08-24-45	C491512	Imperial	66.90	Late Devonian - Frasnian to mid Famennian

to the west in Eagle Plain, where cuttings samples have yielded Ro (random) and equivalent values varying about 1% in several petroleum exploration wells, suggesting the strata are within the oil window at the basal Imperial and Canol stratigraphic level (Link, 1988; Link and Bustin, 1989; Lane *et al.*, 2010). In the Link and Bustin (1989) study, the apparent lack of a maturity discontinuity at the sub-Cretaceous unconformity indicates that the thermal peak was achieved in post-Cretaceous time. However, a lesser, earlier thermal peak is not precluded by the data. The occurrence of immobile pyrobitumen in fractures indicates that hydrocarbons were previously produced and mobilized into the fractures prior to the thermal peak, thus supporting the possibility of an earlier thermal event.

Stratigraphic evidence in Eagle Plain as well as fission track cooling ages from widespread localities across the region (Lane, 1998; O'Sullivan and Lane, 1997) indicate that the dominant uplift/cooling event in the region was latest Cretaceous to Eocene in age, and that inversion of the Richardson trough and uplift of the Richardson anticlinorium was accommodated on outward-directed thrust faults (Lane, 1996). Thermal maturation levels are distinctly higher on the upthrown sides of those faults, which juxtaposed older strata from deeper crustal levels against younger, cooler strata at that time. A candidate mechanism for possible earlier burial and thermal maturation lies in the Late Devonian and Early Carboniferous deposition of some 2-4 km of Ellesmerian foredeep clastic rocks across the Eagle Plain – Richardson trough – Peel Plateau region (Lane, 2010).

Due to the very high thermal maturity (T_{max}) of the cored section, the mineralogy data are the most valuable for shale gas evaluation purposes. High quartz percentages and total organic carbon contents in the Canol Formation suggest that this formation may be the most prospective in terms of shale gas potential, although further studies are required to assess its full potential. The high silica content of these shales is more favourable for fracing the rock than more clay-rich rocks of the Imperial Formation.

Further results are anticipated regarding thermal maturity based on vitrinite reflectance data. These data combined with data from other mineral exploration properties extending over a 170 km length will be presented in supplementary publications.

ACKNOWLEDGEMENTS

Table 4. XRD semi-quantitative analysis (expressed in mineral ratio percent) of black shale core samples. One sample is an iron carbonate concretion (highlighted in grey) (see Fig. 6).

Sample ID	GSC Curation #	M.L.C.*	Mica / Illite	Clinochlore	Gypsum	Quartz	Feldspars	Calcite	Dolomite	Pyrite	Siderite	Others	Total Carbonate	Total Clays	Unit	Depth (m)
RI07-02-1	C491561		1			81	1	14		1		Sphalerite?-2	14	1	Road River	105.60
RI07-02-3	C491563		2			75		19	1	3			20	2	Road River	75.80
RI07-02-5	C491565		3		3	81		11		2			11	3	Road River	44.70
RI07-07A-1	C491515		2			92		4		2			4	2	Road River	166.50
RI07-07A-2	C491516		1			96	1(K)	1		1			1	1	Canol	140.21
RI07-07A-4	C491518		2			95				3			0	2	Canol	114.80
RI07-07A-5	C491519	trace	1			94				5			0	1	Canol	102.30
RI07-07A-6	C491520		1		trace	96		trace		2			1	1	Canol	91.00
RI07-07A-10	C491524		2		2	88				8			0	2	Canol	63.20
RI07-07A-12	C491526		1		1	90			1	8			0	1	Canol	37.80
RI07-16-1	C491554		1			88		10		1			10	1	Road River	121.92
RI07-16-2	C491555		1			61		34	2	2			36	1	Road River	103.10
RI07-16-3	C491556		1			98	trace			1			0	1	Canol	86.00
RI07-16-5	C491558		2			92	2(K)			4			0	2	Canol	58.50
RI07-16-7	C491560		2			95	trace			3			0	2	Canol	25.50
RI07-20-1	C491567		2			96				2			0	2	Canol?	185.93
RI07-20-3	C491569		1			96				2	1	Siderite?-1%	1	1	Canol	152.59
RI07-20-5	C491571		1		trace	98				1			0	1	Canol	119.25
RI07-20-7	C491573		1		1	95				3			0	1	Canol	85.91
RI08-24-1	C486467		trace			99				1			0	0	Canol	565.00
RI08-24-4	C486470		1			93				5		Rutile?-1%	0	1	Canol	531.30
RI08-24-7	C486473		1			93				6			0	1	Canol	507.70
RI08-24-8	C486474		1			95				4			0	1	Canol	494.50
RI08-24-12	C486479		trace			95				4		Hercynite?-1%	0	0	Canol	458.80
RI08-24-14	C486481		1			93				5		Gahnite(ferroan)?-1%	0	1	Canol	425.00
RI08-24-16	C486483		2			91				6		Anhydrite-1%	0	2	Canol ?	401.70
RI08-24-17	C486484		2			96				2			0	2	Canol ?	393.00
RI08-24-18	C486485		2		trace	95				3		Hercynite?-trace	0	2	Canol ?	384.30
RI08-24-19	C486486		1			95			2	2			2	1	Canol ?	376.20
RI08-24-20	C486487	trace	5			88	trace			2			0	5	Imperial	366.80
RI08-24-21	C486488		2			45		2	36	7			38	2	Imperial	360.00
RI08-24-23	C486490	3	3	2		81	2(Na)		4	2	3	Siderite-3%	7	8	Imperial	330.85
RI08-24-25	C486492	2	2	5		36				2	55	Siderite-55%	55	9	Imperial	315.20
RI08-24-26	C486493	3	4	4		85				2	2	Siderite-2%	2	11	Imperial	302.80
RI08-24-28	C486495	3	5	7		83				2			0	15	Imperial	273.20
RI08-24-30	C486497	3	4	7		84				2			0	14	Imperial	244.10
RI08-24-34	C491501	3	4	4		87				2			0	11	Imperial	214.30
RI08-24-37	C491504	3	4	10		81				2			0	17	Imperial	184.50
RI08-24-39	C491506	3	4	5		86				2			0	12	Imperial	155.00
RI08-24-41	C491508	3	4	8		82				3			0	15	Imperial	129.60
RI08-24-43	C491510	2	2	5		85	2(Na)		2	2			2	9	Imperial	96.32
RI08-24-45	C491512	2	3	6		84	3(Na)		1	1			1	11	Imperial	66.90

Table 4 continued.

Sample ID	GSC Curation #	M.L.C.*	Mica / Illite	Clinochlore	Gypsum	Quartz	Feldspars	Calcite	Dolomite	Pyrite	Siderite	Others	Total Carbonate	Total Clays	Unit	Depth (m)
RI08-24-47	C491514	2	3	5	trace	84	4(Na)			2			0	10	Imperial	39.30
RI08-25-1	C491574	3	4	6		85				2			0	13	Imperial	343.51
RI08-25-3	C491576	3	3	7		83	2(Na)			2			0	13	Imperial	314.70
RI08-25-5	C491578	3	4	6		85	trace			2			0	13	Imperial	286.50
RI08-25-8	C491581	3	4	7		84	trace			2			0	14	Imperial	255.70
RI08-25-10	C491583	2	3	6		86				3			0	11	Imperial	225.10
RI08-25-12	C491585	3	3	3		84			2	5		Fe-dolomite	2	9	Imperial	194.40
RI08-25-14	C491587	2	3	7		82	2(Na)		2	2		Fe-dolomite	2	12	Imperial	163.80
RI08-25-16	C491589	2	3	5		87				3			0	10	Imperial	134.50
RI08-25-18	C491591	2	3	5		85	3(Na)			2			0	10	Imperial	105.50
RI08-25-20	C491593	2	3	6		81	trace			2	6	Siderite-6%	6	11	Imperial	77.50
RI08-25-22	C491595	2	3	9		82	2(Na)			2			0	14	Imperial	49.50

* M.L.C means Mixed Layer Clays
Iron carbonate concretion

REFERENCES

Allen, T., 2010. Field Notes on the Upper Devonian Imperial Formation (NTS map sheet 106L), Tetlit Creek, east Richardson Mountains, Yukon. *In:* Yukon Exploration and Geology 2009, K.E. MacFarlane, L.H. Weston and L.R. Blackburn (eds.), Yukon Geological Survey, p. 1-21.

Allen, T.L. and Fraser, T.A., 2008. Hydrocarbon potential of Upper Paleozoic strata, eastern Richardson Mountains, northern Mackenzie Mountains and Peel Plateau, Yukon. *In:* Yukon Exploration and Geology 2007, D.S. Emond, L.R. Blackburn, R.P. Hill and L.H. Weston (eds.), Yukon Geological Survey, p. 91-114.

Allen, T.L., Fraser, T.A. and Osadetz, K.G., 2008. Rock-Eval/ TOC data for 18 wells, Peel Plateau and Plain, Yukon Territory (65°50' to 67°00'N; 133°45' to 135°15'W). Yukon Geological Survey Open File 2008-1, 14 p. plus spreadsheets.

Bassett, H.G., 1961. Devonian stratigraphy, central Mackenzie River region, Northwest Territories, Canada. *In:* Geology of the Arctic, G.O. Raasch (ed.), Alberta Society of Petroleum Geologists and University of Toronto Press, vol. 1, p. 481-498.

Braman, D.R. and Hills, L.V., 1992. Upper Devonian and Lower Carboniferous miospores, western District of Mackenzie and Yukon Territory, Canada. Palaeontolographica Canadiana, no. 8, 97 p.

Cecile, M.P., Hutcheon, I.E. and Gardiner, D., 1982. Geology of the Northern Richardson Anticlinorium. Geological Survey of Canada, Open File 875, scale 1:100 000.

Dixon, J., 1992. Stratigraphy of the Mesozoic strata, Eagle Plain area, northern Yukon. Geological Survey of Canada, Bulletin 408, 58 p.

Dixon, J., 1998. Permian and Triassic Stratigraphy of the Mackenzie Delta, and the British, Barn and Richardson mountains, Yukon and Northwest Territories. Geological Survey of Canada, Bulletin 528, 46 p.

Dolby, G., 2010. Palynological analysis of core, cuttings and outcrop samples from the GEM Yukon Basins Project. Dolby and Associates Report # 2010.9. Internal report prepared for Natural Resources Canada, Calgary, Alberta, 21 p.

Dumala, M.R., 2007. Prospecting, Mapping, Geochemical Sampling, Geophysical Surveys and Diamond Drilling at the RICH Property, Rich 1-46 YC45138-YC45185 and 49-186 YC45388-YC45525, NTS 116I/08, Latitude 66°19'N; Longitude 136°14'W, in the Dawson Mining District, Yukon Territory. Prepared by Archer, Cathro & Associates (1981) Limited for Southampton Ventures Inc. and Strategic Metals Ltd., Government of Yukon, Energy, Mines and Resources.

Espitalié, J., Deroo, G. and Marquis, F., 1985. Rock Eval Pyrolysis and Its Applications. Preprint; Institut Française du Petrole, Geologie No. 27299, 72 p. English translation of, La pyrolyse Rock-Eval et ses applications, Premiere, Deuxieme et Troisieme Parties, in Revue de l'Institut Francais du Petrole, vol. 40, p. 563-579 and 755-784; vol. 41, p. 73-89.

Fraser, T. and Hogue, B., 2007. List of Wells and Formation Tops, Yukon Territory, version 1.0. Yukon Geological Survey, YGS Open File 2007-5, 1 p., plus spreadsheet.

Fritz, W.H., 1985. The basal contact of the Road River Group - a proposal for its location in the type area and in other selected areas in the northern Canadian Cordillera. *In:* Current Research, Part B, Geological Survey of Canada, Paper 85-1B, p. 205-215.

Gal, L.P., Allen, T.L., Fraser, T., Hadlari, T., Lemieux, Y., Pyle, L.J. and Zantvoort, W.G., 2007. Rock-Eval 6 / TOC analyses from outcrop samples in northern Mackenzie Mountains, eastern Richardson Mountains, and southern Peel Plateau and Plain; Northwest Territories and Yukon, Canada. Northwest Territories Geoscience Office, NWT Open Report, 11 p.

Gal, L.P., Allen, T.L., Hadlari, T. and Zantvoort, W.G., 2009. Chapter 10 – Petroleum Systems Elements. *In:* Regional Geoscience Studies and Petroleum Potential, Peel Plateau and Plain, Northwest Territories and Yukon: Project Volume, L.J. Pyle and A.L. Jones (eds.), Northwest Territories Geoscience Office and Yukon Geological Survey, NWT Open File 2009-02 and YGS Open File 2009-25, p. 477-549.

Gregory, D., 20008. Prospecting, Mapping, and Diamond Drilling at the RICH Property, Rich 1-46 YC45138-YC45185 and 49-186 YC45388-YC45525, NTS 116I/08, Latitude 66°19'N; Longitude 136°14'W, in the Dawson Mining District, Yukon Territory. Prepared by Archer, Cathro & Associates (1981) Limited for Southampton Ventures Inc. and Strategic Metals Ltd., Government of Yukon, Energy, Mines and Resources.

Hume, G.S. and Link, T.A., 1945. Canol investigations in the Mackenzie River area, Northwest Territories and Yukon. Geological Survey of Canada, Paper 45-16, 87 p.

Jackson, D.E. and Lenz, A.C., 1962. Zonation of Ordovician and Silurian graptolites of northern Yukon, Canada. American Association of Petroleum Geologists Bulletin, vol. 46, p. 30-45.

Lafargue, E., Espitalié, J., Marquis, F. and Pillot, D., 1998. Rock-Eval 6 applications in hydrocarbon exploration, production and soil contamination studies. Revue de l'Insitut Français du Petrole vol. 53, 421-437.

Lane, L.S., 1996. Geometry and tectonics of early Tertiary triangle zones, northeastern Eagle Plain, Yukon Territory. Bulletin of Canadian Petroleum Geology, vol. 44, p. 337-348.

Lane, L.S., 1998. Late Cretaceous-Tertiary tectonic evolution of northern Yukon and adjacent Arctic Alaska. American Association of Petroleum Geologists Bulletin, vol. 82, p. 1353-1371.

Lane, L.S., 2010. Phanerozoic Structural Evolution of Eagle Plain, Yukon. Canadian Society of Petroleum Geologists, Reservoir, vol. 37, no.1, p.11.

Lane, L. S. and Dietrich, J.R., 1995. Tertiary structural evolution of the Beaufort Sea - Mackenzie Delta region, Arctic Canada. Bulletin of Canadian Petroleum Geology, vol. 43, p. 293-314.

Lane, L.S., Snowdon, L.R. and Obermajer, M., 2010. Rock-Eval/TOC and oil show analyzer data for selected Yukon borehole samples. Geological Survey of Canada, Open File 6652, 1 CD-ROM.

Link, T.A., 1921. Unpublished geological report on the Fort Norman area: Imperial Oil Ltd., Calgary, Alberta, 81 p.

Link, C.M., 1988. A reconnaissance of organic maturation and petroleum source potential of Phanerozoic strata in northern Yukon and northwestern District of Mackenzie. Masters thesis, University of British Columbia, Vancouver, British Columbia, 260 p.

Link, C.M. and Bustin, R.M., 1989. Organic maturation and thermal history of Phanerozoic strata in northern Yukon and northwestern District of Mackenzie. Bulletin of Canadian Petroleum Geology, vol. 37, p. 266-292.

Link, C.M., Bustin, R.M. and Snowdon, L.R., 1989. Petroleum Source Potential and Depositional Setting of Phanerozoic Strata in northern Yukon and northwestern District of Mackenzie. Bulletin of Canadian Petroleum Geology, vol. 37, p. 293-315.

Matthews, W.H., 1986. Physiographic map of the Canadian Cordillera. Geological Survey of Canada, Map 1701A, 1 sheet.

Mazzotti, S., Leonard, L.J., Hyndman, R.D. and Cassidy J.F., 2008. Tectonics, Dynamics, and Seismic Hazard in the Canada–Alaska Cordillera. In: Active Tectonics and Seismic Potential of Alaska. Geophysical Monograph Series 179, American Geophysical Union, p. 297-319.

Morrow, D.W., 1999. Lower Paleozoic Stratigraphy of Northern Yukon Territory and Northwestern District of Mackenzie. Geological Survey of Canada, Bulletin 538, 202 p.

Norris, A.W., 1985. Stratigraphy of Devonian outcrop belts in northern Yukon Territory and northwestern District of Mackenzie. Geological Survey of Canada, Paper 67-53, 287 p.

Norris, A.W., 1997. Devonian. In: Geology and Mineral and Hydrocarbon Potential of Northern Yukon Territory and Northwestern District of Mackenzie, D.K. Norris (ed.), Chapter 7. Geological Survey of Canada, Bulletin 422, p. 163-200.

Norris, D.K., 1997. Geological Setting. In: Geology and Mineral and Hydrocarbon Potential of Northern Yukon Territory and Northwestern District of Mackenzie, D.K. Norris (ed.), Chapter 3. Geological Survey of Canada, Bulletin 422, p. 21-65.

Oil and Gas Resources, 2010. Oil and Gas Basins – Yukon Albers, ESRI shapefile. Department of Energy, Mines and Resources, Government of Yukon, <http://www.emr.gov.yk.ca/oilandgas/mapsdata.html> [accessed May 2010].

Osadetz, K.G., Zhuoheng, C. and Bird, T.D., 2005. Petroleum Resource Assessment, Eagle Plain Basin and Environs, Yukon Territory, Canada. Yukon Geological Survey Open File 2005-2/Geological Survey of Canada, Open File 4922, 88 p.

O'Sullivan, P.B. and Lane, L.S., 1997. Early Tertiary thermotectonic history of the northern Yukon and adjacent Northwest Territories, Arctic Canada. Canadian Journal of Earth Sciences, vol. 34, p. 1366-1378.

Peters, K.E., 1986. Guidelines for evaluating petroleum source rock using programmed pyrolysis. American Association of Petroleum Geologists Bulletin, vol. 70, no. 3, p. 318-329.

Pugh, D.C., 1983. Pre-Mesozoic geology in the subsurface of Peel River Map area, Yukon Territory and District of Mackenzie. Geological Survey of Canada, Memoir 401, 61 p.

Snowdon, L.R., 1988. Petroleum source rock potential and thermal maturation reconnaissance in Eagle Plain, Yukon Territory. Geological Survey of Canada, Open File 1720, 115 p.

Snowdon, L.R., 1990. Rock-Eval/TOC data for 55 Northwest and Yukon Territories wells (60°-69°N). Geological Survey of Canada, Open File 2327, 214 p.

Snowdon, L.R., Brooks, P.W., Williams, G.K. and Goodzrzi, F., 1987. Correlation of the Canol Formation source rock with oil from Norman Wells; Organic Geochemistry, vol. 11, p. 529-548.

Spencer, R.J., Pedersen, P.K., Clarkson, C.R. and Aguilera, R., 2010. Shale Gas Part 3 – Shale Properties, CSPG Reservoir, vol. 37, no. 10, p. 26-29.

Tissot, B.P. and Welte, D.H., 1984. Petroleum Formation and Occurrence. Springer-Verlag, Berlin, Heidelberg, New York, Tokyo, 699 p.

Surficial geology, soils and permafrost of the northern Dawson Range

Jeffrey D. Bond[1] and Panya S. Lipovsky[2]
Yukon Geological Survey

ABSTRACT

New mineral discoveries in the Dawson Range have been heavily supported by soil geochemistry. The use of soil augers to penetrate through loess-rich units and into locally derived weathered bedrock has been important in the successful application of this technique. To assist the mineral exploration industry, we characterized the surficial geology, soils and permafrost of the northern Dawson Range. Mapping indicated that widespread loess is present in the study area and the thickest deposits are located in basins on the south side of the Dawson Range near the Donjek and White rivers. A mantle of weathered bedrock covers virtually the entire landscape. The texture of fluvial deposits is affected by stream order and base level changes along the Yukon River. By understanding the effects of slope, aspect, elevation and permafrost processes on surficial materials, a landscape model can be developed that will facilitate geochemical exploration and mineral development in the region.

[1]*jeff.bond@gov.yk.ca*
[2]*panya.lipovsky@gov.yk.ca*

INTRODUCTION

Recent surficial mapping field work in the northern Dawson Range concludes a three-year surficial mapping project conducted in the Stevenson Ridge map area (NTS 115J; Fig. 1). The objective of mapping the northern Dawson Range was to provide baseline surficial geology information that is applicable to mineral exploration, mineral development, and ecological land classifications. Much of the Dawson Range is underlain by weathered bedrock, so it is assumed that this terrain would be

suitable for exploration using the geochemistry of surficial deposits. In places this is true; however, the periglacial climate of the region, and the widespread Pleistocene eolian deposits, complicate both the collection and interpretation of geochemical data. Furthermore, there will be terrain challenges for mineral development such as building on relatively warm permafrost and dealing with a shortage of high-quality aggregate resources for construction of infrastructure. This paper provides a summary of surficial geology investigations during the 2010 field season.
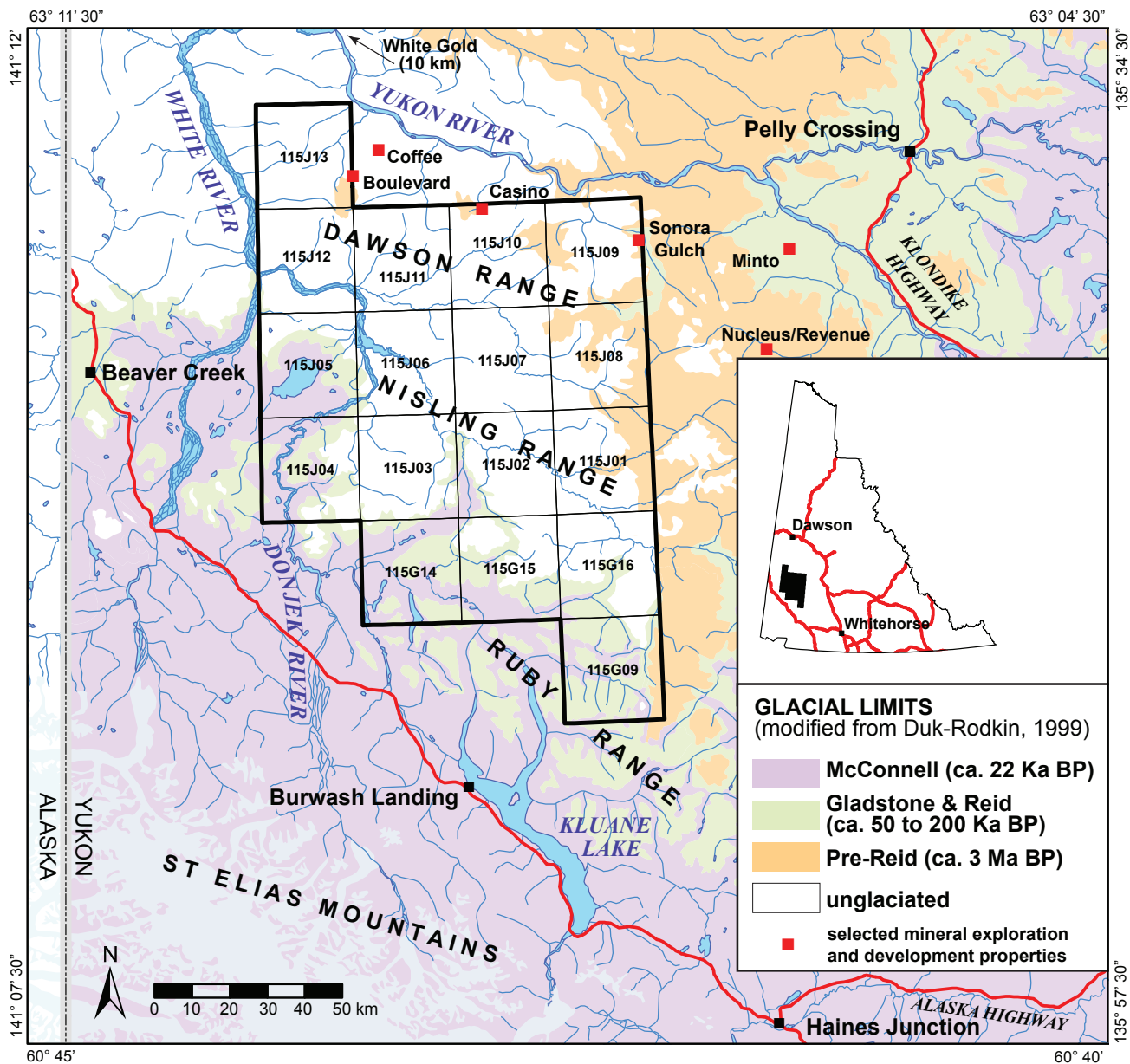

Figure 1. *Location of the Stevenson Ridge (115J) and northern Kluane (115G) study area relative to the glacial limits. The focus for the 2010 field season included 1:50 000-scale map sheets 115J/09-13.*

SETTING

PHYSIOGRAPHY, DRAINAGE AND CLIMATE

The Dawson Range is a northwest-trending mountain range in western Yukon that stretches for over 100 km (Fig. 1). The 2010 study area focused on the northwestern extent of the range in map sheets 115J/09 – 13 (Figs. 1 and 2). With the exception of glaciated massifs, such as Mount Cockfield (1905 m a.s.l.) and Apex Mountain (2022 m a.s.l.), the study area consists mostly of broad, rounded, unglaciated summits that have elevations near 1370 m a.s.l. (Fig. 2). Valley morphology differs depending on proximity to the Yukon River. Streams that flow directly into the Yukon River have experienced a drop in base level, potentially associated with reversal of the Yukon River from a south- to a north-flowing drainage during the early Pleistocene. This Pleistocene base-level change has resulted in deeper incision of third-order reaches of Yukon River tributaries in the Dawson Range. Stream order is

defined as a method of classifying waterways, whereby first order streams are the smallest headwater streams. Where two first-order streams meet, a second-order stream is created (Strahler, 1952). Most tributaries flowing into the Yukon River from the Dawson Range are third or fourth-order drainages. Evidence of the base-level change is most obvious in larger valleys, such as Independence and Carlisle creeks (Fig. 2), where fluvial terraces are preserved near the confluence with the Yukon River. Streams that flow into the Donjek and White rivers however, did not undergo a significant change in base level; in fact, the base levels have possibly risen due to the effects of glaciation in the Wellesley Lake area. As a result, the third and fourth-order streams on the south side of the Dawson Range have wide, low-gradient floodplains.

The climate of the region is described as cold and semi-arid. The mean annual temperature is between -4 and -8°C and the mean annual precipitation is 300 mm (Smith *et al.*, 2004).
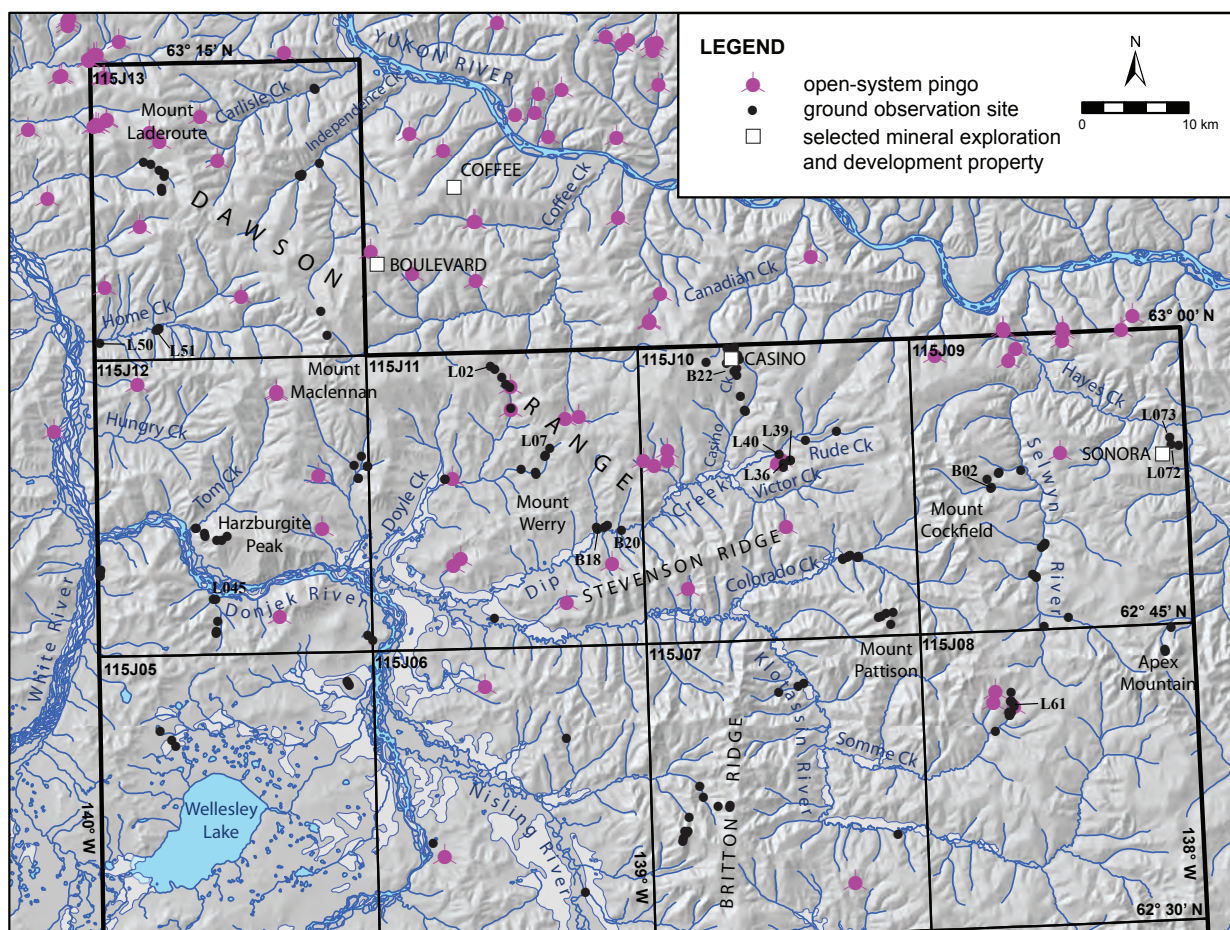

Figure 2. *Location of physiographic features, water bodies, ground observation sites and pingos within the greater study area. Labeled ground observation sites (e.g. L02) are referred to in this report. Relevant mineral exploration properties are also identified.*

BEDROCK GEOLOGY

The bedrock geology of the northern Dawson Range consists of Paleozoic metamorphic rocks of the Yukon-Tanana terrane intruded by Cretaceous and early Cenozoic plutons (Bennett *et al.*, 2010). Regionally, the Cretaceous intrusions are associated with major strike-slip faults that may extend into the Dawson Range, imposing a primary northwest-trending structural trend in the region. Second-order, northeast-trending structures extending up Tom Creek, Doyle Creek and Dip Creek (Murphy *et al.*, 2007) may be associated with extension and local copper-gold mineralization (Bennett *et al.*, 2010).

The northern part of the study area is underlain by the mid-Cretaceous Dawson Range batholith granodiorite (mKW – Whitehorse suite), which was intruded by Late Cretaceous plutons (LKP - Prospector Mountain suite). Upper Cretaceous Carmacks Group volcanics (uKC) are found near Apex Mountain, in the headwaters of the Klotassin River and near the mouth of Nisling River (Fig. 2; Gordey and Makepeace, 2003). Early Cenozoic Skukum/Mount Creedon volcanics outcrop within the Dawson Range batholith and surrounding Britton Ridge which is formed of early Tertiary Nisling Range intrusives (Gordey and Makepeace, 2003). South of Dip Creek, Stevenson Ridge is composed primarily of Paleozoic quartzite and schist of the Yukon-Tanana terrane. Cretaceous mafic volcanics (tuffs and greenstone) and late Paleozoic ultramafics (harzburgite) are found between the mouth of the Donjek River and Mt. Werry (Murphy *et al.*, 2007).

The Dawson Range mineral belt trends northwest through the study area and hosts several copper and gold deposits and prospects (Fig. 1), including:

- White Gold (structurally controlled Au)
- Coffee (Au)
- Boulevard (Au)
- Casino (Au-Cu-Mo-Ag porphyry)
- Sonora Gulch (epithermal/skarn/porphyry Cu-Au-Ag-Mo)
- Revenue (Cu-Mo-Au-Ag-W porphyry)
- Minto (Cu-Au porphyry/IOCG)
- Nucleus (structurally controlled/skarn Cu-Au)

GLACIAL HISTORY

The northern Dawson Range is largely an unglaciated landscape. The only evidence of glacial deposits observed in the study area was on the east side of Mount Cockfield (Figs. 2 and 3). The well developed cirques and end moraine preserved in this area suggests the massif was last glaciated in the late Wisconsin. The glacial limit map of Yukon (Duk-Rodkin, 1999) depicts a series of isolated early Pleistocene ice cap limits on the northern Dawson Range (Fig. 1). While there is evidence of early Pleistocene cirques in this area, we were not able to conclusively identify any depositional glacial landforms. The lack of glacial landform development and the subdued morphology of the cirques suggest this part of the Dawson Range has not been glaciated in over 200 000 years.

McConnell end moraine
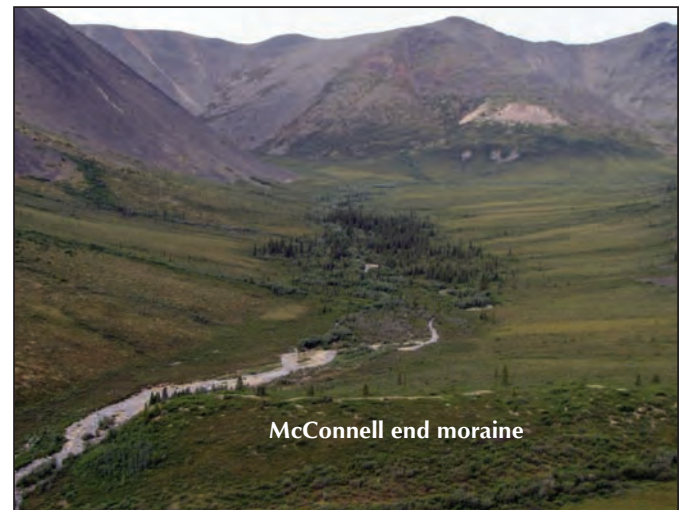
Figure 3. *An alpine glacier end moraine on the east side of Mount Cockfield (see B02 on Figure 2). The moraine is estimated to be McConnell (late Wisconsin) in age based on the distinct sharpness of the ridge crest. View is to the west.*

SURFICIAL GEOLOGY

LOESS

The most widespread glacially derived sediment in the northern Dawson Range is loess, or wind-blown silt. Loess is generated from glaciofluvial flood plains, primarily during glacial and deglacial periods. The Dawson Range has been repeatedly inundated with loess generated from the floodplains of the Donjek and White rivers, and to a lesser extent, the Yukon River (Fig. 2). The northwest orientation of the range provides a perfect barrier for the dominant wind that blows northward from the Pacific. These winds, coupled with katabatic winds generated off the former

St. Elias ice sheet, gathered silt off the Donjek and White river floodplains and deposited it on the upland.

Surficial geology mapping indicates that the loess accumulations are greatest on the southwest-side, or windward side, of the northern Dawson Range. A northeast paleo-wind direction is further supported by a northeast-trending paleo-parabolic dune on the southern flank of the Dawson Range near the Donjek River. The greatest accumulations of loess (>20 m) were observed on tributary valley margins immediately adjacent to the Donjek and White river floodplains (Fig. 4). These deposits are poorly drained and commonly contain permafrost.

WEATHERED BEDROCK

The most common surficial material in the Dawson Range is weathered bedrock (Fig. 5). It varies in texture according to the lithological characteristics of the underlying bedrock, the amount of loess additions to the soil, and the degree of mixing that has occurred between these two material types. Under the current climatic conditions, periglacial and mass wasting processes are the primary means by which bedrock is liberated into the surficial environment. These processes include frost shattering, cryoturbation, solifluction, soil creep and landsliding.
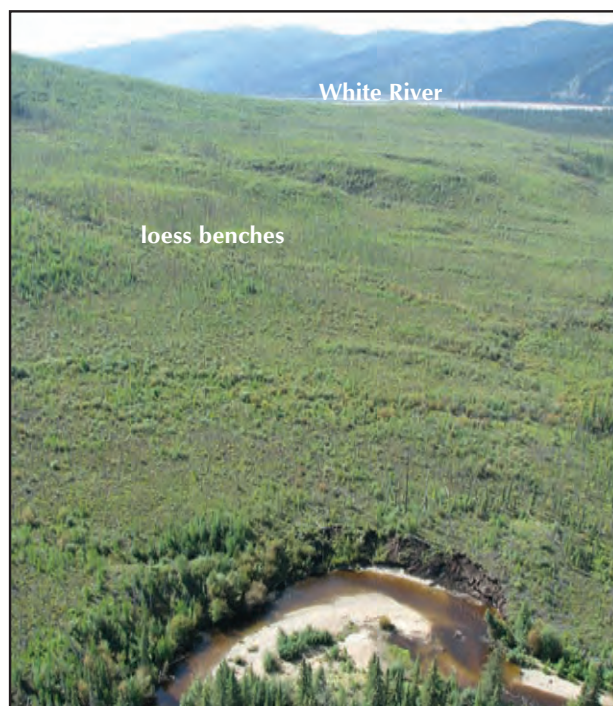

Figure 4. *A view to the southwest over Home Creek; White River is in the background. Thick accumulations (>20 m) of loess (loess benches) are visible along the edge of Home Creek valley.*

Figure 5. *Photograph from the summit of Palton Hill on the Casino property showing a frost-shattered veneer of weathered bedrock (periglacially weathered) overlying bedrock.*

FLUVIAL DEPOSITS

The texture of alluvium in the study area varies according to stream order. First and second order streams are confined to relatively steep, narrow v-shaped valleys. The alluvium in these settings is dominated by locally derived cobbles and boulders; the loess component and fine sediments are largely washed away. Further downstream in third and fourth order reaches, the floodplains widen and stream energy is reduced. The dominant texture in these active channels is sandy, pebble gravel, and the loess component increases. The buildup of colluvial sediments in the high-order valley bottoms confines most streams and limits lateral erosion of the floodplain.

ORGANIC DEPOSITS

Organic deposits are widespread across the study area. Most organic deposits are less than 30 cm thick; however, thicker deposits may be present on poorly drained, north-facing aspects, and in gently sloping valley bottoms. The organic material consists of partially decomposed fibrous peat containing recognizable macrofossils of willow, sedges and rootlets. Buried organic deposits are common in colluvial deposits that are affected by permafrost processes such as cryoturbation and solifluction.

PERMAFROST

Permafrost is widespread but discontinuous in the northern Dawson Range. Permafrost distribution and character (depth, thickness and ice-content) vary widely with local scale variations in both macro and micro-topography, surface cover and soil texture. It is most prevalent on north-facing slopes and in valley bottoms where thick fine-grained slope toe complexes (interbedded loess, colluvium and peat) and alluvial sediments have accumulated.

A variety of landforms that indicate the presence of permafrost were observed throughout the study area including: thermokarst thaw ponds in broad, higher-order valley bottoms; ice-wedge polygons near the confluence of Dip Creek and Klotassin River; and alpine periglacial features such as solifluction lobes and cryoplanation terraces.

Of particular note was the abundance of open-system pingos in the region. Fifty-seven pingos were mapped in the northern Dawson Range study area and hundreds more are found in the unglaciated terrain to the north (Fig. 2). Pingos are ice-cored conical mounds; in the study area, they have dimensions on the order of

10-20 m in height and 100-200 m in width. Hughes (1969) suggested that the distribution of open-system pingos in central Yukon is controlled by topography and permafrost thickness, as well as the appropriate configuration of discontinuous permafrost that allows both groundwater recharge on unfrozen slopes and confinement of artesian pressures beneath frozen valley bottoms.

The pingos in the northern Dawson Range are typically located at the margin of narrow valley floors (Figs. 2 and 6). Most of the pingos have collapse craters suggesting that their ice cores have since thawed. The pingos have developed in a variety of sediment types including fine-grained loess and alluvium, coarser grained grus (grit to pebble-size weathered intrusive fragments), and even bedrock. Establishing the age of pingo formation and collapse was beyond the scope of this study, but warrants further investigation as these landforms are regarded as important habitat islands.

Frost tables were observed in soil pits and stream cut bank exposures at 42 field sites that were visited between July 7 and July 24, 2010. Frost table depths varied between 20 and 170 cm below the ground surface, but were generally less than 1 m. Active layer thicknesses (depth to permafrost table), measured at the end of the summer thaw season, are expected to be of a similar depth or slightly deeper. The frost table was commonly as shallow as 20-40 cm where surface organic cover exceeded 10 cm in thickness.

While permafrost thickness likely varies considerably with topographic position and aspect, several larger subsurface exposures revealed minimum permafrost thicknesses on the order of 10 m in valley bottoms. For example, 12 m of permafrost was exposed in a Sonora Gulch placer excavation (L73); 7 m was exposed in a cut bank on a tributary to the Donjek River (L45); and 9 m was exposed in a Home Creek cut bank (L51).

Volumetric ice contents were visually estimated in the field and were highly variable. Ice contents were generally less than 20% and consisted of thin veins, particle coatings and pore ice. Higher ice contents (up to 50%) were observed in valley bottoms and on mid to upper slopes where groundwater convergence occurred. Thick massive ice lenses consisting of buried aufeis were commonly observed in valley bottoms of low-order drainages. Ice wedges were also observed in a Home Creek cut bank. Clearing or disturbance of organic cover in these areas may lead to rapid thaw and destabilization of ice-rich ground.
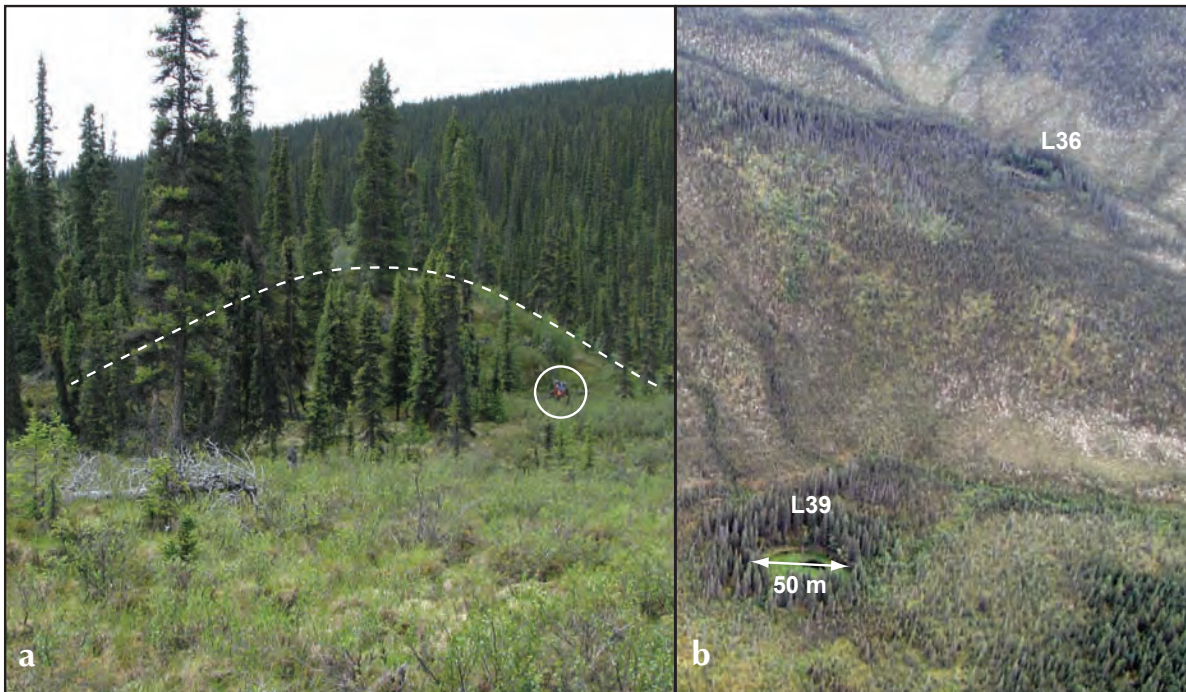
Figure 6. Both uncollapsed *(a)* and collapsed *(b)* open-system pingos were observed in the study area. The uncollapsed pingo is in Somme Creek (L61; Fig. 2) and formed in weathered basalt. The pingo is 5 m high and 45 m in diameter. Note the person circled for scale in Fig. 6a. The collapsed pingos are in a tributary to Rude Creek (L36 and L39; Fig. 2) and both have formed in a silty, colluvial diamicton.

SOIL FORMATION

The term 'soil' can have different meanings depending on its user. For example, in the mineral exploration industry, 'soil sample' is common terminology to describe a near surface sample of unconsolidated sediment. For the purposes of this study, we define a soil sample as the weathered component of parent material that has been altered by chemical, biological, and physical weathering. In the northern Dawson Range, this alteration occurs mainly through decomposition of organic material, translocation of organic matter and silt, enrichment in iron and aluminum oxides and physical weathering by permafrost and periglacial processes. All of these processes, and the extent to which they develop, are affected by topographic position. Lastly, soil properties are affected by the presence of multiple parent materials. In the northern Dawson Range, the most common parent materials include colluvium, alluvium and loess.

General soil horizon characteristics, such as colour, thickness and structure were described based on observations made in the field at hand-dug pits and natural exposures. Due to the cold, semi-arid climate of the region, physical weathering processes like cryoturbation tend to override most other soil forming processes.

Residual soils that formed directly from weathered bedrock contain the least complex parent materials observed in the study area. In the northern Dawson Range, these soils are restricted to flat landscapes typically found on mountain summits and ridges. Detailed soil analyses of high-elevation residual soils was not completed as part of this study; however, recent investigations by Dampier (2010) and Dampier *et al*. (2009) near the southern Dawson Range did characterize the genesis of high-elevation granitic soils. They concluded that periglacial activity, namely cryoturbation, is the most important process affecting upland soils. Chemical analyses indicated that little soil development has occurred, although evidence of alteration of primary minerals demonstrated some chemical weathering. This was present in the form of secondary clay minerals such as kaolinite, vermiculite and minor smectite.

Soil development on slopes is primarily affected by insolation related to aspect (Bond and Sanborn, 2006). On well-drained south-facing slopes, soil horizons are well defined and have not been disrupted by cryoturbation (Fig. 7). The organic horizons and A horizon (incorporated decomposed organic matter) are between 4 and 10 cm thick. The B horizon is emphasized by a zone of iron oxidation that extends up to a depth of 25 cm. The
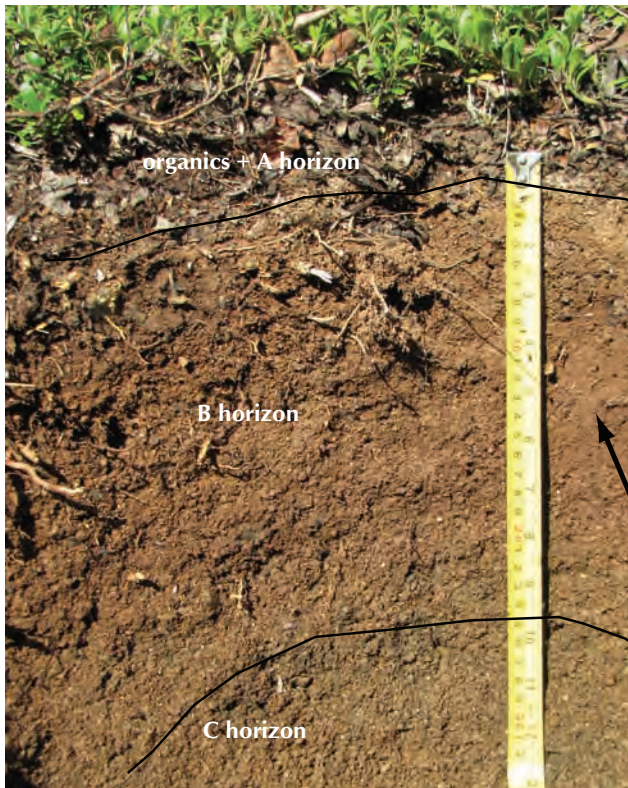
Figure 7. *Soil profile on unfrozen, well-drained bedrock ridge near Dip Creek (B18; Fig. 2). Note the thin surface organic horizon and strongly oxidized colour of the B horizon. The B horizon is siltier and contains fewer coarse fragments (see arrow) compared to the underlying C horizon.*

Figure 8. *Partially thawed Cryosolic soil on Casino property. Note the thick surface organic horizon and absence of oxidized colours. The buried A horizon at the base of the soil pit may have been created by solifluction and/or cryoturbation. The permafrost table is at the contact between the A horizon and the tephra (22 cm depth).*

oxidation often occurs within the loess veneer, although it may extend into the underlying weathered bedrock colluvium. Silt caps are present on the tops of clasts, and build up gradually as silt in suspension is transported downward through the soil horizons via percolating groundwater. These soils are classified as Brunisols based on the absence of permafrost, limited accumulation of organic matter, and strong oxidized colours.

On north-facing slopes, soil development is affected by widespread cryoturbation and near-surface permafrost. Cryoturbation may extend to a depth of 75 cm, mixing both the loess and weathered bedrock parent materials (Smith *et al.*, 2009). Cold soil temperatures reduce the rate of organic matter decomposition, resulting in a surface horizon of partially decomposed organic matter up to 30 cm thick (Fig. 8). The organic horizon insulates the mineral soil and slows the rate of weathering and soil development. As a result, evidence of B horizon weathering is limited to a thickness of 0-10 cm. These soils are classified as Cryosols based on the presence of permafrost.

SURFICIAL GEOLOGY LANDSCAPE MODEL AND EXPLORATION GEOCHEMISTRY SUITABILITY

To summarize the distribution of surficial materials in the northern Dawson Range, an idealized cross-section was developed (Fig. 9). Each of the landscape positions and their suitability for exploration geochemistry are discussed below.

SUMMITS AND RIDGE TOPS

On mountain summits and ridge tops, limited movement of the weathered bedrock has occurred, especially on gentle slopes such as those underlain by the Dawson Range batholith. Tors are common on the batholith and proximity to these bedrock features signifies limited transport of the weathered bedrock sediment (Figs. 9 and 10). These weathered bedrock deposits are typically <1 m in thickness and may be overlain by a veneer of

Figure 9. *An idealized cross-section of the surficial geology across Dip Creek in the northern Dawson Range. This cross-section also illustrates the terrain classification system used for mapping the surficial geology. Regional bedrock map units (DMN5 and mKgW) from Gordey and Makepeace, 2003.*
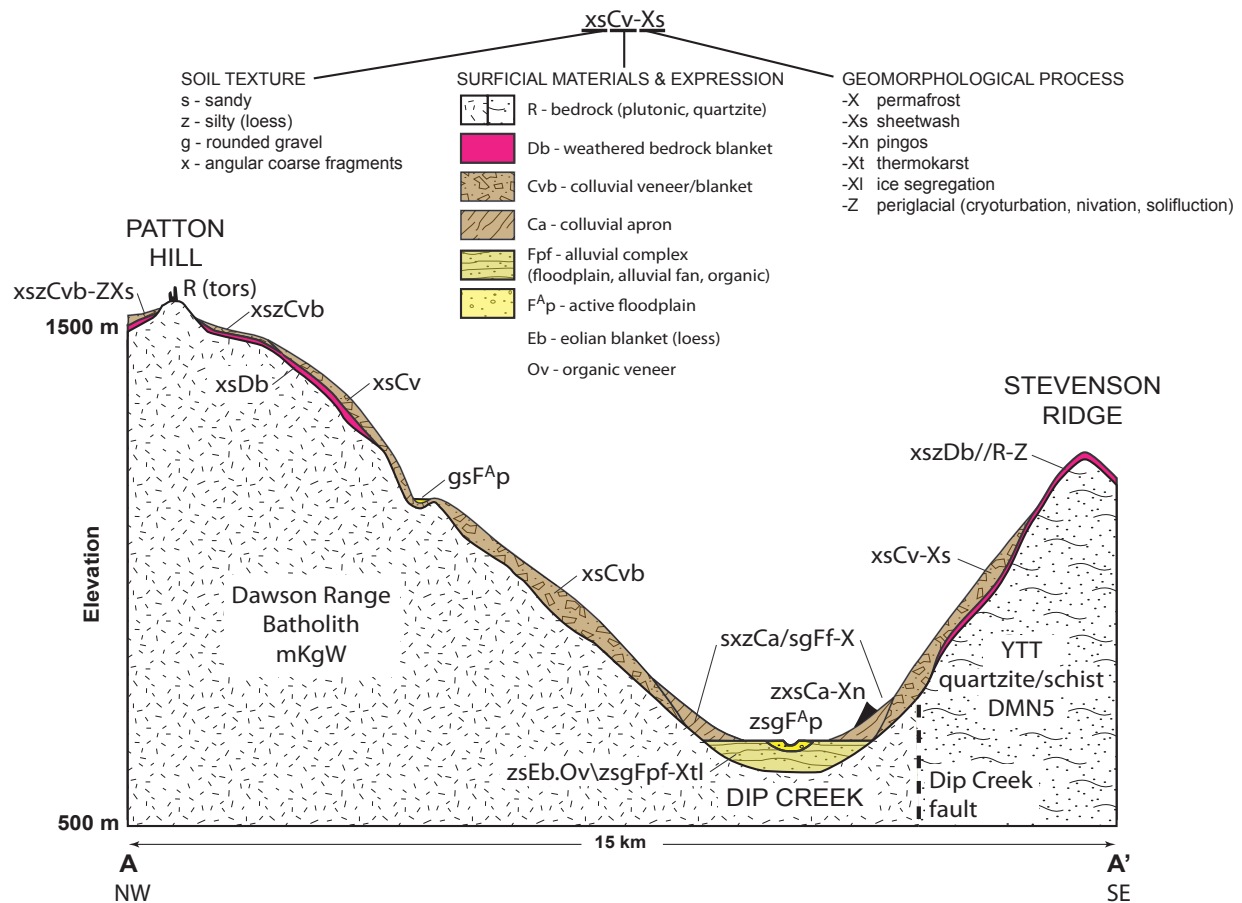
loess (10-20 cm thick) if the site is relatively flat. The loess will be incorporated in the soil profile if cryoturbation has occurred (Dampier *et al.*, 2009; Bond and Sanborn, 2006). Common landforms that signify cryoturbation in alpine environments include sorted stone polygons and mud boils. Soil geochemical samples should be derived from a minimum of 30 cm depth to avoid the loess-enriched soil horizons.

UPPER SLOPES

Immediately downslope from the summit environments are the upper slopes. These landscape environments are spatially extensive over the Dawson Range batholith where much of the landscape has broad, convex, low-angle slopes (Figs. 9 and 11). The primary surficial material on these slopes consists of colluvial veneers (<1 m thick) and blankets (>1 m thick) of transported weathered bedrock fragments. The transport distance of the fragments decreases with depth, although cryoturbation

and solifluction can complicate this pattern by increased mixing of parent materials.

The loess enrichment on these slope positions can be high due to the low slope angles and limited surface erosion. A good example of this was documented on the Casino property. At this site, the intrusive bedrock weathers into coarse angular boulders that become entrained into the upper slope colluvium. Less than 1 km down slope from the summit, on a gentle slope (<10°), the upper 100 cm of the colluvium matrix consisted of ~80% silt and clay based on field estimates (Fig. 11). The matrix of this colluvium is surprisingly fine, given the sandy texture typically associated with weathered granodiorite. For this reason, we suspect that most of the silt was derived from loess deposits. In order to minimize the loess content in soil samples, and potential masking of the weathered bedrock geochemistry, it is recommended to target the sandier components of the colluvium for assaying (Bond and Sanborn, 2006). Soil sampling on upper slopes should therefore be restricted to depths greater than 50 cm.
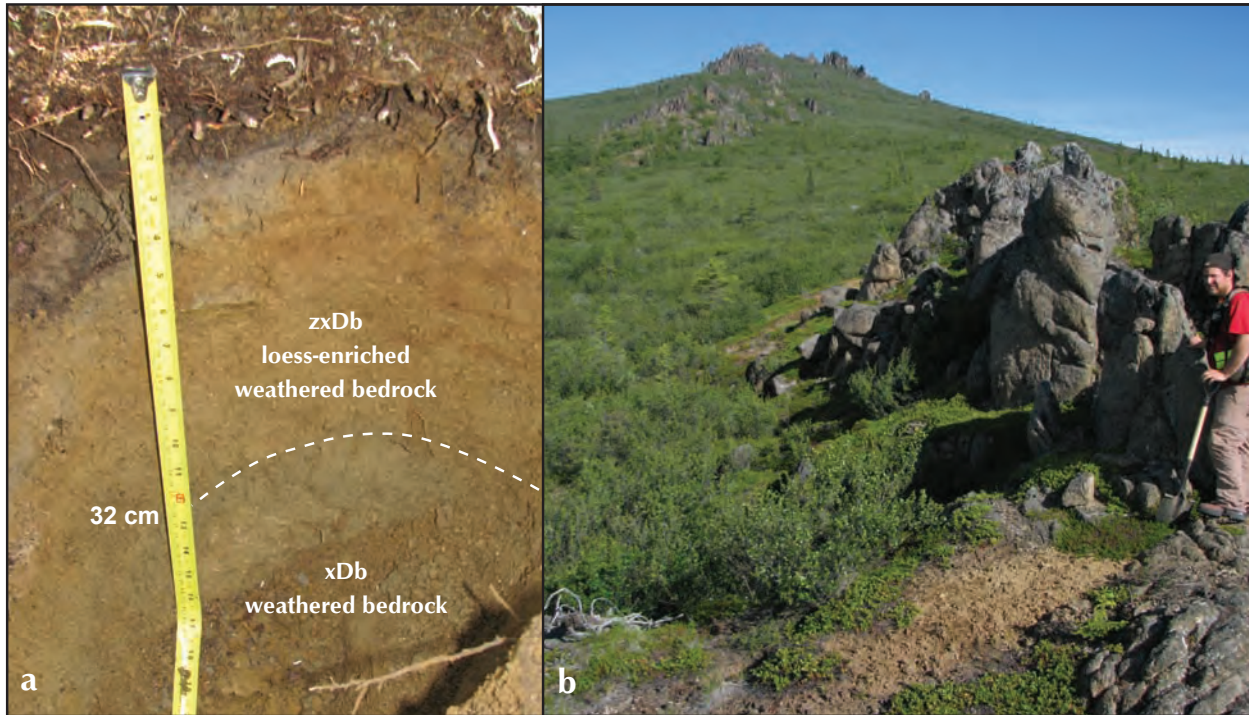
Figure 10. (a) A typical soil profile found near a tor in the Dawson Range summit environment in the study area (L02; Fig. 2). The surficial material exposed in the soil pit consists of loess-enriched weathered bedrock overlying weathered bedrock. For definitions of the classification codes refer to Figure 9. **(b)** Granodiorite tors are a common summit feature within the Dawson Range batholith.
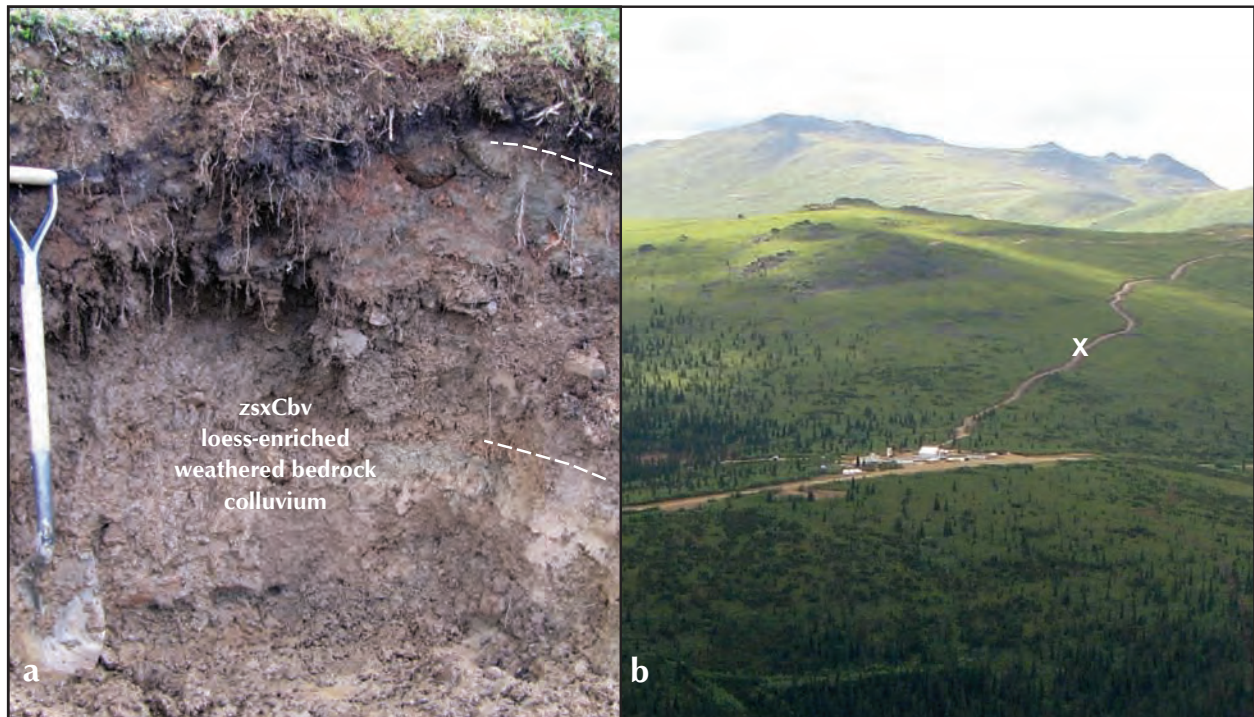
Figure 11. (a) A soil pit illustrating the upper slope position surficial geology (B22; Fig. 2). The surficial material exposed in the soil pit consists of loess-enriched weathered bedrock colluvium that is cryoturbated. The silt content can be as high as 80% in the upper parts of this unit. The zone primarily affected by cryoturbation is identified between the dashed lines. **(b)** An aerial view illustrating the upper slope position near the Casino camp (the "x" marks the location of soil pit in Fig. 11a).

MID-SLOPES

On the mid-slope positions, the slope angles increase into the first-order drainage basins (Fig.12). Similar to the upper slopes, these slopes are mantled with weathered bedrock colluvium (Fig. 9). The colluvium has a stratified appearance, which is accentuated when there are colour variations in the upslope bedrock lithologies. Similar to the upper slope position, the distance of transport of the weathered bedrock fragments decreases with depth (Bond and Sanborn, 2006).

Solifluction lobes are common on these slopes, especially above tree-line. A detailed examination of alpine solifluction lobes on Mount Pattison revealed a decrease in silt content with depth. The internal composition of the lobes consisted primarily of coarse bedrock fragments and little matrix. It appears that much of the movement occurs through deformation within the basal coarse fragment layer.

Loess enrichment is generally lower on mid-slopes because erosion is more active. Some of the loess will get incorporated into the B horizons during the soil creep process, but a significant amount is transported into the valley bottom. Soil geochemical data are more reliable

if sampling occurs at a depth that is greater than 30 cm; however, it is important to account for greater transport distances when interpreting the geochemical data. In addition, large geochemical variations can occur between the colluvial layers depending on the lithological variations and presence of mineralization in the upslope bedrock (Bond and Sanborn, 2006).

LOWER SLOPE COLLUVIAL APRONS

At the base of slopes, significant deposits of colluvial sediment and organic material have accumulated (Figs. 9 and 13). The term colluvial apron is used to describe these deposits because they form a near continuous wedge of sediment at the transition from the hill slopes to the valley bottoms. The colluvial aprons consist mainly of retransported loess mixed with slopewash sediment, which consists of sand and granules that have been carried down slope by water seeping above the permafrost table. Lenses of coarser sediment are common at the base of steeper slopes. In the northern Dawson Range, these landforms cover a significant area, especially along the margins of third and fourth-order valley bottoms. In narrower valleys, the aprons tend to be smaller due to fluvial erosion. Retransported loess

Figure 12. (a) A surficial sediment profile showing the stratified weathered bedrock colluvium that is typical on mid-slope topographic positions (L072; Fig. 2). (b) Aerial view illustrating the mid-slope position in Sonora Gulch. The "X" marks the location of the surficial geology profile.
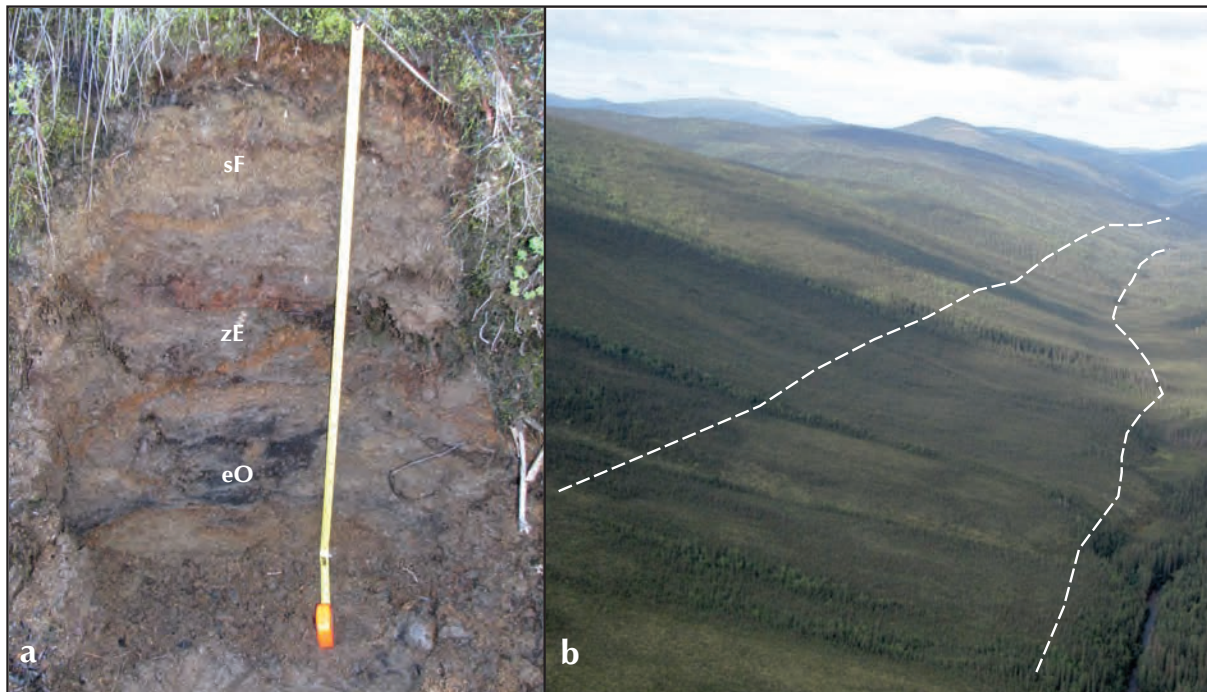
Figure 13. (a) *Surficial sediment profile of typical colluvial apron deposits consisting of retransported loess (zE) mixed with sandy slopewash sediment (sF) and organic matter (eO).* **(b)** *Aerial landscape view of colluvial apron in lower slope position (between dashed lines).*

is the primary sediment type in these landforms and consequently their suitability for exploration geochemistry is low. Ice-rich permafrost is also common in these landforms because of their lower slope position and high silt and organic content, which impedes drainage.

VALLEY BOTTOMS

As described previously, the texture of fluvial deposits vary according to stream order. Alluvium is the main surficial material in valley bottoms of low-order streams, whereas mixed alluvium and colluvium deposits are common in the valley bottoms of broad, high-order streams (Fig. 14). The alluvium in the third and fourth-order valleys is finer and consists of sandy pebble gravel that is typically overlain by silt and widespread organics. Permafrost is continuous in these environments.

Exceptions to this observation include direct tributaries to the Yukon River that have undergone a base-level change. This change has increased stream energy and erosion by increasing the stream gradients and reducing the floodplain width. Fluvial sediment in these drainages is coarse and loess deposits are restricted to blankets on fluvial terraces, or aprons at the base of north-facing slopes. A second exception was found in the valleys on the north side of Stevenson Ridge. Large gravelly fluvial

fans originating from Stevenson Ridge are exposed in cut banks of Dip Creek (B20; Fig. 2). Gravel channels were also noted on the surface of these landforms suggesting active channel avulsion. In terms of aggregate use, the Stevenson Ridge fluvial fans are strategically located for future development in the region.

Mapping the textural variability of fluvial sediment and the relationship to valley morphology is important in stream sediment geochemistry applications. Most stream sediment geochemistry projects assay the silt fraction of the alluvium. This is problematic in the study area because loess is so pervasive. To improve the reliability of stream sediment geochemical exploration, sampling should occur in narrow valleys with high energy streams where the loess content is low. In addition, experimenting with excluding the silt fraction (-230 mesh) from analysis could improve reliability. If this technique is employed, it is important to remember that assay results should not be compared to other surveys where the silt (and clay) fractions were included.

The landscape criteria for obtaining reliable stream sediment samples can also be applied to the regional stream sediment database (RGS). A quick evaluation of the results for arsenic in the study area show that higher values are preferentially found in the first and second
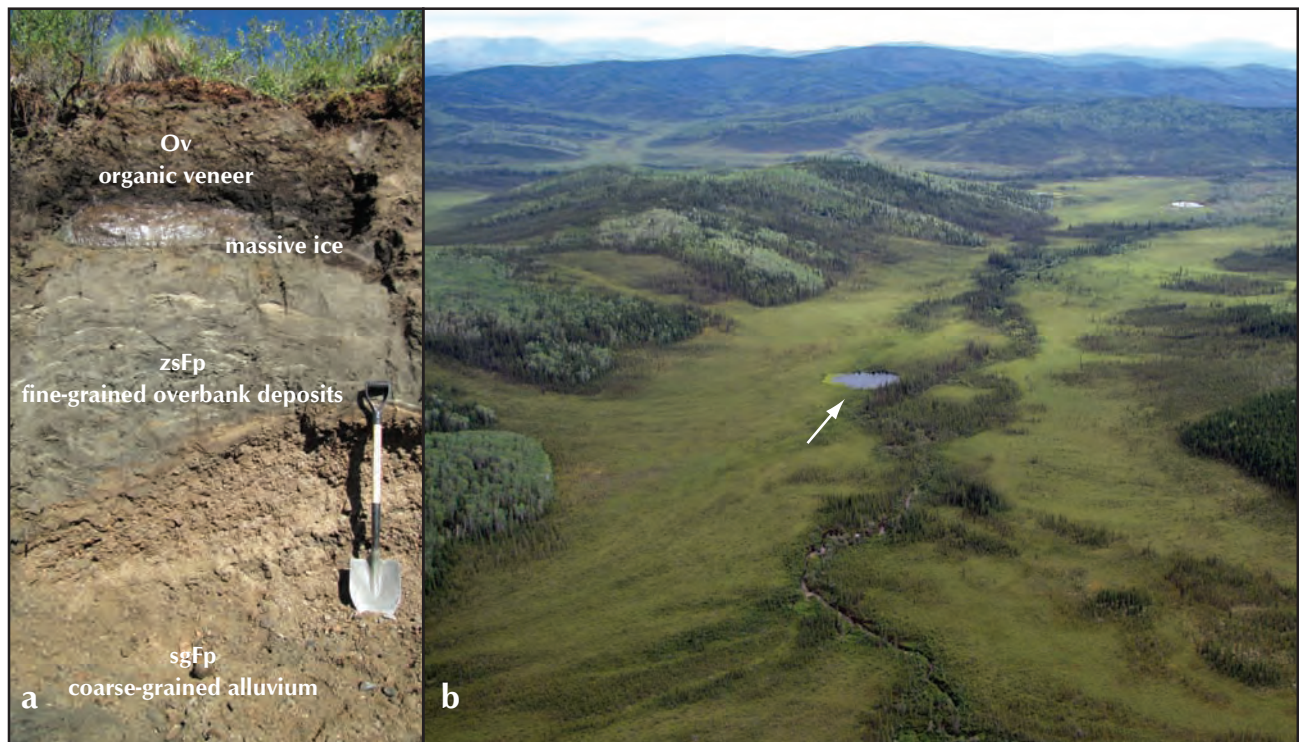
Figure 14. (a) Surficial stratigraphic profile of typical fluvial sediment in third and fourth-order valley bottoms on the south side of the Dawson Range (B18; Fig. 2). Permafrost is common within 30 cm of ground surface. *(b)* Aerial landscape view of the poorly drained third-order valley bottom environments found on the south side of the Dawson Range. A thermokarst thaw pond is denoted by the arrow.

order stream reaches. Anomalies also occur at lower elevations in tributaries to the Yukon River, possibly due to the Pleistocene base-level change. On the south side of the Dawson Range, there are virtually no anomalies in the third or fourth order streams. While this pattern may reflect bedrock geochemistry, it is our impression that it is more likely a function of loess content. In order to prospect the higher-order, low-gradient streams, it is recommended to target coarser alluvium for assaying, apply heavy mineral sampling, or rely strictly on soil geochemistry from adjacent uplands.

SUMMARY

Surficial geology mapping in the northern Dawson Range has emphasized the role that topography and periglacial processes play in affecting unconsolidated material in sub-Arctic unglaciated uplands. The surficial material distribution patterns are somewhat repetitive across the landscape; however, the introduction of loess from nearby braided rivers, and base-level changes in the Yukon River can add local complexities. In terms of mineral exploration, soil geochemical exploration programs need to recognize the distribution and intensity of cryoturbation in order to effectively interpret geochemical data. Stream sediment geochemistry is affected by the ability of streams to effectively mobilize colluvium that reaches the valley bottom. As a result, valley width and gradient, which have a direct relationship to stream order, are important landscape characteristics to consider when planning new stream geochemical surveys or interpreting old data.

Finally, the distribution and character of permafrost in the Dawson Range is affected by the texture of the surficial material, slope aspect and topographic position. Successful development in the northern Dawson Range will require a good understanding of its distribution and character in order to avoid destabilization of ice-rich ground.

ACKNOWLEDGEMENTS

Western Copper Corporation for generously sharing their camp with us this summer. Safe and reliable flight services were provided by HeliDynamics and Alkan Air. Finally, thanks to Paul Sanborn and Leyla Weston for completing a thorough review of this paper.

REFERENCES

Bennett, V., Colpron, M. and Burke, M., 2010. Current thinking on Dawson Range tectonics and metallogeny. Yukon Geological Survey, Miscellaneous Report 2, 12 p.

Bond, J.D. and Sanborn, P.T., 2006. Morphology and geochemistry of soils formed on colluviated weathered bedrock: Case studies from unglaciated upland slopes in west-central Yukon. Yukon Geological Survey, Open File 2006-19, 70 p.

Dampier, L., 2010. Soil genesis in relation to glacial history, central Yukon. Unpublished MSc thesis, University of Northern British Columbia, Prince George, BC, Canada, 244 p.

Dampier, L., Sanborn, P., Bond, J., Clague, J.J. and Smith, S., 2009. Soil genesis in relation to glacial history in central Yukon. *In:* Yukon Exploration and Geology 2008, L.H. Weston, L.R. Blackburn and L.L. Lewis (eds.), Yukon Geological Survey, p. 113-123.

Duk-Rodkin, A., 1999. Glacial limits map of Yukon Territory. Geological Survey of Canada Open File 3694; Exploration and Geological Services Division, Yukon Region, Indian and Northern Affairs Canada, Geoscience Map 1999-2, scale 1:1 000 000.

Gordey, S.P. and Makepeace, A.J. (compilers), 2003. Yukon digital geology, version 2.0. Geological Survey of Canada Open File 1749, and Yukon Geological Survey Open File 2003-9(D), 2 CD-ROMS.

Hughes, O.L., 1969. Distribution of open-system pingos in central Yukon Territory with respect to glacial limits. Geological Survey of Canada, Paper 69, 34 p.

Murphy, D., van Staal, C., Mortensen, J.K., 2007. Preliminary bedrock geology of part of Stevenson Ridge area (NTS 115J/3, 4, 5, 6, 7, 8, parts of 11 and 12; 115K/1, 2, 7, 8, 9, 10, parts of 15 and 16). Yukon Geological Survey Open File 2007-9, scale 1:125 000.

Smith, C.A.S., Sanborn, P.T., Bond, J.D. and Frank, G., 2009. Genesis of Turbic Cryosols on north-facing slopes in a dissected, unglaciated landscape, west-central Yukon Territory. Canadian Journal of Soil Science, vol. 89, p. 611-622.

Smith, C.A.S., Meikle, J.C. and Roots, C.F. (editors), 2004. Ecoregions of the Yukon Territory: Biophysical properties of Yukon landscapes. Agriculture and Agri-Food Canada, PARC Technical Bulletin No. 04-01, Summerland, BC, 313 p.

Strahler, A.N., 1952. Hypsometric (area-altitude) analysis of erosional topography. Geological Society of American Bulletin, vol. 63, p. 1117-1142.

Preliminary stratigraphic and geotechnical investigations of the glaciolacustrine and loess deposits around the city of Whitehorse (NTS 105D/11), Yukon

Marc-André Brideau[1]
School of Environment, University of Auckland, Auckland, New Zealand

Doug Stead
Department of Earth Sciences, Simon Fraser University, Burnaby, BC

Jeffrey D. Bond, Panya S. Lipovsky
Yukon Geological Survey, Whitehorse, YK

Brent C. Ward
Department of Earth Sciences, Simon Fraser University, Burnaby, BC

ABSTRACT

This paper presents the preliminary results of a study investigating the stratigraphy and basic geotechnical properties of the surficial geology deposits observed in the bluffs around the city of Whitehorse. A total of eleven sections were examined on both the east and west banks of the Yukon River. Representative stratigraphic units were analysed for grain size distribution; deposits ranged in size from silt and clay to coarse gravel. Most of the observed sediments represent the glaciolacustrine depositional environment of Glacial Lake Laberge with the exception of a loess unit exposed near the top of the sections. Consistency indices of seven silt and clay-rich samples collected in the bluffs surrounding Whitehorse indicate a low plasticity comparable with other Canadian loess units and the glaciolacustrine bluffs around Kamloops and in the Elk Valley of British Columbia. The soil unconfined compressive strength was estimated using a pocket penetrometer and the dry silt and clay-rich units were found to have strength estimates up to two orders of magnitude greater than the sand-rich units.

[1]m.brideau@auckland.ac.nz

INTRODUCTION

During the last glaciation, large glacier-dammed lakes formed during ice sheet advance and retreat phases (*e.g.,* Teller, 1987; Eyles and Clague, 1991; Bednarski, 2008). Several urban areas of Canada are built on the deposits left behind by these glacial lakes; examples of these developments can be found in Whitehorse (Bond *et al.,* 2005); Prince George (Tipper, 1971); Kamloops (Fulton, 1965); Kelowna (Paradis, 2009); Edmonton (Fredlund and Dahlman, 1971); Calgary (Osborn and Rajewicz, 1998); Regina (Mollard *et al.,* 1998); and Winnipeg (Matile, 2004). Glaciolacustrine deposits have commonly been associated with slope instability and geotechnical problems (*e.g.,* Evans, 2003). In Kamloops, glaciolacustrine deposits are prone to piping erosion and slope failures (Evans and Buchanan, 1976; Lum, 1979), while landsliding in glaciolacustrine sediments due to river undercutting and agricultural irrigation has long been affecting railway lines in the Thompson River Valley (Clague and Evans, 2003; Eshraghian *et al.,* 2007; and Bishop, 2008). Hungr *et al.* (2001) also noted the collapse of a glaciolacustrine bluff near Kelowna that resulted in a dry silt flow which blocked a nearby highway.

This study focuses on the surficial deposits of the area in and around the city of Whitehorse (Fig. 1), where silt bluffs associated with the glaciolacustrine deposits represent a distinct component of the city's landscape (Fig. 2). The objectives of this study were to describe the stratigraphy in the bluffs around the City of Whitehorse; to characterize the basic geotechnical soil properties of the various identified stratigraphic units; and to compare the results with previously published data from similar studies in other Canadian cities.

PHYSIOGRAPHY, CLIMATE AND BEDROCK GEOLOGY

The study area is part of the Yukon Southern Lakes Ecoregion (Smith *et al.,* 2004) and has a physiography characterized by rounded summits and broad valleys. The climate of the ecoregion is arid due to its location in the rain shadow of the St. Elias and Coast Mountains (Smith *et al.,* 2004). Monthly average temperature and precipitation for Whitehorse Airport are presented in Figure 3. The total precipitation for the year averages 267 mm water equivalent (Environment Canada, 2010). Whitehorse is situated within the sporadic discontinuous permafrost zone as defined by Heginbottom *et al.* (1995). Mougeot (1997 and 1998) highlights that the permafrost

distribution around the city of Whitehorse is not well understood; however, at other locations in the Yukon where fine-grained sediment tends to be ice-rich, there can be significant impacts on slope stability. For example, Glacial Lake Laberge glaciolacustrine sediments, which contain ice-rich permafrost, occur beneath and adjacent to the Alaska Highway in the Takhini River Valley, 40-50 km west of Whitehorse in an area of active slumping (Burn, 1998; Huscroft *et al.,* 2004).

The bedrock geology underlying the Whitehorse area consists of Upper Triassic limestone to the east of the Yukon River, and mid-Cretaceous plutons to the west ranging in composition from granodiorite to diorite and tonalite (Hart and Radloff, 1990). To the south, outcrops of Pliocene Miles Canyon Basalt are exposed on the downstream side of the Yukon River dam and upstream at Miles Canyon (Hart and Villeneuve, 1999).

PREVIOUS WORK

GLACIAL LAKE LABERGE

The Whitehorse area was glaciated by the Cassiar lobe of the Cordilleran Ice Sheet. The accumulation zone for this lobe was largely to the south of Whitehorse in northern British Columbia. Ice-flow was directed northwestward and reached a minimum thickness of 1350 m in the Yukon River valley near Whitehorse (Bond, 2004). Deglaciation was punctuated with frontal standstills and possible re-advances, which resulted in the deposition of recessional moraines and larger areas of stagnation moraine. A significant standstill occurred near the north end of Lake Laberge that resulted in the damming of the Yukon River valley. The glacial lake, informally called Glacial Lake Laberge, reached elevations of 716 m (Horton, 2007), 88 m above the modern level (628 m) of Lake Laberge. In the past, the name Glacial Lake Champagne has been used to describe the glacial lake that deposited the sediments exposed in the bluffs around the city of Whitehorse (*e.g.,* Barnes, 1997; Mougeot, 1997 and 1998), but current usage of the term is now restricted to the glacial lake west of Champagne, Yukon that drained north via the Nordenskiold River divide (Bond, 2004). Glacial Lake Laberge expanded with the southward recession of the ice sheet. A standstill in the recession occurred at Whitehorse and resulted in deposition of the Chadburn Lake moraine complex (Chadburn phase; Bond, 2004). At that time, the glacial lake shoreline was at 705 m (Fig. 4; Horton, 2007). It is likely that much of the glaciolacustrine
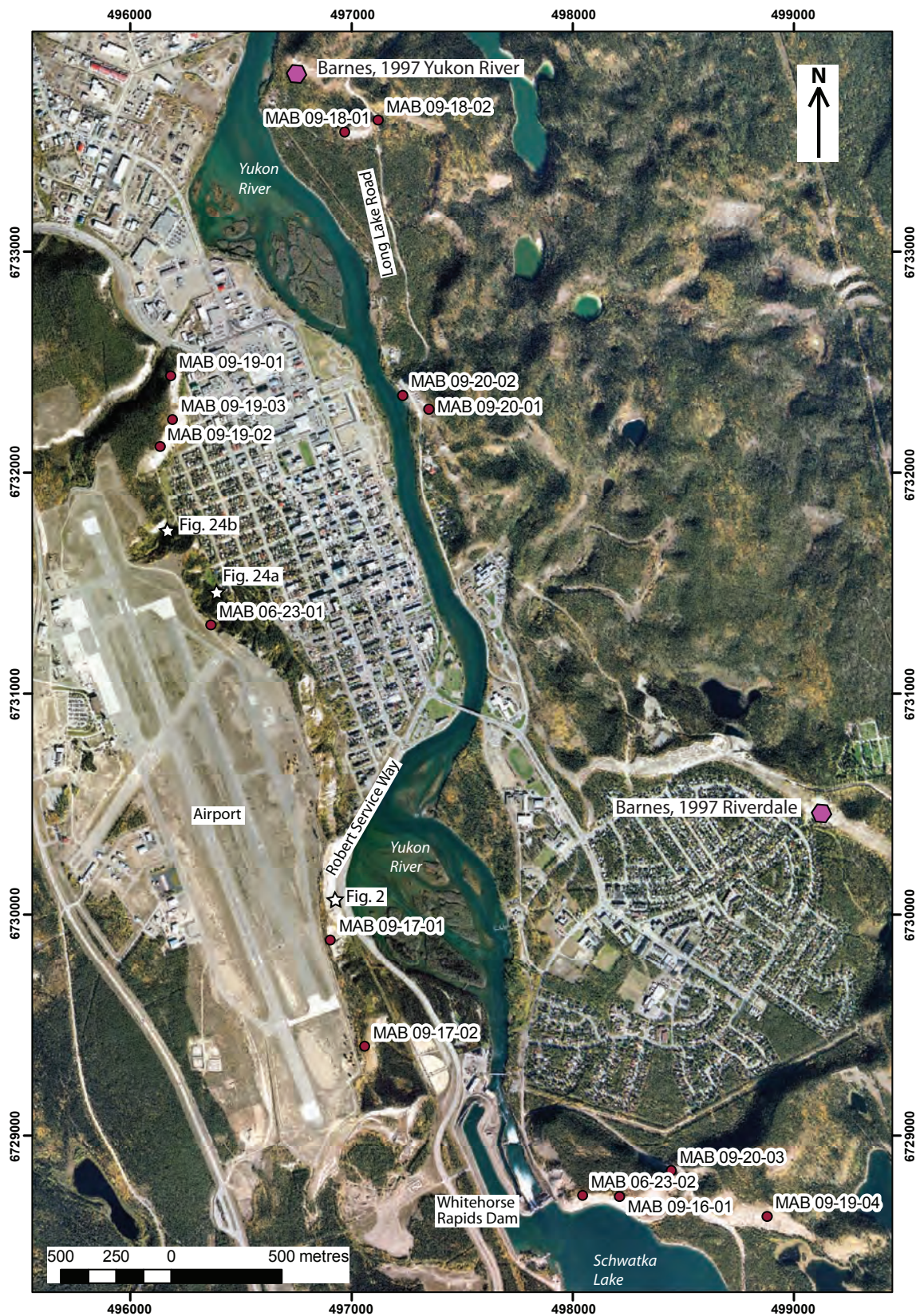
Figure 1. *Study area including the following locations: 1) sections examined in this study; 2) sections studied by previous authors; and 3) photographic sites included in this report.*

Figure 2. (a) *View of a silt bluff at the southern end of town along Robert Service Way, where the road is confined between the base of the bluff and the Yukon River;* ***(b)*** *photo taken at the same location, ca. 1900, where a minor landslide was being cleared from the railroad track (historical photo by H.C. Barley Fonds from the Yukon Archives, #5416).*
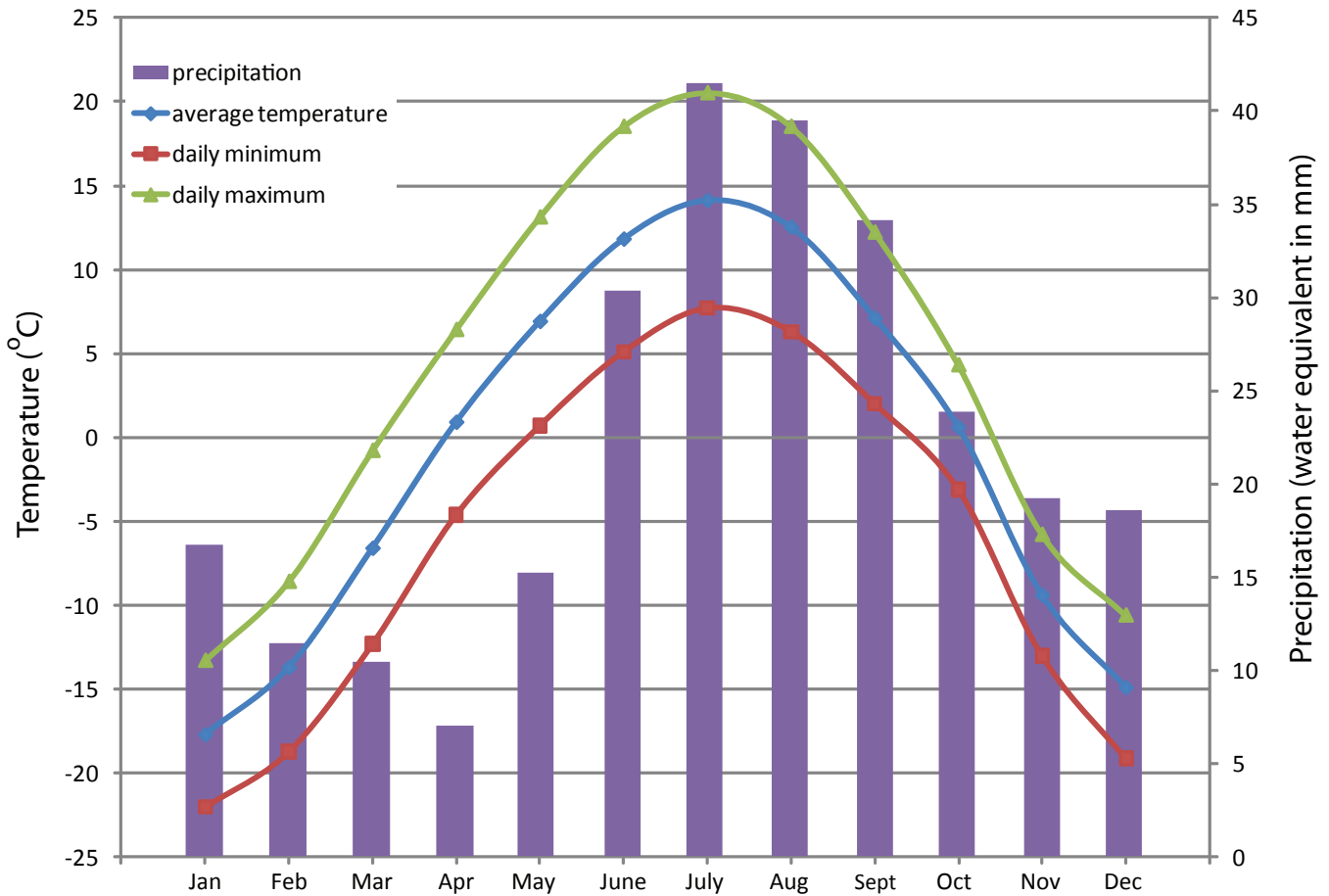
Figure 3. *Average temperature and precipitation recorded at the Whitehorse airport (data from Environment Canada, 2010).*

sedimentation in the Whitehorse area occurred at this time. With continued erosion of the outlet, the glacial lake became shallower and the southern shoreline began migrating northward. This regression continued through the Holocene, causing a drop in base-level for the Yukon River near Whitehorse (Wolfe *et al.*, 2011). The Yukon River has responded to this base-level fall by eroding into Late Wisconsin glaciogenic units and Pliocene basalts in the Yukon River valley bottom.

The glaciolacustrine sediments are well exposed in the city of Whitehorse. Much of the glaciolacustrine deposits on the eastern side of the valley are kettled, suggesting the glacial lake sediments were deposited supraglacially on stagnant ice (*e.g.*, Ward and Rutter, 2000). In contrast, the glaciolacustrine surface on the western side of the valley forms a plain without kettles (Fig. 5). This plain is capped by medium-grained fluvial sand that was likely deposited in a deltaic environment (shallow basin) as the glacial lake regressed northward (Bond, 2004). This sand unit is continuous northward and merges with the contemporary sandy delta at the south end of Lake Laberge. In the early Holocene, the sand cap was reworked into the Whitehorse dune field (Wolfe *et al.*, 2011).
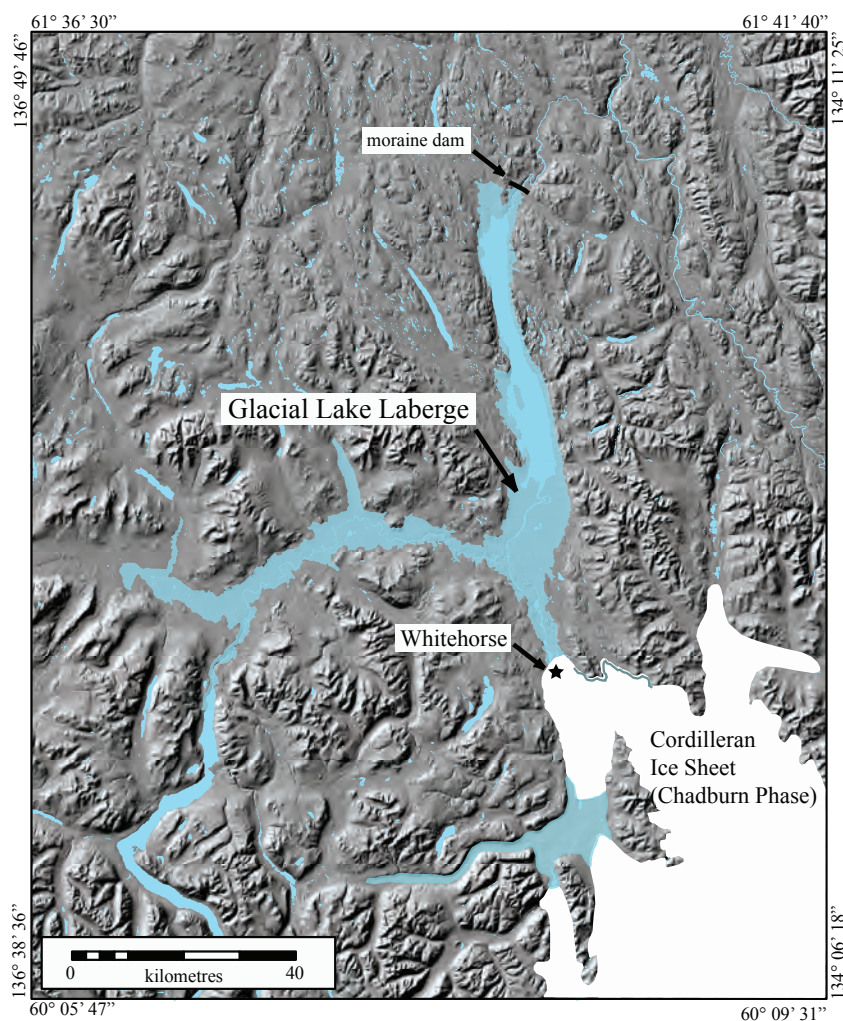
Figure 4. Map of the Yukon River valley depicting Glacial Lake Laberge at its maximum extent (705 m a.s.l.).

Figure 5. A view to the west over Whitehorse showing the glaciolacustrine surfaces remnant from Glacial Lake Laberge. The hummocky and kettled terrain in the foreground is glaciolacustrine sediment that was deposited over stagnant ice and moraine. This is in contrast to the glaciolacustrine plain on the west side of the Yukon River (see airport).

CURRENT INVESTIGATION

The sediments exposed in the bluffs were described at five main locations (including a total of 11 sections and 3 field stations where general observations were made) in and around the City of Whitehorse: Robert Service Way, Schwatka Lake, Downtown Whitehorse, Long Lake Road South, and Long Lake Road North (Fig. 1). The information observed at each section is summarized in geotechnical logs (Figs. 6 to 15) which include a stratigraphic column, a lithological description, and field estimates of the plasticity, water content, Unconfined Compressive Strength (UCS), and colour (Munsell).

OBSERVATIONS ON THE STRATIGRAPHY AND SEDIMENTOLOGY

The two main stratigraphic units observed are a horizontally laminated silt and clay (Figs. 9, 11, 12, 14, and 16a) and a fine to coarse sand that may or may not be horizontally laminated, cross-bedded or interbedded with silty-sand units (Figs. 6, 7, 8, 9, 10, 11, 13, 14, 16b and 16c). The silt and clay-rich unit exhibits rhythmic layering of light and dark lamination, which likely represents suspension settling; colour changes are due to varying silt and clay abundance (Smith and Ashley, 1985; Ashley, 2002). Convolute laminae in interbedded silt and fine sand units are observed at station MAB 09-16-01 (Figs. 6 and 16b). Convolute laminae have previously been reported in glaciolacustrine deposits and are interpreted to be the result of turbid underflow currents and subaqueous fan settings (*e.g.,* Ashley, 2002; Bennett *et al.*, 2000) which cause soft sediment deformation loading during slumping. Crossbeds and climbing ripples have been attributed to turbidity currents in glacial lakes by Shaw and Archer (1978). Rip-up clasts of silt and clay in a medium to coarse sand bed were observed at station MAB 09-16-01 (Figs. 6 and 16c), which are also characteristic of turbidity currents. Similar features were described by Barnes (1997) at his Riverdale section (Fig. 1).

A distinct unit comprising weak red (2.5YR 5/3) silt mixed with some fine sand was observed in the upper parts of sections MAB 09-16-01, MAB 09-19-01 and MAB 09-19-02 (Figs.1, 6, 10 and 11) and has been interpreted by Barnes (1997), Mougeot (1998) and Bond *et al.* (2005) as loess from reworked glaciolacustrine deposits. These aeolian deposits are commonly referred to as 'cliff-top deposits' (David, 1972) and are the result of wind eroding material in the sections and depositing it on top. A tephra layer and several buried organic horizons are associated with the

loess layer (Fig. 17). Based on stratigraphic position, the tephra has been interpreted by Barnes (1997), Mougeot (1997) and Smith *et al.*, (2004) to be White River Ash, which has been dated at ~1150 years BP (Clague *et al.*, 1995). The observed buried organic horizons have also been recognized by Smith *et al.* (2004) as the remnants of large forest fires, but could also represent paleosols not necessarily associated with forest fires. This study represents the first time that 8 buried organic horizons are reported at a single location.

A series of stratigraphic units defined as gap-graded (bimodal), polymictic, well rounded pebble gravel with minor cobbles in a silt and clay matrix were observed only at station MAB 09-20-02 (Figs. 15 and 18). A possible depositional environment for these coarse units could be from melt-out of stranded ice in a lacustrine environment (Mougeot, 1998), resulting in the deposition of large clasts within a fine matrix, while still preserving the horizontal contacts above and below the unit. These units are bounded above and below by silt and clay-rich units that do not contain coarse fragments. These units are exposed just above the level of the Yukon River, and as such, represent the lowest topographic elevation exposure visited in this project; it is unclear however from this study if it also represents the lowest stratigraphic level.

GEOTECHNICAL CHARACTERISTICS

GRAIN SIZE DISTRIBUTION

The grain size distribution of sixteen samples was determined using a stack of ten sieves with openings varying in size from 37.5 mm (#1½) to 0.075 mm (#200). The samples were initially dried in an oven for 24 hours at 100°C after which the soil clumps were broken using a pestle and mortar before being put through the sieve stack. The grain size distribution of four samples containing more than 30% silt and clay was further analysed using a hydrometer, according to the method defined in ASTM (2007). The grain size distributions are presented in Figure 19, demonstrating a wide range of sediment grain sizes associated with the glaciolacustrine environment. The weak red (2.5YR 5/3) fine sand and silt of sample MAB 06-23-0-01 (Fig. 20a) is representative of the grain size distribution and appearance of loess from wind-reworked glaciolacustrine deposits. The clayey silt of sample MAB 09-17-02-01 (Fig. 20b) represents lacustrine deposition in calm water. The cross-bedded coarse to fine sand of sample MAB 09-17-01-03 likely represents underflow current deposition (Fig. 20c), whereas the coarse gravelly

Schwatka Lake section 1
MAB 09-16-01

UTM
0 498 212
6 728 722

Elevation: 755 m a.s.l.

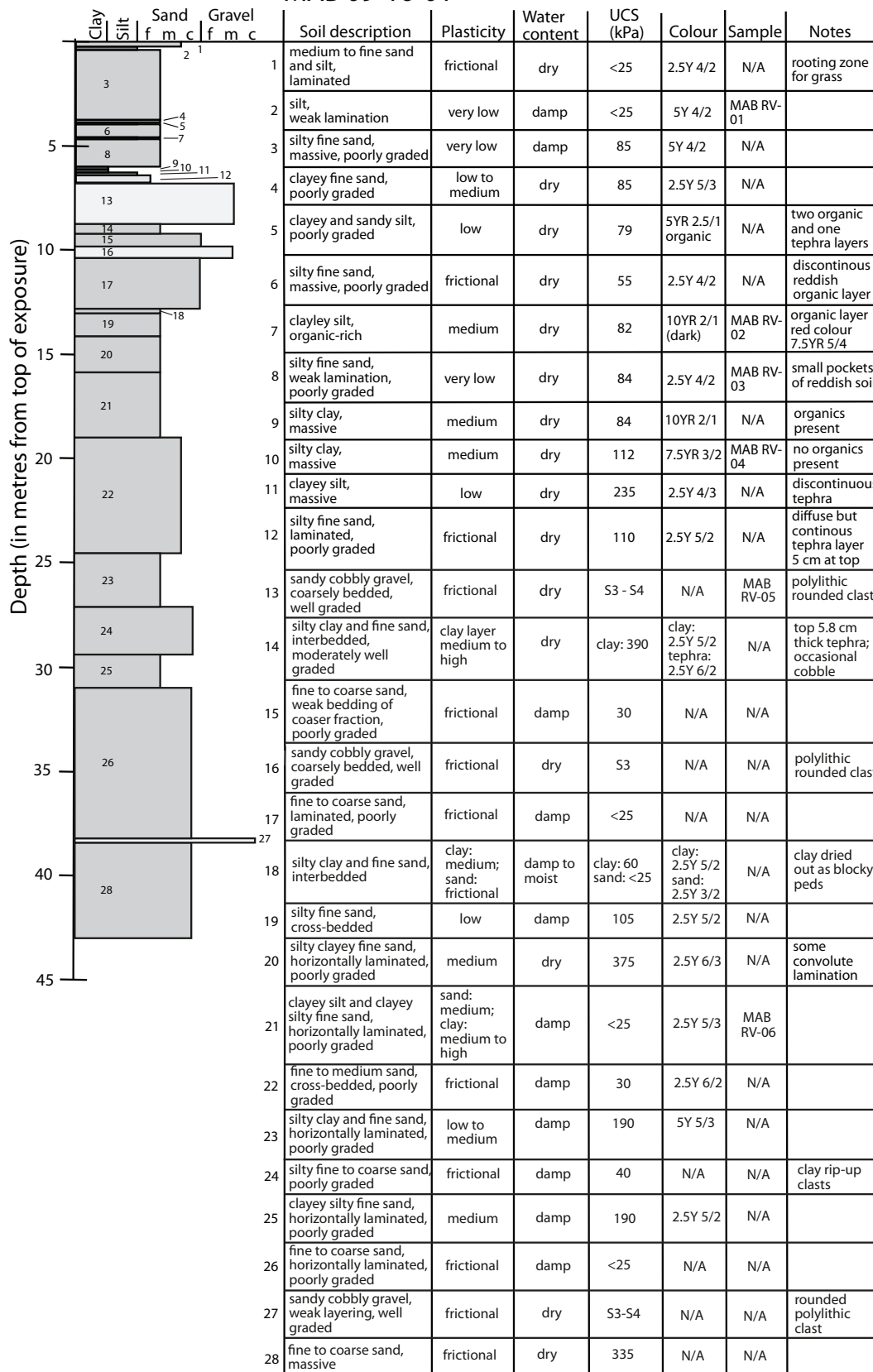| #	Soil description	Plasticity	Water content	UCS (kPa)	Colour	Sample	Notes
1	medium to fine sand and silt, laminated	frictional	dry	<25	2.5Y 4/2	N/A	rooting zone for grass
2	silt, weak lamination	very low	damp	<25	5Y 4/2	MAB RV-01	
3	silty fine sand, massive, poorly graded	very low	damp	85	5Y 4/2	N/A	
4	clayey fine sand, poorly graded	low to medium	dry	85	2.5Y 5/3	N/A	
5	clayey and sandy silt, poorly graded	low	dry	79	5YR 2.5/1 organic	N/A	two organic and one tephra layers
6	silty fine sand, massive, poorly graded	frictional	dry	55	2.5Y 4/2	N/A	discontinous reddish organic layer
7	clayley silt, organic-rich	medium	dry	82	10YR 2/1 (dark)	MAB RV-02	organic layer red colour 7.5YR 5/4
8	silty fine sand, weak lamination, poorly graded	very low	dry	84	2.5Y 4/2	MAB RV-03	small pockets of reddish soil
9	silty clay, massive	medium	dry	84	10YR 2/1	N/A	organics present
10	silty clay, massive	medium	dry	112	7.5Y 3/2	MAB RV-04	no organics present
11	clayey silt, massive	low	dry	235	2.5Y 4/3	N/A	discontinuous tephra
12	silty fine sand, laminated, poorly graded	frictional	dry	110	2.5Y 5/2	N/A	diffuse but continous tephra layer 5 cm at top
13	sandy cobbly gravel, coarsely bedded, well graded	frictional	dry	S3 - S4	N/A	MAB RV-05	polylithic rounded clast
14	silty clay and fine sand, interbedded, moderately well graded	clay layer medium to high	dry	clay: 390	clay: 2.5Y 5/2 tephra: 2.5Y 6/2	N/A	top 5.8 cm thick tephra; occasional cobble
15	fine to coarse sand, weak bedding of coaser fraction, poorly graded	frictional	damp	30	N/A	N/A	
16	sandy cobbly gravel, coarsely bedded, well graded	frictional	dry	S3	N/A	N/A	polylithic rounded clast
17	fine to coarse sand, laminated, poorly graded	frictional	damp	<25	N/A	N/A	
18	silty clay and fine sand, interbedded	clay: medium; sand: frictional	damp to moist	clay: 60 sand: <25	clay: 2.5Y 5/2 sand: 2.5Y 3/2	N/A	clay dried out as blocky peds
19	silty fine sand, cross-bedded	low	damp	105	2.5Y 5/2	N/A	
20	silty clayey fine sand, horizontally laminated, poorly graded	medium	dry	375	2.5Y 6/3	N/A	some convolute lamination
21	clayey silt and clayey silty fine sand, horizontally laminated, poorly graded	sand: medium; clay: medium to high	damp	<25	2.5Y 5/3	MAB RV-06	
22	fine to medium sand, cross-bedded, poorly graded	frictional	damp	30	2.5Y 6/2	N/A	
23	silty clay and fine sand, horizontally laminated, poorly graded	low to medium	damp	190	5Y 5/3	N/A	
24	silty fine to coarse sand, poorly graded	frictional	damp	40	N/A	N/A	clay rip-up clasts
25	clayey silty fine sand, horizontally laminated, poorly graded	medium	damp	190	2.5Y 5/2	N/A	
26	fine to coarse sand, horizontally laminated, poorly graded	frictional	damp	<25	N/A	N/A	
27	sandy cobbly gravel, weak layering, well graded	frictional	dry	S3-S4	N/A	N/A	rounded polylithic clast
28	fine to coarse sand, massive	frictional	dry	335	N/A	N/A	

Figure 6. *Geotechnical logs of stratigraphy and soil properties observed at station MAB 09-16-01 (see Fig. 1 for location).*

sand of sample MAB 09-16-01-05 (Fig. 20d) is interpreted as the proximal part of a large turbidite. An overall fining-upward stratigraphic sequence is illustrated in Figure 20: coarse deposits at the bottom of the section, followed by a sandy unit, which is in turn overlain by a laminated silt and clay unit, and finally capped by a loess unit. This sediment package suggests that the glacier which dammed the valley became progressively more distal to the Whitehorse area.

PLASTICITY

The plasticity of selected soil samples was investigated by determining the liquid and plastic limits of the soil component passing through a sieve having openings of 0.425 mm (#40). The liquid limit (LL) corresponds to the water content at the point at which the remoulded soil starts behaving as a liquid, while the plastic limit (PL) corresponds to the water content at the point at which the soil stops behaving plastically. The plasticity index (PI) is defined as PI = LL- PL and represents the water content range over which the soil behaves plastically (Craig, 2007). The liquid limit was determined using a cone penetrometer, whereas the plastic limit was derived by rolling a wet soil sample into a thread on a frosted glass plate until it crumbled (see Smith, 2006 for details on the methodology).

The results of the seven tested Whitehorse-area samples are plotted on Figure 21 along with published test results from other glaciolacustrine and loess deposits from other areas in Canada. The Whitehorse samples exhibited a low plasticity behaviour that was similar to the range of values reported by Evans and Buchanan (1976) for samples from the Thompson River Valley, and the plasticity of Canadian loess deposits (Sweeney and Smalley, 1988). The low plasticity is attributed to the low clay content (<20% by weight) of the samples collected in this study, as well as those collected by Evans and Buchanan (1976). The high plasticity samples from Mollard *et al.* (1998), Eshraghian *et al.* (2007), and Bishop (2008), all contain 40-80% clay by weight.

Another factor that can influence the plasticity is the clay mineralogy. Mougeot (1994) reported on the clay mineralogy of four samples collected in the Takhini River valley and at the confluence of the M'Clintock River and the Yukon River. X-ray diffraction (XRD) analyses demonstrate that the most common minerals were kaolinite (25-50%) and illite (40-50%), and lesser amounts of montmorillonite (0-20%) and chlorite (10-15%). Very few of the plasticity data from the literature presented in

Figure 21 have accompanying clay mineralogy analyses. Two exceptions are the samples from the Elk Valley region, which are kaolinite and illite-dominated (George, 1986), and the sample from Regina, which contained up to 55% montmorillonite (Mollard *et al.*, 1998). The low montmorillonite content of the Whitehorse-area samples makes them more comparable to the Elk Valley samples.

SOIL STRENGTH

The Unconfined Compressive Strength (UCS) of the soil was estimated using a pocket penetrometer (model EI29-3729 by ELE). The pocket penetrometer is intended to test cohesive (silt and clay-rich) soils; in this study it provides a simple field estimate of frictional (sand-rich) soil strength. To account for the variability associated with the small area sampled during the test, an average of 5 measurements are reported in the geotechnical logs (Figs. 6 to 15). When weak soils (≤5 kPa) were encountered, an adapter foot was used to distribute the force over a larger area. The values listed next to each stratigraphic unit in Figures 6-15 demonstrate that a wide range of strength values was observed even within one section. Figure 22 illustrates that overall, the dry silt and clay-rich units had higher strength estimate values than the sand-rich units. Where a high strength value was observed for the sand-rich units, these results could be attributed to the presence of silt and/or clay cement, as recorded in the lithological description in Figures 6-15. This is consistent with the general expectation that a 'clean', non-cemented dry sand would not have significant cohesive strength. The relationship between soil strength and grain-size distribution may also be demonstrated by field observations whereby the silt and clay-rich units tend to be preferentially exposed in sub-vertical cliffs, while the sandier units tend to be covered in talus. The density of the gravel-rich units (Figs. 6 and 14) was estimated using the field assessment categories listed in Table 1. The observed density categories varied between loose (S2) to the boundary between compact and dense (S3-S4).

Schwatka Lake section 2
MAB 09-20-03

UTM
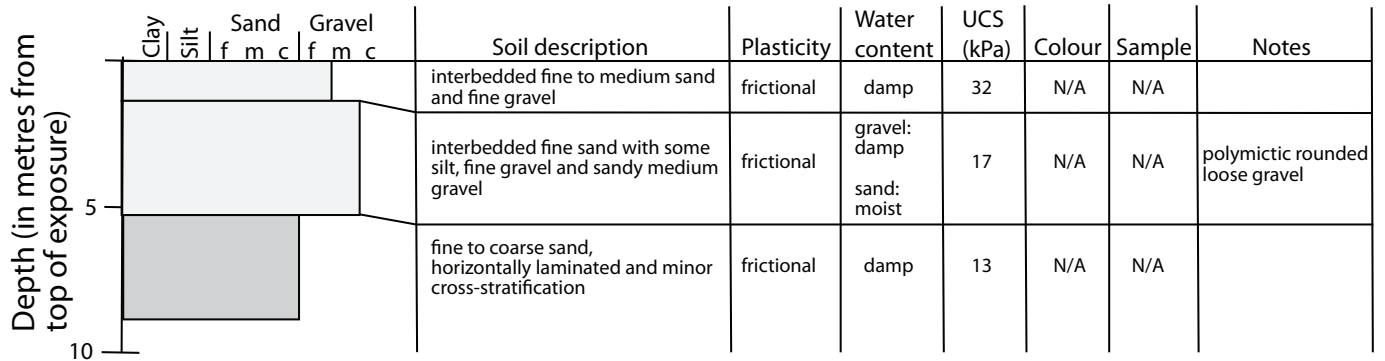0 498 447
6 728 840
Elevation: 681 m a.s.l.

Soil description	Plasticity	Water content	UCS (kPa)	Colour	Sample	Notes
interbedded fine to medium sand and fine gravel	frictional	damp	32	N/A	N/A	
interbedded fine sand with some silt, fine gravel and sandy medium gravel	frictional	gravel: damp sand: moist	17	N/A	N/A	polymictic rounded loose gravel
fine to coarse sand, horizontally laminated and minor cross-stratification	frictional	damp	13	N/A	N/A	

Figure 7. *Geotechnical logs of stratigraphy and soil properties observed at station MAB 09-20-03 (see Fig. 1 for location).*

Robert Service Way section 1
MAB 09-17-01

UTM
0 496 906
6 729 884
Elevation: 674 m a.s.l.

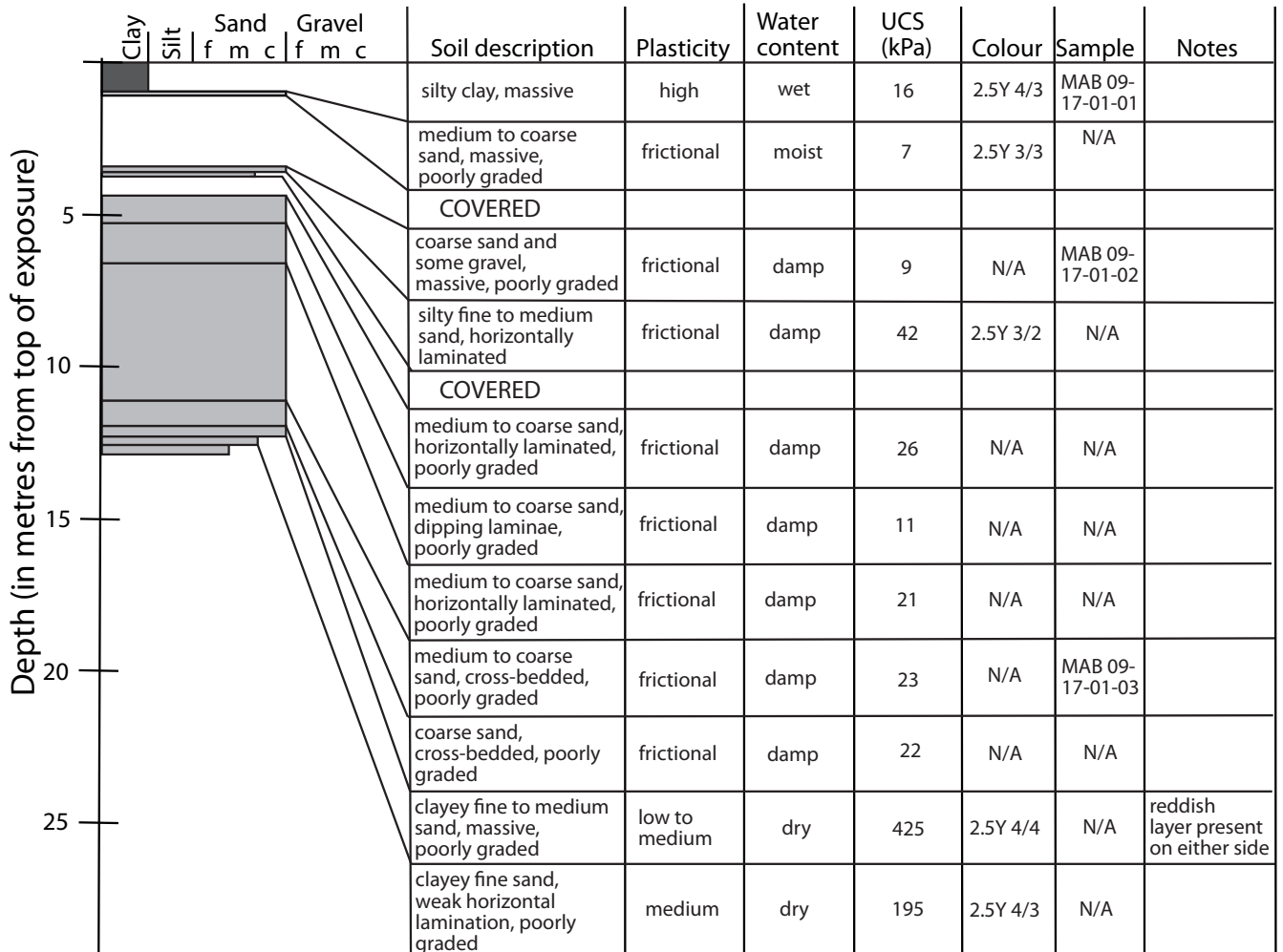| Soil description	Plasticity	Water content	UCS (kPa)	Colour	Sample	Notes
silty clay, massive	high	wet	16	2.5Y 4/3	MAB 09-17-01-01	
medium to coarse sand, massive, poorly graded	frictional	moist	7	2.5Y 3/3	N/A	
COVERED						
coarse sand and some gravel, massive, poorly graded	frictional	damp	9	N/A	MAB 09-17-01-02	
silty fine to medium sand, horizontally laminated	frictional	damp	42	2.5Y 3/2	N/A	
COVERED						
medium to coarse sand, horizontally laminated, poorly graded	frictional	damp	26	N/A	N/A	
medium to coarse sand, dipping laminae, poorly graded	frictional	damp	11	N/A	N/A	
medium to coarse sand, horizontally laminated, poorly graded	frictional	damp	21	N/A	N/A	
medium to coarse sand, cross-bedded, poorly graded	frictional	damp	23	N/A	MAB 09-17-01-03	
coarse sand, cross-bedded, poorly graded	frictional	damp	22	N/A	N/A	
clayey fine to medium sand, massive, poorly graded	low to medium	dry	425	2.5Y 4/4	N/A	reddish layer present on either side
clayey fine sand, weak horizontal lamination, poorly graded	medium	dry	195	2.5Y 4/3	N/A	

Figure 8. *Geotechnical logs of stratigraphy and soil properties observed at station MAB 09-17-01 (see Fig. 1 for location).*

Robert Service Way section 2
MAB 09-17-02

UTM
0 497 065
6 729 401
Elevation: 701 m a.s.l.

Clay / Silt / Sand (f m c) / Gravel (f m c)	Soil description	Plasticity	Water content	UCS (kPa)	Colour	Sample	Notes
	silty fine sand, weakly horizontally laminated, poorly graded	very low	dry	25	2.5Y 4/3	N/A	
	clayey sandy silt, massive	medium	dry	82	2.5Y 5/3	N/A	contains two dark brown and reddish brown layers 7.5YR 4/3
	medium sand with some coarse sand, massive, poorly graded	frictional	damp	4	N/A	N/A	isolated, thin discontinuous silty clayey lenses
	silty clay, prismatic peds	medium to high	dry	dry, strength >450	2.5Y 6/3	N/A	
	clay with some silt, collumnar peds	high	dry	dry, strength >450	2.5Y 6/3	MAB 09-17-02-01	
	clay with some silt, columnar/tabular peds	high	dry	dry, strength >450	5Y 4/3	N/A	some 1cm lenses of darker/wetter material

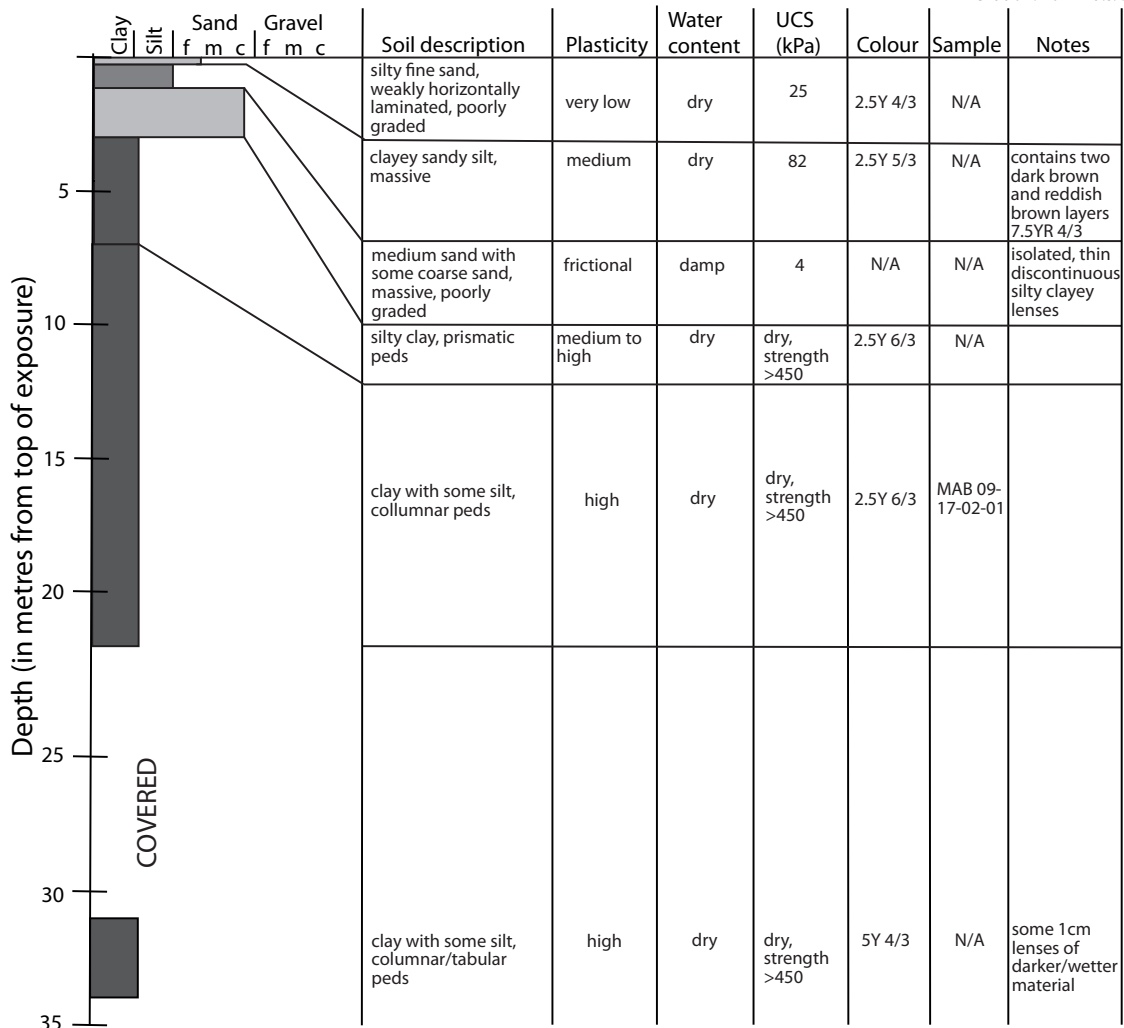Depth (in metres from top of exposure)

COVERED

Figure 9. *Geotechnical logs of stratigraphy and soil properties observed at station MAB 09-17-02 (see Fig. 1 for location).*

Whitehorse section 1
MAB 09-19-01
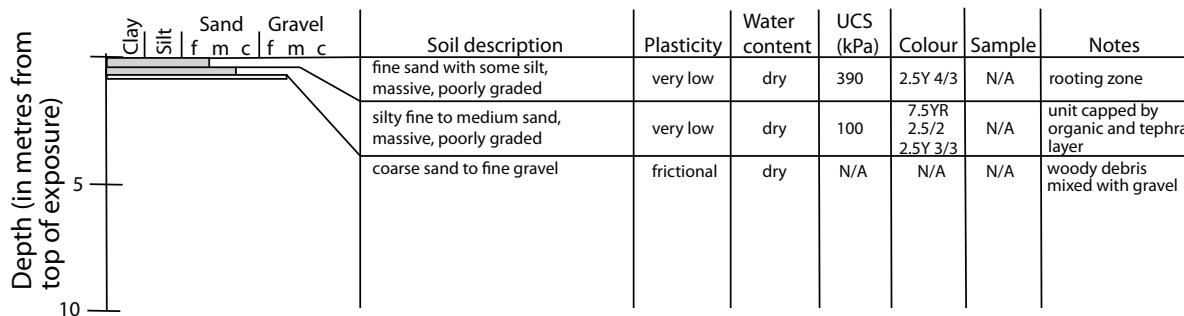
UTM
0 496 183
6 732 436
Elevation: 683 m a.s.l.

Clay / Silt / Sand (f m c) / Gravel (f m c)	Soil description	Plasticity	Water content	UCS (kPa)	Colour	Sample	Notes
	fine sand with some silt, massive, poorly graded	very low	dry	390	2.5Y 4/3	N/A	rooting zone
	silty fine to medium sand, massive, poorly graded	very low	dry	100	7.5YR 2.5/2 2.5Y 3/3	N/A	unit capped by organic and tephra layer
	coarse sand to fine gravel	frictional	dry	N/A	N/A	N/A	woody debris mixed with gravel

Depth (in metres from top of exposure)

Figure 10. *Geotechnical logs of stratigraphy and soil properties observed at station MAB 09-19-01 (see Fig. 1 for location).*

Whitehorse sections 2 and 3
MAB 09-19-02 and MAB 09-19-03

UTM
0 496 135
6 732 116
Elevation: 683 m a.s.l.

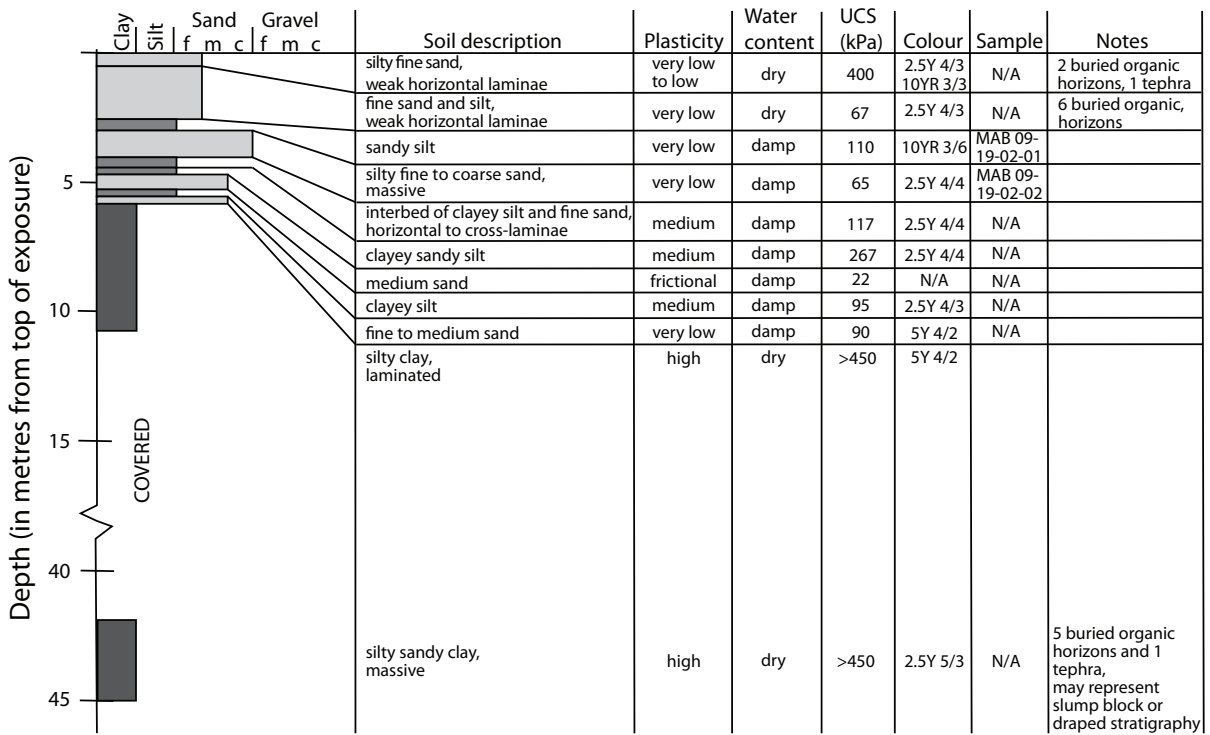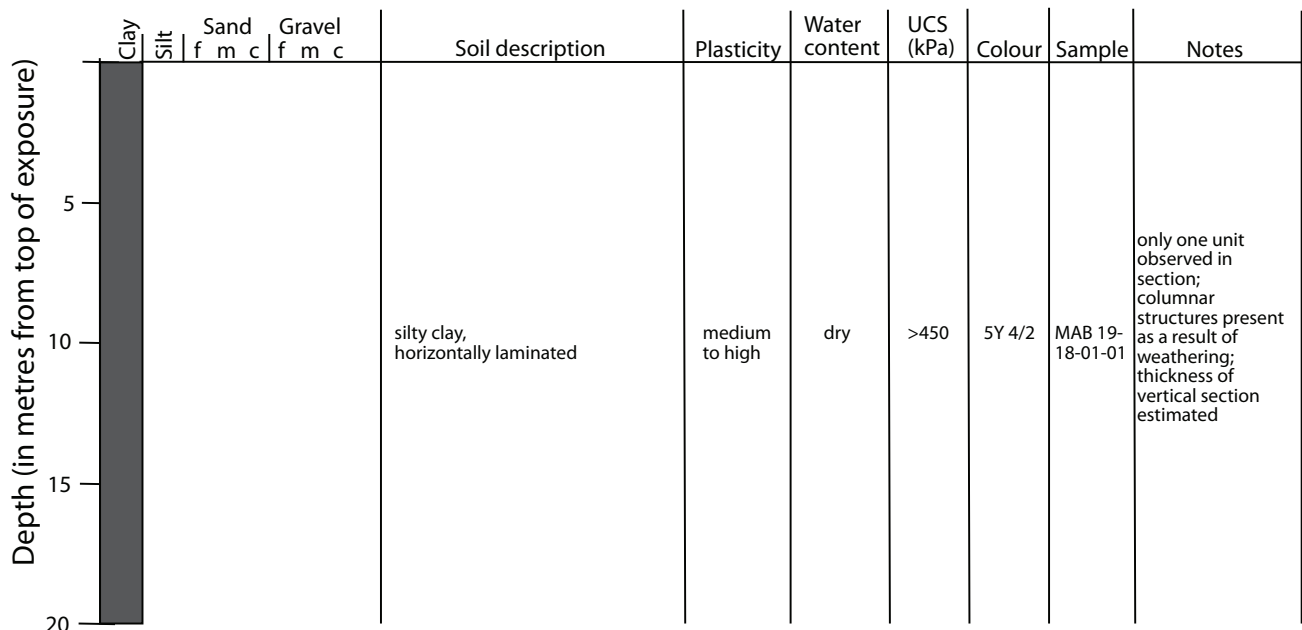UTM
0 496 191
6 732 239
Elevation: 683 m a.s.l.

Soil description	Plasticity	Water content	UCS (kPa)	Colour	Sample	Notes
silty fine sand, weak horizontal laminae	very low to low	dry	400	2.5Y 4/3 10YR 3/3	N/A	2 buried organic horizons, 1 tephra
fine sand and silt, weak horizontal laminae	very low	dry	67	2.5Y 4/3	N/A	6 buried organic, horizons
sandy silt	very low	damp	110	10YR 3/6	MAB 09-19-02-01	
silty fine to coarse sand, massive	very low	damp	65	2.5Y 4/4	MAB 09-19-02-02	
interbed of clayey silt and fine sand, horizontal to cross-laminae	medium	damp	117	2.5Y 4/4	N/A	
clayey sandy silt	medium	damp	267	2.5Y 4/4	N/A	
medium sand	frictional	damp	22	N/A	N/A	
clayey silt	medium	damp	95	2.5Y 4/3	N/A	
fine to medium sand	very low	damp	90	5Y 4/2	N/A	
silty clay, laminated	high	dry	>450	5Y 4/2		
silty sandy clay, massive	high	dry	>450	2.5Y 5/3	N/A	5 buried organic horizons and 1 tephra, may represent slump block or draped stratigraphy

Figure 11. Composite geotechnical logs of stratigraphy and soil properties observed at station MAB 09-19-02 and MAB 09-19-03 (see Fig. 1 for location).

Long Lake Road section 1
MAB 09-18-01

UTM
0 496 970
6 733 541
Elevation: 659 m a.s.l.

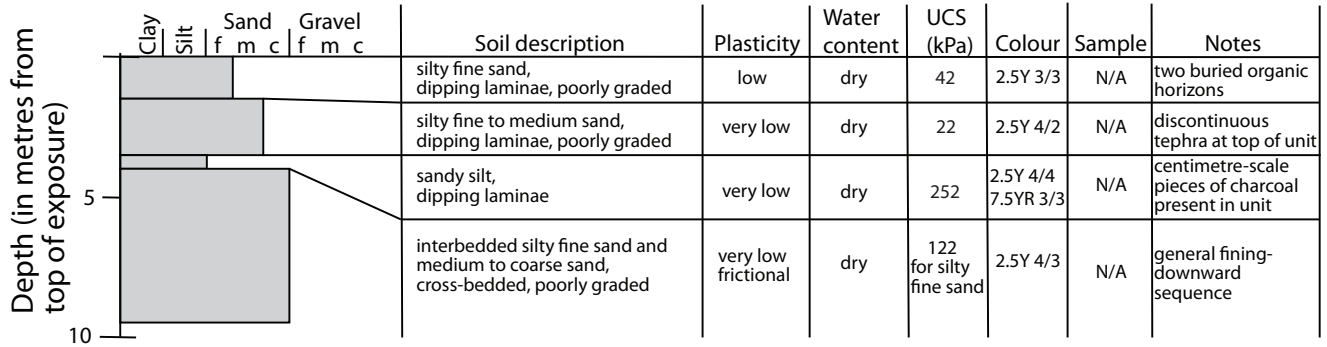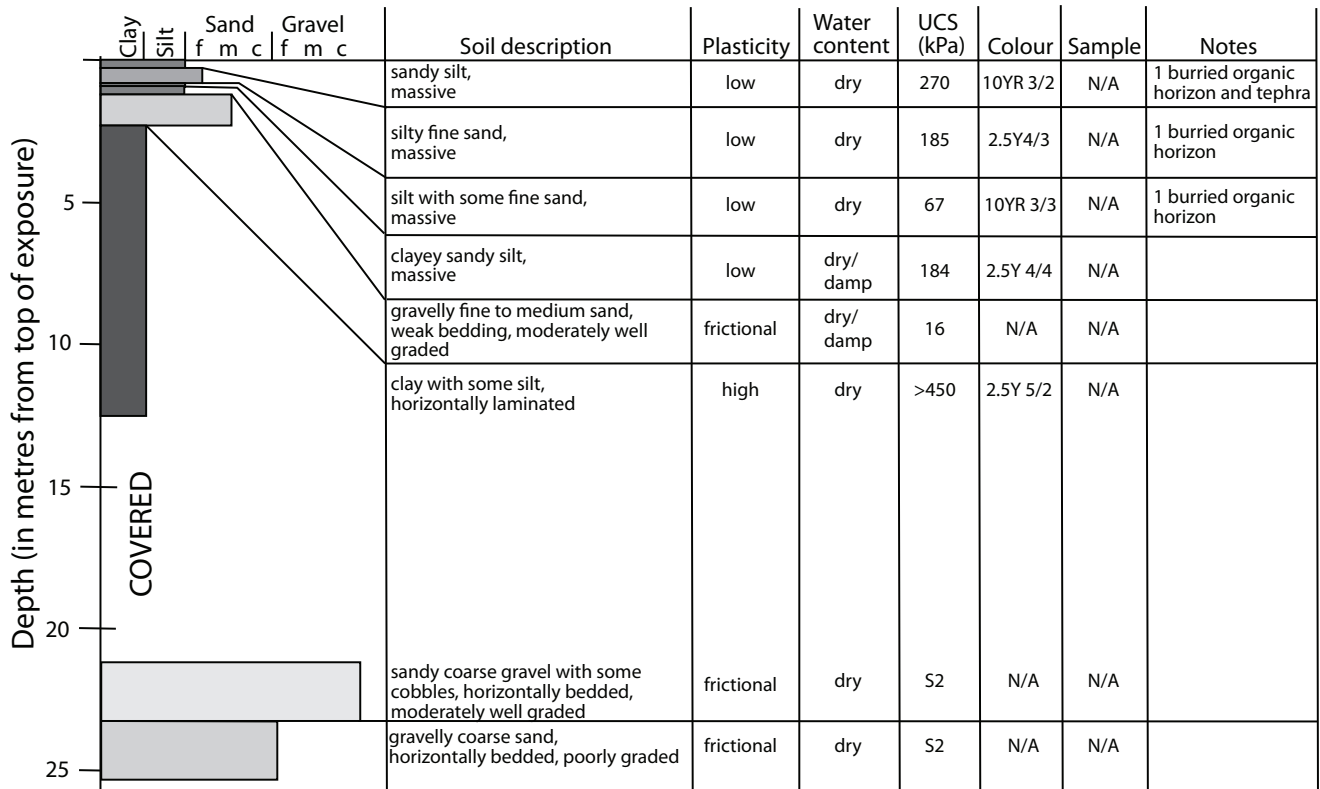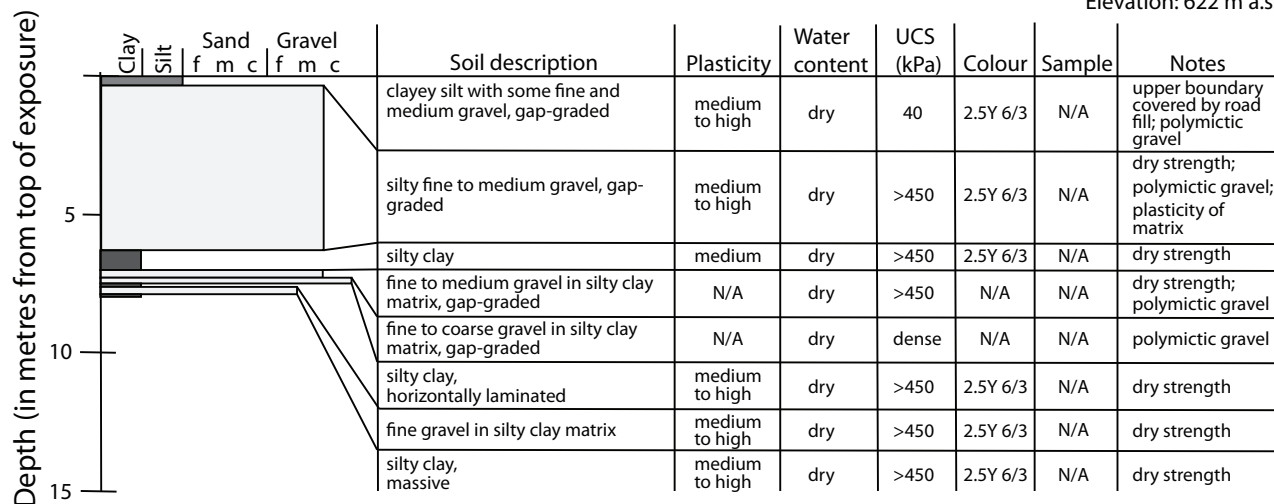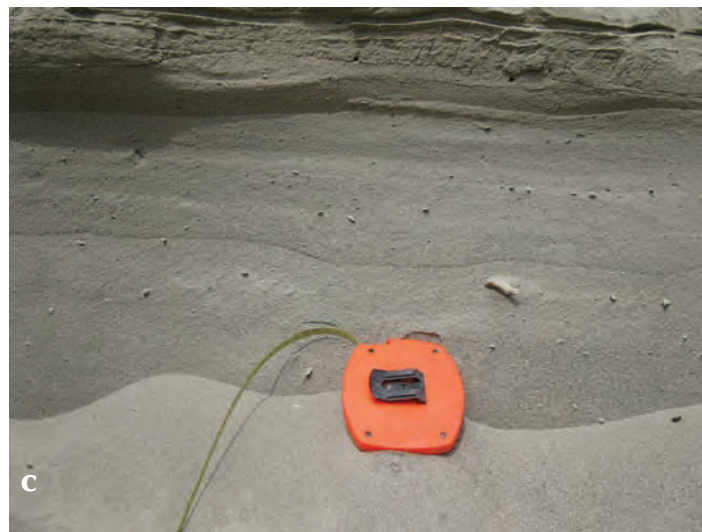| Soil description	Plasticity	Water content	UCS (kPa)	Colour	Sample	Notes
silty clay, horizontally laminated	medium to high	dry	>450	5Y 4/2	MAB 19-18-01-01	only one unit observed in section; columnar structures present as a result of weathering; thickness of vertical section estimated

Figure 12. Geotechnical logs of stratigraphy and soil properties observed at station MAB 09-18-01 (see Fig. 1 for location).

Long Lake Road section 2
MAB 09-18-02

UTM
0 497 121
6 733 593
Elevation: 645 m a.s.l.

			Soil description	Plasticity	Water content	UCS (kPa)	Colour	Sample	Notes
			silty fine sand, dipping laminae, poorly graded	low	dry	42	2.5Y 3/3	N/A	two buried organic horizons
			silty fine to medium sand, dipping laminae, poorly graded	very low	dry	22	2.5Y 4/2	N/A	discontinuous tephra at top of unit
			sandy silt, dipping laminae	very low	dry	252	2.5Y 4/4 7.5YR 3/3	N/A	centimetre-scale pieces of charcoal present in unit
			interbedded silty fine sand and medium to coarse sand, cross-bedded, poorly graded	very low frictional	dry	122 for silty fine sand	2.5Y 4/3	N/A	general fining-downward sequence

Figure 13. Geotechnical logs of stratigraphy and soil properties observed at station MAB 09-18-02 (see Fig. 1 for location).

Long Lake Road section 3
MAB 09-20-01

UTM
0 497 350
6 732 286
Elevation: 676 m a.s.l.

			Soil description	Plasticity	Water content	UCS (kPa)	Colour	Sample	Notes
			sandy silt, massive	low	dry	270	10YR 3/2	N/A	1 burried organic horizon and tephra
			silty fine sand, massive	low	dry	185	2.5Y4/3	N/A	1 burried organic horizon
			silt with some fine sand, massive	low	dry	67	10YR 3/3	N/A	1 burried organic horizon
			clayey sandy silt, massive	low	dry/ damp	184	2.5Y 4/4	N/A	
			gravelly fine to medium sand, weak bedding, moderately well graded	frictional	dry/ damp	16	N/A	N/A	
			clay with some silt, horizontally laminated	high	dry	>450	2.5Y 5/2	N/A	
			sandy coarse gravel with some cobbles, horizontally bedded, moderately well graded	frictional	dry	S2	N/A	N/A	
			gravelly coarse sand, horizontally bedded, poorly graded	frictional	dry	S2	N/A	N/A	

Figure 14. Geotechnical logs of stratigraphy and soil properties observed at station MAB 09-20-01 (see Fig. 1 for location).

Long Lake Road section 4
MAB 09-20-02

UTM
0 497 232
6 732 348
Elevation: 622 m a.s.l.

Depth (in metres from top of exposure)	Clay	Silt	Sand f m c	Gravel f m c	Soil description	Plasticity	Water content	UCS (kPa)	Colour	Sample	Notes
					clayey silt with some fine and medium gravel, gap-graded	medium to high	dry	40	2.5Y 6/3	N/A	upper boundary covered by road fill; polymictic gravel
					silty fine to medium gravel, gap-graded	medium to high	dry	>450	2.5Y 6/3	N/A	dry strength; polymictic gravel; plasticity of matrix
					silty clay	medium	dry	>450	2.5Y 6/3	N/A	dry strength
					fine to medium gravel in silty clay matrix, gap-graded	N/A	dry	>450	N/A	N/A	dry strength; polymictic gravel
					fine to coarse gravel in silty clay matrix, gap-graded	N/A	dry	dense	N/A	N/A	polymictic gravel
					silty clay, horizontally laminated	medium to high	dry	>450	2.5Y 6/3	N/A	dry strength
					fine gravel in silty clay matrix	medium to high	dry	>450	2.5Y 6/3	N/A	dry strength
					silty clay, massive	medium to high	dry	>450	2.5Y 6/3	N/A	dry strength

Figure 15. *Geotechnical logs of stratigraphy and soil properties observed at station MAB 09-20-02 (see Fig. 1 for location).*

Figure 16. *Photos of some of the sedimentological structures observed in the measured sections: (a) horizontally laminated rhythmite of silt and clay at section MAB 09-19-03; (b) convoluted bedding of fine sand and silt at section MAB 09-16-01; (c) silt rip-up clast in silty, fine to coarse sand at section MAB 09-16-01.*

buried organics
buried organics
tephra

buried organics
buried organics

buried organics

buried organics

buried organics
buried organics
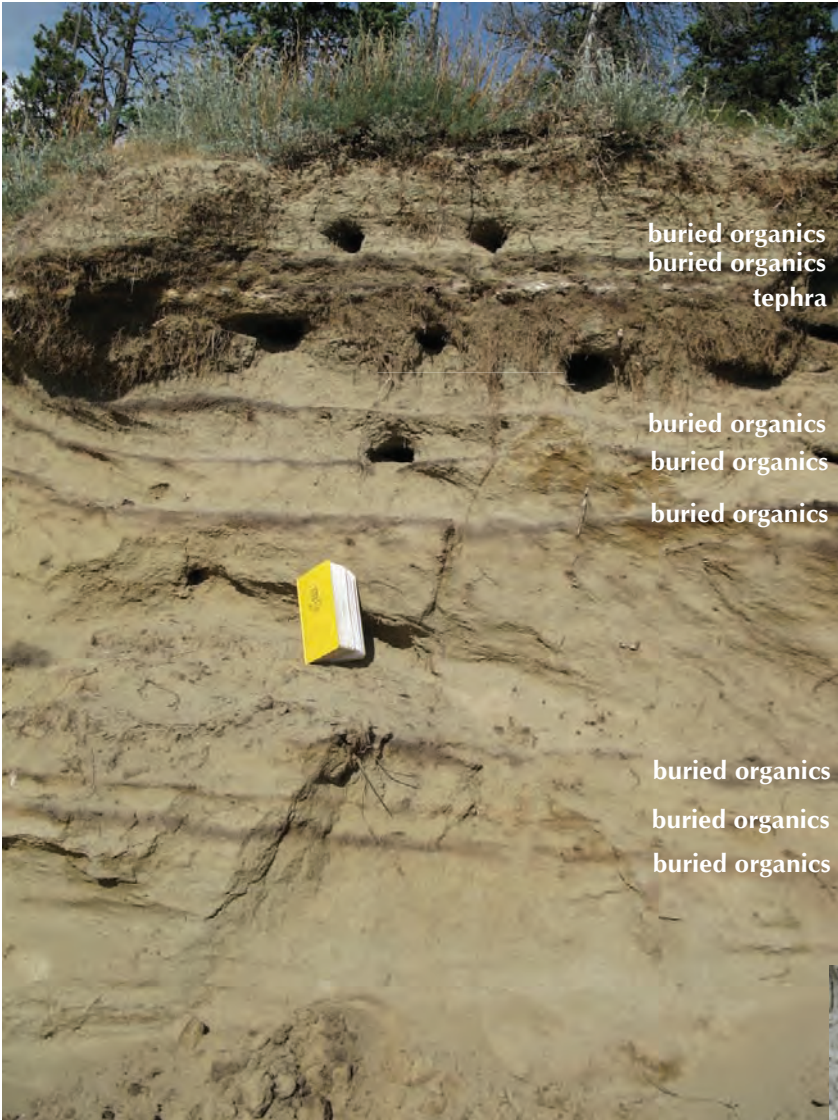
Figure 17. Multiple buried organic horizons and White River Ash (tephra) in the loess deposit at station MAB 09-19-02.

Figure 18. Gap-graded, polymictic, well rounded coarse gravel (including cobbles), in a matrix of silt and clay, at station MAB 09-20-02.
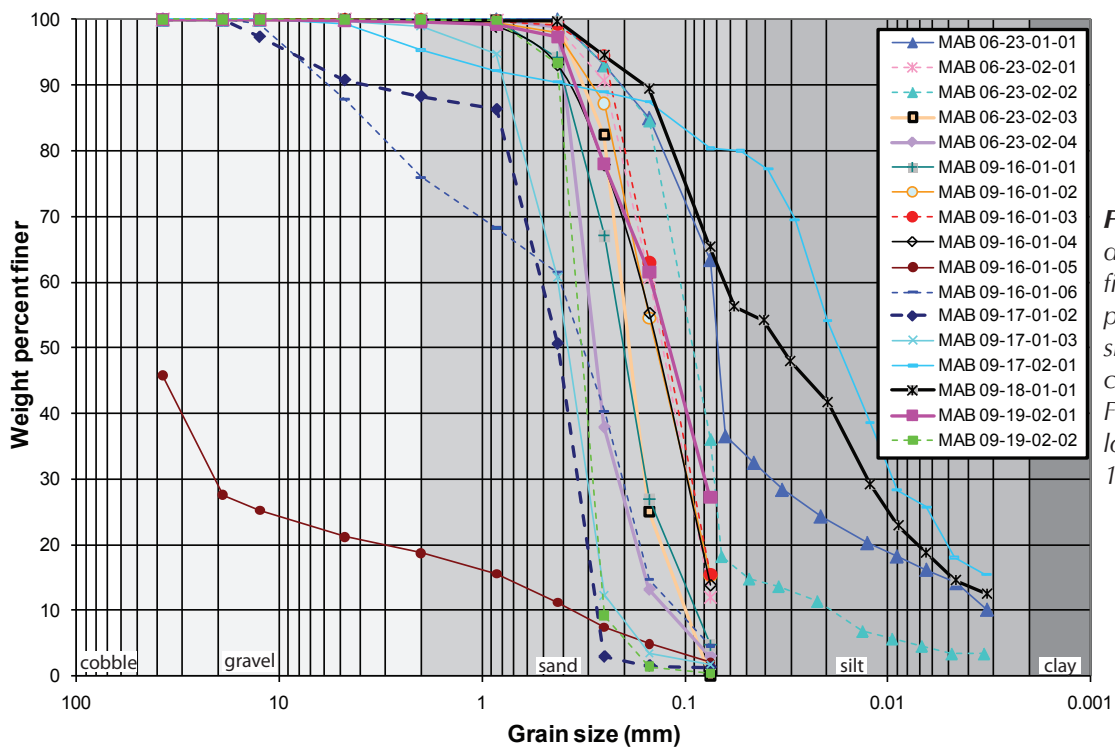
Figure 19. Grain size distribution curve of percent finer (i.e., weight percent passing through a given sieve size) vs. grain size for samples collected during this study. See Figures 6 to 15 for stratigraphic location of samples and Figure 1 for location of stations.

Figure 20. Field photos of selected samples analysed for grain size distribution in Figure19: *(a)* loess unit of sample MAB 06-23-02-01; *(b)* laminated silty clay of sample MAB 09-17-02-01; *(c)* medium cross-bedded sand of sample MAB 09-17-01-03; and *(d)* sandy gravel of sample MAB 09-16-01-05.
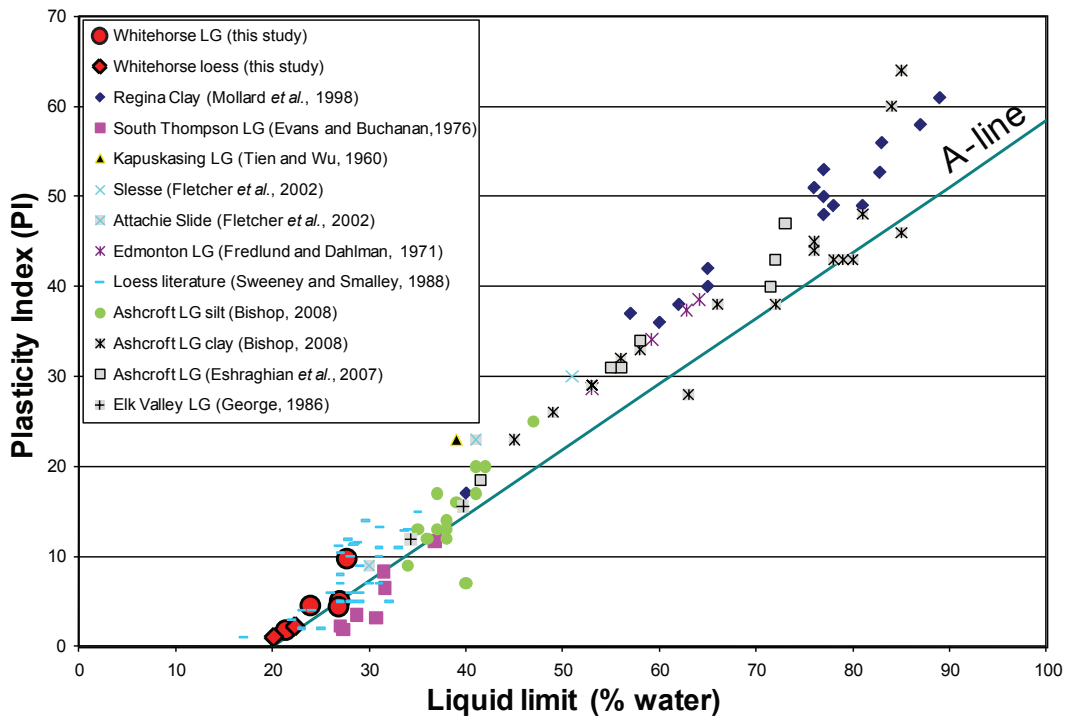
Figure 21. *Plasticity chart comparing samples from this study with plasticity values for samples from other locations in Canada found in the literature. The A-line is an empirical boundary dividing soils with a mechanical behaviour dominated by the presence of clay (above) or silt (below). LG = glaciolacustrine.*
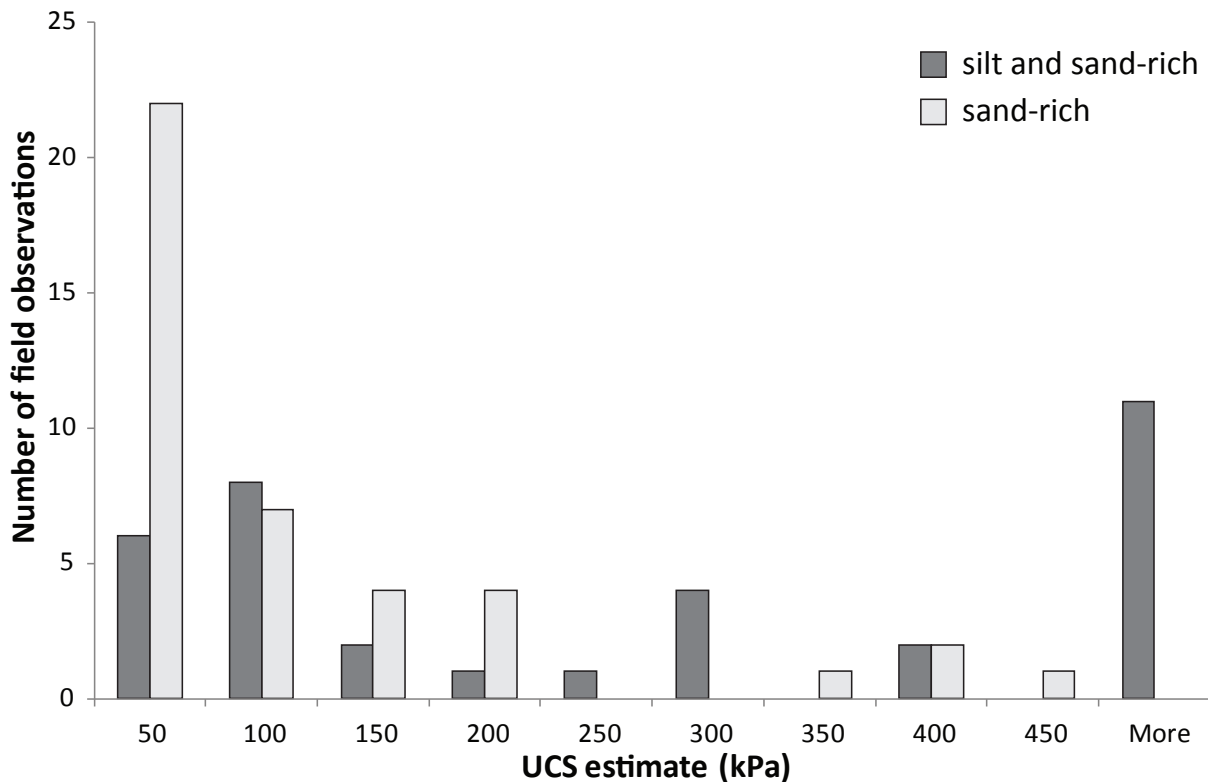
Figure 22. *Histogram of the soil strength estimates obtained from the pocket penetrometer for each of the stratigraphic units in Figures 6 to15.*

Table 1. *Table of soil density class based on field tests (modified from Paddington, 2004).*

Class	Field parameters used in this study to estimate soil density of gravel-rich soils
S1 - very loose	shovel penetrates soil to full length of the blade; easily excavated by hand
S2 – loose	shovel only penetrates soil to half blade length; difficult to excavate by hand
S3 - compact	soil only excavated with shovel with great difficulty; soil excavated without difficulty using pick
S4 - dense	impossible to excavate soil using shovel; pick required
S5 - very dense	soil only excavated with great difficulty using pick

DISCUSSION

Small scale instabilities (such as earth flows and slides (Huscroft *et al.*, 2004, p. 24)) associated with the Whitehorse bluffs have impacted infrastructure (roads, railways and houses) in and around the Whitehorse area (Fig. 2). Their potential hazard has been recognized by the City of Whitehorse which has established geohazard development planning zones, and the City has even purchased properties that are located in high hazard zones (Hopper, 2009). The only obvious sign of active mass movement observed during the period of fieldwork (July 2006 and 2009) conducted for this project, was piping erosion that was noted at station MAB 09-17-02 (Fig. 23); the resulting deposit buried low-lying vegetation with 30 cm of sediment over an area of approximately 20 m by 15 m. To assess the response of the bluffs to the large-scale landscape change due to the raised water table associated with the filling of Schwatka Lake following the construction of the Whitehorse Rapids hydroelectric dam in 1958, aerial photographs from 1950 (A12788-96 to 100; scale 1:15 000) were reviewed. No significant erosion or slope deformation features were observed between the 1950 aerial photographs and the 2006 1-m resolution orthophoto (orthophoto provided by Geomatics Yukon).

The weak strength of the sandy units, and the unvegetated nature of all stratigraphic units in the bluffs, may result in high erosion potential. The low yearly precipitation (Fig. 3) in the Whitehorse region probably minimizes the actual soil erosion; however, as a precaution, sediment erosion control structures such as a series of check dams and interception ditches have been installed at the base of a bluff in downtown Whitehorse (Fig. 24a; see Fig. 1 for location) to facilitate sediment deposition and thereby prevent erosion. In addition, a bio-stabilization attempt was made for the lower section of the bluff by introducing newly planted seedlings (observed during the 2009 fieldwork, Fig. 24b; see Figure 1 for location). Vegetation can increase the soil strength by increasing the root network, and reduce the amount of rainfall reaching the soil and thus moderating surface runoff.

Figure 23. *Photo of piping erosion observed at station MAB 09-17-02.*

Most of the stratigraphic units described in this project were either dry or damp. One sandy unit at station MAB 09-20-03 (Fig. 7) was moist, and one silty clay unit at station MAB 09-17-01 (Fig. 8) was wet. These observations suggest that the heterogeneities of grain size documented in the sections investigated are likely to result in a spatially complex hydraulic conductivity. This could be an important consideration not only for slope stability, but also for contaminant transport (*e.g.,* Soloway *et al.,* 2001).

CONCLUSIONS

Our observations document a larger range of sediment sizes and structures than previously recognized in the Whitehorse area bluffs. This work corroborates the interpretation of previous researchers who noted that the material exposed in the bluffs is dominantly glaciolacustrine sediments associated with Glacial Lake Laberge, which is overlain by a layer of loess. The large range of sediment sizes and structures is evidence for the variety of sediment sources and depositional processes within the glaciolacustrine environment. The loess layer

was found to contain up to 8 buried organic/charcoal layers and at least one tephra layer.

This paper provides a first description of the basic geotechnical properties of the glaciolacustrine and loess deposits around the City of Whitehorse. Samples of the fine, horizontally laminated units typically contain less than 20% clay and their mechanical behaviour is predominantly controlled by the high silt content and consequently low plasticity values. These results are comparable to previously reported values for similar deposits in the Canadian Cordillera, including sites near Kamloops and the Elk Valley areas. Most of the units in the Whitehorse bluffs were observed to be dry, but a few were moist or wet suggesting complex hydrogeological conditions. The dry silt and clay-rich units were found to have strengths up to 2 orders of magnitude greater than the sand-rich units. Minor piping erosion of the silt and clay-rich units was observed during 2009 summer fieldwork.

a

b

Figure 24. *Examples of the remediation effort completed to reduce erosion of the bluffs in downtown Whitehorse: (a) check dam to reduce flow velocity and encourage deposition; and (b) planting of grass and tree saplings in order to reduce erosion due to overland flow, and to increase soil strength by increasing the root network.*

ACKNOWLEDGEMENTS

REFERENCES

Ashley, G.M., 2002. Glaciolacustrine environment. *In:* Modern and Past Glacial Environments, J. Menzies (ed.), Elsevier, p. 335-359.

ASTM, 2007. Standard test method for particle-size analysis of soils. D422-63 (Reapproved 2007), 8 p.

Barnes, S.D., 1997. The sedimentology and paleogeography of Glacial Lake Champagne, southern Yukon Territory. Unpublished MSc thesis, University of Ottawa, Ontario, Canada, 137 p.

Bednarski, J.M., 2008. Landform assemblages produced by the Laurentide Ice Sheet in northeastern British Columbia and adjacent Northwest Territories – constraints on glacial lakes and pattern of ice retreat. Canadian Journal of Earth Sciences, vol. 45, p. 593-610.

Bennett, M.R., Huddart, D. and McCormick, T., 2000. The glaciolacustrine landform-sediment assemblage at Heinabergsjokull, Iceland. Geografiska Annaler, vol. 82A, p. 1-16.

Bishop, N.F., 2008. Geotechnics and hydrology of landslides in Thompson River Valley, near Ashcroft, British Columbia. Unpublished MSc thesis, University of Waterloo, Ontario, Canada, 117 p.

Bond, J.D., Morison, S. and McKenna, K., 2005. Surficial geology of Whitehorse (NTS 105D/11), Yukon. Yukon Geological Survey, Geoscience Map 2005-7, scale 1:50 000.

Bond, J.D., 2004. Late Wisconsinan McConnell glaciations of the Whitehorse map area (105D), Yukon. *In:* Yukon Exploration and Geology 2003, D.S., Emond and L.L. Lewis, (eds.), Yukon Geological Survey, p. 73-88.

Burn, C.R., 1998. The response (1958-1997) of permafrost and near-surface ground temperatures to forest fire, Takhini River valley, southern Yukon Territory. Canadian Journal of Earth Sciences, vol. 35, no. 2, p. 184-199.

Clague, J.J. and Evans, S.G., 2003. Geologic framework of large historic landslides in Thompson River Valley, British Columbia. Environmental & Engineering Geoscience, vol. IV, p. 201-212.

Clague, J.J., Evans, S.G., Rampton, V.N. and Woodsworth, G.J., 1995. Improved age estimates for the White River and Bridge River tephras, Western Canada. Canadian Journal of Earth Sciences, vol. 32, no. 8, p. 1172-1179.

Craig, R.F., 2007. Craig's Soil Mechanics, 7th edition. Spon Press, New York, USA, 447 p.

David, P.P., 1972. Great Sand Hills, Saskatchewan. *In:* Quaternary Geology and Geomorphology Between Winnipeg and the Rocky Mountains, N.W. Rutter and E.A. Christianson (eds.), 24th International Geologic Congress, Field Excursion Guidebook C22, p. 47-50.

Environment Canada, 2010. Canadian Climate Normals or Averages 1971-2000. <http://www.climate.weatheroffice.gc.ca/climate_normals/index_e.html> [accessed October 19, 2010].

Eshraghian, A., Martin, C.D. and Cruden, D.M., 2007. Complex earth slides in the Thompson River Valley, Ashcroft, British Columbia. Environmental & Engineering Geoscience, vol. XIII, p. 161-181.

Evans, S.G. and Buchanan, R.G., 1976. Some aspects of natural slope stability in silt deposits near Kamloops, British Columbia. *In:* Proceedings of the 29th Canadian Geotechnical Conference, Vancouver, BC, p. 1-32.

Evans, S.G., 2003. Characterising landslide risk in Canada. *In:* Proceedings of the 3rd Canadian Conference on Geotechnique and Natural Hazards, Edmonton, Alberta, p. 19-34.

Eyles, N. and Clague, J.J., 1991. Glaciolacustrine sedimentation during advance and retreat of the Cordilleran Ice Sheet in Central British Columbia. Géographie physique et Quaternaire, vol. 3, p. 317-331.

Fletcher, L., Hungr, O. and Evans, S.G., 2002. Contrasting failure behaviour of two large landslides in clay and silt. Canadian Geotechnical Journal, vol. 39, p. 46-62.

Fredlund, D.G. and Dahlman, A.E., 1971. Statistical geotechnical properties of Glacial Lake Edmonton sediments. *In:* Proceedings of the International Conference on Applications of Statistics and Probability to Soil and Structural Engineering, Hong Kong, p. 212-228.

Fulton, R.J., 1965. Silt deposition in late-glacial lakes of southern British Columbia, American Journal of Science, vol. 263, p. 553-570.

George, H., 1986. Characteristics of varved clays of the Elk Valley, British Columbia, Canada. Engineering Geology, vol. 23, p. 59-74.

Hart, C.J.R. and Radloff, J.K., 1990. Geology of the Whitehorse, Alligator Lake, Fenwick Creek, Carcross and Part of Robinson Map Areas (105D/11, 6, 3, 2 & 7). Exploration and Geological Services Division, Yukon Region, Indian and Northern Affairs Canada, Open File 1990-4(G), 4 maps at 1:50 000 scale and report 113 p.

Hart, C.J.R. and Villeneuve, M., 1999. Geochronology of Neogene alkaline volcanic rocks (Miles Canyon basalt), southern Yukon Territory, Canada: The relative effectiveness of laser ^{40}Ar/^{39}Ar and K-Ar geochronology. Canadian Journal of Earth Sciences, vol. 36, p. 1495-1507.

Heginbottom, J.A., Bubreuil, M.A. and Harker, P.A., 1995. Canada permafrost: National Atlas of Canada. Natural Resources Canada, 5th Edition, MCR 4177.

Hopper, T., 2009. Thirty years later, 'mudslide zone' remains inhabited. Yukon News, February 6, 2009, p. 7.

Horton, S., 2007. The paleogeography of Glacial Lake Laberge, south central Yukon Territory. Unpublished B.Sc. thesis, University of Victoria, British Columbia, Canada, 53 p.

Hungr, O., Evans, S.G., Bovis, M.J. and Hutchinson, J.N., 2001. A review of the classification of landslides and flow type. Environmental and Engineering Geoscience, vol. VII, p. 221-238.

Huscroft, C.A., Lipovsky, P.S. and Bond, J.D., 2004. A regional characterization of landslides in the Alaska Highway corridor, Yukon. Yukon Geological Survey, Open File 2004-18, 65 p., report and CD-ROM.

Lum, K.K.Y., 1979. Stability of the Kamloops silt bluffs. Unpublished MSc thesis, University of British Columbia, British Columbia, Canada, 135 p.

Matile, G.L.D., 2004. Surficial geology, Winnipeg, Manitoba. Geological Survey of Canada, Map 2055A, scaler 1:100 000.

Mollard, J., Kozicki, P. and Adelman, T., 1998. Some geological, groundwater, geotechnical and geoenvironmental characteristics of the Regina area, Saskatchewan, Canada. *In:* Urban Geology of Canadian Cities, P.F. Karrow and O.L. White (eds.), Geological Association of Canada Special Paper 42, p. 147-170.

Mougeot, C., 1994. Preliminary assessment of the clay deposits in selected areas of the Whitehorse map sheet area (105D) for the manufacture of clay based products. Mougeot GeoAnalysis, Whitehorse, Yukon, unpublished report prepared for the Yukon-Canada Co-operation Agreement for Small Business, 57 p.

Mougeot, C., 1997. Soil, terrain, and wetlands survey, City of Whitehorse. Mougeot GeoAnalysis, Whitehorse, Yukon, unpublished report prepared for Planning Services, City of Whitehorse, 160 p.

Mougeot, C., 1998. Soil and terrain features of the Yukon River corridor. Mougeot GeoAnalysis, Whitehorse, Yukon, unpublished report prepared for Gartner Lee Consultants Ltd., 29 p.

Osborn, G. and Rajewicz, R., 1998. Urban geology of Calgary. *In:* Urban Geology of Canadian Cities, P.F. Karrow, and O.L. White (eds.), Geological Association of Canada Special Paper 42, p. 93-115.

Paddington, S.R., 2004. The characterization of drainage related landslides on gentle-over-steep forest terrain in the Interior of British Columbia. Unpublished MSc thesis, Simon Fraser University, Burnaby, British Columbia, Canada, 261 p.

Paradis, S.J., 2009. Surficial geology, Kelowna, British Columbia. Geological Survey of Canada, Open File 6146, scale 1:50 000.

Shaw, J. and Archer, J., 1978. Winter turbidity current deposits in Late Pleistocene glaciolacustrine varves, Okanagan Valley, British Columbia, Canada. Boreas, vol. 7, p. 123-130.

Smith, C.A.S., Meikle, J.C. and Roots, C.F., 2004. Ecoregions of the Yukon Territory – Biophysical properties of the Yukon landscapes. Agriculture and Agri-Food Canada PARC Technical Bulletin 04-01, 313 p.

Smith, I., 2006. Elements of Soil Mechanics, 8th edition. Blackwell Publishing, Oxford, UK, 538 p.

Smith, N.D. and Ashley, G., 1985. Proglacial lacustrine environment. *In:* Glacial Sedimentary Environments, G.M. Ashley, J. Shaw and N.D. Smith (eds.), p. 135-215.

Soloway, D.A., Nahir, M., Billowits, M.E. and Whyte, L.G., 2001. In-situ bioremediation of diesel-contaminated soil in Canada's Arctic territory: a case study at the Whitehorse International Airport, Yukon Territory. Polar Record, vol. 37, p. 267-272.

Sweeney, S.J. and Smalley, I.J., 1988. Occurrence and geotechnical properties of loess in Canada. Engineering Geology, vol. 25, p. 123-134.

Teller, J.T., 1987. Proglacial lakes and the southern margin of the Laurentide Ice Sheet, *In:* North American and adjacent oceans during the last deglaciation, W.F. Ruddiman and H.E., Wright (eds.), Geological Society of America, vol. K-3, p. 39-69.

Tien, H. and Wu, M., 1960. Geotechnical properties of glacial lake clays. Transactions of the American Society of Civil Engineers, vol. 125, p. 994-1021.

Tipper, H.W., 1971. Surficial geology of Prince George. Geological Survey of Canada Map 1288A, scale 1:250 000.

Ward, B.C. and Rutter, N.W., 2000. Deglacial valley fill sedimentation, Pelly River, Yukon Territory, Canada. Quaternary International, vol. 68-71, p. 309-328.

Wolfe, S., Bond, J.D. and Lamothe, M, 2011. Dune stabilization in central and southern Yukon in relation to early Holocene environmental change, northwestern North America. Quaternary Science Reviews, vol. 30, p. 324-334.

New bedrock geology of Mount Mervyn map sheet (106C/04) and mineral potential for the South Wernecke mapping project

Joyia Chakungal[1] and Venessa Bennett
Yukon Geological Survey

ABSTRACT

An integrated bedrock mapping and regional soil sampling program in the Mount Mervyn map area (106C/04) was undertaken in 2010. It is the first year of a multi-year initiative called the South Wernecke mapping project (SWP), which will cover ten 1:50K map sheets in the southern Wernecke Mountains area in central Yukon. Field work in the first year served to highlight the complexities of the bedrock geology in the region, and identify areas of mineral potential.

The Mount Mervyn map sheet is underlain by Proterozoic and Paleozoic siliciclastic and carbonate rocks that have been deformed into an east-trending fold-and-thrust belt. Regional soil geochemical data coupled with bedrock observations highlight new areas of mineral potential (*i.e.,* Ni and Au) that have not been previously identified.

[1]joyia.chakungal@gov.yk.ca

INTRODUCTION

In 2010, the Yukon Geological Survey initiated a multi-year mapping program entitled the South Wernecke mapping project (SWP). A core objective of the project is aimed at updating geoscience information available for an area spanning ten 1:50K map sheets in the southern Wernecke Mountains of central Yukon (Figs. 1a,b). The area of interest is situated northeast of the Tintina Fault and includes rocks of the Proterozoic western margin of ancestral North America on which the Paleozoic Selwyn basin subsequently formed. More specifically, the study area is inferred to straddle the boundary between siliciclastic rocks of the Selwyn basin and correlative platform carbonates that unconformably overlie Paleo - Neoproterozoic basement (Fig. 1c). The map area also includes the recently discovered Rackla Gold Belt, a phrase coined by ATAC Resources (property holders), that lies within a structural corridor bounded by the Kathleen Lakes Fault on the north and the Dawson thrust on the south.

Over the next several years the SWP will upgrade the stratigraphy of the area to a standard comparable to that of western Yukon (Fig. 2) and eastern Northwest Territories (NWT), and document the structural elements in order to better understand the area's tectonic evolution. In particular, structures that may have facilitated or controlled development of precious and polymetallic mineral deposits in the area will be examined. A longer-term goal of the SWP is to support regional correlations across Alaska, Yukon, and NWT by integrating the results of this study with work being undertaken across the region by university-based colleagues (Fig. 1; Macdonald *et al.*, this volume; Medig *et al.*, 2010; Nielsen and Thorkelson, this volume; Peters and Thorkelson, this volume; Thiessen and Gleeson, in progress; Turner, this volume). With these goals in mind, field investigations during the summer of 2010 were carried out over six weeks with limited helicopter support. Work was conducted out of eight fly camps positioned throughout the 1:50K Mount Mervyn map sheet (106C/04).

In the following contribution we briefly outline the regional geological context and mineral potential before presenting results of the 2010 bedrock mapping program that was aimed at updating the existing 1:250K map (Blusson, 1974) to 1:50K. Additionally, we report results of a YGS pilot study designed to assess the practical and scientific feasibility of completing regional soil sampling concurrently with regional bedrock mapping.

GEOLOGICAL SETTING

In north and central Yukon, Paleo and Neoproterozoic sedimentary and volcanic rocks of Laurentian affinity are exposed in a series of inliers in the Wernecke and Ogilvie mountains (Fig. 1a). The Selwyn basin, which overlaps the western margin of Laurentia, comprises a sequence of deep-water sediments that range from latest Neoproterozoic to middle Devonian age. Correlative platform rocks associated with the basin unconformably overlie Laurentian basement in the Wernecke and Ogilvie mountains, and give way southward to the deep-water clastic rocks south of the Dawson thrust. Basement rocks on which the deep water sediments of the Selwyn basin have been deposited are unknown. Recent and ongoing research across northern Yukon permit regional stratigraphic correlations between inliers, except in the south Wernecke Mountains where a lack of data preclude such correlations.

While stratigraphic details and associated nomenclature differ from west to east across the Coal Creek, Hart River, and Wernecke inliers, a number of units are common to all three (Fig. 2). From oldest to youngest, Laurentian basement rocks include:

1. Rift-related Paleoproterozoic rocks of the Wernecke Supergroup;

2. Meso - Neoproterozoic rift-related rocks (Pinguicula Group in the Wernecke and Hart River inliers; Fifteenmile Group in the Coal Creek inlier; Mackenzie Mountain supergroup (Wernecke and Northwest Territory);

3. Rift-related (opening of Pacific Ocean at ~ 700 Ma) early Neoproterozoic Windermere Supergroup.

Overlying supracrustal sequences of the Laurentian basement are upper Neoproterozoic - middle Devonian rocks of the Selwyn basin. Lithologies include basinal sediments (Hyland, Gull Lake and Road River groups) and correlative platform carbonate rocks. Stratigraphically overlying sedimentary rocks of the Selwyn basin are late Devonian rift-related clastic rocks of the Earn Group, terrigenous Triassic and younger sedimentary rocks.

Descriptions of the above units and their structural geometry as observed in the Mount Mervyn area are discussed in the bedrock section below.
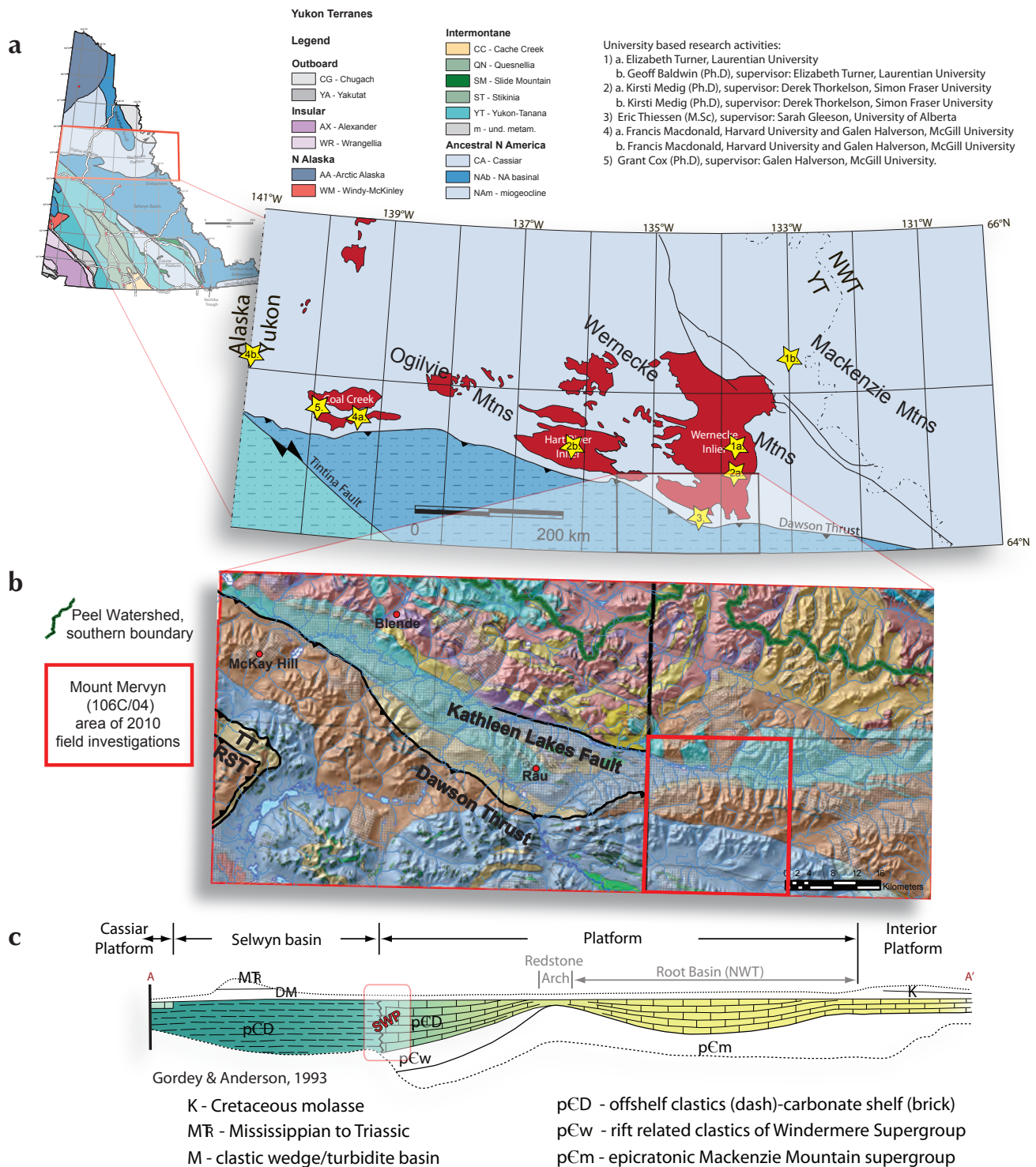
Figure 1. *(a) Terrane map for the central Yukon, highlighting in red the distribution of inliers in which Proterozoic 'basement' rocks are exposed. Yellow stars indicate locations for university based research activities. (b) Regional compilation map of Gordey and Makepeace (2001) for the South Wernecke mapping project and surrounding area. Red circles indicate the position of current exploration targets. The focus of 2010 field work is highlighted by the red box (1:50K, 106C/04). Legend: TT, Tombstone Thrust; RST, Robert Service Thrust. (c) A southwest oriented cross-section that extends from the Paleozoic Mackenzie platform in Northwest Territories, westward into Yukon and the Selwyn basin. The South Wernecke Project (SWP) area straddles the northern boundary between siliciclastics of the Selwyn basin and correlative platform carbonates that sit unconformably on Paleo - Neoproterozoic basement.*
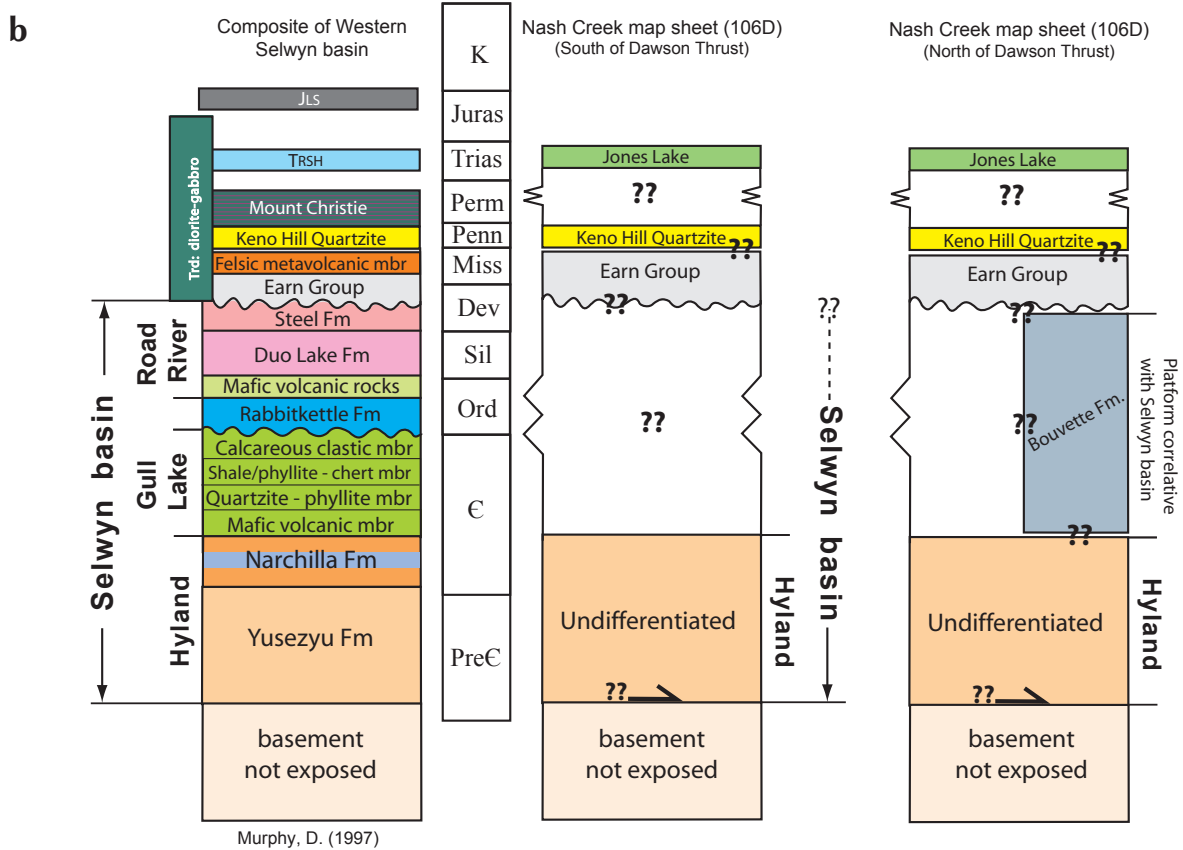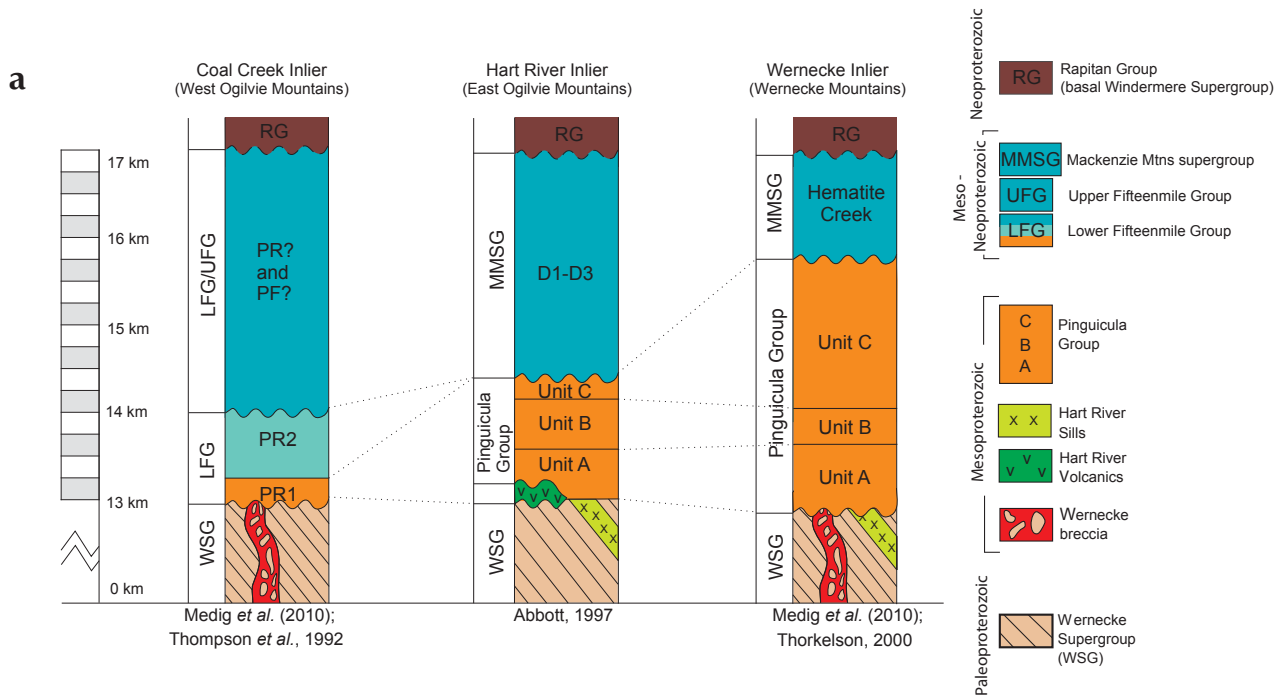
Figure 2. (a) *Stratigraphic correlation charts for Paleoproterozoic – Neoproterozoic stratigraphy across the Yukon, and* **(b)** *stratigraphic column for Neoproterozoic through to Paleozoic stratigraphy in west Yukon as compared to the current stratigraphic understanding of coeval rocks in the area of interest to the South Wernecke mapping project.*

REGIONAL MINERAL POTENTIAL

The SWP is host to a diverse range of mineralization styles. Sixty-five Yukon MINFILE showings, drilled prospects and deposits occur within the footprint of the project area (Yukon MINFILE, 2010). Showings include northeastern extensions of the Ag-Pb-Zn vein faults of the Keno Hill camp (within 106D/03), the Cu-Pb-Ag-Zn Marg deposit (Yukon MINFILE 106D 009), the Pb-Zn-Ag Blende deposit (Yukon MINFILE 106D 064), the past producing polymetallic vein systems of Mckay Hill (Yukon MINFILE 106D 038) and the newly discovered and drilled Au prospect of the Rau property (Yukon MINFILE 106D 098; Fig. 3). Importantly, south and west of the project area (1:50K sheets: 106D/04, 105M/13 and 105M/14), the region is host to the high-grade, past and current-producing Ag-Pb-Zn veins of the Keno Hill mining camp, and Au and W deposits at Dublin Gulch, which is at the pre-feasibility stage of project development (Eagle Au deposit, Yukon MINFILE 106D 025, and Mar Tungsten, Yukon MINFILE 106D 027; Fig. 3).

Among the MINFILE occurrences located in the SWP area, three main mineralization styles are recognized and broadly correlate to host lithology. These styles include: (i) Mississippi Valley-type Ag-Pb-Zn occurrences associated with both Proterozoic and Paleozoic carbonate units; (ii) Syngenetic sedimentary exhalative (SEDEX) and volcanogenic massive sulphide (VMS) occurrences that are host to significant barite, Pb-Zn-Ag and Cu, and interpreted to have formed in Devonian – Mississippian Earn Group and associated volcanic rocks; and (iii) Intrusion-hosted and related W± Cu skarn occurrences that relate to surface and near surface occurrences of Cretaceous intrusions belonging to both the Tombstone and McQuesten magmatic suites. A fourth mineralization style is not associated with a specific host lithology but rather with numerous epigenetic polymetallic vein systems that postdate the polydeformed stratigraphy in the area.

Exploration activity in the project area has significantly increased since the discovery of the carbonate-replacement Au prospects of the Tiger and the Osiris zones within the Rau property of ATAC Resources (Yukon MINFILE 106D 098; Figure 3). The discoveries have highlighted the high Au potential of Paleozoic carbonate platform rocks that are both stratigraphically and tectonically intercalated with Selwyn basin stratigraphy.
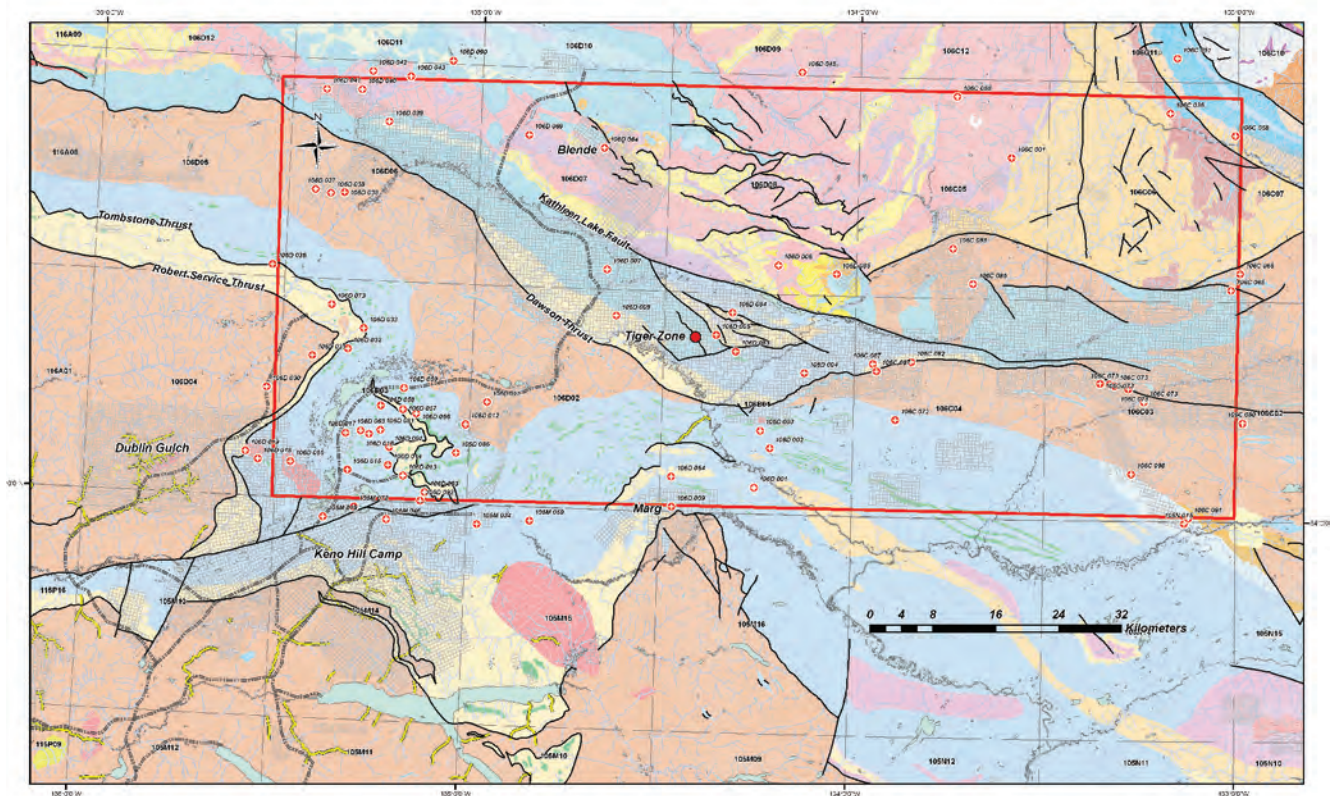

Figure 3. *Distribution of Yukon MINFILE showings, drilled prospects and deposits within the South Wernecke bedrock mapping project area. Major regional faults and thrust systems marked. Carbonate hosted gold drilled prospect of the Tiger zone of ATAC resource also marked for reference.*

Tiger Zone gold mineralization is associated with thrust imbricated packages of the Silurian – Devonian Bouvette Formation (ЄD_B) situated in the foot-wall of the Dawson thrust and south of the Kathleen Lakes fault (Fig. 3). In addition to the main sulphide ore body, Au mineralization is also associated with a series of north-striking oxidizing fault zones (ATAC Corporate presentation; December 2010). Continued regional exploration throughout the property has demonstrated a spatial association of Au occurrences to a prominent west-northwest-trending structural corridor located north of the Dawson thrust and south of the Kathleen Lake Fault (Fig. 3). The new Osiris drilled prospect, located *ca.* 100 km to the east of the Tiger Zone (106C/01), is hosted in a stratigraphically different carbonate package (possibly Cambrian carbonate units associated with the Hyland Group; Fritz *et al.*, 1991) within this regional structural corridor (Fig. 3). Both drilled prospects bear many hallmarks of Carlin-style gold mineralization and consequently the discoveries have resulted in a new staking rush in the region, closely following on the heels of the White Gold staking rush in the Dawson Range.

Analysis of key metals and tracer elements associated with NRCan's Regional Silt Geochemistry (RGS) database (Héon, 2003) within the SWP area has been important for delineating first-order metallogenic domains. The database has also been utilized to identify several areas of significant mineral potential which are currently under explored. Figures 4 –9 represent colour-gradient gridded maps of RGS metal anomalies in the SWP area for Pb, Zn, Cu, Au, W and Mo. Areas in red correspond to 95th percentile (or 2 Standard Deviations) anomalies in the dataset. Integration of RGS data with MINFILE data allow a number of important observations, including:

1. Areas of anomalous Pb (Fig. 4) show a strong spatial correlation with known MVT occurrences. Polymetallic vein systems represent a subordinate contribution to anomalous Pb RGS values.

2. Anomalous Zn domains coincide predominantly with polymetallic vein occurrences (Fig. 5), and to a lesser extent are associated with MVT occurrences and the Marg VMS deposit.

3. Copper anomalies north of the Kathleen Lakes fault coincide spatially with Pb anomalies, in addition to surface occurrences of carbonate hosted MVT mineralization and polymetallic vein prospects (Fig. 6). South of the Kathleen Lakes Fault, domains of anomalous Cu show a stronger spatial correlation with polymetallic vein occurrences. The most anomalous Cu values are associated with drainages proximal to the Marg VMS deposit. Note also that several areas of anomalous Cu are not spatially associated with known mineral occurrences at surface (*e.g.*, within 106D/02 a broad arcuate area of anomalous Cu is defined in the RGS dataset).

4. Elevated Au domains occur within the structural corridor bound by the Dawson Thrust and Kathleen Lakes Fault. Of these, values correlating with the Tiger Zone are most anomalous for gold (Fig. 7). Several Au anomalies are also evident to the north and south of the structural corridor, and are currently not well understood (*e.g.*, two anomalies occur in the Southern and Northern domains of the Mount Mervyn map sheet; Fig. 7).

5. Domains of anomalous W show good correlation with surface occurrences of W ± (Cu) skarn, suggesting W values in the RGS data can be used as a tracer metal for intrusion-hosted and/or related mineralization vectoring (Fig. 8).

6. Five areas of elevated Mo occur in the SWP area, one of which occurs within the Mount Mervyn map sheet and coincides with anomalous Au in the Northern domain (Figs. 7 and 9). The largest anomaly coincides with a strong W anomaly located to the west of the Tiger Zone and immediately south of the Dawson Thrust. Elevated Mo values may correlate with intrusion-related mineralization though a definitive correlation for the remainder of the anomalous regions has yet to be established.

BEDROCK GEOLOGY

STRATIGRAPHY

Field observations permit division of the Mount Mervyn map area into three lithologically and structurally distinct domains herein referred to as the Southern; Central; and Northern domains. Unit descriptions provided below correspond with unit designators as indicated in the legend of Figure 10. Unit names are informal, and are utilized for two reasons: first, not all units are correlated with certainty to stratigraphic units defined by previous workers; and secondly, as noted above, regional stratigraphic correlation studies underway will likely result in revisions to existing nomenclature. As mapping proceeds in the South Wernecke area over the next several years, formal stratigraphic names that are consistent with current nomenclature will be assigned to map units. In the sections below, rocks are tentatively correlated with their named stratigraphic equivalents.
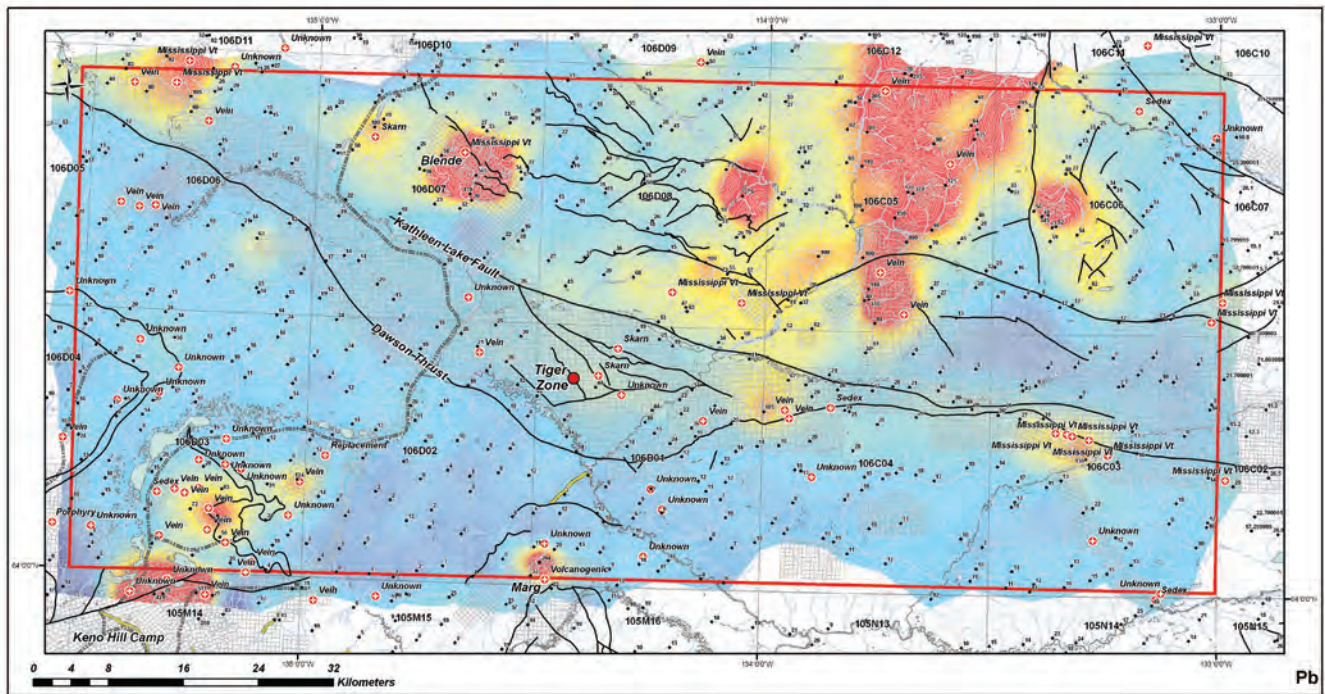
Figure 4. *Colour-gradient gridded map of RGS Pb anomalies in the South Wernecke bedrock project area. Areas in red correspond to 95th percentile (or 2 standard deviations) anomalies in the dataset.*
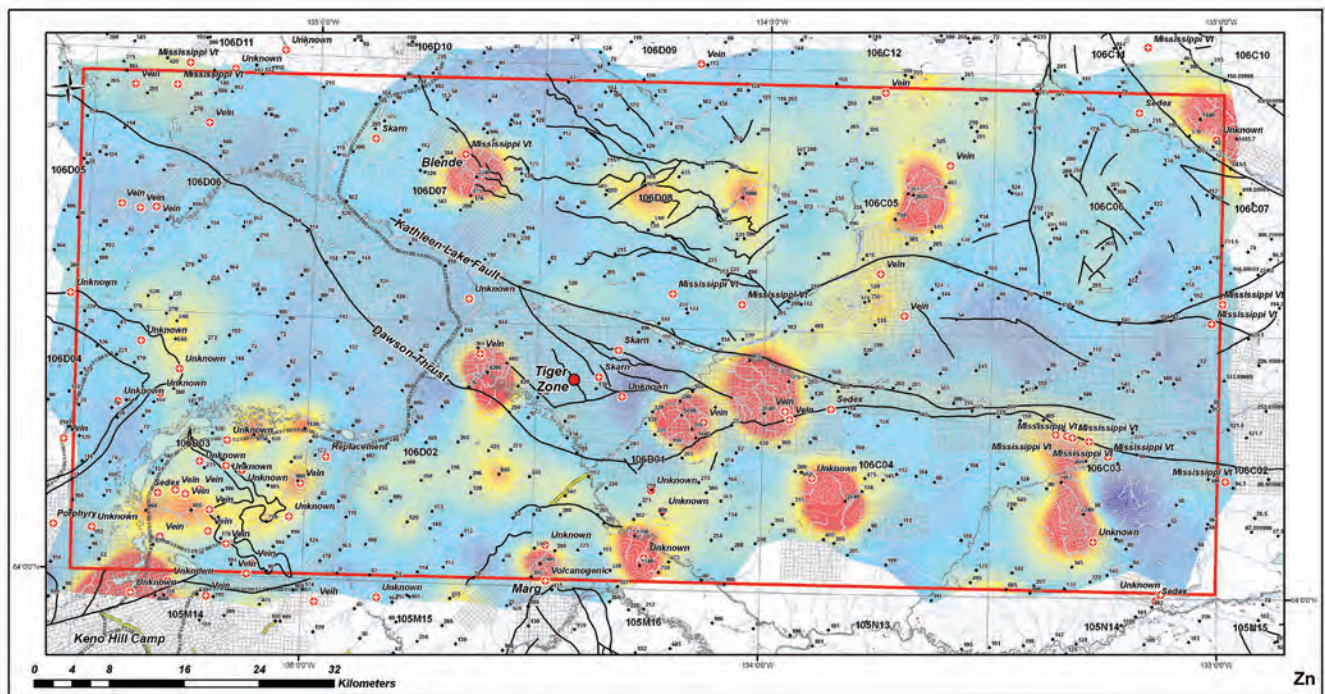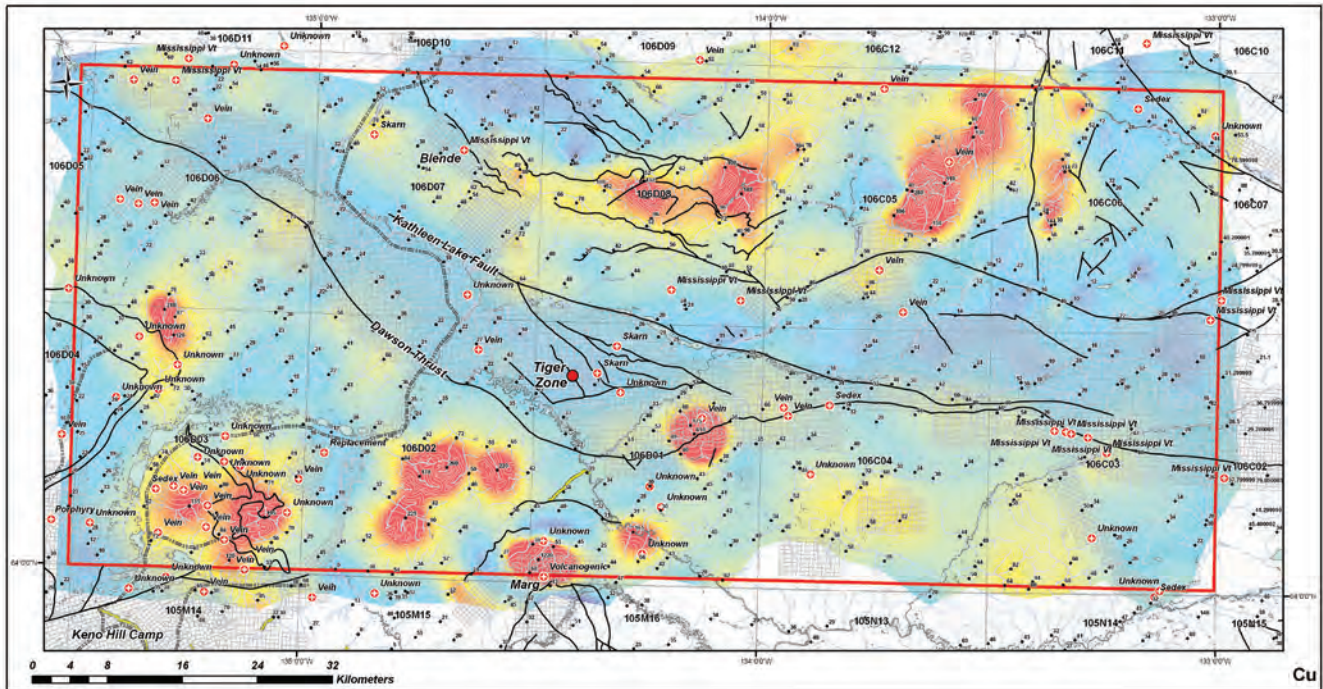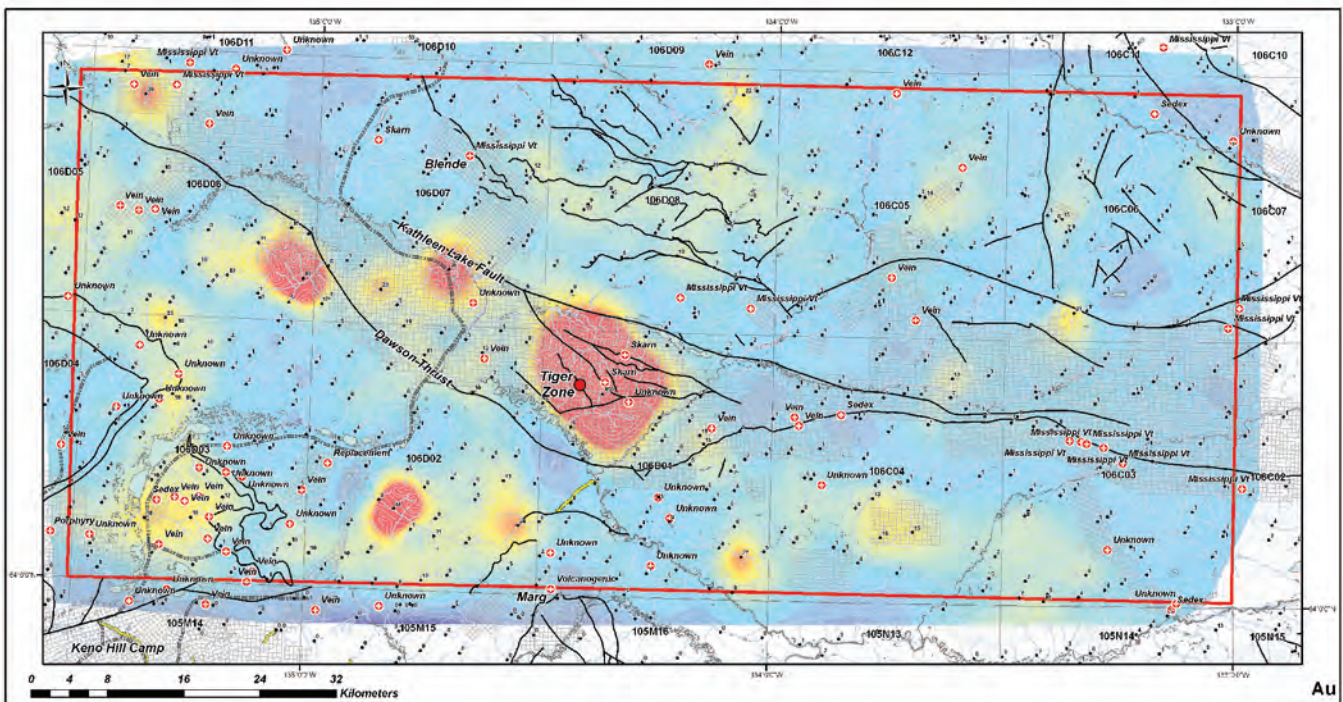

Figure 5. *Colour-gradient gridded map of RGS Zn anomalies in the South Wernecke bedrock project area. Areas in red correspond to 95th percentile (or 2 standard deviations) anomalies in the dataset.*

Figure 6. *Colour-gradient gridded map of RGS Cu anomalies in the South Wernecke bedrock project area. Areas in red correspond to 95th percentile (or 2 standard deviations) anomalies in the dataset.*
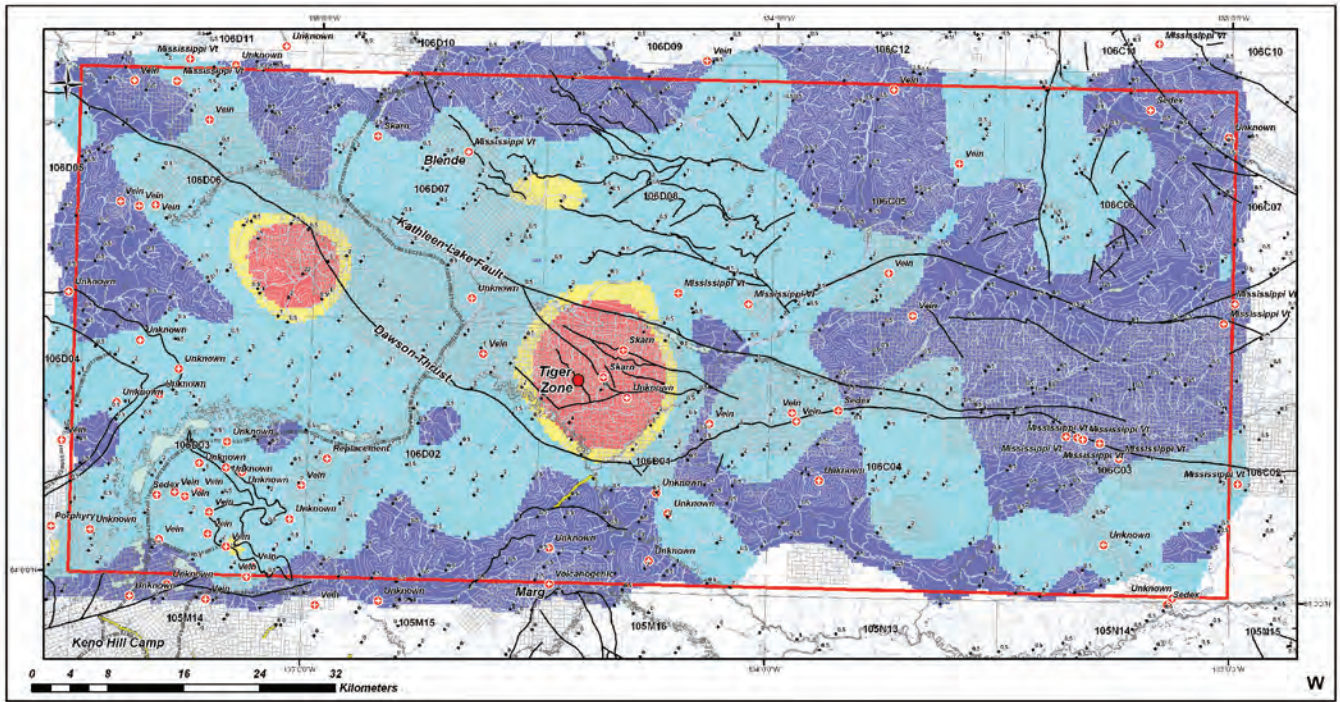

Figure 7. *Colour-gradient gridded map of RGS Au anomalies in the South Wernecke bedrock project area. Areas in red correspond to 95th percentile (or 2 standard deviations) anomalies in the dataset.*
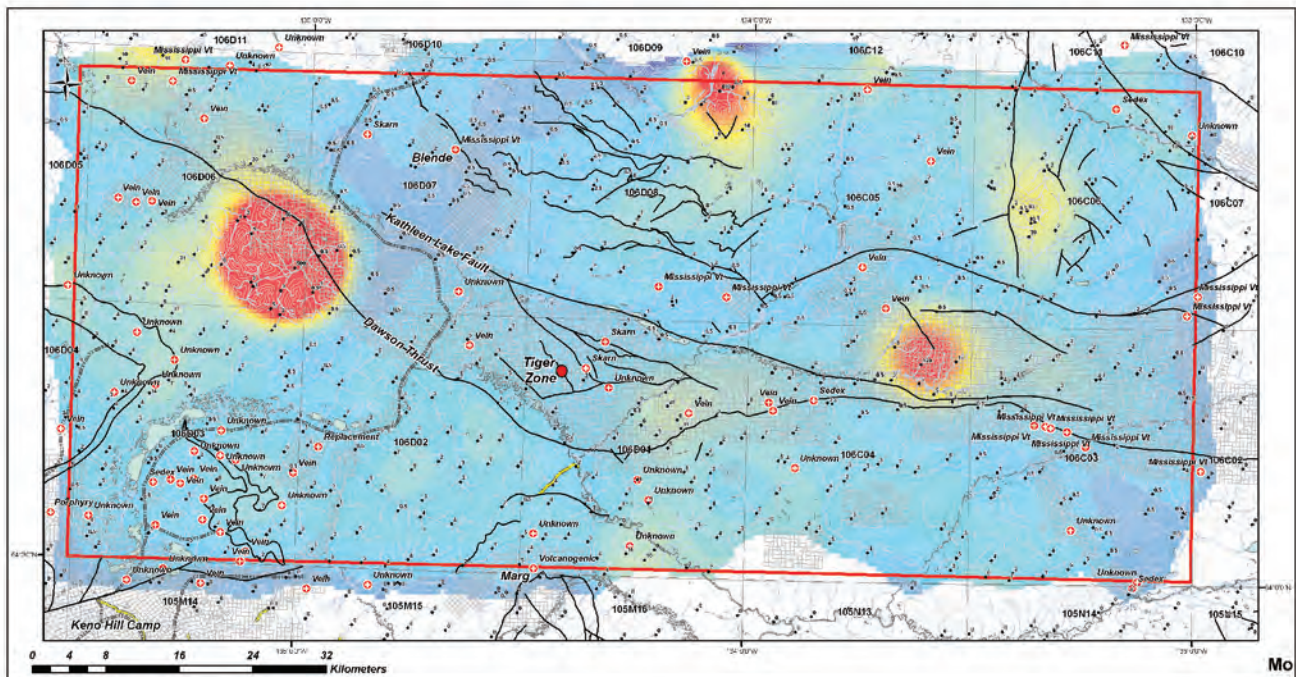
Figure 8. Colour-gradient gridded map of RGS W anomalies in the South Wernecke bedrock project area. Areas in red correspond to 95th percentile (or 2 standard deviations) anomalies in the dataset.

Figure 9. Colour-gradient gridded map of RGS Mo anomalies in the South Wernecke bedrock project area. Areas in red correspond to 95th percentile (or 2 standard deviations) anomalies in the dataset.
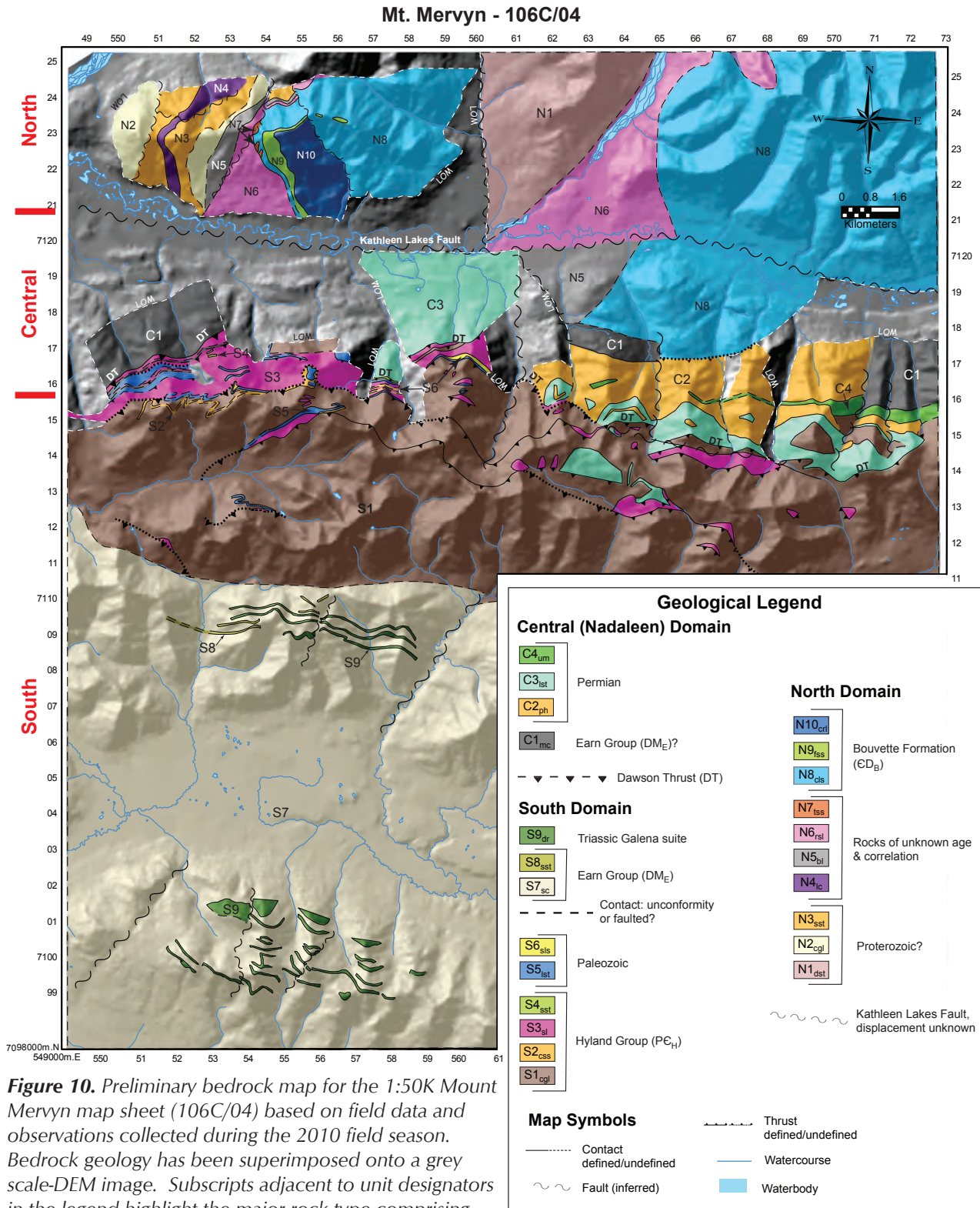
Mt. Mervyn - 106C/04

Figure 10. Preliminary bedrock map for the 1:50K Mount Mervyn map sheet (106C/04) based on field data and observations collected during the 2010 field season. Bedrock geology has been superimposed onto a grey scale-DEM image. Subscripts adjacent to unit designators in the legend highlight the major rock type comprising the unit. Legend: LOM, limit of mapping; cgl, conglomerate; css, calcareous sandstone; sl, slate; sst, sandstone; lst, limestone; sls, siltstone; sc, siliciclastics; dr, diorite; mc, mudstone and chert; ph, phyllite; um, ultramafic; dst, dolostone and sandstone; lc, limestone with chert lenses; bl, brecciated limestone; rsl, finely laminated rosy siltstone; tss, thinly bedded siltstone; cls, cryptically bedded limestone; fss, fossiliferous sand and siltstones; crl, coral bearing limestone.

SOUTHERN DOMAIN

Rocks comprising the Southern domain include all rocks south of the Dawson Thrust. They are exposed along the ridges north of the Stewart River and through much of the Nadaleen Range, where they sit in the hanging wall of the Dawson Thrust. Units S1 – S6 have in part been correlated with the Neoproterozoic – lower Cambrian Hyland Group (Fritz *et al.*, 1983), and form the structurally lower part of the Dawson Thrust sheet. Units S7 – S9 are in part correlated with the Devonian – Mississippian Earn Group that overlie Hyland Group equivalents. Where primary structures could be identified, stratigraphic up is predominantly to the south. The exact nature (unconformity versus thrust fault) of the contact between the two sedimentary sequences is unclear though relative to units S1-S6, Earn Group equivalent rocks are situated structurally higher in the Dawson Thrust sheet.

Hyland Group (Pϵ_H) equivalents

Unit S1 comprises predominantly grey-brown, blocky weathering, thickly bedded ($\geq$1 m) medium to coarse-grained, sandstone and polymictic pebble - cobble conglomerate (Fig. 11a), with minor carbonate and shale. The matrix in coarse-grained sandstones and conglomerates is locally characterized by rusty weathering limonite. Coarse sandstone and conglomerate are locally dolomitic or calcitic, forming massive beds that are separated by intervals of grey-black weathering shales/slates ($\leq$1 m; Fig. 11b). Finer grained sandstones are characterized by the presence of detrital white mi*ca*.

Unit S2 includes orange-brown, blocky weathering; moderately bedded ($\leq$1 m), fine to coarse grained calcareous to dolomitic sandstone with minor polymictic pebble conglomerate (Fig. 11c), and may be equivalent to unit S1 described above. Pebbles include black nodules that may be phosphatic in composition, and rounded quartz and shale chips. Rocks of unit S2 occur most commonly near limestone beds interpreted to belong to the carbonate member of the Hyland Group (Pϵ_{Hc}; Risky Formation?) (Fritz *et al.*, 1991).

Maroon and green, recessive, platy weathering, fine-grained slates comprise unit *S3*. Based on its distinct colour and stratigraphic position, we correlate S3 with the lower Cambrian Narchilla Formation (ϵ_N; Fig. 11d) of Fritz *et al*. (1991). Unlike the Narchilla Formation at its type locality, traces of Oldhamia were not observed in the Mount Mervyn area which may be a consequence of the rocks breaking preferentially along cleavage planes as opposed to bedding.

Unit S4 comprises distinctly green - rusty weathering, fine to medium-grained micaceous sandstones, siltstones and shales (Fig. 11e). Fine-grained sandstone beds are thick ($\leq$1.5 m) while intervening shale beds are thin ($\leq$10 cm). The unit does not appear in outcrop everywhere, but is abundant in the central part of the Nadaleen Range. Abbott (1990) described a coarse-grained member of the Narchilla Formation, to which we tentatively correlate unit S4.

Lower Paleozoic rocks

Unit S5 is made up of light grey-brown, blocky weathering, fine to coarse-grained limestone. In places, outcrops are made up of boulder size (>0.5 m) limestone clasts that have a brecciated appearance. Clasts are cemented by sparry dolomite and calcite, locally preserving tabulate corals and grains interpreted to be ooids (Figs. 12a,b). The corals are tentatively identified as Halysites (E. Turner, personal communication, 2010), implying coral growth on an Ordovician to early Devonian platform. The presence of brecciated clasts indicates disruption and re-deposition of the platform following its formation.

Brown to dark-grey weathering, finely ($\leq$0.25 m) laminated siltstones and phyllites (Fig. 12c) comprise unit S6. The package shows marked similarities to green – orange weathering phyllites described in the eastern half of the Nadaleen Range (see Unit C1).

Earn Group (DM$_E$) equivalents

Units S7 and S8 underlie most of the southern half of map sheet 106C/04. Unit S7 includes grey-black-brown recessive-weathering shale and siltstone of varying carbon content (Fig. 13a), interbedded locally with rare tuffaceous horizons. Siltstone beds are $\leq$0.25 m and commonly characterized by graded, fining upward sequences. Other lithologies include grey chert beds up to 20 cm thick, minor fine-grained sandstone and rare chert-bearing pebble conglomerate. Sandstone beds are typically less than 1 m thick, but locally they are substantially thicker. The thick bedded sandstones were mapped as unit *S8*.

Sedimentary rocks of units S7 and S8 were assigned to the Devonian – Mississippian Earn Group (DM$_E$) by Gordey and Makepeace (2001). This correlation is consistent with our field observations. The interpretation will be further corroborated as U-Pb data becomes available for a tuffaceous shale that was sampled in 2010.
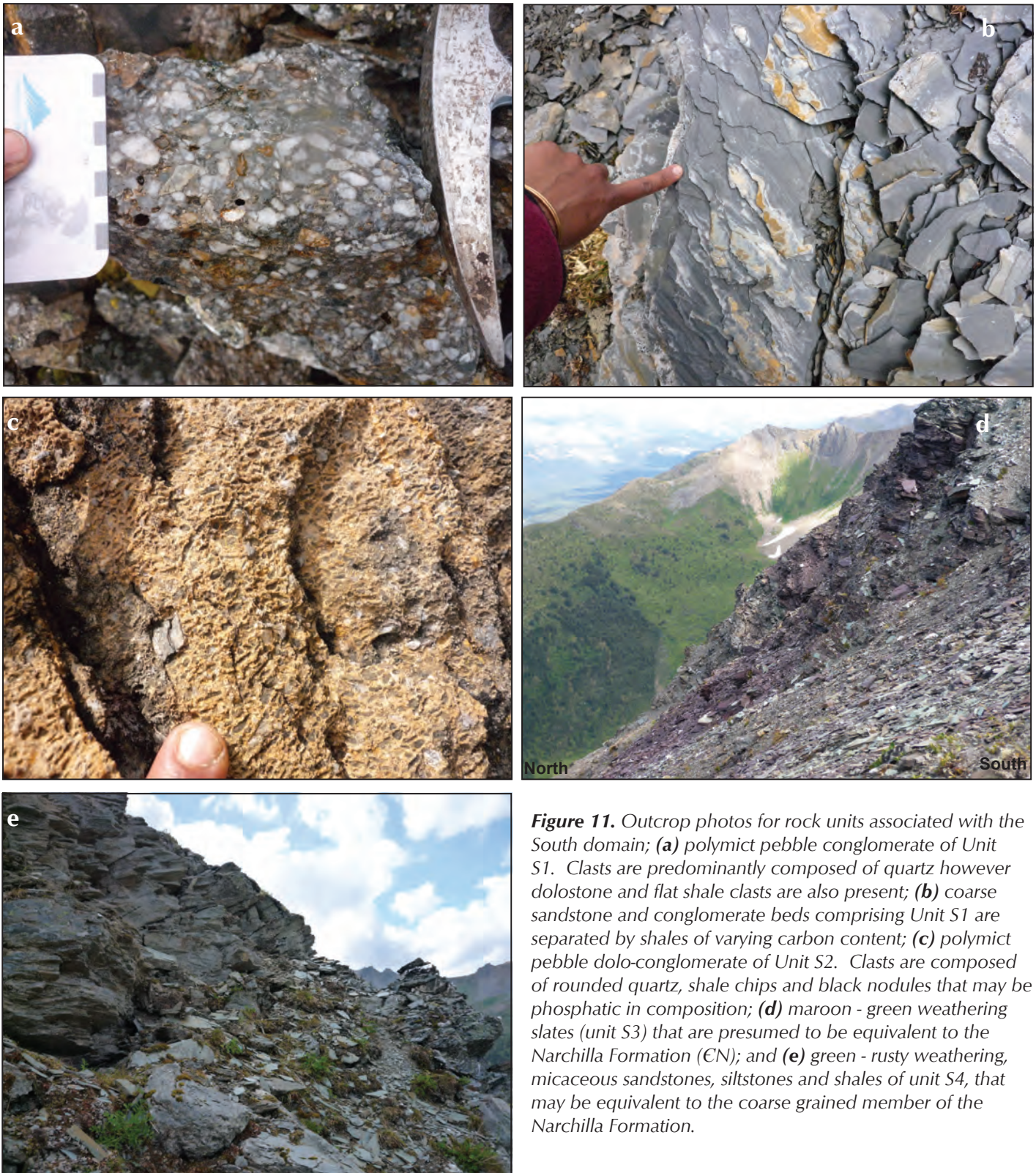
Figure 11. Outcrop photos for rock units associated with the South domain; **(a)** polymict pebble conglomerate of Unit S1. Clasts are predominantly composed of quartz however dolostone and flat shale clasts are also present; **(b)** coarse sandstone and conglomerate beds comprising Unit S1 are separated by shales of varying carbon content; **(c)** polymict pebble dolo-conglomerate of Unit S2. Clasts are composed of rounded quartz, shale chips and black nodules that may be phosphatic in composition; **(d)** maroon - green weathering slates (unit S3) that are presumed to be equivalent to the Narchilla Formation (ЄN); and **(e)** green - rusty weathering, micaceous sandstones, siltstones and shales of unit S4, that may be equivalent to the coarse grained member of the Narchilla Formation.

ooids

Figure 12. *Outcrop photos for Paleozoic and potentially equivalent rock units observed throughout in the lower sheet of the South Domain; (a) tabulate corals (Halysites; E. Turner pers. comm., 2010) weathering out of brecciated limestone clasts of Unit S5; (b) ooid like grains weathering out of brecciated limestone clasts of Unit S5; and (c) brown-grey-green weathering, laminated siltstones and phyllites of Unit S6.*

Triassic rocks

Unit S9 includes dark green - rusty orange/brown, blocky weathering, plagioclase porphyritic intrusions ranging in composition from gabbro to diorite (Fig. 13b). In the southwest corner of the map sheet, the intrusions form tabular bodies that are conformable with bedding in the surrounding sediments. Elsewhere contacts are not as clear and may be discordant with bedding. Mafic rocks of this unit form resistant layers that are visible from kilometres away.

Gordey and Makepeace (2001) included these intrusive rocks with the regionally extensive Triassic Galena Suite. Similar mafic intrusions occur in Lansing Range map area to the south (Roots, 2003), Mount Westman area to the west (Abbott, 1990) and in a west-trending belt from northern Mayo map area (Roots, 1997) to Dawson map area (Green, 1972).

CENTRAL DOMAIN

The Central domain includes rocks north of (*i.e.*, in the footwall of) the Dawson Thrust and south of the Kathleen Lakes Fault. It is divided into four, east-striking units (C1-C4) that are tentatively correlated with Devono – Mississippian and younger rocks to the west, as described by Abbott (1990).

Unit C1 includes rusty-brown to grey weathering, carbonaceous mudstone, black argillaceous chert with minor siltstones and lesser amounts of light grey weathering limestone (Fig. 14a) that resembles unit C3 described below.

Unit C2 comprises phyllitic lithologies that show marked similarities to unit S3. Phyllitic rocks of this unit are characterized by brilliant orange and green and lesser maroon weathering colours (Fig. 14b), that are interbedded with orange weathering siltstones.
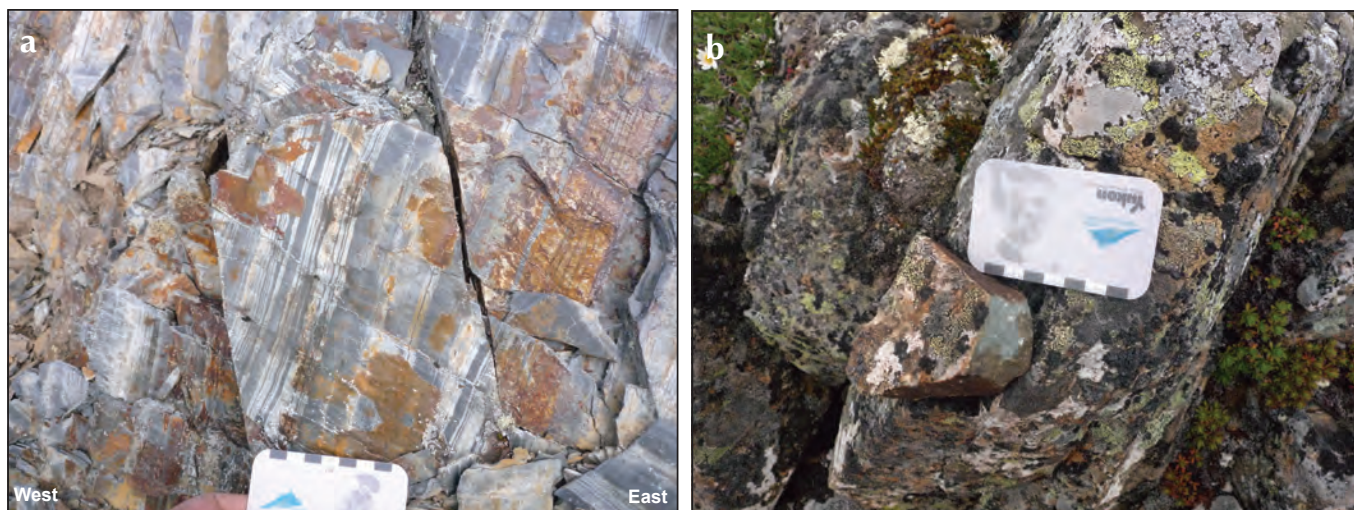
Figure 13. (a) Foliated siltstones and shales of Unit S7 that are presumed equivalent to the Earn Group, **(b)** plagioclase porphyritic gabbro (Unit S9) that has intruded into, and foliated with siliciclastic rocks of Unit S7.

Light grey weathering, dark grey to black, massive limestone comprises unit C3. Locally this unit is brecciated and cemented with calcite. Conodonts extracted from the limestone are of Permian age (Abbott and Orchard, unpublished data.). Limestone occurrences east of the conodont locality are well bedded (≤1 m), characterized by stylolite development and locally preserve lenses of black chert (Fig. 14c).A previously unmapped, apple-green weathering, ultramafic to mafic body comprises unit C4 (Fig. 14d). The rocks, which weather recessively, are pervasively serpentinized, talc bearing and magnetic. The southern boundary of the unit is marked by the presence of brilliant orange weathering dolo-calcareous sandstone that is currently mapped as part of unit C2. The ultramafic unit extends eastward into 106C/03 correlating nicely with the east trending aeromagnetic high that is associated with this unit.

NORTHERN DOMAIN

Rocks of the Northern domain comprise an eastward-younging package of siliciclastic and carbonate rocks. The nature of the contact between the Central and North domains across the Kathleen Lakes structure remains unclear (*i.e.,* thrust or strike-slip). Siliciclastic rocks in the region were previously mapped as Hyland Group that is unconformably overlain by platform carbonate rocks of the Cambrian – Devonian Bouvette Formation (Gordey and Makepeace, 2001). Mapping in 2010 revealed that the siliciclastic rocks do not resemble Hyland Group rocks as mapped in the Southern domain. Further mapping and acquisition of geochronological constrains will be required

before a stratigraphic correlation can be proposed with confidence.

Proterozoic rocks

Unit N1 comprises rhythmically bedded, orange weathering limestone/dolostone, grey weathering calcareous sandstone, and shale. Beds are ~1 m in thickness, separated by relatively thick (≥1 m) shale intervals. Sandstone is fine to medium-grained and characterized by the presence of detrital white mica on bedding planes. Orange dolo- limestone beds preserve fine laminations that may represent algal mats (Fig. 15a).

Green and orange weathering, medium-bedded (≤0.5 m), fine-grained siltstones, fine to coarse-grained sandstones and polymict cobble conglomerate constitute unit N2. Pebble lithologies in the conglomerate include dolostone, limestone, shale and dull grey chert (Fig. 15b). Varying concentrations of dolomitic cement are present in beds of all grain size. Graded bedding in conglomerates indicate locally overturned beds that young to the northwest. The contact between N2 and overlying unit N3 is gradational over 2-5 metres.

Unit N3 comprises red-brown and locally green weathering, medium to thick-bedded (≥1 m; Fig. 15c), fine to medium-grained sandstone, siltstone and lesser shale. Primary sedimentary structures are weakly preserved in coarser grained beds and locally indicate tops to the west-northwest. The distribution of unit N3 in the map area suggests a syncline (cored by the overlying unit N4; Fig. 10); although only west-northwest-younging beds were
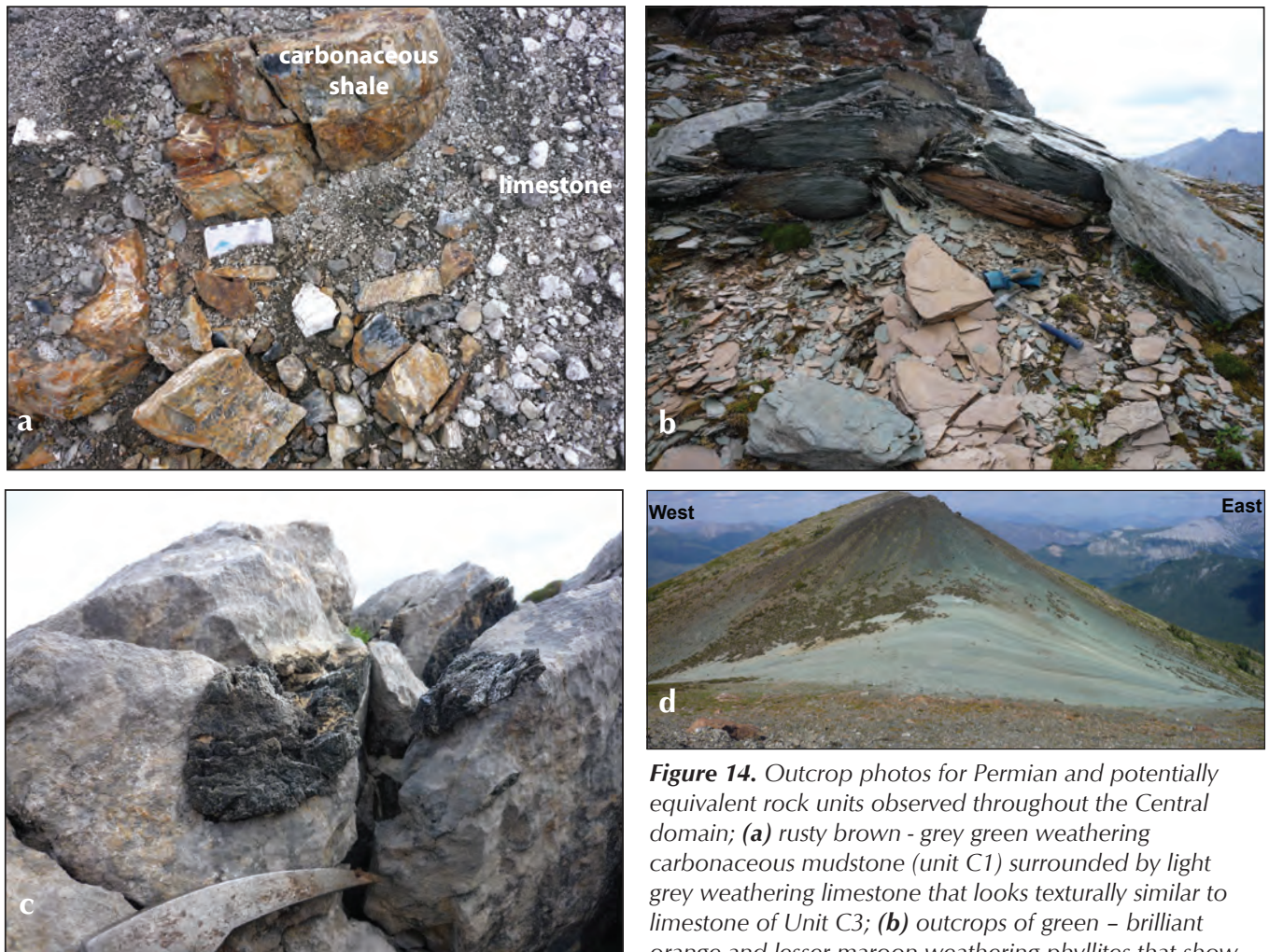
Figure 14. Outcrop photos for Permian and potentially equivalent rock units observed throughout the Central domain; **(a)** rusty brown - grey green weathering carbonaceous mudstone (unit C1) surrounded by light grey weathering limestone that looks texturally similar to limestone of Unit C3; **(b)** outcrops of green – brilliant orange and lesser maroon weathering phyllites that show some similarities to unit S3, but are currently classified as Unit C2 and may be more closely related to Unit S9; **(c)** well bedded limestone of Unit C3 where preservation of black chert lenses was noted and contacts between bedding planes marked by stylolite development; and **(d)** a typical 'outcrop' of the previously unmapped, brilliant apple-green weathering ultramafic – mafic Unit C4.

observed in the field, the geometry, if correct, implies overall eastward younging of the unit.

Unit N4 includes dark grey to grey-white weathering limestone with lenses of finely laminated black chert (Fig. 15d). Bedding is poorly defined but generally less than 0.5 m thick. Chert lenses are 5-10 cm thick and characterized by fine laminations that give a stromatolitic/algal appearance, a feature of chert associated with Proterozoic limestones elsewhere (E. Turner, pers. comm. 2010). Massive (>2 m) chert with siliciclastic clasts occurs locally and may represent a debris flow deposit.

Rocks of unknown age and correlation

Beige to white to orange weathering, massive to chaotic limestone–dolostone constitutes much of unit N5. Rocks are brecciated in places and made up of vuggy limestone boulders locally with ooids up to 0.5 cm in diameter (Fig. 15e). Vugs are filled with calcite and/or quartz.

Elsewhere, more dolomitic lithologies are well bedded (~1 m thick) and preserve cryptalgal laminations. Locally, rocks are characterized by networks of quartz veins (Fig. 15f).

Unit N6 comprises pink to rose coloured, fine-grained siltstone that is finely laminated with beige dolostone and minor limestone (Fig. 16a). In one locality rosy pink weathering rocks grade eastward into texturally identical green-weathering siltstone laminated with beige dolostone and minor limestone. Unit N6 is similar to Precambrian unit 1 of Morrow (1999).
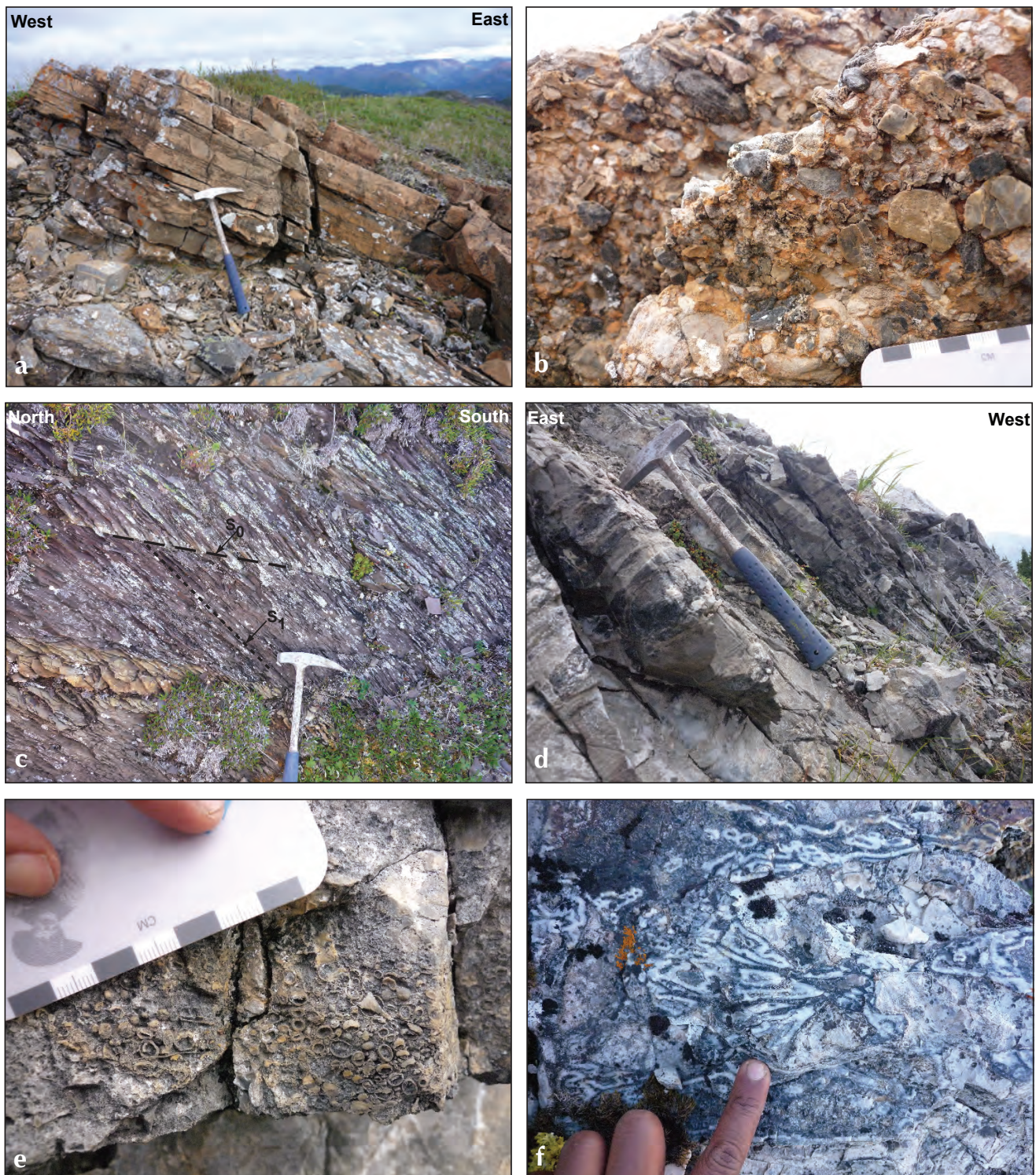
Figure 15. Outcrop photos for rocks comprising the North domain; **(a)** orange dolo- limestone beds of Unit N1. Fine laminations may represent algal mats; **(b)** green and orange weathering polymict cobble conglomerate of Unit N2. Pebble compositions include limestone, dolostone, shale and dull grey chert; **(c)** red-brown silstones and sandstones of Unit N3. Note the well developed cleavage (S1) and its discordance with bedding (S0); **(d)** unit N4 bedded limestones and associated black chert of potential Proterozoic age; **(e)** ooid grains weathering out of brecciated limestone blocks of 'chaotic' of unit N5; and **(f)** epithermal like quartz textures observed locally within seemingly massive and chaotic limestone of unit N5.

Rusty brown weathering, medium-grained, laminated to finely bedded (≤20 cm) sandstone interbedded with siltstone (≥1 m thickness) characterize Unit N7 (Fig. 16b). Centimeter-scale graded beds indicate younging to the southeast. Rocks of this unit are strikingly similar to the siliciclastic component of unit N1 described above. Correlation between the two units will depend on geochronological constraints as they become available. Bedding in Unit N7 is discordant with overlying limestone of unit N8 (see below), suggesting the contact between the two units is either faulted or represents an angular unconformity.

Bouvette Formation (€D$_B$) equivalents:

Unit N8 is well to cryptically bedded, light grey weathering limestone. Beds are less than 1.5 m thick with preservation of black chert locally. In places, limestone beds appear to be graded storm beds (*i.e.*, tempestites?) and/or pelloidal grainstones. Rare fossils include crinoid fragments and gastropods (Fig. 16c). Locally, zones of extensive brecciation up to ~ 100 m thick were observed. Limestone clasts within the brecciated intervals are angular and cemented with sparry calcite and dolomite. While N8 structurally overlies N7, an angular discordance between bedding in the two units suggests that a fault contact or an angular unconformity separates them. The unit underlies a significant area in the eastern part of the Northern Domain and appears also to extend south, across the Kathleen Lakes fault. Conodont samples have been collected from all localities and will provide constraints with which stratigraphic correlations can be made with confidence.

Green to rusty brown weathering, fine to medium-grained, well bedded (≤1 m) quartz sandstone and siltstone of unit N9 overlie limestone of unit N8. The base of the unit is characterized by a medium to coarse-grained, orange weathering, fossiliferous sandstone (~ 1 m thickness) with crinoid and brachiopod fragments (Fig. 16d). Higher up-section, grey-green siltstone beds are blocky-weathering and have been bioturbated (Fig. 16e), in places preserving pyrite filled burrows. Coarser sands preserve climbing ripples (Fig. 16f) and graded bedding that indicates younging to the southeast.

Unit N10 comprises both well bedded (≤1 m thickness) and locally brecciated, light to dark grey weathering limestone (Fig. 17a). The base of the unit is characterized by the presence of crinoid fragments. In outcrops that comprise brecciated limestone boulders, isolated boulders preserve tabulate (Favocites?) ± solitary corals (Rugosian; Figs. 17b,c) and possibly stromatoporoids (Fig. 17d).

Preservation of sponges and horn corals suggests this unit is Ordovician – Devonian in age.

Based on field observations made to date, Units N8 to N10 are interpreted to be part of the Bouvette Formation (Morrow, 1999), If this correlation is correct, the rocks represent platform carbonates deposited on the edge of the Selwyn basin, and are time-equivalents to clastic rocks of the Gull Lake and Road River groups to the south of the study area.

STRUCTURAL GEOLOGY

Structural elements preserved in the map area vary within and between domains, and are not yet well-understood. Evidence for multiple generations of fabric development are locally recognized in outcrop, however correlation of fabrics noted in units of different age and structural level have not yet been established. References to fabrics S_1, S_2, *etc.* are used to describe local overprinting relationships and are not to be applied on the regional scale at this time. In spite of unresolved details, fabrics descriptions and general observations about structural vergence are presented below.

SOUTHERN DOMAIN:

Rocks of the Southern domain make up the hanging wall of the Dawson Thrust. Rocks that occupy the thrust stack are divided into two packages (Fig. 10). The oldest of the sedimentary packages is situated immediately above the Dawson Thrust and includes units S1-S6. Structurally above them is a younger package (S7 to S9) that is in direct contact with the oldest stratigraphic unit (*i.e.*, S1). Based on the inferred correlation of S7 and S8 with Earn Group rocks, the juxtaposition of units S1 and S7 suggests either an angular unconformity or a faulted contact.

Immediately above the Dawson Thrust, older rock units in the structurally lower part of the thrust stack are deformed into north-verging folds and faults (Figs. 18a-c). Where bedding (S_0) and primary sedimentary structures have been identified, stratigraphic 'up' is most commonly to the south. Isolated occurrences for overturned, northward younging beds have also been documented though their occurrence is relatively minor. The main penetrative foliation (S_1) is best developed in less competent lithologies (*i.e.*, shale), and is shallowly to steeply south-dipping. Fold hinges plunge shallowly to moderately to the east and west. Variations in plunge imply more than one phase of folding, although in most outcrops only one penetrative foliation is preserved.

Figure 16. (a) Distinctly rosy pink, finely laminated siltstones interbedded with beige dolostone and minor limestone of Unit N6; **(b)** laminated – finely bedded sandstones that are interbedded with siltstones and together form Unit N7; **(c)** though sparse, gastropod fossils may be found in limestone beds of Unit N8; **(d)** a fossil hash in sandstone at the base of Unit N9 preserving gastropod and crinoid fragments here photographed through a x16 hand lens; **(e)** pyritized burrows preserved in a siltstone bed (Unit N9); and **(f)** climbing ripples preserved in a sandstone bed of Unit N9.

Figure 17. (a) Well bedded limestone of Unit N10 as seen from the helicopter; **(b)** tabulate coral (Favocites?) weathering out of a brecciated limestone horizon in Unit N10; **(c)** potential Rugosian coral weathering out of a brecciated limestone horizon in Unit N10; and **(d)** stromatoporoid fossil also weathering out of a brecciated limestone horizon in Unit N10.

At higher structural levels, immediately south of the contact between units S1 and S7, beds within Earn Group rocks are predominantly east-striking and moderately to steeply south dipping. Primary sedimentary structures indicate southward younging throughout much of unit S7 though minor variations have also been documented (*i.e.*, east- and southeastward younging; Fig. 18d). The main (S_1?) foliation at this locality is similar in orientation to that observed in the underlying units (S1 – S6), dipping moderately to steeply to the south. Locally in outcrop, the main (S_1) foliation surface is characterized by the development of a crenulation (S_2) resulting in a shallowly east – southeast plunging intersection lineation (L_2; Fig. 18d).

In the southwest corner of the Mount Mervyn map sheet, at even higher structural levels of the Southern domain, beds (S_0) in rocks of the Earn Group (S7 and S8) dip moderately to the north. Graded beds generally indicate northward younging, with evidence also for overturned, south-facing beds implying the presence of tight folds (F_1?). Overprinting these rocks is a variably north-dipping penetrative foliation (designated S_2), that is best developed in shale layers and interpreted to be axial planar to large-scale, upright, open (F_2) folds that have refolded the earlier F_1 folds.

Unlike the siliciclastic rocks they intrude, tabular Triassic mafic bodies preserve evidence for only one phase of deformation. They define upright, open folds that plunge gently to the east (Fig. 18e). It is possible that these folds are correlative with a second-generation synform that deforms unit S7 (described above), as their axial surfaces are roughly parallel.

CENTRAL DOMAIN

Green, L. (1972) described rocks in the footwall of the Dawson Thrust as complexly deformed (Fig. 19a). However, the map pattern defined by units in the Central domain does not appear complicated. Similar to the fabrics observed in the immediate hanging wall of the Dawson Thrust fault, bedding and a penetrative bedding-parallel foliation are folded and thrust-imbricated to the north. Both fabrics (bedding and foliation) define asymmetric folds with long shallowly south-dipping limbs and short steeply north-dipping limbs. Hinges plunge shallowly to moderately east and west. Southward younging of beds indicate an upward-facing stratigraphic pile as is also documented in the immediate hanging wall of the overriding thrust (Southern domain).

Variations in fold plunges and the fact that the folds deform a pre-existing foliation suggest the area was subject to more than one phase of deformation. Curved fold plunges (Fig. 19b) suggest the main north-verging folds have been refolded; however, it is possible that the curvature is simply a result of non-coaxial strain, which may be a possibility given the setting of the Central Domain between two major crustal-scale faults.

NORTHERN DOMAIN

Rocks in the Northern domain are situated north of the Kathleen Lakes fault, the kinematics of which is currently unknown. Relative to the domains described above, rocks of the Northern domain are weakly deformed. Bedding orientations are variable though dominantly north-striking and moderately east dipping. Although stratigraphic tops are difficult to decipher in outcrop, the package as a whole youngs eastward.

In the western part of the Northern domain, overturned beds (younging to the northwest) have been identified in units N2 and N3 at two localities east of unit N4. The presence of overturned beds coupled with the symmetrical distribution of N2 and N3 implies the presence of a roughly north trending syncline that is cored by limestone unit N4 (Fig. 10).

Foliation development is restricted to finer grained rocks, and is observed in only three units: the fine layers within units N2, N3 and locally in N6 (Figs. 15c and 16a). Everywhere that it is observed, the foliation is east-striking and dips shallowly to moderately southward. The foliation strikes roughly parallel to the postulated east-trending open folds described above, suggesting a possible correlation.
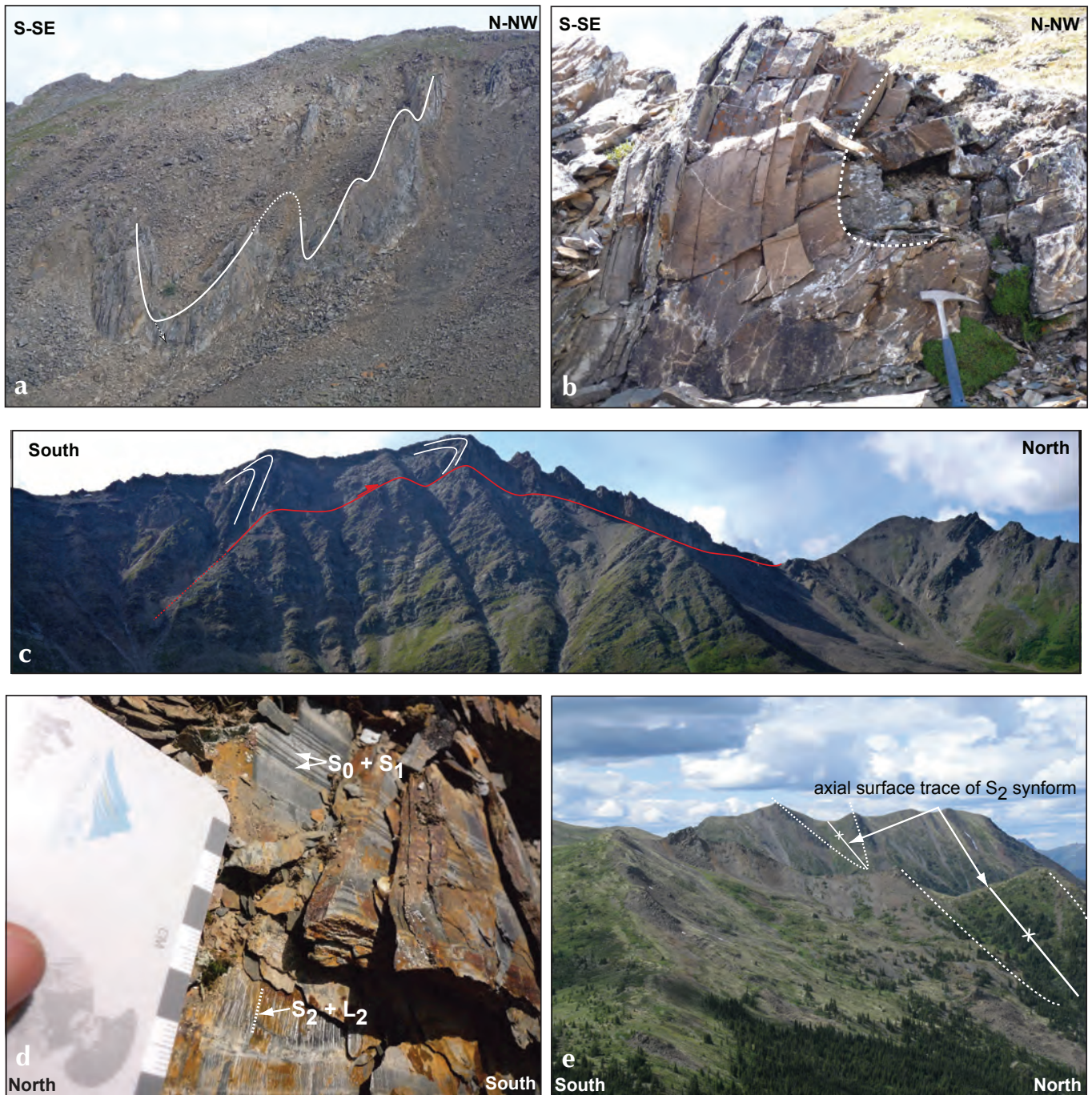
Figure 18. *Photographs illustrating the complex structures observed throughout the South domain; **(a)** northwest verging fold exposed on the southeast side of a mountain in southwestern part of the Nadaleen Range. The fold is developed in Hyland Group equivalent strata of unit S1; **(b)** outcrop scale synform developed in unit S1; **(c)** in addition to intense folding, siliciclastic and carbonate rocks in the 'lower' sheet of the South domain have also been thrust northward on the kilometer scale (photo is ~ 500m in width); **(d)** outcrop of Unit S7 siliciclastic rocks highlighting the relationships between bedding (S0), cleavage (S1 and/or S2) and intersection lineations (L2) between crenulations and the penetrative cleavage; and **(e)** view to the west illustrating the landscape and resistant weathering nature of Unit S9 with respect to surrounding siliciclastic rocks. Also highlighted in the photograph is an S2 synform that can be visibly traced out by following tabular gabbroic bodies from a distance.*

Figure 19. *Photographs illustrating fold development within the Central domain; **(a)** north verging fold developed in Paleozoic limestone of unit C3. For a reference scale, note the author sitting on the hinge of the antiform, and **(b)** an example of folding on the scale of a 'door-stop' sized sample in strata this is currently correlated with unit S1. Note bedding in this sample appears 'twisted'.*

MOUNT MERVYN 2010 REGIONAL SOIL GEOCHEMISTRY SURVEY

In 2010, a regional ridge and spur soil sampling campaign was carried out in parallel with the bedrock mapping of Mount Mervyn map area (106C/04). Reasons for undertaking the survey include i) integration of soil geochemical data with bedrock information collected at the same site, ii) to examine whether a regional scale soil survey might highlight areas of anomalous metal content that would not otherwise be identified by bedrock mapping, and, iii) to assess whether anomalous soil values might relate to existing anomalies identified within the RGS datasets. Results of the survey are presented below, following the description of bedrock geology in the Mount Mervyn area.

METHODOLOGY

Ridge and spur soil samples (C- horizon) were collected using a soil auger and data captured using the 'Dirtbagger' database of Ground Truth Exploration. Data recorded for each soil sample in the pilot study included station number and associated UTM co-ordinates, sampling method

(*i.e.*, auger *vs.* mattic), soil colour, position on slope, sampling depth, soil quality, soil horizon, tree cover, ground cover, other related notes, and photos of each sample site. Including duplicates, a total of 118 *ca.* 2.2 kg soil samples were collected at *ca.* 500 m spacing (Fig. 20). Locations broadly correspond to bedrock station localities. Samples were processed and analyzed by ACME Laboratories, using analytical package 1DX2 (aqua regia digestion of a 15 g sample) and analysed by ICP-MS for 36 elements including Hg. We present results for Au, As, and Ni below. The full geochemical dataset is found in Appendix 1.

RESULTS

The resulting soil geochemistry for Au, As and Ni are graphically presented in Figures 21 – 23 respectively. Interval ranges are based on and defined by the natural breaks in the data sets for each element, and represented as graduated symbols. For ease of comparing the new soil geochemistry with both existing surface geochemical data and bedrock geology, symbols are superimposed on the colour-gradient RGS data and new bedrock geology data.
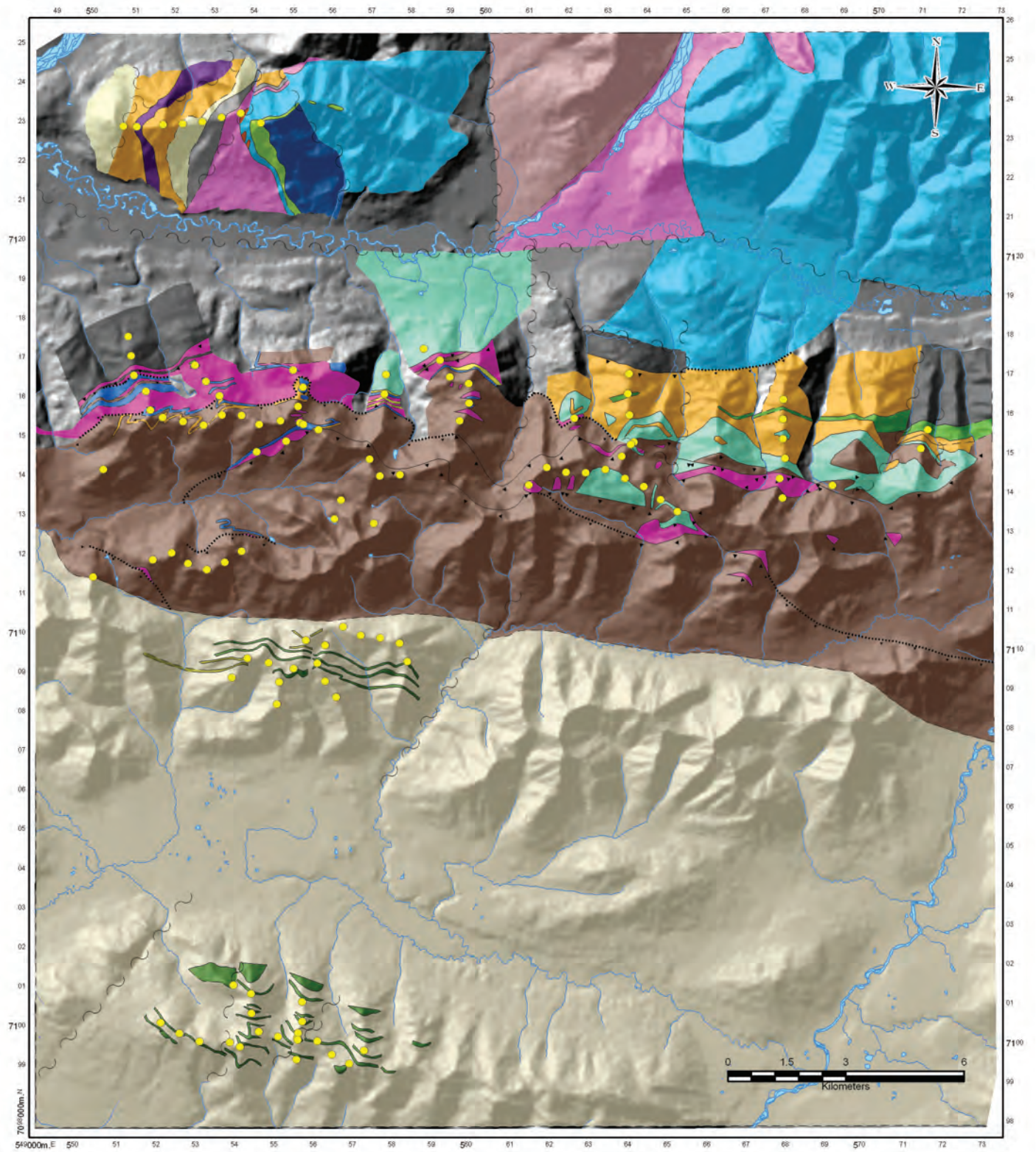
Figure 20. *Soil sampling localities superimposed on preliminary bedrock map for the 1:50K Mount Mervyn map sheet (106C/04). Legend as for Figure 10.*
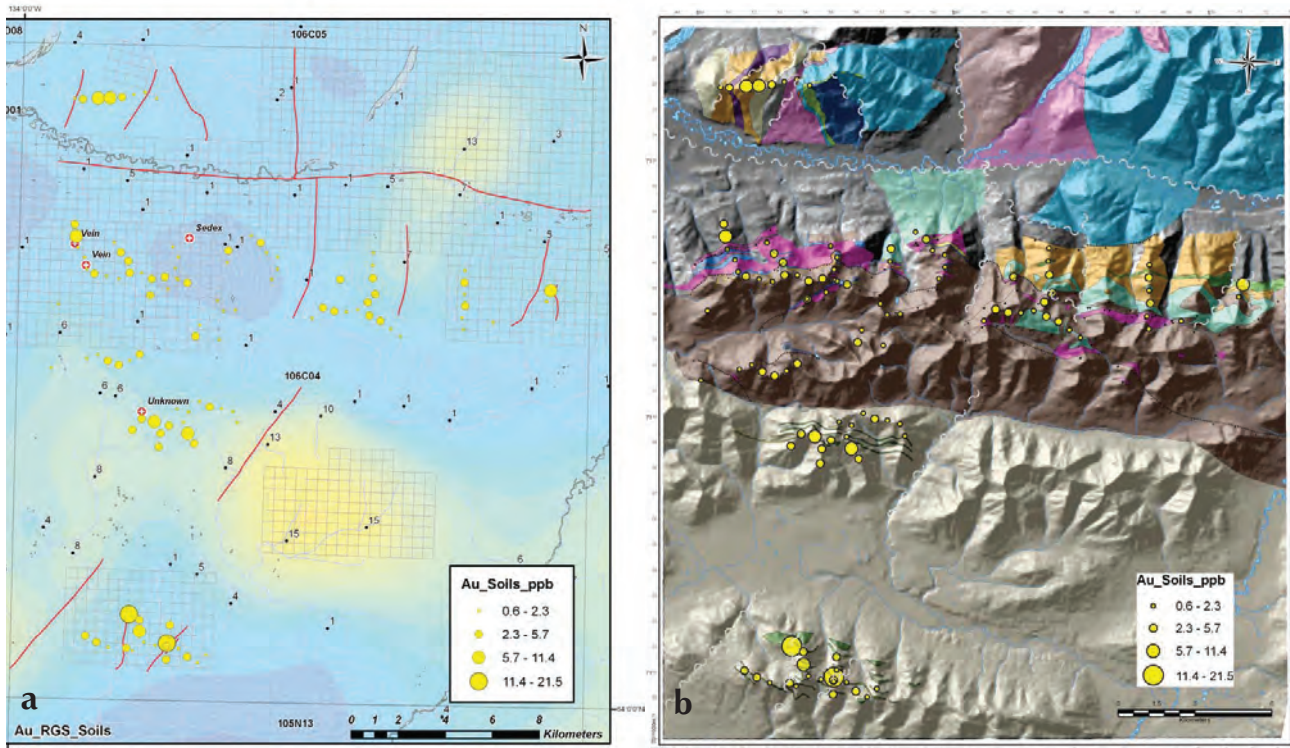
Figure 21. (a) *Graduated symbols of Au-in-soils (natural breaks interval classification) superimposed on colour-gradient gridded map of RGS Au anomalies in the Mt Mervyn map sheet area. Values of Au-in-RGS marked (ppb). Yukon MINFILE occurrences marked. (b) Graduated symbols of Au-in-soils superimposed on new bedrock geology data for Mt Mervyn map sheet area.*
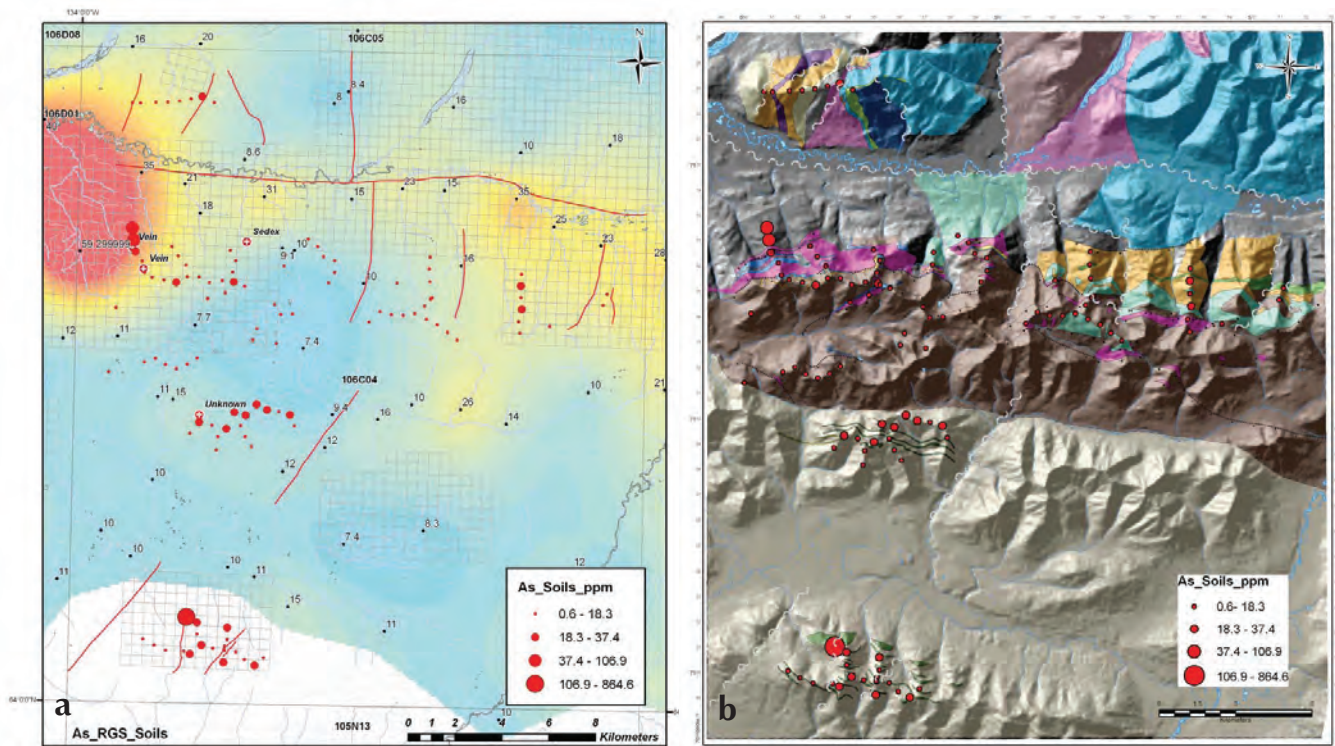
Figure 22. *Graduated symbols of As-in-soils (natural breaks interval classification);* **(a)** *superimposed on colour-gradient gridded map of RGS As anomalies in the Mt Mervyn map sheet area. Values of As-in-RGS marked (ppm). Yukon MINFILE occurrences marked, and* **(b)** *superimposed on new bedrock geology data for Mt Mervyn map sheet area.*

Figure 23. Graduated symbols of Ni-in-soils (natural breaks interval classification); (a) superimposed on colour-gradient gridded map of RGS Ni anomalies in the Mt Mervyn map sheet area. Values of Ni-in-RGS marked (ppm). Yukon MINFILE occurrences marked, and (b) graduated symbols of Ni-in-soils superimposed on new bedrock geology data for Mt Mervyn map sheet area.
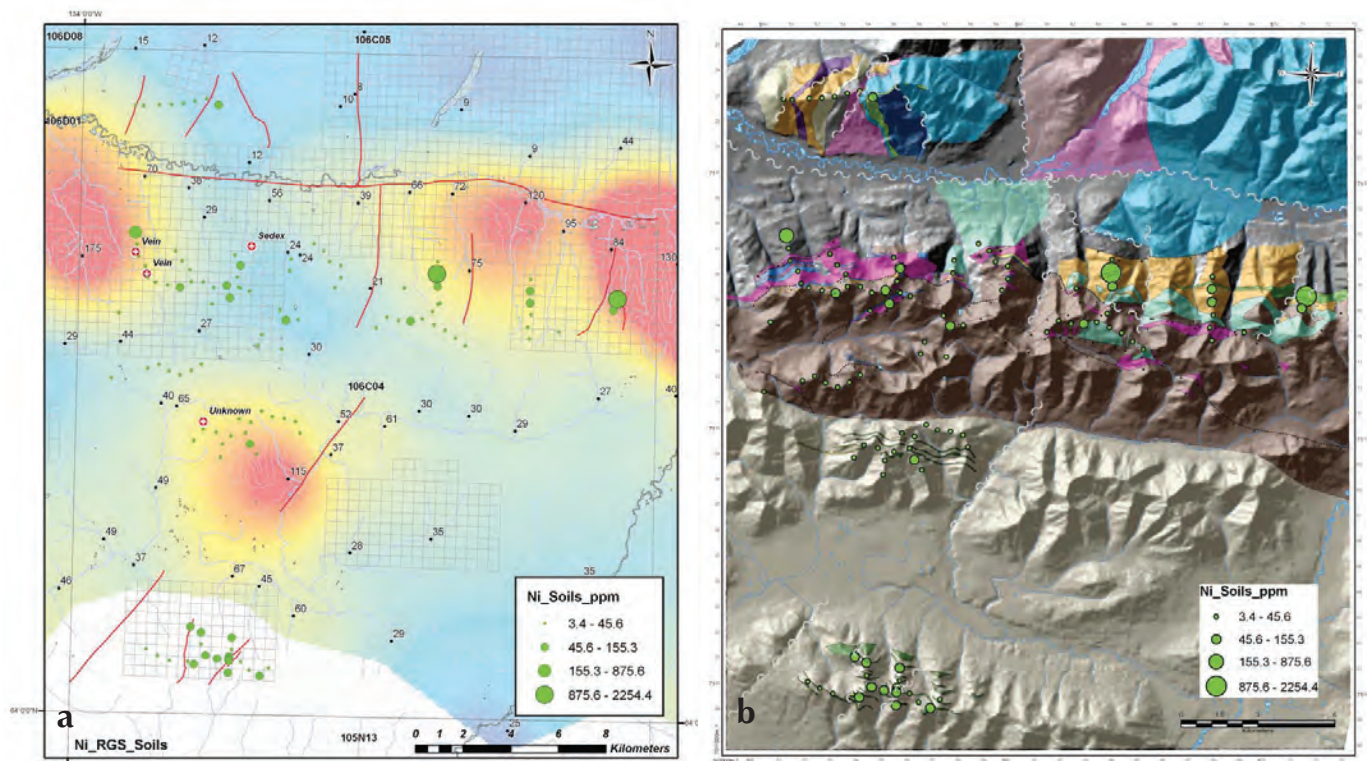
Integration of the three datasets highlights:

1. Elevated Au-in-soil values (Fig. 21) are present in at least two of the structural domains defined above, including three areas with more than one anomalous soil sample. RGS values from watersheds draining the three anomalous soil regions are not elevated in Au (Fig. 21a). Bedrock information for sites with elevated gold-in-soil values coincide with the presence of north and north-northeast-trending late fault zones (Fig. 21b). A single anomalous gold-in-soil value is also identified adjacent to a N-trending fault that cuts unit C4 (mafic to ultramafic body) in the Central domain.

2. Anomalous As-in-soil values (Fig. 22) correspond with elevated Au in the southwestern corner of the Mount Mervyn map area. Elevated As values show a strong spatial correlation with high As in the RGS data in the Central domain of Mount Mervyn, which corresponds to known occurrences of polymetallic veins (106C087; Fig. 22).

3. Anomalous Ni-in-soil values (Fig. 23) correlate directly with the occurrence of the mafic-ultramafic layers (unit C4) in the Central domain, and are substantiated by anomalous Ni in the RGS data (Fig. 23).

SUMMARY AND CONCLUSIONS

Regional ridge and spur soil geochemical data are useful for establishing the baseline geochemical signature of underlying bedrock and is a useful tool to aid in identifying regions of enriched metals that may be overlooked by the RGS database.

With respect to the underlying bedrock geology, field work has highlighted lithological complexities that will require new geochronological data before they can be correlated with confidence to surrounding Proterozoic and Paleozoic units. The division of the study area into three structural domains bounded by the Kathleen Lakes and Dawson Thrust faults highlights the different lithological packages and deformation styles across the study area. New geochronologic data will help to bracket the timing of fabrics in the region and enhance existing tectonic interpretations.

ACKNOWLEDGEMENTS

REFERENCES

Abbott, G., 1990. Preliminary results of the stratigraphy and structure of the Mt. Westman map area, central Yukon. *In:* Current Research, Part E, Geological Survey of Canada, Paper 90-1E, P. 15-22, 1990.

Abbott, G., 1997. Geology of the upper Hart River area eastern Ogilvie Mountains, Yukon Territory (116A/10, 11). Exploration and Geological Services Division, Yukon Region, Indian and Northern Affairs Canada Bulletin 9, 92 p.

Blusson, S., 1974. Bedrock geology of the Nadaleen Range map area (NTS 106C), central Yukon. Geological Survey of Canada, Open File 1974.

Fritz, W.H., Narbonne, G.M. and Gordey, S.P., 1983. Strata and trace fossils near the Precambrian-Cambrian boundary, Mackenzie, Sewlyn and Wernecke mountains, Yukon and Northwest Territories; *In:* Current Research, Part B, Geological Survey of Canada, Paper 83-1B, p. 365-375.

Fritz, W.H., Cecile, M.P., Norford, B.S., Morrow, D. and Geldsetzer, H.H.J., 1991. Cambrian to Middle Devonian assemblages. *In:* Geology of the Cordilleran Orogen in Canada, H. Gabrielse and C.J. Yorath (eds.), Geological Survey of Canada, Geology of Canada, no. 4, p 151-218.

Gabrielse, H., 1967. Tectonic evolution of the northern Canadian Cordillera. Canadian Journal of Earth Sciences, vol. 4, pp. 271-298.

Green, L.H., 1972. Geology of Nash Creek, Larsen Creek, and Dawson map-areas, Yukon Territory (106D, 116A, 116B, and 116C (E½)) Operation Ogilvie. Geological Survey of Canada, Memoir 364, 157 p.

Green, L.H. and Roddick, J.A., 1962. Geology, Nash Creek, Yukon Territory. Geological Survey of Canada, Preliminary Map 15-1962.

Gordey, S.P. and Anderson, R.G., 1993. Evolution of the Northern Cordilleran Miogeocline, Nahanni Map Area (105I), Yukon and Northwest Territories. Geological Survey of Canada, Memoire 428, 214 p.

Gordey, S.P. and Makepeace, A.J., 2001. Bedrock Geology, Yukon Territory; Geological Survey of Canada, Open File 3754, Exploration & Geological Services Division, Yukon Indian and Northern Affairs Canada, Open File 2001-1, scale 1:1 000 000.

Héon, D. (compiler), 2003. Yukon Regional Geochemical Database 2003 – Stream sediment analyses. Exploration and Geological Services Division, Yukon Region, Indian and Northern Affairs Canada.

Macdonald, F.A., Smith, E.F. Strauss, J.V., Cox, G.M., Halverson, G.P. and Roots, C.F., 2011, this volume. Neoproterozoic and early Paleozoic correlations in the western Ogilvie Mountains. *In:* Yukon Exploration and Geology 2010, K.E. MacFarlane, L.H. Weston and C. Relf (eds.), Yukon Geological Survey.

Medig, K.P.R., Thorkelson, D.J. and Dunlop, R.L., 2010. The Proterozoic Pinguicula Group: Stratigraphy, contact relationships and possible correlations. *In*: Yukon Exploration and Geology 2009, K.E. MacFarlane, L.H. Weston and L.R. Blackburn (eds.), Yukon Geological Survey, p. 265-278.

Morrow, D.W., 1999. Lower Paleozoic stratigraphy of northern Yukon Territory and Northwestern District of Mackenzie. Geological Survey of Canada, Bulletin 538.

Murphy, D. C., 1997. Geology of the McQuesten river Region, Northern McQuesten and Mayo Map Areas, Yukon Territory (115P/14, 15,16; 105M/13, 14).

Nielsen, A.B., Thorkelson, D.J., Marshall, D.D. and Gibson, H.D., 2011, this volume. Paleoproterozoic Bonnet Plume River intrusions: Evidence for a calc-alkaline arc at 1.7 Ga and its partial preservation in Yukon, Canada. *In:* Yukon Exploration and Geology 2010, K.E. MacFarlane, L.H. Weston and C. Relf (eds.), Yukon Geological Survey.

Peters, T.J. and Thorkelson, D.J., 2011, this volume. Volcano-sedimentary megaclast in Wernecke breccia, Yukon, and its bearing on the Proterozoic evolution of northwestern Laurentia. *In:* Yukon Exploration and Geology 2010, K.E. MacFarlane, L.H. Weston and C. Relf (eds.), Yukon Geological Survey.

Roots, C.F., 2003. Bedrock geology of Lansing Range map area (NTS 105N), central Yukon (1:250 000-scale). Yukon Geological Survey, Energy Mines and Resources, Government of Yukon, Geoscience Map 2003-1; and Geological Survey of Canada, Open File 1616.

Roots, C.F., 1997. Bedrock geology of Mayo map area, central Yukon (105M). Exploration and Geological Services Division, Indian and Northern Affairs Canada, Geoscience Map 1997-1, 1:50 000 scale.

Tempelman-Kluit, D.J., 1977. Stratigraphy and structural relations between the Selwyn basin, Pelly Cassiar Platform, and Yukon Crystalline Terrane in the Pelly Mountains, Yukon. *In:* Report of Activities, Part A; Geological Survey of Canada, Paper 79-14, 27 p.

Thompson, R.I., Roots, C.F. and Mustard, P.S., 1992. Geology of Dawson map area (116B, C) (northeast of Tintina Trench). Geological Survey of Canada, Open File 2849, 13 sheets, scale 1:50 000.

Thorkelson, D.J., 2000. Geology and mineral occurrences of the Slats Creek, Fairchild Lake and "Dolores Creek" areas, Wernecke Mountains (106D/16, 106C/13, 106C/14), Yukon Territory. Exploration and Geological Services Division, Yukon Region, Indian and Northern Affairs Canada, Bulletin 10, 73 p.

Turner, E.C., 2011, this volume. Stratigraphy of the Mackenzie Mountains supergroup in the Wernecke Mountains, Yukon. *In:* Yukon Exploration and Geology 2010, K.E. MacFarlane, L.H. Weston and C. Relf (eds.), Yukon Geological Survey.

Yukon MINFILE, 2010. Yukon MINFILE – A database of mineral occurrences. Yukon Geological Survey, <http://www.geology.gov.yk.ca/databases_gis.html>.

Appendix 1

Sample	UTM Zone	UTM Easting	UTM Northing	Mo	Cu	Pb	Zn	Ag	Ni	Co	Mn	Fe	As	U	Au	Th	Sr	Cd	Sb	Bi	V	Ca
10CYA-NG001	8	555554	7099772	2.4	44.3	34.6	158	0.1	66	33.6	710	4.78	17.2	1.1	2.1	3.2	29	0.4	1.2	0.4	29	0.12
10CYA-NG002	8	555547	7099829	1.9	220.6	12.7	170	0.2	87.1	51	1223	9.89	7.7	1	4.8	2.3	20	0.4	1.9	0.1	190	0.38
10CYA-NG003	8	555562	7099955	13.8	433.5	118.5	209	0.5	155.3	81.6	1769	13.47	8.8	5.5	18.1	13.1	89	0.8	1.9	0.2	64	0.22
10CYA-NG004	8	555658	7100244	1.7	37.2	39.6	72	0.1	20.9	2.6	151	4.44	16.6	1	0.9	7.6	24	0	0.6	0.4	24	0.08
10CYA-NG005	8	555648	7100744	3.8	53.6	32	101	0.7	47.4	17.1	474	6.61	26.7	1.5	3.6	3.6	47	0.3	2.1	0.3	57	0.12
10CYA-NG006	8	556054	7099748	2.2	34.7	24.1	91	0.1	41.2	15.7	384	4.29	16	1	1.9	5.6	18	0.3	1.1	0.3	51	0.13
10CYA-NG007	8	556429	7099415	2.9	24.6	29.2	80	0	31	9.7	211	4.33	18.1	0.8	2.6	4.9	24	0.2	0.9	0.4	42	0.04
10CYA-NG008	8	556876	7099189	3.4	41.2	39	177	0.2	91.7	34	850	5.3	20.3	1.7	1.1	8.4	65	0.6	1.1	0.5	33	0.12
10CYA-NG009	8	557241	7099531	4.6	57.7	37.4	78	0.1	27	7	308	4.29	17.1	1.1	0.9	5.6	39	0.1	0.7	0.5	18	0.02
10CYA-NG010	8	555056	7099850	2.3	34.2	35.6	101	0.1	50.5	15.6	245	4.35	15.9	1.1	1.2	6.1	24	0.2	0.7	0.4	23	0.09
10CYA-NG011	8	552059	7100147	2.5	31.7	12.2	69	0	25.2	8.8	397	2.99	9.4	0.8	2.4	1.6	13	0.3	0.7	0.2	72	0.16
10CYA-NG012	8	552548	7099893	2.6	21.5	13	60	0	16.8	5.5	239	3.08	12.1	0.8	2.4	0.7	10	0.2	0.9	0.3	71	0.07
10CYA-NG013	8	553055	7099691	2.1	25.1	11.9	39	0.1	17.8	5.1	130	2.48	9.6	0.9	0.7	0.3	10	0.5	0.7	0.2	57	0.06
10CYA-NG014	8	553830	7099679	6	36	15.8	69	0.2	22.5	8.2	285	3.07	12.5	2.1	2.8	0.5	25	0.4	0.9	0.3	62	0.07
10CYA-NG015	8	554089	7099567	14.3	96.6	52.8	151	0.5	51.8	28.3	1231	6.77	31.9	2.7	0.8	7.3	52	0.7	1.6	0.4	46	0.26
10CYA-NG016	8	554568	7099968	3.3	44.9	34.1	107	0.1	52.7	21.2	525	4.08	19	1.1	1.8	3.1	25	0.3	1.1	0.4	32	0.17
10CYA-NG017	8	554365	7100425	2.2	82.2	26	89	0.7	38.2	6.9	227	3.32	11.3	1.2	8.1	1.3	23	0.2	1.3	0.4	35	0.02
10CYA-NG018	8	554348	7100925	6	102.2	63.8	578	0.4	60.2	22.2	575	5.19	34.3	1.8	3.3	1.1	17	2.6	2.7	0.6	135	0.1
10CYA-NG019	8	553894	7101139	3.3	248.3	11.2	846	0.2	81.5	109.7	1315	10.9	864.6	0.6	21.5	2.5	13	3	14	0.3	284	0.21
10CYA-NG020	8	555535	7099271	20.2	79.3	53.2	180	0.4	65.8	51.8	3379	6.7	32.7	2.7	3.8	3.7	44	1.5	2.2	0.3	46	0.15
10CYA-NG021	8	555554	7099772	2.1	43.8	31.2	136	0.1	56.3	31.1	624	4.24	17.5	1.2	1.8	4.1	28	0.4	1.2	0.3	28	0.14
10CYA-NG022	8	556078	7109829	7.9	29.2	23.4	94	0.4	18.1	4.2	130	3.25	28.9	1.2	2	1.4	17	0.2	7.7	0.3	49	0.04
10CYA-NG023	8	553723	7108963	1.7	43.3	14.7	67	0.4	21.7	5.5	161	3.05	12.3	0.9	2.9	1	24	0.2	1.2	0.3	47	0.06
10CYA-NG024	8	554105	7109456	1.9	73.5	18.3	72	1.5	21.2	6.5	156	3.65	21.5	0.8	5	3.4	13	0.2	1.7	0.2	57	0.05
10CYA-NG025	8	554651	7109347	3.5	64.7	21.9	83	0.8	27.4	6	200	2.83	14.7	1.2	9.9	0.5	16	0.2	2.2	0.3	52	0.03
10CYA-NG026	8	555281	7109216	6.1	26.2	22.9	37	1.4	8.9	2.3	97	3.1	19.3	1.2	3.4	0.6	24	0.2	3.2	0.4	51	0.02
10CYA-NG027	8	555882	7109368	2	29.3	15.7	104	0.1	31.5	10.2	345	2.9	15.5	1.1	1.9	2.1	16	0.4	1.6	0.2	46	0.12
10CYA-NG028	8	556092	7108913	3.7	88	17.2	200	1.4	99.5	13.4	1531	4.3	14.4	1.5	9.5	1	22	0.9	2.1	0.2	44	0.17
10CYA-NG029	8	556381	7108503	1.9	29	16.8	95	0.3	23.7	11.2	353	2.93	14.5	1.5	3	2.5	14	0.2	1.2	0.3	57	0.14
10CYA-NG030	8	556078	7109829	8.4	31	24.3	102	0.4	18	4.2	114	3.34	31.2	1.3	2	1.7	18	0.2	8.5	0.3	51	0.04
10CYA-NG031	8	558171	7109448	2.6	15.1	18.2	61	0.2	15.1	5.6	249	3.23	13.6	0.8	1.3	1.1	8	0.2	1.4	0.4	71	0.05
10CYA-NG032	8	557969	7109906	6	41.3	35.5	43	0.1	9.3	1.6	63	3.42	26.4	0.9	1.7	1.8	14	0	6.1	0.5	35	0.01
10CYA-NG033	8	557481	7110031	2	20.7	18.7	79	0	21.4	8.1	308	2.83	14	1	1.6	1.4	11	0.3	2.1	0.3	47	0.06
10CYA-NG034	8	556982	7110086	4.1	22.3	16.9	83	0.6	20.9	8.2	301	2.92	20.8	1.1	2.7	0.9	14	0.4	8.2	0.3	61	0.09
10CYA-NG035	8	556526	7110298	6	60.8	44.5	108	0.4	35.8	2.1	83	4.71	33.5	1.6	0.6	4.2	21	0.6	4.8	0.5	42	<0.01
10CYA-NG036	8	555588	7109939	12.2	41.2	31.2	90	0.3	14.4	2.1	63	3.17	36.9	2	0.8	4.2	19	0.2	12	0.4	44	0.01
10CYA-NG037	8	554873	7108301	2.3	46.3	23.7	76	0.5	24.4	7.9	457	3.5	13.4	0.8	3.4	1.4	8	0.2	1.2	0.4	56	0.06
10CYA-NG038	8	554927	7108863	2.5	33.9	19	80	0.2	22.6	8.8	405	3.42	14.2	0.8	2.6	1.3	10	0	1.3	0.4	71	0.08
10CYA-NG039	8	551660	7111926	1	33.4	23.7	66	0	30	10.6	250	3.13	8	0.7	1.7	7	10	0	0.7	0.3	26	0.1

Sample	UTM Zone	UTM Easting	UTM Northing	Mo	Cu	Pb	Zn	Ag	Ni	Co	Mn	Fe	As	U	Au	Th	Sr	Cd	Sb	Bi	V	Ca
10CYA-NG040	8	552130	7112102	1.3	22.9	21.3	78	0	27.1	9.6	318	2.56	9.9	0.6	1.9	1.6	14	0.2	0.8	0.2	40	0.24
10CYA-NG041	8	552558	7111842	1.4	24.8	85.2	112	0	41.9	20.3	735	4.92	12.4	1	2.7	3.4	15	0	0.8	0.7	20	0.03
10CYA-NG042	8	553036	7111691	1.2	39.8	47.9	80	0	25.8	11.2	407	3.65	14.9	1.7	2.9	1.9	17	0.1	0.9	0.4	25	0.03
10CYA-NG043	8	553495	7111895	1.4	55.4	42.5	96	0	29.7	9.8	248	4.4	13	1.3	2	3.5	17	0.2	0.6	0.5	19	0.02
10CYA-NG044	8	556260	7113044	1.4	34.7	22.5	95	0	27.7	10.8	359	3.24	13.6	1.8	3	1.7	18	0.2	0.8	0.4	53	0.12
10CYA-NG045	8	557258	7112948	1.2	48.4	52.8	69	0	28.2	29.3	954	3.44	13.3	1.5	2.3	3.1	9	0.1	0.7	0.5	30	0.03
10CYA-NG046	8	556415	7113521	1.3	23.5	19.5	80	0	22.8	9.2	423	2.81	8.7	0.7	1.1	0.9	13	0.2	0.6	0.4	32	0.15
10CYA-NG047	8	553855	7115638	0.9	43.4	70.7	98	0	38.3	21.5	1111	4.34	14.4	1.1	0.9	3.4	16	0.1	0.5	0.7	26	0.13
10CYA-NG048	8	555000	7115000	0.3	50.6	24.8	115	0	47	23.4	1469	5.34	10.6	0.8	1.5	5	8	0	0.1	0.6	21	0.07
10CYA-NG049	8	555346	7115474	2.2	34.5	66.4	882	0.2	44	30.5	2168	6.37	37.4	2.1	2.3	3.1	139	0.8	2.2	0.4	15	8.61
10CYA-NG050	8	555424	7115430	1	34.5	29.1	63	0	29	15.8	772	3.65	8.2	1.2	1.5	6.5	16	0	0.4	0.4	12	0.3
10CYA-NG051	8	555819	7115306	1.2	31.9	37.2	68	0.1	22.4	13.6	1212	4.28	5.4	1.5	2.8	3.4	18	0.2	0.4	0.3	16	0.21
10CYA-NG052	8	554848	7115514	1	59.1	41.8	100	0	46.9	23.8	1008	4.11	11.8	0.9	2.5	6.6	65	0	0.7	0.6	14	0.37
10CYA-NG053	8	554300	7115413	1.4	44.4	77.1	87	0.2	42.2	23	1695	3.67	12.8	1.6	4.3	5.9	46	0.3	0.7	0.4	22	0.39
10CYA-NG054	8	550938	7117595	50.2	93.2	45.5	1135	2	875.6	18.4	646	3.36	69.7	11.3	3.7	3	688	12.6	11.1	0.3	574	1.33
10CYA-NG055	8	551013	7117101	6.3	40.8	365.8	324	1.9	19.7	5.4	281	2.54	106.9	1.9	11.4	2.5	37	5.4	27.4	0.3	45	0.08
10CYA-NG056	8	551103	7116608	0.9	47.8	44.3	97	0.3	41.6	21.5	620	3.61	25.3	0.7	2	5.6	19	0.4	1.8	0.6	17	0.23
10CYA-NG057	8	551403	7116208	1	38.8	37.7	61	0.2	39.2	13.6	222	3.23	8.3	1.2	2	5	209	0.2	0.4	0.4	7	4.08
10CYA-NG058	8	551530	7115723	1.1	57.9	28.9	64	0.1	39.6	27.6	576	3.48	9.4	1	1.3	8.1	19	0	0.4	0.7	8	0.23
10CYA-NG059	8	551850	7115541	0.6	40.5	39.9	89	0.1	34.2	18.5	598	3.63	10.1	2.7	2.9	9	26	0	0.6	0.5	7	0.19
10CYA-NG060	8	552363	7115448	1.4	48.5	52.1	79	0.2	40.6	17.7	867	3.67	16.1	1.2	1.5	7.4	169	0.2	0.7	0.6	12	0.4
10CYA-NG061	8	552893	7115363	1.4	50.8	49.9	84	0.1	47.4	19.1	621	3.56	21.4	1.2	0.7	8.5	94	0.1	1.2	0.5	13	0.24
10CYA-NG062	8	553354	7115635	1.7	49.1	45.2	112	0.1	34.9	22.7	280	4.67	9.9	1.5	2.9	5.7	17	0.2	0.8	0.5	21	0.03
10CYA-NG063	8	554258	7114718	0.4	38.1	17.3	96	0	38.9	17.5	515	4.34	1.8	1.3	1.6	6.4	17	0	0.2	0.5	31	0.18
10CYA-NG064	8	554258	7114718	0.4	37.9	18.3	90	0	39.9	17.3	558	4.4	2.5	1.3	2.6	6.7	17	0	0.3	0.5	32	0.18
10CYA-NG065	8	555147	7116809	0.8	40.4	135.2	81	0	45.6	20.8	871	4.26	4	1.4	1.4	6.5	17	0	0.2	0.6	16	0.05
10CYA-NG066	8	555399	7116376	0.6	35.9	53.9	40	0.2	56.3	17.6	348	4.77	9.6	0.5	2.2	8	25	0	0.5	0.4	7	0.59
10CYA-NG067	8	555281	7115890	0.8	50.1	44.6	63	0.1	37.1	23.8	513	3.51	8	1	2.2	7.8	28	0	0.5	0.7	7	0.14
10CYA-NG068	8	552640	7116887	0.7	20.5	67.5	105	0	23.5	30.5	814	5.05	5.4	0.6	1.7	3.2	7	0.2	1.3	0.4	28	0.03
10CYA-NG069	8	552936	7116483	0.6	28.5	29	73	0	26.1	12.4	463	3.33	5.5	1.4	2.5	2.4	12	0	0.3	0.5	28	0.1
10CYA-NG070	8	553280	7116119	0.7	46.4	45.6	89	0	41	23.3	1254	4.6	4.7	0.8	2.6	3.5	14	0	0.3	0.6	23	0.06
10CYA-NG071	8	551722	7122992	1.1	46.3	20.7	68	0	30.9	22.4	846	3.76	6.3	0.7	9.1	2.4	13	0.2	0.8	0.3	48	0.22
10CYA-NG072	8	552229	7123022	1.1	75.3	23.8	80	0.1	39.7	27.6	1093	4.99	4.4	0.6	8.3	3.9	15	0.2	0.7	0.3	47	0.24
10CYA-NG073	8	552728	7123081	0.7	43.4	24.6	70	0.1	27.5	13.3	543	4.52	4.2	0.3	5.3	1.7	33	0.2	0.4	0.3	31	2.07
10CYA-NG074	8	554209	7123083	0.9	32.4	7.1	101	0	76.2	30.2	753	4.85	12.3	0.4	1.3	2.1	78	0.3	0.3	0	27	5.09
10CYA-NG075	8	553702	7123319	2.9	18.7	50.4	119	0.2	24.1	8	496	1.91	27.2	3.2	2.1	2.8	53	0.5	1.1	0.2	30	11.49
10CYA-NG076	8	550720	7122939	1.1	19.3	35.9	85	0.2	22.2	11.6	797	3.17	12.8	0.6	1.7	1.4	22	0.4	1.1	0.2	36	2.41
10CYA-NG077	8	551063	7122930	3.1	11.2	34.1	80	0	10.4	4.6	334	0.95	5	0.3	2.4	0.7	194	0.3	3.1	0	16	11.64
10CYA-NG078	8	553213	7123210	0.2	16.9	13.1	49	0	21.4	8.1	253	1.52	2.1	1.8	1.6	6.6	83	0	0.2	0.2	10	6.92
10CYA-NG079	8	557470	7116239	0.9	26	26.4	48	0	27.8	15.3	1305	3.22	6.4	0.7	2.1	5.2	7	0.1	0.4	0.3	23	0.07
10CYA-NG080	8	557508	7116738	2	22.2	23.5	62	0	22.2	9.5	441	3.09	15.1	1	2.6	4.1	21	0.4	0.7	0.3	36	0.25

Sample	UTM Zone	UTM Easting	UTM Northing	Mo	Cu	Pb	Zn	Ag	Ni	Co	Mn	Fe	As	U	Au	Th	Sr	Cd	Sb	Bi	V	Ca
10CYA-NG081	8	557900	7114198	0.6	28.9	22	53	0	18.3	4.2	123	3.13	5.4	0.8	0.8	3.6	13	0	0.3	0.3	15	0.03
10CYA-NG082	8	557400	7114159	1.2	25.8	43.6	29	0.2	51	16.9	297	2.32	7.2	0.8	1.7	3.8	32	0	0.3	0.3	7	0.92
10CYA-NG083	8	557124	7114579	0.9	40.4	36.4	78	0	38.6	28.4	1258	3.74	13	1.5	2.1	4.4	22	0.1	0.7	0.4	19	0.14
10CYA-NG084	8	558454	7117413	0.9	59.1	26.2	82	0	27.8	17.3	959	3.62	15.3	0.5	2.3	2.7	15	0.2	0.4	0.4	18	0.4
10CYA-NG085	8	558868	7117130	1.2	24.8	32.6	53	0	20.3	19.4	1461	3.5	9.6	0.8	2.9	1.6	9	0.1	0.6	0.4	31	0.03
10CYA-NG086	8	559135	7116707	1.6	27.7	26.3	65	0	23.1	12	486	3.62	9.2	0.8	1.1	1.2	9	0.1	0.8	0.5	42	0.04
10CYA-NG087	8	559608	7116542	1	29.1	40.3	77	0	28.8	20.1	1106	3.65	8.8	0.8	2	3.1	10	0.1	0.6	0.4	32	0.06
10CYA-NG088	8	559629	7116041	1.4	96.8	34.8	67	0	37.6	22.6	2920	3.71	13	1.2	1.7	2.2	32	0.2	0.4	0.4	17	0.64
10CYA-NG089	8	559395	7115597	1.2	40.9	30.2	74	0.1	31.3	13.9	347	3.56	14.7	0.5	1.4	3.5	42	0.1	0.6	0.3	17	0.11
10CYA-NG090	8	550361	7114201	0.5	23.8	21.6	52	0.1	24.9	9.1	239	2.15	5.8	0.4	2.1	4.2	85	0	0.3	0.2	8	1.97
10CYA-NG091	8	550147	7111460	1.1	4.3	28	11	0	3.4	0.4	10	1.21	8.7	0.3	1.9	3.2	5	0	0.8	0.6	5	<0.01
10CYA-NG092	8	553910	7112175	1.9	31.5	21.5	61	0	20.9	8.3	274	2.79	10.1	0.9	2.4	1	10	0.1	0.7	0.3	36	0.06
10CYA-NG093	8	564977	7113381	0.8	27.3	19.3	53	0	26.8	16.1	1253	2.75	6.9	0.8	2.2	2.1	46	0	0.5	0.3	19	2.08
10CYA-NG094	8	564545	7113681	1.5	48	47.1	90	0.2	17.2	6.8	318	5.47	14	0.8	1.5	7.3	55	0	0.6	0.5	17	0.19
10CYA-NG095	8	564107	7114000	1.2	19.2	15.2	64	0	24.2	8.4	285	2.51	8.3	0.7	3.6	1.9	14	0.2	0.9	0.2	38	0.14
10CYA-NG096	8	563628	7114202	1.3	25.3	27.9	137	0.2	39.9	16.1	875	3.37	8.5	0.7	5.2	3.3	28	0.3	0.7	0.3	31	0.3
10CYA-NG097	8	563124	7114426	1.2	21	25	45	0	23.5	9.6	254	2.52	9.7	0.5	1.7	2.1	13	0	0.6	0.3	30	0.06
10CYA-NG098	8	562627	7114333	0.7	35.3	33.9	91	0.1	59.1	20.4	857	3.76	11.5	1	2	4.1	23	0	0.4	0.3	17	0.53
10CYA-NG099	8	562126	7114329	1	26.2	15.4	68	0	21.5	8.6	280	2.54	8.2	1.3	3	3.6	15	0.1	0.6	0.2	32	0.13
10CYA-NG100	8	561639	7114452	0.9	37.5	62	84	0	36.7	20.6	762	3.53	13.2	1.3	3.5	3.7	25	0.2	0.6	0.5	21	0.07
10CYA-NG101	8	561183	7113987	0.7	13.6	19.6	81	0	33.2	14.8	422	3.57	2.2	0.7	1.5	2.3	5	0.1	0.4	0.4	27	0.03
10CYA-NG102	8	563689	7116866	0.7	30.4	40.4	101	0	38.1	16.4	816	4.89	13.9	0.7	1.4	4.4	9	0	0.3	0.6	23	0.04
10CYA-NG103	8	563667	7116358	0	4.4	2.1	12	0	1790.5	89.7	405	2.89	0.6	0	1.7	0	0	0	0.1	0	11	<0.01
10CYA-NG104	8	563713	7115812	0.8	142	13.4	103	0	56.7	39.4	1178	6.79	13.4	0.4	5.7	2.4	9	0.2	0.6	0.2	64	0.08
10CYA-NG105	8	563838	7115126	0.9	58.5	22.4	38	0.1	13.2	16.2	1159	3.95	3.5	0.8	2.4	0.8	5	0.1	0.4	0.5	23	0.03
10CYA-NG106	8	563761	7115066	0.4	27.3	24.7	57	0	18.2	12.9	360	2.37	5.3	2.6	2	3	27	0	0.3	0.5	16	0.58
10CYA-NG107	8	563532	7114763	1.1	21.8	19.8	53	0	12.8	7.6	349	2.46	6.6	0.7	3.1	1.3	6	0	0.5	0.3	33	0.02
10CYA-NG108	8	562315	7115704	1.3	23.4	32.2	66	0	23.5	14.5	558	3.35	12.5	0.7	3.1	4.4	7	0.2	0.7	0.4	38	0.03
10CYA-NG109	8	571298	7115570	0.7	950.1	5.5	323	0	2254.4	250.7	2615	10.12	3.1	0.2	11.3	1	5	1.6	0.1	0.4	37	0.03
10CYA-NG110	8	571139	7115096	0.7	35	35.6	90	0.1	52.8	15.9	707	4.32	18.3	2.3	1.7	6.2	23	0.1	0.6	0.4	23	0.26
10CYA-NG111	8	567617	7116283	1.2	26.1	18.7	59	0	20.2	13.3	469	3.02	6.2	0.6	0.7	5	5	0.2	0.7	0.4	34	0.02
10CYA-NG112	8	567613	7115781	4.4	102.7	31	98	0.1	51.8	30.5	948	5.61	23.3	0.3	2.4	2.2	26	0.4	1.1	0.5	15	1.48
10CYA-NG113	8	567628	7115282	1.5	43.8	15.5	74	0	80.2	28.2	1059	4.98	7.2	0.6	1.1	3.2	13	0.3	0.5	0.2	32	0.19
10CYA-NG114	8	567689	7114782	1.1	21.2	19.6	50	0.2	21	8.6	375	2.14	20.5	2.3	2.5	1.3	485	0.3	0.8	0.2	25	6.48
10CYA-NG115	8	567563	7114270	1.6	24.2	25.8	67	0	20.5	11.1	625	3.51	11.1	0.8	1.9	0.7	7	0.1	0.8	0.4	47	0.05
10CYA-NG116	8	568901	7114113	0.8	45.2	48.3	148	0	34.3	19.6	962	4.2	8.1	1.2	1.5	5.2	12	0.1	0.4	0.6	14	0.06
10CYA-NG117	8	567644	7113777	1	25.9	23.3	67	0	24	12.4	436	3.5	7.1	0.7	1.4	1.9	9	0.2	0.5	0.5	34	0.04
10CYA-NG118	8	567644	7113777	0.9	31.5	27.6	77	0	30	15.4	525	3.84	8.7	0.9	1.7	3.8	10	0.2	0.6	0.5	29	0.05

Sample	P	La	Cr	Mg	Ba	Ti	B	Al	Na	K	W	Hg	Sc	Tl	S	Ga	Se	Te
10CYA-NG001	0.135	15	24	0.3	81	0.007	3	1.03	0.007	0.06	0.1	0.06	2.3	0.2	<0.05	3	1.1	<0.2
10CYA-NG002	0.112	12	64	1.35	331	0.024	2	3.32	0.005	0.03	0	0.61	18.4	0	<0.05	10	0.9	<0.2
10CYA-NG003	0.302	54	52	1	207	0.016	3	3.49	0.081	0.1	0	0.14	8.4	0.3	0.38	7	3.9	0.4
10CYA-NG004	0.091	25	35	0.66	177	0.002	2	1.46	0.013	0.11	0	0.07	1.9	0.2	0.23	5	0.5	<0.2
10CYA-NG005	0.409	20	47	0.68	274	0.044	3	2.06	0.019	0.08	0.4	0.05	3.5	0.2	0.13	6	3	<0.2
10CYA-NG006	0.075	22	39	0.56	105	0.018	3	2.41	0.007	0.07	0.2	0.06	3	0.2	<0.05	6	1.1	<0.2
10CYA-NG007	0.066	15	29	0.42	77	0.016	2	1.29	0.008	0.07	0.1	0.03	2.2	0.2	0.08	6	0.6	<0.2
10CYA-NG008	0.125	19	39	1.18	57	0.002	2	2.29	0.017	0.12	0	0.09	2.5	0.5	0.24	6	1.3	<0.2
10CYA-NG009	0.108	27	39	0.33	133	0.002	3	0.99	0.017	0.08	0	0.3	1.4	0.2	0.15	4	1.2	<0.2
10CYA-NG010	0.081	34	31	0.49	140	0.002	2	1.59	0.008	0.08	0	0.11	2.4	0.2	0.08	5	0.7	<0.2
10CYA-NG011	0.081	14	35	0.43	136	0.05	2	1.34	0.007	0.05	0.2	0.04	2.2	0	<0.05	6	0.7	<0.2
10CYA-NG012	0.063	13	29	0.3	92	0.032	2	1.46	0.006	0.06	0.2	0.05	1.4	0.1	0.05	7	0.6	<0.2
10CYA-NG013	0.085	12	29	0.27	129	0.015	2	1.57	0.008	0.05	0.2	0.06	0.9	0.1	0.06	6	0.8	<0.2
10CYA-NG014	0.126	19	34	0.43	139	0.025	2	1.76	0.012	0.05	0.2	0.06	1.4	0.2	0.12	6	1.4	<0.2
10CYA-NG015	0.205	39	42	0.87	171	0.126	2	1.78	0.048	0.12	0	0.09	4.3	0.2	0.36	6	2.7	<0.2
10CYA-NG016	0.142	24	46	0.49	107	0.005	2	1.53	0.007	0.09	0	0.04	2.1	0.2	0.08	5	0.7	<0.2
10CYA-NG017	0.109	17	43	0.44	153	0.006	2	1.49	0.008	0.05	0	0.08	1.1	0.1	0.08	5	1	<0.2
10CYA-NG018	0.08	13	42	0.64	163	0.027	2	1.87	0.008	0.05	0.2	0.08	3.1	0.1	0.07	7	3.3	<0.2
10CYA-NG019	0.063	10	34	0.78	261	0.042	2	2.35	0.008	0.06	0.1	0.09	13.7	0.1	<0.05	9	4.4	<0.2
10CYA-NG020	0.187	47	43	0.73	178	0.007	2	1.86	0.045	0.09	0	0.17	2.7	0.4	0.2	5	2.9	<0.2
10CYA-NG021	0.123	16	24	0.35	89	0.009	1	1.1	0.006	0.07	0.1	0.06	2.4	0.2	<0.05	3	0.8	<0.2
10CYA-NG022	0.084	12	25	0.3	149	0.011	1	1.19	0.008	0.05	0.1	0.07	1.2	0.5	<0.05	4	4.1	0.2
10CYA-NG023	0.072	12	26	0.29	134	0.016	2	1.31	0.007	0.05	0.2	0.08	1.3	0.1	<0.05	5	1.3	<0.2
10CYA-NG024	0.051	11	32	0.31	106	0.032	2	1.63	0.008	0.04	0.2	0.18	1.9	0.1	<0.05	5	1.8	<0.2
10CYA-NG025	0.081	13	30	0.22	143	0.011	1	1.21	0.003	0.05	0.1	0.26	1	0.2	<0.05	5	2.6	<0.2
10CYA-NG026	0.092	19	24	0.13	171	0.008	2	0.76	0.012	0.05	0.1	0.09	0.7	0.2	0.07	5	3.3	<0.2
10CYA-NG027	0.074	12	28	0.49	118	0.027	2	1.75	0.007	0.05	0.2	0.04	2	0.1	<0.05	5	1.1	<0.2
10CYA-NG028	0.093	18	27	0.18	179	0.016	1	1.01	0.005	0.03	0.2	0.54	3.2	0.2	<0.05	3	3.4	<0.2
10CYA-NG029	0.089	18	33	0.58	193	0.034	3	1.86	0.008	0.06	0.3	0.06	2.8	0.2	<0.05	6	0.8	<0.2
10CYA-NG030	0.087	11	24	0.29	159	0.008	2	1.14	0.008	0.05	0.1	0.08	1.2	0.5	0.06	4	4.7	<0.2
10CYA-NG031	0.039	13	28	0.31	77	0.026	1	1.63	0.005	0.04	0.2	0.04	1.5	0.2	<0.05	8	1.2	<0.2
10CYA-NG032	0.053	6	22	0.13	78	0.008	1	0.71	0.004	0.05	0	0.11	0.8	0.4	<0.05	4	2.6	<0.2
10CYA-NG033	0.048	12	28	0.46	106	0.023	2	1.73	0.006	0.05	0.2	0.05	1.8	0.2	<0.05	5	1.2	<0.2
10CYA-NG034	0.068	14	29	0.41	118	0.024	2	1.67	0.009	0.05	0.2	0.07	1.5	0.3	<0.05	6	4.2	<0.2
10CYA-NG035	0.06	3	37	0.65	112	0.004	1	1.63	0.009	0.07	0	0.12	1.9	0.4	0.07	5	2.6	<0.2
10CYA-NG036	0.055	15	20	0.16	105	0.003	1	0.67	0.005	0.05	0	0.09	1.1	0.6	<0.05	3	5.7	<0.2
10CYA-NG037	0.051	12	27	0.31	123	0.021	2	1.39	0.004	0.04	0.2	0.07	1.3	0.1	0.07	5	<0.5	<0.2
10CYA-NG038	0.039	14	34	0.46	168	0.027	2	2.05	0.005	0.04	0.4	0.05	2.4	0.2	<0.05	7	0.8	<0.2
10CYA-NG039	0.032	26	19	0.37	119	0.014	2	1.07	0.004	0.04	0	0.06	2	0	<0.05	3	<0.5	<0.2

Sample	P	La	Cr	Mg	Ba	Ti	B	Al	Na	K	W	Hg	Sc	Tl	S	Ga	Se	Te
10CYA-NG040	0.052	14	22	0.36	125	0.02	4	1.24	0.007	0.04	0.2	0.04	1.6	0	<0.05	3	0.5	<0.2
10CYA-NG041	0.045	7	25	0.62	91	0.007	2	1.58	0.007	0.06	0	0.04	2.2	0	0.06	4	0.5	0.2
10CYA-NG042	0.076	11	27	0.34	81	0.006	2	1.42	0.008	0.1	0	0.08	1	0.1	0.07	4	0.9	<0.2
10CYA-NG043	0.09	6	24	0.47	47	0.002	1	1.62	0.005	0.06	0.1	0.06	1.5	0	<0.05	4	0.9	<0.2
10CYA-NG044	0.06	16	35	0.59	130	0.025	3	2.09	0.007	0.07	0.2	0.05	2.4	0.2	<0.05	6	0.6	<0.2
10CYA-NG045	0.074	26	27	0.41	99	0.006	3	1.5	0.003	0.12	0	0.03	1.3	0.1	0.07	4	<0.5	0.2
10CYA-NG046	0.064	13	24	0.36	75	0.012	2	1.33	0.005	0.06	0.1	0.04	1.3	0.1	<0.05	4	0.6	<0.2
10CYA-NG047	0.075	10	28	0.62	82	0.007	1	1.85	0.004	0.05	0	0.04	2.1	0	<0.05	6	0.5	<0.2
10CYA-NG048	0.023	6	34	1.09	82	0.003	3	2.55	0.008	0.07	0	0.02	4.1	0	<0.05	7	<0.5	<0.2
10CYA-NG049	0.199	14	10	0.45	1118	0.007	3	0.55	0.005	0.06	0	0.9	2.9	0.2	0.1	2	0.7	<0.2
10CYA-NG050	0.05	10	15	0.11	58	0.002	2	0.36	0.003	0.07	0	0.07	2.6	0	<0.05	0	<0.5	<0.2
10CYA-NG051	0.066	7	17	0.12	153	0.005	3	0.48	0.004	0.07	0	0.06	3.5	0	<0.05	1	<0.5	<0.2
10CYA-NG052	0.16	44	15	0.2	49	0.004	2	0.62	0.005	0.07	0	0.42	2.2	0.1	<0.05	2	0.5	0.2
10CYA-NG053	0.089	25	36	0.39	179	0.009	6	1.28	0.005	0.19	0	0.12	2.1	0.1	<0.05	3	0.9	0.2
10CYA-NG054	0.242	15	79	0.39	>10000	0.089	7	1.14	0.006	0.09	0.5	0.21	7.4	6.7	<0.05	3	8.1	<0.2
10CYA-NG055	0.049	14	17	0.21	497	0.011	2	0.68	0.003	0.08	0.1	0.69	1.8	0.2	0.08	2	4.8	<0.2
10CYA-NG056	0.036	18	15	0.13	532	0.003	2	0.63	0.004	0.06	0	0.05	5.2	0	<0.05	2	<0.5	<0.2
10CYA-NG057	0.091	8	10	0.13	63	0.002	2	0.41	0.003	0.06	0	0.43	3.3	0	0.07	0	0.7	<0.2
10CYA-NG058	0.04	5	11	0.32	84	0.005	2	0.83	0.003	0.09	0	0.05	3	0	<0.05	2	<0.5	<0.2
10CYA-NG059	0.047	7	14	0.32	132	0.001	0	0.93	0.003	0.08	0	0.05	2.2	0	<0.05	2	<0.5	<0.2
10CYA-NG060	0.168	23	20	0.31	209	0.004	2	1.04	0.011	0.15	0	0.13	2.6	0.2	0.25	3	0.7	0.2
10CYA-NG061	0.13	14	14	0.14	120	0.005	2	0.79	0.007	0.13	0	0.15	2.7	0.2	0.19	2	0.7	<0.2
10CYA-NG062	0.048	16	16	0.25	53	0.006	2	1.03	0.005	0.05	0	0.1	2.4	0	<0.05	3	<0.5	<0.2
10CYA-NG063	0.035	9	32	0.72	105	0.01	2	1.91	0.015	0.07	0	0.02	4.1	0	<0.05	6	<0.5	<0.2
10CYA-NG064	0.042	9	32	0.71	108	0.009	2	1.81	0.01	0.06	0	0.02	3.7	0	<0.05	6	<0.5	<0.2
10CYA-NG065	0.031	11	22	0.57	58	0.001	2	1.64	0.005	0.06	0	0.04	3.2	0	<0.05	5	<0.5	<0.2
10CYA-NG066	0.113	27	12	0.33	39	0.001	2	0.82	0.002	0.08	0	0.35	2.4	0	<0.05	2	<0.5	<0.2
10CYA-NG067	0.041	3	12	0.13	74	<0.001	2	0.37	0.006	0.1	0	0.04	2.9	0	0.07	0	<0.5	<0.2
10CYA-NG068	0.035	5	19	0.12	99	0.01	0	0.74	0.004	0.04	0	0.03	2.5	0	<0.05	2	<0.5	<0.2
10CYA-NG069	0.067	8	23	0.45	143	0.004	1	1.64	0.007	0.05	0	0.04	2.6	0	0.07	5	<0.5	<0.2
10CYA-NG070	0.058	4	28	0.64	118	0.005	1	1.63	0.005	0.06	0	0.07	2	0	0.05	5	<0.5	<0.2
10CYA-NG071	0.049	13	28	0.83	151	0.021	2	1.65	0.006	0.07	0.1	0.06	3.9	0	0.05	5	<0.5	0.2
10CYA-NG072	0.046	15	28	1.31	285	0.013	2	2.01	0.004	0.06	0	0.1	6.5	0	<0.05	5	<0.5	<0.2
10CYA-NG073	0.062	8	20	1.75	92	0.005	5	1.49	0.006	0.12	0	0.05	5.9	0.1	<0.05	4	<0.5	<0.2
10CYA-NG074	0.151	25	32	0.48	176	0.004	4	0.8	0.008	0.23	0	0.02	7.2	0.2	0.38	3	<0.5	<0.2
10CYA-NG075	0.04	5	14	6.43	34	<0.001	2	0.17	0.017	0.04	0	0.16	2.3	0.9	<0.05	0	<0.5	<0.2
10CYA-NG076	0.057	12	26	1.54	197	0.01	3	1.11	0.007	0.05	0.1	0.08	3.7	0	<0.05	3	<0.5	<0.2
10CYA-NG077	0.035	2	7	7.2	63	0.004	7	0.24	0.014	0.03	0	0.21	2.2	0	<0.05	0	<0.5	<0.2
10CYA-NG078	0.054	16	20	0.94	173	0.008	3	0.66	0.005	0.13	0	0	2.8	0	<0.05	2	<0.5	<0.2
10CYA-NG079	0.035	13	23	0.39	84	0.006	1	1.56	0.005	0.06	0	0.04	2.3	0	<0.05	3	<0.5	<0.2
10CYA-NG080	0.023	12	18	0.22	148	0.006	2	1.24	0.005	0.04	0.1	0.1	2.8	0.1	<0.05	3	<0.5	0.4

Sample	P	La	Cr	Mg	Ba	Ti	B	Al	Na	K	W	Hg	Sc	Tl	S	Ga	Se	Te
10CYA-NG081	0.029	6	21	0.51	54	0.002	0	1.29	0.004	0.05	0	0.02	1.3	0	<0.05	4	<0.5	<0.2
10CYA-NG082	0.093	16	11	0.11	57	0.004	0	0.66	0.006	0.08	0	0.07	2.2	0	<0.05	0	<0.5	<0.2
10CYA-NG083	0.07	9	19	0.37	79	0.008	1	1.12	0.005	0.07	0	0.03	2.4	0	<0.05	3	<0.5	<0.2
10CYA-NG084	0.048	9	10	0.16	180	0.003	3	0.64	0.005	0.06	0	0.08	5.1	0	<0.05	2	<0.5	0.4
10CYA-NG085	0.064	10	23	0.25	86	0.008	1	1.25	0.006	0.12	0	0.04	1.3	0.1	<0.05	4	<0.5	<0.2
10CYA-NG086	0.05	9	27	0.42	59	0.014	0	1.64	0.006	0.05	0.2	0.05	1.7	0.1	<0.05	6	<0.5	<0.2
10CYA-NG087	0.042	9	27	0.58	54	0.02	0	1.59	0.006	0.04	0.1	0.03	2.7	0	<0.05	6	<0.5	<0.2
10CYA-NG088	0.059	21	14	0.2	144	0.004	2	0.71	0.005	0.1	0	0.06	3.8	0	<0.05	2	<0.5	0.4
10CYA-NG089	0.059	17	16	0.14	98	0.006	0	0.66	0.01	0.07	0	0.46	2.5	0.2	<0.05	2	<0.5	0.3
10CYA-NG090	0.028	15	7	0.12	37	0.004	0	0.39	0.003	0.04	0	0.06	2.4	0	<0.05	0	<0.5	<0.2
10CYA-NG091	0.008	3	4	0.04	278	<0.001	2	0.2	0.004	0.04	0	0.05	0.3	0	<0.05	0	<0.5	<0.2
10CYA-NG092	0.066	8	23	0.34	72	0.011	0	1.22	0.006	0.04	0.2	0.04	1.3	0.1	<0.05	4	0.5	<0.2
10CYA-NG093	0.089	20	14	0.37	122	0.006	1	0.96	0.005	0.07	0	0.05	2.6	0	<0.05	2	<0.5	0.2
10CYA-NG094	0.136	8	26	0.55	80	0.002	0	1.32	0.008	0.07	0	0.07	2.2	0.1	0.06	5	0.8	<0.2
10CYA-NG095	0.054	14	21	0.38	103	0.02	0	1.2	0.008	0.05	0.2	0.03	2	0.1	<0.05	3	<0.5	<0.2
10CYA-NG096	0.085	21	23	0.44	129	0.016	0	1.2	0.008	0.06	0.1	0.05	3.6	0.1	<0.05	3	<0.5	<0.2
10CYA-NG097	0.033	17	16	0.26	69	0.011	0	0.98	0.005	0.05	0.1	0.02	1.3	0	<0.05	3	<0.5	0.2
10CYA-NG098	0.059	20	22	0.54	85	0.007	3	0.9	0.005	0.06	0	0.04	3	0.1	<0.05	2	<0.5	0.3
10CYA-NG099	0.065	11	23	0.45	98	0.027	0	1.19	0.007	0.05	0.1	0.04	2.3	0	<0.05	4	<0.5	<0.2
10CYA-NG100	0.041	6	29	0.49	132	0.008	0	1.3	0.007	0.08	0	0.04	2.1	0	<0.05	4	<0.5	<0.2
10CYA-NG101	0.048	4	24	0.6	45	0.009	0	1.25	0.005	0.05	0	0.02	1	0	<0.05	4	<0.5	<0.2
10CYA-NG102	0.047	6	31	0.86	32	0.003	0	2.36	0.006	0.04	0	0.02	2.5	0	<0.05	8	<0.5	<0.2
10CYA-NG103	0.003	0	612	18.58	5	0.002	45	0.22	0.003	<0.01	0	0	3.8	0	<0.05	0	<0.5	<0.2
10CYA-NG104	0.053	11	25	0.55	315	0.005	1	1.48	0.004	0.06	0	0.12	7.7	0	<0.05	4	<0.5	0.4
10CYA-NG105	0.145	3	21	0.14	58	0.005	2	1.14	0.006	0.11	0	0.1	0.8	0.1	0.09	5	<0.5	<0.2
10CYA-NG106	0.068	16	13	0.19	98	0.003	0	1.08	0.005	0.17	0	0.03	2.1	0	<0.05	3	<0.5	<0.2
10CYA-NG107	0.046	8	16	0.17	51	0.007	0	0.9	0.005	0.09	0	0.02	0.9	0.1	<0.05	4	<0.5	<0.2
10CYA-NG108	0.027	8	23	0.4	47	0.012	0	1.59	0.006	0.04	0.1	0.04	2	0	<0.05	6	<0.5	<0.2
10CYA-NG109	0.021	4	428	12.4	166	0.007	16	0.43	0.003	0.01	0	0.03	5	0	<0.05	0	<0.5	<0.2
10CYA-NG110	0.028	25	23	0.48	113	0.005	2	1.26	0.003	0.04	0	0.07	5.9	0	<0.05	3	<0.5	0.3
10CYA-NG111	0.029	10	20	0.32	54	0.015	0	1.31	0.003	0.04	0.1	0.05	1.5	0	<0.05	5	<0.5	<0.2
10CYA-NG112	0.051	2	5	0.63	83	0.005	6	0.34	0.003	0.09	0	0.44	8.2	0.2	0.05	1	0.6	<0.2
10CYA-NG113	0.09	19	21	0.24	123	0.005	1	1.35	0.003	0.06	0	0.04	5.6	0.1	<0.05	4	<0.5	<0.2
10CYA-NG114	0.227	15	17	0.31	111	0.011	3	0.85	0.008	0.05	0.1	0.26	1.7	0	<0.05	2	<0.5	<0.2
10CYA-NG115	0.058	8	27	0.39	47	0.015	0	1.69	0.004	0.05	0.1	0.03	1.3	0	<0.05	7	0.5	<0.2
10CYA-NG116	0.036	7	18	0.38	67	0.003	4	1.13	0.004	0.06	0	0.08	2.9	0	<0.05	3	<0.5	<0.2
10CYA-NG117	0.047	9	23	0.43	51	0.008	0	1.61	0.004	0.05	0	0.02	1.2	0.1	<0.05	6	<0.5	0.2
10CYA-NG118	0.044	9	26	0.53	55	0.008	1	1.78	0.005	0.05	0.1	0.01	1.6	0.1	<0.05	5	<0.5	<0.2

A field, petrographic and preliminary S isotopic study of the Walt and Tyrala sediment-hosted barite occurrences (105O/7), and associated Ba-Zn-Pb mineralization, MacMillan Pass district, Yukon

N.A. Fernandes[1] and S.A. Gleeson
Department of Earth and Atmospheric Sciences, University of Alberta

ABSTRACT

The MacMillan Pass district (map sheet 105O) located in east Yukon contains several sediment-hosted Ba ± Zn ± Pb deposits including the Tom and Jason deposits, as well as a multitude of 'barren' sediment-hosted barite occurrences. A classic sedimentary-exhalative (SEDEX) model has been postulated for these occurrences in which the barite horizons represent distal expressions of a hydrothermal vent system. Fieldwork was completed at the Walt and Tyrala barite occurrences that occur within the MacMillan Pass district in order to examine the deposit-scale geology and to sample undeformed barite horizons for subsequent geochemical analysis. Samples were also collected from drill core from the Hess barite occurrence. Barium mineralization occurs in both the Devonian Portrait Lake Formation (Lower Earn Group) and in underlying Ordovician-Silurian limestone of the Road River Group. A variety of textures were encountered that were indicative of both synsedimentary deposition of barite, as well as diagenetic to epigenetic barite mineralization. Base metal sulphides that are interpreted to post-date the barite mineralization were encountered at depth in drill core and are primarily hosted by Road River Group carbonates.

[1]nafernan@ualberta.ca

INTRODUCTION

Sedimentary basins host some of the world's major base metal (Zn, Pb, Cu) mineral deposits *e.g.,* McArthur Basin, Australia; the Zambian Copperbelt; and Rammelsburg, Germany. In particular, sedimentary-exhalative (SEDEX) deposits are an important source of these commodities. SEDEX deposits gain their name from the original model proposed by Carne and Cathro (1982), whereby fluids were "exhaled; and precipitated metals on the seafloor". In this model, fluids are sourced from deep within the basin and transported along structures such as synsedimentary faults to the sediment-seawater interface. Upon reaching the seafloor, the mineralizing fluids then interact with the water column, which is thought to be stratified into upper oxygenated and lower anoxic layers (Goodfellow, 1987). In this model, sulphide minerals, mostly occurring as sphalerite ((Zn,Fe)S) and galena (PbS), precipitate due to mixing of anoxic, reduced (H_2S_{aq}-rich) seawater with saline, metaliferous, oxidized (H_2S_{aq}-poor) fluids. Barite ($BaSO_4$) is thought to represent the distal component of the hydrothermal vent associated with SEDEX mineralization, and is precipitated in the upper, oxygenated (SO_4^{2-}- rich) layer. Hence, stratification of the ocean is crucial for both sulphide mineralization and barite precipitation. Minerals precipitated as a result of these reactions, accumulate on the basin floor along with normal marine sediments to form stratiform deposits that contain sulphide-rich and sediment-rich laminations that can often display normal sedimentary features such as bedding and grading. Therefore, barite textures can be used to vector to the sulphide component of the SEDEX system.

One subset of SEDEX deposits is the vent-proximal type (Goodfellow *et al.,* 1993). The conduit for fluids in this case is thought to be a growth fault that creates relief on the sea-floor (Goodfellow and Lydon, 2007). The vent facies can be recognized in paleosystems by brecciation of the basinal units, and the replacement of the host rocks by sulphides and iron carbonates (Fig. 1).

An understanding of SEDEX fluid geochemistry is important for understanding the relationship, if any, between a sulphide ore deposit and possible hydrothermal 'exhalites' that may precipitate at a distance from their source. In Canada, the Selwyn basin, which is located in both Northwest Territories (NWT) and Yukon, contains several economic zinc-lead-silver resources that have been assigned a SEDEX deposit type. Additionally, the Selwyn basin is host to a number of sedimentary barite occurrences whose origins remain unknown. The major

O₂ oxygenated seawater

H₂S anoxic seawater

hydrothermal plume

BaSO₄, PbS and ZnS precipitate from interactions with anoxic seawater

interlaminated barite and base-metal sulphides

interlaminated barite and sediments

stockwork zone and hydrothermal breccias

Is barite a distal expression of a SEDEX mineralizing system?

Early to Middle Devonian sedimentary rocks of the Lower Earn Group

Figure 1. *Idealized cross-section of a vent proximal SEDEX deposit (modified from Goodfellow and Lydon, 2007).*

vent-proximal deposits of the Selwyn basin are thought to have formed in the late Devonian-Mississippian based on the age of host lithologies (Goodfellow and Lydon, 2007). Important sediment-hosted barite sequences that are found in both NWT (Fernandes *et al.*, 2010) and in the MacMillan Pass district, Yukon are interpreted to be in host rocks of the same age (*e.g.*, Turner and Goodfellow, 1990). Barite occurrences and deposits that occur in the MacMillan Pass district include the Hess, Cathy, Walt and Tyrala showings and are found ~30 km northwest of the Tom Ba-Zn-Pb deposit which is also hosted in Lower Earn Group rocks.

This study represents part of a MSc project currently being completed at the University of Alberta, which is focussed on examining sediment-hosted barite mineralization occurring in the Devonian-Mississippian Earn Group in Northwest Territories and Yukon. In this contribution we present preliminary field and analytical results from the barite occurrences examined in Yukon.

Our main objectives of this study are:

1. To sample drill core from the Hess barite occurrence in order to understand the relationship between the barite and sulphide mineralization.

2. To investigate the Walt and Tyrala sediment-hosted barite occurrences (which include the Hess barite occurrence) in the MacMillan Pass district.

3. To analyse the S isotope compositions of sulphides in Hess barite samples in order to better constrain the relationship between sediment-hosted barite and Zn-Pb mineralization in the MacMillan Pass district.

BACKGROUND GEOLOGY

One of the best preserved and documented examples of an epicratonic sedimentary sequence is found in the Selwyn basin in northwestern Canada. This is interpreted to have formed on the passive margin of Ancient North America as a result of erosion of the crystalline basement during continental breakup initiated at ~760 Ma (Eisbacher, 1981). The oldest rocks exposed in the Selwyn basin consist of a thick (4-6 km) sequence of Hadrinian-Cambrian clastic sedimentary rocks of the Windermere Supergroup (Eisbacher, 1981). However, the Windermere Supergroup may also represent the basement to the Selwyn basin and current work by the Yukon Geological Survey (YGS) will refine its regional setting (J. Chakungal, *pers. comm.*, 2010).

The Windermere Supergroup rocks are overlain by deep-water Cambrian-Ordovician carbonate rocks of the Sekwi Formation, which in turn are overlain by Late Ordovician-Silurian basinal facies chert and shale of the Road River Group (Cecile, 1982; Gordey *et al.*, 1982). The basinal sedimentary facies is bounded by the Mackenzie and Macdonald carbonate platforms to the east and north and dissected by the intrabasinal shelf facies of the Cassiar Platform in the south-central part. The regional stratigraphy is illustrated in Figure 2.

Sedimentation changed dramatically in late Devonian time when transgressive shale covered the platform and thick sequences of basin-derived clastic sediments accumulated in a number of submarine fan complexes to the west (Gordey *et al.*, 1982). This was followed by a sequence of arenites and debrites deposited in the early Mississippian. This group of Devonian-Mississippian rocks was first formally defined as the Earn Group in the Nahanni, Sheldon Lake, Niddery Lake and Sekwi Mountain map areas by Gordey *et al.* (1982). They divided the Earn Group into a lower and an upper unit, with the lower unit consisting of basinal siliceous shale, mudstone and shaley siltstone, and the upper unit containing coarser-grained turbiditic siliciclastic rocks.

The focus of this study are the units belonging to the sedimentary rocks of the Earn Group. The Earn Group is subdivided into the Lower Earn Group and the Upper Earn Group (Fig. 3). The Lower Earn Group; known as the Portrait Lake Formation in Yukon and as the Canol Formation in NWT, consists of a package of cherty mudstones, black, siliceous shales and grey siltstones that often weather to a characteristic silver colour.

The Upper Earn Group unconformably overlies the Canol/Portrait Lake formation which is known as the Imperial Formation in NWT and the Prevost Formation in Yukon (more recently called the Itsi Member of the Earn Group (Abbott and Turner, 1990)). The Upper Earn Group comprises coarse-grained, brown debrites and sandstones. The MacMillan Pass district of Yukon also has a chert pebble conglomerate unit, the MacMillan Pass Member, which is not well-constrained stratigraphically, but is thought to occur in the middle of the Lower Earn Group (Fig. 3b; Gordey and Anderson, 1993). Further confusion occurs when reading older literature (*e.g.*, Large, 1980) that originally used the Canol and Imperial Formation nomenclature in Yukon (Fig. 3c).
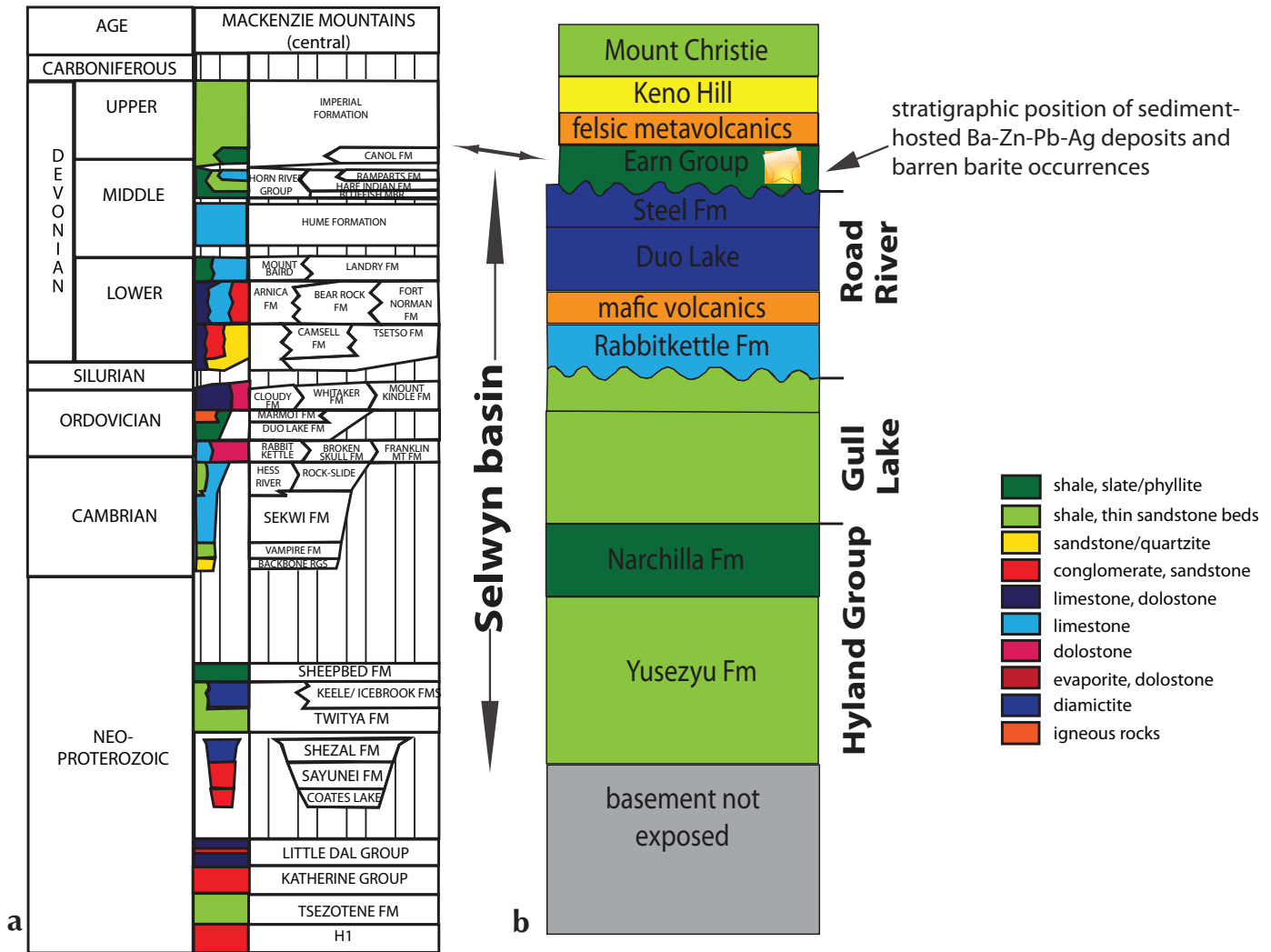
Figure 2. (a) *Regional stratigraphy of the Mackenzie Mountains (modified after Dewing et al., 2006);* **(b)** *regional stratigraphy of the western Selwyn basin (modified after J. Chakungal, pers. comm., 2010)*

For simplicity, we use Yukon stratigraphic nomenclature when describing the geological setting of the barite occurrences in the MacMillan Pass district; however, we recognize that this terminology is different from nomenclature used in NWT and that Portrait Lake Formation is interchangeable with the Canol Formation and that Itsi Member of the Portrait Lake Formation correlates to the Imperial Formation.

GEOLOGICAL SETTING OF STUDY AREA

The Hess occurrence (Yukon MINFILE 105O 021) is found in the MacMillan Pass district, east Yukon and is located in map sheet 105O (Fig. 4). Showing locations (Yukon MINFILE, 2010) are provided on a map of local geology (Fig. 5; J. Chakungal, *pers. comm.*, 2010).

Abbott (1982) divided the MacMillan Fold Belt (MFB) into three tectonostratigraphic domains (North, Central and South blocks) based on style of Mesozoic structures present and distribution of Silurian-Devonian stratigraphy. The Nidd deposit, along with the Jason and Tom stratiform zinc-lead deposits, occur within the Central Block. This block is dominated by west-trending tight folds and steep faults. In the Central Block, lower Earn Group stratigraphy overlies basaltic flows and volcaniclastic rocks as young as late-middle Devonian (Turner and Rhodes, 1990).

Abbott *et al.* (1987) recognized three informal units within the Lower Earn Group: a lower member of carbonaceous chert, a middle turbidite member, and an upper member of carbonaceous siliceous shale. A thick conglomerate unit (MacMillan Pass Member; Fig. 3c) occurs within the middle turbidite member and reflects the development of a Devonian graben (Abbott, 1982). Also restricted to
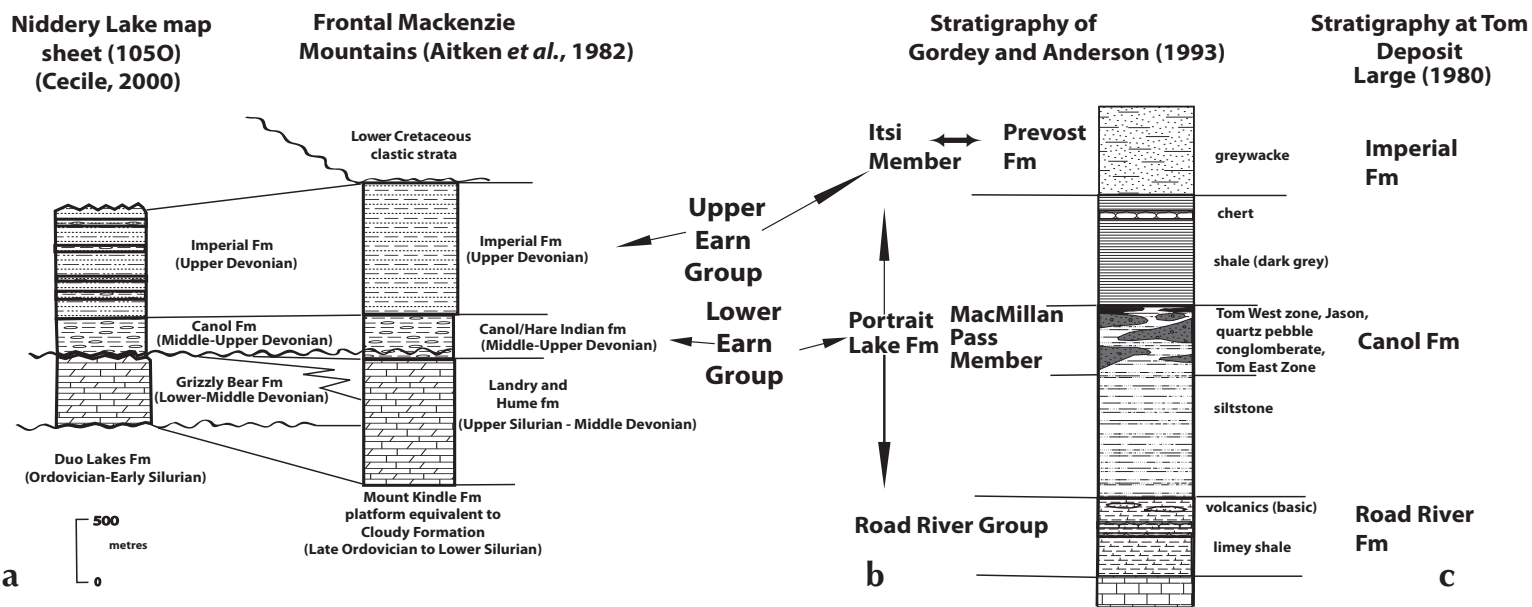
Figure 3. (a) Earn Group Stratigraphy in the Selwyn basin and Frontal Mackenzie Mountains (modified after Aitken et al., 1982; Cecile, 2000); (b) Earn Group stratigraphy in MacMillan Pass district (modified after Gordey and Anderson, 1993); (c) Earn Group stratigraphy at the Tom SEDEX deposit (modified after Large, 1980).

this graben are Silurian and Devonian volcanic rocks, late Devonian faults and upper Devonian stratiform zinc-lead mineralization. The Hess occurrence is located along the southern margin of the North Block, a domain intensely deformed by an imbricate package of south-directed thrust faults (Turner and Goodfellow, 1990).

HESS/WALT/CATHY/TYRALA SEDIMENT-HOSTED BARITE

The sediment-hosted barite showings correspond to Yukon MINFILE 105O 021 and 105O 022 and are located within the Walt and Tyrala claim blocks. These barite occurrences were drilled by Baroid of Canada in 1980, mapped and sampled by Cominco, and later, samples that were anomalous in zinc, lead and copper were re-examined by NDU Resources (Yukon MINFILE, 105O 021). Samples were collected from a single drillhole (Hess Barite) from Hess during fieldwork in 2009 and a field investigation was conducted on the claim blocks during summer of 2010.

FIELD RELATIONSHIPS

Sediment-hosted barite at all occurrences in the study area occurs within interbedded shale and siltstone of the Portrait Lake Formation, and in massive to brecciated limestone of the underlying Road River Group carbonates. The Itsi Member of the Portrait Lake Formation (Upper Earn Group) is absent in the study area. No sulphides were observed in outcrop samples.
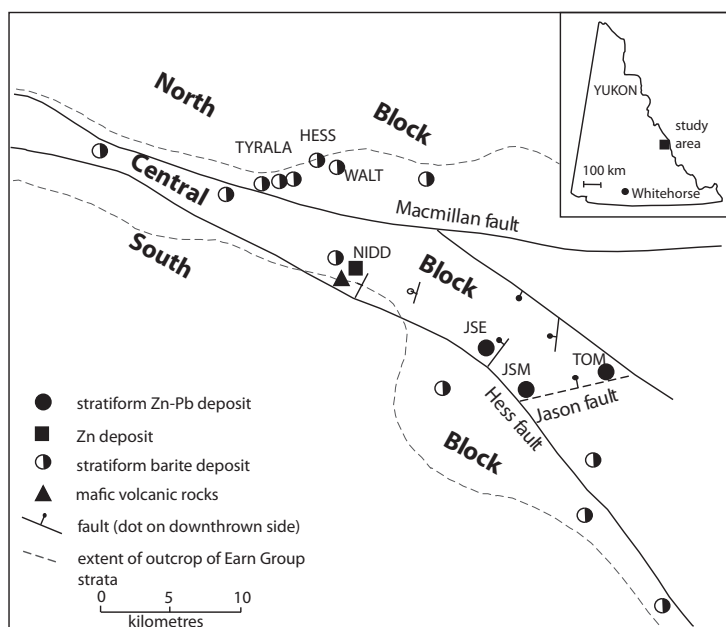
Figure 4. District map of the MacMillan Pass region illustrating major structural blocks, trends and deposits/showings. JSE = Jason Endzone, JSM = Jason Main zone (modified after Turner and Goodfellow, 1990).
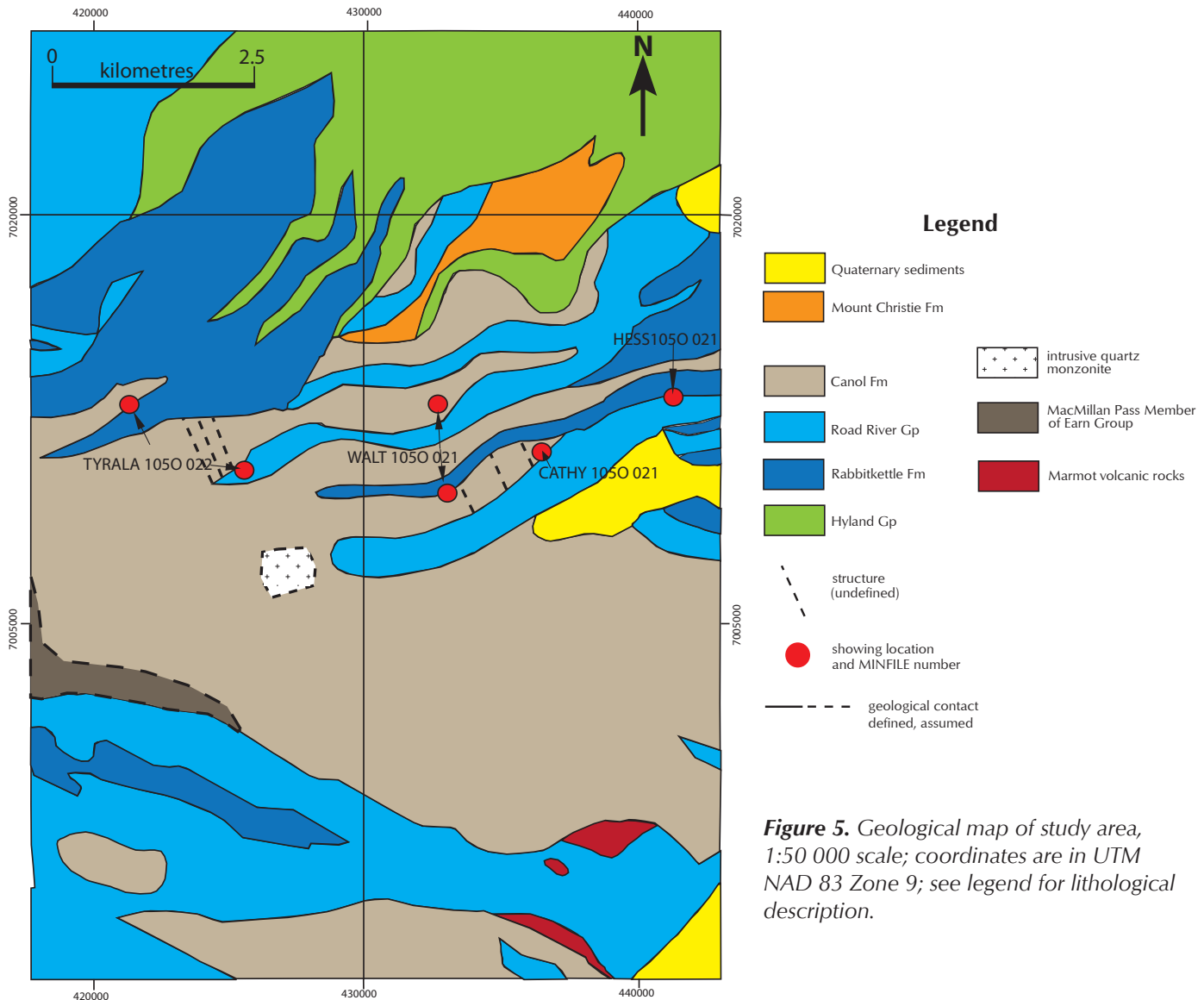
Figure 5. Geological map of study area, 1:50 000 scale; coordinates are in UTM NAD 83 Zone 9; see legend for lithological description.

Barite that is hosted in Portrait Lake Formation shale and mudstone occurs predominantly as fine laminations (Fig. 6a) or in minor, millimetre-sized nodules (Fig. 6b). Tight to isoclinal folding of barite laminations indicates a pre-fold and thrust deformation origin (Fig. 6c). Barite laminae vary from 0.5 to 2 mm in thickness, are dark grey in colour and organic rich. Barium-enriched laminae in the Road River Group carbonates are dark grey, weather to a pale cream colour, and are composed of fine-grained barium carbonate and barite (Fig. 6d). Barite nodules are round, roughly 1 mm in diameter, and are composed of sub-millimetre, radiating barite crystals which make up less than 2% of samples. These primary structures indicate syngenetic to early diagenetic deposition of barium minerals within the Road River Group and Portrait Lake Formation.

Within the study area, the greater majority of barite deposition occurred within the Road River Group carbonates and have a marked fault-related structural control punctuated by sharp contacts (Fig. 6e). X-ray diffraction (XRD) analyses of samples indicates the presence of both barite and numerous barium carbonates such as barytocalcite ($BaCa(CO_3)_2$) and norsethite ($BaMg(CO_3)_2$), in addition to variable amounts of calcite and dolomite. Massive, fine to medium-grained barium carbonate is the principal component of barite lenses, up to 20 m in thickness that form steep, resistant ridges. Barium carbonate breccias range from pale grey, angular to subrounded, and clast-supported, to large, subrounded pale grey clasts up to 50 cm in diameter in a fine-grained, dark grey siliceous matrix (Fig. 6f). Clasts that are composed of fine-grained barium carbonates suggest coeval barium replacement of limestone and brecciation.

HESS BARITE DRILL CORE

Samples were collected from a weathered Cominco Ltd. drillhole at the Hess barite occurrence, which was drilled to a depth of 105.5 m. Textures associated with barium mineralization are similar to those observed in outcrop. Subsequent XRD analysis confirmed the presence of varying amounts of barite and barium carbonates with the Hess barite samples.

The Cominco drillhole was collared in deformed and locally brecciated, non-calcareous, black siltstone and mudstone of the Portrait Lake Formation (Fig. 7a). Minimal barite was observed from 0 to 39 m in the hole. Unmineralized siltstone and mudstone units are underlain (39 – 105.5 m) by increasingly altered, brecciated, and carbonate, sulphide and barite-rich lithologies.

The carbonate units contain barium minerals that exhibit similar epigenetic textures found in outcrop such as breccias (Fig. 7b). Barium minerals are overprinted by disseminated sulphides consisting of coarse-grained, euhedral pyrite and medium-grained galena crystals (Fig. 7c), which can occur as 0.5 cm-patches and as millimetre-thick veinlets that crosscut laminations (Fig. 7d). Sphalerite commonly occurs in these sulphide patches

as fine-grained, light honey-brown anhedral crystals. One sample (~88.65 m depth) has thin laminations of sphalerite interlaminated with host carbonates (Fig. 7e). Late quartz veinlets also crosscut all host rocks and mineralization (Fig. 7f).

SULPHUR ISOTOPE GEOCHEMISTRY

Sulphur (S) is present in nearly all natural environments and is a critical component of ore deposits, where S is the dominant non-metal phase. Fractionation of S isotopes is highly dependent on the process of metal deposition, furthermore S variations in nature are caused by redox reactions involving the isotopic species.

Goodfellow and Lydon (2007) propose that the anoxic part of the seawater column is the source for S in sediment-hosted ore deposits. In this study, we will compare the $\delta^{34}S$ of the sulphides and sulphates from all showings examined to assess whether ore-bearing fluids are genetically related. The $\delta^{34}S$ values of hand-picked sulphides from drill core were analysed in order for future comparison with the $\delta^{34}S$ values of barite from the same locality. These will be compared against established $\delta^{34}S$ values for seawater and sediments during the respective
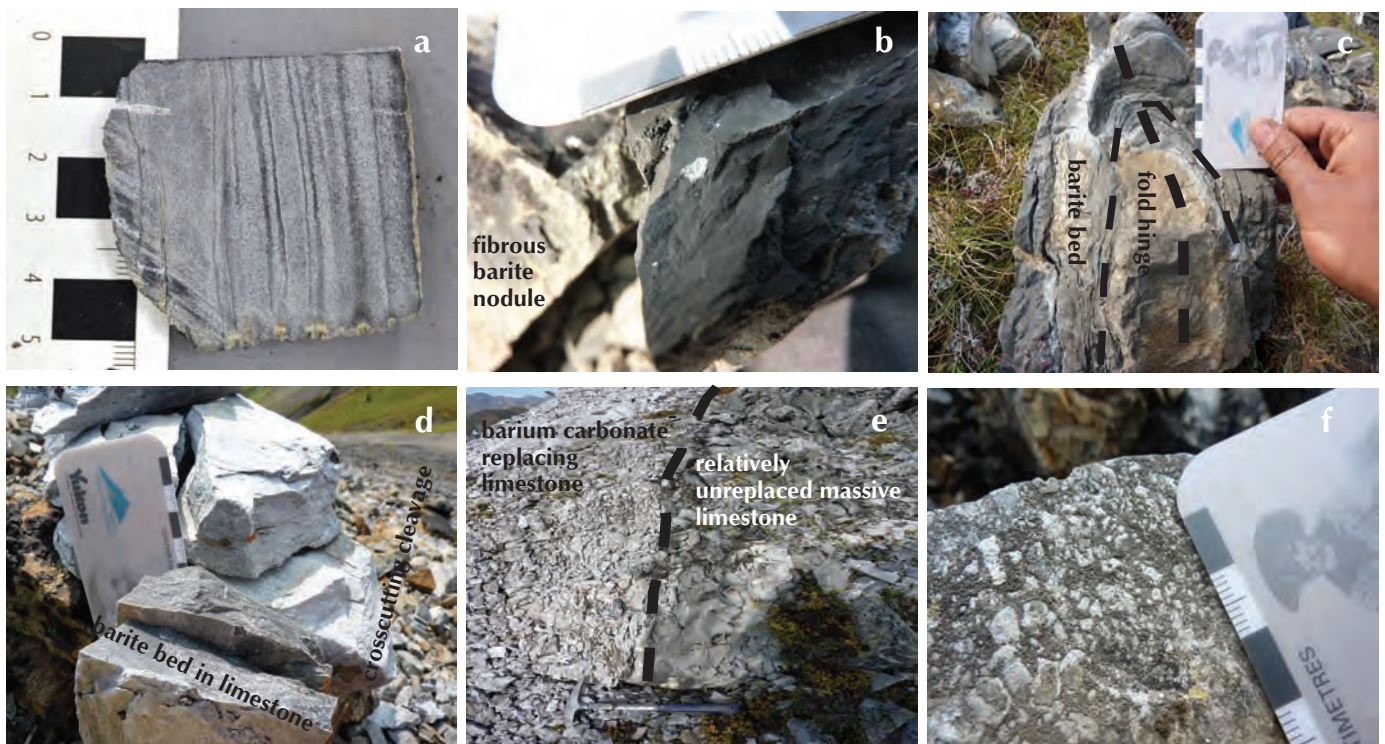
Figure 6. (a) Shale-hosted laminated barite mineralization (sample 10NF42F); **(b)** shale-hosted nodular barite mineralization (sample 10NF40A); **(c)** pre-deformation laminated barite wraps around a fold hinge; **(d)** laminate barium mineralization in Road River Group carbonates at Walt showing; **(e)** sharp contact between barite replacement of Road River Group carbonates at Cathy showing; and **(f)** barium carbonate breccias in Road River Group carbonates.

times of deposition for the Road River Group and Lower Earn Group (*e.g.,* Claypool *et al.,* 1980)

ANALYTICAL TECHNIQUES

The sulphur isotope ratios of sulphides were determined using Continuous Flow Elemental Analyzer Isotope Ratio Mass Spectrometry (CF-EA-IRMS) at the University of Calgary. The instrumentation comprises a Carlo Erba NA 1500 elemental analyzer interfaced to a VG PRISM II mass spectrometer. Samples are packed in tin cups, which are dropped by auto sampler onto a quartz tube combustion reactor. The temperature of this column is maintained at 1020°C and 'flash-combustion' is achieved by injecting a pulse of O_2(gas) exactly at the time of sample drop. The eluent gases are then swept by the helium carrier stream through a gas chromatography column to achieve

separation of SO_2, CO_2 and NO_x's before being focussed through an open split into the ion source of the mass analyzer. $\delta^{34}S$ values are determined by comparing the respective sample peak areas, as [Amp-s], to a reference gas peak inlet from the DI reference bellows of the mass spectrometer during each sample run. Raw data was normalized to the Cody Diablo Troilite (CDT) reference scale. The precision of using the VG Prism II–CE EA1500 technique, is generally better than ± 0.25‰ (n=10).
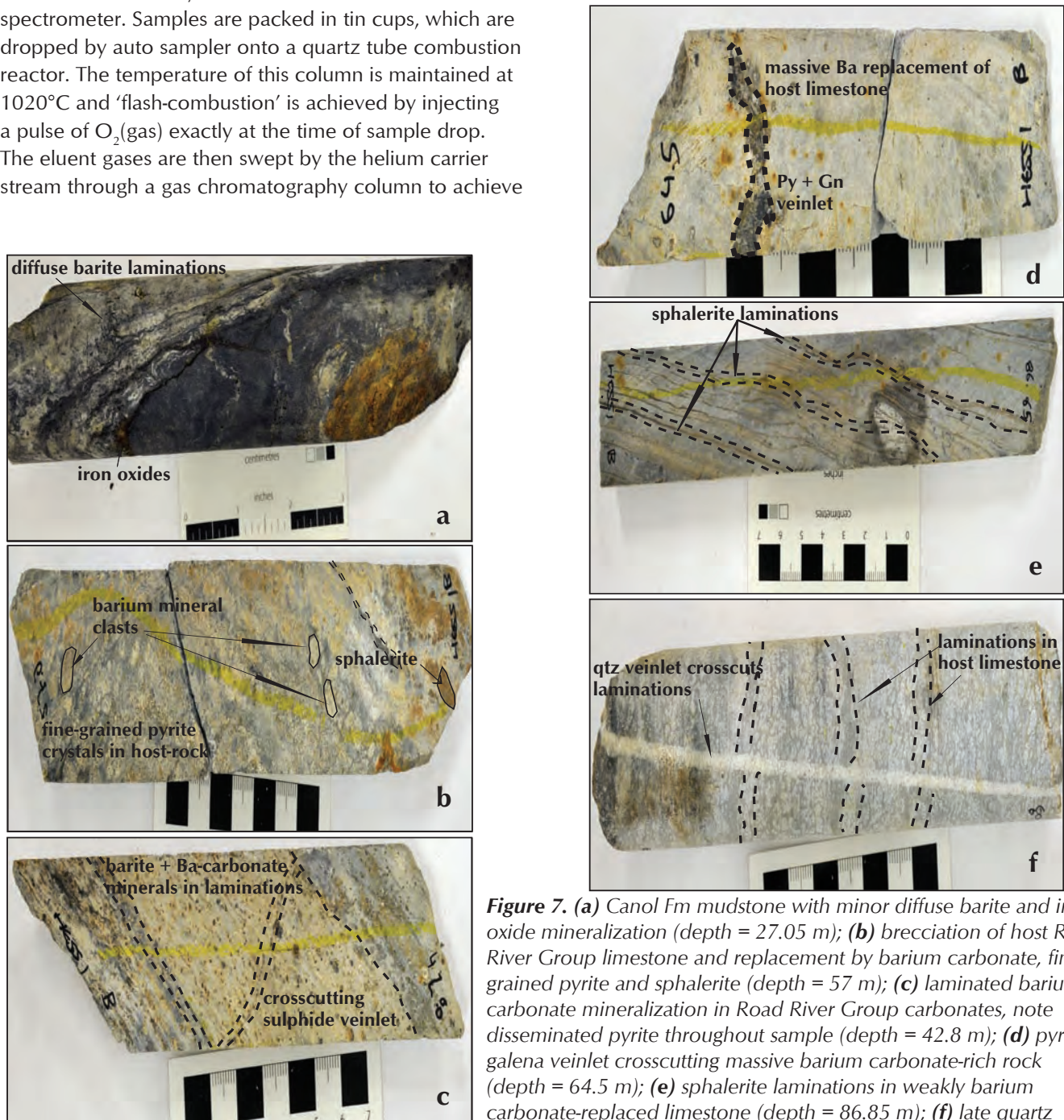
Figure 7. (a) Canol Fm mudstone with minor diffuse barite and iron oxide mineralization (depth = 27.05 m); **(b)** brecciation of host Road River Group limestone and replacement by barium carbonate, fine-grained pyrite and sphalerite (depth = 57 m); **(c)** laminated barium carbonate mineralization in Road River Group carbonates, note disseminated pyrite throughout sample (depth = 42.8 m); **(d)** pyrite + galena veinlet crosscutting massive barium carbonate-rich rock (depth = 64.5 m); **(e)** sphalerite laminations in weakly barium carbonate-replaced limestone (depth = 86.85 m); **(f)** late quartz veinlet crosscuts laminated barium mineralization (depth = 89.5 m).

RESULTS

The δ^{34}S values for sulphides (vCDT) from drill core from the Hess barite occurrence range between +24.3 to +28.4‰ for pyrite, +23.4 to +26.2‰ for galena (one sample at +7.6‰), and 24.6‰ for a single sphalerite sample. Co-existing, intergrown sulphides display similar δ^{34}S values. These results are summarized in Table 1.

SUMMARY

Barium mineralization that occurs at the Walt and Tyrala mineral occurrences in the MacMillan Pass district of Yukon is hosted in carbonates of the Siluro-Ordovician Road River Group, and shale and mudstone belonging to the Portrait Lake Formation (*i.e.,* Lower Earn Group). Barite mineralization pre-dates the ductile deformation that is associated with formation of the MacMillan fold belt.

Barium minerals are predominantly found in the altered limestone lenses of the Road River Group, where they occur as barite and barium carbonates (barytocalcite, norsethite and witherite). These barium phases either massively replace host limestone, or are in the form of breccias, laminations or nodules.

Barite laminations may indicate either synsedimentary depositional textures, or may represent preferential replacement along pre-existing heterogeneities or chemically favourable horizons in the host rock. We consider the majority of the textures observed at these showings to be secondary (*i.e.,* replacing a pre-existing favourable host-rock). Replacement, brecciation and nodule formation are features of diagenetic to epigenetic mineralization that could have only taken place beneath the sediment water interface (SWI).

Additionally, our observations indicate that one protracted episode (or possibly two phases) of barium mineralization may have developed. This occurs by syngenetic to early diagenetic deposition of barite in the Portrait Lake Formation along with contemporaneous epigenetic barium mineral replacement in the Road River Group carbonates related to brittle deformation.

The Road River Group carbonate horizons are the primary host for sulphide mineralization. Sulphide minerals include intergrown coarse-grained pyrite and fine-grained galena ± sphalerite. Sulphide mineralization observed in the Hess barite occurs as disseminations in the host rock, or in crosscutting veins that post-date ductile deformation and barium mineralization.

The δ^{34}S values for sulphides fall within a very tight range from +24 to +28‰ which suggest that S in base-metal sulphides was derived from a single fluid source. Epigenetic sulphide mineralization in the Road River Group and Portrait Lake Formation has δ^{34}S values consistent with seawater evaporite values for the Late Devonian (*e.g.,* Claypool *et al.,* 1980). However, as sulphide mineralization post-dates lithification of the Road River Group, the fluid(s) from which they derived their δ^{34}S values may not necessarily have been seawater, but possibly fluids (*e.g.,* pore waters) derived from basinal sediments.

Importantly, we note that the sedimentary units that host barite mineralization in the MacMillan Pass district are not restricted to the Lower Earn Group as was previously described (Turner and Goodfellow, 1990), but also include the Road River Group carbonates, where mineralization is epigenetic to host limestone.

Table 1. *Summary of δ34S values for sulphides from Hess barite drillhole for pyrite, galena and sphalerite respectively. Number in sample name indicates relative depth of sample downhole. LST = limestone-hosted, SHL = shale-hosted.*

Pyrite	δ^{34}S	Galena	δ^{34}S	Sphalerite	δ^{34}S
H45.0 PY	24.4	H45.0 GN	25.3	H64.5 SPH	24.3
H45.0 PY	24.6	H45.6 GN REP	24.6	H64.5 SPH REP	24.7
H45.0 PY	24.3	H61.6 GN	23.4		
H45.6 PY	23.1	H61.6 GN REP	23.8		
H46.2 LSTPY	24.5	H62.4 GN REP	25.4		
H46.2 SHLPY	24.4	H64.5 GN	7.6		
H57.3 PY	28.4	H66.7 GN	26.2		
H61.6 PY	25.1	H66.7 GN REP	26.0		
H62.4 PY	25.0				
H64.5 PY	25.3				

FUTURE WORK

Future work will include detailed petrography and further stable isotope analysis of sulphides, sulphates and carbonates. The age of pyrite mineralization will also be determined using Re-Os dating techniques and compared to data from other sediment-hosted lead-zinc-barite deposits in the MacMillan Pass district. Petrography will focus on determining whether barite mineralization in the study area is a primary sedimentary event.

ACKNOWLEDGMENTS

REFERENCES

Abbott, J.G., 1982. Structure and stratigraphy of the MacMillan Fold Belt: evidence for Devonian faulting. Northern Affairs Program, Exploration and Geological Services Division, Whitehorse, Open File 1983-1, text and 3 maps.

Abbott, J.G., Gordey, S.P. and Tempelman-Kluit, D.J., 1987. Setting of stratiform, sediment-hosted lead-zinc deposits in Yukon and northeastern British Columbia. *In:* Mineral Deposits of Northern Cordillera Symposium, J.A. Morin (ed.), Canadian Institute of Mining and Metallurgy, Special Volume 37, p. 1-18.

Abbott, J.G. and Turner, R.J.W., 1990. Character and paleotectonic setting of Devonian stratiform sediment-hosted Zn, Pb, Ba deposits, Macmillan fold belt, Yukon. *In:* Mineral deposits of the northern Canadian Cordillera, Yukon, northeastern British Columbia (field trip 14), J.G Abbott and R.J.W. Turner (eds.), Geological Survey of Canada Open File 2169, p. 99-136.

Aitken, J.D., Cook, D.G. and Yorath, C.J., 1982. Upper Ramparts River (106G) and Sans Sault Rapids (106H) map areas, District of Mackenzie. Geological Survey of Canada, Memoir 388, 48 p.

Carne, R.C. and Cathro, R.J., 1982. Sedimentary Exhalative (Sedex) Zinc-Lead-Silver Deposits, Northern Canadian Cordillera, CIM Bulletin, vol. 75, p. 66-78.

Cecile, M.P., 1982. The Lower Palaeozoic Misty Creek Embayment, Selwyn Basin, Yukon and Northwest Territories. Geological Survey of Canada, Bulletin 335, 78 p.

Cecile, M.P., 2000. Geology of the northeastern Niddery Lake map area, East-central Yukon and adjacent Northwest Territories. Geological Survey of Canada, Bulletin 553, 120 p.

Claypool, G.E., Holser, W.T., Kaplan, I.R., Sakai, H. and Zak, I., 1980. The age curves of sulfur and oxygen isotopes in marine sulfate and their mutual interpretation. Chemical Geology, vol. 28, p. 199-260.

Dewing, K., Sharp, R.J., Ootes, L., Turner, E.C. and Gleeson, S.A., 2006. Geological assessment of known Zn-Pb showings, Mackenzie Mountains, Northwest Territories. Geological Survey of Canada, Current Research 2006-A4, 12 p.

Eisbacher, G.H., 1981. Sedimentary Tectonic and Glacial Record in the Windermere Supergroup, Mackenzie Mountains, northwestern Canada. Geological Survey of Canada, Paper 80-27, 40 p.

Fernandes, N.A., Gleeson, S.A., Sharp, R.J., Martel, E. and Fischer, B., 2010. Connecting SEDEX and carbonate-hosted base metal mineralization in the Northwest Territories: Barite as a possible vector. Northwest Territories Geoscience Office, NWT Open Report 2010-003, 26 p.

Goodfellow, W.D., 1987. Anoxic Stratified Oceans as a Source of Sulfur in Sediment-Hosted Stratiform Zn-Pb Deposits (Selwyn Basin, Yukon, Canada). Chemical Geology, vol. 65, p. 359-382.

Goodfellow, W.D. and Lydon, J.W., 2007. Sedimentary-exhalative (SEDEX) deposits. *In:* Mineral Deposits of Canada: A Synthesis of Major Deposit-types, District Metallogeny, the Evolution of Geological Provinces, and Exploration Methods, W.D. Goodfellow (ed.), Geological Association of Canada Special Publication no. 5, p. 163-183.

Goodfellow, W.D., Lydon, J.W. and Turner, R.J.W., 1993. Geology and genesis of stratiform sediment-hosted (SEDEX) zinc-lead-silver sulphide deposits. *In:* Mineral deposit modeling, R.V. Kirkham, W.D. Sinclair, R.I. Thorpe and J.M. Duke (eds.), Geological Association of Canada, Special Paper no. 40, p. 201-251.

Gordey, S.P., Abbott, J.G. and Orchard, M.J., 1982. Devono-Mississipian Earn Group and younger in strata in east-central Yukon. Current Research, Part B, Geological Survey of Canada, Paper 82-1B, p. 93-100.

Gordey, S.P. and Anderson, R.G., 1993. Evolution of the northern Cordilleran Miogeocline, Nahanni map area (105I), Yukon and Northwest Territories. Geological Survey of Canada, Memoir 428, 214 p.

Large, D.E., 1980. On the geology, geochemistry and genesis of the Tom Pb-Zn-Barite deposit, Yukon Territory, Canada. Unpublished PhD thesis, Technische Universität Braunschweig, Institute of Geology and Palaeontology, Germany, 160 p.

Turner, R.J.W. and Goodfellow, W.D., 1990. Barium carbonate bodies associated with the Walt [Cathy] Stratiform barium deposit, Selwyn Basin, Yukon: A possible vent complex associated with a Middle Devonian sedimentary exhalative barite deposit. Geological Survey of Canada, Cordillera and Pacific Margin, Current Research, 90-1E, p. 309-319.

Turner, R.J.W. and Rhodes, D., 1990. Boundary Creek zinc deposit (Nidd property), MacMillan Pass, Yukon: sub-seaflow sediment-hosted mineralization associated with volcanism along a late Devonian syndepositional fault. Geological Survey of Canada Current Research, vol. 90-1E, p. 321-335.

Yukon MINFILE, 2010. Yukon MINFILE – A database of mineral occurrences. Yukon Geological Survey, < *http://www.geology.gov.yk.ca/databases_gis.html*>.

New insights into the geology and mineral potential of the Coast Belt in southwestern Yukon

Steve Israel[1], Don Murphy, Venessa Bennett
Yukon Geological Survey

Jim Mortensen
University of British Columbia, Vancouver BC

Jim Crowley
Boise State University, Boise, Idaho

ABSTRACT

The southwestern Yukon Coast Belt mapping project is a joint Yukon Geological Survey/Geological Survey of Canada initiative operated under Natural Resources Canada's GEM (Geomapping for Energy and Minerals) program. This project is aimed at investigating the geological relationships and mineral potential of the Kluane Schist, the Ruby Range batholith and the Yukon-Tanana terrane in southwestern Yukon. Bedrock mapping at 1:50 000-scale followed a 400 m line-spaced aeromagnetic survey flown in the winter of 2010. Preliminary results indicate the presence of a northeast-dipping structural stack through an ~40 km-thick crustal section, whereby the Kluane Schist occupies the lowest structural level and the Yukon-Tanana terrane the highest. The Ruby Range batholith intruded along the contact between the Kluane Schist and the Yukon-Tanana terrane, and was emplaced late in the deformation history. An orthogneiss/paragneiss unit of unknown tectonic affinity was mapped structurally between the Ruby Range and the Kluane Schist. Detrital zircon analyses from two samples of Kluane Schist indicate that the onset of deposition for this metasedimentary sequence occurred after *ca.* 94 Ma. Two significant metamorphic events, dated at 82 and 70 Ma, affected the Kluane Schist. This indicates that original structural juxtaposition between the Kluane Schist and the Yukon-Tanana terrane pre-dated intrusion of the Ruby Range batholith.

Mineral potential in the Coast Belt area is significant and includes porphyry Cu-Mo-Au, epithermal Au-Ag and orogenic Au occurrences. The upper level of the Ruby Range batholith is most prospective for porphyry and epithermal mineralization, while the Kluane Schist is most prospective for orogenic Au mineralization.

[1]steve.israel@gov.yk.ca

INTRODUCTION

The southwestern Yukon Coast Belt (SYCB) mapping project is a joint Yukon Geological Survey/Geological Survey of Canada initiative operated under Natural Resources of Canada's GEM (Geomapping for Energy and Minerals) program. The mapping project is one of several that comprise the Edges Project. The study area is located in southwest Yukon and extends from the eastern edge of Kluane Lake, north to Rhyolite Creek, east to Aishihik Lake, and south to the Alaska Highway; it encompasses part of the Kluane Lake and Aishihik 1:250 000-scale map area (NTS 115G and 115H, respectively; Fig. 1). Access is mainly by helicopter but the boundaries of the area can be accessed along the Aishihik road in the east, the Cultus Bay road in the west and the Alaska Highway in the south. Much of the area is contained within the Ruby and Nisling ranges that consist of rugged to rounded mountains reaching elevations of up to 2200 m, and separated by large valleys filled with Quaternary deposits. The mountains become less rugged and lower in elevation to the north. Vegetation is limited to scrub grass at higher elevations with open spruce forests occupying areas below ~1200 m and swampy wetlands in the lowest and widest valleys.
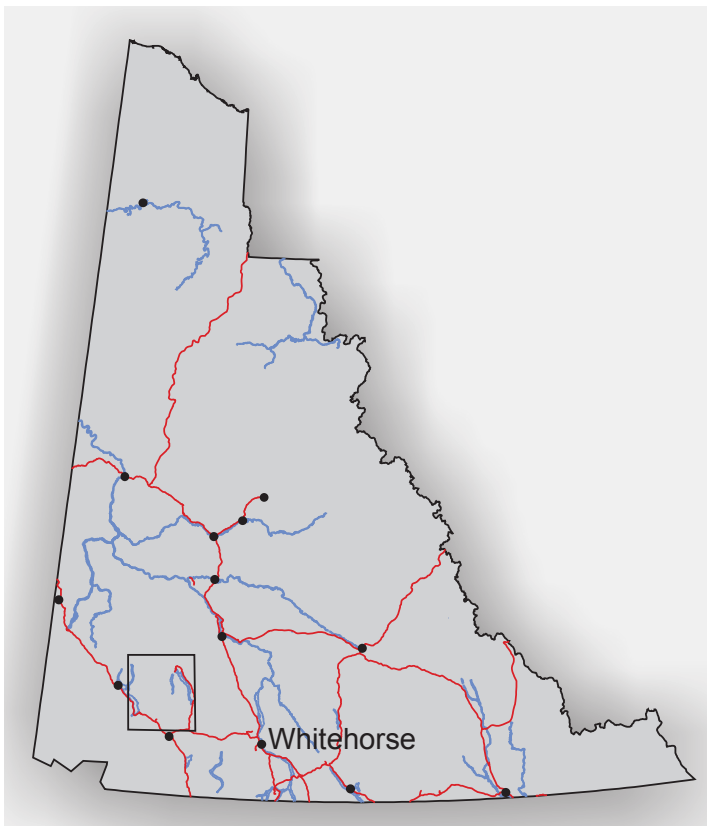
Figure 1. *Location of the Coast Belt project area.*

Bedrock mapping activities were based out of a camp near Silver City and took place over a six week period in June and July 2010. Mapping followed up on a 400 m line-spacing aeromagnetic survey acquired in February and March 2010 (Kiss, 2010) and covering approximately eleven 1:50 000-scale map sheets.

The main goals of the project were to investigate the geological relationships and mineral potential of the Kluane Schist, the Ruby Range batholith and the Yukon-Tanana terrane in southwest Yukon. This paper summarizes bedrock geology data collected during the summer 2010 and presents preliminary results of detrital and igneous zircon analyses from the Kluane Schist and Ruby Range batholith. Key results from this study include:

1. The structural stacking of the tectonic elements creates an exposed section of crust roughly 40 km thick. This section includes an entire batholith from its roots up into the porphyry and epithermal realms, and its overlying volcanic carapace.

2. The Ruby Range batholith is syn-to-post tectonic and becomes more felsic higher in the crustal section.

3. A unit of orthogneiss/paragneiss of uncertain age and correlation occurs along the base of the batholith and structurally above the Kluane Schist.

4. The potential for porphyry and epithermal style mineralization increases up crustal section.

5. The depositional age of the Kluane Schist is constrained by detrital zircons as young as ~95 Ma. The provenance of the Kluane Schist is likely an uplifted Yukon-Tanana terrane and Jurassic to Cretaceous plutons of the Aishihik batholith and the Coast plutonic complex.

6. LA-ICPMS dating of metamorphic rims on Kluane Schist detrital zircons suggest that metamorphism significantly intense enough to cause Pb loss and new zircon growth occurred at ~82 Ma and ~70 Ma.

7. The lithotectonic relationships observed in southwestern Yukon are similar to those in southeastern Alaska, increasing the potential for orogenic-style gold mineralization.

REGIONAL GEOLOGY AND PREVIOUS WORK

The area north of the Denali fault and southeast of the White River in southwestern Yukon is underlain by three main tectonic elements: 1) the Kluane Schist; 2) the Ruby Range batholith; and 3) the Yukon-Tanana terrane. They form a northeast-dipping structural stack that exposes a roughly 40 km-thick section of crust (Fig. 2). This tectonic

configuration continues to the southeast where the Kluane Schist is structurally truncated by an ambiguous fault zone between the Kluane Schist and the Dezadeash Formation, south of the town of Haines Junction. To the southwest, the Kluane Schist is in fault contact with metasedimentary rocks of the Dezadeash Formation and an enigmatic package of highly deformed and metamorphosed mafic volcanic rocks, informally known as the Bear Creek metavolcanic assemblage. To the northwest, the Kluane Schist and the Ruby Range batholith are cut off by the Denali fault. North of the map area, the Yukon-Tanana terrane is extensively intruded by the Early Jurassic Aishihik and mid-Cretaceous Dawson Range batholiths.

Previous geologic studies in the area were either reconnaissance in nature or focussed on specific tectonic elements. The present study is the first to conduct comprehensive bedrock mapping of the entire area at 1:50,000-scale. Previous 1:250 000-scale bedrock mapping by the Geological Survey of Canada was completed by Muller (1967) in the Kluane Lake map sheet (115G) and by Tempelman-Kluit (1974) in the Aishihik map sheet (115H). More detailed, 1:50 000-scale mapping by Johnston and Timmerman (1994) covered map sheets 115H/6-7. Murphy (2007) and Murphy *et al.* (2008; 2009) completed comprehensive 1:50 000-scale mapping of the area northwest of the current study. Their efforts were concentrated on deciphering the tectonic relationships between the Windy-McKinley terrane, mid- to Late Cretaceous igneous rocks and the Yukon-Tanana terrane. Several metamorphic studies have been carried out within the Yukon-Tanana terrane (Aishihik metamorphic complex) and the Kluane Schist (Erdmer, 1991; Johnston and Erdmer, 1995a; Mezger *et al.*, 2001a), as well as larger-scale tectonic analyses (Erdmer and Mortensen, 1993; Mezger *et al.*, 2001b; Johnston and Canil, 2006).

GEOLOGY OF THE STUDY AREA

The Kluane Schist occupies the lowest exposed structural level in the study area, while the Yukon-Tanana terrane occurs at the highest structural level. The Ruby Range batholith intrudes between and across the other two tectonic elements, obscuring the nature of the contact between them. Younger, more felsic and porphyritic phases of intrusive material outcrop at the top of the batholith, where they are interpreted to be the feeders to intermediate to felsic volcanic rocks that unconformably overly the Yukon-Tanana terrane. These intrusive and volcanic rocks have been informally named here the Rhyolite Creek volcano-plutonic complex (Fig. 3).

YUKON-TANANA TERRANE

Rocks in the northern portion of the project area were previously referred to as the Aishihik Lake metamorphic belt (Tempelman-Kluit, 1974), the Nisling terrane (Wheeler and McFeely, 1991) and the Aishihik metamorphic suite (Erdmer, 1991). Murphy *et al.* (2008) correlated similar rocks along strike to the northwest with the Snowcap and Finlayson assemblages of the Yukon-Tanana terrane. Although the rocks in the SYCB project area are more strongly metamorphosed than those described by Murphy *et al.* (2008), we believe that they are part of the Snowcap and Finlayson assemblages.

The Yukon-Tanana terrane in the project area structurally overlies the Ruby Range batholith and locally occurs as isolated roof pendants. The terrane consists of psammitic schist, quartzite, marble, garnet amphibolite and rare metaplutonic rocks. In the western half of the project area, schist and quartzite are variably carbonaceous, and interlayered with at least two similar beige-weathering carbonate units. Overlying the schists and quartzite are amphibolite units that locally contain abundant garnet up to 4 cm across (Fig. 4). In the eastern half of the project area Yukon-Tanana terrane rocks take on a higher degree of metamorphism, possibly lying within the dynamothermal aureole of the Early Jurassic Aishihik batholith (Johnston and Erdmer, 1995a). Yukon-Tanana terrane in this area comprises quartz-muscovite-garnet schist interlayered with carbonaceous quartzite, garnet amphibolite and thick (up to 75 m), beige to white-weathering marble units. Rare metaplutonic rocks are found interfoliated with the schists. These metaplutonic rocks are generally fine to medium-grained and quartz-diorite to diorite in composition. The structurally highest rocks in Yukon-Tanana terrane consist of coarse-grained, quartz-rich 'grits' and grey weathering carbonaceous quartzite (Fig. 5); the nature of the contact between these and underlying rocks is not known.

The age of the Yukon-Tanana terrane in the project area is not well constrained. Ages of 351 to 343 Ma are reported for meta-igneous rocks in the area by Johnston *et al.* (1996). This provides a lower age constraint for the unit. Elsewhere in the Yukon-Tanana terrane, similar ages are characteristic of metaplutonic rocks of the Simpson Range suite that intrudes the Snowcap assemblage, and overlying metavolcanic rocks of the Finlayson assemblage (Colpron *et al.*, 2006; Murphy *et al.*, 2006).
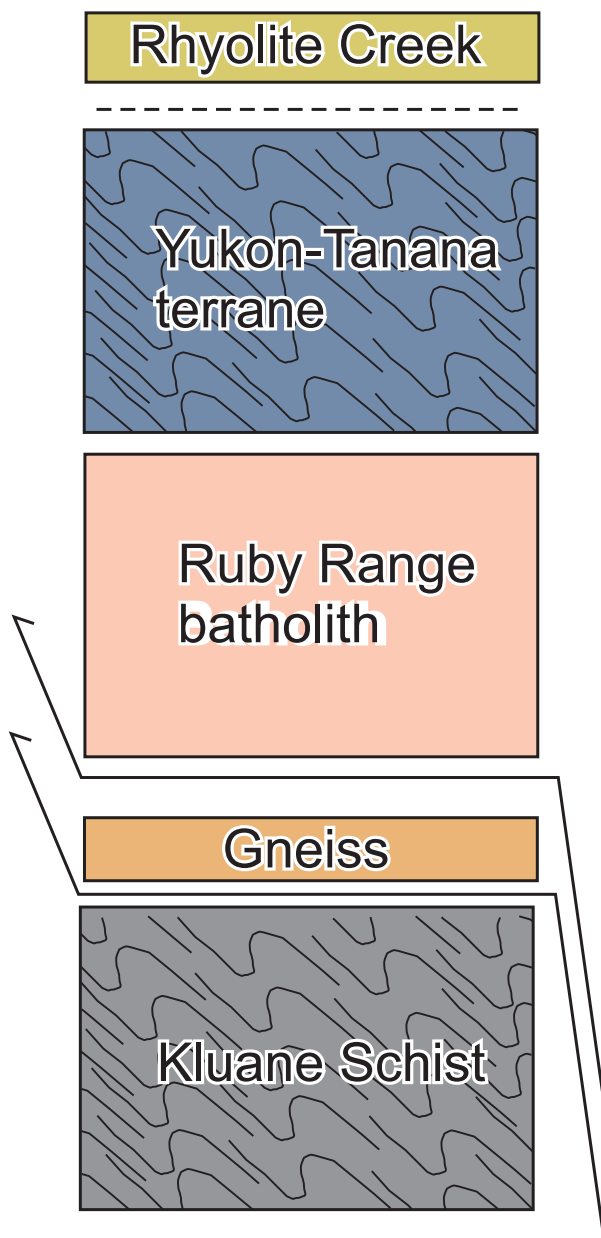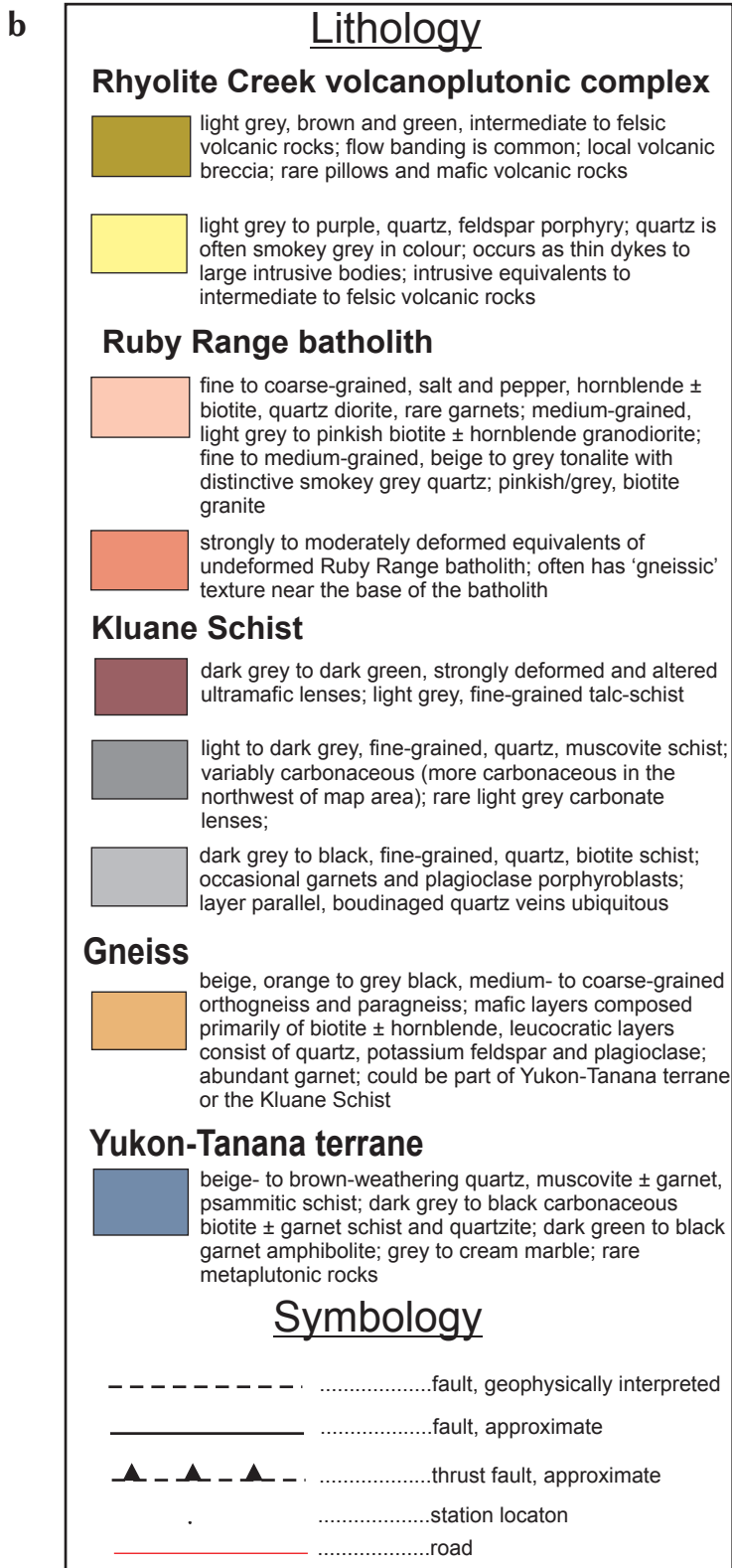
a

Bedrock geology map of the
Coast Belt, southwest Yukon

N

| 0 | 5 | 10 | 20 | 30 | 40 |

kilometres

62°N

138°W

NISLING RANGE

RUBY RANGE

KLUANE RANGES

Rhyolite Creek

Talbot Lake Arm

Denali Lake

Kluane Lake

Slims R.

Cultus Bay

Gladstone Ck

Doghead Point

115G070

Sekulmun Lake

Mt Bisel

Aishihik Lake

Mount Creeden

115H047
115H055
Killermun Lake

Mount Bark

Canyon L.

Otter Falls

Aishihik R.

Kloo L.

Mt Cairnes

Jaime R.

fault

61°N

61°N

Boundary of geophysical survey

Haines Junction

138°W

137°W

b

Lithology

Rhyolite Creek volcanoplutonic complex

light grey, brown and green, intermediate to felsic volcanic rocks; flow banding is common; local volcanic breccia; rare pillows and mafic volcanic rocks

light grey to purple, quartz, feldspar porphyry; quartz is often smokey grey in colour; occurs as thin dykes to large intrusive bodies; intrusive equivalents to intermediate to felsic volcanic rocks

Ruby Range batholith

fine to coarse-grained, salt and pepper, hornblende ± biotite, quartz diorite, rare garnets; medium-grained, light grey to pinkish biotite ± hornblende granodiorite; fine to medium-grained, beige to grey tonalite with distinctive smokey grey quartz; pinkish/grey, biotite granite

strongly to moderately deformed equivalents of undeformed Ruby Range batholith; often has 'gneissic' texture near the base of the batholith

Kluane Schist

dark grey to dark green, strongly deformed and altered ultramafic lenses; light grey, fine-grained talc-schist

light to dark grey, fine-grained, quartz, muscovite schist; variably carbonaceous (more carbonaceous in the northwest of map area); rare light grey carbonate lenses;

dark grey to black, fine-grained, quartz, biotite schist; occasional garnets and plagioclase porphyroblasts; layer parallel, boudinaged quartz veins ubiquitous

Gneiss

beige, orange to grey black, medium- to coarse-grained orthogneiss and paragneiss; mafic layers composed primarily of biotite ± hornblende, leucocratic layers consist of quartz, potassium feldspar and plagioclase; abundant garnet; could be part of Yukon-Tanana terrane or the Kluane Schist

Yukon-Tanana terrane

beige- to brown-weathering quartz, muscovite ± garnet, psammitic schist; dark grey to black carbonaceous biotite ± garnet schist and quartzite; dark green to black garnet amphibolite; grey to cream marble; rare metaplutonic rocks

Symbology

— — — — — ....fault, geophysically interpreted

———————— ....fault, approximate

▲ — ▲ — ▲ — ....thrust fault, approximate

. ...station locaton

——————— ....road

Figure 2. (a) Generalized bedrock geology map of the Coast Belt project area, southwestern Yukon. Red star indicates location of Yukon MINFILE occurrences (2009); *(b)* legend for bedrock map.

Rhyolite Creek

Yukon-Tanana terrane

Ruby Range batholith

Gneiss

Kluane Schist

Figure 3. Schematic stratigraphic column showing general structural relationships. See Figure 2 for lithologic descriptions. Ruby Range batholith is in structural contact with the gneiss and Kluane Schist as well as intrusive into these units.

Figure 4. *Garnet amphibolite of the Yukon-Tanana terrane, from the northern portion of the project area. Garnet is commonly up to 4 cm in diameter.*

Figure 5. *Grey weathering, variably carbonaceous quartzite of the Yukon-Tanana terrane.*

KLUANE SCHIST

The term Kluane Schist is used to describe the metamorphic rocks found between the Denali fault and the Ruby Range batholith in the southern part of the project area (Fig. 2). They have been referred to as the Kluane metamorphic assemblage (Mezger *et al.*, 2001a) and they make up part of the undivided metamorphic rocks of the Coast plutonic complex of Wheeler and McFeely (1991). The unit is composed primarily of monotonous metapelitic quartz-mica schist; rare bodies of ultramafic rocks and carbonate occur locally. Two separate mappable units were delineated in the present study: a muscovite-rich schist and a biotite-rich schist. Muscovite schist occupies a central position between overlying and underlying (?) domains of biotite schist. Both biotite and muscovite schists are variably carbonaceous, with the amount of carbon decreasing from northwest to southeast. Although generally monotonous, grain size variations occur locally, reflecting primary clastic layering. The transition from biotite to muscovite-rich schist is gradational over several hundred metres and in places difficult to identify due to the alteration and/or the weathering of biotite to a brassy colour.

Muscovite schist is fine to medium-grained and light grey weathering (Figs. 2 and 6). It is generally more carbonaceous than biotite schist, with the amount of carbon increasing to the northwest. Porphyroblasts of plagioclase occur locally and rare garnet is present, generally near late intrusions. Several generations of quartz veins are ubiquitous, locally occurring as quartz-rich layers that parallel the main foliation.

Figure 6. *Grey to beige-weathering muscovite schist typical of the Kluane Schist.*

Biotite schist occurs throughout the southern portion of the map area, surrounding the core of muscovite schist and structurally below the orthogneiss/paragneiss unit. Biotite schist is generally, dark grey to black weathering, fine to medium-grained and consists of biotite ± hornblende and quartz (Fig. 7). Biotite ranges in colour from black to brassy. Locally, garnet is observed both as early, deformed porphyroblasts and as late, overprinting porphyroblasts, the latter generally near crosscutting intrusions. Plagioclase porphyroblasts up to 1 mm are common. Quartz veining is ubiquitous and occurs in several generations.

Carbonate and ultramafic rocks are locally observed interleaved with the schist. Carbonate is light bluish-grey weathering, medium to coarse-grained and laterally discontinuous. Carbonate rocks have been observed in only two localities to date, one just north of Cultus Bay, the other just southwest of Killermun Lake. In both localities they are foliated and metamorphosed and have a distinctive weathering appearance, shown in Figure 8.

Ultramafic rocks occur as discontinuous slivers throughout the Kluane Schist. Individual bodies can reach up to 200 m in structural thickness in the project area. The largest ultramafic body is at Doghead Point (Murphy *et al.*, 2009; Fig. 2), on the northern shore of Kluane Lake between Talbot and Brooks arms. In the study area the ultramafic rocks are mainly serpentinite schist with varying amounts of talc (Fig. 9). Within coarser portions of the schist olivine crystals are preserved. Mezger (2000) interpreted these ultramafic bodies as being part of oceanic crust that was tectonically interleaved with the metasedimentary rocks of the Kluane Schist during accretionary processes.

The age of the Kluane Schist is poorly constrained. The youngest detrital zircons from the Kluane Schist suggest an upper age of deposition of ~95 Ma (see detrital zircon section below). The age the first metamorphic event is around 82 Ma (see detrital zircon section) so deposition must have occurred after 95 Ma and before 82 Ma.

Figure 7. *Dark brown to black-weathering, biotite schist of the Kluane Schist. Here outcrop is cut by late axial-planar cleavage associated with latest phase folding.*

Figure 8. *The rounded edges and smooth erosional troughs are distinctive weathering patterns of carbonate pods found within the Kluane Schist.*

Figure 9. *Strongly deformed and altered ultramafic rock, now essentially a talc schist found within the Kluane Schist.*

GNEISS

Gneiss is found in a continuous belt between the Kluane Schist and lowest portions of the Ruby Range batholith (Fig. 2). The unit can be traced for at least 60 km along strike within the project area. It continues to the southeast and northwest outside of the project area for several 10's of kilometres. The gneiss is fine to medium-grained and banded with melanocratic layers composed of biotite and hornblende, and leucocratic layers consisting of plagioclase, quartz, potassium feldspar and biotite (Fig. 10). It is markedly different in appearance from the

Kluane Schist in that the leucocratic layers are composed of igneous appearing material rather than deformed quartz veins. Garnet is locally abundant and ranges in size from <1 mm to 1 cm. In one exposure, the gneiss is structurally interleaved with very strongly deformed and metamorphosed carbonate horizons (Fig. 11). It is not yet apparent whether the gneiss is a highly metamorphosed equivalent of the Kluane Schist or whether it is a portion of the Yukon-Tanana terrane, or perhaps even the metamorphosed crystalline basement to the Yukon-Tanana terrane. Mezger (2001a) included the gneiss with the Kluane Schist, suggesting they are migmatitic versions of the less metamorphosed schist found away from the Ruby Range contact. Wheeler and McFeely (1991) included the gneiss in the Nisling terrane, now considered part of the Yukon-Tanana terrane. Because of the fault-bound nature of the orthogneiss, it considered a distinct tectonostratigraphic entity in this paper.

RUBY RANGE BATHOLITH

The Ruby Range batholith is a large plutonic complex that is found throughout the central portion of the study area (Fig. 2). Muller (1967) used the term Ruby Range batholith to describe all granitic rocks from the White River southeast to the eastern edge of map sheet 115G. Muller's definition included the main intrusive phase of the batholith between the Kluane Schist and the Yukon-Tanana terrane as well as small, compositionally similar intrusions of unknown age within both the Kluane Schist and the Yukon-Tanana terrane, away from the main core

of the complex. We continue this usage but understand that the batholith is a composite body and with more age constraints it may be subdivided into multiple episodes of magmatism.

The Ruby Range batholith is composed largely of quartz-diorite, tonalite and granodiorite with lesser amounts of diorite, gabbro and granite. The base of the Ruby Range batholith is almost entirely characterized by strongly to moderately foliated quartz-diorite that structurally overlies the orthogneiss unit and the Kluane Schist (Fig. 12). The composition becomes more felsic up-section to the north culminating in voluminous amounts of quartz-feldspar porphyry. Several phases of intrusive material can be distinguished purely on crosscutting relationships, and significant evidence for magma mixing can also be observed. Locally, post-tectonic intrusions of unknown age crosscut the foliated phase at the base of the batholith and the underlying orthogneiss unit (Fig. 13). Murphy *et al.* (2009) observed similar relationships outside the study area to the northwest. Several kilometres up from its base, the Ruby Range batholith is relatively undeformed and massive yet still compositionally and texturally variable in that quartz-diorite continues to dominate, but granodiorite and tonalite are common and they are texturally fine-grained to plagioclase and potassium feldspar-porphyritic depending on the composition. Feldspar ranges up to 2 cm in length. The mafic minerals include biotite and hornblende, and magnetite is locally common. Interestingly the presence or absence of magnetite does not appear to be dependant on

Figure 10. *Orthogneiss from the structural top of the Kluane Schist. Leucocratic layers are composed of quartz, plagioclase, biotite and potassium feldspar, while melanocratic layers consist of biotite and hornblende.*

Figure 11. *Strongly deformed and metamorphosed carbonate interleaved with orthogneiss and paragneiss found on the western shore of Talbot Arm.*

composition, but rather is found in all compositions but is not ubiquitous. Tonalite is commonly quartz-porphyritic, with quartz grains up to 0.5 cm and a distinctive smoky grey/blue colour. Miarolitic cavities are common near the upper contact of the batholith where it intrudes Yukon-Tanana terrane. The Ruby Range batholith is only locally foliated near its roof suggesting that much of the accommodated strain within the batholith occurred at its base. Peraluminous quartz-diorite to granodiorite intrusions that include muscovite ± garnet are found within the main batholith, as well as in satellite intrusions well away from the base of the batholith (Fig. 2). These crosscut all ductile structures within the Kluane Schist and are locally mineralized (see below).

Figure 12. *Strongly foliated quartz-diorite typical of the lower contact of the Ruby Range batholith.*

Figure 13. *Massive, undeformed tonalite to granodiorite of the Ruby Range batholith crosscutting fabrics within gneiss of the Kluane Schist.*

Several new U-Pb age determinations suggest a *ca.* 64 to 57 Ma range for the main intrusive phases related to the batholith (Crowley and Murphy, unpublished data; Mortensen and Murphy, unpublished data). The younger ages correspond to the more felsic phases and the older and intermediate ages correspond to more mafic and intermediate phases. Concordant U-Pb ages on zircons from a small boudinaged dyke that cuts the Kluane Schist near the bridge over the Aishihik River, east of Haines Junction, range from 71.8 ± 0.2 to 68.4 ± 0.2 Ma (Fig. 14). This age likely represents a pre-main phase of the Ruby Range batholith.

RHYOLITE CREEK VOLCANO-PLUTONIC COMPLEX

The Rhyolite Creek volcano-plutonic complex refers to the youngest, porphyritic phase of the Ruby Range batholith and its volcanic equivalents. The volcanic rocks were previously included in the Triassic and later (?) unit 4 of Muller (1967) and the Eocene Mount Nansen Group by Tempelman-Kluit (1974). The Mount Nansen Group has since been interpreted as mid-Cretaceous in age (Gordey and Makepeace, 2003) and therefore the volcanic rocks in the project area are no longer considered part of this group. The largest outcrop exposure of this unit in the project area is found in the north, near Rhyolite Creek (Fig. 2). The volcanic rocks consist of intermediate volcanic flows, breccia and tuff, flow-banded rhyolite and felsic tuff, and rare mafic flows, breccia and tuff (Fig. 15). Where volcanic rocks are mafic to intermediate in composition, breccias are almost always found at the base; where felsic, volcanic rocks are usually associated with quartz porphyritic intrusions and dome-like architecture. Porphyritic rocks are purple, brown or beige weathering and contain quartz phenocrysts up to 3 mm in diameter. Quartz porphyritic tonalite occurs extensively, with distinct smokey blue quartz phenocrysts up to 4-5 mm in diameter. The porphyry locally intrudes the overlying volcanic rocks (Fig. 16) and flow-banded rhyolite and quartz-feldspar porphyry from the Rhyolite Creek volcano-plutonic complex are both *ca.* 57 Ma (Crowley and Murphy, unpublished data), affirming the interpretation that porphyries are intruding their coeval volcanic rocks.
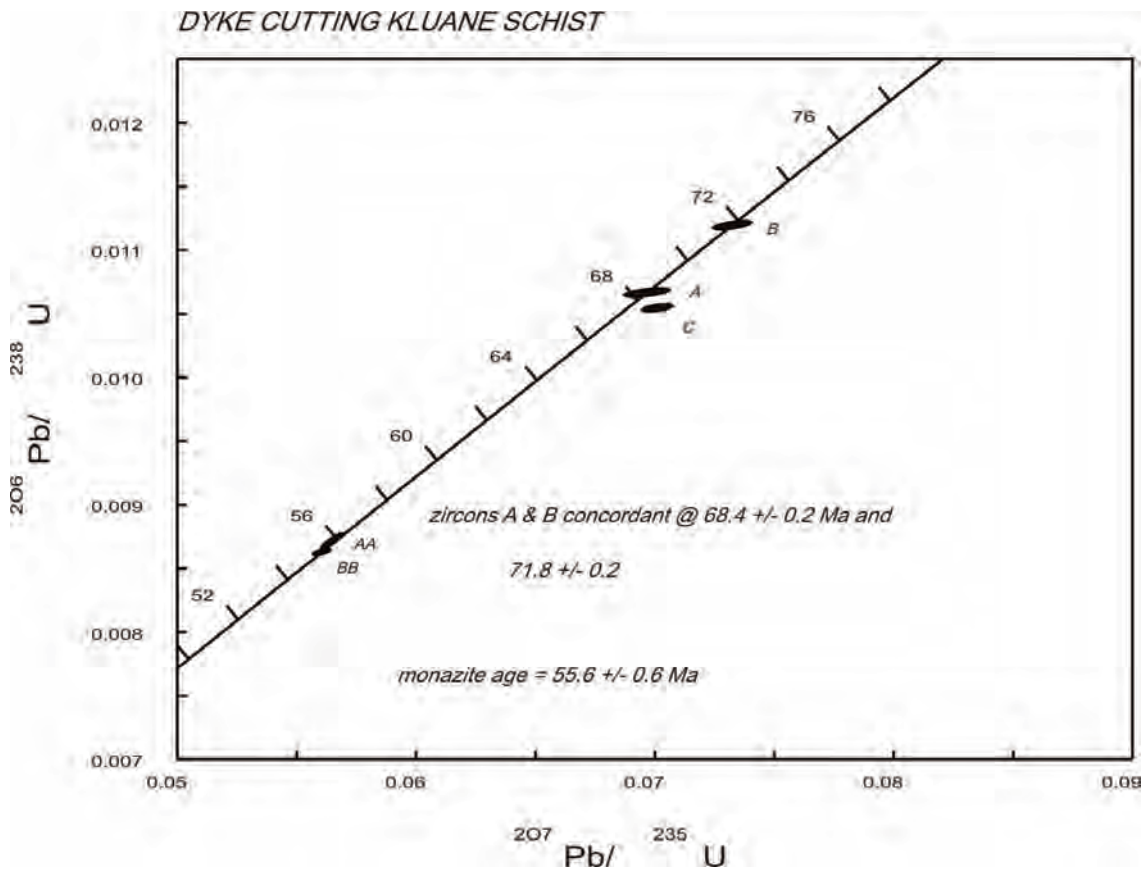
Figure 14. *U-Pb concordia diagram for zircon analyses from a dyke crosscutting main foliation within Kluane Schist. This age likely represents a pre-main Ruby Range batholith phase.*

Figure 15. *Flow banded rhyolite of the Rhyolite Creek volcano-plutonic complex.*

Figure 16. *Flow banded rhyolite being intruded by quartz, feldspar porphyry. The deformation of the flow bands suggest that the rhyolite was not completely cooled before intrusion.*

DETRITAL ZIRCON ANALYSES

Detrital zircon U-Pb analyses were performed on samples from the Kluane Schist to investigate provenance variations and constrain the age of deposition. Two samples were analysed, one without the benefit of cathodoluminescent and backscatter imaging, at the Pacific Centre for Isotopic and Geochemical Research (PCIGR; 08DM126) at the University of British Columbia and one, with imaging, at the Inco Innovation Centre (IIC), Memorial University, St Johns', Newfoundland (09SIT11). Through detailed imaging and subsequent core and rim analyses of sample 09SIT11, we were able to ascertain information relating to provenance and the maximum age for the onset of sedimentation. In addition, we constrained the ages of subsequent thermal events that resulted in extensive Pb loss of the primary detrital zircon population. The following discussion relies predominantly on data collected from sample 09SIT11; however, we provide a comparison of the two samples to highlight the similar provenance variations and the overlap between the ages of youngest accurate detrital zircon populations, after removal of metamorphic ages from the detrital dataset.

ANALYTICAL METHODS

Sample preparation and U-Pb Laser Ablation Microprobe Inductively Coupled Plasma Mass Spectrometry (LAM ICP-MS) geochronology for sample 09SIT11 was completed at the IIC, St Johns', Newfoundland. A detailed outline of the methodology is given in Bennett and Tubrett (2010). U-Pb data are reported in Appendix 1. Zircon separates were extracted using standard crushing techniques, and heavy mineral concentrates were produced using a Wilfley™ table and heavy liquids. To minimize sampling bias, we created a single zircon fraction by doing the initial stages of magnetic separation (Frantz™ isodynamic separator) only, to remove unwanted silicate and accessory phases (*e.g.,* monazite, titanite, garnet). Sampling bias was also minimized by randomly dumping zircon separates onto a grain-mount, as opposed to hand-picking particular grains of interest. Detrital zircon grains were photographed in transmitted light and subsequently mounted in epoxy resin and polished to expose grain cores. Grain mounts were then carbon coated and imaged using backscattered electron (BSE) and cathodoluminescence (CL) image analysis (Fig. 17). Approximately 200 zircon grains were mounted and imaged. Image analysis of 09SIT11 demonstrates variable growth of metamorphic zircon on

Ca. 82 Ma Metamorphic Rims
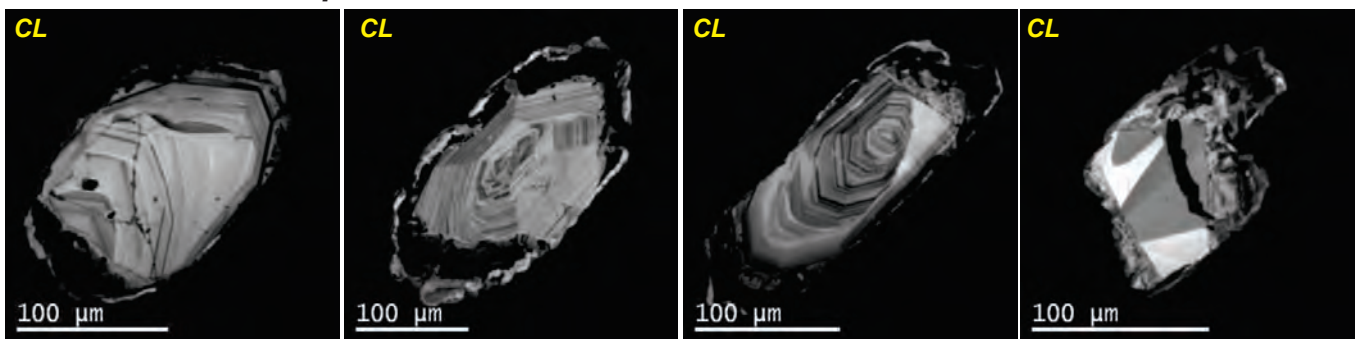
Youngest detrital Zircon Population - ca. 95 Ma
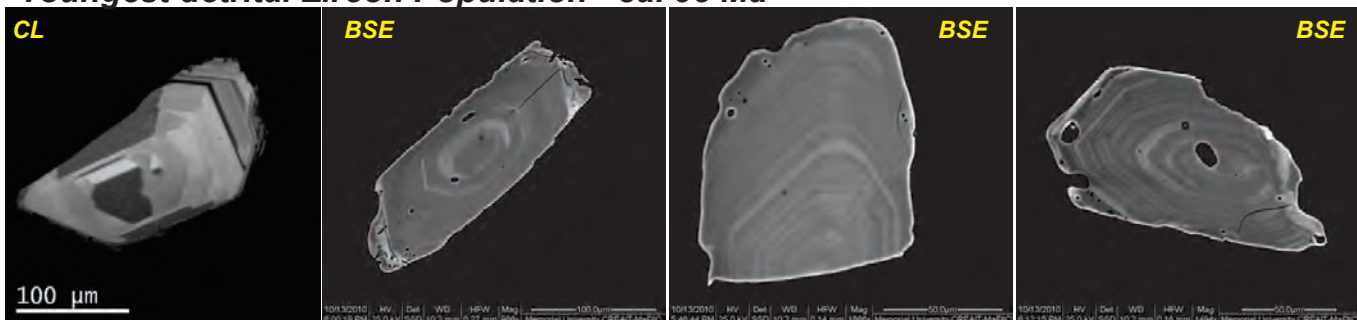
Figure 17. *Cathodoluminescence (CL) and backscatter electron (BSE) images of detrital zircons from sample 09SIT11. Metamorphic rims are the black areas between bright cores and rims. Note the lack of metamorphic rims on the youngest detrital zircons at bottom.*

detrital zircon grains (Fig. 17). A clear understanding of these zircon epitaxial relationships (core *vs.* rim) occurring within 09SIT11 assisted intragrain placement of the laser beam during data collection, which ensured analysis of single discrete age domains (*i.e.*, detrital *vs.* metamorphic) rather than overlapping or mixed age domains. Analysis of multiple age domains within a single zircon grain produces isotopically heterogeneous data which, typically, is a significant contributor to U-Pb discordance using the LAM ICP-MS technique.

Completing U-Pb analyses using LAM ICP-MS for 09SIT11 proved challenging due to the low Pb and U concentrations in grains which had undergone partial to complete Pb loss as a result of younger metamorphic events. In order to acquire useable age data for these grains, background U and Pb levels within the instrument were required to be at their lowest. Additionally, higher laser energy was applied (up to 5J) to analyse the low Pb and U grains to achieve useable, but lower precision age data. For analyses where ^{207}Pb intensity did not exceed background levels, inaccurate and meaningless ^{207}Pb/^{235}U ages result. Consequently, an assessment of concordance could not be made. These data were not included in the final detrital zircon population as the accuracy of the ^{206}Pb/^{238}U could not be determined (*i.e.*, Pb loss or detrital age). The dataset has also been filtered to exclude data exhibiting greater than 10% discordance. Additionally, during data collection the isotope mass 204 (Hg204+Pb204) was monitored. For any individual analysis, where 204 levels exceeded acceptable background levels the data were rejected from the final dataset as these grains have excess common Pb.

The interpreted maximum age of the onset of sedimentation of the sampled bed and the overprinting metamorphic ages for 09SIT11 are based on calculations of concordia ages from individual U-Pb isotopic analyses that have a probability of concordance greater than 0.20 (see Bennett and Tubrett, 2010; Fig. 18). Two-sigma uncertainty levels are reported for all calculated ages and plotted on concordia, unless stated otherwise. Final age calculations include U decay constant uncertainties, which are plotted graphically on concordia plots. Concordia were calculated using Ludwig (1999). Uranium and thorium concentration data and Th/U ratios are also calculated for each zircon analysed in 09SIT11 and reported in Appendix 1. One hundred and thirty-two analyses were completed on 125 zircon grains, 116 from detrital cores and 16 from younger metamorphic rims. Twenty core analyses exceeded the 10% discordance filter
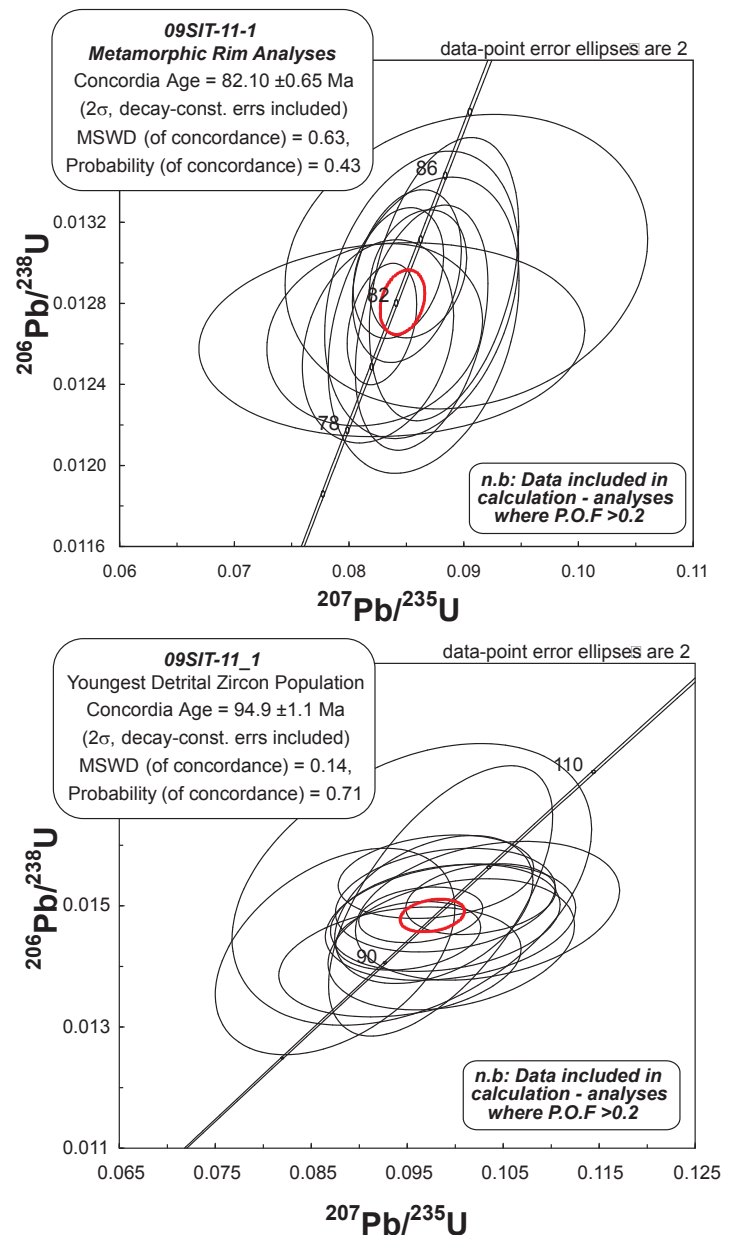
Figure 18. *U-Pb concordia plots from detrital sample 09SIT11; (a) analyses of metamorphic rims, and (b) analyses of the youngest detrital zircons.*

and were excluded from the dataset. Strong Pb loss had affected 22 zircon cores and analyses produced inaccurate and/or meaningless ^{207}Pb/^{235}U ages; these results were subsequently excluded from the final dataset. U-Pb data for the remaining 71 core analyses are presented in Figure 19. U-Pb age data collected for high mean atomic number metamorphic rims and grains interpreted from BSE images to represent new metamorphic zircon growth are presented in Figure 18a.

PROVENANCE OF THE KLUANE SCHIST

Complete detrital populations for both 09SIT11 and 08DM126 are illustrated in Figure 19. The data highlight the predominance of Phanerozoic grains, with subordinate populations occurring at *ca.* 1.2 Ga, 1.8 Ga and a single Archean grain from 09SIT11 (Appendices 1 and 2). Closer examination of the Phanerozoic populations reveals discrete age peaks at ~100 Ma, 200 Ma and 325-350 Ma, with subordinate ages from both samples occurring between the 100 and 220 Ma peaks (Fig. 20).

The detrital age populations in the Kluane Schist from both samples compare closely with known igneous ages from nearby terranes, suggesting that they formed the source area from which these zircons were eroded. The Proterozoic and Archean ages are significant detrital peaks within the Yukon-Tanana terrane (Colpron *et al.*, 2006). The 350-325 Ma ages from the detrital population

are also a well-represented igneous age in Yukon-Tanana terrane (Nelson *et al.*, 2006; Piercey *et al.*, 2006). The ages spanning from ~220 to ~100 Ma are all well-represented within the Aishihik batholith (*ca.* 190-180 Ma) and the Coast plutonic complex (Late Triassic to Eocene; Johnston and Erdmer, 1995a; Gehrels *et al.*, 2009). LAM ICP-MS U-Pb ages ranging from 98 Ma and 104 Ma have been obtained from the Nisling Range granodiorite located about 60 km north-northwest of the study area (Mortensen and Murphy, unpublished data; Tubrett and Murphy, unpublished data). Interestingly, Mezger (2001b), suggested that the only group of rocks in the vicinity that has the same geochemical and isotopic signature of the Kluane Schist is the Nisling Range granodiorite.
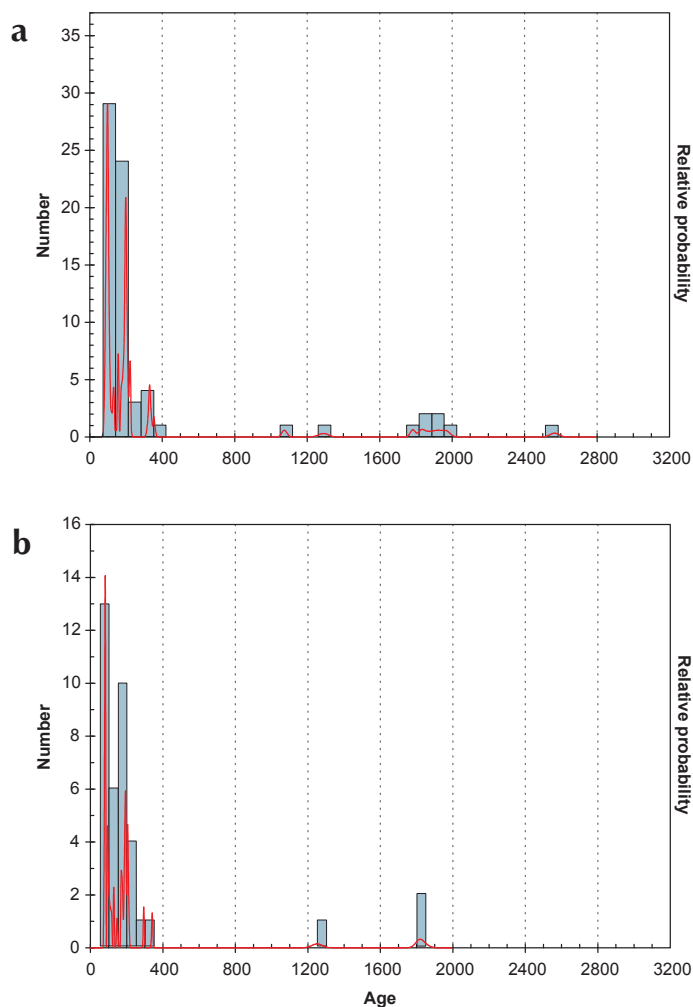
Figure 19. Probability density plots of two detrital zircon samples from the Kluane Schist; *(a)* sample 09SIT11, and *(b)* sample 08DM126.
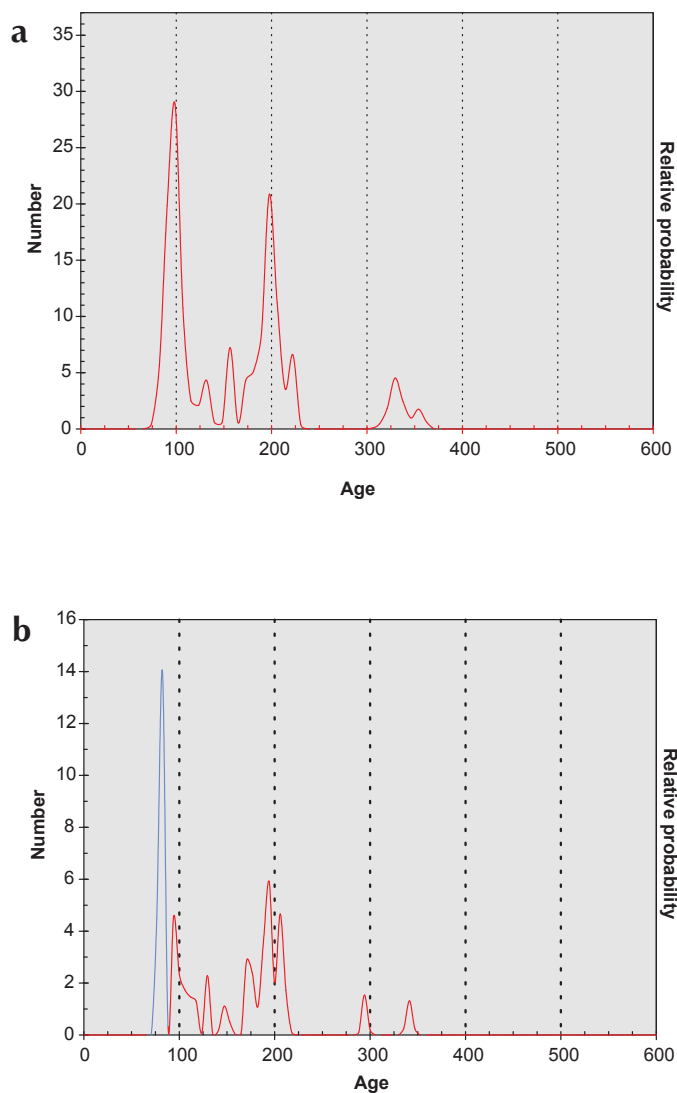
Figure 20. Probability density plots of ages of detrital zircons from the Kluane Schist, showing only the Phanerozoic ages. *(a)* sample 09SIT11, and *(b)* sample 08DM126, the blue peak represents the metamorphic ages from the sample.

AGE OF DEPOSITION AND METAMORPHISM OF THE KLUANE SCHIST

Variable development of metamorphic overgrowth rims is apparent from the images shown in Figure 17. These metamorphic growth zones correspond to domains characterized by high concentrations of U (879–8129 ppm) and very low Th (4-88 ppm; Appendix 1). Analysis of the high U/low Th metamorphic rims yielded a concordia age of 82.10 ± 0.65 Ma (Fig. 18A). Metamorphic ages determined from zircon rims in sample 09SIT11 correlate with the youngest age peak determined for sample 08DM126. Consequently we interpret the youngest age peak in 08DM126 as a metamorphic age rather a detrital age (Fig. 20).

The distinctive high U and low Th composition of the metamorphic growth zones was an important criterion in discriminating them from primary detrital grains. Grains that are detrital in origin were typically characterized by higher concentrations of Th and lower U values. Correspondingly, zircon grains without significant growth of younger metamorphic zircon preserved the original internal zoning structures (*e.g.*, oscillatory, sector, diffuse; Fig. 17). The youngest accurate age from this population of detrital grains from sample 09SIT11 is 94.9 ± 1.1 Ma (Fig. 18b). After stripping away the metamorphic peak from 08DM126 the age of the youngest peak is very close to the ~95 Ma age for the youngest detrital grain from 09SIT11 (Fig. 20b). We therefore interpret this age as the maximum age of the onset of deposition of this part of the Kluane Schist.

STRUCTURAL GEOMETRY AND RELATIONSHIPS

The project area is characterized by three separate fault-bound domains that include, from highest structural level to lowest, the Yukon-Tanana terrane, the gneiss unit, and the Kluane Schist (Fig. 21). We consider the Ruby Range batholith to be a late kinematic intrusion that overprints the original structural contact between the Yukon-Tanana

terrane, the orthogneiss and the Kluane Schist. The structural character of each domain is described separately below. The relationships between each domain are discussed in the context of younger structural elements that affect all domains.

YUKON-TANANA TERRANE

Structural trends within the Yukon-Tanana terrane generally define a northeast-dipping structural panel of Paleozoic rocks that is interpreted to be in thrust contact with underlying gneiss and/or the Late Cretaceous Kluane Schist. The lower contact of the Yukon-Tanana terrane is obscured by the Ruby Range batholith. Pre-Jurassic and Jurassic deformation and metamorphism within the Yukon-Tanana terrane was responsible for the initial northeast to east dip of the main foliations (Johnston and Erdmer, 1995a). These foliations have been kinked and overprinted by lower grade metamorphism related to thrusting over the Kluane Schist and intrusion of the Ruby Range batholith (Johnston and Erdmer, 1995a). More than one phase of folding is evident. The first phase is related to pre-Jurassic deformation, with later isoclinal re-folding of these during the Jurassic (Johnston and Erdmer, 1995a; Johnston and Erdmer, 1995b). The resulting folds generally verge to the southwest, with plunges towards both the northwest and southeast with some folds verging to the northeast. Stretching lineations occur on northeast dipping foliations; these trend towards the northeast; however, these are likely related to Jurassic deformation and syn-tectonic intrusion of the Aishihik batholith (Johnston and Erdmer, 1995a).

KLUANE SCHIST

Deformation within the Kluane Schist is expressed by a pervasive northwest-striking, northeast-dipping foliation. This foliation is likely a composite of two progressive phases of deformation related to southwest-verging deformation associated with thrusting of Yukon-Tanana terrane over the Kluane Schist. It is difficult to see
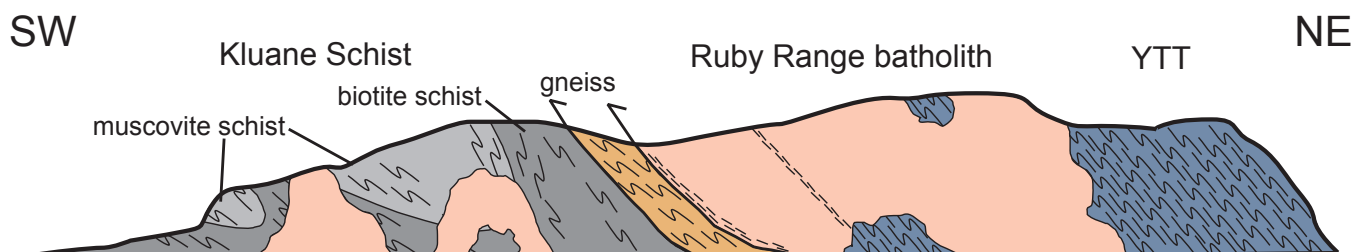
Figure 21. *Schematic cross section drawn from southwest to northeast, through the middle of the Coast Belt project area.*

these folds in outcrop and they are best observed in F2 fold hinges or expressed by pre and syn-deformation quartz veins (Fig. 22). These quartz veins are commonly boudinaged and tight to isoclinally folded and refolded. In the southeastern exposure of the Kluane Schist, late-stage south-to-southeast trending open-to-closed folds of the main foliation are preserved (Fig. 23). These late folds deform the main foliation so that it locally dips towards the southeast and southwest rather than the northeast. Timing of these structures is not well constrained. They must be post-95 Ma, the maximum depositional age of the Kluane Schist, and pre-57 Ma, the age for crosscutting porphyritic dykes. The 84 Ma metamorphic overgrowths on the detrital zircons likely reflect the main metamorphic event related to thrusting of Yukon-Tanana over the Kluane Schist. The early northeast-dipping foliation is most certainly related to this event and, as this foliation is seemingly crosscut by a 70 Ma late-syn-kinematic dyke (at the Aishihik River), southwestward thrusting was likely over by this time.

ORTHOGNEISS/PARAGNEISS

The structural relationships within the orthogneiss unit and its relationships with the other domains are not clear. The contact with the underlying Kluane Schist is interpreted as a north to northeast-dipping shear zone, based upon an increase in intensity of fabrics towards to the lower contact of the gneisses. The upper contact is either a shear zone that places strongly deformed Ruby Range quartz diorite over the gneiss or an intrusive contact

where younger phases of the batholith crosscut both sheared quartz diorite and orthogneiss. Rootless, isoclinal, southwest-verging folds within the orthogneiss/paragneiss unit are ubiquitous and help define the overall northeast dip of the penetrative foliation. Locally the main foliation is quite discordant with the sheared base, suggesting a more complex nature to the internal structural relationship.

RUBY RANGE BATHOLITH

Structural relationships within the Ruby Range batholith are purely time dependant, in that earlier phases are foliated and are therefore interpreted as pre to syn-tectonic, whereas later phases crosscut earlier formed fabrics and are interpreted as post-tectonic. Fabrics within the Ruby Range batholith are most strongly developed at the base of the batholith where it is in contact with the gneiss unit. The textures of the fabrics grade from proto-mylonitic and gneissic to magmatic away from the base. A magmatic age from an early, foliated phase of the Ruby Range batholith suggests that deformation was occurring at *ca.* 64 Ma (Crowley and Murphy, unpublished data). As mentioned earlier, it is likely that deformation between the Yukon-Tanana terrane and the Kluane Schist was taking place prior to intrusion of the main phase of the Ruby Range batholith, based on the Late Cretaceous age from a boudinaged dyke from the Aishihik River and *ca.* 84 and 70 Ma metamorphic overprints on detrital grains from the Kluane Schist.

Figure 22. *Tight to isoclinally folded quartz veins found within the Kluane Schist. These folds are likely F2 regional folds.*

Figure 23. *Late F3 folds within the Kluane Schist. These folds verge to the west-southwest.*

POST-64 MA DEFORMATION

Faults in the area are not well exposed, as they generally occur in the heavily overburdened filled valleys. The steep, regionally crosscutting faults are imaged on the regional and finer scale aeromagnetic surveys over the project area, and some are defined based on discontinuities in rock types and structures across valleys. The largest of these structures is the Denali fault, found in the southwestern-most portion of the field area. This structure has accommodated at least 450 km of right-lateral offset, likely in the latest Cretaceous to Eocene (Eisbacher, 1976; Lowey, 1998). North to northeast and northwest-striking faults are common, many of which do not penetrate the base of the Ruby Range batholith (Fig. 2). Kinematic interpretation of these structures is difficult to resolve because of a lack of good marker horizons. Similar fault patterns are observed to the northwest of the study area and have been interpreted to be related to hangingwall damage during pluton emplacement over the Kluane Schist (Murphy, 2007; Murphy *et al.*, 2008). These faults are likely important for mineralization as many of the gold bearing quartz-carbonate veins near Killermun Lake are found within north to northeast-striking structural zones (Wengzynowski, 1995; Eaton, 2003). East-striking faults cut by the Denali fault dissect the southern part of the project area and are interpreted to crosscut young, unfoliated phases of the Ruby Range batholith and some of the north-striking faults (Fig. 2).

Preliminary results from bedrock mapping and geochronological studies within the Coast Belt area of southwest Yukon indicate that the present day structural stacking and lithotectonic relationships are the result of southwestward (today's coordinates) thrusting of Yukon-Tanana terrane over the Kluane Schist and syn to post-tectonic intrusion of the main phase of the Ruby Range batholith. The *ca.* 70 Ma age from the boudinaged dyke near Aishihik River that crosscuts the main foliation in the Kluane Schist suggests that deformation related to thrusting was well underway by this time. The age of the dyke coincides with some metamorphic rims and some completely reset detrital grains from the Kluane Schist. Given that deposition of the Kluane Schist likely is constrained to post-*ca.* 95 Ma there is a maximum window of 25 My between deposition and peak (?) metamorphism of the Kluane Schist. Intrusion of the earliest dated phase of the Ruby Range batholith occurred late in the deformational history, at least 6 My after the boudinaging of the dyke at *ca.* 64 Ma (Crowley and Murphy, unpublished data). It is possible that much of the later strain was accommodated near the base of the intruding batholith in the Paleocene. Later stage intrusions that crosscut foliation in the Kluane Schist appear to be more peraluminous in composition and may reflect the tapping of a different source of magma along deep penetrating faults like the Denali fault and related structures.

METALLOGENIC IMPLICATIONS

Mineral potential in the project area is separated into two generalized categories: 1) porphyry and epithermal mineralization; and 2) orogenic gold.

PORPHYRY/EPITHERMAL OCCURRENCES

In the early 1970's a few companies had small exploration programs within the project area focussing mainly on Casino type Cu-Mo porphyries. These programs included only limited drilling and geochemical and geological ground surveys and assaying was restricted to molybdenum and copper (*e.g.*, Smith, 1971; Trigg, Woolet and Associates, 1971). From this era several new Cu-Mo porphyry showings were identified in the upper portion of the Ruby Range batholith and overlying Yukon-Tanana terrane. The newly-recognized crustal section described here allows for a more comprehensive look at the porphyry and epithermal potential of the area, as the geologic setting and structural levels of the batholith are better understood.

Widespread, mainly potassic and localized silicic alteration associated with the Raft Creek/Meloy prospect (Yukon MINFILE 115G070) near the top of the Ruby Range batholith is highly visible from the surrounding ridges and mountain tops. Similar reddish colour anomalies can be seen in other areas along the top of the Ruby Range batholith. Most of these are associated with other MINFILE occurrences. At the time of discovery, these mineral occurrences were described as Cu-Mo-Au porphyry systems similar to the Casino deposit located northwest of the study area. The occurrences in the study area are associated with the upper-most fractionated portion of the Ruby Range batholith, which is now known to be younger than Casino mineralization. At least one of the younger (based on crosscutting relationships with the Kluane Schist), peraluminous intrusions is known to host significant mineralization. An example of this late mineralization was discovered in a quarry along the Alaska Highway late in the field season. The occurrence consists of molybdenite, which occurs along a series of altered subvertical joint surfaces in the southern part of the project area (Fig. 24).

Silica ± potassic alteration was observed at the plutonic-volcanic transition (Fig. 25) in the upper part of the batholith. This alteration has the appearance of high sulfidation, epithermal style mineralization, found above and adjacent to deeper porphyry systems. The silica alteration is likely the result of highly acidic, low pH fluids infiltrating the host rock, dissolving everything but the silica.

Figure 24. *Parallel, strongly altered joint surfaces found in a peraluminous intrusion found within a quarry along the Alaska Highway. Molybdenum mineralization is often found within the alteration zones.*

Figure 25. *Massive silica alteration of quartz-feldspar porphyry from the top of the Ruby Range batholith. The alteration is likely the result of a high sulfidation epithermal system.*

OROGENIC GOLD - ANALOGIES WITH JUNEAU GOLD BELT

The tectonic framework observed within the project area is very similar to that of the Juneau Gold Belt in southeast Alaska (Fig. 26). In Alaska, around Juneau, the east-west juxtaposition of terranes includes the Yukon-Tanana terrane, thrust to the west over the late Paleozoic Taku terrane (a Late Paleozoic to Triassic metasedimentary and metavolcanic assemblage), which is itself thrust over the Jura-Cretaceous sedimentary rocks of the Gravina belt (McClelland and Mattinson, 2000; Miller *et al.*, 2000). Paleocene to Eocene intrusive rocks of the Coast plutonic complex occur between the Yukon-Tanana rocks and the Taku terrane. These plutonic rocks are thought to have intruded during deformation. Gold mineralization has been found in abundance within the plutonic rocks, leading to the use of the term Juneau gold belt when describing the metallogenic character of the area (Goldfarb *et al.*, 1988).

Southwestern Yukon comprises lithotectonic panels of similar age and affinity to those in southeastern Alaska, and preserves the same structural juxtaposition, with Yukon-Tanana terrane being thrust to the southwest over rocks of the Kluane Schist (Taku terrane analog). The Kluane Schist is interpreted to have been thrust to the southwest over Jura-Cretaceous rocks of the Dezadeash Formation. The Ruby Range batholith is age-equivalent to the Coast plutonic complex, and occurs at the same structural level as the complex.

The similarities between the two areas are striking and a metallogenic comparison between the two areas has previously been suggested (Wengzynowski, 1995). In southeastern Alaska there has been mining of several gold deposits for about 100 years, the most recent, the Kensington mine, opening in 2010. The numerous deposits have been interpreted as orogenic gold systems directly related to the tectonic processes active in southeast Alaska during the latest Cretaceous to Eocene (Miller *et al.*, 1994; Miller *et al.*, 1995). A generalized description of orogenic gold systems is one where regional hydrothermal fluids focus within crustal weaknesses in metamorphic rocks that are spatially associated with large-scale compressional to transpressional structures and abundant syn-tectonic plutonism (Groves *et al.*, 1998; Goldfarb *et al.*, 2001). The deposits typically consist of abundant quartz-carbonate veins formed over a broad range of temperatures and pressures, somewhere between 200-650°C and 1-5 kbar (Groves, 1993). The veins generally form late in the deformational-metamorphic-magmatic evolution and

mineralization is strongly structurally controlled, related to faults, shear zones and folds (Hodges, 1989; Groves *et al.*, 2003).

Known lode-gold occurrences in the Kluane Schist, although not well studied, have characteristics indicative of orogenic style mineralization. The vein system at Rockhaven Resources Ltd. Kluane project (Yukon MINFILE 115H 055, 115H 047) shares many of the characteristics of the orogenic-type gold veins found in the Juneau gold belt. Quartz-carbonate ± muscovite, arsenopyrite veins that host gold mineralization in the Kluane Schist have been described by Wengzynowski (1995) and Eaton (2003), and are similar to those observed within the Juneau gold belt (Miller *et al.*, 1995).

CONCLUSIONS

While only one summer of mapping has been completed in the area and most analytical data are not yet available to evaluate, a number of conclusions can be drawn from the work completed to date:

1. The structural stacking of the tectonic elements creates an exposed section of crust roughly 40 km thick. This section includes an entire batholith from its roots up into the porphyry and epithermal realms, and its overlying volcanic carapace.

2. The Ruby Range batholith is syn-to-post tectonic and becomes more felsic higher in the crustal section.

3. A unit of orthogneiss/paragneiss of uncertain age and correlation occurs along the base of the batholith and structurally above the Kluane Schist.
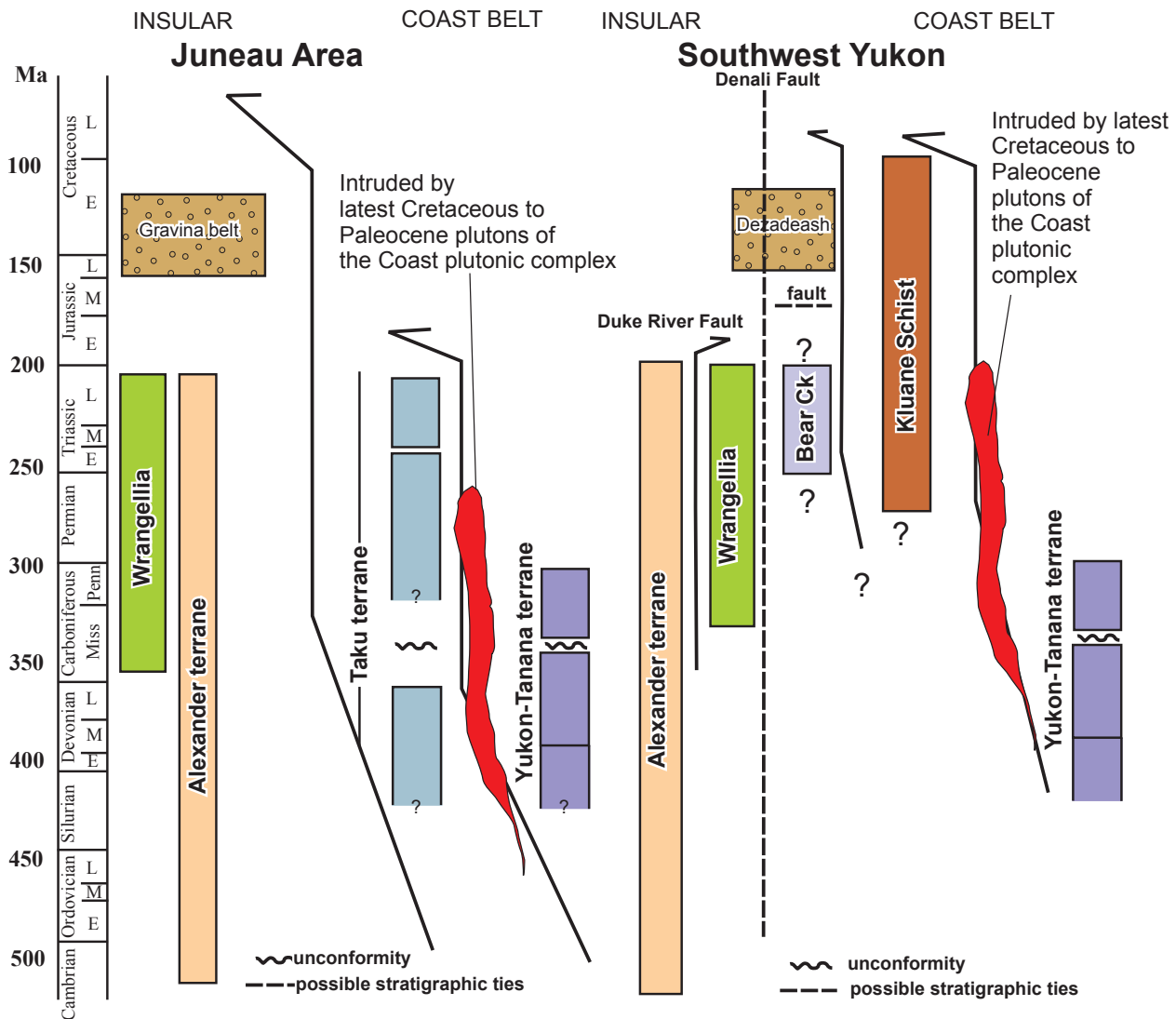
Figure 26. *Schematic stratigraphic sections from the Juneau area, southeast Alaska and the Coast Belt area, southwest Yukon. Alaska data modified from McClelland and Mattinson (2000) and Miller et al. (2000).*

4. The potential for porphyry and epithermal style mineralization increases up crustal section.

5. The depositional age of the Kluane Schist is constrained by detrital zircons as young as ~95 Ma. The provenance of the Kluane Schist is likely an uplifted Yukon-Tanana terrane and Jurassic to Cretaceous plutons of the Aishihik batholith and the Coast plutonic complex.

6. LA-ICPMS dating of metamorphic rims on Kluane Schist detrital zircons suggest that metamorphism significantly intense enough to cause Pb loss and new zircon growth occurred at ~82 Ma and ~70 Ma.

7. The lithotectonic relationships observed in southwestern Yukon are similar to those in southeastern Alaska, increasing the potential for orogenic-style gold mineralization.

ACKNOWLEDGEMENTS

REFERENCES

Bennett, V. and Tubrett, M., 2010. U-Pb isotopic age dating by LAM ICP-MS, INCO Innovation Centre, Memorial University: Sample preparation methodology and analytical techniques. *In:* Yukon Exploration and Geology 2009, K.E. MacFarlane, L.H. Weston and L.R. Blackburn (eds.), Yukon Geological Survey, p. 47-55.

Colpron, M., Mortensen, J.K., Gehrels, G.E. and Villeneuve, M.E., 2006. Basement complex, Carboniferous magmatic arcs and Paleozoic deformation in Yukon-Tanana terrane of central Yukon: Field, geochemical and geochronological constraints from Glenlyon map area. *In:* Paleozoic evolution and metallogeny of pericratonic terranes at the ancient Pacific margin of North America, Canadian and Alaskan Cordillera, M. Colpron and J.L. Nelson (eds.), Geological Association of Canada, Special Paper 45, p. 131-152.

Eaton, W.D., 2003. Hand trenching, propecting and soil geochemistry at the Ruby Range Project. Yukon Territorial Assessment Report 094415, 102 p.

Eisbacher, G.H., 1976. Sedimentology of the Dezadeash flysch and its implications for strike-slip faulting along the Denali fault, Yukon Territory and Alaska. Canadian Journal of Earth Sciences, vol. 13, p. 1495-1513.

Erdmer, P., 1991. Metamorphic terrane east of Denali fault between Kluane Lake and Kusawa Lake, Yukon Territory. *In:* Current Research, Part A, Geological Survey of Canada, Paper 91-1A, p. 37-42.

Erdmer, P. and Mortensen, J.K., 1993. A 1200-km-long Eocene metamorphic-plutonic belt in the northwestern Cordillera: Evidence from southwet Yukon. Geology, vol. 21, p. 1039-1042.

Gehrels, G.E., Rusmore, M.E., Woodsworth, G.J., Crawford, M.L., Andronicos, C.L., Hollister, L.S., Patchett, P.J., Ducea, M., Butler, R.F., Klepeis, K.A., Davidson, C., Friedman, R.M., Haggart, J., Mahoney, J.B., Crawford, W.A., Pearson, D. and Girardi, J., 2009. U-Th-Pb geochronology of the Coast Mountains batholith in north-coastal British Columbia: Constraints on age and tectonic evolution. Geological Society of America Bulletin, vol. 121, p. 1341-1361.

Goldfarb, R.J., Groves, D.I. and Gardoll, S., 2001. Orogenic gold and geologic time: a global perspective. Ore Geology Reviews, vol. 18, p. 1-75.

Goldfarb, R.J., Leach, D.L., Pickthorn, W.J. and Paterson, C.J., 1988. Orogin of lode-gold deposits in the Juneau gold belt, southeastern Alaska. Geology, vol. 16, p. 440-443.

Gordey, S.P. and Makepeace, A.J., 2003. Yukon Digital Geology (version 2). Geological Survey of Canada, Open File 1749.

Groves, D.I., 1993. The crustal continuum model for the late-Archean lode-gold deposits of the Yilgarn Block, Western Australia. Mineralia Deposita, vol. 28, p. 366-374.

Groves, D.I., Goldfarb, R.J., Robert, F. and Hart, C.J.R., 2003. Gold deposits in metamorphic belts: Overview of current understanding, outstanding problems, future research, and exploration significance. Economic Geology, vol. 98, p. 1-29.

Groves, D.I., Goldfarb, R.J., Grebre-Mariam, H., Hagemann, S.G. and Robert, F., 1998. Orogenic gold deposits-a proposed classification in the context of their crustal distribution and relationship to other gold deposit type. Ore Geology Reviews, vol. 13, p. 7-27.

Hodges, C.J., 1989. The structure of shear-related, vein-type gold deposits: A review. Ore Geology Reviews, vol. 4, p. 231-273.

Johnston, S.T. and Timmerman, J.R., 1994. Geology of the Aishihik Lake and Hopkins Lake map areas (115H6/7), southwestern Yukon. *In:* Yukon Exploration and Geology 1993, S.R. Morison (ed.), Indian and Northern affairs Canada, Exploration and Geological Services Division, p. 93-110.

Johnston, S.T. and Erdmer, P., 1995a. Hot-side-up aureole in southwest Yukon and limits on terrane assembly of the northern Canadian Cordillera. Geology, vol. 23, p. 419-422.

Johnston, S.T. and Erdmer, P., 1995b. Magmatic flow and emplacement foliations in the Early Jurassic Aishihik batholith, southwest Yukon: Implications for northern Stikinia. *In:* Jurassic magmatism and tectonics of the North American Cordillera, D.M. Miller and C. Busby (eds.), Geological Society of America, Special Paper 299, p. 65-82.

Johnston, S.T. and Canil, D., 2006. Crustal architecture of SW Yukon, northern Cordillera: Implications for crustal growth in a convergent margin orogen. Tectonics, vol. 26, p. 18.

Johnston, S.T., Mortensen, J.K. and Erdmer, P., 1996. Igneous and meta-igneous age constraints for the Aishihik metamorphic suite, southwest Yukon. Canadian Journal of Earth Sciences, vol. 33, p. 1543-1555.

Kiss, F., 2010. Residual total magnetic field, Kluane area aeromagnetic survey, Parts of NTS 115A, 115B, 115G and 115H, Yukon. Geological Survey of Canada, Open Files 6584 to 6591; Yukon Geological Survey Open Files 2010-21 to 2010-28.

Lowey, G., 1998. A new estimate of the amount of displacement on the Denali Fault system based on the occurence of carbonate megaboulders in the Dezadeash Formation (Jura-Cretaceous), Yukon, and the Nutzotin Mountains sequence (Jura-Cretaceous), Alaska. Bulletin of Canadian Petroleum Geology, vol. 46, p. 379-386.

Ludwig, K.R., 1999. IsoplotEX v.2.6. Berkeley Geochronological Center Special Publication 1a.

McClelland, W.C. and Mattinson, J.M., 2000. Cretaceous-Tertiary evolution of the western Coast Mountains, central southeastern Alaska. *In:* Tectonics of the Coast Mountains in southeast Alaska and British Columbia, H.H. Stowell and W.C. McClelland (eds.), Geological Society of America, Special Paper 343, p. 159-182.

Mezger, J.E., 2000. 'Alpine-type' ultramafic rocks of the Kluane metamorphic assemblage, southwest Yukon: Oceanic crust fragments of a late Mesozoic back-arc basin along the northern coast Belt. *In:* Yukon Exploration and Geology 1999, D.S. Emond and L.H. Weston (eds.), Exploration and Geological Services Division, Yukon Region, Indian and Northern Affairs Canada, p. 127-138.

Mezger, J.E., Chacko, T. and Erdmer, P., 2001a. Metamorphism at a late Mesozoic accretionary margin: a study from the Coast Belt of the North American Cordillera. Journal of metamorphic Geology, vol. 19, p. 121-137.

Mezger, J.E., Creaser, R., Erdmer, P. and Johnson, S.E., 2001b. A Cretaceous back-arc basin in the Coast Belt of the northern Canadian Cordillera: evidence from geochemical and neodynium isotope characterisitics of the Kluane metamorphic assemblage, southwest Yukon. Canadian Journal of Earth Sciences, vol. 38, p. 91-103.

Miller, L.D., Stowell, H.H. and Gehrels, G.E., 2000. Progressive deformation associated with mid-Cretaceous to Tertiary contractional tectonism in the Juneau gold belt, Coast Mountains southeastern Alaska. *In:* Tectonics of the Coast Mountains, Southeastern Alaska and British Columbia, H.H. Stowell and W.C. McClelland (eds.), Geological Society of America, Special Paper 343, p. 193-233.

Miller, L.D., Goldfarb, R.J., Gehrels, G.E. and Snee, L.W., 1994. Genetic links among fluid cycling, vein formation, regional deformation and plutonism in the Juneau gold belt, southeastern Alaska. Geology, vol. 22, p. 203-206.

Miller, L.D., Goldfarb, R.J., Gent, C.A. and Kirkham, R.A., 1995. Structural geology, age, mechanisms of gold formation at the Kensington deposits, Berners Bay district, southeast Alaska. Economic Geology, vol. 90, p. 343-368.

Muller, J.E., 1967. Kluane Lake map-area, Yukon Territory. Geological Survey of Canada, Memoir 340, p. 137.

Murphy, D.C., 2007. The three 'Windy McKinley' terranes of Stevenson Ridge (115JK), western Yukon. *In:* Yukon Exploration and Geology, D.S. Emond, L.L. Lewis and L.H. Weston (eds.), Yukon Geological Survey, p. 223-236.

Murphy, D.C., van Staal, C.R. and Mortensen, J.K., 2008. Windy McKinley terrane, Stevenson Ridge area (115JK), western Yukon: composition and proposed correlations, with implications for mineral potential. *In:* Yukon Exploration and Geology, D.S. Emond, L.R. Blackburn, R.P. Hill and L.H. Weston (eds.), Yukon Geological Survey, p. 225-235.

Murphy, D.C., Mortensen, J.K. and van Staal, C.R., 2009. 'Windy-McKinley' terrane, western Yukon: new data bearing on its composition, age, correlation and paleotectonic settings. *In:* Yukon Exploration and Geology, L.H. Weston, L.R. Blackburn and L.L. Lewis (eds.), Yukon Geological Survey, p. 195-209.

Murphy, D.C., Mortensen, J.K., Piercey, S.J., Orchard, M.J. and Gehrels, G.E., 2006. Mid-Paleozoic to early Mesozoic tectonostratigraphic evolution of Yukon-Tanana and Slide Mountain terranes and affiliated overlap assemblages, Finlayson Lake massive sulphide district, southeastern Yukon. *In:* Paleozoic evolution and metallogeny of pericratonic terranes at the ancient Pacific margin of North America, Canadian and Alaskan Cordillera, M. Colpron and J.L. Nelson (eds.), Geological Association of Canada, Special Paper 45, p. 75-105.

Nelson, J.L., Colpron, M., Piercey, S.J., Dusel-Bacon, C., Murphy, D.C. and Roots, C.F., 2006. Paleozoic tectonic and metallogenic evolution of the pericratonic terranes in Yukon, northern British Columbia and eastern Alaska. *In:* Paleozoic evolution and metallogeny of pericratonic terranes at the ancient Pacific margin of North America, Canadian and Alaskan Cordillera, M. Colpron and J.L. Nelson (eds.), Geological Association of Canada, Special Paper 45, p. 323-360.

Piercey, S.J., Nelson, J.L., Colpron, M., Dusel-Bacon, C., Simard, R.-L. and Roots, C.F., 2006. Paleozoic magmatism and crustal recycling along the ancient Pacific margin of North America, northern Cordillera. *In:* Paleozoic evolution and metallogeny of pericratonic terranes at the ancient Pacific margin of North America, Canadian and Alaskan Cordillera, M. Colpron and J.L. Nelson (eds.), Geological Association of Canada, Special Paper 45, p. 281-322.

Smith, F.M., 1971. Geological and geochemical report on the Alaskite project claims Ed and Add groups, Claim sheet 115G8, Rockslide and Alaskite Ck area Yukon Territory. Yukon Territorial Assessment Report 060194, 33 p.

Tempelman-Kluit, D.J., 1974. Reconnaissance geology of Aishihik Lake, Snag and part of Stewart River map areas, west-central Yukon. Geological Survey of Canada, Paper 73-21.

Trigg, Woollett and Associates., 1971. Exploration 1971- Max Mineral Claim Group, Ryholite Creek, Yukon Territory. Yukon Territorial Mineral Assessment Report 060991, 90 p.

Wengzynowski, W., 1995. Prospecting, soil geochemistry, trenching and geophysical surveys at the Ruby Range project. Yukon Territorial Assessment Report 093250, 148 p.

Wheeler, J.O. and McFeely, P., 1991. Tectonic assemblage map of the Canadian Cordillera and adjacent parts of the United States of America. Geological Survey of Canada, scale 1:2 000 000.

Yukon MINFILE, 2009. Yukon MINFILE – A database of mineral occurrences. Yukon Geological Survey, <*http://www.geology.gov.yk.ca/databases_gis.html*>.

Appendix 1. Detrital zircon data for sample 09SIT11

	CONCORDIA COLUMNS 207/235	7/5 err	206/238	6/8 err	Rho	207/206	7/6 err	2 s % 207/235	2 s % 206/238	2 s % 207/206	AGES Ma 7/5 age	1 sigma	6/8 age	1 sigma	7/6 age	1 sigma	Concordia age (Ma)	2σ error Ma	MSWD (of concordance)	Probability (of concordance)	ppm Th232	ppm U238	Ratio Th/U
Phanerozoic Ages																							
no09a07	0.0998	0.0055	0.0129	0.0008	0.5920	0.0698	0.0081	10.9	13.0	23.2	97	5	83	5	922	238	90.4	9.2	8.76	0.003	15	34	0.42
no09a08	0.0985	0.0048	0.0151	0.0009	0.6237	0.0508	0.0033	9.7	12.1	12.9	95	6	96	4	233	149	95.6	8.7	0.06	0.809	25	68	0.36
no09a09	0.2469	0.0107	0.0307	0.0009	0.2812	0.0602	0.0027	8.7	4.9	9.0	224	6	195	9	611	97	198.5	9.1	11.26	0.001	82	220	0.37
no09a11	0.2014	0.0088	0.0298	0.0006	0.2292	0.0513	0.0027	8.8	4.0	10.6	186	4	189	7	255	122	188.7	7.2	0.14	0.706	66	135	0.49
no09a12	0.1734	0.0066	0.0243	0.0004	0.2228	0.0535	0.0024	7.6	3.4	8.8	162	3	155	6	352	100	155.4	5.1	1.84	0.175	271	558	0.49
no09a15	0.3875	0.0188	0.0524	0.0015	0.2848	0.0549	0.0024	9.7	5.5	8.8	333	9	329	14	407	98	330.0	16.7	0.05	0.822	61	128	0.48
no09a24	0.2169	0.0076	0.0318	0.0007	0.3184	0.0512	0.0023	7.0	4.5	9.1	199	4	202	6	252	105	201.1	8.3	0.14	0.713	66	252	0.26
no09a25	0.2198	0.0068	0.0318	0.0006	0.2989	0.0518	0.0019	6.2	3.7	7.2	202	4	202	6	278	83	201.6	6.9	0.00	0.974	96	253	0.38
no09a27	0.1201	0.0037	0.0185	0.0004	0.3697	0.0488	0.0020	6.2	4.6	8.0	115	3	118	3	138	94	117.0	4.8	0.61	0.436	35	331	0.29
no09a30	0.2175	0.0078	0.0313	0.0008	0.3752	0.0527	0.0023	7.2	5.4	8.8	200	5	199	7	316	100	199.1	9.6	0.03	0.866	95	114	0.31
no09a34	0.1035	0.0076	0.0149	0.0007	0.3133	0.0566	0.0069	14.6	9.2	24.2	100	4	95	7	476	268	96.0	8.2	0.51	0.476	45	73	0.61
no09a36	0.1886	0.0083	0.0279	0.0005	0.1910	0.0504	0.0021	8.8	3.4	8.2	175	3	177	3	213	95	177.3	5.7	0.08	0.783	114	278	0.41
no09a37	0.1907	0.0094	0.0282	0.0006	0.2274	0.0492	0.0028	9.8	4.6	9.3	177	4	179	4	203	108	179.0	7.6	0.07	0.798	168	338	0.50
no09a49	0.0990	0.0047	0.0151	0.0003	0.2450	0.0502	0.0023	9.5	4.5	11.2	96	2	97	2	158	131	96.5	4.3	0.03	0.863	317	688	0.46
no09a50	0.2283	0.0166	0.0330	0.0015	0.3068	0.0536	0.0042	14.5	8.9	15.6	209	9	209	14	356	177	209.1	17.1	0.00	0.974	43	91	0.48
no09a51	0.1334	0.0186	0.0194	0.0022	0.4043	0.0538	0.0096	27.9	22.6	35.7	127	14	126	17	363	403	126.7	25.4	0.00	0.965	37	81	0.46
no09a52	0.1882	0.0082	0.0294	0.0010	0.2472	0.0472	0.0020	8.7	6.8	8.5	175	6	187	7	58	101	182.1	10.9	2.67	0.102	197	489	0.40
no09a54	0.0990	0.0049	0.0148	0.0004	0.3158	0.0491	0.0023	9.9	4.9	9.2	96	2	95	5	153	108	94.9	4.4	0.08	0.806	353	662	0.53
no09a60	0.1805	0.0082	0.0247	0.0007	0.3158	0.0550	0.0030	9.0	5.7	11.0	169	4	157	7	411	123	159.3	8.4	2.65	0.104	79	303	0.26
no09a62	0.1040	0.0063	0.0135	0.0004	0.2482	0.0570	0.0032	12.0	6.0	11.1	100	3	87	6	428	123	87.9	5.0	5.81	0.016	191	291	0.65
no09a64	0.1100	0.0064	0.0153	0.0004	0.2248	0.0554	0.0041	10.4	6.2	14.9	106	3	98	5	555	166	99.3	5.8	2.33	0.127	113	238	0.47
no09a70	0.1167	0.0066	0.0152	0.0004	0.2533	0.0587	0.0039	11.3	5.1	13.5	112	2	97	6	510	147	98.2	4.8	6.23	0.013	137	222	0.62
no09a74	0.2717	0.0124	0.0349	0.0008	0.2522	0.0575	0.0025	9.1	4.6	8.5	244	5	221	10	218	94	224.1	9.7	5.17	0.023	54	154	0.35
no09a75	0.1027	0.0032	0.0151	0.0002	0.2307	0.0483	0.0017	6.2	3.2	6.7	99	2	97	3	112	77	97.0	2.9	0.76	0.384	116	395	0.29
no09a76	0.0964	0.0026	0.0149	0.0002	0.2452	0.0488	0.0016	5.5	2.5	6.7	93	2	95	2	95	79	94.8	2.3	0.41	0.522	351	1087	0.32
no09a86	0.4050	0.0091	0.0523	0.0007	0.2990	0.0567	0.0013	4.5	2.7	4.8	345	4	329	7	482	52	332.5	8.1	5.92	0.015	123	378	0.33
no09a88	0.0951	0.0031	0.0145	0.0002	0.2452	0.0488	0.0017	6.5	3.2	7.2	92	1	93	3	138	84	92.7	2.8	0.04	0.838	154	528	0.29
no09a95	0.1317	0.0118	0.0200	0.0003	0.2525	0.0491	0.0035	18.0	9.1	14.4	126	6	128	11	154	168	127.5	11.0	0.05	0.830	45	131	0.35
no09a98	0.0980	0.0042	0.0155	0.0003	0.2139	0.0472	0.0021	8.5	3.6	9.1	95	2	99	4	60	108	98.5	3.5	1.12	0.291	125	336	0.37
no09a100	0.4087	0.0301	0.0523	0.0017	0.2139	0.0576	0.0049	14.8	6.3	17.0	348	10	329	22	514	187	330.8	19.6	0.76	0.383	14	91	0.16
no09a101	0.2318	0.0111	0.0340	0.0008	0.2407	0.0501	0.0023	9.5	4.6	9.0	212	5	215	9	200	104	214.8	9.3	0.16	0.689	48	260	0.18
no09a107	0.3953	0.0173	0.0533	0.0012	0.2624	0.0547	0.0020	8.7	4.6	7.3	338	7	335	13	400	82	335.6	14.2	0.07	0.798	241	765	0.32
no09a109	0.1843	0.0071	0.0270	0.0005	0.2223	0.0503	0.0017	7.7	3.4	6.9	172	3	172	6	208	79	172.0	5.6	0.00	0.965	171	487	0.35
no09a112	0.1369	0.0064	0.0206	0.0005	0.2586	0.0554	0.0027	9.4	4.9	10.8	130	3	131	6	186	126	131.3	6.0	0.04	0.838	122	301	0.41
no09a113	0.0939	0.0040	0.0130	0.0004	0.3955	0.0566	0.0017	8.6	6.8	9.6	91	3	83	4	477	106	85.5	5.2	4.39	0.036	53	120	0.44
no09a119	0.2291	0.0065	0.0320	0.0005	0.2699	0.0534	0.0032	5.7	3.1	6.2	209	3	203	5	348	70	203.9	5.9	1.50	0.221	108	259	0.42
no09a120	0.0978	0.0042	0.0149	0.0005	0.3870	0.0531	0.0029	8.6	5.0	12.2	95	3	96	5	333	138	95.3	5.8	0.05	0.827	52	123	0.43
no09a121	0.2113	0.0100	0.0308	0.0008	0.2616	0.0522	0.0027	9.5	5.6	11.0	195	5	196	8	296	126	195.6	9.1	0.02	0.894	41	157	0.26
no09a122	0.1100	0.0057	0.0158	0.0005	0.2966	0.0520	0.0029	10.4	6.2	10.4	106	3	101	5	318	119	102.1	5.9	0.80	0.371	187	385	0.49
no09a123	0.2128	0.0119	0.0308	0.0009	0.2518	0.0527	0.0033	11.2	5.6	12.6	196	5	196	10	387	143	195.6	10.4	0.00	0.974	29	121	0.24
no09a126	0.4178	0.0129	0.0567	0.0008	0.2256	0.0544	0.0018	6.2	2.8	6.4	354	3	355	9	224	72	355.3	9.2	0.01	0.921	101	270	0.37
no09a130	0.2108	0.0071	0.0313	0.0005	0.2466	0.0506	0.0035	6.8	3.3	7.0	194	3	199	6	339	81	198.2	6.2	0.59	0.442	58	239	0.24
no09a131	0.0996	0.0052	0.0144	0.0004	0.2922	0.0532	0.0021	10.5	6.2	13.2	96	3	92	5	240	150	92.7	5.4	0.85	0.356	136	480	0.28
no09a132	0.2121	0.0084	0.0312	0.0007	0.2811	0.0513	0.0012	7.9	4.4	8.3	195	4	198	7	255	96	197.6	8.2	0.17	0.681	98	225	0.43
no09a133	0.2416	0.0050	0.0351	0.0006	0.3166	0.0530	0.0018	4.1	1.9	4.6	220	2	222	4	-63	53	221.9	4.0	0.37	0.544	99	718	0.14
no09a137	0.2234	0.0066	0.0318	0.0006	0.2572	0.0449	0.0017	5.9	3.7	6.9	205	4	202	5	124	78	202.7	6.9	0.24	0.626	100	303	0.33
no09a138	0.1011	0.0042	0.0167	0.0004	0.3861	0.0553	0.0047	8.2	4.2	7.5	98	2	107	4	422	91	105.1	4.3	5.35	0.021	43	680	0.06
no09a139	0.0955	0.0077	0.0154	0.0010	0.4191	0.0501	0.0040	16.0	12.4	14.6	93	6	98	7	199	230	96.1	10.8	0.59	0.393	51	142	0.36
no09a144	0.1034	0.0056	0.0149	0.0007	0.2580	0.0517	0.0015	10.9	6.3	15.7	100	3	95	5	271	163	96.2	5.7	0.73	0.442	46	119	0.39
no09a145	0.0875	0.0051	0.0142	0.0004	0.2471	0.0477	0.0037	11.7	6.3	5.9	85	4	91	4	83	182	88.5	7.7	1.48	0.224	33	85	0.38
no09a146	0.2031	0.0053	0.0292	0.0009	0.2658	0.0608	0.0018	5.2	2.7	5.9	188	4	185	7	630	67	185.8	4.7	0.25	0.614	184	497	0.37
no09a151	0.1076	0.0029	0.0168	0.0004	0.2164	0.0507	0.0014	5.5	2.5	5.9	104	1	108	6	225	70	107.0	2.7	2.02	0.156	452	842	0.54
no09a152	0.2623	0.0137	0.0324	0.0009	0.2800	0.0513	0.0037	12.2	5.5	12.2	237	6	205	11	256	131	209.0	10.9	7.91	0.005	24	104	0.23
no09a153	0.2118	0.0073	0.0312	0.0005	0.2164	0.0503	0.0028	7.1	3.0	7.1	195	3	198	6	209	83	197.9	5.7	0.29	0.593	116	383	0.30
no09a156	0.2114	0.0112	0.0309	0.0004	0.2800	0.0509	0.0018	10.6	5.9	10.6	195	6	196	9	238	125	195.8	10.8	0.02	0.892	63	234	0.27
no09a157	0.1046	0.0060	0.0156	0.0004	0.1988	0.0498	0.0031	11.4	5.9	12.2	101	2	100	5	188	142	100.1	4.4	0.03	0.857	98	400	0.24
no09a159	0.1663	0.0032	0.0243	0.0003	0.2929	0.0501	0.0011	3.8	2.2	4.3	156	2	155	3	199	50	155.0	3.2	0.29	0.588	483	1472	0.33
no09a160	0.0942	0.0052	0.0141	0.0004	0.2406	0.0515	0.0032	10.9	5.3	10.1	91	2	90	5	262	149	90.3	4.6	0.08	0.776	77	384	0.20
no09a161	0.0995	0.0053	0.0147	0.0004	0.2488	0.0529	0.0025	10.7	5.3	6.2	96	2	94	6	323	118	94.5	4.8	0.18	0.675	178	482	0.37
no09a162	0.2224	0.0069	0.0319	0.0006	0.1982	0.0515	0.0016	6.2	2.4	10.3	204	2	202	6	262	71	202.3	4.7	0.09	0.765	132	978	0.14
no09a163	0.1014	0.0051	0.0144	0.0006	0.3840	0.0529	0.0027	10.1	7.8	6.5	98	4	92	5	324	117	93.6	6.6	1.73	0.189	18	409	0.04
Precambrian Ages																							
no09a38	4.7953	0.0527	0.3185	0.0027	0.3808	0.1113	0.0011	2.2	1.7	2.0	1784	13	1782	9	1821	18	1783.7	17.4	0.02	0.891	82	184	0.45
no09a39	5.3082	0.1200	0.3354	0.0056	0.3678	0.1181	0.0032	4.5	3.3	5.5	1870	27	1865	19	1928	49	1868.8	36.2	0.04	0.836	29	34	0.85
no09a48	5.1197	0.0782	0.3282	0.0035	0.3512	0.1148	0.0017	3.1	2.1	2.9	1839	17	1830	13	1877	26	1836.5	23.8	0.30	0.587	83	144	0.58
no09a56	11.4497	0.1563	0.4888	0.0057	0.4275	0.1735	0.0026	2.7	2.3	3.0	2560	25	2566	13	2592	25	2560.8	25.4	0.05	0.818	30	57	0.53
no09a73	6.2866	0.0687	0.3577	0.0042	0.5312	0.1288	0.0021	2.2	2.8	2.6	2017	20	1971	10	2082	23	2017.9	19.1	7.41	0.006	130	233	0.56
no09a83	1.8404	0.0508	0.1813	0.0026	0.2570	0.0746	0.0011	5.5	5.7	5.7	1060	14	1074	18	1058	57	1069.2	24.7	0.48	0.487	48	180	0.27
no09a85	5.5991	0.1407	0.3439	0.0070	0.4069	0.1193	0.0022	5.0	4.1	3.8	1916	34	1905	22	1946	34	1914.2	42.0	0.11	0.740	120	145	0.83
no09a148	6.9175	0.1411	0.3487	0.0052	0.3660	0.1463	0.0022	4.1	3.0	3.0	2101	25	1929	18	2303	26	2048.6	34.8	48.12	0.000	111	190	0.58
no09a149	3.3930	0.1105	0.2215	0.0052	0.3581	0.1127	0.0019	6.5	4.7	3.4	1503	27	1290	26	1844	31	1389.4	45.5	48.53	0.000	123	207	0.59

Appendix 2. *Detrital zircon data for sample 08DM126.*

Analysis No.	$^{207}Pb/^{235}U$ Ma	$^{207}Pb/^{235}U$ +/- 1σ Error	$^{206}Pb/^{238}U$ Ma	$^{206}Pb/^{238}U$ +/- 1σ Error	$^{207}Pb/^{206}Pb$ Ma	$^{207}Pb/^{206}Pb$ +/- 1σ Error	Preferred Age Ma *	+/- 1σ Error	Discordancy %
08DM-126L2	104.2	2.16	104.5	1.01	112.5	53.27	**104.5**	**1.0**	7.1
08DM-126L3	83.1	22.65	83.1	4.54	89.1	565.96	**83.1**	**4.5**	6.7
08DM-126L4	80	0.96	79.7	0.69	85.9	35.03	**79.7**	**0.7**	7.2
08DM-126L5	195	3.55	191.4	1.86	211.7	46.72	**191.4**	**1.9**	9.6
08DM-126L6	86	3.62	81.7	1.26	199	100.8	**81.7**	**1.3**	58.9
08DM-126L7	79.6	3.7	79.5	1.14	77.5	113.42	**79.5**	**1.1**	-2.6
08DM-126L8	191.4	2.93	190.6	1.75	199.6	40.61	**190.6**	**1.8**	4.5
08DM-126L9	87.4	4.26	87.4	1.35	85.5	118.87	**87.4**	**1.4**	-2.2
08DM-126L10	112	1.76	111.7	1.05	109.3	41.95	**111.7**	**1.1**	-2.2
08DM-126L11	193.3	3.02	191.5	1.8	191.4	41.13	**191.5**	**1.8**	-0.1
08DM-126L12	88	5.26	88.1	1.61	88.4	143.95	**88.1**	**1.6**	0.3
08DM-126L13	167.4	5.63	166.1	2.08	180.1	82.27	**166.1**	**2.1**	7.8
08DM-126L15	78.2	4.19	78	1.18	75.7	129.55	**78.0**	**1.2**	-3.0
08DM-126L16	80	2.01	80.4	0.86	85.8	64.32	**80.4**	**0.9**	6.3
08DM-126L17	328.1	3.64	328.3	2.87	335.4	31.07	**328.3**	**2.9**	2.1
08DM-126L18	180.2	2.33	180.5	1.63	180.5	35.49	**180.5**	**1.6**	0.0
08DM-126L19	207	4.85	199.4	2.31	201.9	57.58	**199.4**	**2.3**	1.2
08DM-126L20	101	1.58	101.2	0.96	102.1	41.58	**101.2**	**1.0**	0.9
08DM-126L21	108.2	4.29	112.4	1.83	131.9	96.11	**112.4**	**1.8**	14.8
08DM-126L22	105.1	7.33	79.7	2.06	797.6	149.09	**79.7**	**2.1**	90.0
08DM-126L23	117.3	2.58	116	1.27	130.8	55.65	**116.0**	**1.3**	11.3
08DM-126L24	187.5	3.11	185.1	1.83	186.1	42.97	**185.1**	**1.8**	0.5
08DM-126L25	95.2	2.73	94.4	1.08	92.4	72.46	**94.4**	**1.1**	-2.2
08DM-126L26	126.8	3.93	128.5	1.56	122.8	76.79	**128.5**	**1.6**	-4.6
08DM-126L27	197.2	2.69	195	1.86	201	36.26	**195.0**	**1.9**	3.0
08DM-126L28	91.1	2.41	87.3	1.1	103.5	66	**87.3**	**1.1**	15.7
08DM-126L29	187.9	2.05	185.8	1.68	205.4	30.62	**185.8**	**1.7**	9.5
08DM-126L30	295.4	3.61	294.5	2.72	301.2	33.06	**294.5**	**2.7**	2.2
08DM-126L31	78.8	3.26	78.6	1.12	79.9	101.53	**78.6**	**1.1**	1.6
08DM-126L32	1823.2	22.18	1807	16.74	1835.4	27.22	**1835.4**	**27.2**	1.5
08DM-126L33	146.1	11.83	148.2	3.64	164.3	188.99	**148.2**	**3.6**	9.8
08DM-126L34	97.3	4.67	96.6	1.59	107.9	115.69	**96.6**	**1.6**	10.5
08DM-126L35	81.1	1.76	79.7	0.88	77.6	55.74	**79.7**	**0.9**	-2.7
08DM-126L36	1822.7	10.25	1819.4	14.53	1813.5	20.95	**1813.5**	**21.0**	-0.3
08DM-126L37	106.2	1.13	105.9	0.97	120.1	29.65	**105.9**	**1.0**	11.8
08DM-126L38	85.6	4.34	84.6	1.36	86.4	123.32	**84.6**	**1.4**	2.1
08DM-126L39	213.1	13.72	207.6	4.91	215.7	149.79	**207.6**	**4.9**	3.8
08DM-126L40	206.9	8.9	205.8	3.58	204.3	101.89	**205.8**	**3.6**	-0.7
08DM-126L41	1168.1	13.18	1142.9	10.67	1251.2	28.42	**1251.2**	**28.4**	8.7
08DM-126L42	82	3.21	83.2	1.32	85.5	96.34	**83.2**	**1.3**	2.7
08DM-126L43	83.7	6.82	83.8	2.01	92.6	192.37	**83.8**	**2.0**	9.5
08DM-126L44	173.6	6.08	171.6	2.56	174.6	84.52	**171.6**	**2.6**	1.7
08DM-126L45	197.4	6.11	192.8	2.62	189.7	75.18	**192.8**	**2.6**	-1.6
08DM-126L46	194.4	3.92	192.8	2.18	194.5	50.01	**192.8**	**2.2**	0.9
08DM-126L47	103.5	3.02	101.3	1.39	111.8	71.62	**101.3**	**1.4**	9.4
08DM-126L48	342.4	3.68	341.1	3.22	337.2	29.3	**341.1**	**3.2**	-1.2
08DM-126L49	195	7.12	198.1	3.02	205.8	87.67	**198.1**	**3.0**	3.7
08DM-126L50	121.6	3.39	119.5	1.46	125.3	68.57	**119.5**	**1.5**	4.6
08DM-126L51	207.6	5.04	205.6	2.64	218.9	59.85	**205.6**	**2.6**	5.6
08DM-126L52	170.4	5.14	174.5	2.49	172.6	74.03	**174.5**	**2.5**	0.1
08DM-126L53	82.8	9.76	82.6	2.02	80.3	270.69	**82.6**	**2.0**	-3.0
08DM-126L54	104.9	6.86	105.9	2.46	100.5	156.48	**105.9**	**2.5**	-4.9
08DM-126L55	206.8	6.53	208.3	2.95	200.5	77.44	**208.3**	**3.0**	-3.5
08DM-126L56	110.8	1.78	110.1	1.22	112.6	40.93	**110.1**	**1.2**	1.9
08DM-126L57	77.8	2.79	77.5	1.23	81.7	88.94	**77.5**	**1.2**	5.0
08DM-126L58	82.6	1.49	82.4	0.94	87.7	46.4	**82.4**	**0.9**	5.9
08DM-126L59	188.9	3.91	189.4	2.28	190.7	51.48	**189.4**	**2.3**	0.8
08DM-126L60	114.8	5.29	103.2	1.72	382.8	106.66	**103.2**	**1.7**	71.5
08DM-126L61	170.5	6.14	173.6	2.71	183.1	87.41	**173.6**	**2.7**	6.0
08DM-126L62	79.9	3.41	80.3	1.27	87	104.68	**80.3**	**1.3**	7.9
08DM-126L63	81.8	9.05	82	2.35	92.2	255.9	**82.0**	**2.4**	11.2
08DM-126L64	76.9	3.73	78.2	1.38	77.7	118.23	**78.2**	**1.4**	0.2
08DM-126L65	83.4	2.61	84	1.24	83.4	77.87	**84.0**	**1.2**	-0.4

Preliminary observations on stratigraphy and hydrocarbon potential of middle to Upper Cretaceous strata, Eagle Plain basin, northern Yukon

Kevin Jackson[1], Michael McQuilkin, Per Kent Pedersen, and Rudi Meyer
Department of Geoscience, University of Calgary, Calgary, Alberta

Larry S. Lane
Geological Survey of Canada, Calgary, Alberta

ABSTRACT

The Eagle Plain basin, having proven hydrocarbon potential, is a relatively underexplored intermontane basin located in northern Yukon . Previous studies of the middle Albian-Cenomanian Parkin Formation and the Turonian Fishing Branch Formation are based on broad lithostratigraphic correlations. The primary goal of the study is to refine the sequence stratigraphic framework of the middle to Upper Cretaceous succession based on sedimentological observations. New findings from this study require subdivision of the stratigraphic nomenclature by defining new informal lithological members. Facies transitions, paleoflow indicators and isopach maps indicate overall westward deepening of the basin. Large-scale, sand-prone mass transport deposits observed in the upper part of the lower Parkin shale member in western Eagle Plain indicate the presence of shelf-to-basin floor relief of at least 100 m. Recognition of significant shelf-to-basin floor topography greatly increases the potential for hydrocarbon reservoirs (gas-dominated) in stratigraphic traps associated with the shelf edge.

[1]kwjackso@ucalgary.ca

INTRODUCTION

This project is part of the Geo-mapping for Energy and Minerals (GEM) program conducted by the Geological Survey of Canada in collaboration with the Yukon Geological Survey and universities. GEM is a five year program (concluding in 2013) intended to provide new public domain geoscience information to identify the energy and mineral resource potential of northern Canada.

The objective of this study is to refine the stratigraphic framework for the middle to Upper Cretaceous succession of the Eagle Plain basin by integrating seismic, outcrop, core, well log and petrographic data, and to present some initial sedimentological interpretations. A concurrent biostratigraphic study will be incorporated to publish an updated hydrocarbon resource assessment of the succession. Comparison of new data with research from adjacent basins is also a priority, as it is vital to understanding regional-scale sedimentation patterns and paleogeography in northern Yukon and Northwest Territories.

FIELD RESEARCH

Eight weeks of cumulative field work was carried out in the summers of 2009 and 2010 in the Eagle Plain area. Eagle Plain consists of low-lying, rolling topography dominated by north-trending Laramide-aged structures of the Eagle foldbelt. The study area is located roughly between latitudes of 65°N and 67°N, and longitudes of 136°W and 139°W (Fig. 1).

The middle Albian-Cenomanian Parkin Formation and the Turonian Fishing Branch Formation are the primary units investigated in this study (Fig. 2). Over one hundred field samples were collected, from which key specimens were slabbed and sectioned for petrographic analysis. Shale samples were collected to study foraminiferal assemblages and Rock-Eval pyrolysis for organic geochemistry and thermal maturity.

REGIONAL STRATIGRAPHY

The Eagle Plain basin is a relatively unexplored intermontane basin with proven hydrocarbon potential located in northern Yukon. Out of 34 exploratory wells drilled in Eagle Plain since 1957, five encountered significant hydrocarbons. Well control is largely concentrated in the southern and eastern parts of the

basin, and large gaps exist in our understanding of the subsurface.

Proterozoic to Quaternary-aged strata are preserved in the sedimentary record of Eagle Plain basin. The Cretaceous succession is up to 2 km thick and underlies the majority of the study area at surface. The middle to Upper Cretaceous succession of Eagle Plain consists of two major transgressive-regressive clastic cycles of the Eagle Plain Group, as defined by Dixon (1992a). Mountjoy (1967) assigned the type section of the Eagle Plain Group to outcrops along the Fishing Branch River in the western part of Eagle Plain basin (Fig. 3).

Eagle Plain was located at the northern terminus of the Cordilleran Foreland Basin during the middle to Late Cretaceous. Provenance is interpreted to be from the encroaching Cordilleran orogen to the south, while open-marine and offshore conditions prevailed to the north (Dixon, 1992a). Extensional tectonism was dominant during the middle Cretaceous, and syndepositional faulting may have had a significant influence on the basin profile.

Existing interpretations of Cretaceous basin morphology were based on lithostratigraphic correlations and suggested deposition in a broad, low-angle shelf setting in the Cordilleran Foreland Basin (Dixon, 1992a). However, observations from this study indicate greater stratigraphic complexity than previously recognized, necessitating subdivision of the current nomenclature (Fig. 4). Several new informal stratigraphic members are defined and discussed briefly in this report.

PRELIMINARY RESULTS AND DISCUSSION

DEVELOPMENTS IN STRATIGRAPHIC FRAMEWORK

PARKIN FORMATION

The Parkin Formation is described by Dixon (1992a) as consisting of a basal transgressive sandstone member and an overlying shale member which lies unconformably on lower Albian shales of the Whitestone River Formation. It is overlain gradationally by the regressive Fishing Branch Formation. Dixon (1992a) divided the Parkin Formation into a basal sandstone member and overlying shale member; the unit is further subdivided herein, based on observations from this study.
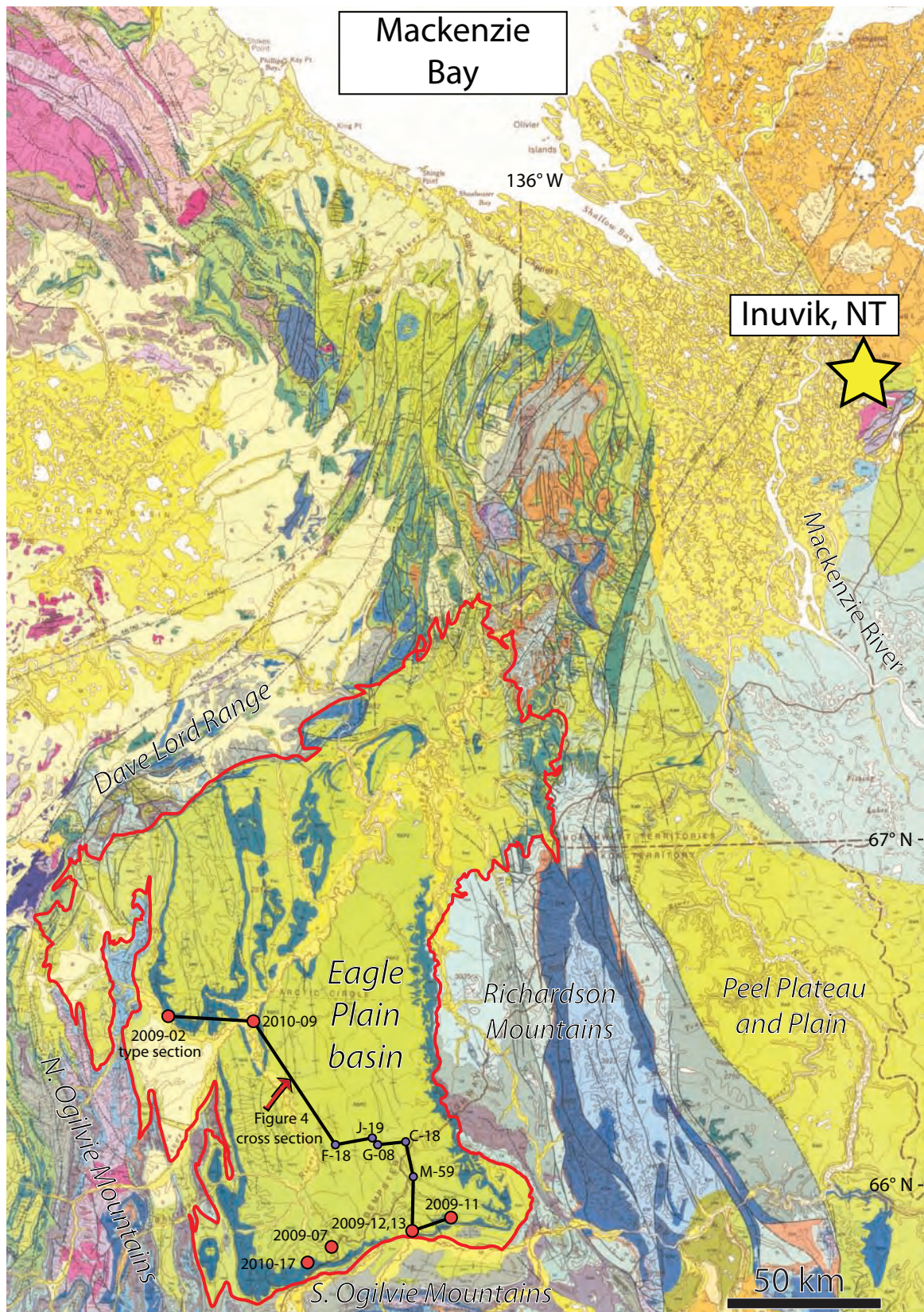
Figure 1. *Geological map of northern Yukon Territory and adjacent Northwest Territories indicating location of the Eagle Plain basin (outlined in red) and major geomorphological elements. Cretaceous bedrock (green and blue-green on map) underlies the majority of Eagle Plain at surface. (Modified from Norris, 1984)*
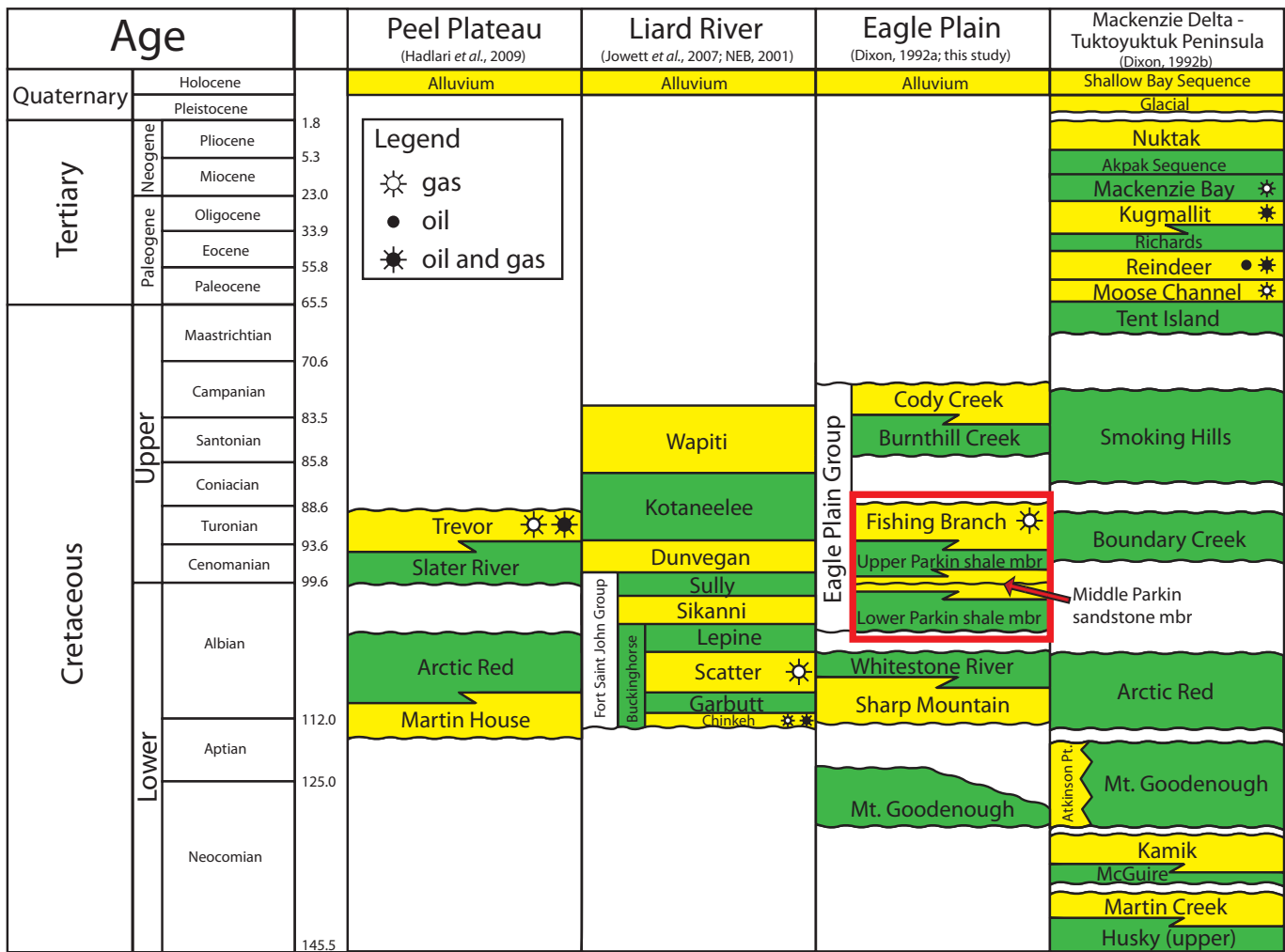
Figure 2. *Cretaceous to recent stratigraphy of Eagle Plain area and other basins of northern Canada. Red box outlines the units investigated in this study.*

Basal Parkin sandstone member

The basal Parkin sandstone member is a transgressive unit consisting of coarse-grained fluvial and fine to medium-grained shoreface sandstones (Fig. 5). The basal sandstone member exhibits porosities of up to 22% in core from the North Parkin D-61 well. It is overlain abruptly at a major flooding surface by the newly defined lower Parkin shale member.

Prior to this study the basal Parkin sandstone member was documented only in the subsurface; however, several sections of the unit were measured in this study along a 20-km outcrop belt in southern Eagle Plain (Stations 2009-11, 2009-12, 2009-13; see Figure 1). A westward change in facies from a fluvial to a marine environment is apparent along the exposures. Interfingering of the marine and non-marine facies suggests an eastward stepwise transgression, although the true shoreline orientation is not known.

Ammonites collected from the basal sandstone member at Station 2010-12 have been dated as middle Albian (Haggart, 2010), indicating that the basal Parkin sandstone is older than the Cenomanian age suggested by Dixon (1992a).

New unit: Lower Parkin shale member

The lower Parkin shale member is a siltstone and shale-dominated succession overlying the basal Parkin sandstone member at a major flooding surface. It is separated from the newly defined upper Parkin shale member by the middle Parkin sandstone member in southern Eagle Plain and equivalent sand-prone mass transport deposits identified from outcrop in the western part of the study area.
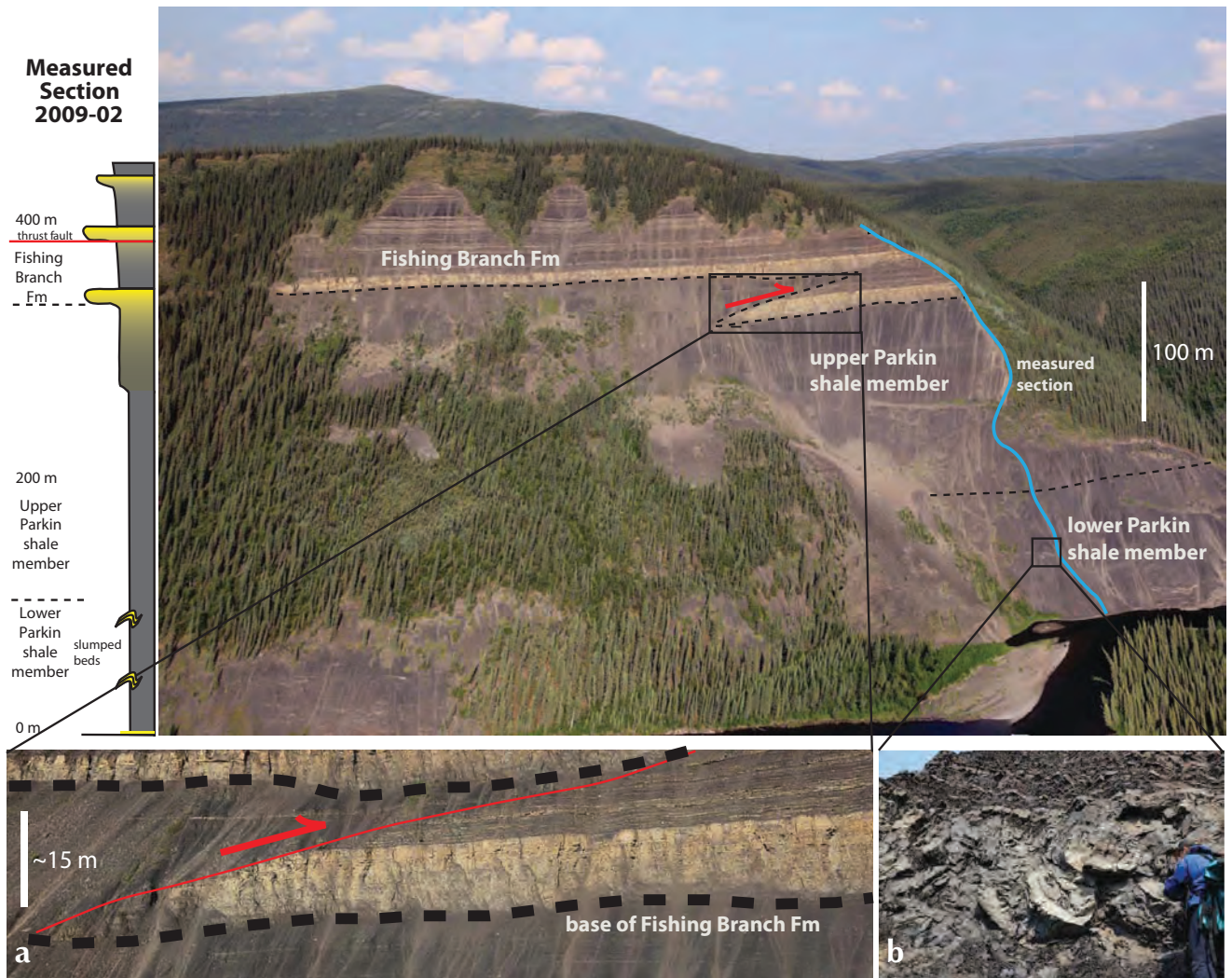
Figure 3. *Measured section at Eagle Plain Group type section (Station 2009-02, 7W 586947 7374123). Insets: (a) thrust fault offsetting the lowest upward coarsening sandstone cycle of the Fishing Branch Formation; (b) convoluted sand-prone unit in the lower Parkin Formation shale member interpreted as slump deposits;*
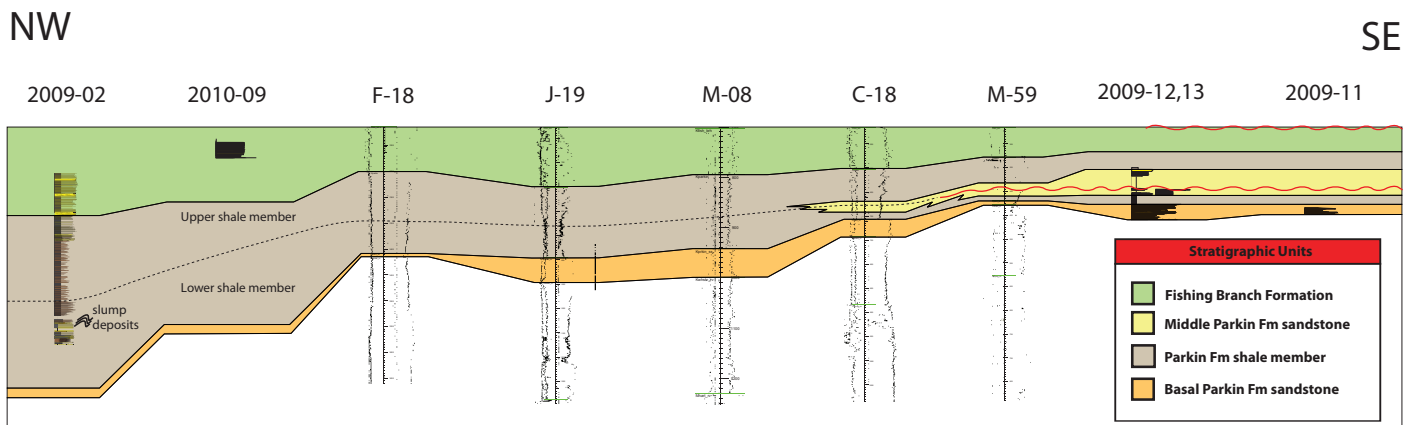
Figure 4. *Cross section with correlation of outcrop and well data from the Parkin and Fishing Branch transgressive-regressive formations cycle showing updated stratigraphic framework. Transect is shown in Figure 1.*
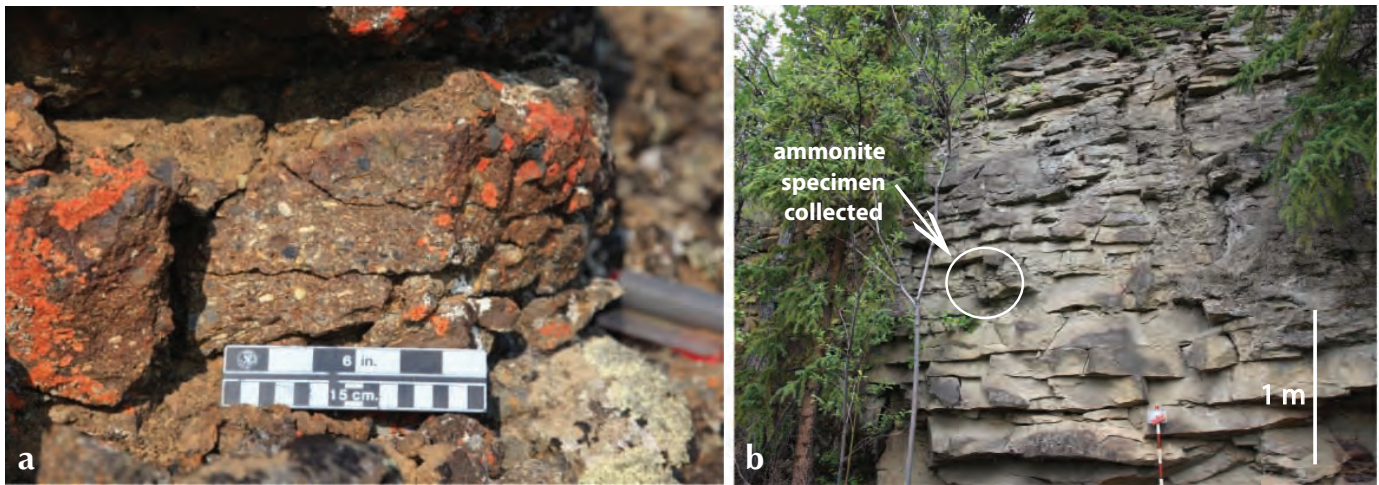
Figure 5. *Outcrops of the lower Parkin Formation sandstone member in southern Eagle Plain: (a) Coarse-grained fluvial sandstones and channel base conglomerates with black and white chert pebbles (Station 2009-11, UTM 8W 412908 7309651); (b) medium and coarse-grained shoreface sandstones (Station 2009-12, UTM 8W 401623 7305779). Ammonite specimen is identified as Middle Albian-aged Cleogastroplites aberrans (Haggart, 2010).*

Large-scale mass transport complexes involving packages of sediments up to 100 m thick are observed in outcrop at the top of the lower Parkin shale member in western Eagle Plain (Station 2009-02), indicating a shelf-to-basin floor relief of at least 100 m (Fig. 6). Mass transport processes of this magnitude occur due to oversteepening and failure of shelf-edge clinoforms (Fig. 7); examples of these deposits are well-documented in both ancient and modern analogues around the world (*e.g.*, Armitage *et al.*, 2009; Gee *et al.*, 2006). The intensely convoluted slump deposits are dominated by interbeds of very fine grained sandstones and siltstone, and are interpreted as the distal expression of the same regression which deposited the middle Parkin sandstone member. Limited paleoflow data from tool marks and current ripples in the overlying undeformed bedding indicate westward-directed paleocurrents in this part of the basin.

Overall westward-thickening trends observed in Cretaceous isopachs also reflect conditions with increasing accommodation space and subsidence to the west (Fig. 8).

New unit: Middle Parkin sandstone member

In outcrop in southern Eagle Plain (Station 2010-13), hummocky sandstones and a chert-rich pebble conglomerate layer are overlain by an upward-coarsening cycle of at least 15 m of clean quartz-rich shoreface sandstones (Fig. 9). The conglomerate lag marks a newly recognized intraformational sequence boundary; the middle Parkin sandstone member is interpreted to be stratigraphically equivalent to the sand-prone mass

transport deposits in western Eagle Plain. Well log responses indicating coarse-grained facies in the middle of the Parkin Formation in wells Blackie No. 1 M-59 and East Chance C-18 become more subdued to the north, suggesting a southern source for coarser grained sediments to the south of the Eagle Plain basin. The middle sandstone member is overlain abruptly by the upper Parkin shale member.

New unit: Upper Parkin shale member

The upper shale member of the Parkin Formation is dominated by interbedded shales and siltstone and is gradationally overlain by the Fishing Branch Formation. The upper contact of the upper Parkin shale member is taken at the base of the lowest sandstone bed, above which the succession consists of at least 30% sandstone and is dominated by thicker, more prominent sandstone beds (Dixon, 1992a).

FISHING BRANCH FORMATION

The Fishing Branch Formation is described by Dixon (1992a) as an overall upward-shallowing fine to medium-grained marine sandstone unit consisting of stacked coarsening upward cycles, individually up to 30 m thick.

At the Eagle Plain Group type section (Station 2009-02; see Figures 1 and 3) in western Eagle Plain, two upward-coarsening cycles capped by flooding surfaces represent the lowest parasequences of the Fishing Branch Formation. The sand-rich units consist of interbedded very fine to fine-grained sandstone and siltstone with unidirectional current
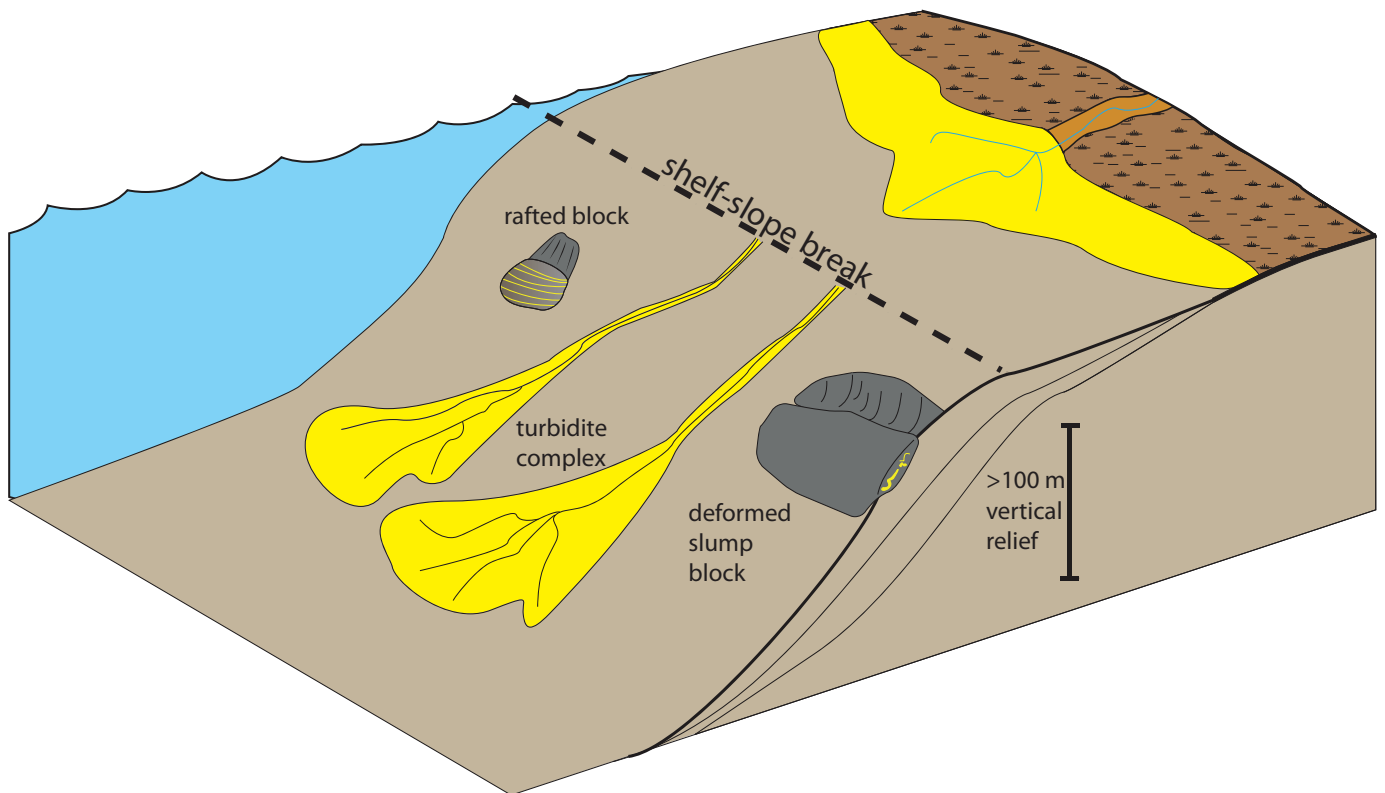
Figure 6. *Block diagram depiction of slope failure and mass wasting processes that occur as a result of increased accommodation and changing depositional parameters at the shelf-slope break. Diagram is vertically exaggerated; a slope angle of 1-2 degrees is sufficient for mass transport processes to occur.*

ripples and tabular beds, interpreted as being deposited in the prodelta of a fluvial-dominated delta. Towards the east, at Station 2010-09, the Fishing Branch cycles are thicker, coarser grained, sandier and show a *Teichichnus* and *Planolites*-dominated ichnofabric; this outcrop is interpreted to represent a more proximal deltaic setting *i.e.*, the delta front.

Outcrops of the Fishing Branch Formation in southern Eagle Plain (*e.g.*, Station 2009-07) are generally shalier and sandstone beds are dominated by storm-generated bedforms including large hummocks. This change in facies suggests a transition to a more distal storm-dominated environment in the south, possibly in the windward side of a deltaic complex.

New unit: Fishing Branch fluvial sandstone member

In southern Eagle Plain (*e.g.*, Stations 2009-07, 2010-23), medium to coarse-grained cross-bedded sandstones with channel lag conglomerates and abundant clay clasts overlie interbedded fine hummocky sandstones and shales. This previously undocumented fluvial unit represents an unconformity and period of sea level lowstand capping

the Fishing Branch Formation, and is unconformably overlain by marine shales of the Santonian Burnthill Creek Formation.

PETROLEUM SYSTEMS AND IMPLICATIONS FOR HYDROCARBON POTENTIAL

Eagle Plain has recognized petroleum potential, and the most significant hydrocarbon occurrences are found in structures in the Chance and Birch fields in the southern part of the basin. Mesozoic source rocks in Eagle Plain are dominated by Type III gas-prone kerogen (Link *et al.*, 1989). Potential source rocks in the lower Albian Whitestone River Formation are largely immature in the southern part of Eagle Plain becoming increasingly mature towards the northwest as the Cretaceous succession thickens (Dixon, 1992a). Biogenic activity may also contribute to gas generation.

The Cretaceous strata were commonly considered a secondary target to deeper Paleozoic reservoirs; however, the sandstone of the Fishing Branch Formation flowed 3300 Mcf of gas per day on a production test at the
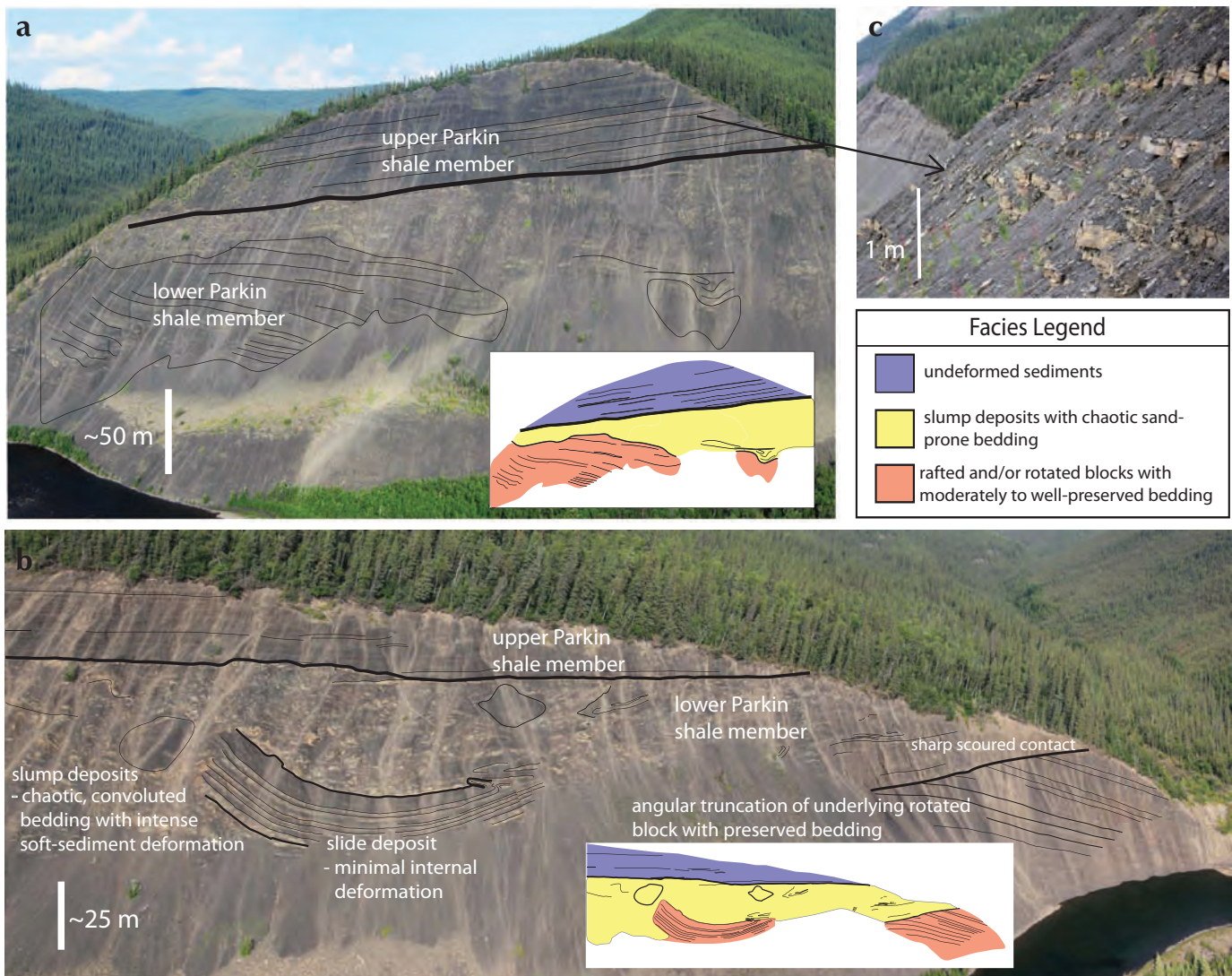
Figure 7. (a) and **(b)** Outcrops along Fishing Branch River (south of Station 2009-02) exhibiting very large (>100m in scale) mass transport complexes with convoluted sand-prone bedding. Select beds are traced to show varying degrees of soft sediment deformation. Insets show line drawing of bedding and colours indicate facies. **(c)** Photograph of undeformed bedding of the upper Parkin shale member which overlies the slump deposits with overlying sandstones.

Chance G-08 well, and oil and gas-cut mud was recovered at several other wells. A recent petroleum assessment (Osadetz *et al.*, 2005) estimated 349 Bcf of natural gas and 108 MMbbls of oil in Cretaceous reservoirs.

Recognition of the presence of a shelf-slope break in the Cretaceous basin adds potential for large new hydrocarbon plays in stratigraphic traps. Sand-prone slump deposits in the upper Parkin shale member indicate transport of sandy sediments across the shelf and deposition at the shelf edge, resulting in oversteepening and failure of shelf edge clinoforms. Increased subsidence and accommodation at the shelf-edge allows potential space for the accumulation of thick sandstone bodies.

The mass transport deposits may represent the distal expression of a shelf-margin delta complex located farther landward at the shelf edge. Shelf-margin delta complexes are often associated with slope failures due to oversteepening of the delta front along the shelf edge. There is also potential for a turbidite fan complex basinward of the slope break by sandy gravity-driven flows. Very large oil and gas fields have been discovered within shelf-margin delta and turbidite fan sandstones around the world. Such high-yield reservoirs in stratigraphic traps could easily have been overlooked in northwest Eagle Plain where well control is sparse.
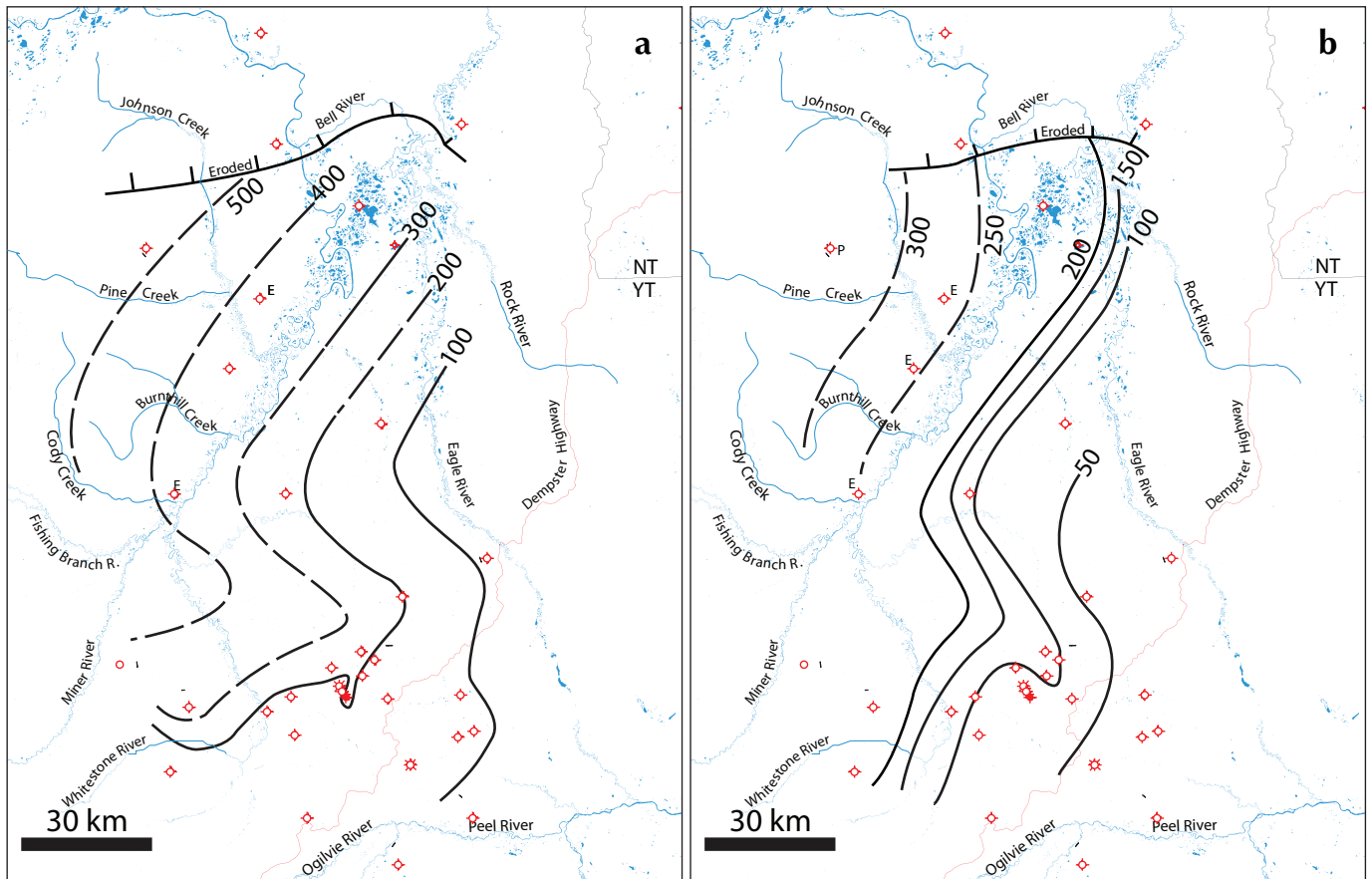
Figure 8. *Isopach maps of (a) Parkin Formation and (b) Fishing Branch Formation, demonstrating overall trend of thickening sediments basinward to the west; P, partial section; E, eroded (after Dixon, 1992a; base-map from geoSCOUT Systems).*
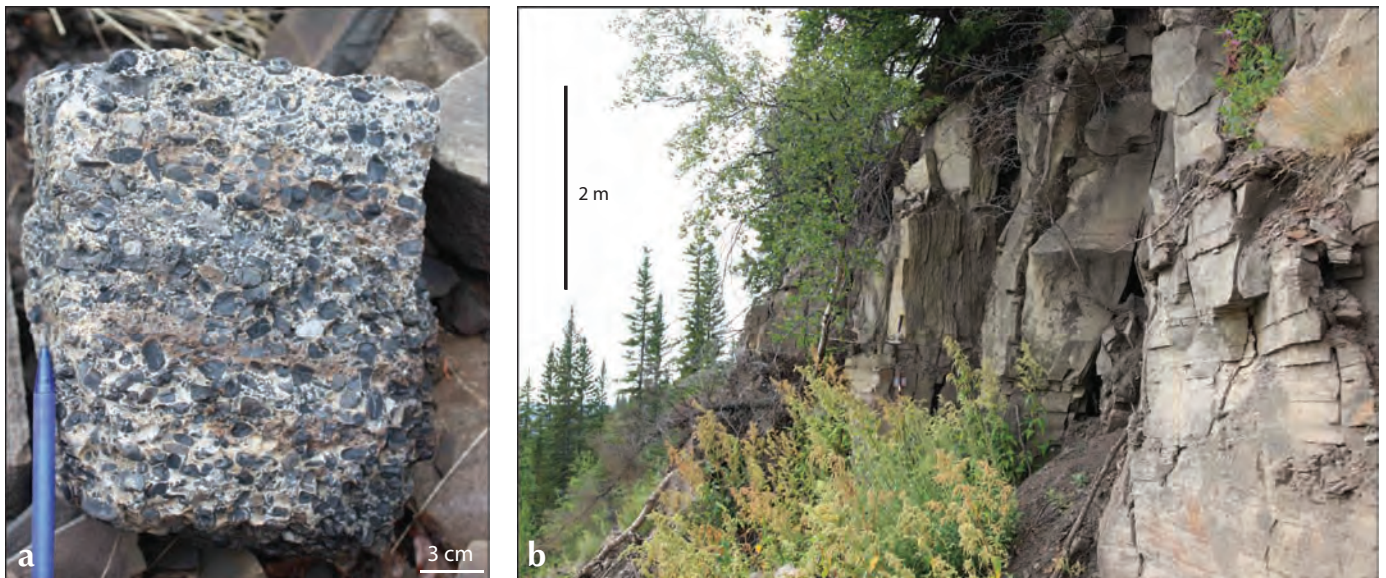
Figure 9. *Outcrops of middle Parkin Formation sandstone member at Station 2009-13, UTM 8W 400748 7306350. The unit consists of (a) Chert pebble-rich transgressive lag, which is overlain by (b) at least 5 m of fine to medium-grained shoreface sandstones.*

SUMMARY

The stratigraphic complexity of the Parkin and Fishing Branch formations is undoubtedly greater than the scope of prior studies of the succession, and thus further investigation is required. Subdivision of the stratigraphic nomenclature is required to reflect previously unrecognized intraformational unconformities. Thus far the following important observations are highlighted:
1) facies trends, paleoflow indicators, and isopachs suggest a broadly westward-deepening basin; 2) southeastern Eagle Plain received periodic input of coarse-grained sediment; and 3) mass transport deposits in western Eagle Plain indicate the presence of a significant shelf-to-basin floor relief (>100 m), which boosts the potential for stratigraphically confined play types associated with the shelf edge.

ACKNOWLEDGEMENTS

REFERENCES

Armitage, D.A., Romans, B.W., Covault, J.A. and Graham, S.A., 2009. The influence of mass-transport deposit surface topography on the evolution of turbidite architecture: The Sierra Contreras, Tres Pasos Formation (Cretaceous), Southern Chile. Journal of Sedimentary Research, vol.79, p. 287-301.

Dixon, J., 1992a. Stratigraphy of Mesozoic Strata, Eagle Plain Area, Northern Yukon. Geological Survey of Canada, Bulletin 408, 58 p.

Dixon, J., 1992b. A Review of Cretaceous and Tertiary Stratigraphy in the Northern Yukon and Adjacent Northwest Territories. Geological Survey of Canada, Paper 92-9, 79 p.

Gee, M.J.R., Gawthorpe, R.L. and Friedman, S.J., 2006. Triggering and evolution of a giant submarine landslide, offshore Angola, revealed by 3D seismic stratigraphy and geomorphology. Journal of Sedimentary Research, vol. 76, p. 9-19.

Hadlari, T., Thomson, D., Schröder-Adams, C.J., Lemieux, Y., MacLean, B.C. and Gal, L.P., 2009. Chapter 9 – Cretaceous Strata and Basal Cretaceous Sandstone Play. In Regional Geoscience Studies and Petroleum Potential, Peel Plateau and Plain: Project Volume, L.J. Pyle and A.L. Jones (eds.), Northwest Territories Geoscience Office, NWT Open File 2009-02 and and Yukon Geological Survey Open File 2009-25, p. 410-476.

Haggart, J.W., 2010. Report on Cretaceous fossils from Eagle Plain, Yukon Territory (NTS 116H). Unpublished Geological Survey of Canada Paleontological Report JWH-2010-02, 2 p.

Jowett, D.M.S., Schröder-Adams, C.J., and Leckie, D., 2007. Sequences in the Sikanni Formation in the frontier Liard Basin of northwestern Canada – evidence for high frequency late Albian relative sea-level changes. Cretaceous Research, vol. 28, p. 665-695.

Link, C.M., Bustin, R.M. and Snowdon, L.R., 1989. Petroleum source potential and depositional setting of Phanerozoic strata in northern Yukon and northwestern District of Mackenzie. Bulletin of Canadian Petroleum Geology, vol. 37, no. 3, p. 293-315.

Mountjoy, E.W., 1967. Upper Cretaceous and Tertiary stratigraphy, northern Yukon Territory and District of Mackenzie. Geological Survey of Canada, Paper 66-16, 70 p.

National Energy Board, 2001. Petroleum Resource Assessment of the Liard Plateau, Yukon Territory, Canada. Oil and Gas Resources Branch. Department of Economic Development, Government of the Yukon, 63 p.

Norris, D.K., 1984. Geology of the northern Yukon and northwestern District of Mackenzie. Geological Survey of Canada, Map 1581A, scale 1:500 000.

Osadetz, K.G., Chen, Z. and Bird, T.D., 2005. Petroleum Resource Assessment, Eagle Plain Basin and Environs, Yukon Territory, Canada. Yukon Geological Survey Open File 2005-2 and Geological Survey of Canada Open File 4922, 100 p.

Geophysical and borehole investigations of permafrost conditions associated with compromised infrastructure in Dawson and Ross River, Yukon

Sarah Laxton[1]
Yukon Geological Survey

Jim Coates

ABSTRACT

The effects of permafrost degradation in Yukon have serious negative implications for the structural integrity of vertical infrastructure. This is especially pertinent for critical buildings such as hospitals, schools, etc., in small communities that are situated on top of warm, ice-rich permafrost. Projections of mean annual air temperature over the next few decades, based on regional climatic models, indicate that air temperature will rise, hastening the thaw of permafrost. The combination of rising of air temperatures and buildings situated on warm permafrost has prompted this investigation into the vulnerability of Yukon Government vertical infrastructure. The application of DC resistivity and ground penetrating radar in conjunction with borehole drilling indicates that in Dawson there is warm ice-rich permafrost beneath the Palace Grand Theatre; the Old Territorial Administration building is underlain by primarily unfrozen sediment; and permafrost under the St. Andrew's Church is characterized by high variability. A deep active layer was observed at Ross River School and geophysical surveys indicate that warm water drainage from the roof is contributing to the thaw of the underlying permafrost.

[1]*sarah.laxton@gov.yk.ca*

INTRODUCTION

Degrading permafrost continues to have devastating impacts on critical community infrastructure including schools and health centres in northern regions. It is anticipated that projected temperature increases and changes in precipitation will accelerate the warming and thawing of permafrost (ACIA, 2004). Regional scale trend analyses generated by the Pacific Climate Impact Consortium (PCIC) indicate a projected mean air temperature increase of 6.2°C per century (Werner *et al.*, 2009).

The projected warming of mean annual air temperature and variations in precipitation patterns will induce further disruptions in the equilibrium of warm permafrost. Permafrost is defined as ground which has remained below zero degrees Celsius for two consecutive years (Harris *et al.*, 1988). Since permafrost is defined as a thermal condition, subtle perturbations to the ground thermal regime, such as increases in ambient air temperature, changes to the micro-hydrologic regime, vegetation clearing, and depth of snow pack may have serious implications for its long-term sustainability. This has important implications for the maintenance of the structural integrity for infrastructure located on permafrost vulnerable to warming-induced degradation.

Yukon is divided into three permafrost zones: continuous (90-100%); extensive discontinuous (50-90%); and sporadic (10-50%) (Heginbottom *et al.*, 1995) (Fig. 1). The extensive and sporadic permafrost zones contain the warmest permafrost within the territory. It is this warm permafrost that is the most susceptible to thaw due to factors such as ambient air temperature increase, disturbance of insulating surface vegetation, and changes to snow cover. The City of Dawson and the community of Ross River are both located within the zone of extensive discontinuous and typically warm permafrost (Fig. 1).

The impacts of permafrost degradation on vertical infrastructure are evident at numerous building locations throughout Yukon. Evidence of this degradation is visible from the historic wooden structures built in the early 20th century within the City of Dawson, and at other locations such as the Ross River School, where the heating of the buildings has contributed to the warming and subsequent thaw and destabilization of the supporting permafrost.

In order to address the costs associated with the effects of permafrost degradation on infrastructure, initiatives such as the development of the Canadian Standards
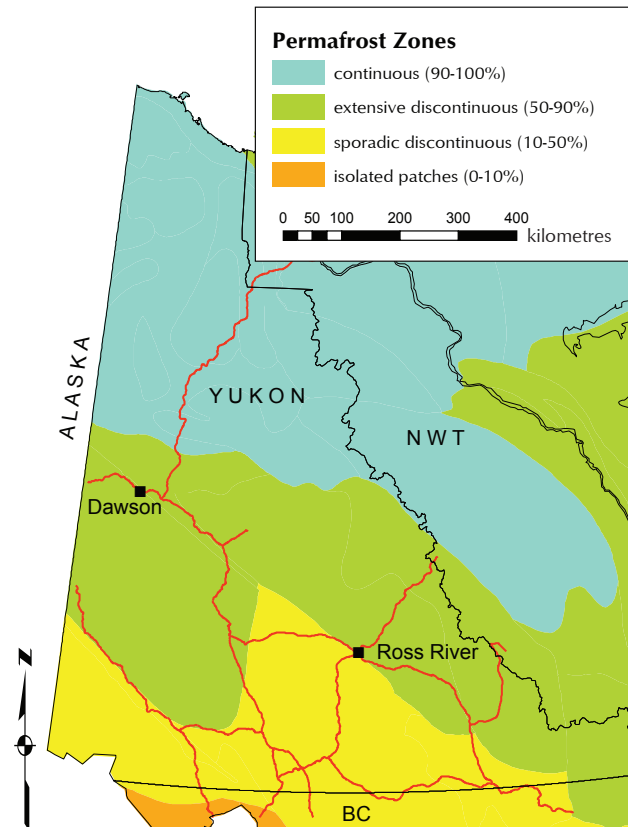
Figure 1. *Location of Dawson and Ross River in the extensive discontinuous permafrost zone.*

Association (2010) *Technical guide for infrastructure foundations in permafrost: A practice guide for climate change adaptation for building in permafrost areas;* and *True North: Adapting Infrastructure to Climate Change in Northern Canada* (NRTEE, 2009) have been developed. Yukon Government's *Climate Change Action Plan* (2009) has also identified that the adaptation of infrastructure to climate change is a priority and noted that actions should be taken. The *True North* (NRTEE, 2009) paper noted that ensuring the resiliency of infrastructure throughout its designed lifespan is one of the most critical aspects of climate change adaptation. The findings brought forward by the *True North: Adapting Infrastructure to Climate Change in Northern Canada* (NRTEE, 2009) report highlight some of the past hindrances to addressing the adaptation of building practices to changing climatic conditions. Three of the most applicable findings to this study include:

1. The limited interaction among scientists and data providers, designers and builders of infrastructure, and policy-makers are barriers to problem identification and the application of solutions.

2. Significant gaps exist in the availability and accessibility of data and information that form the basis for infrastructure risk management and loss prevention, including information on current and projected impacts of climate change, as well as data on the stock of, and demand projections for infrastructure.

3. The capacity across and within northern jurisdictions to assess climate risks to infrastructure, and to develop, deploy, and enforce standards and risk reduction measures is uneven and lacking.

This paper aims to: 1) employ a combination of non-destructive geophysical and traditional borehole methods to identify the condition of permafrost adjacent to, and underneath buildings vulnerable to permafrost degradation at case study locations in the City of Dawson and the community of Ross River, Yukon; and 2) establish a baseline of permafrost conditions to monitor and assess the response of buildings to future climatic regimes.

STUDY SITES

To gain a better understanding of how buildings are responding to permafrost degradation within the zone of extensive discontinuous permafrost, the communities of Dawson and Ross River, Yukon were selected. Although these communities are both situated within the Klondike Plateau Ecoregion, a constituent of the larger Boreal Cordillera Ecozone, and within the Central Yukon Basin Yukon climatic zone, they are each characterized by unique geologic and climatic characteristics (Yukon Ecoregions Working Group, 2004a,b; Wahl et al., 1987) (Fig. 1). The selection of buildings at these two locations within the extensive discontinuous permafrost zone enables the comparative analyses of the effects of thawing

permafrost on buildings situated in different physiographic conditions.

DAWSON

Dawson City, Yukon, (64°03'34N, 139°25'50W; 320 m a.s.l.) is situated along the banks of the Yukon River and is home to ~1,891 residents (Yukon Bureau of Stats., 2010) (Fig. 2a). The climate of Dawson is characterized by continental conditions with the 1971-2000 climate normals recording an annual daily average temperature of -4.4°C and a yearly precipitation total of 324.3 mm (Fig. 3) (Environment Canada, 2010). Mean annual air temperature measured in 2007-2008 in the townsite was -3.16°C. Projected annual mean temperature trends generated by the Canadian Global Climate Model (CGCM3), following the A2 emissions scenario, indicate a mean annual temperature increase of 2.5 to 3.5°C in Dawson for the 2050s compared with the 1961-1990 baseline (Werner et al., 2009). The surficial geology is characterized by fluvial deposits overlain by muck (frozen organic sediment), and capped in locations by eolian sediments (Duk-Rodkin, 1996; Duk-Rodkin et al., 2000; Froese et al., 2000, 2001).

ROSS RIVER

Ross River, Yukon, (61°58'47N, 132°27'03W; 650 m a.s.l.) is situated along the banks of the Pelly River and is home to ~361 residents (Yukon Bureau of Stats., 2010) (Fig. 2b). Located in the Tintina Trench rain shadow, Ross River experiences drier continental conditions with more variation between winter and summer temperatures than regions further to the west where the climatic conditions are moderated by the close proximity to the Pacific Ocean. The greatest amount of precipitation occurs during
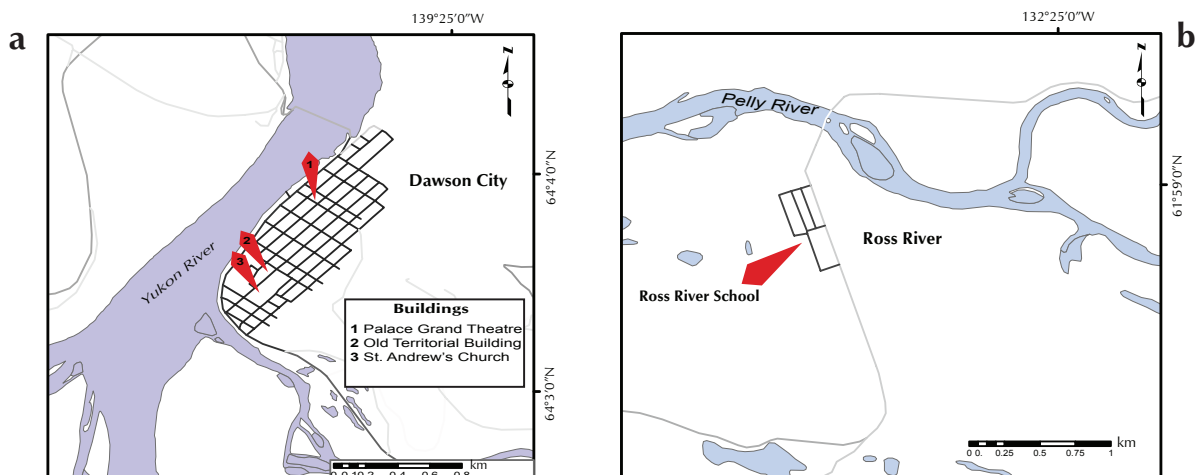
Figure 2. Locations of the study sites in **(a)** Dawson and **(b)** Ross River, Yukon.

the summer months of July and August (Fig. 3). The 1967-1994 climate averages are an annual daily average temperature of -4.6°C and yearly precipitation total of 258.7 mm (Fig. 3) (Environment Canada, 2010). The mean annual air temperature for 2008 was -3.7°C. The average annual ground surface temperature for 2008 was 0.4°C and the average annual temperature recorded at 19 m below surface was -0.14°C (Fig. 4), both temperatures were recorded from the Ross River School borehole. The surficial geology of the area is characterized by hill slopes and low-valleys blanketed in silt-rich till and coarse-grained glaciofluvial sediments that have been deposited in main valley meltwater channels and outwash plains (Lipovsky and Huscroft, 2007).
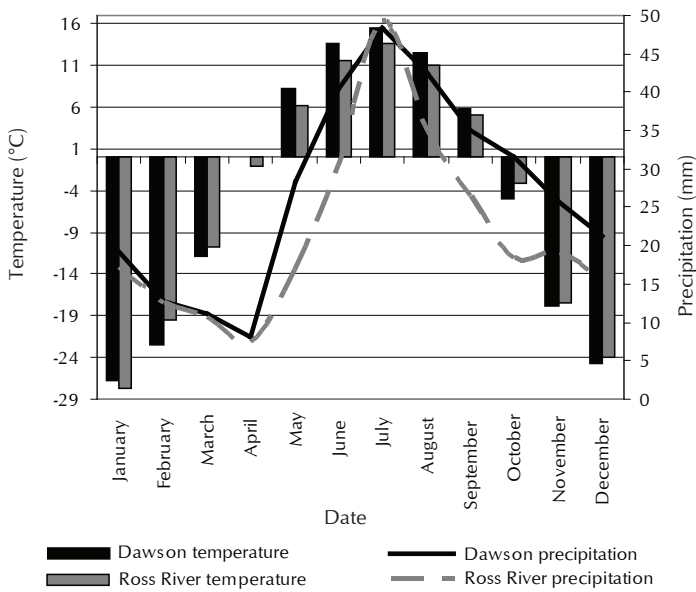
Figure 3. *Climatic data for Dawson City and Ross River, Yukon.*

METHODS

The subsurface adjacent to the buildings was investigated using a combination of geophysical and physical techniques. The Dawson sites were sampled July 19-23, 2010, and the Ross River site was sampled on August 26, 2010.

GROUND PENETRATING RADAR

Ground-penetrating radar (GPR) was used to gain a two dimensional image below ground surface. A TerraSIRch Subsurface Interface Radar (SIR) System 3000® with a 200-MHz antenna (Geophysical Survey Systems, Inc. (GSSI)) was employed for the field investigation. The SIR-3000 control unit was set to record at 64 scans per second, which translates to 10 scans per metre, and a dielectric constant set at 13. Post collection processing was conducted using RADAN™ (version 6.6, GSSI) software.

BOREHOLE DRILLING

Drilling was conducted at selected sites using a combination of two drilling systems. A truck-mounted J.K. Smit rotary rig was used in areas where coarse gravel were encountered near the surface. This drill uses 2.5" solid-stem augers and carbide-tipped fishtail or offset-tooth bits. A Bosch rotary percussion electric drill was used to retrieve core from ice-rich permafrost. This uses a 1" or 3" diamond-tipped high-speed coring barrel. Intact core samples were retrieved from ice-rich fine-grained permafrost with this tool. However, the coring is ineffective in gravel and sandy soils with poor core recovery and can cause damage to the equipment. The Bosch electric drill was used indoors to recover core within the St. Andrew's Church to a depth below ground surface of 3.8 m.

Figure 4. *Ground Surface temperature data from Ross River School borehole 2007-2010.*

ELECTRICAL RESISTIVITY TOMOGRAPHY

Electrical resistivity is an effective method for determining the presence of frozen ground (Hauck *et al.,* 2003). Resistivity is a measure of the degree of conductivity of soil materials and their inverse, which is measured as resistance or resistivity. The resistivity varies according to the material type, composition and moisture content. Temperature and the state of water have an exponential effect on resistivity; liquid water has an exponentially lower resistivity than frozen ice. Resistivity works by injecting a current into the ground at one location, then measuring the voltage in the ground at another location. Using a large number of electrodes and multi-core cables, many combinations of transmitting and receiving electrodes are activated and voltages measured. These measurements are then inverted and processed using well-defined geometric factors to produce a tomogram, which is a one, two, or three dimensional image of the subsurface resistivity patterns.

Mapping of the horizontal extent of permafrost has been reliably established using galvanically and capacitively coupled resistivity (Hauck *et al.*, 2003; Kneisel, 2004; Fortier *et al.*, 2008). The system used for these investigations is the Advanced Geosciences SuperSting R1/IP. This equipment uses 28 electrodes, an automatic switchbox and processor, and can conduct a survey in less than 20 minutes. Array lengths of 120 and 60 m were used, giving a depth of penetration from 10 to 20 m.

Wenner arrays were used for near-surface resolution as well as speed of survey. Results were processed using AGI EarthImager2D software.

RESULTS

DAWSON CITY

Palace Grand Theatre

Building history

The Palace Grand is a flagship building of the Klondike Gold Rush Historical Complex and as such has great cultural, historical and civic value (Fig. 2a). The Palace Grand is built on a flat, level site, with one building adjacent on the east and a large graveled parking lot on the west. The Palace Grand is a wood-framed, three-storey building which was built in 1899 and heavily refurbished in 1962 (Coutts, 1984). The structure is supported on wooden piles. These piles have concrete pads poured around their uppers. Wooden beams are placed on top of the piles. Beneath the building, and extending 0.5 m out from the building's sides, is a 1.2 m ventilated crawlspace.

Surficial geology, ice content

The area behind the building, on the north side, is disturbed but re-vegetated with grass and 3 to 4 m-high willows. The areas immediately adjacent to the building on the north and west sides are covered with White Channel gravel fill brough in from the Klondike River Valley southeast of the town site. Drilling, GPR and resistivity surveys were conducted on the White Channel gravel adjacent to the building.

At the time of inspection on July 20, 2010, the crawlspace had 5 to 10 cm of water in a depressed area near the centre of the building (Fig. 5). The floor of the crawlspace appears to have subsided almost 40 cm since the piles were poured, as evidenced by suspended concrete slabs which originally rested on grade. The piles do not appear to be settling and the building appears to have remained level.

Figure 5. *Water in crawl space beneath Palace Grand Theatre, July 25, 2010; note the exposed piling below concrete pad indicating the presence of ground surface subsidence.*

Drilling at the rear of the building, on the north side, revealed 1.6 m of gravel, silt and debris fill over almost 1 m of nearly pure ice. Ice contents decreased in silt and sand until alluvial gravel were encountered at a depth of 3.4 m. The transition from silt to sand was gradational, and coarse-grained particles were found lower in the borehole. DC resistivity geophysics were then used to reveal a large region of ice-rich permafrost extending for several metres (Fig. 6). GPR was used to survey the subsurface site stratigraphy and to detect areas of massive ice and groundwater seepage (Fig. 7).

Geophysics

Drilling and resistivity showed a relatively consistent active layer approximately 1.5 m thick (Fig. 6). Deeper thaw was observed beneath a drainage ditch in a parking lot to the west of the structure (Fig. 6). Several ice-rich or pure ice lenses were detected by the resistivity and drilling at depths from 1.4 to 5.0 m. These were characterized by high resistivities of 800-1200 Ωm. This roughly corresponds with the depth of the silt unit. Frozen gravel layers beneath the ice-rich silt have lower resistivities due to lower ice contents (200-300 Ωm). The thawed active layer, which is largely composed of White Channel gravel fill, has a very low resistivity (40-50 Ωm). This indicates high groundwater content between the highly resistive quartz cobbles. Standing water was observed in the crawlspace below the building. The source of this water is likely groundwater moving through the permeable active layer.

The GPR output indicates an active layer which is approximately 2 m thick (Fig. 7). Above this level, the signal is attenuated and blurry, indicating groundwater presence. Several regions of chaotic GPR signals may indicate massive ice or very ice-rich conditions.

Old Territorial Building

Building history

The Old Territorial Administration Building is located near the permafrost boundary south of Church Street (Fig. 2a). It is a wood-framed three story building that currently houses the museum and several government offices. It was built in 1901 and has been in continuous service to present day. The building is supported on posts with a ventilated crawlspace. Evidence of subsidence is indicated by the presence of 0.5 m-deep depressions in the lawn surrounding the building, and damage to various porches and boardwalks has also occurred.
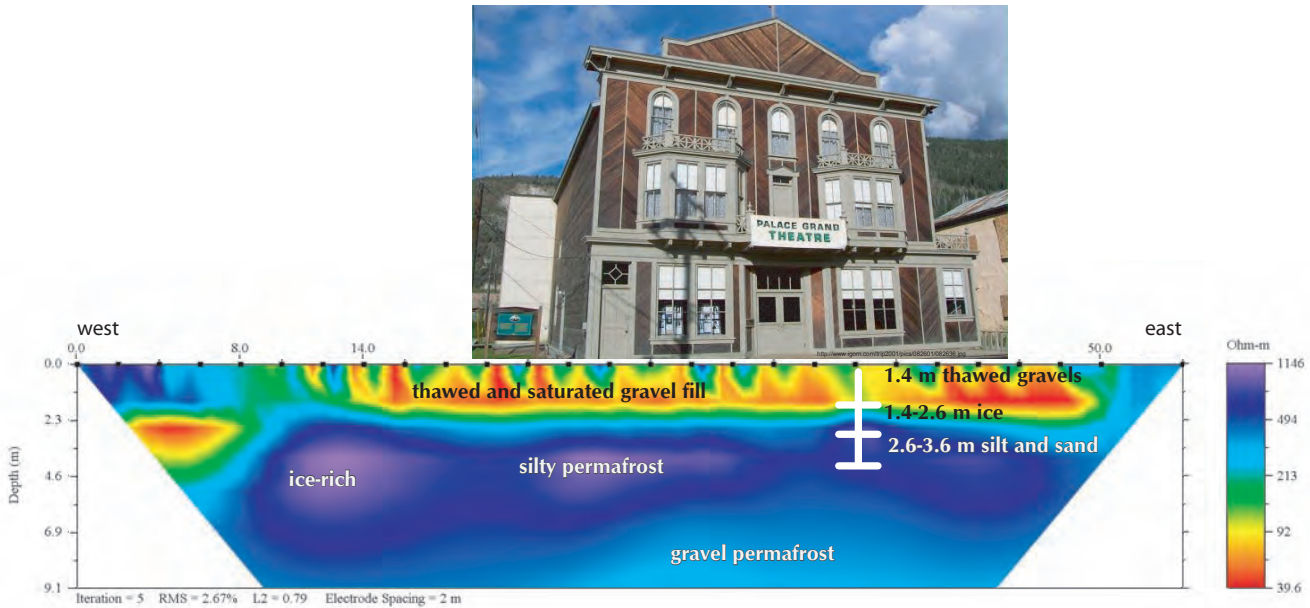
Figure 6. *The Palace Grand Theatre resistivity tomogram run on the north side of the building, and borehole data.*
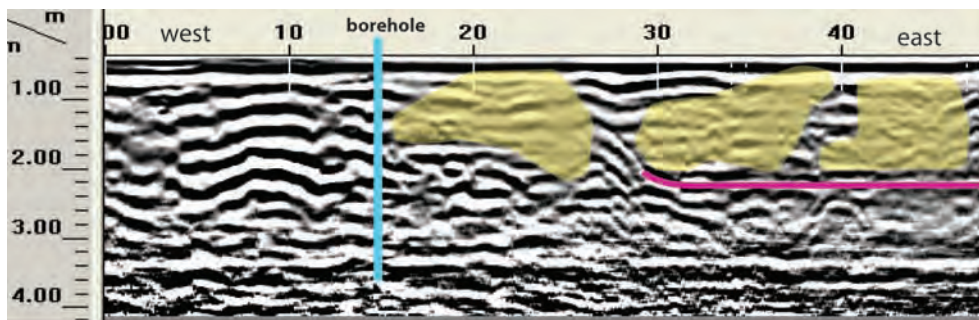
Figure 7. *GPR image along same path as resistivity transect located on the north side of the Palace Grand Theatre. Yellow areas demark zones with higher ground water content; the blue line indicates the location of the borehole; and the pink line is the interpreted upper contact of the silty sand unit.*

Geophysics

Resistivity transects were performed on the south, north and east-facing sides of the building. Excavation for the new hospital, on the east side of the building, allowed for ground-truthing of the results, as did one shallow borehole to a depth of 1.6 m on the south side of the building.

No permafrost was detected within the top 10 m of the subsurface on the south side of the building (Fig. 8a). While higher resistivities were present near the base of the image, there is no sharp boundary which is generally found at the top of the permafrost table. Thawed silt were encountered in the upper 2 to 5 m (100-200 Ωm). Gravel is likely found below 5 m. Low resistivities within the gravel indicate that they are probably thawed (200-350 Ωm). Borehole BH01 was drilled to a depth of 1.3 m; sticky unfrozen clay bound the Bosch drill auger stem and prevented further drilling.

The transect on the east side of the building was run along the east side of the parking lot adjacent to the foundation excavation for the new hospital construction site (Fig. 8b). Possible permafrost was encountered at the north end of the transect within local alluvial gravel (300-500 Ωm). The hospital foundation excavation allowed for observation of materials to a depth of 4 m, which consisted of 2 to 3 m of silt (50-200 Ωm) overlaying gravel. No permafrost was found by equipment operators during excavation for the new hospital's foundation; however, the resistivity showed a strong contrast between high and low resistance materials. This is likely ice-poor gravel permafrost which equipment operators may not have recognized. As the ice content in the sediments are low, thaw and subsidence are not expected at this site.

The transect on the north side of the building ran parallel to the structure at the edge of the Fifth Ave. entrance boardwalk (Fig. 8c). Several regions of very low resistivity may be groundwater channels, rotting wooden pilings or buried metallic debris (10-30 Ωm). Low resistivities near the surface are likely thawed silt (25-200 Ωm). A high resistance buried object (2000-8000 Ωm) was found beneath the centre of the porch. Permafrost appears to be present at depths below 7 m with high resistivities (1000-3000 Ωm), likely in alluvial gravel. This area may have been subject to permafrost thaw and surface subsidence in the past; however, with such a deep active layer and ice-poor gravel, further subsidence is unlikely.
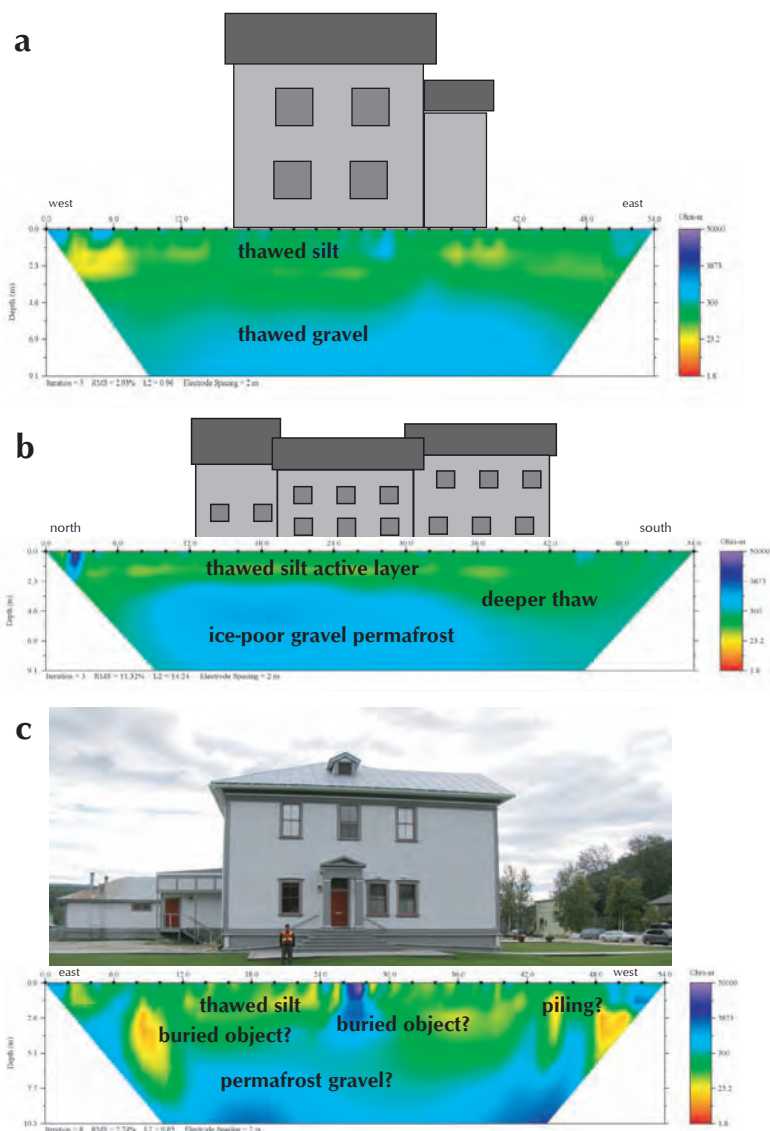
Figure 8. Resistivity tomograms at the Old Territorial building: *(a)* run on the south side; *(b)* run on the east side; and *(c)* run on the north side.

St. Andrew's Church

Building history

St. Andrew's Church is one of the best examples in the area of a historical building which has been rendered unusable due to permafrost degradation (Fig. 2a). The building was constructed in 1901 and abandoned in 1932 due to permafrost thaw and subsequent structural collapse (Commonwealth, 1984). This collapse may have been caused by the installation of a furnace in a cellar excavated in permafrost. The inside of the structure was shored using large timbers during the mid-1980s. There is currently no floor in the structure, and large gaps in the foundation allow for air and water flow into the interior.

Geophysics

Resistivity and GPR were run on four transects around the perimeter of the building. Boreholes were drilled on the west side, north side and within the structure itself. PVC plastic casings (25 mm) were placed in the 75 mm boreholes to facilitate thermistor installation. Boreholes were drilled to refusal on frozen gravel, which varied from 3.0 to 4.5 m depth. This is consistent with other boreholes around the Dawson town site.

The west side of the church appears to be underlain by permafrost within alluvial silt (300-4000 Ωm; Fig. 9a). Permafrost degradation has taken place, as evidenced by tilting of the structure. The permafrost on this side of the church has the lowest resistivity in the building area, indicating low ice contents or high unfrozen water content. Several isolated bodies of high-resistivity material (4000-30000 Ωm) were surrounded by low-resistivities (300-500 Ωm), suggesting that there are relict patches of ice-rich silt surrounded by ice-poor degraded permafrost. Deep thaw depths of >6 m beneath the south face of the bell tower may account for some of the lean evident in the structure. This side of the church may experience more thaw due to its westerly aspect, which receives increased summer evening insolation.

A large region of ice-rich silt underlies the west end of the transect, beneath the bell tower (~30 000 Ωm) (Fig. 9b). Degraded permafrost is found towards the east end of the structure, where surface subsidence is visible (100-200 Ωm). Regions of low resistivity found in the thaw depression at the left end of the image are likely due to saturated silt (<20 Ωm). However, they may also be interpreted as buried metallic debris. Borehole STA02 was drilled to a depth of 4.5 m through ice-rich silt before refusal was encountered on frozen gravel.

Along the east side of the structure, permafrost has a relatively consistent depth of thaw to 2.5 m along the south end of the transect (<300 Ωm; Fig. 9c). Towards the thaw depression at the north side of the building, the active layer becomes much deeper as indicated by the area of increased thaw (<200 Ωm; Fig. 9c). This is an area where surface water pools. This will trap heat and transfer it to the underlying permafrost causing continued thaw. Much of the damage to the structure appears to be as a result of the building 'leaning' into this thaw depression. Permafrost appears to be colder and/or more ice-rich than at other locations beneath the structure as is evidenced by the high resistivities (80 000 to 100 000 Ωm).

The permafrost table is deep and uneven across the south side of the structure; it ranges in depth from 2 m in an adjacent lawn area to 4.0 m directly in front of the structure on 4th Ave. (Fig. 9d). Deep thaw in front of the building (30-100 Ωm) is likely due to the south-facing wall absorbing solar energy and re-emitting that energy into the ground. Ice-rich permafrost is present in the shaded area to the east (3000-30 000 Ωm) of the church, but ice-poor or high water content permafrost with an uneven active layer surface and low resistivities (300-400 Ωm) was found on the west side.

GPR was run along the same path as the resistivity array on the north side of the church. Results from the GPR survey yielded data which support the resistivity results that suggest the presence of a thawed active layer (Figs. 9b,e). Zones with a higher ground water content are identified by a decrease in the GPR signal strength and are highlighted by the yellow areas in Figure 9e. The active layer is also visible on the GPR image as a strong horizontal linear layer at a depth of ~ 2 m below the ground surface.

Active layer depths near the shaded sides of the buildings ranged from 0.9 to 1.4 m. Within St. Andrew's Church, the permafrost table had rebounded to 0.56 m. An area of very ice-rich soil was found at a depth of 1.2 m, which may have been the historical maximum depth of thaw beneath the church. The silt below this region is visually interpreted as containing 50-80% ice, while the silt above had lower ice contents with wood and metal debris.

The thickness of ice-rich silt was remarkably consistent between the Palace Grand and St. Andrew's Church sites, ranging from 3.0-3.6 m in depth. If this soil was to thaw by the projected 1 m depth due to climatic warming surface, subsidence of up to 0.5 m could be reasonably expected.

Dawson Downtown Street Survey

GPR transects were run over many of the main streets of downtown Dawson. The transects revealed a strong reflector at a depth of 2.6 m, which was consistent across the town. It is likely that this is the top of the active layer. This was similar to active layer depths detected by drilling (Table 1) and resistivity around St. Andrew's Church, Front Street and the Palace Grand Theatre. The suspected active layer reflector was observed beneath many streets and all alleyways, but almost never beneath intersections.
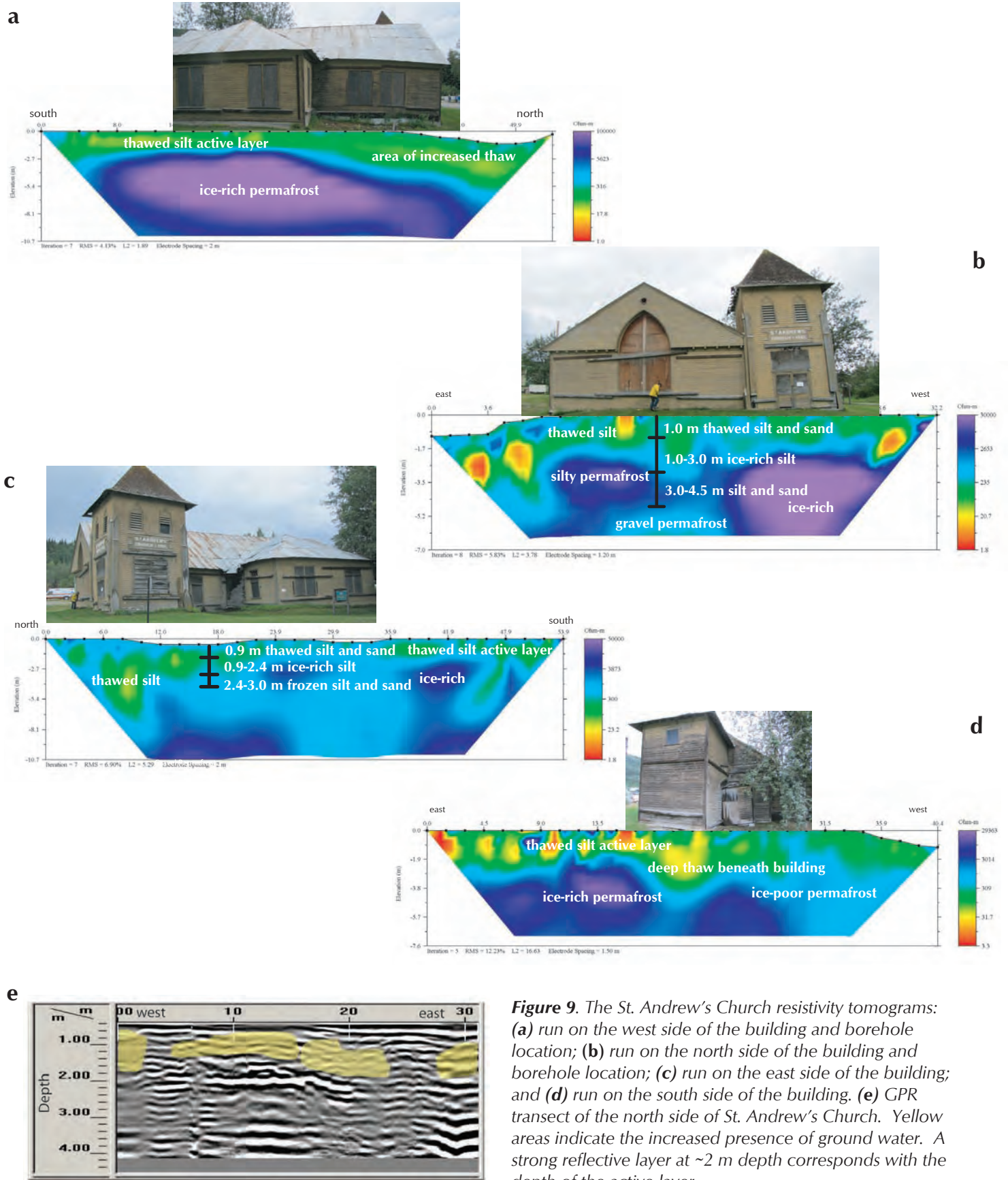
Figure 9. The St. Andrew's Church resistivity tomograms: *(a)* run on the west side of the building and borehole location; *(b)* run on the north side of the building and borehole location; *(c)* run on the east side of the building; and *(d)* run on the south side of the building. *(e)* GPR transect of the north side of St. Andrew's Church. Yellow areas indicate the increased presence of ground water. A strong reflective layer at ~2 m depth corresponds with the depth of the active layer.

Table 1. Summary of borehole results, July 2010.

Borehole	Active layer depth (m)	Ice-rich silt thickness (m)	Depth to gravel (m)
St. Andrew's east side	0.9	0.9-3.6	3.6
St. Andrew's north side	1.0	1.0-3.0	4.5
St. Andrew's inside	0.56	1.4-3.0	3.8
Palace Grand east side	1.4	1.4-?	N/A
Palace Grand north side	1.4	1.4-3.4	3.4

ROSS RIVER

Ross River School

Building history

The Ross River School has experienced damage relating to foundation settlement for over 10 years (Fig. 2b). An insulated crawlspace and thermosiphons are being used to prevent thaw of the underlying ice-rich permafrost; however, continued thaw and settlement is occurring (Fig. 10a).

Surficial geology, ice content

A borehole drilled adjacent to the building in 2007 by EBA Engineering, and observed by J. Coates, revealed that deep active layers (up to 4.5 m in depth) occur in the area, which is underlain by up to 20 m of ice-rich silt below 4-5.0 m of silty gravel.

Ground temperature

Ground temperatures at the Ross River School are warm. At depths of 4.5 m, adjacent to the school, the active layer fluctuated between -0.3 and 2°C. This is near the base of the active layer, and agrees well with the resistivity. At depths of 13 m, temperature varied between -0.2 and -0.5°C. This is very vulnerable permafrost that is often within 0.1°C of thawing.

Geophysics

The two high-resistance regions labeled as ice-rich (500-1000 Ωm) are separated by a lower resistance region (200-300 Ωm) that is likely the same temperature as the surrounding permafrost, but may have much higher unfrozen water content (Fig. 10a). In this case, future thaw and subsidence may take place in this region, which

lies beneath an area of already deep thaw. A region of very low resistivity (40-100 Ωm) near the centre of the image may indicate the presence of a large buried metal object or an area of groundwater infiltration. Groundwater infiltration is the more likely explanation, as a drain pipe from the roof eaves trough disgorges in this area. GPR was used along the same transect and revealed an area of increased signal attenuation over the resistivity anomaly, an indication of groundwater presence (Fig. 10b).

Interpretations of the geophysical data indicate that water drainage from the roof may be a contributing factor for the deep thaw in the very warm permafrost adjacent to the west side of the school.

DISCUSSION

DAWSON

Geothermal Modeling

Permafrost conditions in Dawson City were modeled as part of a YG Transportation Engineering Study (Coates, 2009) using the MUT 1D, a finite element analysis geothermal modeling program designed by the Alaska Department of Transportation. Results from Coates (2009) indicate that active layer depths are expected to increase by up to 1 m, from 2.6 to 3.6 m, by 2020 in ice-rich permafrost in the Dawson town site due to anticipated climatic warming rates of 0.1˚C per year (Fig. 11).

Projected impacts on infrastructure

Palace Grand Theatre

The permafrost beneath the Palace Grand Theatre is extremely ice-rich and warm with an approximate temperature above -1.0˚C, making it very prone to thaw. Active layer depth increases in this area will lead to subsidence of the surface and to the reduction of bearing capacity of the soils. A region of nearly pure buried ice has been identified immediately adjacent to the north side of the Palace Grand Theatre. This poses a significant structural risk to the foundations of the building. Should the massive ice body located behind the Palace Grand Theatre thaw, a surface subsidence of up to 0.75 m can be expected. This would have serious consequences for the integrity of the structure. With projected active layer depth increases due to climatic warming, some thaw of ground ice may be anticipated (Coates, 2009). Surface subsidence and structural damage would likely follow.
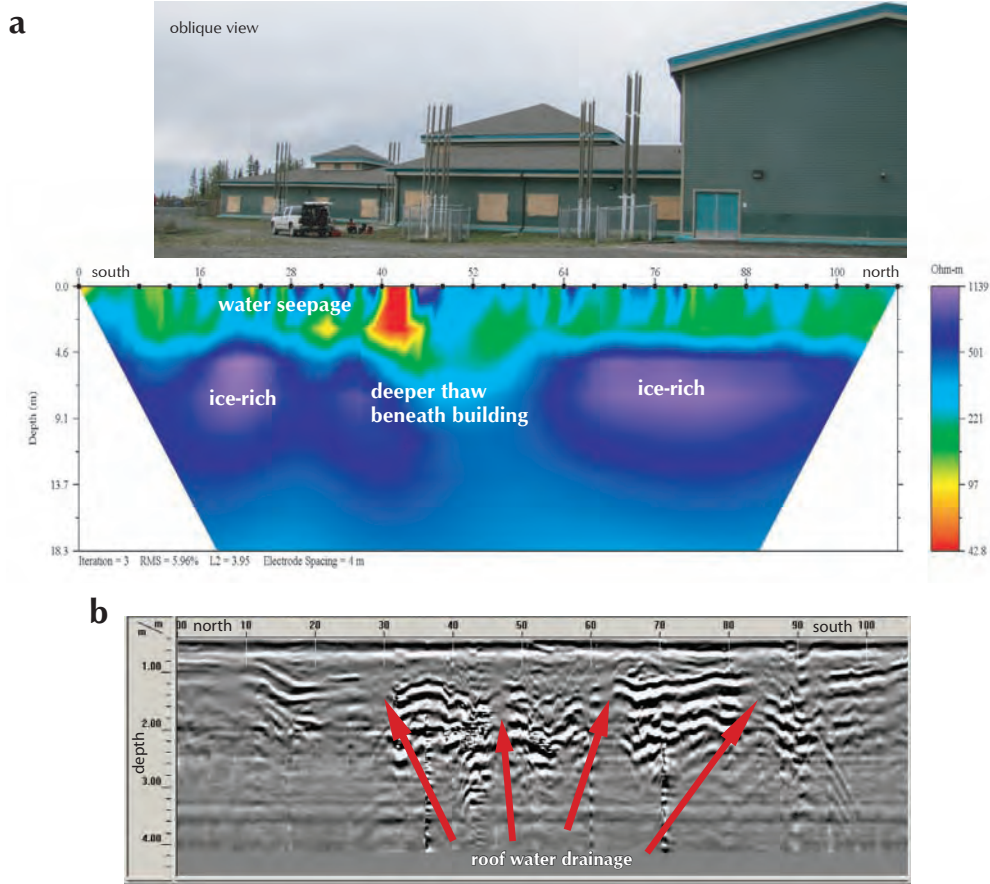
Figure 10. (a) Ross River School resistivity profile on the west side of the building; (b) GPR transect following the same path as the resistivity profile. The red arrows indicate regions where water runoff from the roof of the school has infiltrated into the ground.
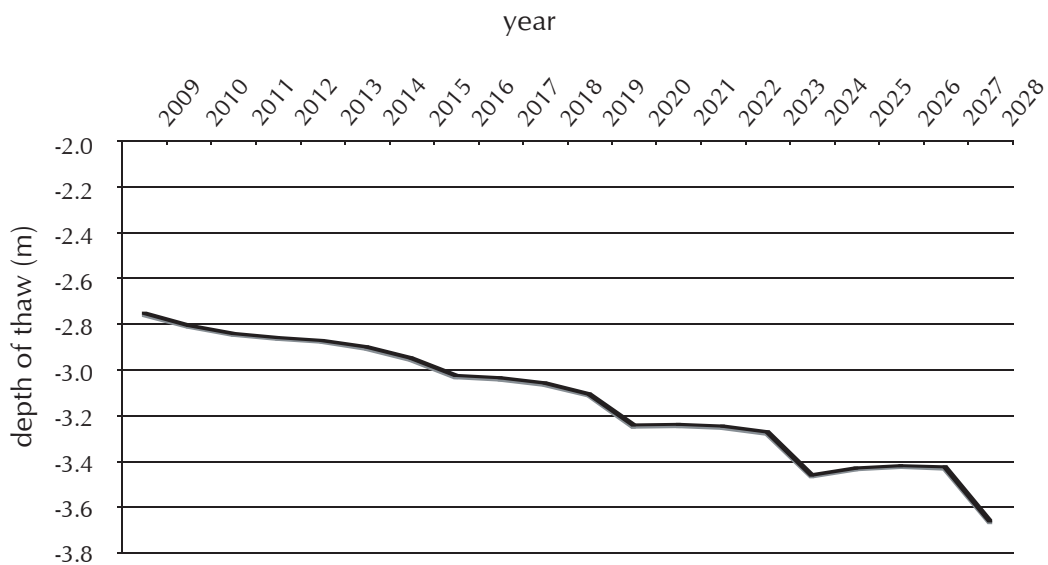
Figure 11. Projected increase in maximum depth of seasonal permafrost thaw by 2020 for Dawson (Coates, 2009).

Old Territorial Building

The Old Territorial Administration Building appears to be underlain by mostly unfrozen sediments. Resistivities in these sediments on the north and east sides of the structure are within the range expected for ice-poor silt and gravel. However, the lack of sharp boundaries between higher resistance materials at depth and lower resistance materials at the surface indicate that ice-rich silt are not expected. Therefore, this structure is not expected to experience further permafrost thaw or damage due to settlement.

St. Andrew's Church

St Andrew's Church is underlain by degraded ice-rich permafrost which has caused significant damage to the structure in the past. However, the permafrost table has recovered within the unheated and unoccupied structure to within 50 cm of the surface. An increase in active layer depths due to climatic warming may cause increased subsidence of certain parts of the structure where ground and surface water collection occurs.

Ross River School

The Ross River School has a very deep active layer. The depth of the active layer adjacent to the school ranges from 4.5 to 8.0 m. Future permafrost thaw will likely occur due to warm water drainage from the roof. The heat transfer from this water through the granular materials beneath the school is a very effective method of permafrost thaw. Increases in thaw depth and subsidence may be expected until water is rerouted away from the building.

CONCLUSIONS

Resistivity and GPR were successfully used to identify regions of permafrost beneath structures located in the extensive discontinuous zone of central Yukon. Regions of high resistivity were interpreted as ice-rich permafrost. Regions of low resistivity within permafrost regions were interpreted as high unfrozen water content within permafrost. Interpretations of the geophysical investigations were confirmed by boreholes drilled along the geophysical transects. GPR was successful in delineating the permafrost table and identifying areas of groundwater within the active layer. The Palace Grand Theatre and Ross River School are identified as regions where projected climatic warming may lead to permafrost thaw and structural damage.

The impacts of climatic warming are likely to be more pronounced in urban areas than forested terrain as there is no insulating organic mat to shield permafrost from temperature increases. Comprehensive monitoring of permafrost conditions within townsites will be required in order to mitigate damage to buildings and other infrastructure.

Baseline conditions have now been established using two-dimensional DC electrical resistivity. Future measurements at the sites may provide insight into changing active layer depths, regions of increased thaw, groundwater movement and areas where increased unfrozen water content signals imminent thaw of ice-rich permafrost. The installation of four PVC pipe casings in the ice-rich materials will allow for future thermal measurements of the permafrost temperature and monitoring of thaw.

ACKNOWLEDGEMENTS

REFERENCES

ACIA, 2004. Impacts of a Warming Arctic: Arctic Climate Impact Assessment. Cambridge University Press.

Canadian Standards Association, 2010. Technical Guide: Infrastructure in permafrost: A guideline for climate change adaptation. PLUS 4011-10, 112 p.

Coates, J., 2009. Dawson City Front Street Thaw Depth Model. Report delivered to Yukon Highways and Public Works Transportation Engineering. Prepared by Kryotek Arctic Innovation.

Commonwealth Historic Resource Management Limited. 1984. St. Andrew's Presbyterian Church, Dawson: A Structural and Land Use Study. Parks Canada, MRS # 171, 206 p.

Coutts, R., 1984. The Palace Grand Theatre, Dawson City, YT: An Interpretive History. Parks Canada, MRS # 428, 121 p.

Duk-Rodkin, A.,1996. Surficial Geology, Dawson, Yukon Territory. Geological Survey of Canada, Open File 3288, scale 1:250 000.

Duk-Rodkin, A., Barendregt, R.W., White, J.M. and Singhroy, V.H., 2000. Geologic evolution of the Yukon River: implications for placer gold. Quaternary International, vol. 82, p. 5-31.

Environment Canada, 2010. National Climate Data and Information Archive. http://www.climate.weatheroffice. gc.ca/Welcome_e.html [accessed Dec. 8, 2010].

Fortier, R., LeBlanc, A., Allard M., Buteau S. and Calmels, F., 2008. Internal structure and conditions of permafrost mounds at Umiujaq in Nunavik, Canada, inferred from field investigation and electrical resistivity tomography. Canadian Journal of Earth Sciences, vol. 45, p. 367–387.

Froese, D.G., Barendregt, R.W., Enkin, R.J. and Baker, J., 2000. Paleomagnetic evidence for Multiple late Pliocene – early Pleistocene glaciations in the Klondike area, Yukon Territory. Canadian Journal of Earth Sciences, vol. 37, p. 863-877.

Froese, D.G., Duk-Rodkin, A., Bond, J.D. (eds.), 2001. Field guide to the Quaternary Research in the central and western Yukon Territory, CANQUA 2001. Occasional Papers in Earth Sciences, vol. 2, Heritage Branch, Government of Yukon.

Harris, S.A., French, H.M., Heginbottom, J.A., Johnston, G.H., Ladanyi, B., Sego, D.C. and van Everdingen, R.O. 1988. Glossary of permafrost and related ground ice terms. Permafrost Subcommittee, Associate Committee on Geotechnical Research, National Research Council of Canada, Ottawa.

Hauck, C., Vonder Mühll, D. and Maurer, H., 2003. Using DC resistivity tomography to detect and characterize mountain permafrost. Geophysical Prospecting, vol. 51, p. 273-284.

Heginbottom, J.A., Dubreuil, M.A. and Harker, P.A., 1995. Canada – Permafrost, In: National Atlas of Canada, 5th Edition, National Atlas Information Service, Natural Resources Canada, MCR 4177.

Kneisel, C., 2004. New Insights into mountain permafrost occurrence and characteristics in glacier forefields at high altitude through the application of 2D resistivity imaging. Permafrost and Periglacial Processes, vol. 15, p. 221-227.

Leverington, D.W. and Duguay, C.R., 1997. A Neural Network Method to Determine the Presence or Absence of Permafrost near Mayo, Yukon Territory, Canada. Permafrost and Periglacial Processes, vol. 8, p. 205-215.

Lipovsky, P. and Huscroft, C., 2007. A reconnaissance inventory of permafrost-related Landslides in the Pelly River watershed, central Yukon. In: Yukon Exploration and Geology 2006, D.S. Emond, L.L. Lewis and L.H. Weston (eds.), Yukon Geological Survey, p.181-195.

Munroe, J.S., Doolittle, J.A., Kanevskiy, M.Z., Hinkle, K.M., Nelson, F.E., Jones, B.M., Shur, Y. and Kimble, J.M., 2007. Application of Ground-Penetrating Radar Imagery for Three-Dimensional Visualization of Near-Surface Structures in Ice-Rich Permafrost, Barrow, Alaska. Permafrost and Periglacial Processes, vol. 18, p. 309-321.

National Round Table on the Environment and the Economy (NRTEE), 2009. True North: Adapting Infrastructure to Climate Change in Northern Canada. Ottawa, ON.

Plouffe, A. and Jackson, L.E., Jr., 1995. Quaternary stratigraphy and till geochemistry in the Tintina Trench, near Faro and Ross River, Yukon territory. In: Drift Exploration In the Canadian Cordillera, P.T. Bobrowsky, S.J. Sibbick, J.M. Newell and P.F. Matysek, (eds.), British Columbia Ministry of Energy, Mines, and Petroleum Resources, Paper 1995-2, p. 53-66.

Ross, N., Harris, C., Christiansen, H. and Brabham, P.J., 2005. Ground penetrating radar Investigations of open system pingos, Adventdalen, Svalbard. Norsk Geografisk Tidsskrift – Norwegian Journal of Geography, vol. 59, p. 129-138.

Wahl, H.E., Fraser, D.B., Harvey, R.C. and Maxwell, J.B., 1987. Climate of the Yukon. Atmospheric Environment Service. Environment Canada, Ottawa, Ontario.

Werner, A.T., Jaswal, H.K. and Murdock, T.Q., 2009. Climate Change in Dawson City, YT: Summary of Past Trends and future Projections, Pacific Climates Consortium, University of Victoria, Victoria, BC, 40 p.

Yukon Bureau of Statistics, 2010. Yukon fact sheet. http://www.eco.gov.yk.ca/stats/yukonfactsheet.html [accessed Nov.21, 2010].

Yukon Ecoregions Working Group, 2004a. Klondike Plateau. *In:* Ecoregions of the Yukon Territory: Biophysical properties of Yukon landscapes. C.A.S. Smith, J.C. Meikle and C.F. Roots (eds.), Agriculture and Agri-Food Canada, PARC Technical Bulletin no. 04-01, Summerland, BC, p. 159-168.

Yukon Ecoregions Working Group, 2004b. Yukon Plateau-North. *In:* Ecoregions of the Yukon Territory: Biophysical properties of Yukon landscapes. C.A.S. Smith, J.C. Meikle and C.F. Roots (eds.), Agriculture and Agri-Food Canada, PARC Technical Bulletin no. 04-01, Summerland, BC, p. 197-206.

Yukon Government, 2009. Yukon Government Climate Change Action Plan, 45 p.

Quartz vein gold mineralization in the Klondike Schist: The Mitchell-Sheba system, central Klondike district, Yukon

Tim Liverton[1]
Consultant

William Mann[2]
Klondike Star Mineral Corporation

ABSTRACT

The Mitchell-Sheba occurrence is a gold, silver and base metal-bearing quartz vein system contained within a thrust slice of mafic schist that forms part of the Klondike Schist. The vein system formed late in the D4 folding event or subsequently thereafter. Mineralization occurs as gold + silver, base metal sulphides and sulphosalts within quartz veins. Low-grade gold associated with pyrite mineralization is hosted within the surrounding chlorite schist. The mafic rocks are interpreted to be metavolcanic in origin and have reached upper greenschist facies metamorphism. Hydrothermal sericite-carbonate alteration of the host rocks is associated with mineralization and is reflected in the whole rock geochemistry. The prospect underlies one of the larger soil geochemical anomalies in the Klondike region.

[1]timliv@northwestel.net
[2]mann@klondikestar.ca

INTRODUCTION

This paper describes the geological setting of one of the most significant gold-silver bedrock occurrences in the Klondike goldfields, the Mitchell-Sheba vein system. The structural setting, lithology and lithogeochemistry of this system are described in this paper. Mafic metavolcanic rocks that are interpreted to have reached upper greenschist facies metamorphism host the gold-silver mineralization, which occurs in the hanging wall of a regional thrust fault that locally contains slivers of ultramafic rock. The authors explored the property in the period between 2006 and 2008 for Klondike Star Mineral Corp. (Liverton, 2007) whom held the property under option.

In the two decades following the discovery of placer gold in Bonanza Creek in 1896, drainages radiating from King Solomon Dome were thoroughly prospected. Many prospectors sought a bedrock source for the gold, and one of their early finds was a gold-bearing quartz vein system about 1200 m north-northeast of the King Solomon Dome summit. The Mitchell and Sheba veins are rumoured to have initially yielded spectacular surface samples; occurrences on these veins, the KSD, J.A.E. and others (Yukon MINFILE 115O 068), have been intermittently trenched and bulk-sampled since their discovery. The Mitchell-Sheba veins are one of two Klondike area prospects where significant gold has been extracted from bedrock and therefore are likely an important source of placer gold.

REGIONAL GEOLOGY AND STRUCTURE

The Mitchell, Sheba and Orekon prospects (herein the study area) are 30 km southeast of Dawson City. The regional bedrock unit is the Klondike Schist, a widespread Middle to Late Permian unit of the Yukon-Tanana terrane. The greenschist facies siliciclastic metasedimentary and bimodal metavolcanic rocks form a thrust stack (Mortensen, 1990, 1996; Mackenzie *et al.*, 2007; Mackenzie *et al.*, 2008a). These rocks and the coeval Sulphur Creek orthogneiss, located 15 km to the southwest, are remnants of a short-lived arc overlying the north and west-dipping subduction of the Slide Mountain Ocean (269 to 253 Ma Klondike cycle of Nelson *et al.*, 2006), which represents the last magmatic cycle of Yukon-Tanana terrane before its accretion to the margin of Laurentia.

Less than 1 km east of the study area (Fig. 1), a road-cut exposes a thrust slice of Klondike Schist overlying altered ultramafic rocks interpreted as a sliver of Slide Mountain terrane (Mortensen, 1996). The rocks within the study area are structurally near the base of the hanging wall. The dominant lithology is chloritic schist (here referred to as the mafic schist unit), one of the three broad lithologic groupings of the Klondike Schist (Mortensen, 1990, 1996).

The structural geology of the Klondike district as described by MacKenzie *et al.* (2007) hosts four generations of deformation. D_1 isoclinal folding (S_1) transposes original bedding (S_0) such that hinges of this generation appear as intrafolial cm-scale folds. The second ductile deformation event produced isoclinal recumbent folds (Fig. 2a) and pervasive penetrative foliation (S_2). Hinges of these folds have decimetre-scale wavelength and are locally apparent within the Klondike Schist and are particularly well developed at the Orekon prospect (Fig. 1). Ductile folding (D_3) during thrust stacking produced recumbent folds with a spaced cleavage (S_3) that are well developed in the muscovite-rich schist (Fig. 2b). A phacoidal cleavage is exhibited in some thrust fault zones.

Folding of D_4 generation is of mesoscopic-scale kink or box-fold style that has axial trends from ten to eighty degrees different to those of F_3 axes. D_3 folding occurred in a ductile regime whereas D_4 folding formed near the brittle-ductile transition. Quartz veins were formed locally during D_2 to late D_4. Only the undeformed late D_4 mesothermal quartz veins contain obvious gold mineralization. Younger brittle faults with gouge zones are exposed in several trenches throughout the Klondike. The Klondike region has not been glaciated, and outcrops in the study area are variably oxidized.

MAFIC SCHIST UNIT

LITHOLOGY

Outcrops in the study area vary from quartz-feldspar-muscovite ± chlorite in the eastern slopes, to chlorite-quartz-feldspar-epidote-actinolite ± biotite (Fig. 3a) at the ridge crest along the Mitchell-Sheba trend. The most mafic schist, containing quartz, feldspar, chlorite, epidote and actinolite, is consistent with derivation from a basic volcanic protolith. Analyses of major oxide contents and trace elements (Table 1) are consistent with basaltic protoliths. The muscovite schist is interpreted to have been derived from clay-rich siliciclastic metasediments which contained a volcanic component. The chlorite schists are likely metavolcanic flows with possible sub-volcanic intrusions.
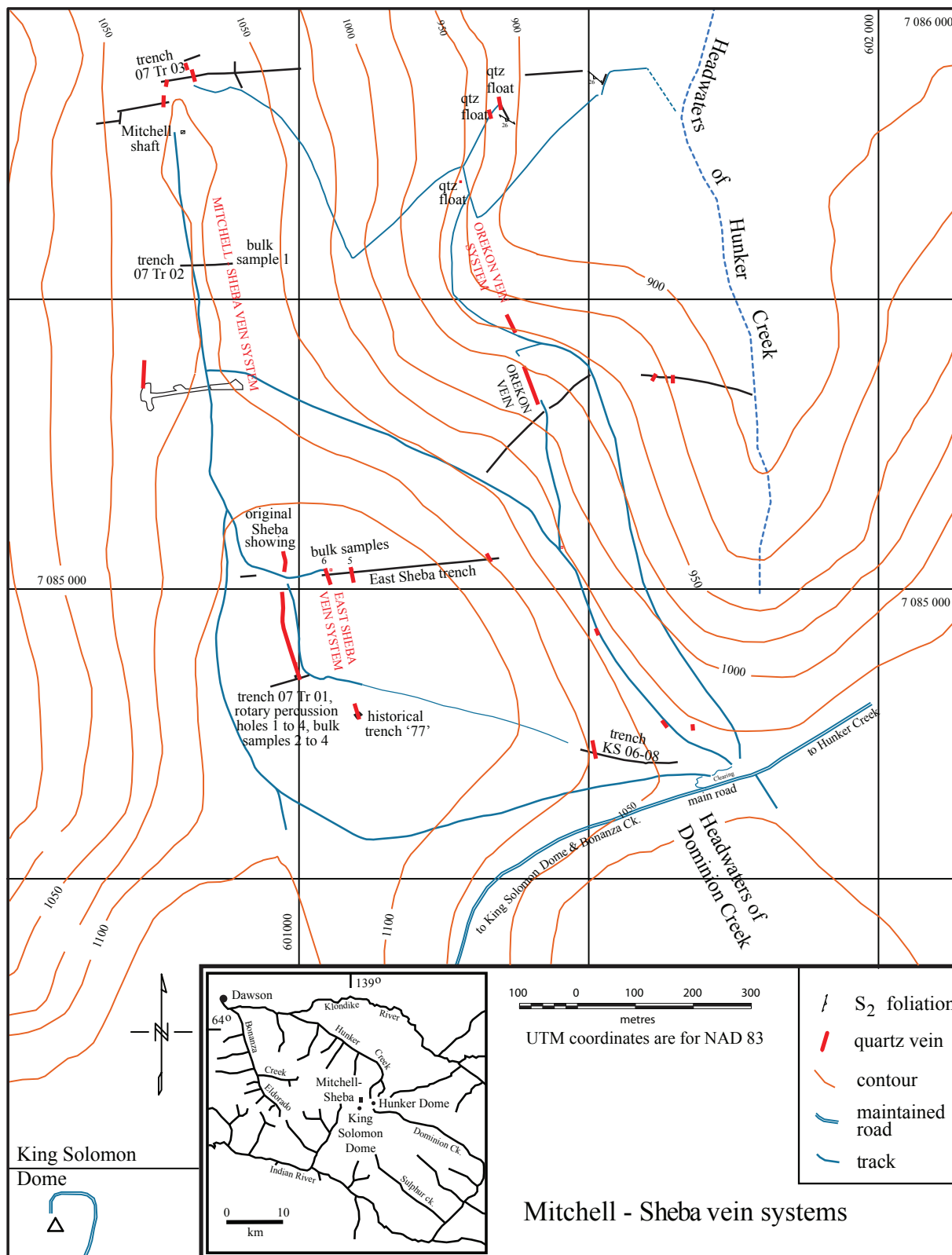
Figure 1. *Quartz vein systems at the JAE property.*
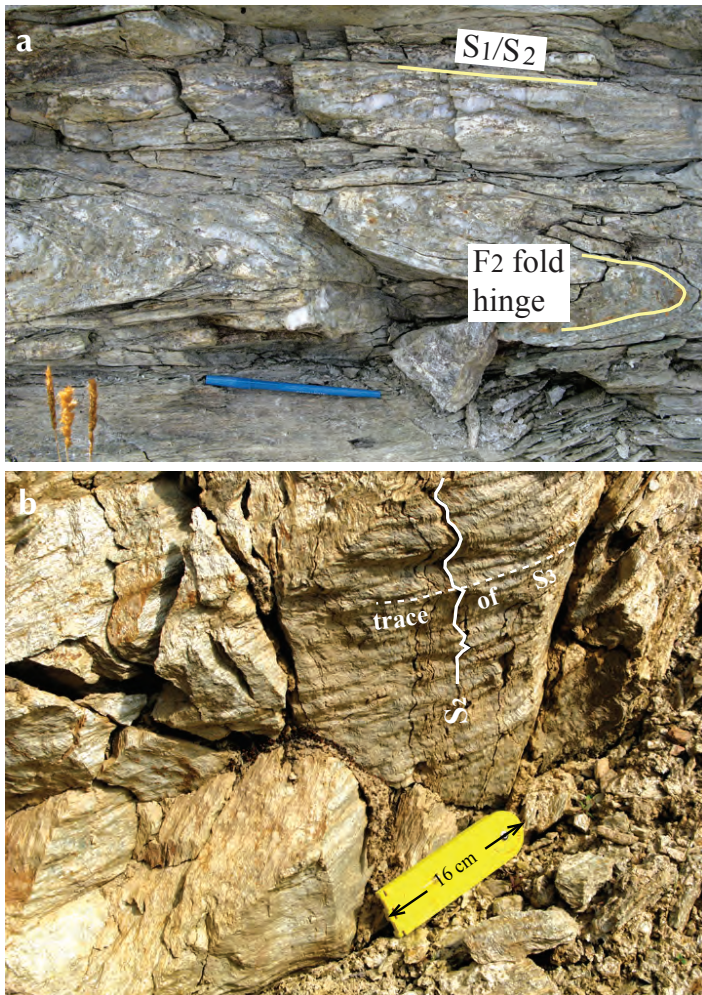
Figure 2. (a) *Recumbent F_2 folds at the Orekon prospect. Pen is 16 cm long.* **(b)** *F_3 crenulation folding; trench is 185 m northeast of the Mitchell shaft.*

PETROGRAPHY

The mafic schists comprise quartz, feldspar, chlorite, epidote, plus bluish actinolite in some lithologies (Figs. 3a,b), notably along the crest of the Mitchell ridge. A strong metamorphic foliation (S_2) was observed and where euhedral amphiboles are present, they are aligned within this fabric. The amphibole crystals are interpreted to be metamorphic in origin rather than porphyroblasts derived from original phenocrysts. Biotite occurs infrequently within the mafic schist unit that comprises the thrust sheet present at the JAE property.

In the most 'mafic' schist the S_2 foliation, defined by preferred orientation of biotite and chlorite, curves around spherical masses of epidote that are interpreted to be retrogressed garnet (Fig. 3c). This indicates that the rocks reached upper greenschist facies metamorphism. Relatively coarse plagioclase porphyroblasts with myrmekitic rims (Fig. 3d) are interpreted to be relict phenocrysts.

DISCUSSION

It is uncertain whether the emplacement of the Klondike's largest late-tectonic quartz vein system was due to the mafic schist behaving in a more brittle manner compared to the more incompetent quartz-rich muscovite schist. It is plausible that during the late to post-D_4 deformation (*i.e.*, in a brittle regime) the basic rocks had accommodated extension and possibly strike-slip movement which resulted in the formation of a major vein system. Another possibility is that the Sheba vein system has followed the axial plane of a major F_4 fold whereby one wavelength is in the order of hundreds of metres. The lack of rock exposure to the west of the ridge does not allow for adequate determination of fabric elements that could establish or refute these interpretations.

Table 1. *Major oxide and trace element analyses.*

Sample number	Metres from west end	SiO2 %	Al2O3 %	Fe2O3 %	CaO %	MgO %	Na2O %	K2O %	Cr2O3 %	TiO2 %	MnO %	P2O5 %	SrO %	BaO %	C %	S %	LOI %	Total %	Ba ppm	Ce ppm	Co ppm	Cs ppm	Dy ppm	Er ppm	Eu ppm
B26	35.1	51.37	17.99	10.50	1.99	6.18	5.38	0.34	0.005	0.82	0.1	0.11			0.42	0.04	5.20	100.02	124.4	16.2	32.0	0.2	3.48	2.11	0.81
B28	30.0	48.56	18.76	12.04	1.83	6.03	4.07	1.86	0.006	0.98	0.11	0.14			0.40	0.26	5.40	99.88	549.2	18.6	42.2	1.4	3.71	2.37	1.03
C35	38.6	51.00	19.85	9.63	1.73	4.81	6.08	1.15	<0.01	0.72	0.11	<0.01	0.01	0.02	0.28	0.01	4.31	99.40	202.0	8.8	32.9	1.4	2.29	1.41	0.74
B18	45.5	48.36	17.64	8.90	5.08	5.02	1.72	3.83	0.005	0.84	0.14	0.05			1.22	0.21	8.30	100.02	892.9	16.1	18.7	1.4	3.43	2.17	0.84
B11	48.3	40.52	18.22	10.97	7.43	6.00	0.63	4.54	0.007	0.92	0.16	0.12			1.73	0.30	10.30	100.03	1401.4	16.2	36.1	2.9	3.21	2.01	0.66

	Ga ppm	Gd ppm	Hf ppm	Ho ppm	La ppm	Lu ppm	Nb ppm	Nd ppm	Ni ppm	Pr ppm	Rb ppm	Sm ppm	Sr ppm	Ta ppm	Tb ppm	Th ppm	Tm ppm	U ppm	V ppm	W ppm	Y ppm	Yb ppm	Zr ppm
B26	18.4	2.98	1.8	0.68	6.5	0.29	1.6	11.1	31	2.22	10.1	2.7	48.9	0.1	0.60	1.30	0.30	0.60	275	6.5	20.70	1.87	58
B28	23.1	3.30	2.5	0.75	7.1	0.34	1.9	11.8	26	2.51	68.9	3.0	67.3	0.1	0.66	1.80	0.34	0.90	401	10.3	22.60	2.20	75
C35	16.1	2.01	1.7	0.46	3.6	0.23	1.2	6.1	21	1.31	38.9	1.7	75.0	0.1	0.37	1.17	0.24	0.41	218	16.0	12.00	1.37	59
B18	17.2	2.95	2.1	0.71	6.0	0.30	1.5	10.5	21	2.18	102.0	2.7	239.7	0.1	0.57	1.20	0.28	0.50	274	9.4	20.10	1.92	61
B11	21.1	2.92	2.1	0.66	6.0	0.29	1.6	10.6	28	2.24	114.9	2.7	358.4	0.1	0.55	1.50	0.29	0.60	335	13.4	19.30	1.91	66

Analyses were obtained by Li metaborate fusion/ICPMS for major elements, with fusion/ICPMS for traces. 'B' prefix specimens were analysed by Eco Tech laboratory and 'C' by ALS Chemex
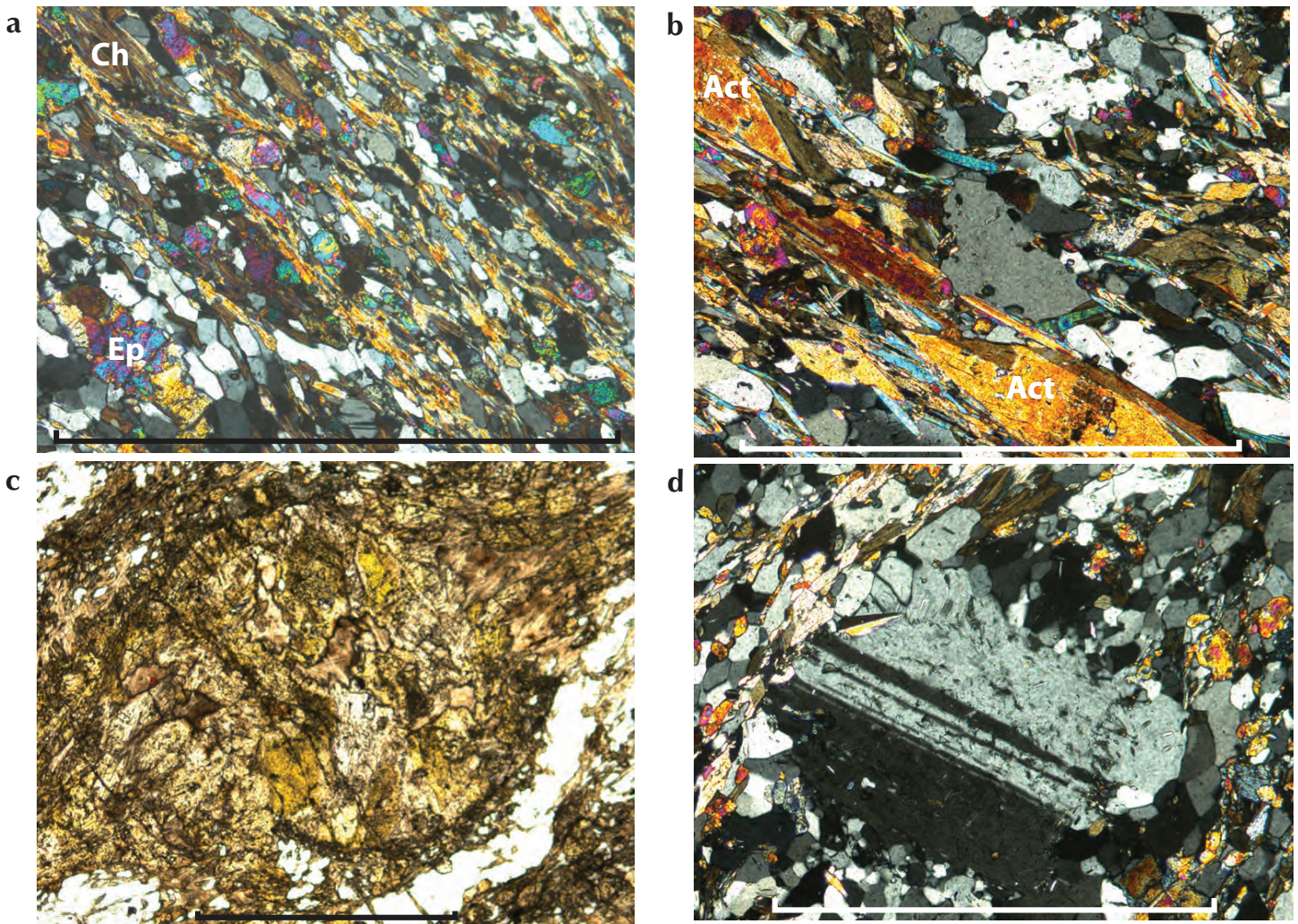
Figure 3. (a) *Epidote-chlorite-quartz-feldspar schist. Trench 07Tr03 at the Mitchell prospect, 47.7 m from west end of trench. Thin section under crossed polarizers. Epidote (Ep) and chlorite (Ch, dark and showing cleavage in the monochrome image) define the S2 foliation.* **(b)** *Euhedral actinolite (Act) in quartz-feldspar-epidote-chlorite-amphibole schist. Trench 07Tr03 35.1m from west end of trench. Thin section under crossed polarizers. Presence of actinolite amphibole which is blue under plane polarized light in this lithology is likely a reflection of protolith chemistry rather than an indicator of high pressure metamorphism.* **(c)** *Spherical mass of epidote (pseudomorph after garnet?) in carbonate-altered, epidote-chlorite quartz feldspar schist. The various thrust sheets of the Klondike Schist show some evidence of variation in metamorphic grade. Trench 07Tr03 at the Mitchell prospect, 46.7 m from west end of trench. Thin section under plane polarized light.* **(d)** *Plagioclase porphyroblast in quartz-feldspar-epidote-chlorite-amphibole schist. This is interpreted to be a remnant phenocryst in a basalt protolith. Same specimen as (3c). Thin section under crossed polarizers. Scale-bar on these images represents 1 mm.*

QUARTZ VEIN SYSTEMS

The Mitchell-Sheba system is a kilometre-long zone of anastomosing and stockwork veins that coalesce into massive 2 m-thick veins over tens of metres strike length at the Mitchell and Sheba prospects. The East Sheba and Orekon veins are parallel structures located 80 and 500 m to the east, respectively (Fig. 1). Orientation of these veins is consistent with their formation late in the D_4 ductile to brittle folding parallel to the northwesterly axial planes of this fold generation (Mackenzie *et al.*, 2008b). In the South Sheba area several examples of centimetre-scale quartz veins following axial planes of mesoscopic-scale F_4 kink folds may be observed. One such example from Trench 07Tr01 is shown in Figure 4. Also note various S_4 orientations and similarity to vein attitudes shown in Figure 5.
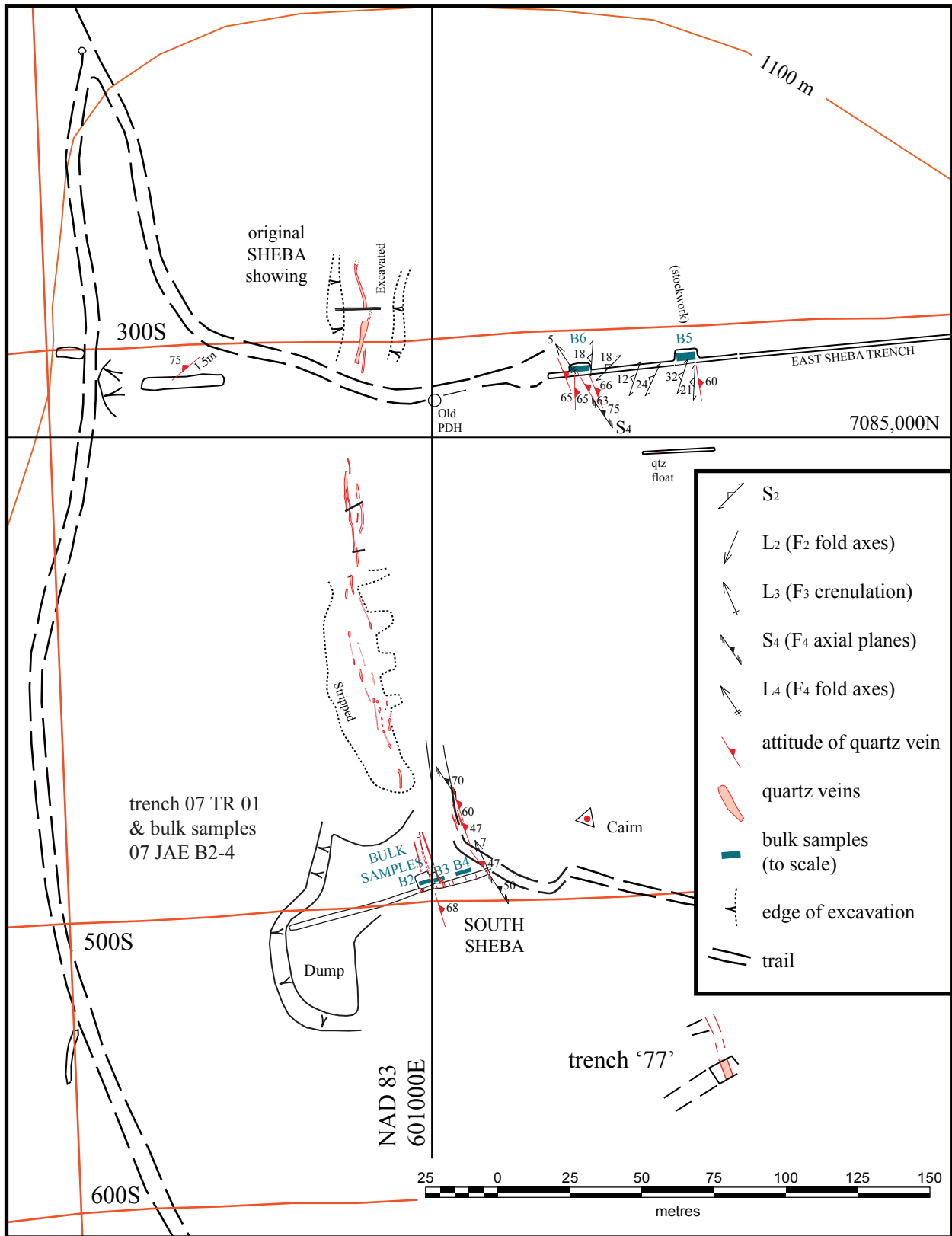
Figure 4. *Detailed map of the Sheba prospect.*
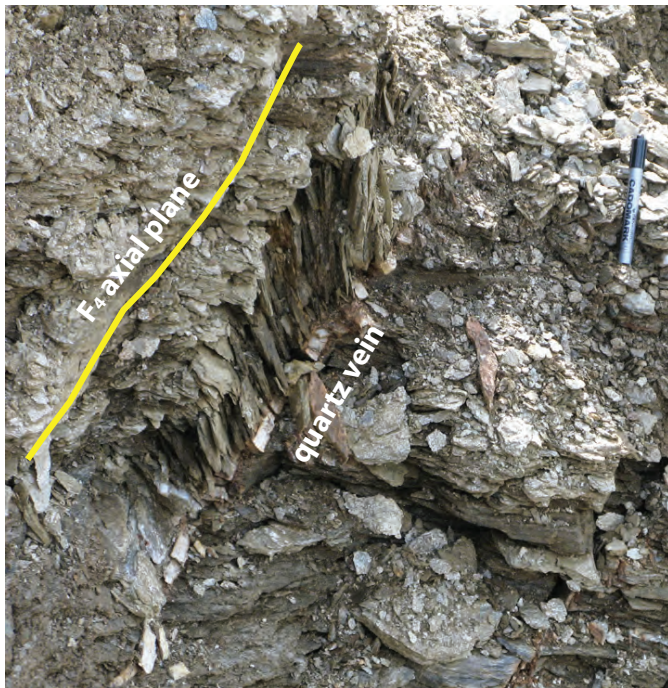
Figure 5. *Example of a quartz vein following the orientation of F$_4$ axial surfaces. East end of trench 07Tr01. Several examples of quartz veins following the orientation of S$_4$ may be seen in the South Sheba area. Marker pen is 13 cm long.*

In addition to the obvious north-northwest-striking, near vertical structures that form the Mitchell-Sheba, East Sheba and Orekon veins, a set of flat-lying, northwest-dipping, intersecting veins have also been observed adjacent (33 m south) to the Mitchell shaft and at the stockwork system in the East Sheba trench. Although these veins are <10 cm thick, they are economically significant because they contain free gold.

The largest vein in the East Sheba stockwork has a 20 cm-wide gouge zone along its western margin indicating late movement under a brittle faulting regime. Fault movement with gouge zones along vein margins is also observed at the Orekon vein and un-named veins to the east of the Mitchell prospect.

The Dome Lode vein occurrence (Yukon MINFILE 115O 067), located about 2 km south-southeast of the Mitchell-Sheba system, occurs in a similar geological setting.

MINERALIZATION WITHIN THE VEIN SYSTEMS

The historical Mitchell and Sheba prospects produced small tonnages of spectacular Au and Ag grades from 'pods' of massive sulphides that were <15 m in strike length. A small tonnage of hand-sorted high-grade ore was shipped from the Mitchell shaft (Yukon MINFILE 115O 068) and Sheba prospect (Hulstein, 1988). Detailed mapping of the Sheba prospect (Fig. 4 - north end) indicates that the 'pod' of high-grade galena-chalcopyrite-tetrahedrite mineralization occurred at a bend in the massive part of the vein system. This could indicate that minor strike-slip motion (a releasing bend) produced an extensional environment that allowed for formation of the more massive portion of the vein system.

In the East Sheba trench, two mineralized vein systems are exposed. Four decimetre-scale quartz veins are found at the west end of the trench and a stockwork zone 5.5 m wide is formed by steep east-dipping veins parallel to the Sheba vein, with shallow west-dipping cm-scale veins. The separate vein system at the west end of the trench contains ≤1 mm grains and crystals of pyrite, arsenopyrite, galena, chalcopyrite and tetrahedrite. Selvedges to these veins contain pyrite crystals that penetrate up to 10 cm into the muscovite schist wallrock. The stockwork zone veins extend 42 to 50 m from the west end of the East Sheba trench and are formed in comparatively massive mafic schist. Carbonate alteration is obvious in hand specimen, and occurs 2 m on either side of the zone, with petrographic specimens indicating up to 20% modal carbonate for a further 2 m on the eastern side. Within the stockwork, the metamorphic fabric (S$_2$) of the country rock has been completely obliterated by randomly oriented sericite and brown carbonate alteration. Both pyrite (up to 20 mm across) and finer grained arsenopyrite are common (Figs. 6a,b). In comparison, the relatively unaltered chlorite schist and muscovite schist elsewhere in the East Sheba trench show a strong foliation (Figs. 6c,d). Assays of the selvedge rock (single hand specimens selected for petrography) reported from trace amounts to 12.2 g/t gold.

Gold grade of the schist between individual quartz veins (selvedges) appears highly variable. Analyses of the petrographic specimens from the East Sheba stockwork zone indicate grades from 0.03 to 12 g/t Au for samples that contain no quartz vein material. At the South Sheba zone, Trench 07Tr01, chip samples were taken across the zone that contains four major and fifteen minor east-dipping quartz veins. The intervening schist assayed up to 0.11 g/t. Additional subparallel veins, with thicknesses ranging from a few cm to 1.5 m, are exposed in road cuts and trenches in the study area, but have unknown extents. Gold on the property is often coarse, as it is elsewhere in the Klondike, creating a 'nugget effect' making gold resource evaluation challenging. A program
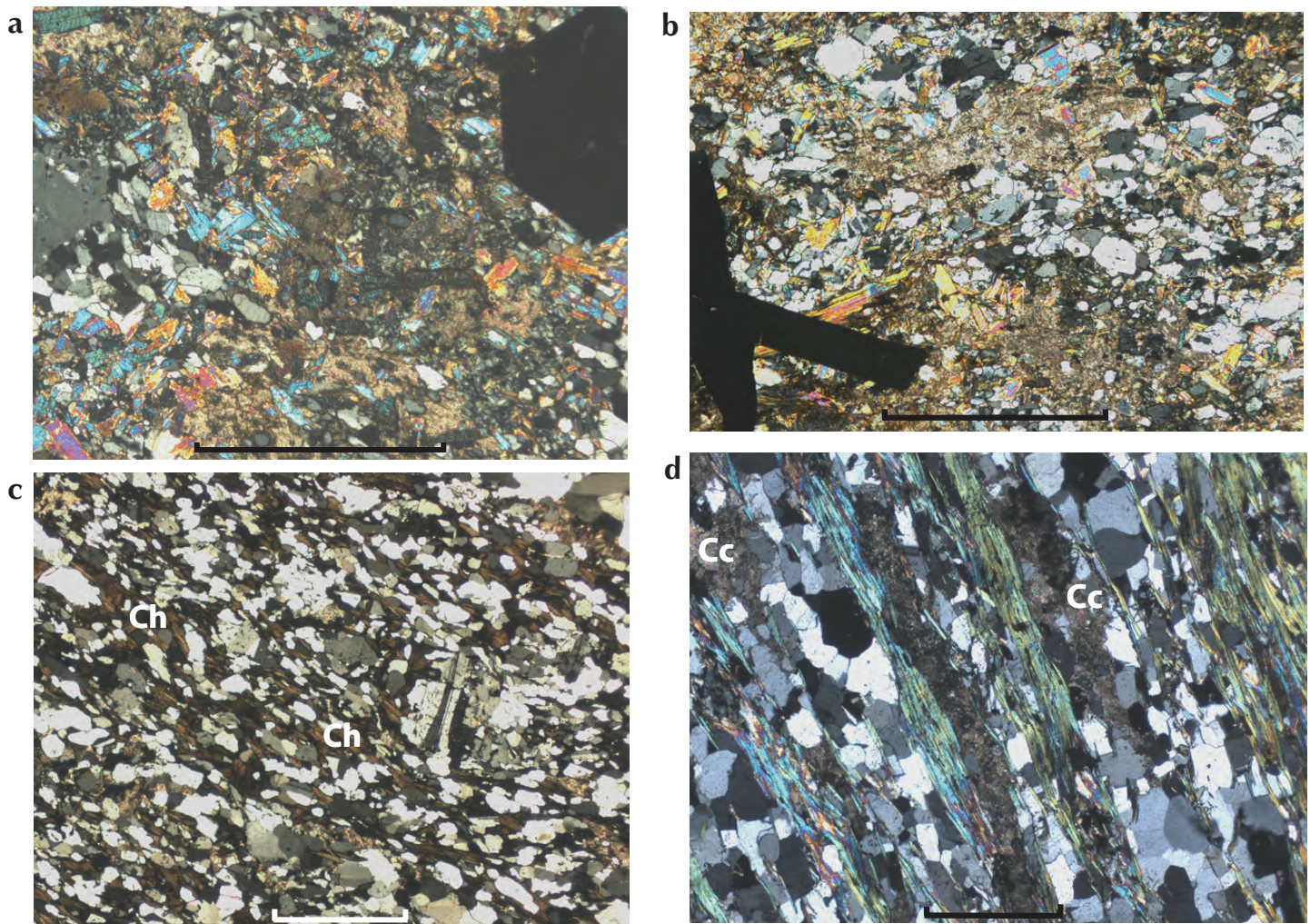
Figure 6. (a) *Pyrite crystal in heavily carbonate-sericite altered schist. East Sheba trench, 47.7 m from west end. Thin section under crossed polarizers. Note that the muscovite 'flakes' are coarse-grained and randomly oriented rather than defining a S2 foliation as in unaltered schist – they are interpreted to be sericite alteration. **(b)** Arsenopyrite crystals in heavily carbonate altered schist. East Sheba trench, 39.0 m from west end. Thin section under crossed polarizers. As in (a) the metamorphic foliation has been destroyed. **(c)** Unaltered chlorite-quartz-feldspar schist. The S2 foliation is produced by preferred orientation of chlorite (Ch, dark, showing cleavage in the monochrome image). East Sheba trench, 28.0 m from west end. One plagioclase porphyroblast may be seen. Thin section under crossed polarizers. **(d)** Muscovite-quartz-feldspar schist with slight carbonate alteration. East Sheba trench, 25.1 m from west end. Thin section under crossed polarizers. A distinct S2 foliation is produced by the mica layers. Cc = carbonate. The scale-bar in these images is 1 mm.*

Table 2. *Results from bulk sampling.*

Sample no.	Zone	UTM (NAD 83) Easting	UTM Northing	Weight kg	Au g/t	Rock type
06-JAE-B1	Hunker Dome Trench	601510	7084727	2276	3.99	quartz vein in rusty schist
06-JAE-B2	Mitchell	600790	7085815	5729	1.30	pyritic schist, no veins
07-JAE-B1	Speed Bump (Meneluk)	600852	7085574	4211	0.26	quartz vein with galena
07-JAE-B2	South Sheba	600999	7084844	6103	0.27	quartz veins and rusty schist
07-JAE-B3	South Sheba	601004	7084844	5862	0.09	quartz veins and rusty schist
07-JAE-B4	South Sheba	601013	7084847	2095	0.10	quartz veins and rusty schist
07-JAE-B5	Sheba East	601090	7085028	7249	0.73	quartz veins and rusty schist
07-JAE-B6	Sheba East	601050	7085024	6088	0.50	quartz veins and rusty schist

of bulk sampling, with gravity concentration and analysis of products, was undertaken to accurately assess gold grade and size distribution. The bulk sampling results are summarized in Table 2.

Elsewhere on the property, other ≤1 m-thick veins (*e.g.*, Orekon and the veins dubbed 'trench 77' in Figure 1; possibly the southern extension of the east Sheba system) have quartz with massive galena cores. This Pb precipitation is interpreted as the last mineralizing event in the vein system.

GEOCHEMISTRY

GEOCHEMISTRY OF THE MAFIC HOST ROCK

The composition of the chlorite schists was determined by analysis of slightly altered to unaltered schist from the East Sheba trench. Five of these analyses are presented in

Table 1. These rocks are believed to have a basaltic protolith and therefore, the results are plotted on trace element discrimination diagrams (Fig. 7) to determine the paleotectonic setting. The chlorite schist analyses plot in the field for island arc tholeiites or volcanic arc basalts on the diagrams.

GEOCHEMISTRY OF THE VEIN WALLROCK AND ALTERATION

Analyses of chip samples from the East Sheba trench indicate that gold values correlate strongly with arsenic (Fig. 8), which is consistent with the observation of arsenopyrite or tetrahedrite-tennantite within the quartz veins and within the sericite-carbonate alteration zone of the stockwork. Increase in the sulphur and 'total carbon' content of the rock reflects pyrite-arsenopyrite mineralization and carbonate alteration within this zone. However, when the ratio C/S is plotted, the carbonate
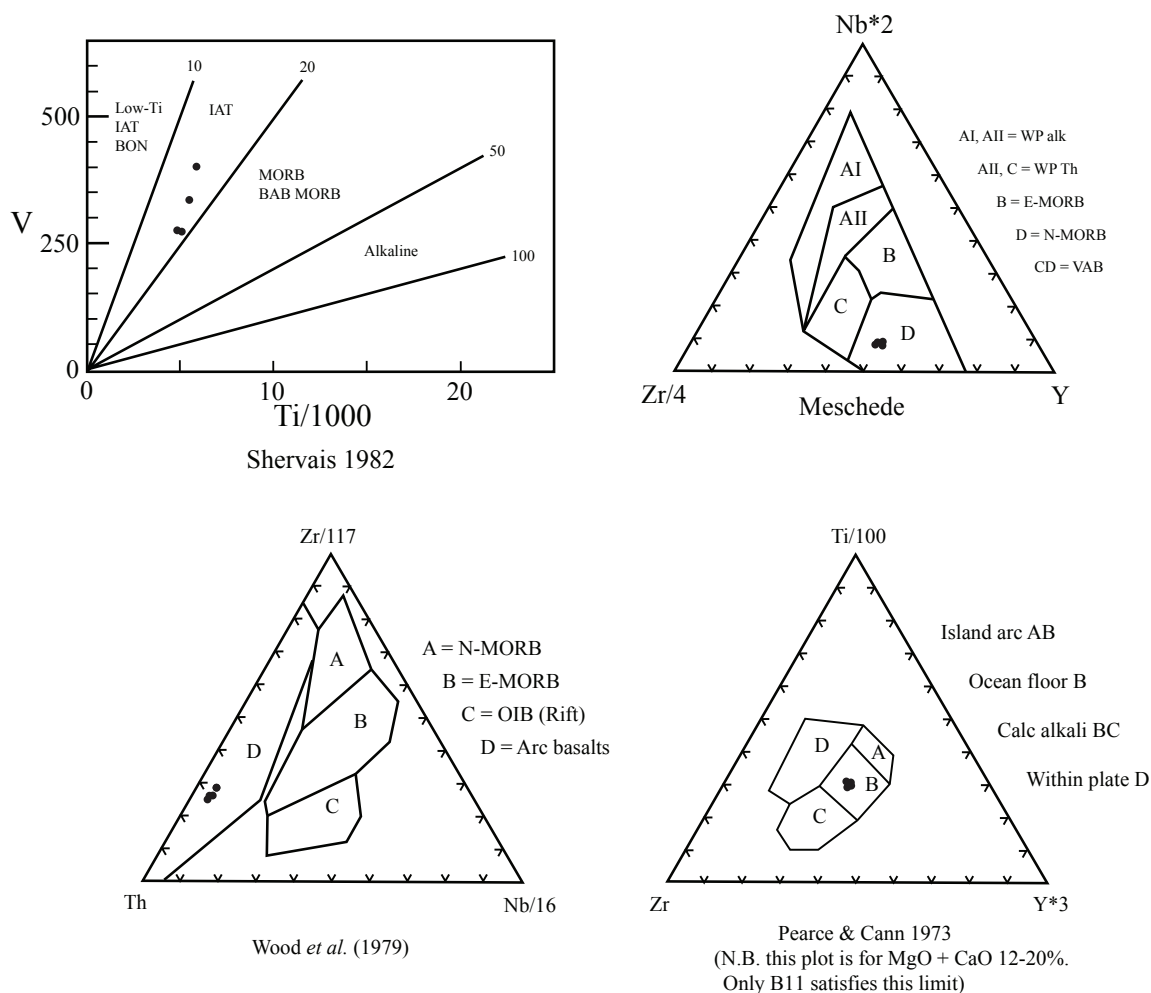
Figure 7. *Trace element discriminant diagrams for relatively unaltered chlorite schist.*
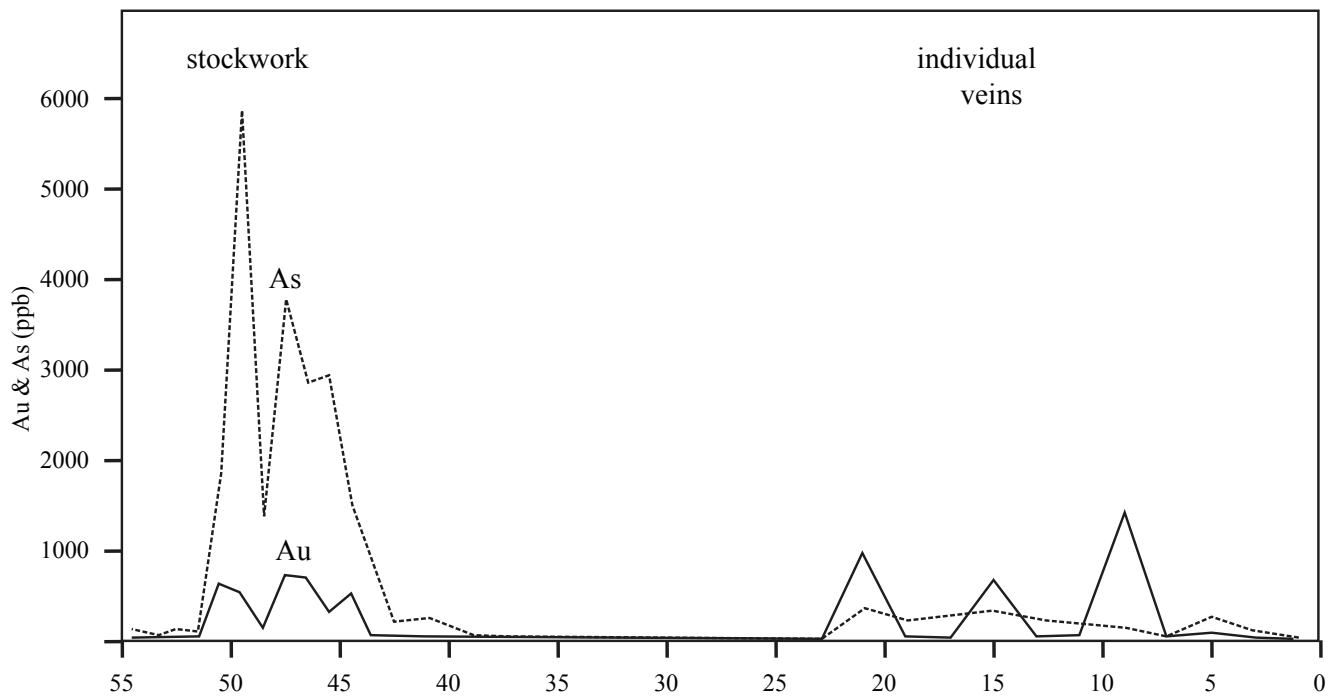
Figure 8. *Gold (Au) and arsenic (As) values from analyses of rock chip samples for the East Sheba trench, including both the stockwork and western vein zones.*

alteration at the margin of the zone is emphasized (Figs. 9a,b). Where whole-rock analysis is employed, this element ratio could prove a useful indicator for mineralized zones; however, typically exploration geochemistry trace element analytical packages are preferred due to cost considerations. The sericite alteration is reflected in the K/Na ratio for the whole-rock analyses (Fig. 9c). Increase in K relative to Na is obvious in samples analysed from within the region of intense quartz veining (42 to 48 m from the west end of the trench). No metre-scale potassic selvedge to the stockwork is indicated by this ratio. At the detailed rock sampling scale, Cu, Pb, Zn, Ag, Sb and As show a close relationship with anomalous gold. Furthermore, all of these elements could potentially indicate mineralized zones.

EXPLORATION GEOCHEMISTRY OF THE VEIN AREA

These prospects are contained within one of the largest soil geochemical anomalies found in the Klondike (Stevens, 1997). This previous work reports results from over 1700 samples of -80 mesh soil collected from the B or C soil horizons in the area. Samples were analysed by multi-element inductively coupled plasma mass-spectrometry (ICP-MS). The anomaly consists of elevated Au, As, Ag and Pb (and to a lesser extent elements such as

Cu, Ba, Zn), which are coincident with the Mitchell and Sheba zones and the Dome Lode area, extending over an area roughly 2 by 4 km. The anomaly comprises broad but erratic gold (<20 ppb to 915 ppb), strong arsenic near Sheba and Dome Lode, weaker arsenic near Mitchell and strong silver and lead along the Sheba trend. Lead is also elevated near the Orekon vein. The anomaly extends beyond the study area to the northwest and southeast.

For regional soil sampling Pb may be the best indicator of the location of vein systems. However, correlation with gold content may not be strong since the larger veins have cores of massive galena that are related to the latest mineralizing event. Gold would have been introduced early in the vein-forming process and in the vein selvedges (*e.g*, Hoymann and Friedrich, 1992).

DISCUSSION

EXPLORATION SIGNIFICANCE

The vein systems of the JAE offer two targets for mineralization: 1) small, very high-grade 'pods' such as those at the original Mitchell and Sheba showings; and 2) quartz vein plus disseminated mineralization that is of low-grade but has potential for large bulk tonnages. Pyritic alteration zones associated with the vein systems

are considered important for the economic potential of the gold-bearing system as they have greater width and continuity than the quartz veins. The pyritic zones show continuity in induced polarization (IP) geophysical surveys and additional IP work is recommended (Mark, 1991).

The Mitchell and Sheba vein system occurs roughly on trend with the Hunker Dome or Dome Lode occurrence (Yukon MINFILE 115O 067), approximately 2 km to the south-southeast. Four quartz-gold veins are reported at Dome Lode, and a 790 m adit was driven under these veins during 1909 and 1910. The veins at Dome Lode are not as well exposed as those at Mitchell and Sheba, and bedrock is covered by overburden between them; however, the geochemical anomaly connects the two occurrences.

These veins are considered to be of orogenic or mesothermal nature (Mortensen, 1996).

The vein system was emplaced either late in the D_4 deformation of the Klondike Schist or subsequently as a brittle extensional event. Mineralization consists of Au with Ag, Pb, Cu, As and Sb sulphides and sulphosalts in the quartz veins and lower grade Au + pyrite within the immediately surrounding schist.

The well mineralized Mitchell and Sheba trend is one of the strongest gold-bearing structures in the Klondike region and occurs within one of the strongest geochemical anomalies. This property is located at the headwaters of some very rich placer gold streams, but has been minimally tested by drilling. None of the drilling has targeted the Mitchell prospect, which appears to be the best gold target on the claims. Considerable exploration potential exists to the southeast towards the Dome Lode prospect, and on trend in both directions.

ACKNOWLEDGEMENTS
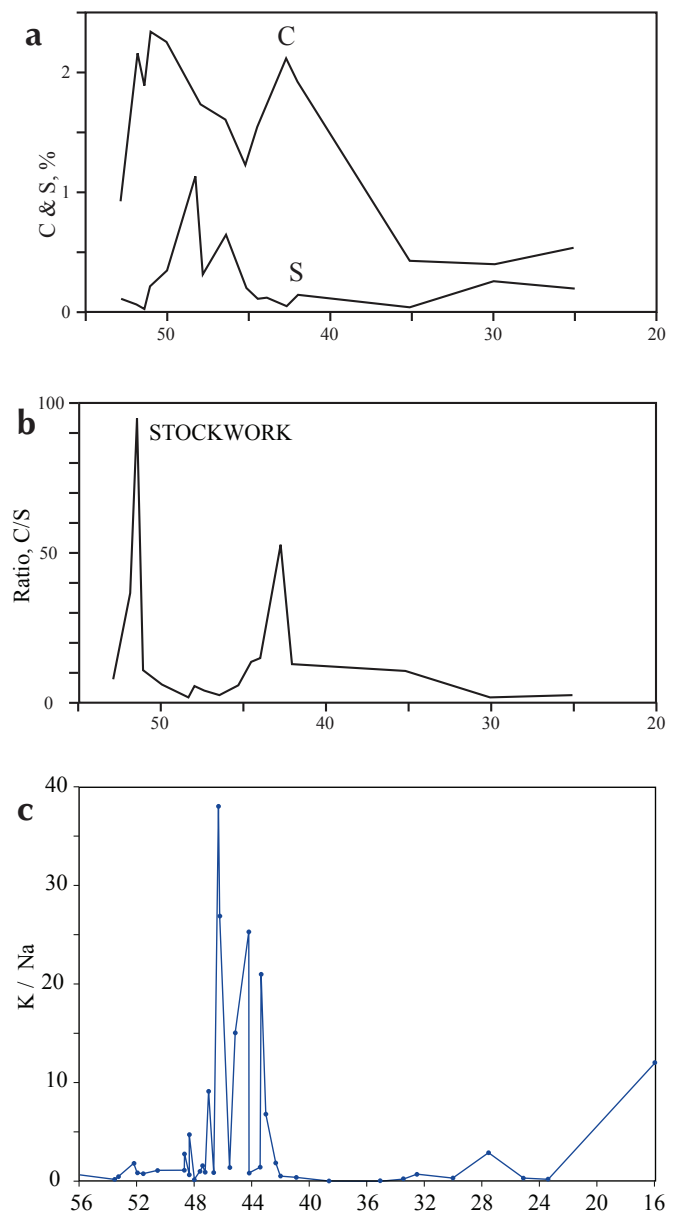
Figure 9. (a) Total sulphur (S) and carbon (C) values and their ratios from whole-rock analyses of petrographic specimens (single ≤1 kg hand samples) taken across the East Sheba stockwork zone. Increase in total C indicates carbonate alteration and S predominantly the pyrite mineralization. **(b)** The element ratio emphasizes the carbonate alteration at the margin of this mineralized zone. **(c)** The K/Na ratio also emphasizes the sericite alteration within the stockwork zone.

REFERENCES

Hoymann, K-H. and Friedrich, G., 1992. Gold and sulphide mineralization in the Hunker Creek area, Yukon Territory, Canada. *In*: Yukon Geology, vol. 3, Exploration and Geological Services Division, INAC, p. 12-326.

Hulstein, R., 1988. 1988 work on the JAE claims. Yukon mining assessment report number 092517.

Liverton, T., 2007. Geological mapping, trenching, rock sampling, bulk sampling and grid preparation on the JAE property. Klondike Star Mineral Corp. Yukon mining assessment report.

MacKenzie, D., Craw, D. and Mortensen, J.M., 2008a. Thrust slices and associated deformation in the Klondike goldfields, Yukon. *In:* Yukon Exploration and Geology 2007, D.S. Emond, L.R. Blackburn, R.P. Hill and L.H. Weston (eds.), Yukon Geological Survey, p. 199-213.

MacKenzie, D., Craw, D., Mortensen, J.M. and Liverton, T., 2008b. Disseminated gold mineralization associated with orogenic veins in the Klondike Schist, Yukon. *In:* Yukon Exploration and Geology 2007, D.S. Emond, L.R. Blackburn, R.P. Hill and L.H. Weston (eds.), Yukon Geological Survey, p. 215-234.

MacKenzie, D., Craw, D., Mortensen, J.M. and Liverton, T., 2007. Structure of schist in the vicinity of the Klondike goldfield. *In:* Yukon Exploration and Geology 2006, D.S. Emond, L.L. Lewis and L.H. Weston (eds.), Yukon Geological Survey, p. 197-212.

Mark, D., 1991. Geophysical Report on Induced Polarization, Resistivity and Magnetic Surveys over portions of the JAE and Dawson claims, Hunker Creek, Dawson City area, Dawson M.D., Yukon Territory. Yukon mining assessment report number 092974.

Mortensen, J.K., 1996. Geological compilation maps of the northern Stewart River map area, Klondike and Sixtymile districts (115N/15,16; 115 O/13,14 and parts of 115 O/15, 16), 1: 50 000 scale. Exploration and Geological Services, Yukon Region, Indian and Northern Affairs Canada, Open File 1996-1 (G), 43 p. and 6 maps.

Mortensen, J.K., 1990. Geology and U-Pb geochronology of the Klondike district, west-central Yukon Territory. Canadian Journal of Earth Sciences, vol. 27, p. 903-914.

Nelson, J.L., Colpron, M., Piercey, C.J., Dusel-Bacon, C., Murphy, D.C. and Roots, C.F., 2006. Paleozoic tectonic and metallogenic evolution of pericratonic terranes in Yukon, northern British Columbia and Alaska. *In:* Paleozoic Evolution and Metallogeny of Pericratonic Terranes at the Ancient Pacific Margin of North America, Canadian and Alaskan Cordillera, M. Colpron and J.L. Nelson (eds.), Geological Association of Canada, Special Paper 45, p. 323-360.

Stevens, R., 1997. JAE Soil Survey Report – 1996. Yukon mining assessment report number 093711.

Yukon MINFILE, 2009. Yukon MINFILE – A database of mineral occurrences. Yukon Geological Survey, <http://www.geology.gov.yk.ca/databases_gis.html>.

Neoproterozoic and early Paleozoic correlations in the western Ogilvie Mountains, Yukon

F.A. Macdonald[1], E.F. Smith and J.V. Strauss
Department of Earth and Planetary Sciences, Harvard University, Cambridge, MA, USA

G.M. Cox and G.P. Halverson
Department of Earth and Planetary Sciences, McGill University, Montreal, QC

C.F. Roots[2]

ABSTRACT

Continued investigations of sedimentary units in the Tatonduk and Coal Creek inliers of the western Ogilvie Mountains have resulted in a refinement of the regional Neoproterozoic and early Paleozoic stratigraphy. The proposed correlations simplify Yukon stratigraphic nomenclature and promote synthesis of geological data.

Strata of the Fifteenmile, Rapitan and Hay Creek groups, as well as the upper Windermere Supergroup are present in both inliers. Prominent unconformities within the Fifteenmile Group, and between the Windermere Supergroup and the variable overlying Paleozoic stratigraphy, represent at least three distinct tectonic events and basin-forming episodes.

We propose redefinition of the Fifteenmile Group, abandonment of the Tindir Group, and recognition of strata equivalent to the Coates Lake Group and Mackenzie Mountains supergroup. This refined nomenclature across the Ogilvie, Wernecke and Mackenzie mountains is a step toward enhanced regional correlation of exposures in the northern Cordillera and Proterozoic inliers of the western Arctic.

[1]*fmacdon@fas.harvard.edu*
[2]*charlie.roots@gov.yk.ca*

INTRODUCTION

The Proterozoic stratigraphic record in the northwestern Canadian Cordillera is preserved in erosional windows through Phanerozoic strata (here termed 'inliers'; Fig. 1). Since early recognition of analogous sequences among these inliers (*e.g.,* Gabrielse, 1972; Eisbacher, 1978; Young *et al.,* 1979), correlation of units, particularly those with stratabound mineral potential, has been a principal goal in geological mapping and stratigraphic analysis. Correlations of early Neoproterozoic strata in the Ogilvie Mountains of the Yukon Territory (Abbott, 1997; Thorkelson *et al.,* 2005), the Mackenzie Mountains of the Northwest Territories (*e.g.,* Aitken, 1981; Eisbacher, 1981), and Victoria Island of Nunavut and Northwest Territories (Rainbird *et al.,* 1996; Young, 1981) were recently refined with chemo and litho-stratigraphy calibrated with U/Pb geochronology on zircons (Jones *et al.,* 2010; Macdonald *et al.,* 2010b; Medig *et al.,* 2010). We agree with previous researchers that the Lower Tindir and Fifteenmile groups are at least, in part, correlative with the Mackenzie Mountains supergroup (Abbott, 1997; Macdonald *et al.,* 2010b; Thorkelson *et al.,* 2005). We further extend stratigraphic correlations into the Cryogenian and Ediacaran periods and suggest that the Rapitan, Hay Creek and 'upper' groups of the Windermere Supergroup extend westward across Yukon.

In this paper, the Neoproterozoic and earliest Paleozoic strata are described based upon measured sections in the two western inliers (Coal Creek and Tatonduk; Fig. 2) of the western Ogilvie Mountains, about 100 km north of Dawson. Correlation of the Proterozoic strata has been challenging due to the paucity of age-defining fossils, the scarcity of isotopically dateable lithologies, and the unknown structural complications beneath broad valleys and between inliers that are 70 km apart. We systematically collected samples of carbonate rocks for stable isotope analysis, as well as igneous rocks for geochemistry and geochronology. Results will provide quantitative evidence to more conclusively determine the equivalency of regional units. Towards this goal, we herein describe the lithologic character of the many locally named units and seek to streamline the nomenclatures by using fewer and more wide-ranging stratigraphic terms.

THE COAL CREEK INLIER

Neoproterozoic strata in the Coal Creek inlier were separated from the Wernecke Supergroup by Norris (1981) and later mapped as the Mount Harper Group (Mustard and Roots, 1997) and the Fifteenmile Group

(named after the headwaters of Fifteenmile River; Thompson *et al.,* 1987 and 1994). This latter informal unit was a provisional measure to distinguish older Neoproterozoic strata in the Coal Creek inlier from the Lower Tindir Group of the Tatonduk inlier and the Pinguicula Group in the Wernecke Mountains. The relationship of all these units to the Coates Lake Group and the Mackenzie Mountains supergroup of the Yukon-NWT border area was unclear. Our recent mapping, coupled with geochronologic and chemostratigraphic studies, provides a framework for correlating the Fifteenmile Group with other Neoproterozoic rocks throughout northwestern Canada (Macdonald and Roots, 2010; Macdonald *et al.,* 2010a).

Here we subdivide the Fifteenmile Group into two informal formations, the 'lower' assemblage and the Craggy dolostone. Overlying these is the Callison Lake dolostone (Abbott, 1997; Macdonald and Roots, 2010), which we propose should be grouped with the Lower Mount Harper Group and the Mount Harper volcanic complex. Furthermore, we believe the Upper Mount Harper Group (Mustard and Roots, 1997) should be dissolved and strata re-assigned to two existing groups (Rapitan, Hay Creek) and the 'upper' part of the Windermere Supergroup (James *et al.,* 2001).

FIFTEENMILE GROUP

The Fifteenmile Group was originally subdivided into upper and lower subgroups, containing three (PF1–PF3) and five (PR1–PR5) informally defined units, respectively (these units are shown on the regional map of Thompson *et al.,* 1994; suffix 'P' refers to Proterozoic). These authors suggested that the lower Fifteenmile Group was intruded by breccia equivalent to the *ca.* 1600 Ma Wernecke breccia (age reported in Abbott, 1997). However, Medig *et al.* (2010) demonstrated that PR1 overlies a regolith formed within the breccia, and that all of the lower subgroup is younger. Moreover, a tuff recovered within strata previously mapped as PR4 (revised to PF1a to reconcile inconsistencies of previous mapping) was dated at 811.51 ± 0.25 Ma (U/Pb ID-TIMS; Macdonald and Roots, 2010; Macdonald *et al.,* 2010b). Thus the lower Fifteenmile Group is considered much younger than the Wernecke breccia as noted by Thorkelson *et al.* (2005). Medig *et al.* (2010) suggested that PR1-PR2 are correlative with units A-C of the Pinguicula Group, however, this correlation remains to be tested with further mapping, geochemistry, and geochronology.
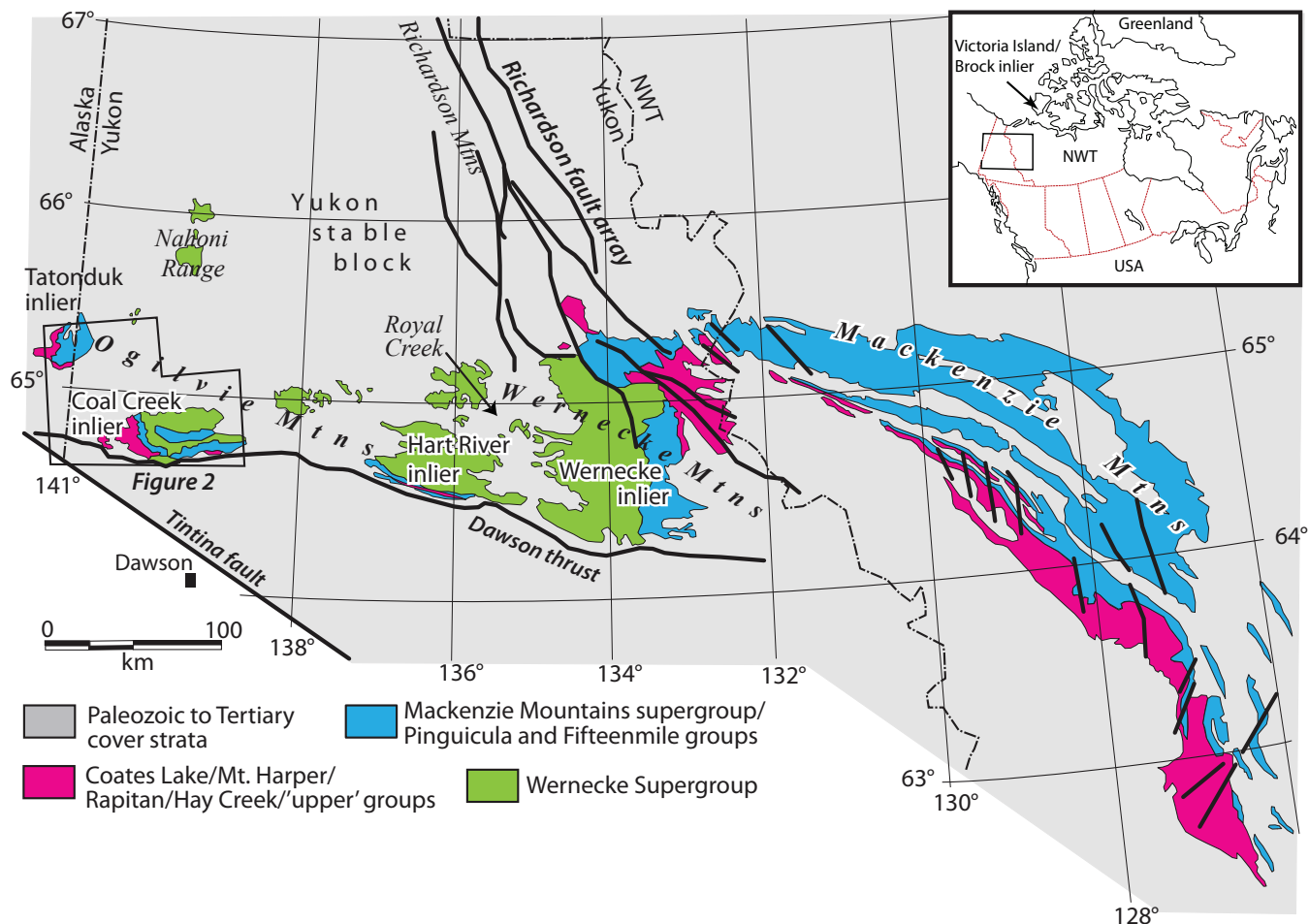
Figure 1. *Distribution of Proterozoic strata in the Ogilvie, Wernecke and Mackenzie Mountains. Modified from Abbott (1997) and Young et al. (1979).*

The former map units PR3-PR5, and PF1a are here discarded for two reasons. First, they represent a complex stratigraphic package with prominent lateral facies changes that are unsuited for lithostratigraphic correlation. Second, we have found them to be significantly mis-mapped throughout the Coal Creek inlier. Therefore we refer to this package, >1000 m of mixed carbonate and siliciclastic rocks, as the 'lower' assemblage of the Fifteenmile Group, pending resolution of its lowermost extent. A tuff within the upper portion of the 'lower' assemblage constrains its depositional age to 811.51 ± 0.25 Ma (Macdonald *et al.*, 2010b). These strata are succeeded by the Craggy dolostone (informal term; formerly PF1), which is in turn unconformably overlain by the Callison Lake dolostone (Abbott (1997), correlated with former PF2 and PF3 by Macdonald and Roots (2010)). The Callison Lake dolostone consists of >300 m of microbially bound dolostone bracketed by intervals of shale.

In the 2008–2010 field seasons we measured ten detailed stratigraphic sections of the Fifteenmile Group. Our work outlined a network of stromatolitic buildups that occur between the inner shelf and upper slope facies on a northwest-facing (present coordinates) margin. In the south-central part of Coal Creek inlier, the lowermost unit of the 'lower' assemblage (formerly PR1) is exposed in a syncline to the northwest of Mt. Gibben, and in minor exposures occurring along strike to the west. On the north limb of the syncline, this lower siliciclastic unit is ~320 m thick (Fig. 4, section E1003), and consists primarily of weakly foliated, brown to grey-coloured siltstone and shale, as well as large carbonate blocks and conglomerates interpreted as olistostromes (Fig. 5a) and debris flows, respectively. Carbonate blocks are over 10 m in diameter and bedding is discordant to the supporting siliciclastic matrix. Deposition appears to be fault-controlled and the unit thickens along a syn-sedimentary northwest side-down fault (Roots and Thompson, 1992). This interpretation is
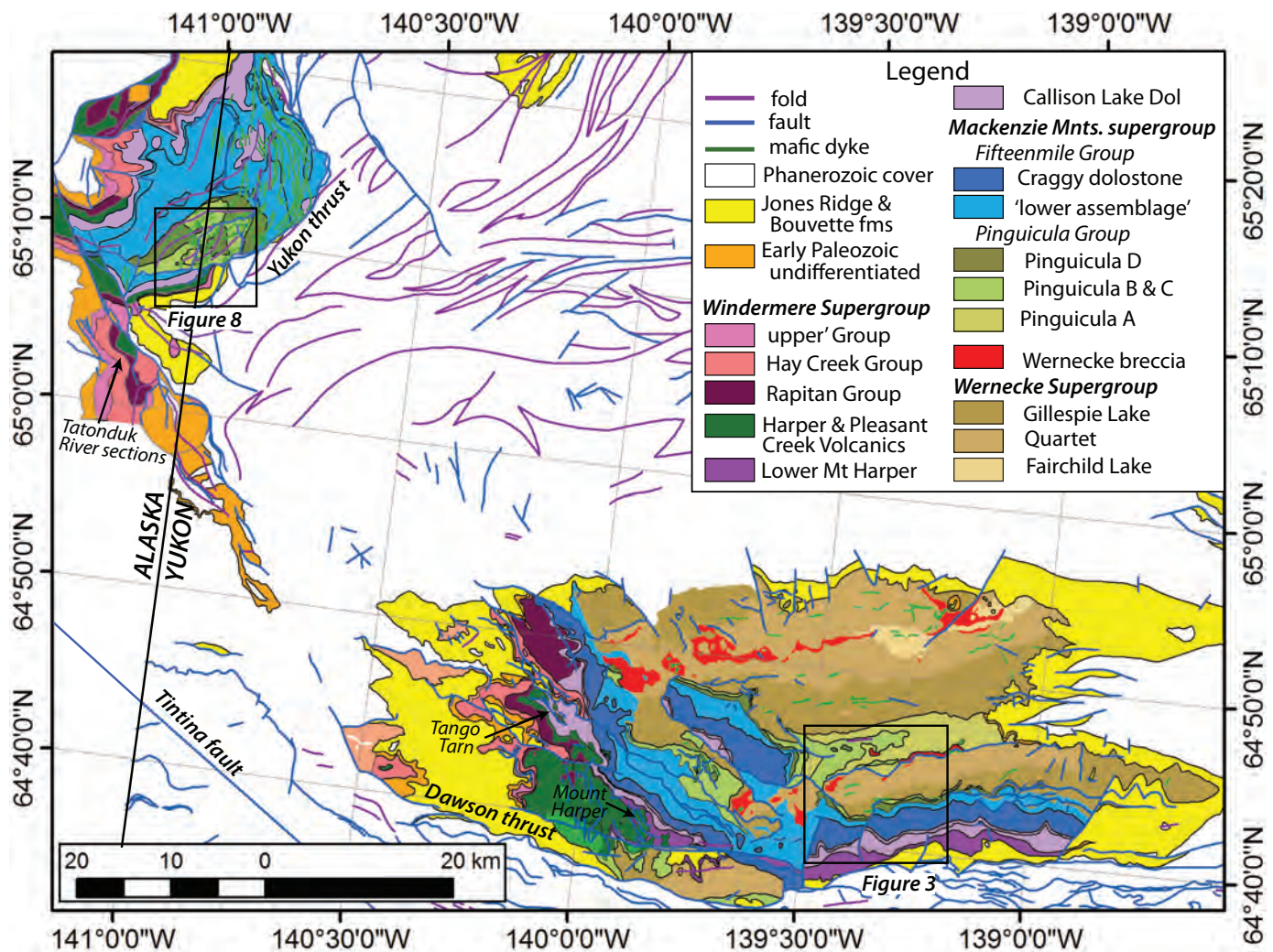
Figure 2. Distribution of Neoproterozoic units in the Tatonduk and Coal Creek inliers of the southern Ogilvie Mountains. Map units are based on Thompson and et al. (1994) and Van Kooten et al. (1997), and revision and assignment of names are discussed in the text.

supported by the abundance of larger olistostromes in the southernmost exposures. The olistostrome-bearing carbonates are overlain by >500 m of yellow to blue-grey weathering carbonate rocks (Fig. 5b). These strata were previously mapped as PR2 (Thompson et al., 1994) and correlated with the Pinguicula Group (Medig et al., 2010), but it is unclear if they represent a distinct rock package or are facies change of the lower assemblage. Consequently, pending further study we herein map these units as 'Fifteenmile Group undifferentiated' (Figs. 2 and 3).

In the most proximal section (E1002; Fig. 5c), the 'lower' assemblage begins with ~100 m of blue-grey dolomite with oolitic grainstone and stromatolites. These are overlain by ~500 m of lilac to black-coloured shale and coarse clastic rocks, and an additional ~500 of carbonate mudstone, grainstone and stromatolites. The carbonate mudstone

includes dark-coloured limestone and commonly contains molar tooth structures. The grainstone and stromatolite beds are typically light grey to buff-coloured dolostone. At the northwest end of the Coal Creek inlier, measured sections reveal symmetric transgressive-regressive sequences defined by the northwest progradation of stromatolitic buildups in low-stand sequence tracts.

These sequences culminate with the deposition of the Craggy dolostone (PF1), a regionally extensive, conspicuous white dolostone that is >500 m thick (Fig. 5c). The Craggy dolostone consists predominantly of massive, recrystallized and silicified grainstone. Occasionally, microbialaminites and low-relief stromatolites (up to 10 cm of relief) are visible. Recrystallized ooids, coated grains, brecciated teepee structures, flat-chip conglomerates, interclast breccias and low-angle crossbeds are also
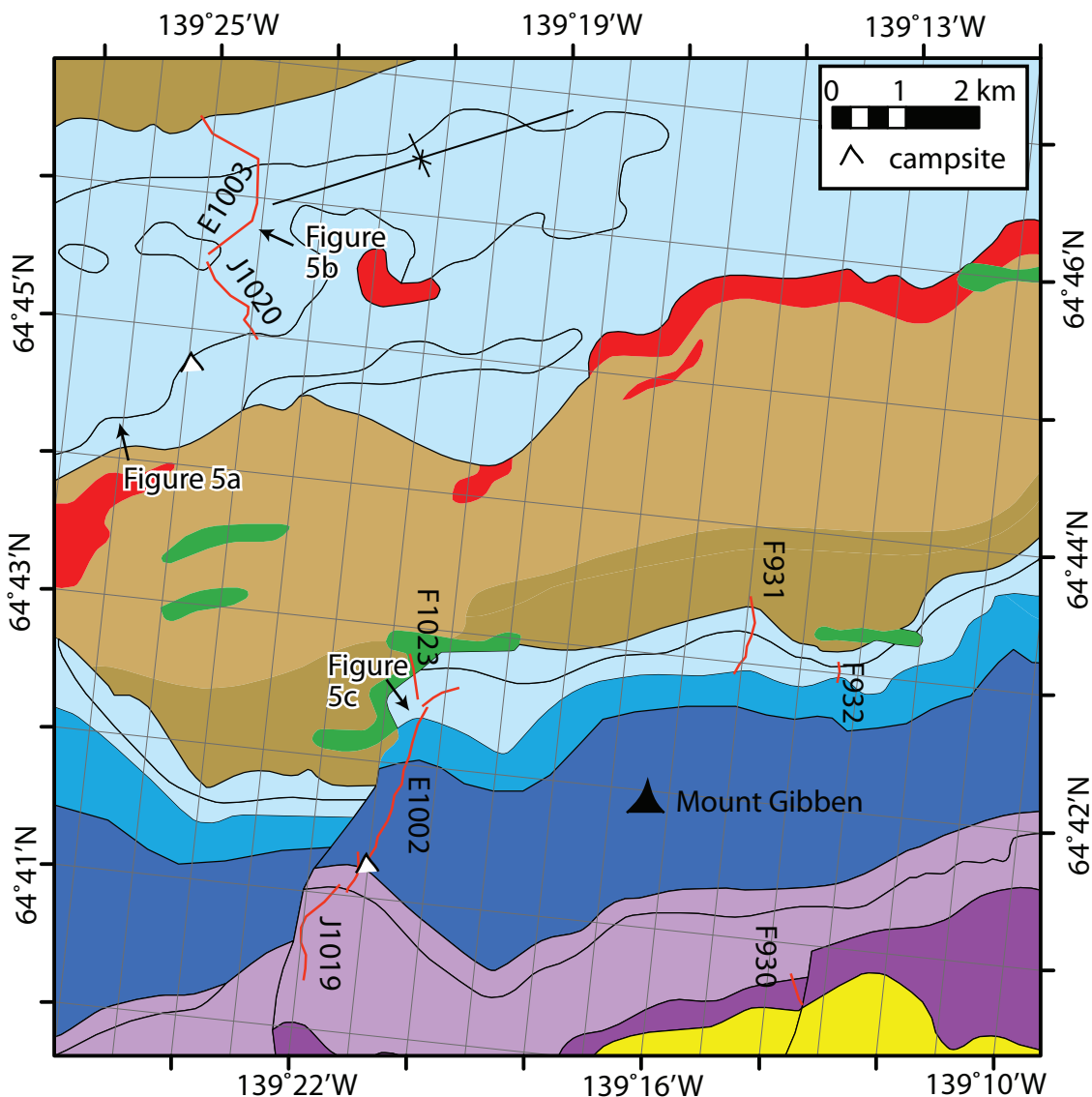
Figure 3. *Geological map of a part of the Coal Creek inlier, illustrating the locations of sections displayed in Figure 4. Modified from Thompson et al. (1994) with new mapping. Colour of units matches the legend in Figure 2.*

sometimes present. The Craggy dolostone does not contain any siltstone, mudstone, or shale, and its base is defined by the contact between the last black shale and the massive dolostone. This is an important point because in the most proximal sections, large, massive stromatolitic buildups in the overlying Callison Lake dolostone resemble the Craggy dolostone.

The Craggy dolostone is succeeded by the Callison Lake dolostone (previously part of the Upper Fifteenmile Group; Macdonald and Roots, 2010). Near Mt. Gibben, the Callison Lake dolostone is well exposed and measures over 500 m thick (Fig 4; section J1019). Here,

the basal ~75 m consists of siltstone and shale with laterally discontinuous bioherms. The black shale has a peculiar waxy luster, which consists almost exclusively of sedimentary talc (Macdonald and Roots, 2010). The black shale also contains talc rip-up clasts supported in a nodular dolomicrite matrix and abundant black chert nodules. This shale was previously mapped as unit PF2 and is succeeded gradationally by over 400 m of silicified dolostone of PF3, which is characterized by stromatolites, microbialaminite and intraclast conglomerate. An additional ~25 m of interbedded black talc and dolomitic microbialite is present at the top of these strata. We consider the entire shale-carbonate sequence as the Callison Lake dolostone

Figure 4. *Measured stratigraphic sections of the Fifteenmile Group west, and south of Mt. Gibben, in the Coal Creek inlier. Locations of the sections are shown on Figure 3. Section on the left is a composite of six measured sections indicated to the right of the column. LMHG: Lower Mount Harper Group*
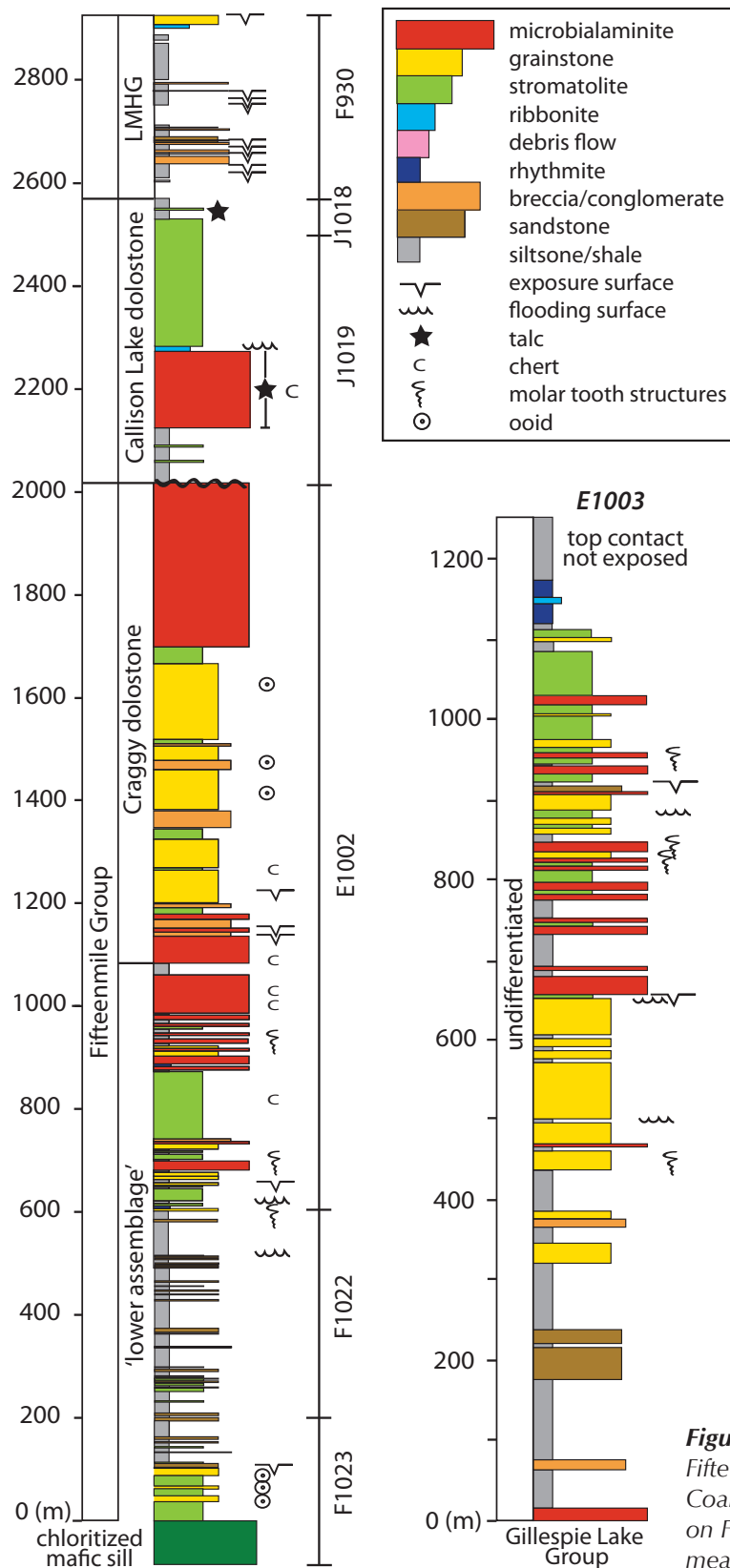
because we interpret them to be genetically related. This nomenclature minimizes new terminology and allows straightforward stratigraphic correlations between the Coal Creek and Hart River inliers.

The low-angle unconformity at the base of the Callison Lake dolostone in the Hart River inlier (Abbott, 1997; Macdonald and Roots, 2010) suggests the commencement of an additional basin-forming episode. It is at an equivalent stratigraphic position, and possibly analogous to, the Coates Lake Group of the Mackenzie Mountains. Stratigraphic sections measured through this map unit in the Ogilvie Mountains reveal significant thickness and facies variations. Furthermore, in the western Coal Creek inlier, a wedge of proximal conglomerate and hematitic siltstone were deposited atop the Callison Lake dolostone by an adjacent normal fault, which was overstepped by subaqueous to subaerial volcanism (Lower Mount Harper Group and volcanic complex of Mustard and Roots, 1997; see below).

LOWER MOUNT HARPER GROUP

The Lower Mount Harper Group (LMHG) conformably overlies the Callison Lake dolostone. Near Mount Harper it is exposed on the north side of a syn-depositional fault scarp (the Mount Harper fault; Mustard and Roots, 1997) where it consists of up to 1100 m of talus breccia and debris flow conglomerate interpreted to represent coalescing alluvial fans (Mustard, 1991; Mustard and Donaldson, 1990). To the east, in the Mt. Gibben area, the LMHG is as thick as 300 m and consists predominantly of red beds commonly containing mudcracks, and conglomerate interbedded with minor carbonate rocks that were deposited in a distal fan environment (Fig. 4; Section F930).

THE MOUNT HARPER VOLCANIC COMPLEX

The Mount Harper volcanic complex (MHVC) is divided into six informal units that are defined both stratigraphically and compositionally (Mustard and Roots, 1997; Roots, 1987). A lower suite, constituting members A–C, are basaltic and comprise several hundreds of metres of pillowed and massive flows in both subaqueous and subaerial breccia. The lower flows overlie sandstone, siltstone and cobble conglomerate north of the Harper fault (Fig. 5d), a pre-volcanic, north side-down scarp. Soft-sediment roll-ups, dolostone rip-ups and spiracles (steam-generated cavities) attest to the soft, damp substrate encountered by the initial lava flow (Fig. 5d). The basal flows on the south side of the Harper fault disconformably overlie thickly bedded dolostone of Pinguicula unit B or C, attesting to uplift and erosion of the fault block prior to volcanism.

Volcanic members A and B formed an edifice up to 1200 m thick. Some of the later eruptions were subaerial, producing agglutinate spatter cones and hematitic, autobrecciated massive flows. Holocene erosion has provided cross sectional views of the edifice in which outward dipping paleo-slopes and tapering eruption units are discernible. Other steep exposures reveal that the edifice was unevenly dissected during, or shortly after, members A and B were extruded, resulting in overlaps by tuff-breccia, lapilli tuff, and block-and-ash breccia deposits of member C. The clasts are either primary basaltic, or derived from erosion.

Member A has the highest Mg/Fe ratio and is considered the most primitive magma although its high large-ion lithophile (LIL) concentrations suggest some crustal contamination. Subsequent flows and sheeted intrusions within member B have decreased Mg/Fe and more uniform composition. Incompatible element abundance diagrams yield patterns that approximate those of typical ocean island volcanic suites, such as Hawaii (Mustard and Roots, 1997).

The Upper suite consists of three members: D (rhyolite), E (andesite) and F (andesite). They are three distinct units, but their relative timing and original distribution remain unclear. In different places, each unit unconformably overlies members A–C. Despite their different rock types, members D and E are similarly enriched in large-ion lithophile elements and may have erupted from a compositionally differentiated magma chamber. The rhyolite is exposed as thick flows and probable domes. Member E forms cliff exposures of columnar-jointed and shattered massive flows; these prograde over an apron of angular flow shards ('hydroclastic breccia') that is extensive atop the older edifice. Epiclastic sedimentary units preserved as erosional outliers in the complex contain abundant clasts derived from members D and E.

Member F andesites form pillowed flows, breccias, tuffs and invasive flows that interfinger with, and intrude into, diamictites of the Rapitan Group. The scarcity of mafic minerals and relatively high concentration of most incompatible elements could have resulted from mixing a relatively primitive magma pulse with an evolved andesite such as member E. Sedimentary strata that overlie the western and northwestern part of the volcanic complex contain thin flows believed to be compositionally related to member F (*e.g.*, Green Shelter section; Fig. 7). In summary, a period of unknown duration separates the lower from the upper suite, during which time a fractionated magma evolved, and the last phase of volcanism was sporadic. Member D was dated at 717.43 ± 0.14 Ma (U/Pb ID-TIMS; Macdonald *et al.*, 2010b), but the age of the lower members of the MHVC is unknown.

RAPITAN GROUP

At Tango Tarn and on the south flank of Mount Harper (Macdonald *et al.*, 2010a, supplementary online material at www.sciencemag.org/content/327/5970/1241/suppl/DC1), a maroon-coloured mudstone with pebble to cobble-sized lonestones of dolomite and volcanic rocks forms the base of the Rapitan Group (formerly PH1; Thompson *et al.*, 1987; Mustard and Roots, 1997). These strata resemble, in colour, texture and stratigraphic position, the glacially influenced Sayunei Formation of the Rapitan Group in the Mackenzie Mountains (Eisbacher, 1978; Yeo, 1984). An ~1 m-thick, green to pink, brecciated tuff that is above the maroon stratified diamictite yielded a 716.47 ± 0.24 Ma U/Pb ID-TIMS zircon age (Macdonald *et al.*, 2010b). The tuff interfingers with a massive diamictite unit that is >10 m thick and consists of dolomite and volcanic boulder clasts suspended in a carbonate matrix. Above the massive diamictite is an additional ~10 m of fine-laminated, yellow-weathering carbonate mudstone with bed-penetrating dropstones that are interpreted as glacial in origin (Fig. 5e). Approximately 10 km north of Tango Tarn, ice till pellets (Fig. 5e) and striated clasts were also identified (Fig. 5f), further supporting a glacial origin for this deposit. In both the Coal Creek and Hart River inliers, plow structures and highly convoluted soft-sedimentary deformation suggest the presence of grounded ice (Macdonald *et al.*, 2010b). Furthermore, a granitic clast was discovered in the Rapitan Group in the Coal Creek inlier testifying to an exotic origin of some clasts.

Figure 5. *Field photos from the Coal Creek inlier. Figures 5a-c are from localities near Mt. Gibben with locations shown in Figure 3.* **(a)** *Large carbonate olistostromes (outlined in red) in siltstone of the 'lower' assemblage of the Fifteenmile Group; view is to the north.* **(b)** *Measured section E1003 through the undifferentiated Fifteenmile Group; view is to the west.* **(c)** *Measured section E1003 through the 'lower' assemblage; view is to the south; students for scale.* **(d)** *The lowest flow of the Mount Harper volcanic complex directly overlies (at scale card in circle) red and tan siltstone and sandstone beds of the Lower Mount Harper Group. Contact is conformable and exposed in north-facing gully 1 km north of Mount Harper.* **(e)** *Carbonate dropstone and grit in laminated orange dolomicrite matrix. Note the till pellet in the top right corner of the sample. This sample was extracted from outcrop of the Rapitan Group ~12 km north of Tango Tarn.* **(f)** *Striated clasts of the Rapitan Group, from subcrop ~10 km north of Tango Tarn. Coin is 2.5 cm across.*

HAY CREEK GROUP

The Hay Creek Group (Yeo, 1978; Young *et al.*, 1979) was proposed to encompass the Twitya and Keele formations in the Mackenzie Mountains. In its original usage, it was essentially a clastic to carbonate grand cycle. Later studies in the region defined the Icebrook Formation (Aitken, 1991) and documented 'cap carbonate' lithologies that were first referred to as the Tepee dolostone (Eisbacher, 1985) and later as the informal Hayhook and Ravensthroat formations (James *et al.*, 2001). All of these units should be included in a contemporary definition of the Hay Creek Group (R. MacNaughton, pers. comm., 2010).

In the Coal Creek inlier, the Rapitan Group is succeeded by <100 m of poorly exposed siltstone and limestone (formerly PH2) herein assigned to the Hay Creek Group. This unit commences with <10 m of dolomite breccia. While a genetic interpretation of this breccia is unclear, it is overlain by a white to buff-coloured, fine-laminated dolostone with abundant bed-parallel cements (sheet-crack) that shares textural and geochemical similarities with the Hayhook formation (James *et al.*, 2001) and basal Ediacaran cap carbonates world-wide (Hoffman *et al.*, 2007).

THE 'UPPER' GROUP

In the Mackenzie Mountains, the Sheepbed, Gametrail, Blueflower and Risky formations (*e.g.*, Aitken, 1989; Dalrymple and Narbonne, 1996; MacNaughton *et al.*, 2000; MacNaughton *et al.*, 2008) have provisionally been considered to comprise the informal 'upper' group of the Windermere Supergroup. Although details of correlation are controversial (see summary in MacNaughton *et al.*, 2008), these units have been considered to form two clastic-carbonate grand cycles that predate the deposition of Cambrian sandstone (Backbone Ranges Formation). This group completes Windermere Supergroup sedimentation.

In the Coal Creek inlier, the 'upper' group (formerly PH3-PH5) is exposed along the ridge and saddle due north of Tango Tarn (Fig 6; section F838) where it begins with ~250 m of black shale that directly overlie brecciated dolomite beds. The thick shale succession is succeeded by ~25 m of massive white to buff-coloured dolostone and an additional ~100 m of thinly bedded, pink dolorhythmite, ribbonite and grainstone with hummocky cross-stratification. The 'upper' group culminates with ~10 m

of dark-coloured, nodular, organic-rich limestone. These carbonate beds are overlain disconformably by as much as 170 m of siliciclastic rocks (formerly PH5) that include simple trace fossils such as *Cruziana* and *Rusophycus*, thought to be early Cambrian in age (Mustard *et al.*, 1988); in some instances, the beds are unconformably overlain by the Cambrian-Devonian Bouvette Formation.

BOUVETTE FORMATION

The Bouvette Formation was formally named by Morrow (1999) to describe a thick sequence of Cambrian to Devonian dolostone and limestone that outcrops extensively throughout central and northern Yukon. These strata characterize the geographic limits of the Yukon Stable Block (YSB) and encompass all strata mapped as unit CDb of Operation Porcupine (Norris, 1997; Morrow, 1999) and Unit 8 of the Nash and Larsen Creek map areas (Green, 1972). The Bouvette Formation commonly overlies a variety of Proterozoic strata in the southwestern parts of the YSB and conformably overlies the Cambrian Taiga Formation (or its equivalents) in the southeastern parts of the YSB (Morrow, 1999). The Ordovician to Silurian Road River Formation commonly succeeds Bouvette Formation and is laterally equivalent to parts of it, except in the Dave Lord region (Morrow, 1999). The type section of the Bouvette Formation was chosen by Morrow (1999; MTA-86-11; #36) 80 km north of Mount Harper in the northern Ogilvie Mountains.

Only two stratigraphic sections of the Bouvette Formation have been measured in the southern Ogilvie Mountains (Morrow, 1999, sections MTA-86-5 (4) and MTA-86-25 (7)). These strata unconformably overlie variable Proterozoic strata and record incomplete thicknesses ranging from 432 to 987 m. They predominantly consist of highly silicified, thick-bedded, very light grey dolomitic grainstone with abundant vugs and occasional microbial fabrics. Revisional mapping and preliminary descriptions of various outcrops of the Bouvette Formation in the Coal Creek inlier and further north in the Nahoni Ranges was carried out in 2010. However, the lack of significant relief and characteristic blocky weathering of the Bouvette Formation precluded logging detailed stratigraphic sections. Future study near Morrow's type section and near Royal Creek in northeastern Ogilvie Mountains will establish the sedimentological and chemostratigraphic characteristics of this map unit.
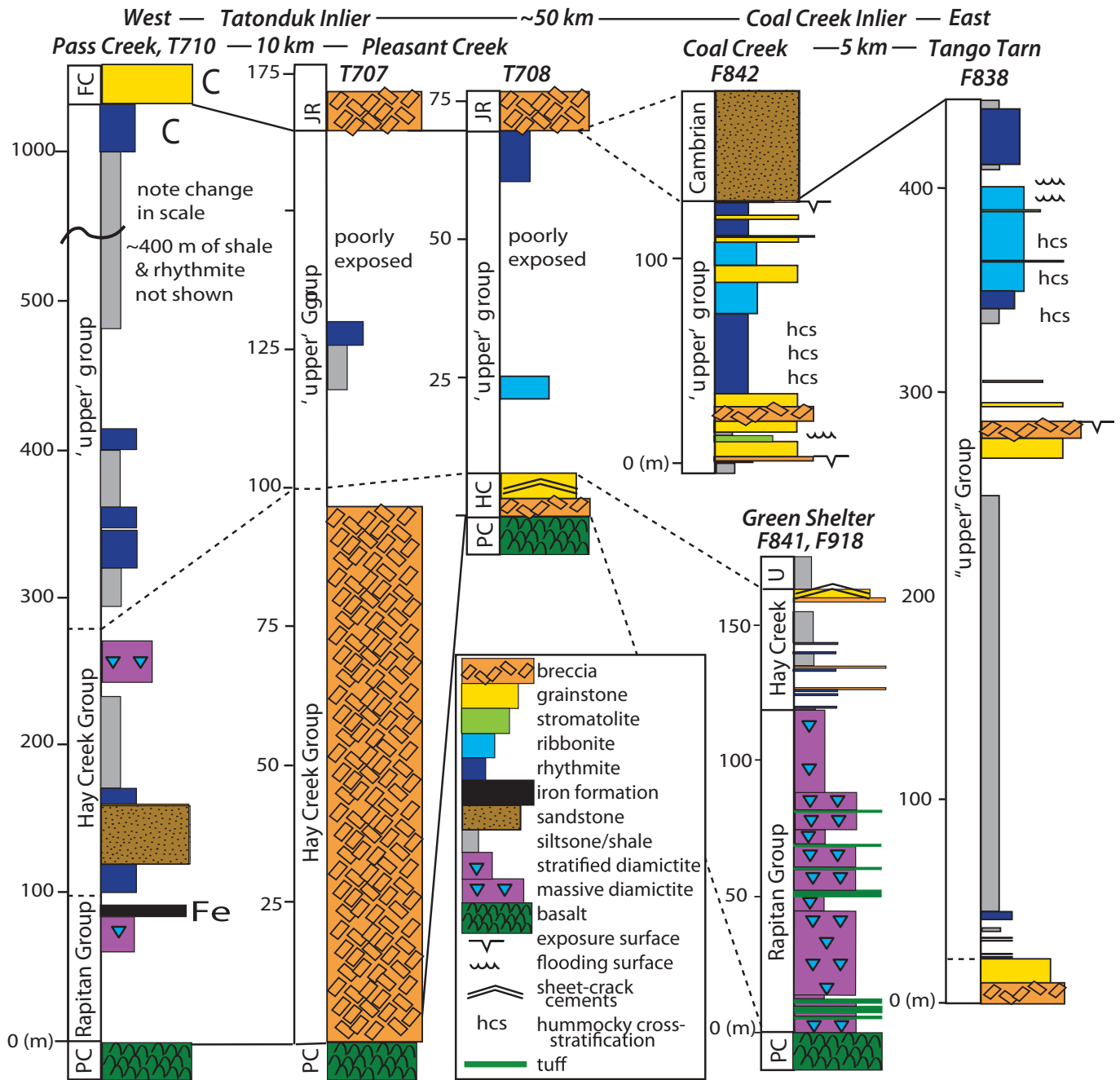
Figure 6. *Measured stratigraphic sections of the Rapitan Group, Hay Creek Group and 'upper' group. Locations are shown on Figures 3 and 8, and in Macdonald et al. (2010a,b). Vertical scale varies. 'FC' = Funnel Creek limestone; 'JR' = Jones Ridge limestone; 'PC' = Pleasant Creek volcanics.*

Figure 7. *Measured stratigraphic sections of the Pinguicula Group near Pleasant Creek and at Mt. Slipper in the Tatonduk inlier. Locations are shown on Figure 8 and coordinates for the base are in Appendix 1.*
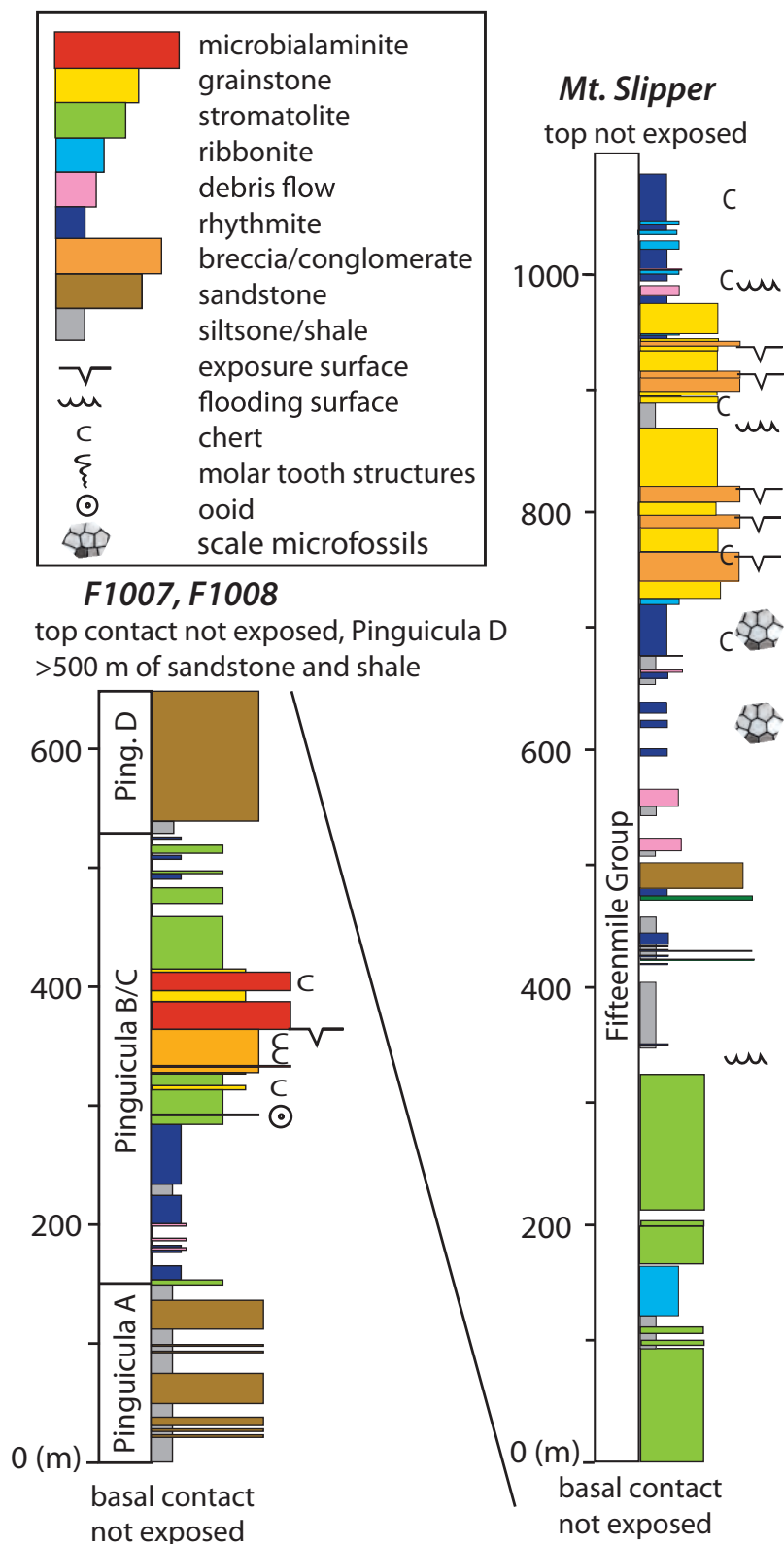
THE TATONDUK INLIER

Cairnes (1915) referred to Precambrian stratigraphy exposed along the international border as the Tindir Group. Mertie (1930 and 1933) described the stratigraphy (and natural history) of the region in remarkable detail and recognized seven units in the Tindir Group. Brabb and Churkin (1969) produced a detailed geologic map of the Tindir Group on the Alaskan side of the border. The same stratigraphy was mapped on the Yukon side by Norris (1979). However, exact correlations of specific units of the Tindir Group across the border remained ambiguous until the completion of more recent mapping and compilation (Van Kooten *et al*., 1997) and integrated litho and chemostratigraphy (Macdonald *et al*., 2010a,b).

The informal division of the Tindir Group into the Upper and Lower Tindir groups was first distinguished by Payne and Allison (1981), despite the fact that no unconformable contacts had been observed between them. Young (1982) extended their work by separating the Lower Tindir Group into six informal units and the Upper Tindir Group into five informal units. The Lower Tindir Group units of Young (1982) were further modified by Van Kooten *et al*. (1997) and Macdonald *et al*. (2010a). Importantly, Van Kooten *et al*. (1997) identified an angular unconformity within the Lower Tindir Group. We have examined these units in part of the inlier drained by Pleasant Creek, on the Alaska-Yukon border (Fig. 8). Here we correlate and redefine individual units of the Lower Tindir Group below the unconformity, with units of the Pinguicula Group and units above the unconformity, with the Fifteenmile Group.

PINGUICULA GROUP

The Pinguicula Group was originally defined in the Wernecke Mountains near Pinguicula Lake and separated into
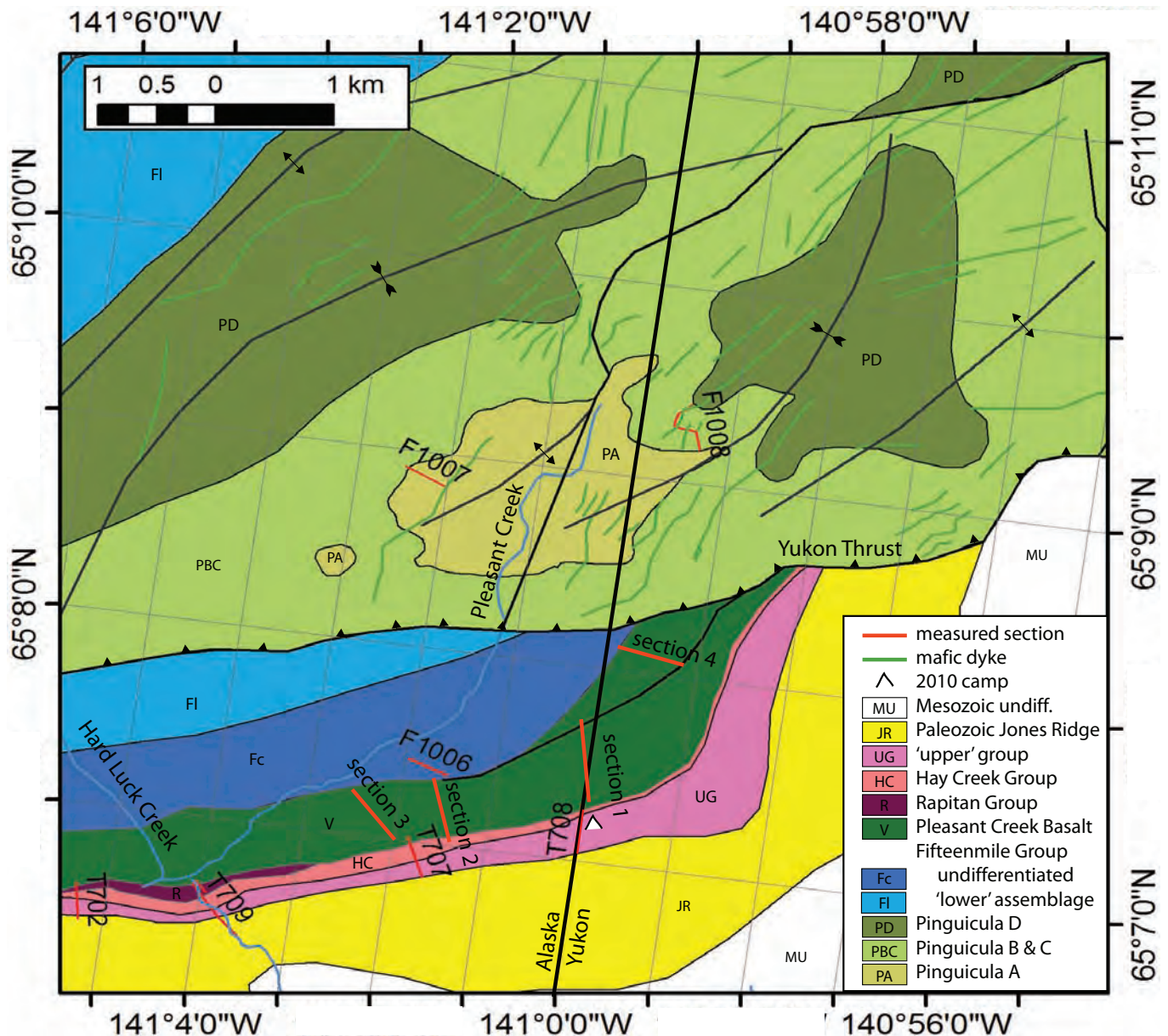
Figure 8. *Geological map of the Pleasant Creek area of the Tatonduk inlier.*

units A-F (Eisbacher, 1981). Although precise correlations were uncertain, Aitken and McMechan (1991) suggested the Pinguicula Group was in part correlative with the Mackenzie Mountains supergroup (MMSG). Abbott (1997) later described Proterozoic strata in the Hart River inlier of the eastern Ogilvie Mountains, correlating them with units A-D of the Pinguicula Group in the Wernecke Mountains. Furthermore, he recognized that unit D included strata equivalent to both the Tsezotene Formation and Katherine Group of the MMSG. Refining earlier work in the Wernecke Mountains, Thorkelson (2000) upheld units A-C in the Pinguicula Group, but

reassigned units D-F to the Hematite Creek Group. The more restricted definition of Pinguicula Group allowed for its correlation with the pre-1270 Ma Dismal Lake Group in the Coppermine homocline. This correlation stemmed from the identification of a dyke assigned to the *ca.* 1380 Ma Hart River Sills that cuts fine-grained clastic strata assigned to Pinguicula A in the Wernecke Mountains (Thorkelson, 2000). However, the intruded strata were later reassigned to the Wernecke Supergroup (Medig *et al.*, 2010), which raised the possibility that Pinguicula A-C is younger than 1380 Ma.

In the Tatonduk inlier the Pinguicula Group (formerly the lower portion of the Lower Tindir Group) is exposed in a faulted anticline oblique to the international border. The base of the Pinguicula Group and underlying Wernecke Supergroup are not exposed. The stratigraphically lowest outcrop, ~150 m of grey to dark brown shale, siltstone and sandstone ('mudstone' unit of Young, 1982), is assigned to unit A of the Pinguicula Group. The units are succeeded by ~375 m of carbonate ('cherty-stromatolitic dolostone' and 'dolostone-shale' units of Young, 1982) that we recognize as equivalent to unit B/C of the Pinguicula Group (we choose to group units B and C of the Pinguicula Group together because laterally these buildups occur at different positions and represent facies changes, rather than a distinct temporal progression). In the F1008 measured section (Fig. 7), unit B/C begins with ~100 m of thinly bedded orange to light blue coloured dolomicrite, followed by ~275 m of shallow-water carbonates dominated by stromatolitic buildups (Figs. 9a,b). Again, Unit B/C is overlain by black shale and an additional >500 m of interbedded sandstone and shale that is correlated with Pinguicula unit D.

FIFTEENMILE GROUP

In the Tatonduk inlier, the Pinguicula Group is unconformably overlain by the Fifteenmile Group (formerly the upper part of the Lower Tindir Group), which is exposed near the international border at Mt. Slipper and along Pleasant Creek (Fig. 8). The exposures at Mt. Slipper, previously mapped as the Cambrian Jones Ridge limestone (Morrow, 1999; Norris, 1979; Young, 1982) are reinterpreted, based upon new mapping and carbon and strontium chemostratigraphy, as Tonian in age, lying stratigraphically below the Rapitan Group (Macdonald *et al.*, 2010a; Van Kooten *et al.*, 1997). The pre-Rapitan stratigraphy, including the exposures at Mt. Slipper, is intruded by numerous dykes (Fig. 9a), whereas the Rapitan Group and overlying stratigraphy are not (Macdonald *et al.*, 2010a). The 'lower' assemblage of the Fifteenmile Group at Mount Slipper consists of >350 m of carbonate, dominated by branching to massive domal stromatolites and an additional ~500 m of fissile black shale with interbedded quartzite and carbonate (Fig. 6). Microfossils were located within the top 10 m of the 'lower' assemblage at Mt. Slipper (Macdonald *et al.*, 2010a). These strata are succeeded by a yellow-weathering dolostone with common intraclast breccias, black chert nodules, and green shale interbeds that are tentatively assigned to the Callison Lake dolostone.

PLEASANT CREEK VOLCANICS AND TINDIR DYKE SWARM

The Pleasant Creek volcanics (formerly Upper Tindir unit 1) are a series of pillowed and massive basalt lava flows (Fig. 9c) along with substantial volcaniclastic breccia (Fig. 9d). Maximum thickness of the volcanic pile is ~330 m (Fig. 10). Stratigraphically, the volcanics are comformably on top of shallow-water carbonates and have a sharp, but comformable, upper contact with either carbonate or ironstone correlated with the Rapitan Group. The sub-vertical dykes are mapped throughout an area extending 15 km to the north and constitute a swarm. A direct relationship between the dykes and volcanics was not observed in the field, but preliminary geochemical analyses are consistent with a co-magmatic relationship. Trace element analyses are currently being carried out to determine the tectonic setting of these volcanic rocks and assess petrogenetic similarities to the Mount Harper Volcanic Complex, the Little Dal basalt, the sills within the Tsezotene Formation of the Mackenzie Mountains and/or the Natkusiak basalts of Victoria Island.

RAPITAN GROUP

The Rapitan Group (formerly Upper Tindir unit 2) is exposed near the international border along Pleasant Creek and in outcrops close to the Tatonduk River (Macdonald *et al.*, 2010a). The stratigraphy of the Rapitan Group in this region was reviewed by Allison *et al.* (1981) and described in detail by Young (1982). The basal contact of the Rapitan Group was not seen; however, volcanic fragments similar in composition to the underlying Pleasant Creek Volcanics are common in the lower half of the massive diamictite. These strata are chiefly composed of fine-laminated, purple and red mudstone and siltstone speckled with dolomite gravel lonestones. These layers also contain faceted clasts and boulders with striations (Young, 1982), also indicating a glacial origin. The upper ~15 m of the Rapitan Group hosts multiple ~10 cm-thick beds of iron formation, which are interbedded with a laminated diamictite containing bed-penetrating, outsized clasts (Macdonald *et al.,* 2010a,b). The majority of clasts in the Rapitan Group consist of dolomite derived from the Fifteenmile Group. Where the upper contact is exposed, it is overlain by a well sorted carbonate matrix diamictite including abundant dolostone clasts of variable size, interpreted as a debris flow. This is overlain by a parallel-laminated siltstone and sandstone of the Hay Creek Group. Samples of the hematitic section of the Rapitan Group were systematically collected for further study and

Figure 9. *Field photos from the Tatonduk inlier.* **(a)** *Measured stratigraphic section F1008 of Pinguicula B/C looking north. Stratigraphic log shown in Figure 4. Arrows mark dykes of the Tindir dyke swarm.* **(b)** *Discrete columnar stromatolites from Pinguicula B/C in section F1008 at 160 m (see Fig. 4).* **(c)** *Massive and columnar jointed basalt flow, near the top of the volcanics exposure in Pleasant Creek. The flows dip 65° to the southeast, similar to the overlying ironstone.* **(d)** *Angular to subrounded, pebble to cobble-sized basaltic fragments with glassy texture, stratigraphically above massive lava flow at the top of Section 1, Pleasant Creek volcanics (see Fig. 8).* **(e)** *Measured section of the Jones Ridge limestone along the international border, looking east.*

comparison with other Neoproterozoic iron formation. The thickness of the Rapitan Group varies greatly from <50 m near Pleasant Creek, to >700 m, ~20 km to the northwest (Young, 1982). Paleocurrent measurements in the interbedded siltstone suggest a west-facing margin (present coordinates; Young, 1982).

HAY CREEK GROUP

Along the Tatonduk River, the Hay Creek Group (formerly unit 3 and a part of unit 4 of the Upper Tindir Group, Young, 1982) consists of >100 m of flat-bedded, graded siltstone and sandstone interbedded with minor dolomitic mudstone, and overlain by a massive dolomite-matrix diamictite and dolo-grainstone (Fig. 7; section T707). On the Yukon side of the international border, the diamictite is either absent or represented by a dolomite clast breccia suspended in a fine-grained dolomite matrix. No foreign

clasts were noted with the exception of some clasts of the Pleasant Creek volcanics near the base. The breccia is overlain by another massive dolomite that is <5 m thick and is disconformably on units of the Hay Creek Group as well as the Pleasant Creek volcanics and Rapitan Group strata. It is a white to buff-coloured dolostone with bed-parallel cements and pseudo-teepee structures (Young, 1982). These pseudo-teepees do not show a polygonal plan-form or a concentration of cements along the broken pieces, as is typical of teepees that form as a result of sub-aerial exposure (Kendall and Warren, 1987). Instead, cements are isopachous and bed-parallel and the geometry of the beds are contorted and irregularly buckled, suggesting intraformational detachment during deposition. Similar 'sheet-crack' cements are globally present in basal Ediacaran cap carbonates (Hoffman and Macdonald, 2010).
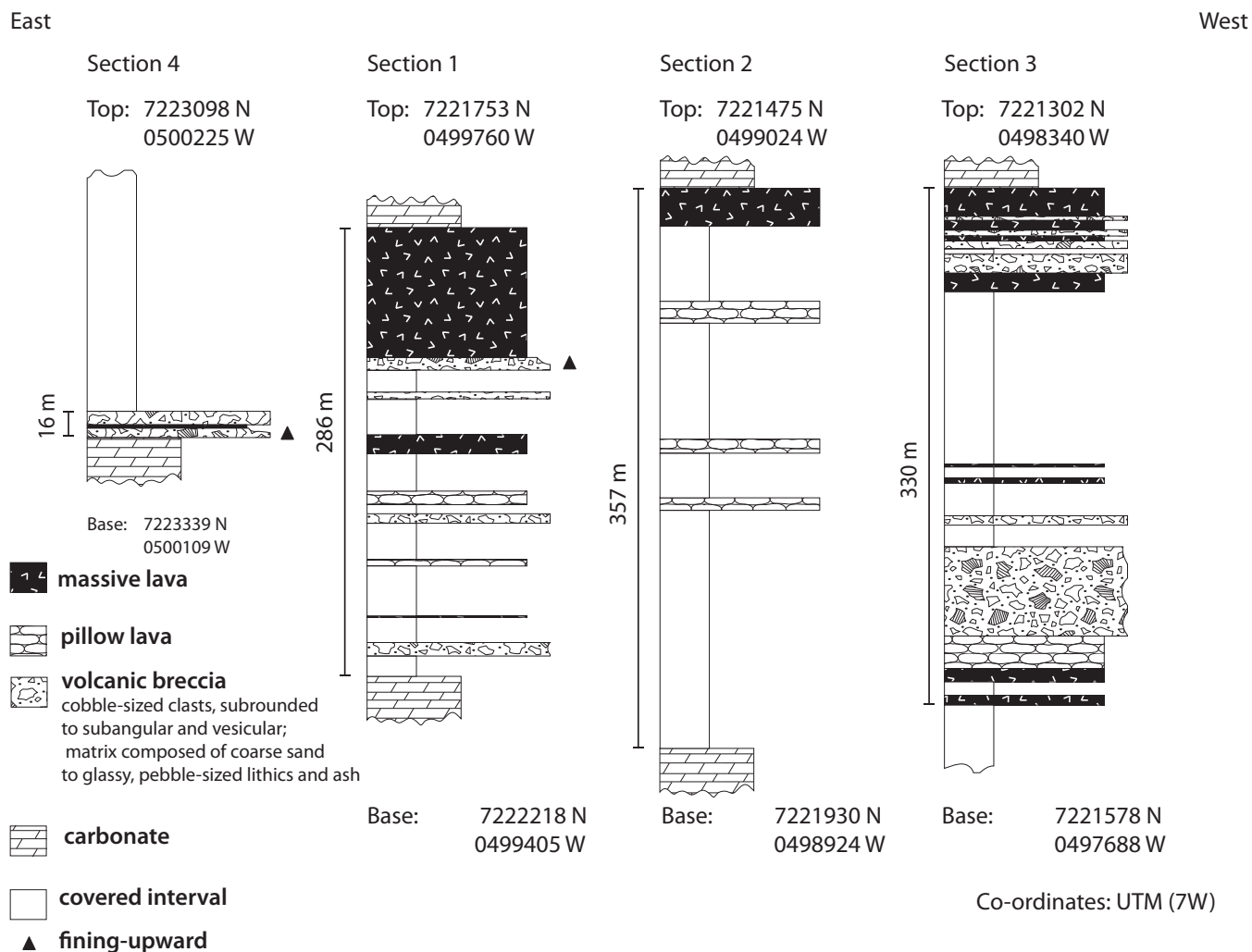
Figure 10. *Measured sections of the Pleasant Creek basalt. Locations of sections are shown in Figure 8.*

THE 'UPPER' GROUP

The Hay Creek Group is overlain by the 'upper' group (formerly units 4b and 5 of the Upper Tindir Group), which consists of <50 m of parallel-laminated siltstone, sandstone and dolomitic marl, and an additional sequence of black shale interbedded with minor organic-rich limestone (Fig. 7; section T707). Like the underlying units, the 'Upper' group displays a major stratigraphic expansion to the southwest ranging from 40 to 75 m thick in Yukon, to ~700 m thick along the Tatonduk River in Alaska (Macdonald *et al.*, 2010a). Both the Hay Creek and 'upper' group strata are consistent with deposition along a southwesterly facing margin (present coordinates).

JONES RIDGE LIMESTONE

The type locality of the Jones Ridge Limestone is the Jones Ridge-Squaw Mountain area of the Tatonduk inlier of eastern Alaska, adjacent to the border with Yukon (Brabb, 1967). It is also exposed in the southwest corner of the Ogilvie River map area where it has been mapped as a lateral equivalent to the Bouvette Formation (CDb map unit of Norris, 1982). The Jones Ridge Limestone contains archeocyathids, trilobites, brachiopods, sphinctozoan sponges and conodonts which indicate an age-span of the Early Cambrian to Late Ordovician, with prominent hiatuses in the Middle Cambrian and Middle Ordovician (Brabb, 1967; Palmer, 1968; Blodgett *et al.*, 1984; Rigby *et al.*, 1988; Allison, 1988; Harris *et al.*, 1995). Coeval but deeper water equivalents to the Jones Ridge Limestone are variably exposed to the southwest of the Jones Ridge-Squaw Mountain area and consist of the Funnel Creek limestone, Adams argillite and Hillard limestone. Diachronous Early Ordovician to Silurian (middle Wenlock) siltstone and shale of the Road River Formation unconformably or disconformably overlie the Jones Ridge limestone and its local equivalents (Blodgett *et al.*, 1984; Harris *et al.*, 1995).

We examined the Jones Ridge Limestone in the Ogilvie River map area north of the Yukon thrust at Mt. Slipper (Morrow, 1999; his section 21) and south of the Yukon thrust along the Jones Ridge. The Mt. Slipper section is cut by multiple dykes of unknown age, which is inconsistent with other outcrops of Jones Ridge Limestone in which intrusive bodies are absent. Therefore, along with geochemical argument, Macdonald *et al.* (2010a) reassigned these strata to the Fifteenmile Group. Along the Jones Ridge, the Jones Ridge Limestone is certainly age-equivalent in part to Cambrian-Ordovician strata of the Yukon Stable Block (Bouvette Fm, Taiga Fm, Slats

Creek Fm and Illtyd Fm), Richardson Trough (Illtyd Fm, Slats Creek Fm, Rabbitkettle Fm and Vunta Fm), and parts of the Mackenzie-Peel Shelf (Backbone Ranges Fm, Sekwi Fm and Franklin Mountain Fm). In 2010, three detailed stratigraphic sections were measured near the type section of the Jones Ridge Limestone, spanning the lower and upper members (Fig. 9e). These sections were sampled at 1–2 m intervals for carbon isotope chemostratigraphy and approximately 30 bulk-rock samples were collected to search for conodonts. Five separate trilobite collections were also made.

DISCUSSION

The stratigraphic observations outlined above have allowed refinement and expansion of Neoproterozoic correlations presented in Macdonald and Roots (2010) and the development of consistent nomenclature within Yukon (Fig. 11). These correlations facilitate the synthesis of geological data throughout northwest Canada.

In the western Ogilvie Mountains we have reassigned the lower part of the Lower Tindir Group to the Pinguicula Group. We have included a part of the Lower Tindir Group, and units PR4, PR5 and PF1a of the Coal Creek inlier to the 'lower' assemblage of the Fifteenmile Group. The distribution of the 'lower' assemblage of the Fifteenmile Group in the western Ogilvie Mountains is consistent with deposition along northwest side-down normal faults. Detailed correlations between the Fifteenmile Group and the MMSG in the Mackenzie Mountains await further stratigraphic and chemostratigraphic description.

Additional detailed stratigraphic sections of the Callison Lake dolostone will provide better constraints on the depositional environment of this unit and its relationship with the metalliferous Coates Lake Group. The Callison Lake dolostone should possibly be separated from the underlying Fifteenmile Group because it appears more closely related to the overlying Lower Mt. Harper Group. One option is that the Callison Lake dolostone, Lower Mt. Harper Group and the Mt. Harper Volcanic Complex could be included in a separate group in recognition of possible correlation with the Coates Lake Group in the Mackenzie Mountains.

The Pleasant Creek Volcanics are geochemically and petrographically similar to members A-C of the Mount Harper Volcanic Complex. Whether these volcanics and the potentially correlative Tindir dyke swarm are coeval

Ogilvie Mountains					
		Tatonduk Inlier		Coal Creek Inlier	
this paper	Macdonald et al., 2010b	Van Kooten et al., 1997	Young, 1992	Macdonald et al., 2010a; Macdonald & Roots, 2010	Thompson et al. 1994; Mustard & Roots, 1997
Jones Ridge & Bouvette Fms, Cambrian Undiff.	Paleozoic undiff.	Funnel Ck., Adams, Hillard, Jones Ridge Fms	Jones Ridge Formation	Bouvette Formation	CDb
				PH5	PH5
"upper" group	5	pCtl	5	PH4	PH4
	4b			PH3	PH3
Hay Creek Group	4a / 3b / 3a	pCtss	4	PH2	
Rapitan Gp	2	pCtr	2	PH1	PH1/PH2
Pleasant Creek/ Mt Harper Vol	1	pCtbs	1	MHVC	MHVC
Lower Mt Harper				L Mt Harper	L Mt Harper
Callison Lake Dol	Upper Carb.	pCtds	dolostone	PF3	PF3
Craggy				PF2	PF2
				PF1	PF1
'lower' assemblage	Upper Shale	pCts	black shale	PF1a	PF1a / PR5
	Lower Shale	pCtsl			
P-D		pCtq	quartzite -shale		PR4
P-B/C	Lower Shale	pCtsd	dolostone -shale		PR3
			chert-strom dolostone		PR2
P-A		pCtlc	mudstone		PR1

Left-margin group labels (this paper column): Windermere Supergroup / Coates Lake / Mackenzie Mts supergroup; Upper Tindir Group / Lower Tindir Group; Pinguicula Gp / Fifteenmile; Upper Harper Group / U Fifteenmile Gp / L Fifteenmile Gp.

Legend:
🔶 scale microfossils (Allison *et al.*, 1986)
☆ U/PB ID-TIMS age (Macdonald et al., 2010a)
▼▼ major exposure surface
〰 angular unconformity

Figure 11. *Correlation of nomenclature and stratigraphic units previously used to describe the Tatonduk and Coal Creek inliers. Regionally consistent units proposed in this publication are shown in the left column.*

with the *ca.* 717 Ma members D-F of the Mount Harper Volcanic Complex and the Franklin Large Igneous Province (Macdonald *et al.*, 2010b), the Little Dal basalt (Dudás and Lustwerk, 1997), and/or the *ca.* 778 Ma Gunbarrel event (Harlan *et al.*, 2003) remains to be tested with further geochemical and geochronological analyses.

The Rapitan Group in the Tatonduk inlier consists of clast-poor siltstone and iron formation (Yeo, 1984; Young, 1976), reminiscent of the Sayunei Formation of the Rapitan Group in the Mackenzie Mountains. A glaciomarine depositional setting for the Rapitan Group in the Ogilvie Mountains is confirmed by the presence of faceted and striated clasts, bed-penetrating dropstones, common outsized and exotic clasts, and glacial push structures, along with evidence for subaqueous slumping in the form of graded grain and chaotic debris flows. A 716.47 ± 0.24 Ma U/Pb ID-TIMS zircon age (Macdonald *et al.*, 2010b) from a tuff near the base of the Rapitan Group in the Coal Creek inlier provides a direct age constraint on deposition.

Above the Rapitan Group, the Cryogenian stratigraphy of the Hay Creek Group is very condensed and commonly absent in the western Ogilvie Mountains. The diamictite and breccia at the top of Hay Creek Group may be correlative with the Ice Brook Formation in the Mackenzie Mountains. A discontinuously exposed dolostone above the Hay Creek Group in both the Coal Creek and Tatonduk inliers shares sedimentological and isotopic characteristics with the Ravensthroat dolomite in the Mackenzie Mountains (Aitken, 1991; James *et al.*, 2001) and with basal Ediacaran cap carbonates globally (Hoffman *et al.*, 2002; Kennedy, 1996). The Ice Brook Formation has long been correlated with the Marinoan glaciation in Australia, (Eisbacher, 1985; Halverson *et al.*, 2005). If this correlation is confirmed, the overlying black shale of the Hay Creek Group in Tatondul inlier is most likely correlative with the Sheepbed Formation in the Mackenzie Mountains.

This development and expansion of the stratigraphic framework for correlating Neoproterozoic strata in the Ogilvie Mountains will facilitate correlations with the Wernecke and Mackenzie Mountains and will aid in giving context to future geochemical, geochronological, paleontological, paleomagnetic and tectonic studies.

ACKNOWLEDGEMENTS

REFERENCES

Abbott, G., 1997. Geology of the Upper Hart River Area, Eastern Ogilvie Mountains, Yukon Territory (116A/10, 116A/11). Exploration and Geological Services Division, Yukon Region, Bulletin 9, p. 1-76.

Aitken, J.D., 1981. Stratigraphy and Sedimentology of the Upper Proterozoic Little Dal Group, Mackenzie Mountains, Northwest Territories. In: Proterozoic Basins of Canada, F.H.A. Campbell (ed.), Geological Survey of Canada Paper 81-10, p. 47-71.

Aitken, J.D., 1989. Uppermost Proterozoic formations in central Mackenzie Mountains, Northwest Territories. Geological Survey of Canada, Bulletin 368, 26 p.

Aitken, J.D., 1991. The Ice Brook Formation and Post-Rapitan, Late Proterozoic glaciation, Mackenzie Mountains, Northwest Territories. Geological Survey of Canada, Bulletin 404, 43 p.

Aitken, J.D. and McMechan, M.E., 1991. Middle Proterozoic assemblages. *In:* Geology of the Cordilleran Orogen in Canada, H. Gabrielse and C.J. Yorath (eds.), Series no. 4, Geological Survey of Canada, p. 97-124.

Allison, C.W.A., Young, G.M., Yeo, G.M. and Delaney, G.D., 1981. Glaciogenic rocks of the Upper Tindir Group, east-central Alaska. *In:* Earth's Pre-Pleistocene glacial record, M.J. Hambrey and W.B. Harland (eds.), Cambridge University Press, p. 720-723.

Allison, C.W., 1988. Paleontology of Late Proterozoic and Early Cambrian rocks of east-central Alaska. United States Geological Survey Professional Paper 1449, 46 p.

Brabb, E.E., 1967. Stratigraphy of the Cambrian and Ordovician rocks of east-central Alaska. United States Geological Survey Professional Paper 559-A, 30 p.

Brabb, E.E. and Churkin, M.J., 1969. Geologic map of the Charley River Quadrangle, east-central Alaska. United States Geological Survey, Miscellaneous Investigations 573, 1 sheet, scale 1:250 000.

Blodgett, R.B., Potter, A.W. and Clough, J.G., 1984. Upper Ordovician-Lower Devonian biostratigraphy and paleoecology of the Jones Ridge-Squaw Mountain area, east-central Alaska. Geological Society of America Abstracts with Programs, vol. 16, p. 270.

Cairnes, D.D., 1915. The Yukon-Alaska international boundary between Porcupine and Yukon Rivers. Geological Survey of Canada, Memoir no. 67, 161 p. and accompanying map 140-A, scale 1:126 720.

Dalrymple, R.W. and Narbonne, G.M., 1996. Continental slope sedimentation in the Sheepbed Formation (Neoproterozoic, Windermere Supergroup), Mackenzie Mountains, N.W.T. Canadian Journal of Earth Sciences, vol. 33, p. 848-862.

Dudás, F.O. and Lustwerk, R.L., 1997. Geochemistry of the Little Dal basalts: continental tholeiites from the Mackenzie Mountains, Northwest Territories, Canada. Canadian Journal of Earth Sciences, vol. 34, p. 50-58.

Eisbacher, G.H., 1978. Redefinition and subdivision of the Rapitan Group, Mackenzie Mountains. Geological Survey of Canada Paper 77-35, p. 1-21.

Eisbacher, 1981. Sedimentary tectonics and glacial record in the Windermere Supergroup, Mackenzie Mountains, northwestern Canada. Geological Survey of Canada Paper 80-27, p. 1-40.

Eisbacher, 1985. Late Proterozoic rifting, glacial sedimentation, and sedimentary cycles in the light of Windermere deposition, western Canada. Palaeogeography Palaeoclimatology Palaeoecology, vol. 51, p. 231-254.

Gabrielse, H., 1972. Younger Precambrian of the Canadian Cordillera. American Journal of Science, vol. 272, p. 521-536.

Green, L.H., 1972. Geology of Nash Creek, Larsen Creek, and Dawson Map-Areas, Yukon Territory. Geological Society of Canada, Memoir 364, 157 p.

Harris, A.G., Dumoulin, J.A., Repetski, J.E. and Carter, C., 1995. Correlation of Ordovician rocks of Northern Alaska. *In:* Ordovician odyssey, Short Papers for the 7th International Symposium on the Ordovician system, J.D. Cooper, M.L. Droser and S.C. Finney (eds.), Pacific Section for Sedimentary Geology (SEPM), Book 77, p. 21-26.

Halverson, G.P., Hoffman, P.F., Schrag, D.P., Maloof, A.C. and Rice, A.H.N., 2005. Toward a Neoproterozoic composite carbon-isotope record. Geological Society of America Bulletin, vol. 117, p. 1181-1207.

Harlan, S.S., Heaman, L.M., LeCheminant, A.N. and Premo, W.R., 2003. Gunbarrel mafic magmatic event: a key 780 Ma time marker for Rodinia plate reconstructions. Geology, vol. 31, p. 1053-1056.

Hoffman, P.F., Halverson, G.P., Domack, E.W., Husson, J.M., Higgins, J.A. and Schrag, D.P., 2007. Are basal Ediacaran (635 Ma) post-glacial "cap dolostones" diachronous? Earth and Planetary Science Letters, vol. 258, p. 114-131.

Hoffman, P.F., Halverson, G.P., Grotzinger, J.P., Kennedy, M.J., Christie-Blick, N. and Sohl, L.E., 2002. Are Proterozoic cap carbonates and isotopic excursions a record of gas hydrate destabilization following Earth's coldest intervals? Discussion and reply. Geology, vol. 30, p. 286-288.

Hoffman, P.F. and Macdonald, F.A., 2010. Sheet-crack cements and early regression in Marinoan (635 Ma) cap dolostones: Regional benchmarks of vanishing ice-sheets? Earth and Planetary Science Letters, vol. 300, p. 374-384.

James, N.P., Narbonne, G.M. and Kyser, T.K., 2001. Late Neoproterozoic cap carbonates: Mackenzie Mountains, northwestern Canada: precipitation and global glacial meltdown. Canadian Journal of Earth Sciences, vol. 38, p. 1229-1262.

Jones, D.S., Maloof, A.C., Hurtgen, M.T., Rainbird, R.H. and Schrag, D.P., 2010. Regional and global chemostratigraphic correlation of the early Neoproterozoic Shaler Supergroup, Arctic Canada. Precambrian Research, vol. 181, p. 43-63.

Kendall, C.G.S.C. and Warren, J., 1987. A review of the origin and setting of teepees and their associated fabrics. Sedimentology, vol. 34, p. 1007-1027.

Kennedy, M.J., 1996. Stratigraphy, sedimentology, and isotope geochemistry of Australian Neoproterozoic postglacial cap dolostones: deglaciation, $\partial^{13}C$ excursions, and carbonate precipitation. Journal of Sedimentary Research. vol. 66, p. 1050-1064.

Macdonald, F.A., Cohen, P.A., Dudás, F.O. and Schrag, D.P., 2010a. Early Neoproterozoic scale microfossils in the Lower Tindir Group of Alaska and the Yukon Territory. Geology, vol. 38, p. 143-146.

Macdonald, F.A., Schmitz, M.D., Crowley, J.L., Roots, C.F., Jones, D.S., Maloof, A.C., Strauss, J.V., Cohen, P.A., Johnston, D.T. and Schrag, D.P. 2010b. Calibrating the Cryogenian. Science, vol. 327, p. 1241-1243.

Macdonald, F.A. and Roots, C.F., 2010. Upper Fifteenmile Group in the Ogilvie Mountains and correlations of early Neoproterozoic strata in the northern Cordillera. *In:* Yukon Exploration and Geology 2009, K.E. MacFarlane, L.H. Weston and L.R. Blackburn (eds.), Yukon Geological Survey, p. 237-252.

MacNaughton, R.B., Narbonne, G.M. and Dalrymple, R.W., 2000. Neoproterozoic slope deposits, Mackenzie Mountains, northwestern Canada: implications for passive-margin development and Ediacaran faunal ecology. Canadian Journal of Earth Sciences, vol. 37, p. 997-1020.

MacNaughton, R.B., Roots, C.F. and Martel, E., 2008. Neoproterozoic-(?)Cambrian lithostratigraphy, northeast Sekwi Mountain map area, Mackenzie Mountains, Northwest Territories: new data from measured sections. Geological Survey of Canada, Current Research 2008, vol. 16, 17 p.

Medig, K.P., Thorkelson, D.J. and Dunlop, R.L., 2010. The Proterozoic Pinguicula Group: stratigraphy, contact relationships, and possible correlations. *In:* Yukon Exploration and Geology 2009, K.E. MacFarlane, L.H. Weston and L.R. Blackburn (eds.), Yukon Geological Survey, p. 265-278.

Mertie, J.B., 1930. Geology of the Eagle-Circle district, Alaska. U.S. Geological Survey Bulletin, vol. 816, p. 121-122.

Mertie, 1933. The Tatonduk-Nation district, Alaska. U. S. Geological Survey Bulletin, vol. 836-E, p. 345-454.

Morrow, D.W., 1999. Lower Paleozoic stratigraphy of northern Yukon Territory and northwestern District of Mackenzie. Geological Survey of Canada, Bulletin 538, 202 p.

Mustard, P.S., 1991. Normal faulting and alluvial-fan deposition, basal Windermere Tectonic Assemblage, Yukon, Canada. Geological Society of America Bulletin, vol. 103, p. 1346-1364.

Mustard, P.S. and Donaldson, J.A., 1990. Paleokarst breccias, calcretes, silcretes and fault talus breccias at the base of upper Proterozoic "Windermere" strata, northern Canadian Cordillera. Journal of Sedimentary Petrology, vol. 60, p. 525-539.

Mustard, P.S., Donaldson, J.A. and Thompson, R.I., 1988. Trace fossils and stratigraphy of the Precambrian-Cambrian boundary sequence, upper Harper group, Ogilvie Mountains, Yukon. Current Research, Part E, Geological Survey of Canada Paper 88-1E, p. 197-203.

Mustard, P.S. and Roots, C.F., 1997. Rift-related volcanism, sedimentation, and tectonic setting of the Mount Harper Group, Ogilvie Mountains, Yukon Territory. Geological Survey of Canada Bulletin 492, 92 p.

Norris, D.K., 1979. Geological map of the Porcupine River area. Geological Survey of Canada Map Sheets 116J and 116K (E1/2), GSC Open File Report 621, scale 1:250 000.

Norris, D.K., 1981. Geology, Porcupine River area. Geological Survey of Canada Map 1522A, scale 1:250 000.

Norris, D.L., 1982. Geology, Ogilvie River, Yukon Territory. Geological Survey of Canada, Map 1526A, scale 1:250 000.

Norris, D.K., 1997. The Geology, Mineral, and Hydrocarbon Potential of Northern Yukon Territory and Northwest District of Mackenzie. Geological Survey of Canada Bulletin 422, 401 p.

Palmer, A.R., 1968. Cambrian trilobites of east-central Alaska. United States Geological Survey Professional Paper 559-B, 115 p.

Payne, M.W. and Allison, C.W.A., 1981. Paleozoic continental-margin sedimentation in east-central Alaska. Geology, vol. 9, p. 274-279.

Rainbird, R.H., Jefferson, C.W. and Young, G.M., 1996. The early Neoproterozoic sedimentary Succession B of Northwestern Laurentia: Correlations and paleogeographic significance. Geological Society of America Bulletin, vol. 108, p. 454-470.

Rigby, J,K., Potter, A.W. and Blodgett, R.B., 1988. Ordovician sphinctozoan sponges of Alaska and Yukon Territory. Journal of Paleontology, vol. 62, p. 731-746.

Roots, C.F., 1987. Regional tectonic setting and evolution of the Late Proterozoic Mount Harper volcanic complex, Ogilvie Mountains, Yukon. Unpublished PhD thesis, Carleton University, Ottawa, Ontario, Canada.

Roots, C.F. and Thompson, R.I., 1992. Long-lived basement weak zones and their role in extensional magmatism in the Ogilvie Mountains, Yukon Territory. *In:* Basement Tectonics and Characterization of Ancient and Mesozoic Continental Margins, M.J. Bartholomew, D.W. Hyndman, D.W. Mogk and R. Mason (eds.), Proceedings of the 8th International Conference in Basement Tectonics, Kluwer Academic Publishers, p. 359-372.

Thompson, R.I., Mercier, B. and Roots, C.F., 1987. Extension and its influence on Canadian Cordilleran passive-margin evolution. *In:* Continental Extensional Tectonics, M.P. Coward, J.F. Dewey, and P.L. Hancock (eds.), Geological Society Special Publication, vol. 28, p. 409-417.

Thompson, R.I., Roots, C.F. and Mustard, P.S., 1994. Geology of Dawson map area 116B, C, northeast of Tintina Trench: Geological Survey of Canada, Open File 2849, scale 1: 50 000.

Thorkelson, D.J., 2000. Geology and mineral occurrences of the Slats Creek, Fairchild Lake and "Dolores Creek" areas, Wernecke Mountains, Yukon Territory, 106D/16, 106C/13, 106C/14. Exploration and Geological Services Division, Yukon Region, Bulletin 10.

Thorkelson, D.J., Abbott, G.J., Mortensen, J.K., Creaser, R.A., Villeneuve, M.E., McNicoll, V.J. and Layer, P.W., 2005. Early and Middle Proterozoic evolution of Yukon, Canada. Canadian Journal of Earth Sciences, vol. 42, p. 1045-1071.

Van Kooten, G.K., Watts, A.B., Coogan, J., Mount, V.S., Swenson, R.F., Daggett, P.H., Clough, J.G., Roberts, C.T. and Bergman, S.C., 1997. Geological Investigations of the Kandik Area, Alaska and Adjacent Yukon Territory, Canada. Alaska Division of Geological and Geophysical Surveys, Report of Investigations 96-6A, 3 sheets, scale 1:125 000.

Yeo, G.M., 1978. Iron-formation in the Rapitan Group, Mackenzie Mountains, Yukon and Northwest Territories. DIAND Mineral Industry Report 1975, NWT Economic Geology Series 1978-5, p. 170-175.

Yeo, G.M., 1984. The Rapitan Group: relevance to the global association of Late Proterozoic glaciation and iron-formation. Unpublished PhD. thesis, University of Western Ontario, London, Ontario, Canada, 599 p.

Young, G.M., 1976. Iron-formation and glaciogenic rocks of the Rapitan Group, Northwest Territories, Canada. Precambrian Research, vol. 3, p. 137-158.

Young, 1981. The Amundsen Embayment, Northwest Territories: Relevance to the Upper Proterozoic evolution of North America. *In:* Proterozoic Basins of Canada, F.H.A. Campbell (ed.), Geological Survey of Canada Paper 81-10, p. 203-218.

Young, 1982. The late Proterozoic Tindir Group, east-central Alaska; Evolution of a continental margin. Geological Society of America Bulletin, vol. 93, p. 759-783.

Young, G.M., Jefferson, C.W., Delaney, G.D. and Yeo, G.M., 1979. Middle and Upper Proterozoic evolution of the northern Canadian Cordillera and Shield. Geology, vol. 7, p. 125-128.

Appendix 1. Locations of the base of stratigraphic sections described in text.

Section	Latitude	Longitude
E1002	64.708	139.340
E1003	64.705	139.341
E1006	65.123	141.033
F1007	64.149	141.034
F1008	65.152	140.989
F1022	64.712	139.325
F1023	64.714	139.346
F838	64.726	140.040
F841	64.756	140.115
F842	64.693	140.113
F918	64.762	140.107
F930	64.682	139.232
F931	64.725	139.249
F932	64.718	139.225
J1018	64.663	139.397
J1019	64.689	139.353
Section 1	65.119	141.005
Section 2	65.116	141.020
Section 3	65.115	141.035
Section 4	65.131	140.995
T708	65.119	141.004
T710	65.051	141.174

Paleoproterozoic Bonnet Plume River intrusions: Evidence for a calc-alkaline arc at 1.7 Ga and its partial preservation in Yukon, Canada

Alexander B. Nielsen[1], Derek J. Thorkelson, Daniel D. Marshall and H. Daniel Gibson
Department of Earth Sciences, Simon Fraser University

ABSTRACT

The 1.71 Ga Bonnet Plume River intrusions (BPRI) and related volcanics are preserved only as clasts in the 1.60 Ga Wernecke breccias of Yukon that host iron-oxide copper gold (IOCG) occurrences. Field work conducted in 2009 confirmed that they did not intrude the surrounding <1.64 Ga Wernecke Supergroup. Petrography shows that they are extensively altered and/or metasomatized, although relicts of primary igneous minerals remain. The major oxides are of little use in classification. Trace element geochemistry however, reveals a mafic to intermediate, calc-alkaline volcanic arc signature. Geochemical modelling has demonstrated that crystal fractionation was dominated by pyroxenes, plagioclase and olivine. The BPRI and related volcanic rocks are thought to have originated in a calc-alkaline volcanic arc that was obducted onto the Wernecke Supergroup, subsequently partially brecciated, and finally sank within the Wernecke breccias to the level of the Wernecke Supergroup.

[1]onielsen@sfu.ca

INTRODUCTION

LOCATION, ACCESS AND METHODS

Fieldwork in 2009 was undertaken in order to investigate and sample the Bonnet Plume River intrusions (BPRI) and other igneous rocks at known mineral occurrences across the Yukon (Fig. 1). With the exception of 'Spectacular Creek' (Yukon Olympic MINFILE occurrence 116G/082), all locations are remote and accessible only by helicopter. The Spectacular Creek location is most easily accessed by crossing the Blackstone River by small watercraft. BPRI exposures were examined at each of the field locations (investigation sites, Fig. 1). Volcanic and plutonic rocks correlated with the BPRI were examined at the Spectacular Creek locality. At two locations, near the Bel and Pika MINFILE occurrences, detailed maps were made to show the relationship between the igneous clasts and the surrounding breccias (Figs. 2 and 3).

Figure 1. Map of central Yukon illustrating the distribution of Proterozoic inliers and locations where field work was conducted.

REGIONAL GEOLOGY

The Paleoproterozoic (1725 -1705 Ma) BPRI comprise bodies of metamorphosed diorite, gabbro, basalt and andesite, as well as minor anorthosite and quartz-albite syenite (Thorkelson *et al.*, 2001a). Diorite clasts are most common. These bodies of igneous rock are present only as clasts within the Mesoproterozoic Wernecke breccia systems (1595 Ma; Thorkelson *et al.* 2001b). Unbrecciated examples of the Bonnet Plume River intrusions are not known.

Zones of Wernecke breccia are exposed in Proterozoic inliers in the Wernecke, Ogilvie and Richardson mountains throughout the central and northern Yukon (Fig.1). They intrude the Mesoproterozoic (minimum age 1595 Ma, maximum age 1640 Ma; Thorkelson *et al.,* 2001b; Furlanetto *et al.*, 2009a) Wernecke Supergroup (Fig.1), a 13 to 14 km-thick sedimentary succession (Delaney, 1981; Norris, 1997; Thorkelson, 2000). Prior to brecciation, the Wernecke Supergroup was deformed and locally metamorphosed to middle-upper greenschist grade during the Racklan orogeny (Thorkelson *et al.,* 2000; Brideau *et al.*, 2002). The Wernecke breccias and the BPRI host numerous iron-oxide copper gold (IOCG) occurrences (Thorkelson, 2000).

PREVIOUS WORK

The remote locations and difficult access has meant that the BPRI have received only cursory investigation in the past. The first major study was conducted by Thorkelson (2000), and was expanded upon in Thorkelson *et al.* (2001a,b), following regional mapping by Thorkelson and Wallace (1998a,b,c) in the Wernecke Mountains. Key results include that the BPRI crystallized between 1725 Ma and 1705 Ma, and that the crystallization preceded their inclusion in the Wernecke breccias.

Laughton *et al.* (2002) studied the Slab volcanics, which comprise a series of mafic volcanic clasts, including a megaclast at Slab Mountain consisting of 35 amygdaloidal basaltic pahoehoe flows. Laughton *et al.* (2002) concluded that they are probably correlative with the BPRI. Following this, Hunt and Thorkelson (2007) studied mafic igneous rocks in the Wernecke breccias in the eastern Ogilvie Mountains and Nor inlier (Fig. 1). On the basis of field relationships, and major and trace element geochemistry, it was determined that these rocks are probably correlative with the BPRI.

WHY REINTERPRET THE ORIGINS OF THE BPRI?

A previous model of geological events described the BPRI as igneous intrusions hosted by the Wernecke Supergroup (Thorkelson, 2000; Thorkelson *et al.*, 2001a,b), with both intrusions and host affected by hydrothermal activity and formation of Wernecke breccia. However, a detrital mineral study by (Furlanetto *et al.*, 2009a) indicated that the Wernecke Supergroup is <~1640 Ma, which is ~75 m.y. younger than the BPRI. This age difference indicates that the BPRI could not have intruded the Wernecke Supergroup, and that a different explanation is required to account for the presence of the BPRI in the Wernecke breccias.

Figure 2. *Geological map of the Bel MINFILE occurrence (106C/14 097).*

FIELD RELATIONSHIPS

The BPRI are the oldest known rocks in the Yukon at 1710 Ma (Thorkelson *et al.*, 2001a). They exist only as clasts within the Wernecke breccias. Thorkelson *et al.* (2001a) proposed that there are BPRI bodies with igneous contact relationships with the Wernecke Supergroup; however, the age relationship between the BPRI (1710 Ma) (Thorkelson *et al.*, 2001a) and the Wernecke Supergroup (maximum 1640 Ma, Furlanetto *et al.*, (2009a)) casts doubt on this relationship. More detailed work during the 2009 field season was carried out at many of the locations where igneous contact relationships between the BPRI and Wernecke Supergroup were inferred in the original mapping by Thorkelson and Wallace (*e.g.*, 1998a,b,c). In all cases, the BPRI were not in igneous contact with the Wernecke Supergroup; they were separated by a zone of Wernecke breccia. This separation was commonly on the order of 1-10 m (Figs. 2 and 3). Furthermore, the BPRI do not show grain size variations consistent with chilling along their margins, and the Wernecke breccias are not contact-metamorphosed by

the BPRI. This understanding is consistent with the isotopic age of the Wernecke breccias (~1595 Ma; Thorkelson, 2000), which is ~115 Ma younger than the BPRI.

Clasts of BPRI are up to 900 m long and 200 m wide. The BPRI are not metamorphosed above middle greenschist grade. The Wernecke breccias lack any clasts which would suggest derivation from a basement source under the Wernecke Supergroup such as gneiss and peridotite.

PRIMARY AND SECONDARY MINERALOGY

The mineralogy of the BPRI reflects both primary (igneous) and secondary (metasomatic and metamorphic) mineral growth. The observed mineral assemblage of the Bonnet Plume River intrusions may be divided into three groups: primary igneous minerals; secondary minerals that are pseudomorphs of the primary minerals; and secondary minerals that occur in veins, mats and mineral overgrowths (Table 1).
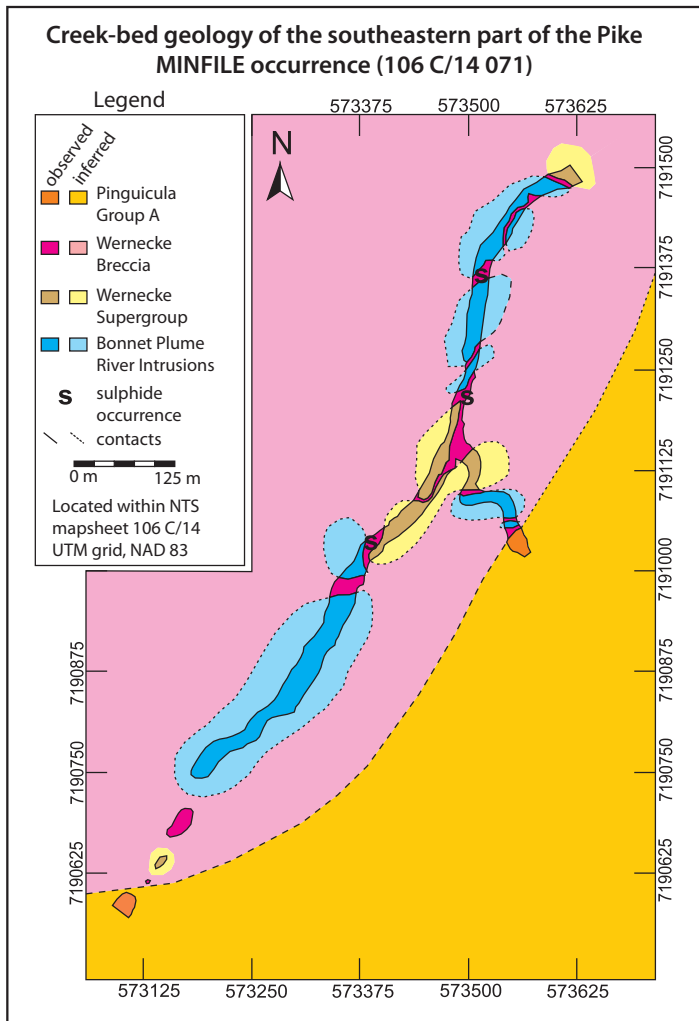
Figure 3. *Geological map of part of the Pika MINFILE occurrence (106C14 071).*

The inferred primary mineralogy of the BPRI, without metasomatic minerals, consists of pyroxenes, plagioclase and olivine, as well as rare quartz and potassium feldspar. Based on the quartz-alkali feldspar-plagioclase-feldspathoid classification system of LeMaitre (2002), the BPRI are primarily diorites and gabbros with minor quartz diorite, tonalite, granodiorite and quartz monzodiorite.

The mineralogy of the BPRI is dominated by secondary minerals, primarily chlorite, epidote, sericite, Na-Ca zeolites and iron oxides. Potassium feldspar is commonin more potassically altered samples. Veins in the BPRI are composed primarily of calcite, commonly with quartz and other minor phases.

Sericite, scapolite and Na-Ca zeolites form partial to complete replacements of plagioclase (Fig 4a). Chlorite is present as pseudomorphs of euhedral phenocrysts (former pyroxene or olivine crystals) in fine-grained BPRI, or as well defined zones bounded by plagioclase pseudomorphs (Fig. 4b), and also in groundmass and undefined parts of the rock. Commonly, the chlorite pseudomorphs include grains of hematite. Hematite also forms pseudomorphs of magnetite and possibly ilmenite, as well as newly formed metasomatic porphyroblasts (Fig. 4c). These relationships are summarized in Table 2.

Table 1. *Occurrence of minerals observed in thin section. Dots indicate known occurrence; question marks indicate uncertain presence.*

Mineral	Occurs as a primary mineral	Occurs as a pseudomorph	Occurs as overgrowths	Occurs in veins
plagioclase	*			*
alkali feldspar	*	*		
Na-Ca zeolites		*		
muscovite (sericite)		*		
hornblende		*		
chlorite		*	*	*
scapolite		*		
epidote			*	*
biotite			*	
calcite			*	*
quartz	*			*
apatite				*
hematite		*	*	
magnetite	?		*	
pyrite	?		*	
chalcopyrite			*	
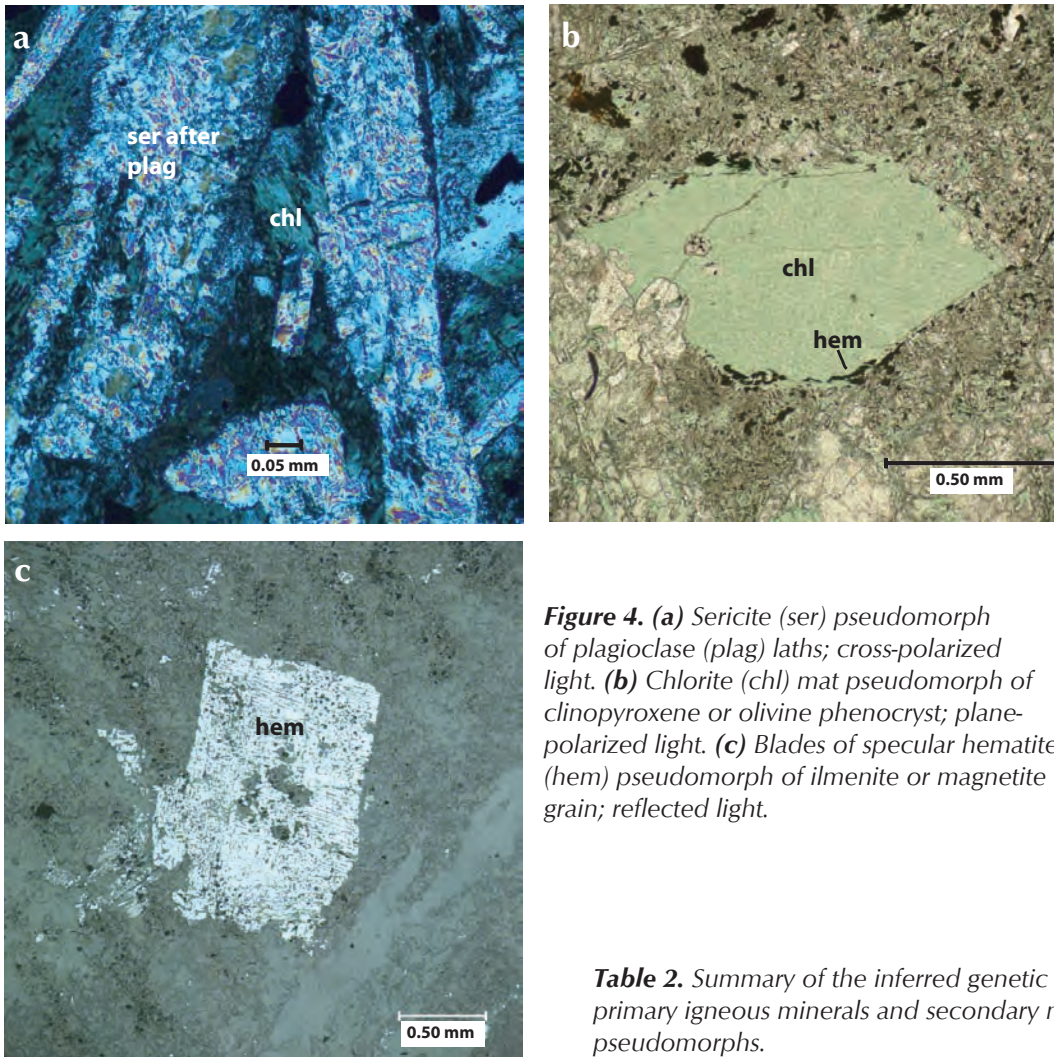
Figure 4. (a) *Sericite (ser) pseudomorph of plagioclase (plag) laths; cross-polarized light.* **(b)** *Chlorite (chl) mat pseudomorph of clinopyroxene or olivine phenocryst; plane-polarized light.* **(c)** *Blades of specular hematite (hem) pseudomorph of ilmenite or magnetite grain; reflected light.*

Table 2. *Summary of the inferred genetic relationships between primary igneous minerals and secondary minerals that are present as pseudomorphs.*

Primary minerals	Secondary minerals
igneous crystallization	metamorphism and metasomatism
plagioclase	Na-Ca zeolites sericite scapolite alkali feldspar
olivine pyroxene amphibole	chlorite
magnetite ilmenite	hematite

GEOCHEMISTRY

Thirty samples of BPRI were analysed for major and trace elements at Activation Laboratories in Ancaster, Ontario, and the resulting data have been added to previously collected data for the BPRI from Thorkelson (2000) and unpublished data from the Slab volcanics (Laughton, 2004) in order to create a more robust data set.

MAJOR ELEMENT COMPOSITIONS

Silica concentrations for BPRI cluster in the range of 45-55% and a few samples to almost 70% (Fig. 5). When plotted against hafnium (Hf) (Fig. 5), a relatively immobile element, most major oxides display a high degree of scatter, particularly those that are mobile in hydrothermal solution such as the alkalis and alkaline earths. In contrast, alumina forms a relatively tight linear array. Given that alumina is relatively immobile in hydrothermal conditions, much of the scatter of the other oxides is probably the result of metasomatic alteration rather than igneous processes such as fractional crystallization. The main cause of the hydrothermal alteration is probably fluid activity during Wernecke breccia formation, which is widely recognized in wallrock and clasts of Wernecke breccia (Thorkelson *et al.*, 2001b).
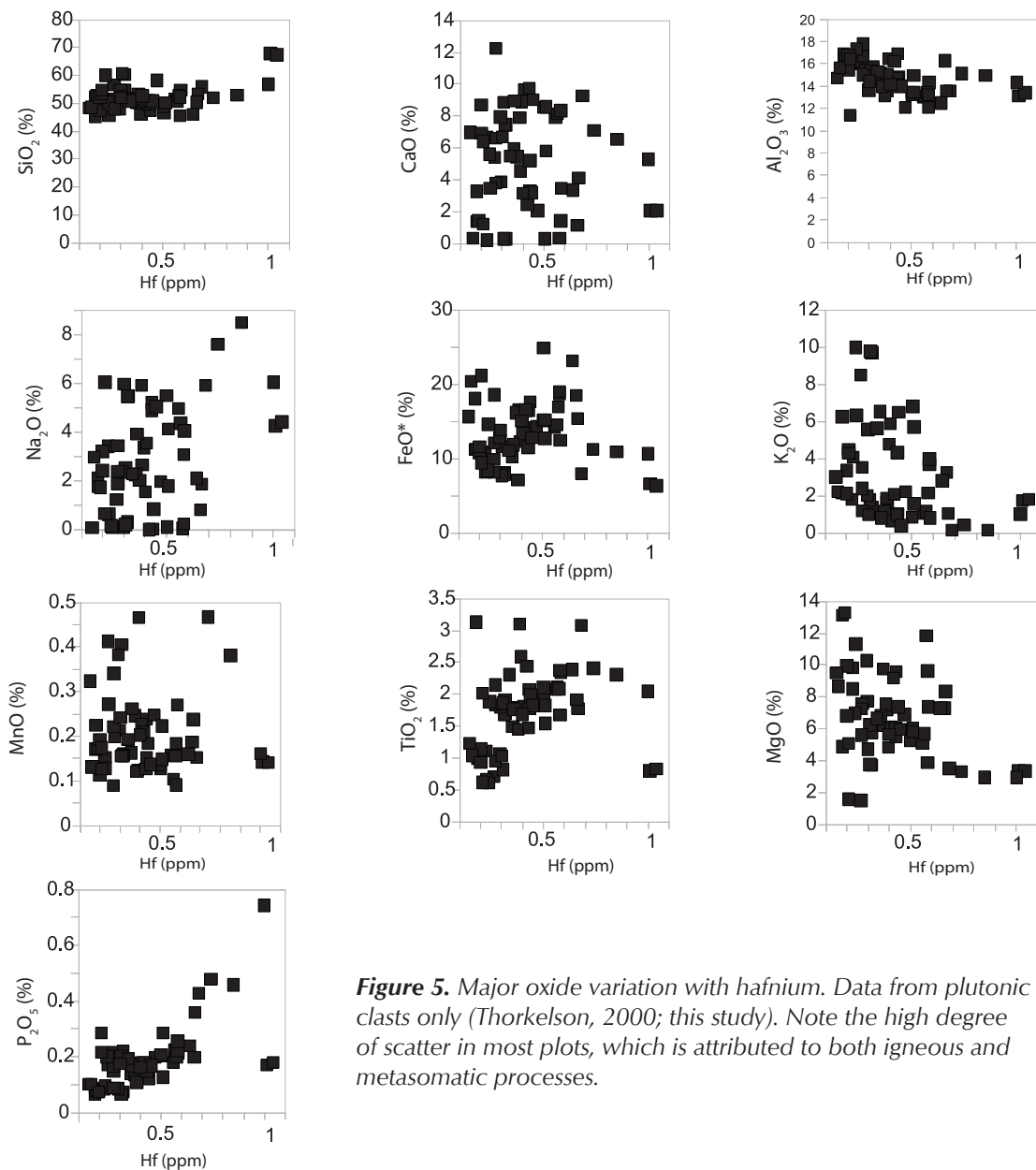
Figure 5. *Major oxide variation with hafnium. Data from plutonic clasts only (Thorkelson, 2000; this study). Note the high degree of scatter in most plots, which is attributed to both igneous and metasomatic processes.*

The CIPW normative mineralogy of the BPRI is highly variable, largely due to major element mobility. Samples range from 22% quartz to 15% nepheline and 6% leucite in their normative mineralogies. Plagioclase compositions range from An_0 to An_{96}. Whole-rock Mg numbers range from 29 to 69. Samples are peraluminous to metaluminous. These compositional variations likely reflect the original igneous compositions with significant modifications from brecciating fluids.

CALC-ALKALINE DIORITES AND GABBROS

DIFFICULTIES IN GEOCHEMICAL DISCRIMINATION OF THE BPRI AND RELATED VOLCANICS

Systems of classifying, determining rock series, and assigning tectonic affinity of rocks are commonly based on major elements and/or mobile trace elements. These elements do not generally retain their primary concentrations after metasomatism by hydrothermal fluids; therefore, systems based on these concentrations are likely to produce results with a wide and meaningless scatter. In order to address this issue, systems based on immobile elements have been applied to the BPRI (Floyd and Winchester, 1978; Rollinson, 1993; Gifkins *et al.,* 2005).

ROCK CLASSIFICATION

The system of Winchester and Floyd (1977) has been used for classifying the BPRI. In this system, the BPRI are predominantly subalkaline basalt and andesite, and minor rhyodacite-dacite, rhyolite, trachyandesite and alkali basalt (Fig. 6). Given that many of the BPRI are phaneritic, plutonic rock names of comparable composition are generally more appropriate. Accordingly, the BPRI should be regarded as mostly diorite and gabbro, and minor granodiorite, tonalite and quartz monzonite.

The commonly used TAS method of Le Maitre (2002) was not used due to the open-system behaviour of the alkalis and to a lesser degree, silica, in the BPRI. When the TAS system is applied, it produces an extremely wide array of rock types, with samples plotting evenly among the basalt to trachydacite fields, in all three levels of silica saturation.

ROCK SERIES

In order to further describe the composition of the BPRI, the method of Ross and Bédard (2009) was applied. This method demonstrates that the BPRI follow the calc-alkaline to transitional series trend, as opposed to a tholeiitic one (Fig. 7). This differentiation method is more robust than
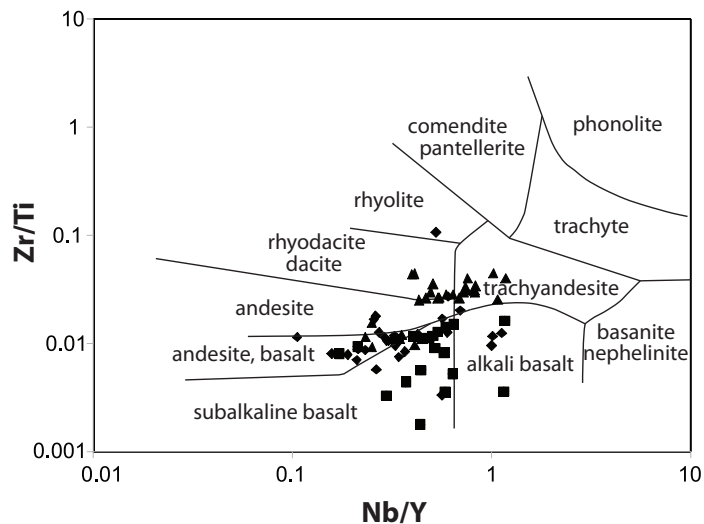
Figure 6. *Rock classification after Winchester and Floyd (1977). Diamonds indicate data from this study, squares indicate data from Thorkelson (2000), and triangles indicate data from Laughton et al. (2002).*
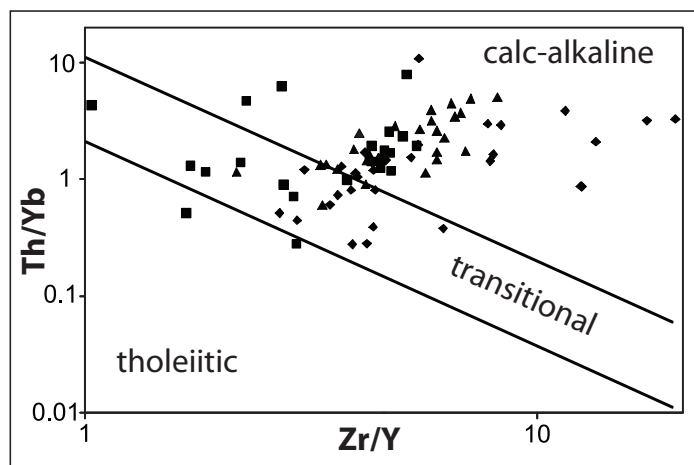
Figure 7. *Rock series classification after Ross and Bédard (2009); logarithmic scale. Diamonds indicate data from this study, squares indicate data from Thorkelson et al. (2001a), and triangles indicate data from Laughton et al. (2002).*

the standard methods of differentiating the magma series of rocks (*e.g.*, Irvine and Baragar, 1971; Miyashiro, 1974; Pecerillo and Taylor, 1976) because it is based on the ratios of relatively immobile trace elements.

ARC AFFINITY OF THE BPRI

An N-MORB-normalized spider diagram including the BPRI and related volcanics is illustrated in Figure 8 (normalizing values Cs-Lu after Sun and McDonough, 1989; Gd-Ti order reversed after Pearce and Parkinson, 1993; Co to Ni after Pearce and Parkinson, 1993, except Zn and Cu, estimated

by D.J. Thorkelson (unpublished data), and from Basaltic Volcanism Study Group, 1981). The strongly enriched large-ion lithophile elements, relative Nb-Ta depletion, and gently right-sloping rare-earth element pattern that approaches unity, indicate that the BPRI probably formed in an arc to back-arc setting. The scatter on the diagram may reflect fluid-induced remobilization, but the general shape of the pattern reflects original igneous compositions.

ARC AFFINITY REVEALED BY IMMOBILE ELEMENTS

Thorkelson *et al.* (2001a) attempted to characterize the tectonic affinity of the BPRI based on the Ti/V ratio of Shervais (1982) and the La/Th, La/Ba and Nb/La ratios of Gill (1981). This attempt was inconclusive because Ba and Ti have a large scatter, probably due to metasomatism during the emplacement of the Wernecke breccias. Immobile element (Th, Nb, La, Hf, Ta and Yb) ratio plots

of the BPRI and associated lavas demonstrate a strong geochemical similarity to calc-alkaline arcs (Figs. 9 and 10; Wood, 1980; Gill, 1981).

GEOCHEMICAL MODELLING

Geochemical modelling was performed on the BPRI in order to investigate whether their major and trace element characteristics can be explained by closed-system Rayleigh fractionation and if metasomatic processes could be recognized. This was done with (1) a numerical model of major element trends-based mineral compositions, and (2) models of mineral-specific partition coefficients for the trace elements. The modelling demonstrated that the geochemical patterns of the BPRI can be explained by Rayleigh fractionation, and that metasomatism and other open-system processes, such as crustal assimilation and mixing, play a significant role.
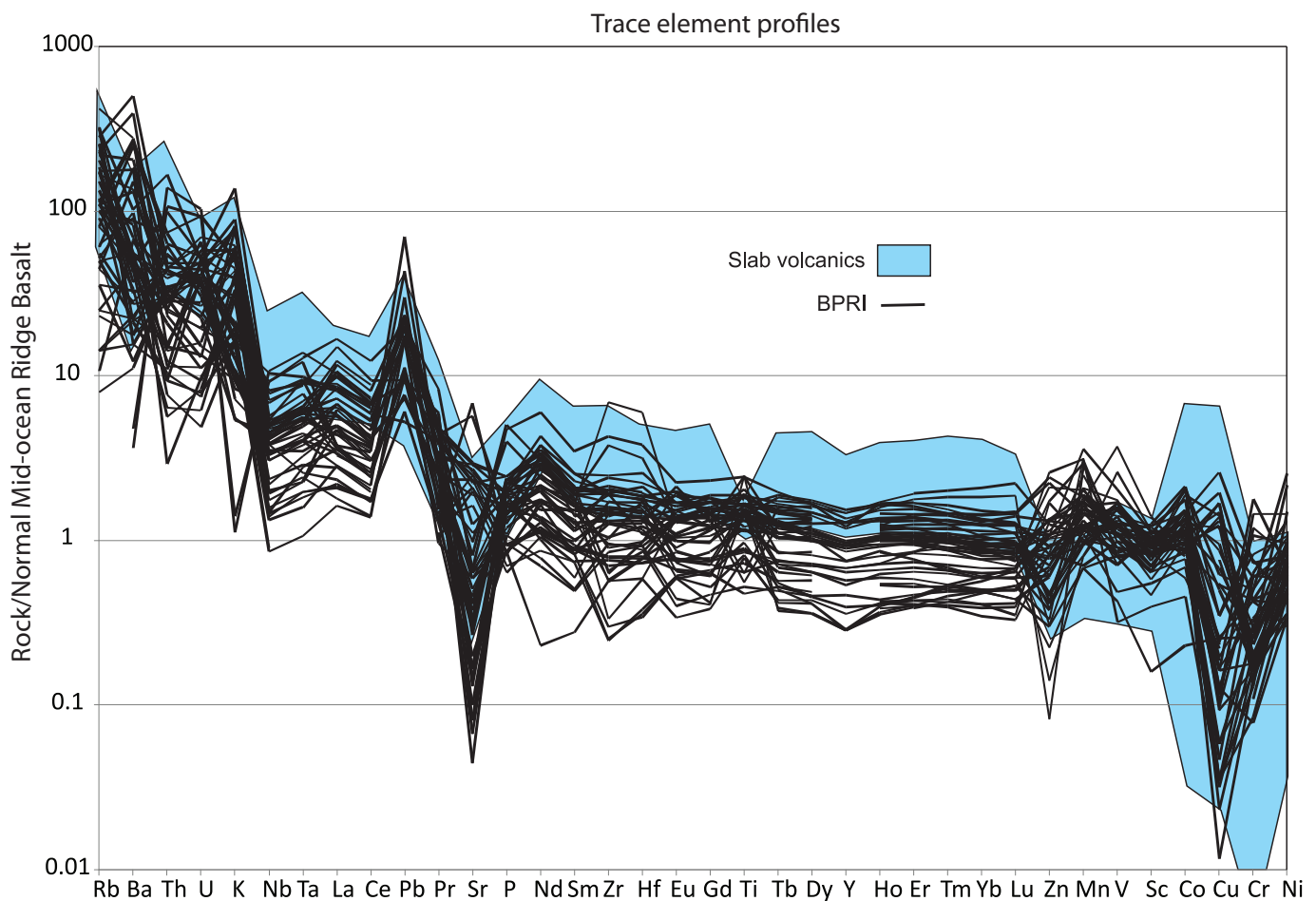
Figure 8. *N-MORB normalized (normalizing values Cs-Lu after Sun and McDonough (1989); Gd-Ti order reversed after Pearce and Parkinson (1993); Co to Ni after Pearce and Parkinson (1993) except Zn and Cu, estimated by D.J. Thorkelson (unpublished data) and from Basaltic Volcanism Study Group (1981)) spider diagram illustrating data from this study and Thorkelson et al., (2001a; black lines), and the Slab volcanics (light blue field).*
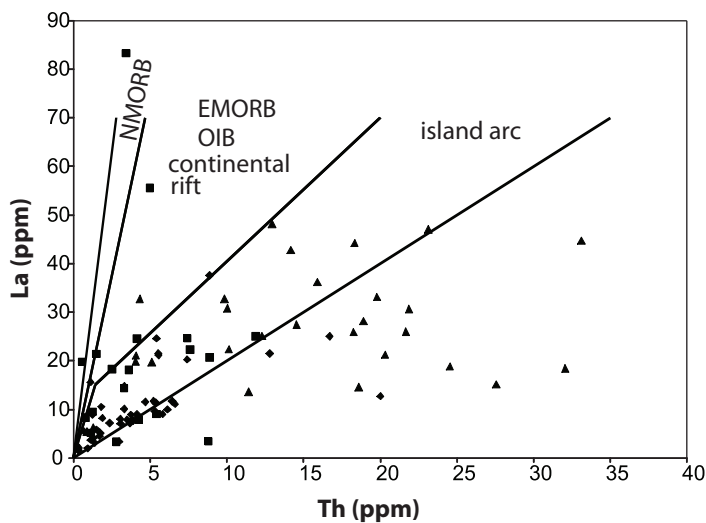
Figure 9. *Tectonic affinity plot, modified after Gill (1981), based on La and Th. Samples plot predominantly in the arc volcanics field. Diamonds indicate data from this study, squares indicate data from Thorkelson et al. (2001a), and triangles indicate data from Laughton et al. (2002).*

Figure 10. *Tectonic affinity plot, after Wood (1980), based on Hf, Th and Ta. Samples plot predominantly in the calc-alkaline arc basalt field. Diamonds indicate data from this study, squares indicate data from Thorkelson (2000), and triangles indicate data from Laughton et al. (2002).*

METHODS

Major element geochemical modelling is preliminary and reflects a first attempt to model rock evolution using two of the least metasomatized samples of BPRI, as determined petrographically. One sample had high levels of Mg, Cr, Ni and Sc and was therefore regarded as a possible parent to other BPRI units. The other had lower levels of these elements and a high level of potassium. Zr was used as a conserved element against which igneous and open-system processes were gauged. The parental composition plots as a horizontal line and has a value of 1; geochemical losses and gains relative to variations in Zr plot below and above the parental composition in Figure 11, respectively. Elemental losses from the primary composition were modelled by removal of stoichiometrically appropriate molar quantities of major elements based on the compositions of minerals that were hypothesized to have crystallized and subsequently removed from the magma system (except for Na which could only be modeled by metasomatic and igneous depletion). Elemental gains were modelled using individual elements without stoichiometric constraints. This procedure was deemed to be the most suitable approach because there is no necessity for metasomatic processes to add or remove mineralogically defined molar quantities of elements.

The trace element modelling used all available data for the BPRI. Differentiation trends were defined by ratios of trace element partition coefficients into olivine, orthopyroxene, clinopyroxene, plagioclase, and hornblende, plotted as fractionation vectors in Figure 12. A model differentiation trend was defined using an appropriate weighted average of the differentiation trends of these minerals. This trend was defined visually in order to approximate the distribution of data points. The mineral proportions defining this trend reflect the relative abundances of dominant phases that fractionated during the evolution of the BPRI.

IGNEOUS AND METASOMATIC PROCESSES

Major element modeling indicates that geochemical variations were produced mainly by augite, orthopyroxene and plagioclase fractionation, and only minor removal of magnetite, rutile, titanite and apatite (Fig. 11). The total amount of fractionation was nearly 50%. However, despite using the least altered samples in the major element modelling, it was necessary to invoke open-system processes such as metasomatism, crustal assimilation, or variable primary magma systems in order to model the calculated bulk composition differentiation trend. Specifically, concentrations of K_2O, Na_2O, TiO_2 and P_2O_5 could not be modelled by mineral fractionation alone, and required elemental additions or subtractions. The alkali elements showed the greatest divergence from closed-system processes, and the high level of potassium in the rock was modeled with an open-system gain of 3.33 mol%, and Na_2O modeled with a loss of 2.6 mol% (Fig. 11). Most of the open-system variability was probably caused by breccia fluid activity.

Trace element geochemical modelling indicates a similar suite of fractionating minerals and range of fractionation percentages. The full range of fractionation was greater than 90%. Across various trace element systems, the minerals that consistently define the model trend were orthopyroxene, clinopyroxene, olivine and plagioclase (Yb-Nb illustrated in Fig. 12). Metasomatism, crustal assimilation, and differences in primary magmas may explain the large range of trace element compositions, because the full range cannot be explained by fractional crystallization alone.

IGNEOUS AND TECTONIC HISTORY

Wernecke breccias, and the clasts contained within, have been the subject of considerable debate, and various
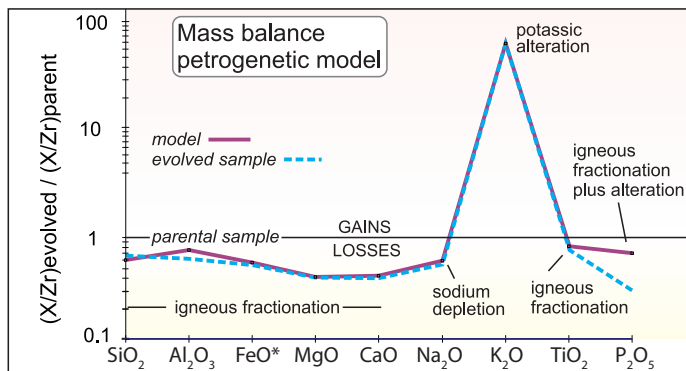
Fractionation phases	Mineral compositons	Percent of phase
plagioclase	anorthite in plagioclase = 60	14.9
augite	diopside in augite = 61	43.6
orthopyroxene	enstatite in orthopyroxene = 61	35.8
magnetite	TiO_2 in magnetite = 15	3.0
rutile		0.9
titanite		0.1
apatite		1.8
Percentage of fractionation		48

Metasomatic gains and losses	Percent of component
Fe_2O_3	0.33
K_2O	3.33
Na_2O	(loss) -2.66

Figure 11. *Stonergram using mass balance and conserved element logic (using Zr) to model igneous and metasomatic processes between a sample that is inferred to be of parental composition (having high Mg, Sc, Cr and Ni), and a sample that is evolved. Tables summarize the model fractionation assemblage and components added or removed by metasomatizing fluids.*

models have been proposed including mud diapirs, salt diapirs, epiclastic deposits, diatremes and hydrothermal breccias (see reviews in Thorkelson, 2000 and Thorkelson *et al.*, 2001b). Recent advances in understanding have occurred through the acquisition of new field and analytical data, which confirm that the breccia system was generated by hydrothermal processes but require revisions to regional models of tectonic, magmatic and hydrothermal activity. New information about the BPRI provides constraints on an emerging model of the Paleo-Mesoproterozoic history of the northwestern margin of ancestral North America (present coordinates; Furlanetto, *et al.*, 2009b).

Any model that attempts to explain the assemblage of Paleo-Mesoproterozoic units in the study area should take into account the following key points: (1) field relationships indicate that the BPRI did not intrude the Wernecke Supergroup or Wernecke breccia; (2) the BPRI are located entirely within zones of Wernecke breccia; (3) Wernecke breccia zones are noted within all stratigraphic units of the Wernecke Supergroup; (4) Wernecke breccia formed after Racklan deformation and metamorphism; (5) the BPRI crystallized ~75 Ma before the onset of Wernecke Supergroup deposition, and ~115 Ma before Wernecke breccia formation at 1595 Ma; (6) the geochemical compositions of the BPRI, the Slab volcanics, and other volcanic clasts in Wernecke breccia indicate formation in a calc-alkaline volcanic arc
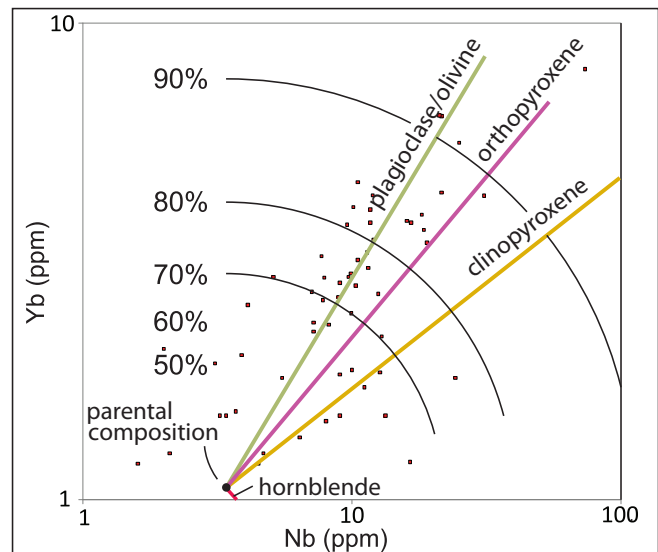
Figure 12. *Distribution of incompatible elements (Nb and Yb) in relation to Rayleigh fractionation vectors. Lines illustrate the fractionation trend away from the same inferred parental sample as in Figure 11. Arcs depict approximate percentage of fractionation.*

(see Peters and Thorkelson (this volume) for additional information); (7) no gneiss or peridotite clasts have been reported from Wernecke breccia; and (8) clasts of the BPRI are up to 900 m in length, and 200 m in width.

The BPRI were not emplaced as magma into either the Wernecke Supergroup, or the Wernecke breccias. They must have been present either above, or below the Wernecke Supergroup at the time of Wernecke breccia formation. Clasts of the BPRI would have been enclosed by Wernecke breccia and transported either upward or downward, and some clasts may have become cemented within zones of breccia at the level of the Wernecke Supergroup. Transport of the BPRI from beneath the Wernecke Supergroup would require upward translation of clasts through nearly the entire succession, *i.e.*, nearly 13 km. This scenario is problematic because it would require hydrothermal solutions to upwardly drive megaclasts which approach 1 km in length. It is also unappealing because clasts of the BPRI are not accompanied by clasts of other rock types that might be situated beneath the Wernecke Supergroup, such as peridotite and high-grade schist and gneiss.

Derivation of BPRI clasts from above the Wernecke Supergroup is more plausible because it would require smaller transport distances and could rely on gravity as the main driving force. Smaller transport distances are permissible because the Wernecke Supergroup had been previously deformed during the Racklan orogeny. This deformational event would allow all units of the Wernecke Supergroup to occupy the same crustal level and, upon exhumation, to be exposed at the same erosional surface, much as they are today. Therefore, emplacement of BPRI clasts to positions alongside all units of the Wernecke Supergroup could occur with little vertical displacement.

To accommodate these observations and constraints, a modified version of the tectonic model of Furlanetto *et al.* (2009b) is presented. In the Furlanetto *et al.* (2009b) model, the BPRI were part of an offshore terrane at ~1.71 Ga. Our geochemical analyses of the BPRI, and the petrologic findings of Peters and Thorkelson (this volume), indicate that the igneous megaclasts were derived from a mature volcanic arc. This igneous environment is consistent with the proposed model for the emplacement of the BPRI, because there are numerous modern examples of arc terranes being obducted onto continental cratons such as the Spong arc in the Ladahk-Zanskar Himalaya (Cornfield *et al.* 2001), the Semail supra-subduction zone ophiolite of the Oman Mountains (Shervais, 2001), and the ophiolitic nappe in New

Caledonia (Aitchison *et al.*, 1995). It is also possible that the volcanic arc was built on the leading edge of a larger landmass or continent that collided with, and overrode, northwestern North America.

This model is illustrated in Figure 13, which depicts the genesis of the BPRI in an offshore arc assemblage at 1.71 Ga (Fig. 13a). After ~75 m.y., the Wernecke Supergroup began to be deposited onto ancestral North America (Fig. 13b). After sedimentation, the region was affected by contractional deformation and metamorphism, and exhumation, exposing all units of the Wernecke Supergroup (Fig. 13c). At 1.60 Ga, the volcanic arc overrode the continental margin, followed by, and possibly triggering, surges of hydrothermal fluids and the formation of Wernecke breccia. The brecciating fluids affected both the Wernecke Supergroup and the overthrust arc complex, leading to metasomatism and iron-oxide copper gold mineralization. Megaclasts of the BPRI, the Slab volcanics and other volcanic units from the nappe travelled downward in the breccia zones, some coming to rest at the level of the Wernecke Supergroup (Fig. 13d). Subsequent erosion removed the nappe and exposed BPRI-bearing breccia zones within the Wernecke Supergroup (Fig. 13e).

CONCLUSIONS

i. The BPRI consist primarily of subalkaline diorite and gabbro that are related by plagioclase and pyroxene fractionation.

ii. Clasts of the BPRI were affected by hydrothermal alteration and widespread development of iron-oxide copper gold occurrences.

iii. The BPRI and related volcanics were not derived from the Wernecke Supergroup. They were probably derived from above the Wernecke Supergroup and transported downward within Wernecke breccia to the level of the Wernecke Supergroup.

iv. The geochemical signature of the BPRI indicates that they were derived from a calc-alkaline volcanic arc that was active at ~1.71 Ga.

v. The volcanic arc was obducted over the Wernecke Supergroup after the Racklan orogeny and subsequently fragmented during hydrothermal activity of Wernecke breccia at 1.60 Ga; many clasts were dropped down to the level of the Wernecke Supergroup within zones of Wernecke breccia (Fig. 13).

1.71 Ga: Volcanic arc crust is formed separately from ancestral North America (Laurentia).

1.64 Ga: Wernecke Supergroup is deposited as three groups on the ancestral North American margin.

1.61 Ga: Racklan orogeny causes uplift and erosion of the Wernecke Super-group, exposing all three groups.

1.60 Ga: Obduction of volcanic arc and penecon-temporaneous brecciation transports fragments of arc rocks downward into the crust.

Present day: Several cycles of sedimentation/erosion with renewed tectonic activity denude the magmatic arc and expose the Wernecke breccias.

fault
Wernecke breccia
Wernecke Supergroup
volcanic arc
North American craton

Figure 13. *Schematic history of the Bonnet Plume River intrusions, related volcanics, and the Wernecke Supergroup.*

ACKNOWLEDGEMENTS

REFERENCES

Aitchison, J.C., Clarke, G.L., Meffre, S. and Cluzel, D., 1995. Eocene arc-continent collision in New Caledonia and implications for regional southwest Pacific tectonic evolution. Geology, vol. 23, p. 161-164.

Basaltic Volcanism Study Project, 1981. Basaltic Volcanism on the Terrestrial Planets., Pergamon Press Inc., New York, 1286 p.

Brideau, M.-A., Thorkelson, D.J., Godin, L. and Laughton, J.R., 2002. Paleoproterozoic deformation of the Racklan Orogeny, Slats Creek (106D/16) and Fairchild Lake (106C/13) map areas, Wernecke Mountains, Yukon. *In:* Yukon Exploration and Geology 2001, D.S. Edmond, L.H. Weston and L.L. Lewis (eds.), Exploration and Geological Services Division, Yukon Region, Indian and Northern Affairs Canada, p. 65-72.

Delaney, G.D., 1981. The mid-Proterozoic Wernecke Supergroup, Wernecke Mountains, Yukon Territory. *In:* Geological Survey of Canada Paper, F.H.A. Campbell (ed.), Geological Survey of Canada, vol. 81-10, p. 1-23.

Floyd, P.A., and Winchester, J.A., 1978, Identification and discrimination of altered and metamorphosed volcanic rocks using immobile elements: Chemical Geology, vol. 21, p. 291-306.

Furlanetto, F., Thorkelson, D.J., Davis, W.J., Gibson, H.D., Rainbird, R.H. and Marshall, D.D., 2009a. Preliminary results of detrital zircon geochronology, Wernecke Supergroup, Yukon. *In:* Yukon Exploration and Geology 2008, L.H. Weston, L.R. Blackburn and L.L. Lewis (eds.), Yukon Geological Survey, p. 125 – 135.

Furlanetto, F., Thorkelson, D.J., Davis, W.J., Gibson, H.D., Rainbird, R.R. and Marshall, D.D., 2009. A new Model of Terrane Accretion in Northwestern Laurentia required by U-Pb SHRIMP Analysis of Detrital Zircons from the Paleoproterozoic Wernecke Supergroup, Wernecke Mountains, Yukon [Abstract U74A-04]. Geological Association of Canada, Joint Assembly, 24-27 May 2009, Toronto, Canada.

Gifkins, C.C., Herrmann, W. and Large, R.R., 2005. Altered volcanic rocks: a guide to description and interpretation. Centre for Ore Deposit Research, University of Tasmania, Hobart, Tasmania, 275 p.

Gill, J.B., 1981. Orogenic Andesites and Plate Tectonics. Springer-Verlag, Berlin, 390 p.

Hunt, J.A. and Thorkelson, D.J., 2007. Are mafic dykes in the Nor and Hart River areas of the Yukon correlative to the Bonnet Plume River Intrusions? Constraints from geochemistry. *In:* Yukon Exploration and Geology 2006, D.S. Emond, L.L. Lewis and L.H. Weston (eds.), Yukon Geological Survey, p. 127-137.

Irvine, G.J. and Baragar, W., 1971. A guide to the chemical classification of the common volcanic rocks. Canadian Journal of Earth Sciences, vol. 8, p. 523-584.

Laughton, J.R., 2004. The Proterozoic Slab Volcanics of Northern Yukon, Canada: Megaclasts of a Volcanic Succession in Proterozoic Wernecke Breccia, and Implications for the Evolution of Northwestern Laurentia, Earth Sciences. Simon Fraser University, Burnaby, p. 81.

Laughton, J.R., Thorkelson, D.J., Brideau, M.-A. and Hunt, J.A., 2002. Paleoproterozoic volcanism and plutonism in the Wernecke Mountains, Yukon. *In:* Yukon Exploration and Geology 2001, D.S. Emond, L.H. Weston and L.L. Lewis (eds.), Exploration and Geological Services Division, Yukon Region, Indian and Northern Affairs Canada, p. 139-145.

LeMaitre, R.W., 2002, Igneous Rocks: A Classification and Glossary of Terms. Recommendations of the International Union of Geological Sciences Subcommission on the Systematics of Igneous Rocks, Cambridge University Press, Cambridge, UK, 256 p.

Miyashiro, A., 1974. Volcanic rock series in island arcs and active continental margins. American Journal of Science, vol. 274, p. 321-355.

Norris, D.K., 1997. Geology and mineral and hydrocarbon potential of northern Yukon Territory and northwestern district of Mackenzie. Geological Survey of Canada Bulletin, vol. 422, 401 p.

Pecerillo, A. and Taylor, S.R., 1976. Geochemistry of Eocene calc-alkaline volcanic rocks from the Kastamonu area, Northern Turkey. Contributions to Mineralogy and Petrology, vol. 58, p. 63-81.

Peters, T.J. and Thorkelson, D.J., (this volume). Volcano-sedimentary megaclast in Wernecke breccia, Yukon, and its bearing on the Proterozoic evolution of northwestern Laurentia. *In:* Yukon Exploration and Geology 2010, K.E. MacFarlane, L.H. Weston and C. Relf (eds.), Yukon Geological Survey.

Rollinson, 1993. Using Geochemical Data: Evaluation, Presentation, Interpretation. Longman Scientific and Technical, London, UK, 352 p.

Ross, P. and Bédard, J.H., 2009. Magmatic affinity of modern and ancient subalkaline volcanic rocks determined from trace-element discriminant diagrams. Canadian Journal of Earth Sciences, vol. 46, p. 823-839.

Shervais, J.W., 1982. Ti-V plots and the petrogenesis of modern and ophiolitic lavas. Earth and Planetary Science Letters, vol. 59, p. 101-118.

Shervais, J.W., 2001. Birth, death, and resurrection: The life cycle of suprasubduction zone ophiolites. Geochemistry Geophysics Geosystems, vol. 2, no. 1, 1010, 45 p. doi:10.1029/2000GC000080

Thorkelson, D.J., 2000. Geology and Mineral Occurrences of the Slats Creek, Fairchild Lake and "Dolores Creek" Areas, Wernecke Mountains (106D/16, 106C/13, 106C/14), Yukon Territory. Exploration and Geological Services Division, Yukon, Indian and Northern Affairs Canada, Bulletin 10, 73 p.

Thorkelson, D.J. and Wallace, C.W., 1998a. Geological map of Slats Creek area, Wernecke Mountains, Yukon (106D/16). Exploration and Geological Services Division, Yukon, Indian and Northern Affairs Canada, Geoscience Map 1998-9, scale 1:50 000.

Thorkelson, D.J. and Wallace, C.W., 1998b. Geological map of Fairchild Lake area, Wernecke Mountains, Yukon (106C/13). Exploration and Geological Services Division, Yukon, Indian and Northern Affairs Canada, Geoscience Map 1998-10, scale 1:50 000.

Thorkelson, D.J. and Wallace, C.W., 1998c. Geological map of Dolores Creek area, Wernecke Mountains, Yukon (106C/14). Exploration and Geological Services Division, Yukon, Indian and Northern Affairs Canada, Geoscience Map 1998-11, scale 1:50 000.

Thorkelson, D.J., Mortensen, J.K., Creaser, R.A., Davidson, G.J. and Abbott, J.G., 2001a. Early Proterozoic magmatism in Yukon, Canada: constraints on the evolution of northwestern Laurentia. Canadian Journal of Earth Sciences, vol. 38, p. 1479 – 1494.

Thorkelson, D.J., Mortensen, J.K., Davidson, G.J., Creaser, R.A., Perez, W.A. and Abbott, J.G., 2001b. Early Mesoproterozoic intrusive breccias in Yukon, Canada: the role of hydrothermal systems in reconstructions of North America and Australia. Precambrian Research, vol. 111, p. 31-55.

Winchester, J.A. and Floyd, P.A., 1977. Geochemical discrimination of different magma series and their differentiation products using immobile elements. Chemical Geology, vol. 20, p. 325-343.

Wood, D.A., 1980. The Application of a Th-Hf-Ta diagram to problems of tectonomagmatic classification and to establishing the nature of crustal contamination of basaltic lavas of the British Tertiary Volcanic Province: Earth and Planetary Science Letters, vol. 50, issue 1, p. 11-30.

Yukon MINFILE, 2010. Yukon MINFILE – A database of mineral occurrences. Yukon Geological Survey, <http://www.geology.gov.yk.ca/databases_gis.html>, [accessed November 2010]

Volcano-sedimentary megaclast in Wernecke breccia, Yukon, and its bearing on the Proterozoic evolution of northwestern Laurentia

Timothy J. Peters[1] and Derek J. Thorkelson
Department of Earth Sciences, Simon Fraser University

ABSTRACT

A group of hydrothermal breccias, collectively known as Wernecke breccia, formed at approximately 1.60 Ga in Yukon. The breccias consist of a hydrothermally precipitated matrix that cements clasts derived mainly from the metasedimentary Wernecke Supergroup. Locally, clasts and megaclasts of the Bonnet Plume River intrusions, the Slab volcanics, and other volcanic rocks are also present within the breccias. This paper describes a volcano-sedimentary succession interpreted as a megaclast within Wernecke breccia. The succession consists of pyroclastic and epiclastic rocks that formed in a volcanic environment in a region of evolved crust. This finding adds detail to the character of a postulated Proterozoic terrane that may have collided with the northwestern margin of ancestral North America toward the end of the Paleoproterozoic.

[1]tjp5@sfu.ca

INTRODUCTION

The Wernecke breccias are a group of early Mesoproterozoic hydrothermal breccias located in Yukon (Thorkelson, 2000; Thorkelson *et al.,* 2001b). The breccias formed within meta-sedimentary rocks of the Wernecke Supergroup and are unconformably overlain by the Pinguicula and Fifteenmile groups (Thorkelson, 2000). In addition to the clasts of dolostone, siltstone, slate, phyllite, and schist derived from the Wernecke Supergroup, which is the predominant clast source, the breccias contain fragments of plutonic and volcanic rock including the Bonnet Plume River intrusions and the Slab volcanics (Thorkelson *et al.,* 2001a; Laughton *et al.,* 2005). The model for brecciation proposed by Thorkelson (2000) involves incorporation of the plutonic, volcanic and sedimentary clasts and megaclasts into the breccias zones during surges of hydrothermal fluids that occurred after deformation and metamorphism of the Wernecke Supergroup.

The area studied in the summer of 2010 (Fig. 1) is near the Yukon Olympic mineral occurrence (Yukon MINFILE 116G 082) along the Dempster Highway, approximately 150 km north of its junction with the Klondike Highway. The work was carried out over an interval of three days and yielded two sample sets west of the Blackstone River. The first set consists of 25 samples of Wernecke breccia collected from talus and rip-rap along the Dempster Highway. The second set was obtained on a traverse atop a ridge in the area, and consists of 16 samples from a succession of lapillistone, volcaniclastic wacke and volcano-sedimentary breccia. The succession is interpreted as a megaclast within Wernecke breccia, herein informally named the Blackstone River megaclast. This paper provides hand specimen and thin section descriptions of selected samples from both localities to provide an interpretation of the provenance of the sediment, environment of formation, and origin of the volcano-sedimentary megaclast.

REGIONAL GEOLOGICAL FRAMEWORK

WERNECKE SUPERGROUP

The Wernecke Supergroup (Delaney, 1981) is a metasedimentary succession that was deposited as two cycles of basinal siliciclastic to platformal carbonate rock during two corresponding intervals of extension and subsidence that formed the Wernecke basin (Thorkelson,

2000; Thorkelson *et al.,* 2005; Hunt *et al.,* 2006). Delaney (1981) and Thorkelson (2000) place the minimum thickness of the Wernecke Supergroup between 13 and 14 km. The Wernecke Supergroup consists of the Fairchild Lake Group, which represents the first cycle of basin infill and the conformably overlying Quartet and Gillespie Lake groups, which represent the second cycle (Delaney, 1981; Thorkelson, 2000; Thorkelson *et al.,* 2005). The Fairchild Lake Group is inferred to lie on >1.84 Ga basement rock of cratonic Laurentia (ancestral North America), although this relationship is nowhere exposed and drilling in mineral exploration projects has not been deep enough to test this theory. At present, the Proterozoic rocks of the Wernecke Supergroup are exposed as inliers in Yukon (Fig. 1b; Thorkelson *et al.,* 2005). The age of the Wernecke Supergroup was previously thought to be >1.71 Ga (Thorkelson *et al.,* 2001a), but recent detrital zircon studies by Furlanetto *et al.* (2009a,b) indicate that the Wernecke Supergroup is <1.64 Ga.

RACKLAN OROGENY

The Wernecke Supergroup was deformed to greenschist grade metamorphism by the compressional Racklan Orogeny before 1.60 Ga (Thorkelson, 2000; Brideau *et al.,* 2002; Laughton *et al.,* 2005; Thorkelson *et al.,* 2005). Deformation occurred first as easterly contraction, resulting in fold and foliation development in the Wernecke Supergroup, and was followed by additional folding and kink-banding (Thorkelson, 2000). The results of the Racklan Orogeny are especially evident in the Fairchild Lake Group near Slab Mountain, where schist, exhibiting crenulations and kink-banding, is present (Brideau *et al.,* 2002). Racklan deformation is not observed in Wernecke breccia except in individual breccia clasts with random foliation orientations, indicating that deformation occurred before breccia formation (Thorkelson, 2000; Brideau *et al.,* 2002; Laughton *et al.,* 2005).

WERNECKE BRECCIA

Wernecke breccia is a group of numerous breccia occurrences in the Wernecke and Ogilvie mountains, and one local occurrence in the Richardson Mountains, in Yukon (Thorkelson, 2000; Thorkelson *et al.,* 2001b). Several models for the formation of the breccias have been proposed, but the most plausible model according to the most recent evidence is that structurally influenced hydrothermal fluid ascent and volatile-induced expansion caused brecciation of host rocks (Hitzman *et al.,* 1992; Thorkelson, 2000; Thorkelson *et al.,* 2001b). This process occurred at depths of 7.5-9 km and involved
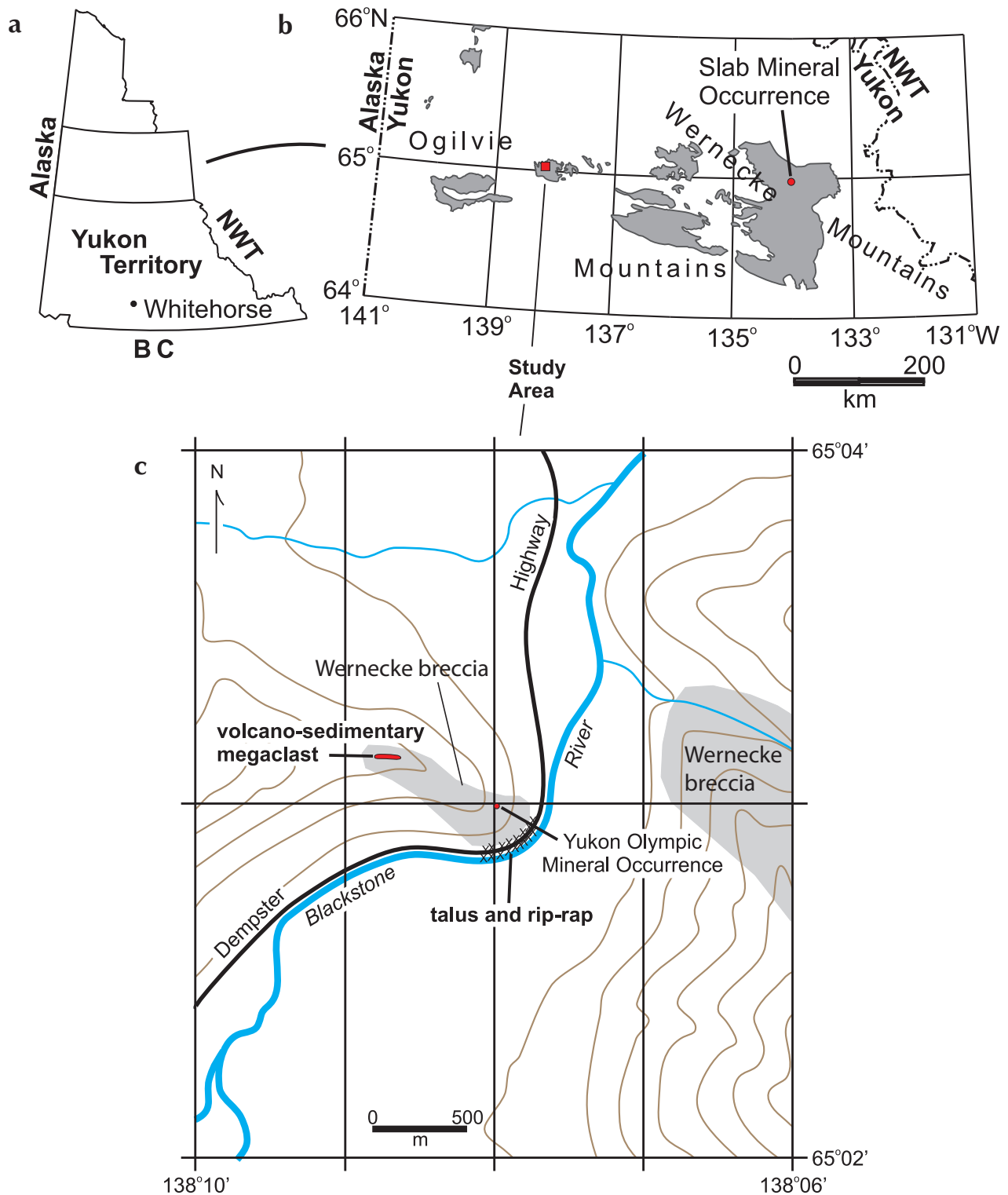
Figure 1. *Location of the study area. Longitude and latitude in (b) and (c), are expressed as NAD27 coordinates. (a) Map of Yukon illustrating the locations of inliers (b) of the Early Proterozoic Wernecke Supergroup (inliers are shaded in grey; modified from Thorkelson et al., 2001a). (c) Map of the study area depicting the minimum extent of Wernecke breccia and the location of the volcano-sedimentary megaclast.*

non-magmatic fluids that were generally present in only modest amounts (Hunt *et al.*, 2005; Hunt *et al.,* 2007). Most of the brecciation occurred at approximately 1.59 Ga during several hydrothermal 'pulses' that crosscut each other and their host rocks (Thorkelson *et al.,* 2001b; Hunt *et al.*, 2005; Hunt *et al.*, 2007). The hydrothermal processes that created the breccias produced abundant iron oxide copper-gold-type (IOCG) mineralization and hydrothermally precipitated material in veins, fractures and among matrix rock fragments, as well as metasomatic alteration, to a variable extent, within breccia clasts (Hitzman *et al.*, 1992; Thorkelson *et al.*, 2001b; Hunt *et al.*, 2005). Breccia clasts are commonly granule to cobble in size, but are locally as large as boulders; they are dominantly derived from the Wernecke Supergroup, but igneous clasts of Bonnet Plume River intrusions and Slab volcanics (described later) are common at many localities (Thorkelson, 2000; Thorkelson *et al.*, 2001b). Alteration is commonly either potassic (yielding mainly pink and red colours) or less commonly sodic (grey), and late carbonate veins are typically present (Thorkelson *et al.,* 2001b; Hunt *et al.*, 2005; Laughton *et al.*, 2005; Hunt *et al.*, 2007). Clasts that may be interpreted as basement rock are nowhere observed (Thorkelson *et al.*, 2001b).

BONNET PLUME RIVER INTRUSIONS

The Bonnet Plume River intrusions are dominantly dioritic to gabbroic igneous rocks that occur as clasts of variable size within zones of Wernecke breccia (Thorkelson, 2000; Laughton *et al.,* 2002). Clasts typically range in size from a few centimetres to tens of metres wide, but can be as large as 0.2 km by 1 km (Thorkelson *et al.,* 2005). Lithification of the rocks occurred before their incorporation into the breccias (Thorkelson, 2000). Many clasts are hydrothermally altered, veined, and mineralized (magnetite, hematite, chalcopyrite and gold), but most lack foliation (Thorkelson *et al.,* 2005). The intrusions were dated at ≥1.71Ga based on four U-Pb zircon dates (Thorkelson *et al.*, 2001a). These intrusive bodies were previously thought to be dykes and stocks that intruded the Wernecke Supergroup (Thorkelson, 2000; Thorkelson *et al.,* 2001a) and were later dismembered during Wernecke breccia formation. However, Furlanetto *et al.* (2009b) demonstrated that the Bonnet Plume River intrusions are ~70 m.y. older than the Wernecke Supergroup and that the intrusive rocks were probably derived from a terrane that was thrust over the Wernecke Supergroup and involved with subsequent Wernecke breccia development.

SLAB VOLCANICS

The informal term 'Slab volcanics' refers to several occurrences of volcanic clasts within Wernecke breccias that are proximal to each other, the largest being a 160x380 m megaclast at the Slab mineral occurrence (Fig. 1b; Thorkelson, 2000; Laughton *et al.*, 2002; Laughton *et al.*, 2005). Their presence in the Wernecke breccia indicates that they are older than 1.60 Ga (Thorkelson, 2000). The incorporation of the volcanic rocks into the Wernecke breccia may have been facilitated by hydrothermal venting at the surface that ejected host rock material and allowed clasts to move to stratigraphically lower positions by several hundred metres (Thorkelson *et al.*, 2001b; Laughton *et al.*, 2005). Thorkelson (2000) suggested a possible comagmatic relationship between the Slab volcanics and the Bonnet Plume River intrusions based on geochemical affinity.

RESULTS

WERNECKE BRECCIA

The samples of Wernecke breccia taken from talus and rip-rap in the study area display compositional and textural characteristics that are typical of the widespread Wernecke breccias in Yukon described by Thorkelson (2000), Thorkelson *et al.* (2001b) and Hunt *et al.* (2005; 2007). Although the samples were not derived from outcrop, they are similar to (and were probably derived from) a zone of Wernecke breccia that is exposed in nearby outcrops and road-cuts.

The breccia samples consist of clasts, matrix, and younger veins. They commonly contain disseminated specular hematite. Some samples contain macroscopic chlorite. The matrix of the samples consists mainly of dark purple mud, sand and silt-sized quartz grains and rock fragments, carbonate cement, and opaque minerals such as hematite. Locally, the matrix also contains sericite and possible titanite. In some samples, the matrix is dark greenish-grey, but is compositionally similar to the purple matrix, including quartz sand and silt fragments, polycrystalline quartz, carbonate and hematite.

Clast size is highly variable and ranges from sand to boulders. The clasts are mainly light brown-weathering, light pink to medium purple, very fine grained sandstone and siltstone and dark green volcanic rock. The sedimentary clasts are commonly laminated and some display trough cross-lamination. They are composed of dominantly angular and subangular quartz, but also

contain biotite and muscovite (ranging in size from silt to very fine sand), hematite and possibly other metallic minerals, carbonate minerals, and possible titanite and zircon. The volcanic clasts consist predominantly of feldspar laths, secondary chlorite (probably after pyroxene), and accessory hematite and/or titanite. Some clasts also contain sericite or muscovite flakes, and some contain quartz and/or calcite amygdules.

VOLCANO-SEDIMENTARY MEGACLAST

The volcano-sedimentary megaclast is surrounded by a zone of Wernecke breccias (Fig. 1c). It is approximately 125 x 15 m in size and outcrops approximately 0.7 km west of the Dempster Highway. The succession consists of pyroclastic rock, including lapillistone and lapilli tuff, and epiclastic rock, including wacke and volcaniclastic breccia. Most of the clasts consist of fine-grained volcanic rock, but some are epiclastic, including quartz-rich siltstone and fine-grained sandstone. The clasts are typically ≤1 cm in diameter and rarely >2 cm in diameter. The stratigraphic order is not evident, although the succession appears to be structurally intact. Contacts with Wernecke breccia are not exposed, although Wernecke breccia appears to surround the outcrop, implying that the succession is megaclast engulfed by breccia. Such a relationship between igneous clasts and breccia is common in many other localities (Thorkelson *et al.*, 2001a,b; Nielsen *et al.*, this volume). Four samples from the outcrop were chosen to be examined critically based on the variability of lithologic textures.

SAMPLE 1

Sample 1 is a lapillistone. It consists of volcaniclastic fragments, lesser sedimentary rock fragments and minor monocrystalline and polycrystalline quartz, and a matrix of clay, quartz silt, and local very fine volcanic quartz. The rock is clast-supported and almost all of the clasts are lapilli (pebble-sized fragments). The volcanic clasts consist of an isotropic groundmass with variable amounts of feldspar and quartz microphenocrysts, and abundant chlorite patches (Fig. 2a). These patches are interpreted as variably collapsed vesicles that were subsequently converted to amygdules by chlorite precipitation. The direction of elongation of the amygdules is interpreted as the plane of flattening that developed perpendicular to the orientation of maximum compressive stress during vesicle collapse. The planes of flattening among the grains are remarkably similar, typically differing from one another by only a few degrees and seldom by more than 25˚ (Fig. 2b). Several of

these volcanic grains also display extensive replacement by calcite. The sedimentary rock fragments are very fine grained sandstone and siltstone, composed of quartz and feldspar, and lesser mudstone or accretionary lapilli clasts. Some of the sedimentary clasts contain minor mica and at least one contains zircon (Fig. 2c). Many of the grains share concavo-convex or curviplanar contacts, and display greater amounts of vesicle flattening near such contacts (Fig. 2b).

SAMPLE 2

Sample 2 is a lapillistone. It consists mainly of granule-sized, variably shaped volcaniclastic fragments with secondary chlorite. It contains deformed and chloritized vesicles similar to those in Sample 1. There are also subangular to rounded grains of crystalline volcanic rock containing feldspar laths and chlorite (possibly as grain replacements), very fine sandstone and siltstone fragments, and monocrystalline and polycrystalline quartz. Also present are clasts of mud or volcanic ash that display ductile fabrics (Fig. 2d). The sample has a muddy matrix.

SAMPLE 3

Sample 3 is a succession of poorly sorted granule and pebble breccia that is interlaminated with wacke and mudstone. The matrix is composed of clay and silt to sand-sized quartz grains. Breccia layers consist of a variety rock fragment types, including clasts of laminated siltstone, mudstone and volcanic rock deposited as lava or coarse tephra. The siltstone clasts are composed of quartz and feldspar with lesser amounts of muscovite and biotite. Some of the volcanic fragments are dominated by feldspar laths and locally contain chlorite and quartz amygdules (Fig. 3a). Other fragments consist mainly of isotropic groundmass, which probably originated as volcanic glass; the groundmass is composed of microlites, devitrified glass and chlorite alteration. Clast sizes range from mud, to a maximum of approximately 1 cm diameter. The breccia layers are clast-supported, and are approximately 0.5 mm to nearly 1 cm thick. The rock is compositionally and texturally immature due to relatively high clay content, the abundance of volcanic rock fragments, the high range in grain size from clay matrix to pebble-sized conglomerate clasts, and the variability in grain rounding from angular to rounded. The rock shows evidence of dewatering of fine-grained layers and subsequent compaction around competent grains within coarse-grained layers (Fig. 3b). There are also dark brown cataclastic foliations at high angles to bedding (Fig. 3c), as well as local concavo-convex grain contacts.
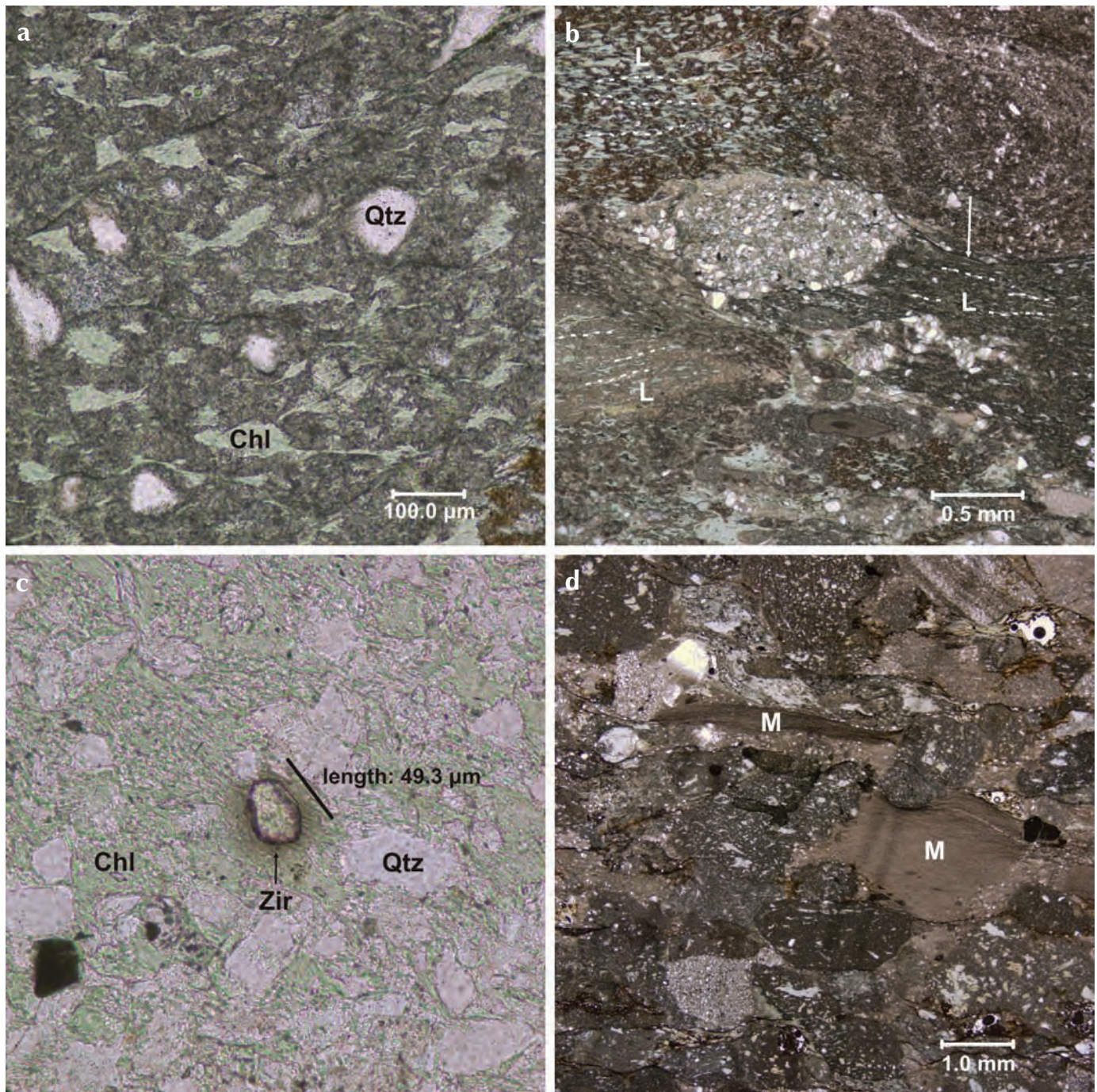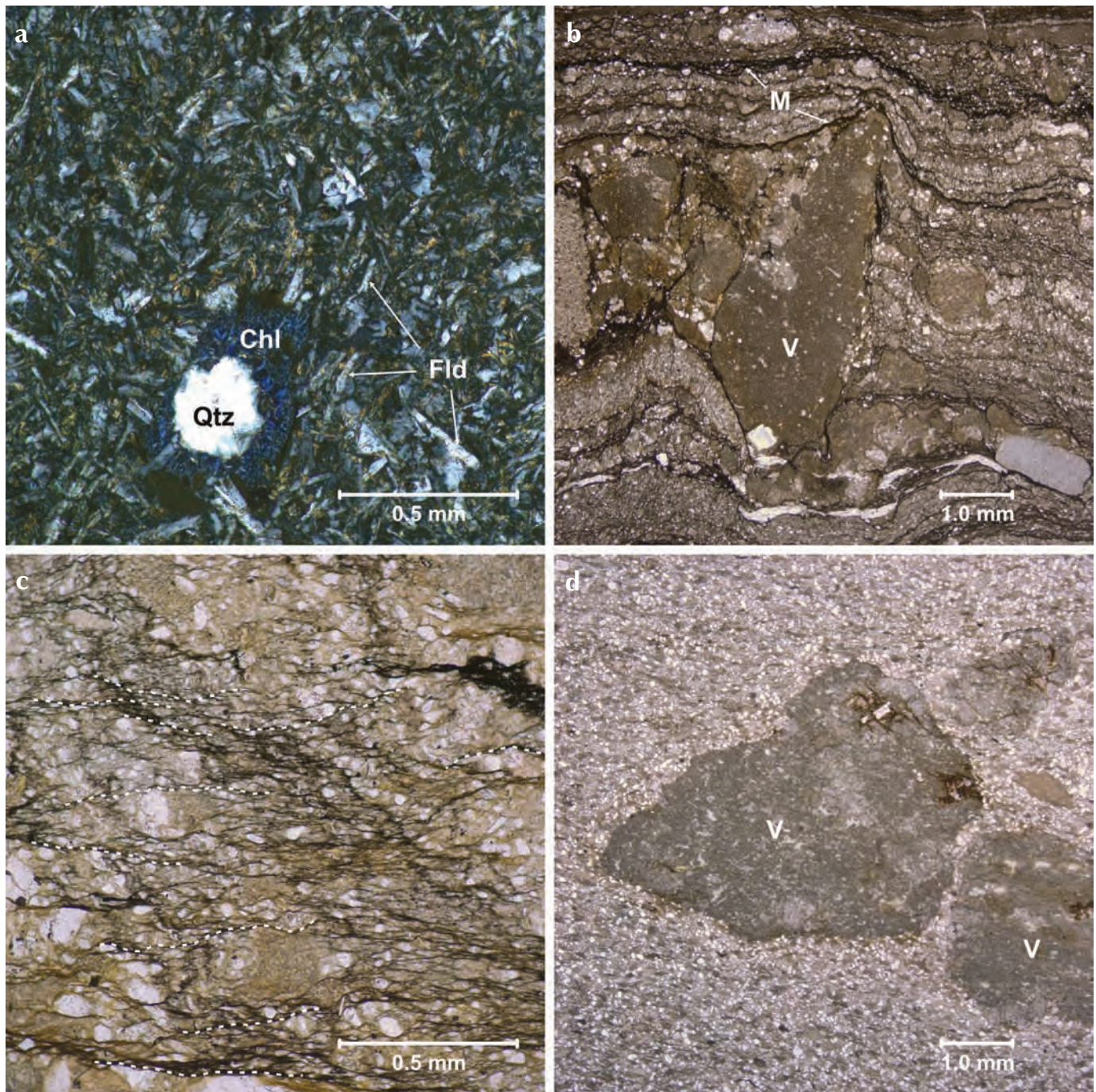
Figure 2. Photomicrographs of pyroclastic rock samples: (a) to (c) from Sample 1, and (d) from Sample 2. **(a)** A lapillus consisting of isotropic groundmass, quartz microphenocrysts (Qtz) and chlorite amygdules (Chl); and **(b)** lapilli (L) with similarly oriented amygdule flattening fabrics (outlined with dashed white lines). The white arrow indicates the location of a concavo-convex grain contact. **(c)** An accidental siltstone clast that contains zircon (Zir); and **(d)** clasts of mudstone or volcanic ash (M) displaying ductile fabrics.

SAMPLE 4

Sample 4 is a lithic wacke. Clasts are dominantly angular, subangular and occasionally subrounded, monocrystalline, very fine sand and silt-sized quartz, but the rock contains subangular to rounded, granule to pebble-sized volcaniclastic fragments (none larger than about 1 cm in diameter) that display calcite replacement (Fig. 3d). The rock also contains small (<0.6 mm diameter) mudstone fragments. Secondary calcite is abundant in the sandstone as cement and as grain replacements. Although the rock contains volcanic rock fragments, there is also a high proportion of quartz sand suggesting that the rock is compositionally submature to mature. Texturally, the sample is immature due to the bimodal grain size distribution and angularity of many of the quartz grains. Subparallel alignment of linear, dark brown concretions and locally linear bands of secondary chlorite (possibly as mica replacement), suggest that a deformational event produced minor foliation.

DISCUSSION

The volcano-sedimentary succession occurs within a zone of typical, hematitic Wernecke breccia and is interpreted as a large breccia clast, herein informally named the Blackstone River megaclast. Numerous clasts of volcanic rock (mostly or entirely derived from lava) occur in this breccia zone and are abundant in the talus and rip-rap located along the Dempster highway (Fig. 1), and east of the Blackstone River (A. Nielsen, pers. comm, 2009). Megaclasts of lava and subordinate sedimentary rock also occur in a zone of Wernecke breccia located at Slab Mountain in the Wernecke Mountains (Fig. 1b; Slab mineral occurrence; Yukon MINFILE 106D 070; Laughton *et al.*, 2005).

The Blackstone River megaclast can be distinguished from the other volcanic megaclasts in Wernecke breccia on the basis of its felsic composition, and association with quartz-rich sediment. A felsic magma composition is implied by the abundance of micro-phenocrysts of quartz and/or potassium feldspar in some of the lapilli. Other volcanic clasts in the enclosing breccia, and at Slab Mountain (Laughton *et al.*, 2005), are mafic in composition. The Blackstone River megaclast is the only known clast in Wernecke breccia to contain quartz-rich sediment. The quartzose material occurs in two forms: as crude laminations in the volcaniclastic wacke; and as accidental clasts in the lapillistone (Fig. 2c).

The Blackstone River megaclast is also characterized by a subaerial origin, as implied by the elongated amygdules in the lapilli, and the consistent orientation of the inferred flattening fabric among lapilli in the same sample (Fig. 2b). The consistent direction of flattening in the lapilli may be explained by flattening upon impact. Alternatively, the flattening could have been caused by the weight of an overlying and rapidly accumulating layer of tephra, soon after the grains were deposited; the grains would have remained hot enough to deform ductilely in a manner similar to welding of fiamme in pyroclastic flow deposits (Fisher and Schmincke, 1984). The slight inter-grain variation in the orientation of planes of flattening may be the result of grain rotation during, or after, deformation. Regardless of whether impact and/or penecontemporaneous welding were the cause(s), the ductile deformation of the lapilli is indicative of subaerial deposition.

The relative coarseness of the volcanic clasts (up to 2 cm in diameter) suggests a transport distance of no more than a few kilometres from the volcanic vent. The inferred hot, ductile character of the volcanic clasts upon deposition also suggests a short aerial transport time after their expulsion from the volcano. The volcano may have been a cinder cone or a large, explosive composite volcano, but in either case the minimal amount of lapilli transport implies a volcanic environment of deposition. The presence of mud as matrix and as laminae within the epiclastic, quartz-rich sediment suggests an environment capable of low-energy transport and deposition, perhaps on the gently sloping base of the volcano.

This interpretation is important for the refinement of a new model that explains the origin of the igneous clasts in Wernecke breccia (Furlanetto, 2009a). The new model involves obduction of a terrane onto the western margin of Laurentia, followed by Wernecke breccia formation that involved downward movement of igneous rocks of the terrane. The terrane was considered to consist of mafic volcanic rocks and associated mafic intrusions, as indicated by the composition of the igneous clasts in Wernecke breccia. With the recognition of felsic volcanism and quartz-rich sediment in the Blackstone River megaclast, the obducted terrane of Furlanetto *et al.* (2009a) should be adjusted to include not only felsic, explosive volcanoes, but also a source of quartz-rich sediment hosting rounded and possibly long-travelled detrital zircon grains. The age and origin of the zircon grains has not yet been determined, and it is possible that they were derived from local rhyolitic igneous rocks, or

Figure 3. Photomicrographs of epiclastic rock samples: (a) to (c) from Sample 3, and (d) from Sample 4. **(a)** A volcanic rock fragment consisting of feldspar laths (Fld) and quartz (Qtz) and chlorite (Chl) amygdules. **(b)** A volcanic rock fragment (V) with dewatered mud layers (M) that have been compacted around it. **(c)** Cataclastic foliations at high angles to bedding (outlined with dashed white lines). **(d)** Volcanic rock fragments (V) surrounded by very fine sand and silt-sized quartz grains.

from older basement exposures. The now-vanished terrane may have been part of another landmass such as Australia. Additional work on this megaclast may provide solutions to this question, and further refine the understanding of the obducted terrane.

CONCLUSIONS

The Blackstone River megaclast is a clast within the Wernecke breccia in Yukon. It consists of felsic, subaerially deposited pyroclastic rocks and lesser quartz-rich epiclastic rocks. Flattening textures in the pyroclasts and overall felsic composition of the megaclast imply that the succession was deposited in a volcanic environment in an area of evolved crust. These observations augment the terrane model of Furlanetto *et al.* (2009a), which involves obduction of a terrane onto Laurentia in late Paleoproterozoic time.

ACKNOWLEDGEMENTS

REFERENCES

Brideau, M-A., Thorkelson, D.J., Godin, L. and Laughton, J.R., 2002. Paleoproterozoic deformation of the Racklan Orogeny, Slats Creek (106D/16) and Fairchild Lake (106C/13) map areas, Wernecke Mountains, Yukon. *In*: Yukon Exploration and Geology 2001, D.S. Emond, L.H. Weston and L.L. Lewis (eds.), Exploration and Geological Services Division, Yukon Region, Indian and Northern Affairs Canada, p. 65-72.

Delaney, G.D., 1981. The mid-Proterozoic Wernecke Supergroup, Wernecke Mountains, Yukon Territory. *In:* Proterozoic Basins of Canada, F.H.A. Campbell (ed.), Geological Survey of Canada, Paper 81-10, p. 1-23.

Fisher, R.V. and Schmincke, H.-U., 1984. Pyroclastic rocks. Springer-Verlag, Berlin, Heidelberg, Germany.

Furlanetto, F., Thorkelson, D.J., Davis, W.J., Gibson, H.D., Rainbird, R.R. and Marshall, D.D., 2009a. A New Model of Terrane Accretion in Northwestern Laurentia required by U-Pb SHRIMP Analysis of Detrital Zircons from the Paleoproterozoic Wernecke Supergroup, Wernecke Mountains, Yukon [Abstract U74A-04]. Geological Association of Canada, Joint Assembly, 24-27 May 2009, Toronto, Canada.

Furlanetto, F., Thorkelson, D.J., Davis, W.J., Gibson, H.D., Rainbird, R.H. and Marshall, D.D., 2009b. Preliminary results of detrital zircon geochronology, Wernecke Supergroup, Yukon. *In*: Yukon Exploration and Geology 2008, L.H. Weston, L.R. Blackburn and L.L. Lewis (eds.), Yukon Geological Survey, p. 125-135.

Laughton, J.R., Thorkelson, D.J., Brideau, M-A. and Hunt, J.A., 2002. Paleoproterozoic volcanism and plutonism in the Wernecke Mountains, Yukon. *In*: Yukon Exploration and Geology 2001, D.S. Emond, L.H. Weston and L.L. Lewis (eds.), Exploration and Geological Services Division, Yukon Region, Indian and Northern Affairs Canada, p. 139-145.

Laughton, J.R., Thorkelson, D.J., Brideau, M-A., Hunt, J.A. and Marshall, D.D., 2005. Early Proterozoic orogeny and exhumation of Wernecke Supergroup revealed by vent facies of Wernecke breccia, Yukon, Canada. Canadian Journal of Earth Sciences, vol. 42, p. 1033-1044.

Hitzman, M.W., Oreskes, N. and Einaudi, M.T., 1992. Geological characteristics and tectonic setting of Proterozoic iron oxide (Cu-U-Au-REE) deposits. *In*: Precambrian Metallogeny Related to Plate Tectonics, G. Gall and K. Schulz (eds.), Precambrian Research, vol. 58, p. 241-287.

Hunt, J.A., Abbott, J.G. and Thorkelson, D.J., 2006. Unconformity-related uranium potential: Clues from Wernecke breccia, Yukon. *In*: Yukon Exploration and Geology 2005, D.S. Emond, G.D. Bradshaw, L.L. Lewis and L.H. Weston (eds.), Yukon Geological Survey, p. 127-137.

Hunt, J., Baker, T. and Thorkelson, D., 2005. Regional-scale Proterozoic IOCG-mineralized breccias systems: examples from the Wernecke Mountains, Yukon, Canada. Mineralium Deposita, vol. 40, p. 492-514.

Hunt, J.A., Baker, T. and Thorkelson, D.J., 2007. A review of iron oxide copper-gold deposits, with focus on the Wernecke breccias, Yukon, Canada, as an example of a non-magmatic end member and implications for IOCG genesis and classification. Exploration and Mining Geology, vol. 16(3-4), p. 209-232.

Nielsen, A.B., Thorkelson, D.J., Marshall, D.D. and Gibson, H.D., this volume. Paleoproterozoic Bonnet Plume River intrusions: Evidence for a calc-alkaline arc at 1.7 Ga and its partial preservation in Yukon, Canada. *In:* Yukon Exploration and Geology 2010, K.E. MacFarlane, L.H. Weston and C. Relf (eds.), Yukon Geological Survey.

Thorkelson, D.J., 2000. Geology and mineral occurrences of the Slats Creek, Fairchild Lake and "Dolores Creek" areas, Wernecke Mountains (106D/16, 106C/13, 106C/14), Yukon Territory. Exploration and Geological Services Division, Yukon Region, Indian and Northern Affairs Canada, Bulletin 10.

Thorkelson, D.J., Abbott, J.G., Mortensen, J.K., Creaser, R.A., Villeneuve, M.E., McNicoll, V.J. and Layer, P.W., 2005. Early and Middle Proterozoic evolution of Yukon, Canada. Canadian Journal of Earth Sciences, vol. 42, p. 1045-1071.

Thorkelson, D.J., Mortensen, J.K., Creaser, R.A., Davidson, G.J. and Abbott, J.G., 2001a. Early Proterozoic magmatism in Yukon, Canada: constraints on the evolution of northwestern Laurentia. Canadian Journal of Earth Sciences, vol. 38, p. 1479-1494.

Thorkelson, D.J., Mortensen, J.K., Davidson, G.J., Creaser, R.A., Perez, W.A. and Abbott, J.G., 2001b. Early Mesoproterozoic intrusive breccias in Yukon, Canada: the role of hydrothermal systems in reconstructions of North America and Australia. Precambrian Research, vol. 111, p. 31-55.

Yukon MINFILE, 2010. Yukon MINFILE – A database of mineral occurrences. Yukon Geological Survey, <*http://www.geology.gov.yk.ca/databases_gis.html*> [accessed November 1, 2010].

Stratigraphy of the Mackenzie Mountains supergroup in the Wernecke Mountains, Yukon

Elizabeth C. Turner[1]
Laurentian University

Turner, E.C., 2011. Stratigraphy of the Mackenzie Mountains supergroup in the Wernecke Mountains, Yukon. *In:* Yukon Exploration and Geology 2010, K.E. MacFarlane, L.H. Weston and C. Relf (eds.), Yukon Geological Survey, p. 207-231.

ABSTRACT

Mackenzie Mountains supergroup (MMSG) strata in the Wernecke Mountains are described in detail. Three new formations are assigned to the revised and formalized Hematite Creek Group, which forms the base of the MMSG. The Dolores Creek Formation (black mudrocks and microbial dolostone) is the basal unit of the MMSG. The Black Canyon Creek Formation (cyclic peritidal dolostone) and Tarn Lake Formation (desiccation-cracked, shallow-marine siltstone and sandstone) are probably equivalent to the 'H1 unit' and Tsezotene Formation in NWT, respectively. The Hematite Creek Group is overlain by the Katherine Group (thick quartz arenite-dominated succession). The highest MMSG strata documented belong to the Basinal assemblage (Little Dal Group). Regional thickness and lithofacies variations in two of the new formations suggest that the basin had considerable paleobathymetric variation that is not consistent with patterns established in NWT. The economic potential of the succession is unknown.

[1]*eturner@laurentian.ca*

YUKON EXPLORATION AND GEOLOGY 2010

207

INTRODUCTION

Although suggested correlation schemes for Neoproterozoic stratigraphic units in northwestern Canada are numerous, a lack of detailed stratigraphic knowledge of units in the Wernecke Mountains and other locations in Yukon has precluded both definitive correlations and interpretation of basin evolution. Rainbird *et al.* (1996, 1997), Abbott (1997), Cook and MacLean (2004), Thorkelson *et al.* (2005) and Long *et al.* (2008) proposed that stratigraphic units originally assigned to the upper part of the Proterozoic Pinguicula Group (Eisbacher, 1978, 1981) in the Wernecke Mountains are equivalent to some part of the Mackenzie Mountains supergroup (MMSG; Young *et al.*, 1979). The present project was undertaken to ascertain whether this is valid, to determine what parts of

the MMSG have stratigraphic equivalents in the Wernecke Mountains, and to establish preliminary interpretations of basin evolution for the MMSG west of known exposures in Northwest Territories (NWT). Four units that form much of the MMSG were examined in the Dolores Creek – Pinguicula Lake area, and are here compared to their equivalents in NWT. Strata of the MMSG were examined in detail on the flanks of an un-named mountain near the junction of 'Dolores Creek' with the Bonnet Plume River (Fig. 1), and on a ridge approximately 7 km southsouthwest of Mount Profeit (both locations in NTS 106C).

HEMATITE CREEK GROUP (REVISED)

The entire succession described here (including Katherine Group and Little Dal Group strata) was at one point named Hematite Creek Group (Thorkelson, 2000), a term that was subsequently abandoned (Thorkelson *et al.*, 2005). This stratigraphic name is here re-introduced, and revised to refer only to the basal three formations of the MMSG (Fig. 2). These three formations form an internally conformable succession that appears to lie unconformably on Pinguicula Group unit 'C' and to underlie the Katherine Group conformably. The MMSG in the Wernecke Mountains consists, therefore, of three groups: the Hematite Creek Group (comprising three new formations), the Katherine Group, and at least part of the Little Dal Group (Fig. 3). The revised Hematite Creek Group is widespread in the Pinguicula Lake – Dolores Creek area. Three representative sections are presented below. It is proposed that the Dolores Creek Formation and Black Canyon Creek Formation measured sections become their type sections, but that the measured section of the Tarn Lake Formation be considered a reference section until a stratigraphically complete type section can be documented.
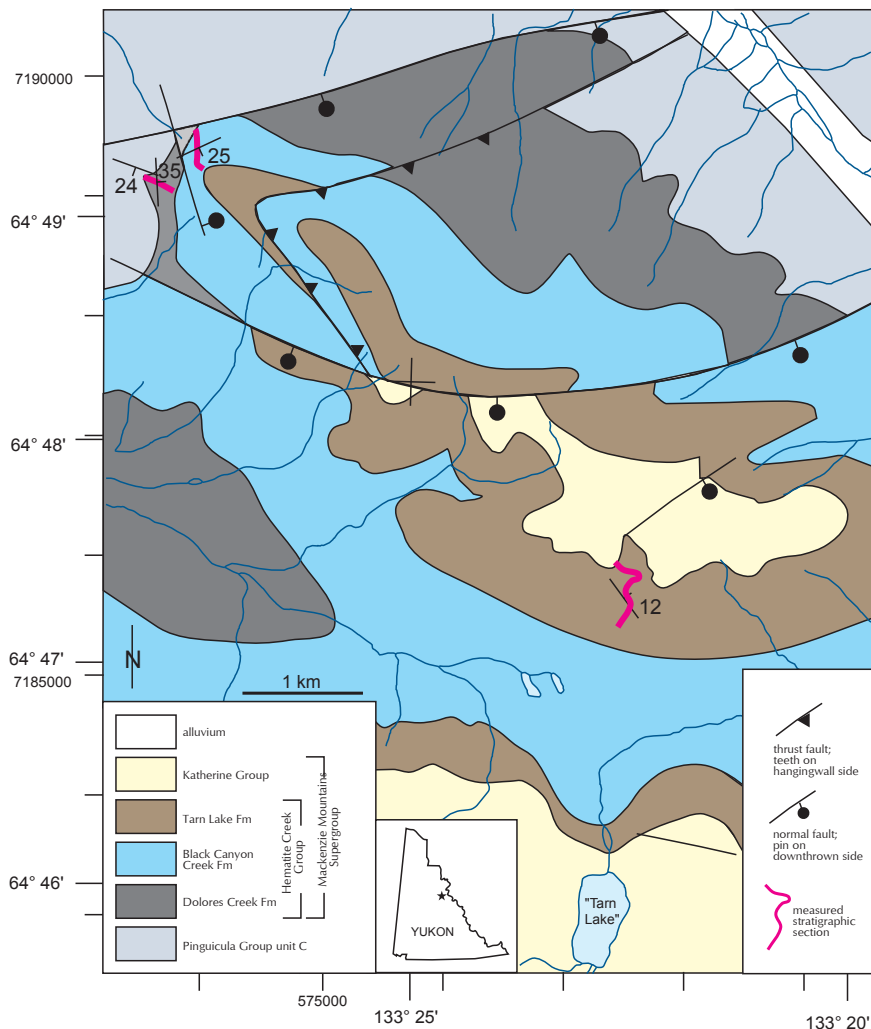
Figure 1. Geologic map of a mountain exposing strata of the lower MMSG near the junction of 'Dolores Creek' and Bonnet Plume River. The locations of type sections of three new formations in the (revised) Hematite Creek Group (=basal MMSG) are indicated.
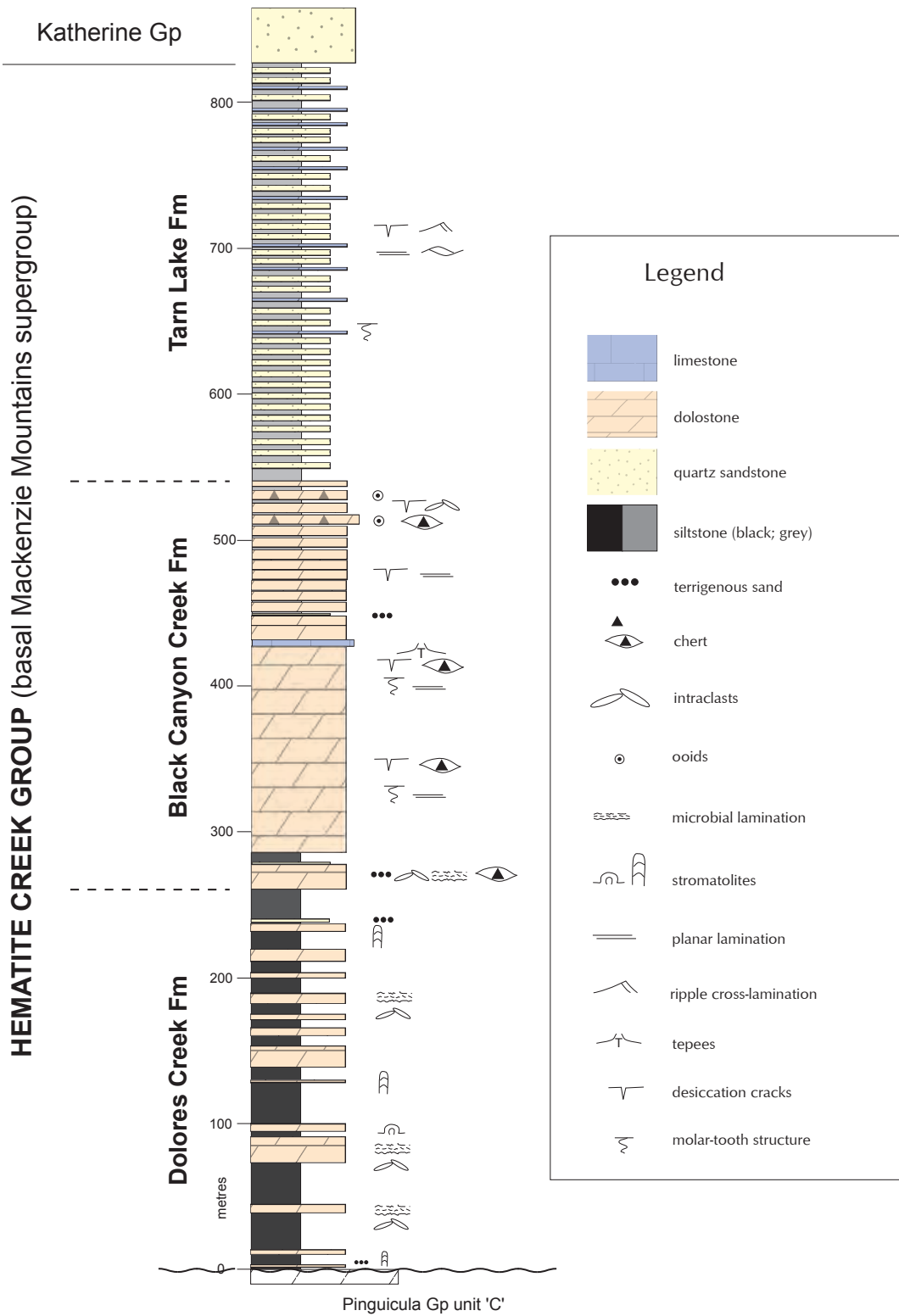
Figure 2. *Schematic stratigraphy for the (revised) Hematite Creek Group in the Dolores Creek – Pinguicula Lake area. Basal contact is an unconformity with dolostone of Pinguicula Group unit 'C'. Contacts between formations of the Hematite Creek Group are conformable and gradational.*

Figure 3. (a) Proposed correlation of Hematite Creek Group, Katherine Group and Little Dal Group strata of the Wernecke Mountains. Radiometric bracketing dates are from Jefferson and Parrish (1989), Heaman et al. (1992), and Leslie (2009). (b) A less probable alternative correlation. (c) Revised correlation of MMSG units in the Mackenzie Mountains and Wernecke Mountains inlier, with Shaler Supergroup units (Amundsen Basin, after Rainbird et al., 1996 and Long et al., 2008).
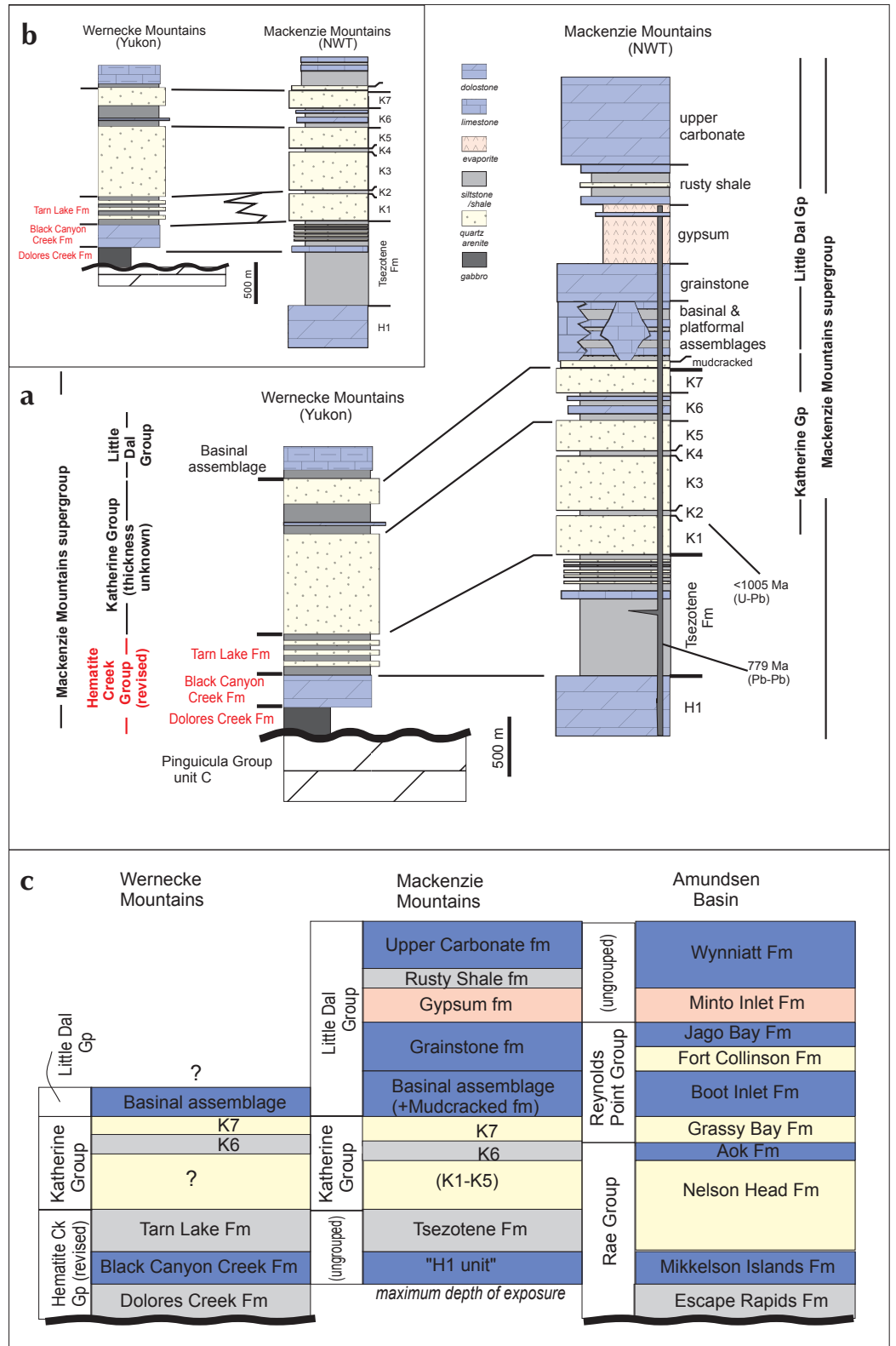
DOLORES CREEK FORMATION (NEW)

The basal unit of the MMSG is extensively exposed east of the Bonnet Plume River in north-central NTS 106C (Nadaleen River map sheet). A detailed section was measured on an un-named, 15 km-long mountain ridge, at a location approximately 12 km east of the Bonnet Plume River and 6 km south of 'Dolores Creek' (Thorkelson and Wallace, 1998), an informally named west-flowing tributary of the Bonnet Plume River, after which the formation is named. The ridge section measured in this study (Figs. 4 and 5; ~260 m thick) is the best of the generally recessive exposures of this formation in the Dolores Creek area, and is proposed as the type section of the Dolores Creek Formation. Much of the section consists of stratigraphically intact rubble along the ridge-line.

The Dolores Creek Formation is dominated by recessive dark grey to black-weathering, variably pyritic siltstone and mudstone with conspicuous, commonly bright orange-weathering microbial carbonate intervals. Covered intervals are numerous, but most can be inferred to be underlain by grey to black siltstone or mudstone based on the composition of ridge-line scree. Minor quartz sandstone units are present in the upper one-third of the formation.

The basal contact of the Dolores Creek Formation appears to be an angular unconformity at the top of massive, pale grey-weathering, laminated to thinly layered dolostone of unit 'C' of the Pinguicula Group (Figs. 1 and 6a). Strata of Pinguicula Group 'unit C' at this location exhibit no obvious evidence of meteoric alteration or geomorphic structures that would be consistent with karstification. No evidence of faulting is present at the contact. Less well-exposed sections of this formation on other flanks of the same large mountain (Fig. 7) exhibit the same stratigraphic
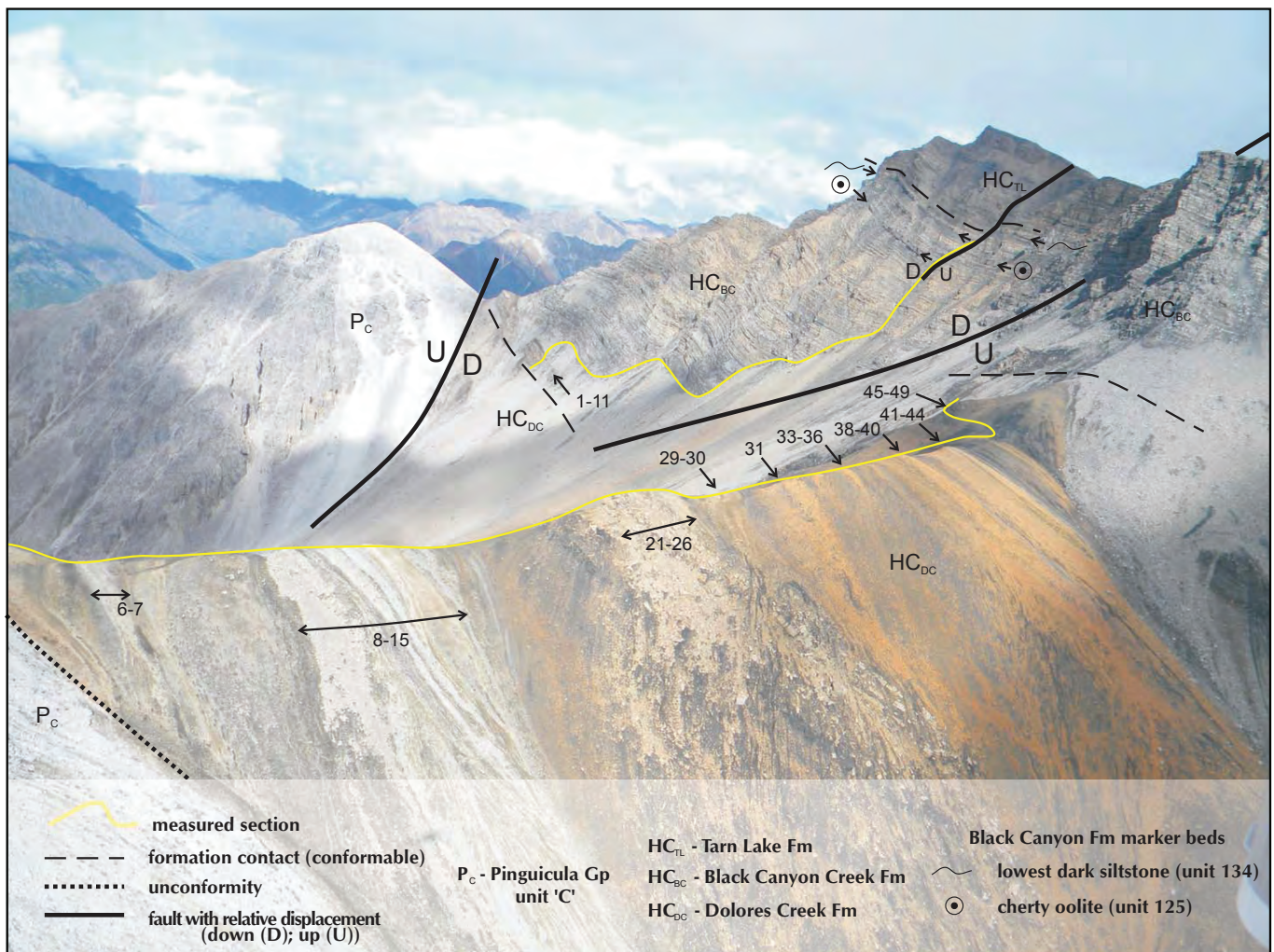
Figure 4. Type sections of the Dolores Creek and Black Canyon Creek formations. Unit numbers for prominent layers in the measured sections are indicated.

Type Section of Dolores Creek Fm
64°49'09" / 133°27'00" NTS 106C

~20 m to base of
Black Canyon Creek Fm

Legend

dolostone

quartz sandstone

siltstone

••• terrigenous sand

silty

limestone, dolostone
interlayers

intraclasts & catagraphs

microbial lamination

stromatolite (columnar)

stromatolite (domal)

planar lamination

asymmetrical ripples or
ripple cross-lamination
(with apparent paleocurrent)

normal grading

desiccation cracks

fenestral fabric

bit   bitumen

Q   void-filling quartz

Figure 5. *Type section of the
Dolores Creek Formation,
as shown in Figures 1 and
4. Column width indicates
weathering profile. Coloured
fills indicate weathering colour.*

colour pattern in the disposition of distinctive, orange-weathering dolostones above the contact with Pinguicula unit 'C', supporting the inference that the contact at the measured section is structurally intact.

The upper contact with the Black Canyon Creek Formation (new) is at the top of a covered interval underlain by black siltstone and fissile mudstone (shale; Fig. 6b). The contact is probably conformable, based on the presence in the lowermost Black Canyon Creek Formation of microbial carbonate rocks identical to those that predominate in the Dolores Creek Formation, and the gradual loss of quartz sandy and silty interlayers across the transition into the basal Black Canyon Creek Formation.

The lowest 2 m of the Dolores Creek Formation are covered, but ridgeline scree indicates that they consist of dark grey siltstone. The lowest exposed unit (0.6 m) is bright orange-weathering microbially laminated dolostone with millimetric intraclasts and minor quartz silt. After another covered interval (siltstone), a 1 m-thick orange-weathering stromatolitic dolostone contains robust, branching, unwalled columnar stromatolites (form genus *Baicalia*). From 10 m to 132 m, the succession consists of thick (1 to 30 m) covered intervals of dark grey to black siltstone (70% of the interval's total thickness) with interlayered pale grey to yellow-buff-weathering microbial intraclastic dolostone (30%) identical to those below. Dolostones in this interval contain conspicuous intercrystalline and pore-filling bitumen. A 0.2 m-thick, bright orange-weathering unwalled, unbranching stromatolite (form genus *Colonella*; Fig. 6c) is conspicuous at 132 m. The stromatolite is overlain by a further 98 m of interlayered dark grey to black siltstone (60%) with orange-yellow, grey or brown–weathering, microbially laminated, intraclastic dolostone layers (40%); each typically 1 to 5 m thick (Fig. 6d,e). In this 98 m-thick interval from 132 to 230 m, thin, sparse quartz sandstone layers first appear 168 m above the formation's base, increasing over the next 30 m and then disappearing (Fig. 6f). This 98 m-thick interval has 10 m of black-weathering siltstone at its top. The overlying 11.5 m consist of ripple cross-laminated medium brown-weathering quartz sandstone with dark grey-weathering siltstone interbeds and sparse, graded intraclastic dolostone. A 1.6 m-thick unit of orange-brown-weathering, non-branching, unwalled columnar stromatolite (form genus *Boxonia*) occurs at the base of this interval (~230 m). The sandstone and siltstone of the uppermost exposure of the Dolores Creek Formation is overlain by approximately 20 m of cover (Fig. 6b), but

appears to consist predominantly of black siltstone and fissile mudstone.

A preliminary stratigraphic survey of the metal composition of the black mudrocks was conducted using a portable, hand-held x-ray fluorescence (XRF) analyser (Thermo Scientific Niton® XL3t), in the analyser's "soils" software mode. Metals such as Zn, Pb and Ni show concentrations at some stratigraphic levels that are elevated above post-Archean average shale values (PAAS; Taylor and McLennan, 1985).

INTERPRETATION

The basal contact of the measured section appears to be a pronounced angular unconformity with massive strata of the underlying unit 'C' of the Pinguicula Group. It is possible, however, that the angularity of the unconformity is an artifact caused by differential strain in the weak, mudrock-dominated Dolores Creek Formation relative to that of rigid, massive dolostone of Pinguicula Group unit 'C'. A proper understanding of the configuration and implications of this important contact will require further investigation.

Inundation of the unconformity surface of the Pinguicula Group was not accompanied by deposition of high-energy facies. Although the unconformity surface may have been irregular, in this section there is no evidence for pronounced topography or syndepositional faulting that would have been reflected in marked lateral lithofacies variation and local shedding of coarse detritus from topographic highs. Strongly evaporative conditions are not indicated, and the microbial and intraclastic carbonate lithofacies record comparatively shallow-water to possibly emergent conditions (although no desiccation cracks were evident). At the same time, however, the black siltstone and mudstone that dominate this formation suggest that the shallow water of the incipient MMSG basin was anoxic and restricted from circulation with the open ocean. The black colour may reflect a high organic content, which probably accounts for the conspicuous bitumen in some of the formation's carbonate rocks. These attributes would be consistent with an incipient extensional basin that may not have been well connected to the global ocean. Three subtle transgressive intervals are suggested by the three columnar stromatolitic carbonates (at 7.4, 132.1, and 230.2 m), which differ markedly from the intraclastic, microbial dolomudstone that characterizes the remainder of the carbonate units.
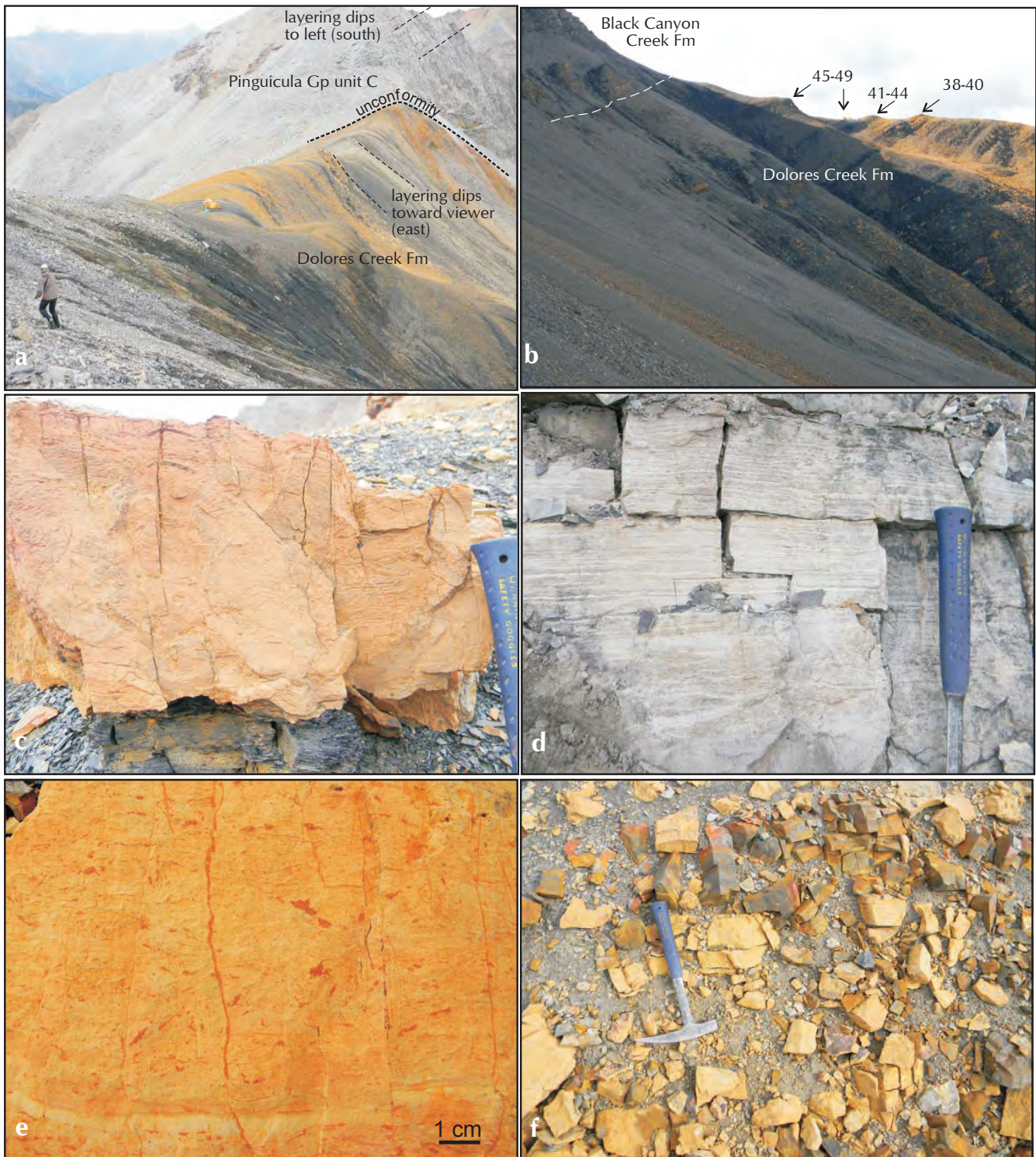
Figure 6. Exposures and typical lithofacies of the Dolores Creek Formation. (a) View to west from top of Dolores Creek Formation, showing conspicuous black and orange weathering colours, and angular relationship between bedding in Pinguicula Group unit 'C' and that of the Dolores Creek Formation. (b) Gradational upper contact of Dolores Creek Formation and Black Canyon Creek Formation. Two 1 m-high tents on ridge (arrow) give scale. (c) Orange-weathering columnar stromatolite (unit 20) overlies grey-weathering siltstone (unit 19). (d) Planar-laminated (above) and intraclastic (below) grey-weathering dolostone of unit 28. (e) Bright orange-weathering microbial, intraclastic dolostone of unit 31. (f) Units 38 (orange-weathering dolomudstone) and 39 (rusty brown-weathering quartz sandstone).

DISTRIBUTION AND MAPPING

The Dolores Creek Formation is easily recognized in the Dolores Creek-Pinguicula Lake area owing to its bright orange dolostones and dark grey to black, recessive mudrocks. It forms slopes and poorly exposed ridges beneath the evenly bedded, grey-weathering carbonate succession of the Black Canyon Creek Formation, and overlies massive, pale grey-weathering dolostone of Pinguicula Group unit 'C'. The extent of exposure beyond this area is unknown.

CORRELATION

The Dolores Creek Formation is equivalent to the lower part of abandoned Pinguicula Group unit 'D' of Eisbacher (1978). It is the basal unit of the MMSG, and has never before been described in detail. Equivalent strata are not exposed in the Mackenzie Mountains because that area is not as deeply exhumed. Basal strata of the Shaler Supergroup (Amundsen Basin, Arctic coastal NWT and Victoria Island) consist of the Escape Rapids Formation (Fig. 3c), which comprises a variety of storm-dominated marine to supratidal terrigenous siliciclastic facies (Long *et al.*, 2008). From this description, it appears that, although the Dolores Creek Formation and Escape Rapids Formation may be in part time-equivalents, they appear to represent different environmental and tectonic settings (isolated rift basin(s) for Dolores Creek Fm; storm-dominated, stable, open-marine shelf for Escape Rapids Fm; Long *et al.*, 2008). If the Dolores Creek Formation can be demonstrated to be the regional base of the MMSG, and it is accepted that the overlying Black Canyon Creek Formation (described below) is equivalent to the 'H1 unit', interpretations of seismic data from the interior plains of NWT (Cook and MacLean, 2004) that invoke approximately 2.3 km of MMSG-related strata beneath the inferred 'H1' unit may require revision.

ECONOMIC POTENTIAL

The economic potential of the Dolores Creek Formation is unknown. No economic mineral occurrences have been reported from these strata. Bitumen and quartz are locally present in carbonate porosity in the measured section, indicating migration of heated fluids at some time after sediment lithification.

BLACK CANYON CREEK FORMATION (NEW)

In the Dolores Creek - Pinguicula Lake area, the Black Canyon Creek Formation (~285 m thick) forms recessive hillsides and consists of evenly bedded, intermittently cherty, pale grey dolostone with silty interbeds, between more recessive siliciclastic strata of the Dolores Creek and Tarn Lake formations (Fig. 7). Although most exposures are extensively rubble-covered, exposure in cliffs above the type section of the Dolores Creek Formation (5 km south of Dolores Creek; 12.5 km east of Bonnet Plume River; Figs. 4 and 8) is almost complete, though complicated by numerous small normal faults. The section measured here (Fig. 8) is complete except for the uppermost ~10 m, which record the transition to the overlying Tarn Lake Formation; this upper part of the formation was deemed too dangerous to measure at the type locality. The Black Canyon Creek Formation is named for a tributary of Hematite Creek in NTS 106C.

The base of the Black Canyon Creek Formation is placed above the 20 m-thick covered interval at the top of the underlying Dolores Creek Formation (Figs. 4 and 6b), at the base of the lowest resistantly weathering interval of orange-buff and grey-weathering dolostone. Dolostones in the lowermost 17.3 m-thick interval are microbially laminated, mechanically plane-laminated, or intraclastic (mm to cm-scale), and have graded centimetric layers of quartz-rich, sandy to silty dolostone, and local, minor black chert nodules. This dolostone interval is overlain by 1.1 m of quartz sandstone and a 6.8 m-thick covered interval inferred to consist of fissile mudstone or siltstone similar to that of the underlying Dolores Creek Formation. The next ~148 m of the formation consist of approximately 11 decametre-scale cycles, each typically consisting of molar-tooth dolomudstone (MTS; generally <1 m thick; Fig. 9a), overlain by mechanically laminated to banded, desiccation-cracked and tepeed dolomudstone (Fig. 9b), locally with thin interlayers of intraclast dolopackstone. Chert nodules are locally common in the upper parts of cycles (Fig. 9b). MTS is not evident in the upper ~35 m of this interval, although cyclicity persists. From 140 to 144 m is the only calcareous interval in the succession: slightly argillaceous dolostone riddled with calcareous MTS crack-fills. The succession from 144 to 220 m consists of metre-scale cycles, each with siltstone or argillaceous dolostone (with MTS in the lower 30 m) overlain by mechanically laminated, desiccation-cracked and tepeed, locally intraclastic dolomudstone (Fig. 9c). At ~220 m is a prominent 3.5 m-thick marker bed of massive, dark-weathering, partly silicified, cross-bedded oolite (Figs. 9d-f). Above the oolite are 22 m of variably argillaceous dolostone with ooids and chert. The measured section ends at a conspicuous, 1.2 m-thick marker bed
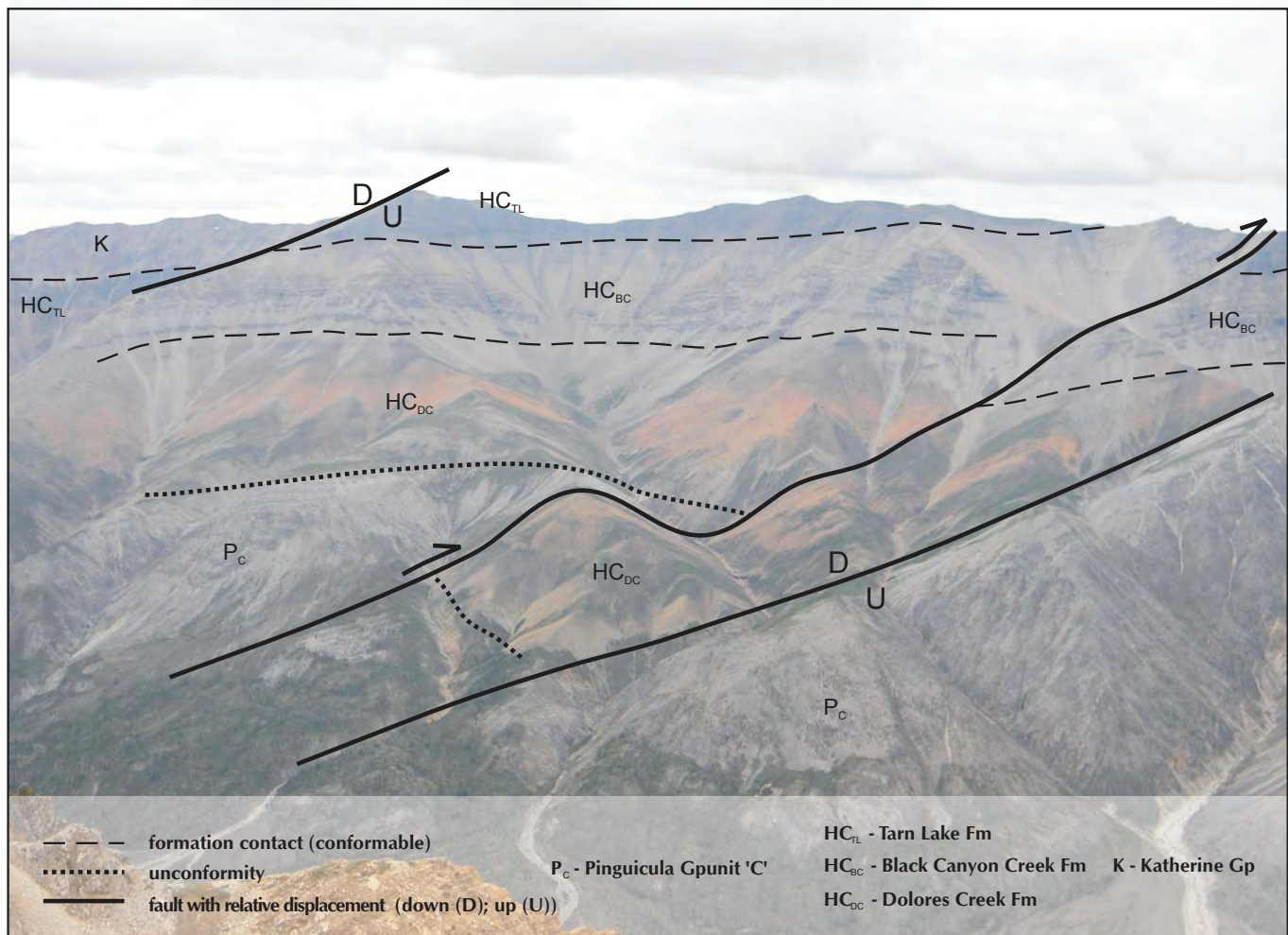
Figure 7. *A typical exposure of the Hematite Creek Group, here on the northeastern flank of the un-named mountain on which the type sections were measured (type sections not seen in this view).*

of dark grey-weathering siltstone (Figs. 9e,f). Although the remaining few metres of the formation were not measured, they are estimated from photos (Figs. 9e,f) to be about 10 m thick, and consist of interlayered siltstone/ sandstone and dolostone, and represent a gradational zone between the Black Canyon Creek Formation and Tarn Lake Formation.

INTERPRETATION

The Black Canyon Creek Formation is markedly cyclic. Decametric cycles in the lower part of the formation record normal-marine subtidal conditions (molar-tooth dolostone) repeatedly shallowing to arid supratidal environments. This regime is then gradually superseded by silty-based supratidal cycles an order of magnitude thinner (metre-scale). Both cyclic intervals exhibit stability throughout many tens of metres of section, reflecting depositional equilibrium with subsidence, yet they differ

markedly in composition and paleoenvironment: lower, normal-marine cycles are followed by upper, argillaceous, supratidal cycles. The change in cyclicity appears to reflect an adjustment in the subsidence regime that was coeval with the introduction of terrigenous silt. Abrupt transgression recorded by the oolite marker did not significantly alter the depositional regime and may not be part of the eustatic signal that is reflected in the rest of the formation. Although its lateral extent is not known, the marker unit is present in other exposures up to at least 5 km away. The transition to the overlying Tarn Lake Formation is a change from carbonate-dominated to terrigenous-clastic-dominated composition, but the depositional environment remains very shallow marine to supratidal through the entire Tarn Lake Formation. Apparently, this transition reflects a change in terrigenous source dynamics, which had been presaged by introduction of terrigenous silt in the upper Black Canyon Creek Formation.
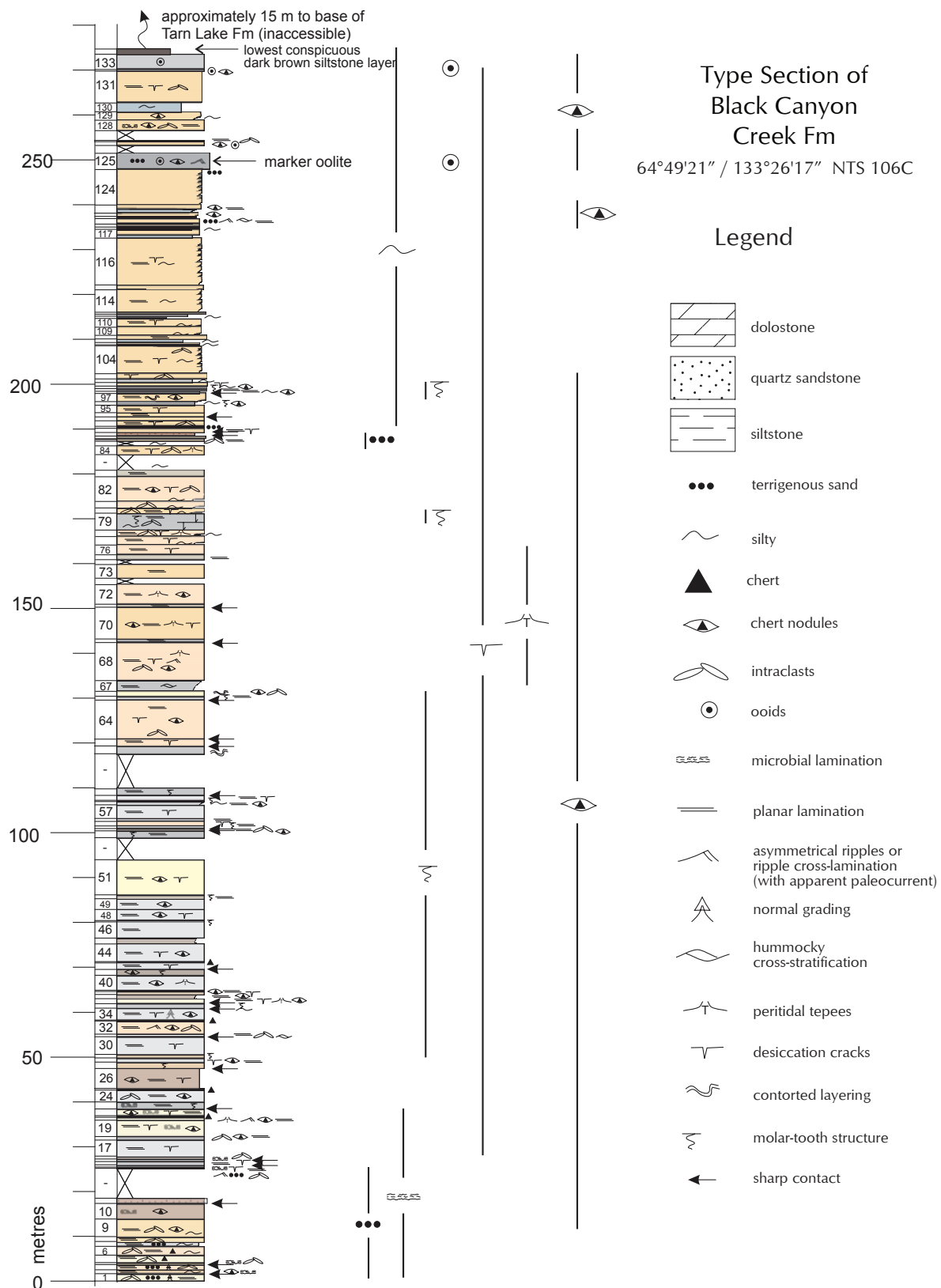
Figure 8. *Type section of the Black Canyon Creek Formation, as shown in Figures 1 and 4. Column width indicates weathering profile. Coloured fills indicate weathering colour. Range bars to right of section summarize stratigraphic distribution of paleoenvironmentally significant sedimentary components and structures.*
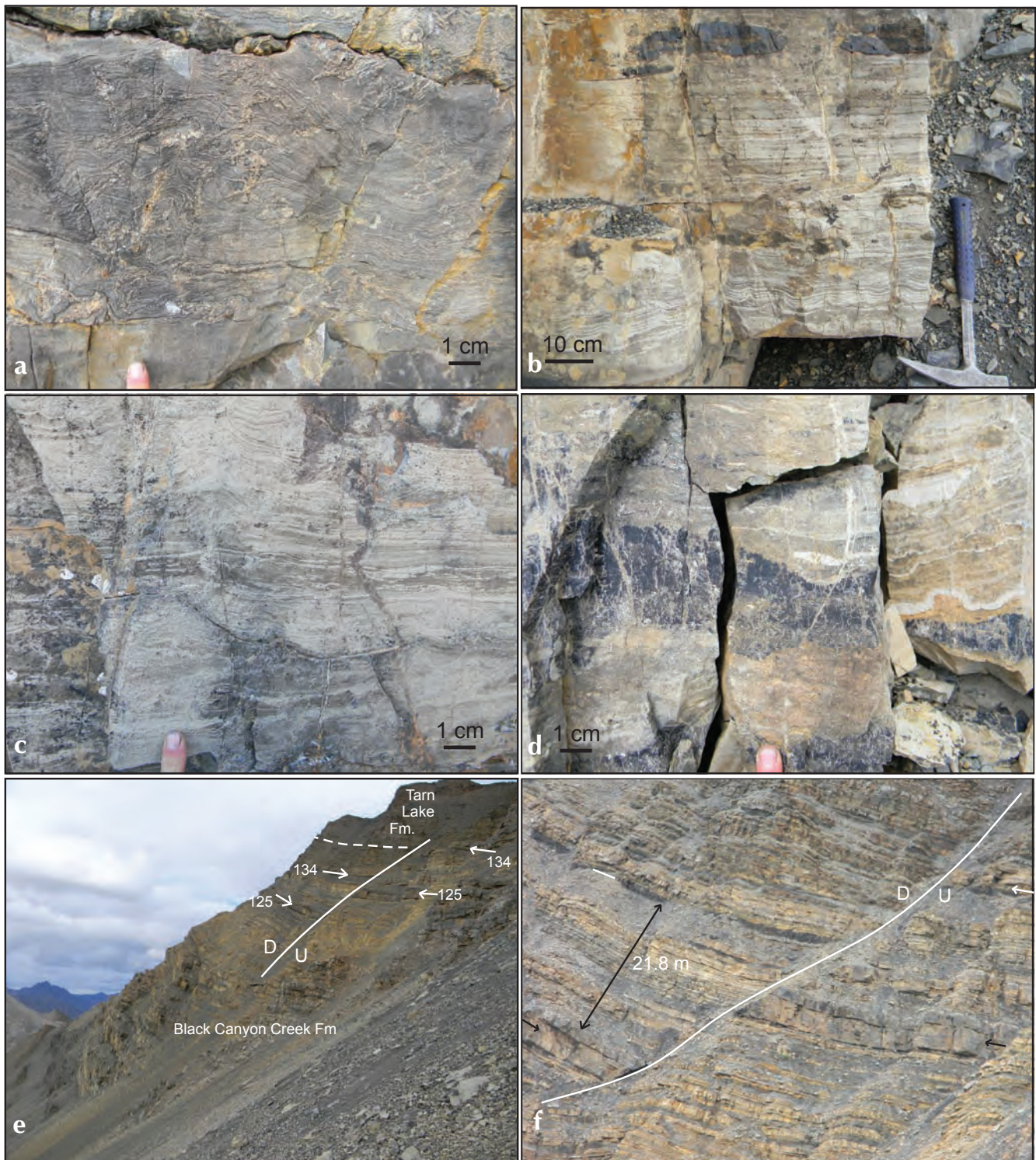
Figure 9. Typical exposures, lithofacies, and marker units of the Black Canyon Creek Formation. **(a)** Recrystallized molar-tooth structure (unit 29). **(b)** Cherty, laminated supratidal dolostone (unit 68). **(c)** Laminated, tepeed supratidal dolomudstone (unit 78). **(d)** Interlayered cherty oolite and dolomudstone of marker bed 128. **(e)** Upper part of the Black Canyon Creek Formation, with marker beds 125 (oolite) and 134 (dark siltstone), just below transition to Tarn Lake Formation. **(f)** Close-up view of transition interval in (e), illustrating gradational nature of contact. Marker units 125 and 134 are indicated with black and white arrows, respectively.

DISTRIBUTION AND MAPPING

The Black Canyon Creek Formation is widespread in the Dolores Creek-Pinguicula Lake area, where it is easily distinguished from other formations in the MMSG (and Pinguicula Group) by its conspicuous, regular layering and pale grey to buff colour, and by its stratigraphic position between the black and orange-weathering Dolores Creek Formation and the dark brown-weathering Tarn Lake Formation. No other unit in this area contains abundant chert nodules. Uppermost strata of the Black Canyon Creek Formation are commonly yellow-orange-weathering from a distance. The extent of exposure beyond this area has not been ascertained.

CORRELATION

The Black Canyon Creek Formation is equivalent to the upper part of Pinguicula Group unit 'D' of Eisbacher (1978). It may be stratigraphically equivalent to the Mikkelson Islands Formation of the Shaler Supergroup (Rainbird *et al.*, 1996) and is probably equivalent to the 'H1 unit' in the Mackenzie Mountains, NWT (Fig. 3c; Turner, in press a). Neither the Black Canyon Creek Formation nor the 'H1' unit exhibits any similarity to strata of Pinguicula Group unit 'C', other than their dolomitic composition.

This proposed correlation of the Black Canyon Creek Formation and 'H1 unit' is made despite pronounced differences in the lithofacies and stratigraphic expression of the carbonate successions in the two areas, which are separated by about 150 km (oblique to strike, and not palinspastically restored). The 'H1 unit', the lowest part of the MMSG exposed in the Mackenzie Mountains is known in only three localities in NWT, of which two are of poor quality or negligible thickness. At the third locality, in NTS 106G, the uppermost ~480 m of the formation are exposed (Turner, in press a), but what lies beneath is unknown. The 'H1 unit' is strikingly non-cyclic and is not peritidal throughout most of its thickness (Turner, in press a). It does not contain a significant amount of terrigenous silt. Nonetheless, some similarities with the Black Canyon Creek Formation are present, including the presence of chert (upper 'H1 unit'; throughout Black Canyon Creek Formation). The Black Canyon Creek Formation may be a shallow-water equivalent to the 'H1 unit'. Their apparent lateral equivalence but stratigraphic and sedimentologic dissimilarity suggest that they are best considered to be different formations. The 'H1' will be formalized in a separate publication.

An alternative correlation of the Hematite Creek Group is that the entire group consists of lateral facies equivalents of the Tsezotene Formation and lowermost Katherine Group (Thorkelson *et al.*, 2003; 2005; Fig. 3b). The Dolores Creek Formation would be equivalent to the lower 'Grey member' of the Tsezotene Formation (Long *et al.*, 2008; Turner and Long, 2008), the Black Canyon Creek Formation would be a shallower-water equivalent of carbonate rocks in the lower part of the upper 'Red member' of the Tsezotene Formation, and the Tarn Lake Formation would be a shallow-marine facies equivalent of the lowermost fluvial unit (K1) of the Katherine Group (Long, in press a). If the lower two formations of the Hematite Creek Group were correlated with the Tsezotene Formation in NWT, the westward thinning of time-equivalent units would be significantly less marked than in the correlation scheme that is favoured here.

ECONOMIC POTENTIAL

No occurrences of economic minerals are known from this unit, and the economic potential of the Black Canyon Creek Formation is unknown. Minor occurrences of copper minerals and fluorite are present in the 'H1 unit' in the Mackenzie Mountains approximately 150 km to the east-northeast (personal observation).

TARN LAKE FORMATION (NEW)

A terrigenous-clastic-dominated unit that lies stratigraphically between the Black Canyon Creek Formation and quartz arenite of the Katherine Group was measured up a creek incised into the south flank of an un-named mountain about 10 km south of Dolores Creek and 16 km east of the Bonnet Plume River (Fig. 10). The name for this stratigraphic unit is after the informal name given by hunters to a small lake 2.5 km south of the type section.

The lower contact with the Black Canyon Creek Formation is covered at this location, and probably occurs a few tens of metres below the lowest exposed strata, based on Black Canyon Creek Formation exposures elsewhere in the valley, a negligible dip angle, and the geomorphology of the broad valley in which the section is based (Fig. 10). Lowermost Tarn Lake Formation strata are exposed above the Black Canyon Creek Formation where the latter was measured on a ridge on the northwestern part of the same mountain. The uppermost ~10 m of strata of the Black Canyon Creek Formation were not measured, but the excellent exposure of this inaccessible transitional interval clearly demonstrates a gradational contact through interlayering of dolostone, siltstone, and sandstone.
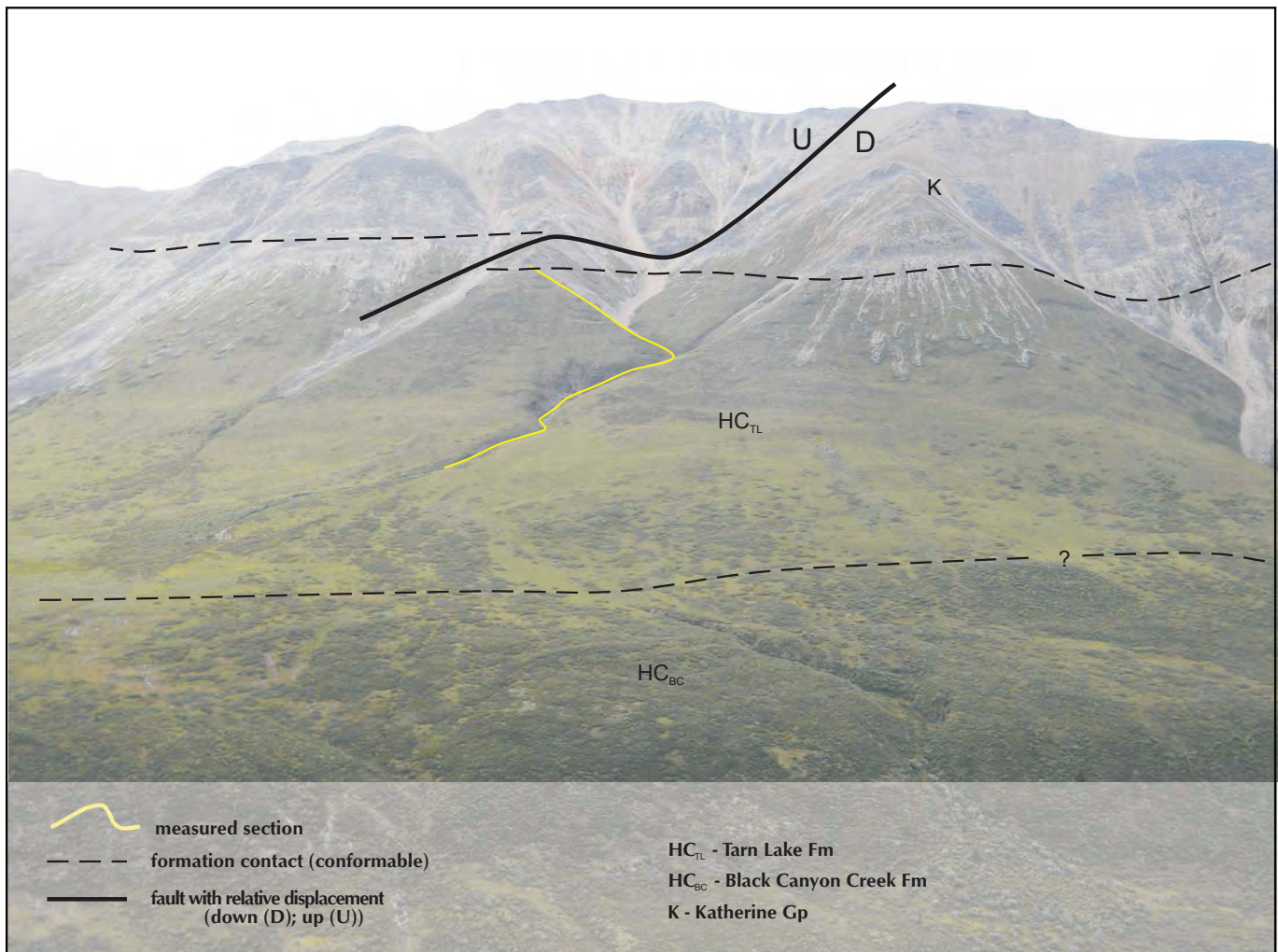
Figure 10. *Measured section of the Tarn Lake Formation on the south flank of the un-named mountain where all Hematite Creek Group sections were measured. To right (east) of marked fault, the lowest marine interval of the Katherine Group is down-faulted against the lowest fluvial interval.*

The measured section of the Tarn Lake Formation is approximately 265 m thick, and the full thickness of the formation in this area is probably approximately 300 m. The upper contact with resistant, white-weathering, massive quartz arenite of the Katherine Group is covered, but appears to be abrupt (Figs. 10 and 11).

The Tarn Lake Formation consists of generally medium-bedded quartz sandstone interlayered with siltstone (Figs. 12a,b). Sedimentary structures in sandstone and siltstone throughout most of the succession include hummocky cross-stratification (HCS), desiccation cracks, plane lamination and parting lineations, wave and current-ripple cross-lamination, trough cross-bedding, and less commonly, synaeresis cracks, scour structures, and gutter casts (Fig. 12c). Centimetric to millimetric siltstone clasts

locally form lags at bed bases. Orange-brown-weathering dolostone interlayers first appear approximately one-fifth of the way through the exposed part of the succession. Although the lowest of these dolostone units contains recrystallized molar-tooth structure (Fig. 12d), all other dolostone units consist of millimetric to centimetric layers of dolomudstone to dolosiltstone (Fig. 12e), locally with desiccation cracks, wave-ripples, contorted layering, or grading expressed in quartzose silt to very fine sand. One carbonate unit two-thirds of the way through the exposed succession exhibits two layers of centimetric nodules of medium grey chert. The uppermost 50 m of the formation (Fig. 12f) are slightly more recessive and contain a lower proportion of quartz sandstone, although carbonate interbeds persist. Sedimentary structures are difficult to discern in this upper interval of dark grey-weathering

Representative Section of
Tarn Lake Fm
64°47'13" / 133°22'11" NTS 106C

Legend

Katherine Group

dolostone

quartz sandstone

sandy siltstone

siltstone

••• terrigenous sand

~ silty

chert (black; white)

chert nodules

carbonate intraclasts

mudstone clasts

planar lamination

asymmetrical ripples or ripple cross-lamination

normal grading

hummocky cross-stratification

synaeresis cracks

desiccation cracks

contorted layering

molar-tooth structure

scour

trough crossbedding

symmetrical ripples

gutter cast

* carbonate rock present

unknown thickness (<100 m) to top of Black Canyon Creek Fm

metres

Figure 11. Measured section of the Tarn Lake Formation, as shown in Figure 1. Column width indicates weathering profile. Coloured fills indicate weathering colour.
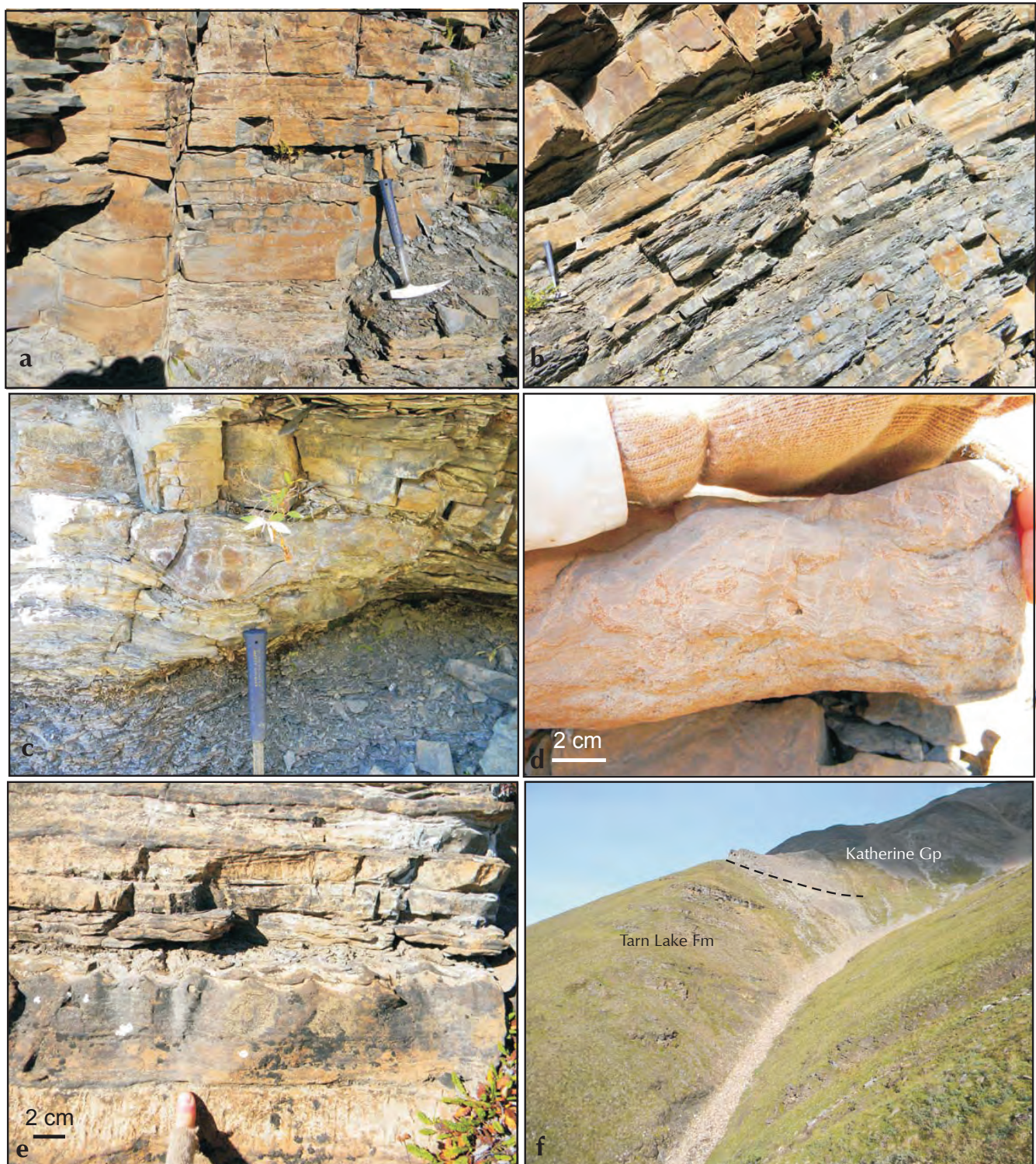
Figure 12. Exposure and typical lithofacies of the Tarn Lake Formation. **(a)** and **(b)** Typical exposures of sandstone and siltstone interlayers, from sandstone-dominated intervals. **(c)** Gutter cast (unit 8). **(d)** The only molar-tooth interval in the section is 1 m thick (unit 12). **(e)** Interlayered wave-rippled sandstone and dolomudstone (unit 38). **(f)** Uppermost ~120 m of the Tarn Lake Formation, and its abrupt upper contact with the Katherine Group.

siltstone, but there is some suggestion of desiccation cracks. Cyclicity is not well developed in this formation, but may be expressed in decametre-scale variation in the relative proportions of siltstone to sandstone. A detailed study of paleocurrent indicators was not undertaken, but sparse measurements of wave-ripple crests suggest a north-trending shoreline, and ripple cross-lamination and gutter casts in tempestites are oriented roughly south-southwest, suggestive of shore-parallel geostrophic currents.

The maximum depositional age of the Tarn Lake Formation in the Wernecke Mountains is constrained by the age of youngest detrital muscovite (1033 ± 9 Ma Ar-Ar; Thorkelson, 2000; Thorkelson et al., 2005). This concurs with detrital zircon ages for the Katherine Group in the Mackenzie Mountains: Rainbird et al. (1996) reported a youngest detrital zircon age of 1083 Ma, and Leslie (2009) obtained a 1005 Ma youngest zircon.

INTERPRETATION

The Tarn Lake Formation in the study area contains abundant sedimentary structures indicative of deposition in a very shallow-water, storm-dominated marine environment. Desiccation cracks are ubiquitous, indicating that the bathymetric differential between the sea-floor, where subaqueous deposition of storm-influenced sand (HCS; gutter casts) took place, and subaerial zones (desiccation cracks) was minimal (perhaps less than a metre), or that sediment deposition took place predominantly during storm surge over surfaces that were subaerially exposed during calm weather. The presence of one thin interval of molar-tooth structure indicates that the environment was, at least for a brief time, a geochemically normal (unrestricted) subaqueous setting. The combination of dominant attributes, however, depicts a very near-shore to subaerial environment in an arid or semi-arid environment strongly affected by storms. For storm waves to persist across shallow-water areas such as this, a strong fetch is required, which implies a large area of open water over which storm winds could build.

DISTRIBUTION AND MAPPING

Although strata of the Tarn Lake Formation are readily recognized as a recessive, medium brown-weathering interval beneath resistant quartz arenite of the Katherine Group and are widespread on recessive slopes of the Pinguicula Lake – Dolores Creek area, the full exposure area has not been demonstrated by mapping. Tarn Lake Formation strata superficially resemble silty marine

intervals in the Katherine Group, and care should be taken that the two are not mistaken for one another.

CORRELATION

The Tarn Lake Formation consists of recessive siliciclastic rocks between the abandoned units 'D' and 'E' of the Pinguicula Group (Eisbacher, 1978, 1981). Although this unit appears to be stratigraphically equivalent to the Tsezotene Formation of NWT (Fig. 3c), and has been mapped as such in NTS 106E and 106F (Norris, 1982a,b; Thorkelson et al., 2003), strata described here are similar to the Tsezotene Formation of NWT only in their terrigenous clastic composition. The comparatively thin, shallow-water Tarn Lake Formation in the Pinguicula Lake – Dolores Creek area contrasts markedly with the thick, deep-water mudstone and siltstone succession of the Tsezotene Formation of the Mackenzie Mountains, and for this reason, the shallow-water unit in the Wernecke Mountains requires a distinct formation name. The Tsezotene Formation in the Mackenzie Mountains (Gabrielse et al., 1973; Long et al., 2008; Long in press b), is interpreted to have been deposited in a sub-storm-wave-base, distal shelf environment dominated by siliciclastic mud (Long et al., 2008). Thickness of the Tsezotene Formation in the Mackenzie Mountains is typically in excess of 1 km (Long, in press b); the type section, in the Tsezotene Range in NTS 95L (Glacier Lake) is approximately 1100 m thick (Gabrielse et al., 1973).

There are no distinctive stratigraphic units in the measured section with which to correlate this formation locally or regionally. The only stratigraphically distinctive variability in the formation is the appearance of sparse carbonate interlayers in the upper three-quarters of the measured section.

The lower contact of the Tsezotene Formation is covered at the three known localities where the underlying 'H1 unit' is exposed in the Mackenzie Mountains, but exposure patterns and lithostratigraphy at these locations suggest that the transition is abrupt (major flooding surface; Long et al., 2008; Turner and Long, 2008) and possibly unconformable (Turner, in press a). In the Wernecke Mountains, however, the lower contact of the Tarn Lake Formation is compositionally gradational (from carbonate-dominated to quartz sandstone-dominated), and depositional environments appear to be consistently shallow water to emergent. The Tsezotene Formation consists of grey mudrocks in the thick, lower 'grey member', and red-weathering mudrocks and subordinate carbonates and sandstones of the thinner, upper 'red

member' (Long, in press b). The Tarn Lake Formation cannot be subdivided into meaningful, informal members, although the sparse carbonate layers are limited to the upper three-quarters of the exposed section.

Sediment grain size of the Tarn Lake Formation is markedly coarser than that of the Tsezotene Formation, and all sedimentary structures in the former point to extremely shallow-water deposition. In the context of paleotectonic conditions inferred by Turner and Long (2008), this suggests that, during deposition of the Tsezotene Formation, the MMSG basin may have deepened westward from a basin margin somewhere beneath the Mackenzie Plain to an area of maximum depth somewhere in the Mackenzie Mountains, then shallowed westward into the present-day area of the Wernecke Mountains. A different sediment supply and dispersal regime than that of the Tsezotene Formation in the Mackenzie Mountains would be necessary, and it is possible that the study area represents the western side of the early MMSG basin. Further work is required to establish the basin configuration at that time and determine the implications for tectonostratigraphic evolution of the basin and for inter-regional correlation.

Interpretation of the Tarn Lake Formation in a regional context is complicated by identification of strata that are clearly its equivalent in nearby NTS 106E and 106F as Tsezotene Formation (Norris 1982a,b; Thorkelson *et al.*, 2003). Norris (1982a,b) described the rocks as being of marine and non-marine origin, perhaps owing to the prevalence of desiccation cracks, and Thorkelson *et al.* (2003) described abundant indications of subaerial exposure. Although the lithofacies described for 'Tsezotene Formation' strata in NTS 106E by Thorkelson *et al.* (2003) are of a shallow-marine to subaerial origin that agrees with the Tarn Lake Formation, the unit's thickness is reported to be >1.2 km, which is roughly three times the inferred thickness of the Tarn Lake Formation exposed in this NTS 106C. Validation of marked thickening in the Tarn Lake – 'Tsezotene Formation' interval between NTS 106C and NTS 106E would imply a very significant geographic variation in subsidence rate that would support previous interpretations of basin segmentation in the MMSG (Turner and Long, 2008).

For proposed correlations to inliers west of the Wernecke Mountains, the reader is referred to Rainbird *et al.* (1996, 1997), Abbott (1997), Cook and MacLean (2004), Thorkelson *et al.* (2005), Long *et al.* (2008), and Macdonald and Roots (2009).

ECONOMIC POTENTIAL

No mineral occurrences are known from the Tarn Lake Formation or its equivalent in NWT (Tsezotene Formation). This is the first documentation of this unit, and so its regional economic potential is unknown.

KATHERINE GROUP

Thick strata of the Katherine Group are extensively exposed in the Dolores Creek - Pinguicula Lake area, where these quartz arenites were known for a time as unit E of the Pinguicula Group (Eisbacher, 1978), and the 'Corn Creek quartz arenite' or 'Corn Creek quartzite' (Eisbacher, 1981; Thorkelson, 2000). No sections were measured in this unit for this study, but some general characteristics can be established.

In the Mackenzie Mountains, the Katherine Group comprises seven formation-scale units (K1 to K7). Odd-numbered units are white, pink- and purple-weathering fluvial-dominated quartz arenite, whereas even-numbered units consist of dull brown marine siltstone and sandstone with minor orange-brown-weathering carbonate rock. The recessive marine intervals are commonly covered by blocky quartz arenite talus, but the uppermost marine interval, unit K6, is commonly conspicuous. Unit K6 siltstone is marked by an orange-weathering stromatolitic dolostone throughout the exposure area of the Katherine Group in the Mackenzie Mountains, and indeed in correlative strata of the Shaler Supergroup (Jefferson and Young, 1989; Long *et al.*, 2008).

This general description also applies to the Katherine Group in the Wernecke Mountains. Although it has not been ascertained that seven units are expressed, thick marine and fluvial units clearly alternate (Figs. 13a,b,c), and units K6 (including its characteristic stromatolite; Fig. 13d) and K7 clearly underlie strata of the lower Little Dal Group where they were documented 15 km east of Pinguicula Lake near a tributary of Corn Creek (Figs. 14 and 15a).

The Katherine Group is correlated with the Nelson Head, Aok and Grassy Bay formations in the Shaler Supergroup, Amundsen Basin (Fig. 3c; Rainbird *et al.*, 1996). Unit K6 is directly equivalent to the Aok Formation of the Shaler Supergroup (Jefferson and Young, 1989; Rainbird *et al.*, 1996; Long *et al.*, 2008). For suggested correlations westward to other Proterozoic inliers in the Yukon, the reader is referred to Rainbird *et al.* (1996, 1997), Abbott (1997), Cook and MacLean (2004), Thorkelson *et al.* (2005), Long *et al.* (2008), and Macdonald and Roots (2009).
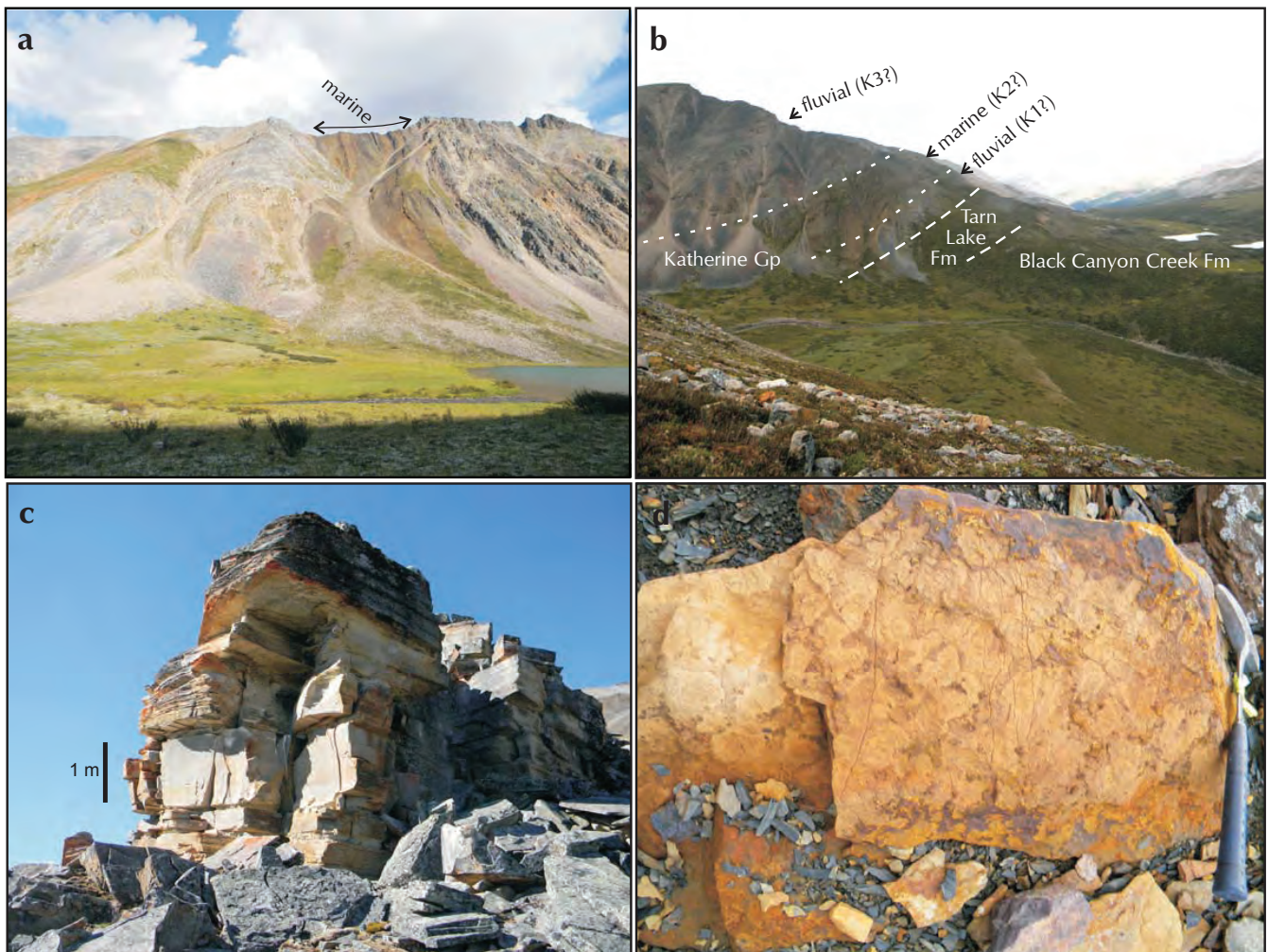
Figure 13. Katherine Group. **(a)** Interlayered fluvial quartz arenite (pale purplish-grey) and marine siltstone – mudstone. It is unknown which of the marine intervals is depicted here. **(b)** Fluvial and marine intervals of the Katherine Group overlie strata of the Hematite Creek Group. If no structural features are present, this exposure would suggest that unit K1 is thin in this area. **(c)** Massive, cross-bedded and planar-bedded quartz arenite of the basal Katherine Group (marine) above Tarn Lake Formation type section (see Fig. 12f). **(d)** Orange-weathering stromatolite (Inzeria) is a widespread marker in unit K6 and equivalent unit of the Shaler Supergroup. This exposure is in upper Katherine Group near Mount Profeit.

The abrupt base of the Katherine Group in the Wernecke Mountains resembles the same contact in the Mackenzie Mountains. The contact's abruptness is a function of the contrasting depositional processes and sediment grain sizes in marine (Tarn Lake/Tsezotene) versus fluvial (Katherine) systems, and reflects the progradation of a fluvial-dominated system over a near shore marine system at the beginning of Katherine Group deposition. The volumetric importance of quartz sand in the Tarn Lake Formation (and indeed the minor influxes of quartz sand that are intermittently present all the way to the base of the Hematite Creek Group) also emphasizes the similarity in source material in the two formations and

the conformable nature of the transition between the two stratigraphic units, in spite of marked differences in structure and composition associated with their contrasting marine and fluvial environments.

LITTLE DAL GROUP – BASINAL ASSEMBLAGE

Strata of the lower Little Dal Group were examined on a ridge near Corn Creek, approximately 15 km east of Pinguicula Lake and 7 km south-southwest of Mount Profeit (Fig. 14). The abrupt basal contact with Katherine Group quartz arenite is overlain by approximately 20 m of poorly exposed, dark grey to black siltstone and shale followed by three metres of interlayered siltstone and
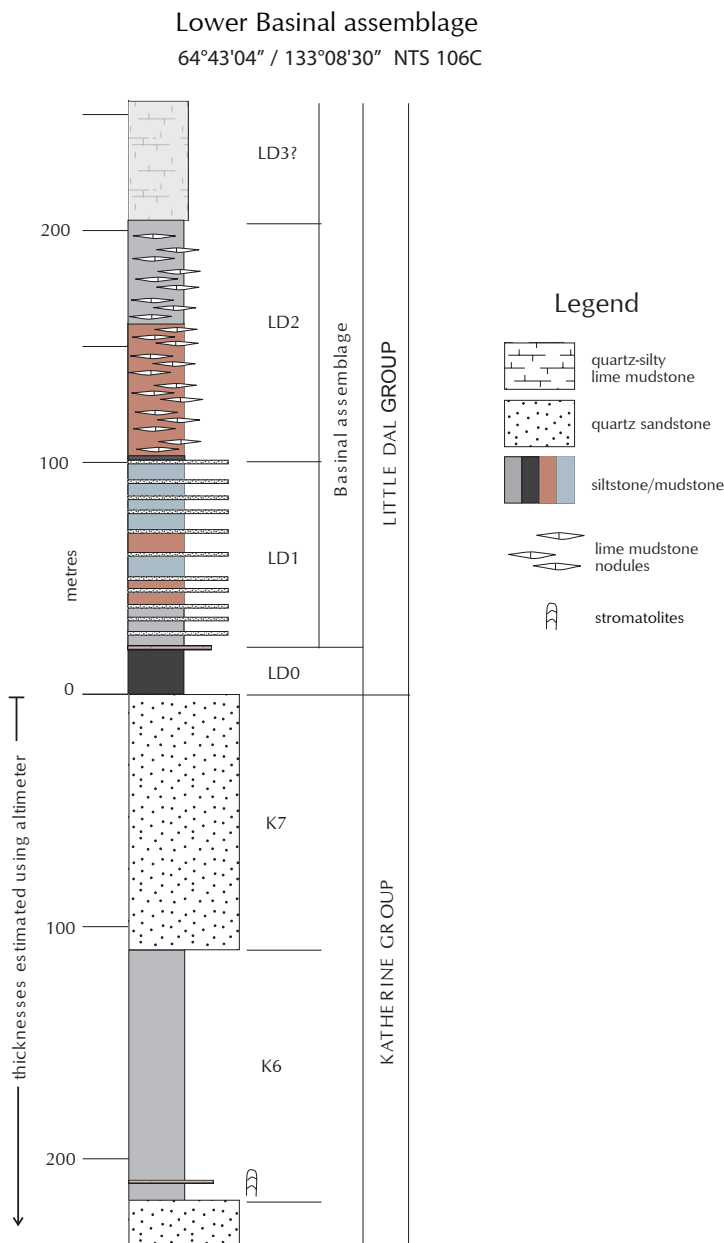
Figure 14. *Measured section of the lower part of the Basinal assemblage at a ridge location 7 km south-southwest of Mount Profeit. Column width indicates weathering profile. Coloured fills indicate weathering colour. Sequence-stratigraphic interpretations are based on the strikingly similar stratigraphy of the Basinal assemblage in the NWT (Turner and Long, 2008). Katherine Group talus below the ridge was crudely measured using an altimeter. Rough position of orange-weathering stromatolite (Fig. 13d) in unit K6 is indicated.*

quartz sandstone, capped by a thin, medium brown-weathering dolomudstone. The interval from 23 to 102 m consists of dark grey, brown, maroon, green, and tan-weathering siltstone (Fig. 15b) with subordinate ripple cross-laminated quartz sandstone. At 102 m is a thin but conspicuous (<1 m) black shale, which is then overlain by 102 m of maroon and greenish-tan-weathering siltstone with abundant lime mudstone nodules and local thin lime mudstone layers (Fig. 15c-e). This is overlain gradationally over 3 m by 50 m of platy, fissile, calcareous siltstone (Fig. 15f). The section (254 m total thickness) ends at a mountain peak.

INTERPRETATION

This succession is strikingly similar to the lower Basinal assemblage of the Little Dal Group (probably up to the middle of Basinal member 3; Turner *et al.*, 1997; Turner and Long, 2008; Turner, in press b). Like the underlying Katherine Group strata in this area, but unlike the units below the Katherine Group, paleoenvironments and stratigraphic expression closely resemble those of equivalent units in the Mackenzie Mountains. The Basinal assemblage consists of deeper-water carbonate rocks and terrigenous mudrocks. Deposition took place below the photic zone and below storm wave-base. The silt and clay-grade terrigenous material represents hemipelagic deposition and possibly very weak turbidity currents, whereas much of the carbonate mudstone was probably contributed by the settling of carbonate mud that precipitated in the overlying water column (Turner *et al.*, 1997).

The lowermost 23 m are interpreted as the first third-order stratigraphic cycle of the Little Dal Group (LD0; Turner and Long, 2008), and are equivalent to the Mudcracked formation. These siltstones lack the abundant shallow-water sedimentary structures of the Mudcracked formation, and the capping carbonate, so conspicuously developed as a marker oolite in NWT, is here limited to a ferruginous dolomudstone. The overlying 79 m-thick interval of siltstone and sandstone is equivalent to the second third-order cycle in the Little Dal Group (LD1; Basinal assemblage member 1); the stromatolitic carbonate that punctuates the top of this unit in NWT is absent. Multi-coloured siltstone with nodular lime mudstone (103 m) is characteristic of the third Little Dal cycle (LD2; Basinal assemblage member 2). It is unclear whether platy-weathering silty limestone of the uppermost exposed unit belongs to Basinal assemblage member 2 or member 3.
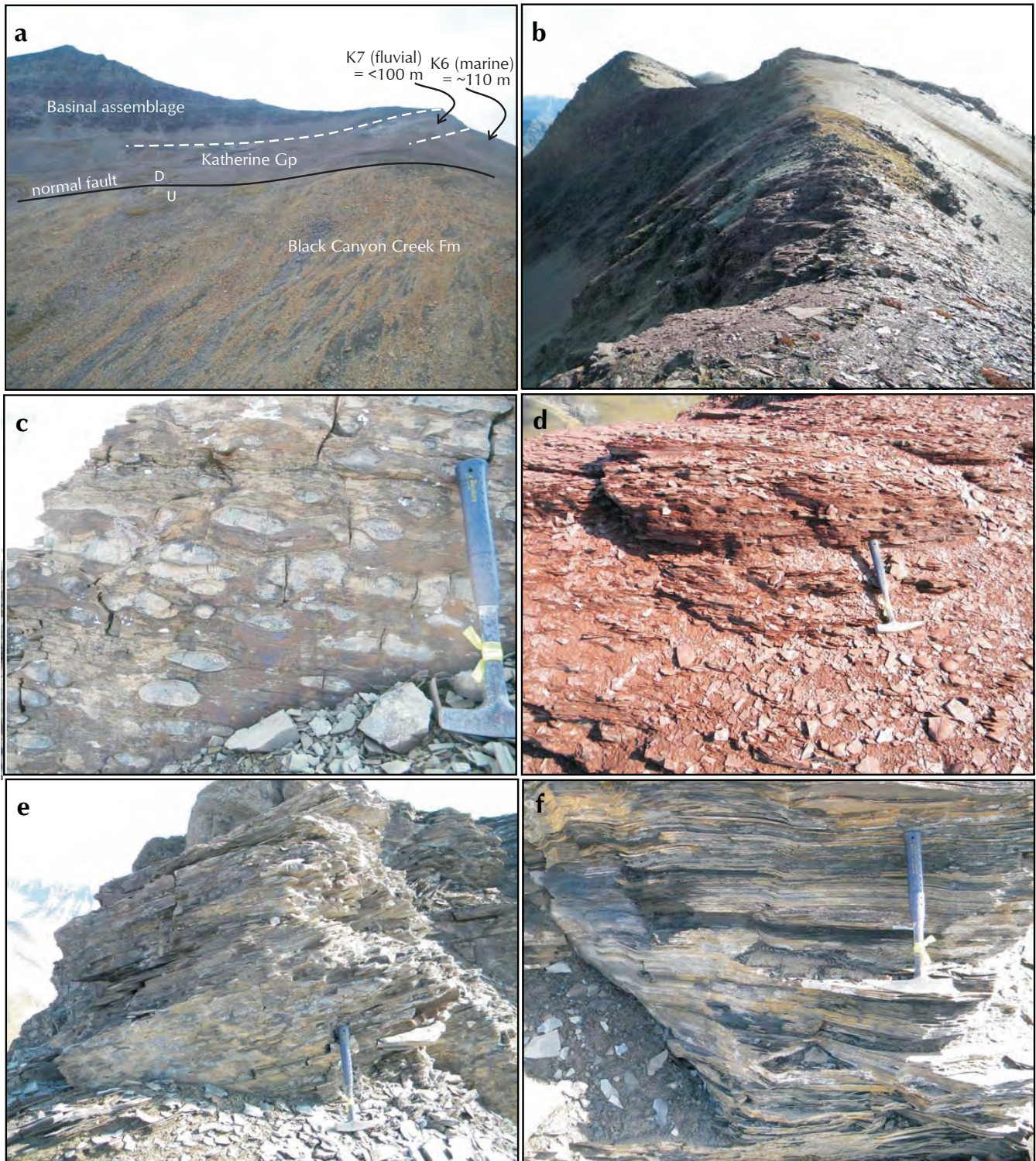
Figure 15. *Exposures and typical lithofacies of the Basinal assemblage of the Little Dal Group at location of measured section (Fig. 14).* ***(a)*** *Basal Little Dal Group overlies Katherine Group talus south of a normal fault, in the only Little Dal Group exposure in the Wernecke Mountains that has been documented to date (view to south).* ***(b)*** *View up-section from 50 m above section base shows maroon siltstone-dominated interval of lower Basinal assemblage.* ***(c)*** *Lime mudstone nodules in grey-weathering siltstone at 100 m stratigraphic elevation.* ***(d)*** *Maroon siltstone with thin beds and nodules of lime mudstone at 150 m stratigraphic elevation.* ***(e)*** *Lime mudstone nodules become less abundant at about 200 m stratigraphic elevation.* ***(f)*** *Uppermost ~50 m of the measured section consist of fissile, argillaceous limestone.*

Thorkelson *et al.* (2003) described Little Dal Group strata from NTS 106E as consisting of approximately 500 m of carbonate mudstone and black shale. Such a composition is typical of the deepest-water areas of the Basinal assemblage of the Little Dal Group in NWT (Aitken, 1981; Turner *et al.*, 1997; Turner and Long 2008). Previous interpretations of the basin configuration during this time interval were based on sections from NWT, with the northwestern-most section in NTS 106F just east of the Yukon-NWT border, where there exists indications of westward-shallowing and an absence of the deep-water black shale facies. The presence in the Basinal assemblage of black shale in NTS 106E, but of red and grey-weathering siltstone in NTS 106C (this study) points to a complex basin-floor paleotopography that lay at a variety of depths below a water column that was redox-stratified (Turner and Long, 2008).

CORRELATION

The Basinal assemblage is equivalent to abandoned Pinguicula Group unit 'F' (Eisbacher, 1981). It correlates northeastward from the Mackenzie Mountains to the Boot Inlet Formation of the Shaler Supergroup of Victoria Island and adjacent mainland (Fig. 3c). For proposed correlations to inliers west of the Wernecke Mountains, the reader is referred to Rainbird *et al.* (1996, 1997), Abbott (1997), Cook and MacLean (2004), Thorkelson *et al.* (2005), Long *et al.* (2008), and Macdonald and Roots (2009).

DISTRIBUTION AND MAPPING

The lack of detailed mapping in the MMSG in the Wernecke Mountains precludes assessment of the areal extent of this unit, or determination of the highest Little Dal Group stratigraphic unit present in the area.

ECONOMIC POTENTIAL

The economic potential of the lower Little Dal Group in the Wernecke Mountains is unknown. In NWT, part of the Basinal assemblage (equivalent to lower part of the nodular lime mudstone and siltstone interval) consists of black shale that probably accumulated under euxinic basin water. Although black shale is limited in the measured section of this study to <1 m in thickness, strata of the same interval to the northwest (NTS 106E; Thorkelson *et al.*, 2003) are reported to contain black shale, which may reflect the development of deep-water euxinia in more than one area of the basin. The extent and cause of basin extension and excessive subsidence during this time is as yet unknown, and the composition and origin

of black shale of this interval in NWT are currently being studied. It remains unknown whether the black shale may have economic potential on its own, or whether it may have contributed metals to known showings in associated carbonate strata in NWT.

Parts of the Gayna River deposit in NWT (Hewton, 1982; Turner, 2007) are hosted by the upper Basinal assemblage, and vein-filling sphalerite is known in reefs of the Basinal assemblage away from the Gayna River deposit (personal observation). It is not known whether any of the four thick formations that overlie the Basinal assemblage may be present somewhere in the Wernecke Mountains. A superficial assessment of the economic potential of the Little Dal Group in Yukon is not possible without knowledge of its full stratigraphic expression and areal extent.

FUTURE WORK

This project has identified numerous aspects of the MMSG in the Wernecke Mountains that merit further investigation. Among these, the nature of the basal contact is critical; this is the long-sought interface between two major intervals in the Proterozoic evolution of northwestern Laurentia. Is this contact truly an angular unconformity, and does it exhibit evidence of extensive exposure, erosion, or tectonism? Is there facies variation in the basal Dolores Creek Formation that would reflect paleotopographic variation associated with rifting? The lateral continuity of the Dolores Creek Formation's stratigraphy requires investigation, to determine whether extensional basin segmentation took place.

The proposed correlation of the Black Canyon Creek Formation with the 'H1 unit' in NWT should be tested using stable isotope stratigraphy. A full section of the Tarn Lake Formation needs to be documented in detail. Perplexing thickness and facies patterns in the Tarn Lake Formation suggest significant syndepositional tectonic activity, and require documentation to establish the location of sedimentary depocentres and possible synsedimentary faults.

The Katherine Group remains undescribed; its basic stratigraphy needs to be established to determine whether its 7 formation-scale units are expressed in Yukon. Paleocurrent and isopach studies in the Katherine Group will help to establish basin deepening directions, which will reflect the regional basin configuration and add to the growing understanding of this tectonostratigraphically complex succession.

Areas south of Pinguicula Lake need to be examined to determine whether Little Dal Group strata younger than the Basinal assemblage may be present. All of these future endeavours will be fundamental to both understanding how the MMSG strata in the Wernecke Mountains correlate eastward to NWT and westward to other inliers in Yukon, and to evaluating the economic potential of the MMSG.

SUMMARY

Strata of the MMSG were examined in detail on the flanks of an un-named mountain near the junction of 'Dolores Creek' with the Bonnet Plume River, in NTS 106C (Fig. 1) and on a ridge approximately 7 km south-southwest of Mount Profeit. The Dolores Creek Formation (~260 m thick; Fig. 2) represents the basal strata of the MMSG, which have remained hitherto unknown. This unit is conformably overlain by a carbonate succession (Black Canyon Creek Formation; ~285 m thick) that is probably stratigraphically equivalent to the 'H1 unit' in the Mackenzie Mountains. Gradationally overlying the Black Canyon Creek Formation is a siltstone-dominated unit (Tarn Lake Formation; >265 m thick) and a thick succession dominated by quartz arenite (Katherine Group; unmeasured). The highest MMSG unit discovered to date in this area belongs to the Basinal assemblage of the lower Little Dal Group (>250 m). It is unknown how much of the upper part of the MMSG may be present in the Wernecke Mountains (Little Dal Group is 2-3 km thick in the Mackenzie Mountains). The economic potential of the MMSG in the Wernecke Mountains is unknown and requires further investigation.

ACKNOWLEDGEMENTS

REFERENCES

Abbott, G., 1997. Geology of the upper Hart River area, eastern Ogilvie Mountains, Yukon Territory (116A/10, 116A/11). Exploration and Geological Services Division, Yukon Region, Indian and Northern Affairs Canada, Bulletin 9, 91 p.

Aitken, J.D., 1981. Stratigraphy and sedimentology of the Upper Proterozoic Little Dal Group, Mackenzie Mountains, Northwest Territories. In: Proterozoic Basins of Canada, F.H.A. Campbell (ed.), Geological Survey of Canada, Paper 81-10, p. 47-71.

Cook, D.G. and MacLean, B.C., 2004. Subsurface Proterozoic stratigraphy and tectonics of the western plains of the Northwest Territories. Geological Survey of Canada, Bulletin 575, 91 p.

Eisbacher, G.H., 1978. Two major Proterozoic unconformities, northern Cordillera. Geological Survey of Canada, Paper 78-1A, p. 53-58.

Eisbacher, G.H., 1981. Sedimentary tectonics and glacial record in the Windermere Supergroup, Mackenzie Mountains, northwestern Canada. Geological Survey of Canada, Paper 80-27, 40 p.

Gabrielse, H., Blusson, S.L. and Roddick, J.A., 1973. Flat River, Glacier Lake, and Wrigley Lake map areas (95E, L, M), District of Mackenzie and Yukon Territory. Geological Survey of Canada, Memoir 366, 153 p. and 3 maps.

Heaman, L.M., LeCheminant, A.N. and Rainbird, R.H., 1992. Nature and timing of Franklin igneous events, Canada: Implications for a late Proterozoic mantle plume and the break-up of Laurentia. Earth and Planetary Science Letters, vol. 109, p. 117-131.

Hewton, R.S., 1982. Gayna River: A Proterozoic Mississippi Valley-type zinc-lead deposit. In: Precambrian Sulphide Deposits, R.W. Hutchinson, C.D. Spence and J.M. Franklin (eds.), Geological Association of Canada, Special Paper 25, p. 667-700.

Jefferson, C.W. and Parrish, R.R., 1989. Late Proterozoic stratigraphy, U-Pb zircon ages, and rift tectonics, Mackenzie Mountains, northwestern Canada. Canadian Journal of Earth Sciences vol. 26, p. 1784-1801.

Jefferson, C.W. and Young, G.M., 1989. Late Proterozoic orange-weathering stromatolite biostrome, Mackenzie Mountains and western Arctic Canada. *In:* Reefs, Canada and adjacent area, H.H.J. Geldsetzer, N.P. James and G.E. Tebbut (eds.), Canadian Society of Petroleum Geologists, Memoir 13, p. 72-80.

Leslie, C.D., 2009. Detrital zircon geochronology and rift-related magmatism: central Mackenzie Mountains, Northwest Territories. Unpublished MSc thesis, University of British Columbia, Vancouver, BC, 236 p.

Long, D.G.F., *in press* a. Katherine Group. *In:* Geology of the Northern Cordillera, central Mackenzie Mountains; Sekwi Mountain (105P), Mount Eduni (106A), and northwestern Wrigley (95M) Lake map areas, Northwest Territories; Northwest Territories Geoscience Office, NWT Open File, 2011.

Long, D.G.F., *in press* b. Tsezotene Fm. *In:* Geology of the Northern Cordillera, central Mackenzie Mountains; Sekwi Mountain (105P), Mount Eduni (106A), and northwestern Wrigley (95M) Lake map areas, Northwest Territories, Northwest Territories Geoscience Office, NWT Open File, 2011.

Long, D.G.F., Rainbird, R.H., Turner, E.C. and MacNaughton, R.B., 2008. Early Neoproterozoic strata (Sequence B) of mainland northern Canada and Victoria and Banks islands: a contribution to the Geological Atlas of the Northern Canadian Mainland Sedimentary Basin. Geological Survey of Canada, Open File 5700, 27 p.

Macdonald, F.A. and Roots, C.F., 2009. Upper Fifteenmile Group in the Ogilvie Mountains and correlations of early Neoproterozoic strata in the northern Cordillera. *In:* Yukon Exploration and Geology 2009, K.E. MacFarlane, L.H. Weston and L.R. Blackburn (eds.), Yukon Geological Survey, p. 237-252.

Norris, D.K., 1982a. Geology, Wind River, Yukon Territory. Geological Survey of Canada, Map 1528A, scale 1:250 000.

Norris, D.K., 1982b. Geology, Snake River, Yukon-Northwest Territories. Geological Survey of Canada, Map 1529A, scale 1:250 000.

Rainbird, R.H., Jefferson, C.W. and Young, G.M., 1996. The early Neoproterozoic sedimentary Succession B of northwestern Laurentia: correlations and paleogeographic significance. Geological Society of America Bulletin, vol. 108, p. 454-470.

Rainbird, R.H., McNicoll, V.J., Thériault, R.J., Heaman, L.M., Abbot, J.G., Long, D.G.F. and Thorkelson, D.J., 1997. Pan-continental river system draining Grenville Orogen recorded by U-Pb and Sm-Nd geochronology of Neoproterozoic quartz arenites and mudrocks, northwestern Canada. Journal of Geology, vol. 105, p. 1-17.

Taylor, S. and McLennan, S.M., 1985. The Continental Crust: Its Composition and Evolution. Blackwell Scientific Publications, 312 p.

Thorkelson, D.J., 2000. Geology and mineral occurrences of the Slats Creek, Fairchild Lake and 'Dolores Creek' areas, Wernecke Mountains (106D/16, 106C/13, 106C/14), Yukon Territory. Exploration and Geological Services Division, Yukon Region, Indian and Northern Affairs Canada, Bulletin 10, 73 p.

Thorkelson, D.J. and Wallace, C.A., 1998. Geological map of 'Dolores Creek' map area (106C/14), Wernecke Mountains, Yukon. Exploration and Geological Services Division, Yukon, Indian and Northern Affairs Canada Geoscience Map 1998-11, scale 1:50 000.

Thorkelson, D.J., Laughton, J.R., Hunt, J.A. and Baker, T., 2003. Geology and mineral occurrences of the Quartet Lakes map area (NTS 106E/1), Wernecke and Mackenzie mountains, Yukon. *In:* Yukon Exploration and Geology 2002, D.S. Emond and L.L. Lewis (eds.), Exploration and Geological Services Division, Yukon Region, Indian and Northern Affairs Canada, p. 223-239.

Thorkelson, D.J., Abbott, J.G., Mortensen, J.K., Creaser, R.A., Villeneuve, M.E., McNicoll, V.J. and Layer, P.W., 2005. Early and Middle Proterozoic evolution of Yukon, Canada. Canadian Journal of Earth Sciences, vol. 42, p. 1045-1071.

Turner, E.C., 2007. Lithofacies and structural controls on Zn-Pb mineralization at Gayna River, NWT. GAC-MAC Joint meeting 32, May 23-25, 2007.

Turner, E.C., *in press* a. 'H1 unit'. *In:* Geology of the Northern Cordillera, central Mackenzie Mountains; Sekwi Mountain (105P), Mount Eduni (106A), and northwestern Wrigley (95M) Lake map areas, Northwest Territories Geoscience Office, NWT Open File, 2011.

Turner, E.C., *in press* b. Little Dal Group. *In:* Geology of the Northern Cordillera, central Mackenzie Mountains; Sekwi Mountain (105P), Mount Eduni (106A), and northwestern Wrigley (95M) Lake map areas, Northwest Territories Geoscience Office, NWT Open File, 2011.

Turner, E.C. and Long, D.G.F., 2008. Basin architecture and syndepositional fault activity during deposition of the Neoproterozoic Mackenzie Mountains supergroup, N.W.T., Canada. Canadian Journal of Earth Sciences, vol. 45, p. 1159-1184.

Turner, E.C., James, N.P. and Narbonne, G.M., 1997. Growth dynamics of Neoproterozoic calcimicrobial reefs, Mackenzie Mountains, northwest Canada. Journal of Sedimentary Research, vol. 67, p. 437-450.

Young, G.M., Jefferson, C.W., Delaney, G.D. and Yeo, G.M., 1979. Middle and Upper Proterozoic evolution of the northern Canadian Cordillera and Shield. Geology, vol. 7, p. 125– 128.

Geology of new gold discoveries in the Coffee Creek area, White Gold District, west-central Yukon

Alan J. Wainwright[1], Adam T. Simmons, Craig S. Finnigan, Tim R. Smith and Robert L. Carpenter
Kaminak Gold Corp.

ABSTRACT

A new widespread, structurally controlled gold mineralizing system has been identified during the 2010 exploration drilling program at the Coffee Project, west-central Yukon. The Coffee Creek area is underlain by a sequence of shallowly to moderately south to southwest-dipping Paleozoic metamorphic rocks that are considered to be part of the Yukon-Tanana terrane and are intruded by the Cretaceous Coffee Creek granite along a west to northwest-trending contact. During the 2010 drilling program, structurally controlled gold mineralization was discovered in all major lithological units underlying the Coffee property. Importantly, these mineralized zones correspond to a number of discrete structural corridors. The gold zones are steeply dipping and characterized by extensive silicification in addition to sericite and clay alteration accompanied by variable As-Ag-Sb-Ba-Mo enrichment. Polyphase breccias of both hydrothermal and tectonic origin, in addition to andesite-dacite dykes, are common within the gold-bearing structural corridors. The dominant sulphide is pyrite, although trace arsenopyrite, chalcopyrite and stibnite are observed locally. The similarity of breccia textures and alteration/sulphide mineralogy between all gold zones currently defined on the Coffee property implies a common mineralizing event.

[1]alanw@kaminak.com

INTRODUCTION

Economic accumulations of gold that occur in the Dawson Range of west-central Yukon include the historic and producing placer deposits of the Klondike, in addition to numerous auriferous bedrock deposits related to fossil magmatic-hydrothermal systems (*e.g.,* the Mesozoic Casino and Minto porphyries; Mortensen and Hart, 2010). A surge of exploration activity in the region, in part spurred by the recent discovery of 'Golden Saddle' on the White Gold property by the former Underworld Resources, has led to several new discoveries that indicate the emergence of a new gold district in Yukon. The Coffee property (Fig. 1a), located 130 km south of Dawson City and 30 km south of the Golden Saddle deposit, represents the southernmost known gold occurrence of this new district. Significant and widespread gold mineralization has been identified during the 2010 exploration drilling program at the Coffee Project. Gold is hosted in steeply dipping structures outlined by a 15 km-long, east to northeast-trending array of gold-in-soil anomalies. In this contribution we describe the geology of the Coffee property, as well as breccia textures, alteration, sulphide phases and the nature of mineralization that occurs within the gold zones discovered to date. The mineralized zones are referred to as Supremo, Latte, Double Double, Americano, Espresso and Kona (Fig. 2). Details of the host lithologies, style of gold mineralization and important mineralized intersections are summarized for each zone in Table 1.

REGIONAL GEOLOGY

The Coffee Project is located in the Yukon-Tanana terrane (YTT), an accreted pericratonic sequence that covers a large part of the northern Cordillera from northern British Columbia to east-central Alaska (Colpron *et al.,* 2006; Fig. 1a). The YTT hosts several gold deposits and occurrences that are genetically related to Mesozoic intrusions, including the Mt Nansen past-producing mine, the Nucleus deposit at Freegold Mountain, and the Casino Cu-Au-Mo porphyry deposit, located southeast of the Coffee property (Fig. 1b; Bennett *et al.,* 2010; Bineli Betsi and Bennett, 2010). The YTT consists of Paleozoic schists and gneisses that were deformed and metamorphosed in the late Paleozoic, and intruded by several suites of

Mesozoic intrusions that range in age from Jurassic to Eocene (Mortensen, 1992; Colpron *et al.,* 2006; Fig. 1b). The Paleozoic rocks are pervasively foliated and contain at least two overprinting rock fabrics (Ryan and Gordey, 2004; Mackenzie and Craw, 2010; MacKenzie *et al.,* 2008). From Late Permian to Early Jurassic, the rocks were tectonically stacked along foliation-parallel thrust faults (Mortensen, 1996; Berman *et al.,* 2007). Extensional (or at least partly tensional) tectonics, although not described in the Dawson Range, may have occurred during the mid-Cretaceous in western Yukon, similar to that documented in east-central Alaska (Pavlis *et al.,* 1993).

PROPERTY GEOLOGY

For simplicity, we have subdivided the geology of the Coffee property into two main west to northwest-trending, south to southwest-dipping panels of metamorphic rocks that border a third intrusive panel to the south. From north to south, these include (i) an augen gneiss-mafic schist sequence (augen gneiss panel) that is overlain by (ii) a heterogeneous package of intercalated biotite-feldspar schist, highly-strained felsic rocks, metagabbro, talc schist and metacarbonate (biotite schist panel). The foliated rock sequences are intruded by (iii) mid to Late Cretaceous equigranular granite along a west to northwest-trending contact located in the south end of the property (Fig. 2a). Both the Paleozoic metamorphic rocks and the mid to Late Cretaceous intrusive complex are cut by intermediate to felsic dykes of unknown age. Numerous structures are interpreted based on mapping, drill core logging and ground magnetic survey interpretation (Fig. 2b). The main rock units are briefly described below and summarized in Table 2.

AUGEN GNEISS

Augen gneiss, which represents an important host rock lithology in the Supremo area, is characterized by variable amounts of quartz, alkali feldspar augens (typically 0.5-1.5 cm in length), biotite and muscovite (Fig. 3a). Augen gneiss is structurally intercalated with subordinate biotite-feldspar (±quartz, ±muscovite) schist (Fig. 3b). Discontinuous lenses of biotite schist vary from 0.3 to 10 m apparent width as observed in drill core, and represent approximately 30% of the overall rock volume within the unit.
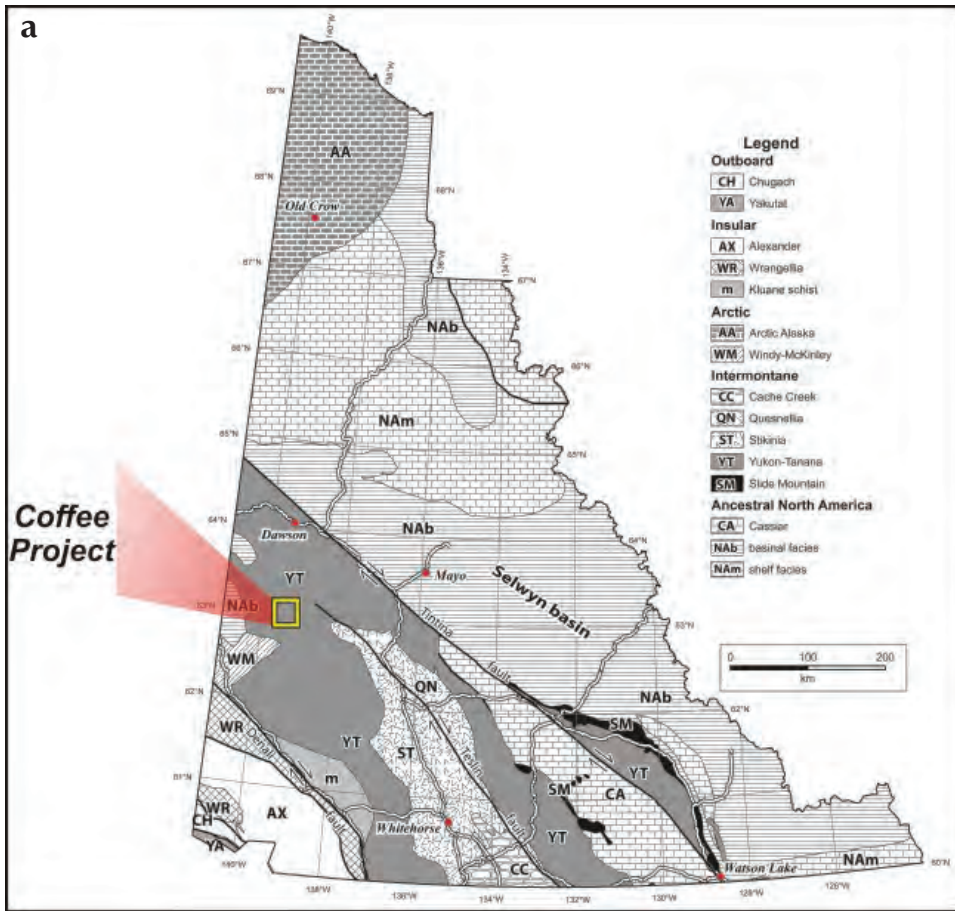
Figure 1. (a) Regional terrane and location map, and *(b)* regional geology map for the Dawson Range.
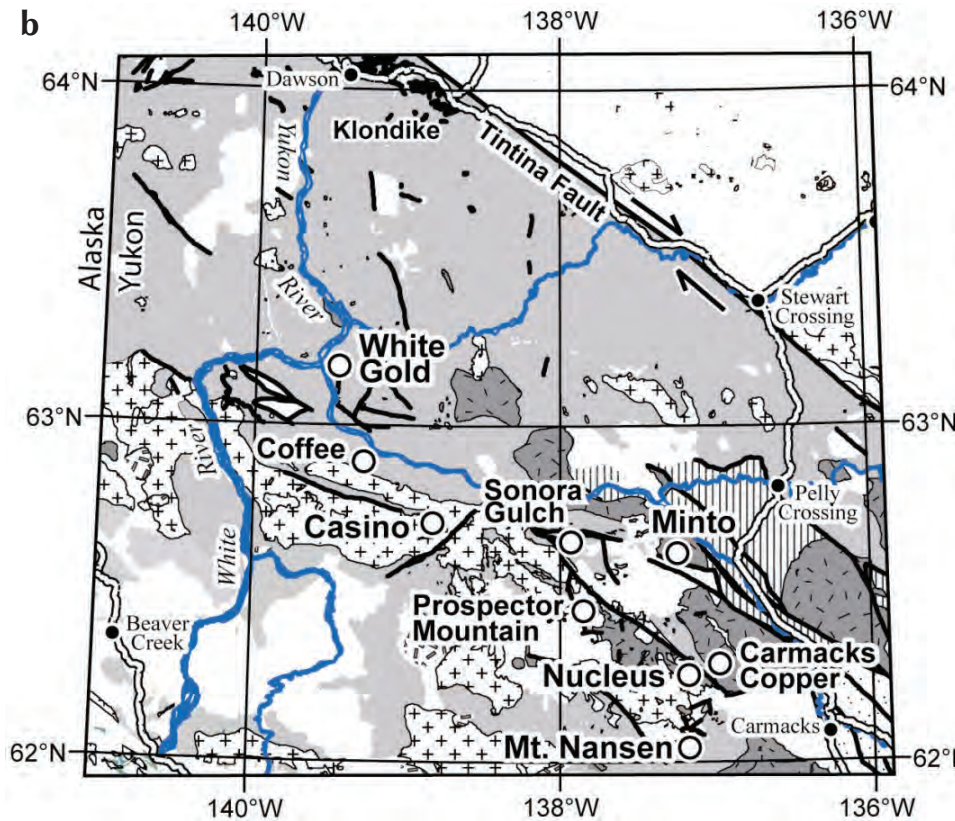
Table 1. Discrete mineralized areas at the Coffee property.

Zone	Host rock panel	Au occurrence and representative grade	Comment
Supremo Zone	augen gneiss	narrow Au-bearing brittle structures; *e.g.,* CFD001, 17.07g/t over 15.50 m; CFD016, 12.43g/t Au over 14 m	gold commonly hosted in matrix-supported breccia and dacite dykes
Latte Zone	biotite-feldspar schist	**UPPER LATTE**: wide zones of disseminated and fracture controlled sulphide and oxide; *e.g.,* CFD011, 2.35g/t over 51 m; CFD044, 1.83g/t over 58 m **LOWER LATTE**: narrow zones of high grade gold along discrete structures; *e.g.,* CFD010, 3.71g/t over 16 m; CFD012, 17.4g/t over 1 m; CFD048, 5.55g/t over 9 m	gold hosted in limonitic high-strain rocks; Fe-oxides replace disseminated and fracture-controlled pyrite (Upper Latte); sooty-pyrite rich gold zones in narrow, high-grade shear zones (Lower Latte)
Double Double Zone	biotite-feldspar schist	narrow gold bearing brittle structures; *e.g.,* CFD027, 6.3g/t over 35 m; CFD028, 15.91g/t over 5 m	gold hosted in matrix-supported breccia including dacite porphyry fragment breccia
Kona Zone	granite	broad zones of fracture-controlled and disseminated pyrite associated with dacite dykes; *e.g.,* CFD053, 2.21g/t over 56.75 m and 1.92g/t over 23 m	gold hosted in quartz-sericite altered granite; Fe-oxides after disseminated pyrite, pyrite veinlet stockworks and sooty-pyrite rich shear zones
Americano Zone	granite	zones of fracture-controlled and disseminated pyrite; *e.g.,* CFD064, 2.36g/t over 18 m	gold hosted in quartz-sericite altered granite similar to Kona
Espresso Zone	granite	zones of fracture-controlled and disseminated pyrite; low-grade gold encountered	gold hosted in quartz-sericite altered granite similar to Kona

Table 2. Rock units mapped in drill core and outcrop at the Coffee property.

Rock unit	Location	Comment
augen gneiss	Supremo area	intercalated with biotite-feldspar schist; dominant host rocks surrounding high-grade breccias in the Supremo zone
ribbon quartz mylonite	Upper Sequence at Latte zone; rare thin intervals in the Lower Sequence	favourable gold host in the Upper Latte zone
feldspar-muscovite schist	occurs in the Latte zone; most commonly in the Upper Sequence	favourable gold host in the Upper Latte zone
biotite-feldspar schist	dominant unit in central panel	minor intercalated metacarbonate; host for high-grade gold in the Lower Latte zone; host for Double Double zone
talc schist	talc schist occurs in the vicinity of metagabbro; possible strained mafic-ultramafic intrusions	not associated with gold
metagabbro	below Lower Sequence at Latte	not associated with gold
dacite dykes	cuts all rock units	strong spatial association with gold zones
andesite dykes	cuts all rock units	weaker spatial association with gold zones
granite	Kona area	large Coffee Creek granite batholith trends west-northwest. mid to Late Cretaceous

BIOTITE SCHIST

Biotite-feldspar (± quartz, ± muscovite) schist dominates the central rock panel in the Coffee property area (Figs. 2 and 3b). Mineralogy varies from biotite-feldspar dominant to quartz-muscovite dominant, defining compositional layering in the schist, which ranges from a few centimetres to >10 cm in thickness. Biotite-feldspar schist is locally intercalated with metacarbonate bands that range in width from 3 cm to >1 m and which increase in volumetric significance to the south. The degree of penetrative strain development is also variable, but increases significantly to the south, particularly within close proximity to the Latte zone.

Biotite schist is structurally interleaved locally with mylonite (comprising predominantly feldspar-quartz-muscovite) and metagabbro lenses. The highly strained feldspar-quartz-muscovite rocks are characterized by a thinly banded texture that includes pale mica-rich layers alternating with feldspar-rich and ribbon-quartz layers (Fig. 3c). Highly strained metagabbro is common within the biotite schist unit and locally exhibits intense foliation development and compositional banding (Fig. 3d). The high-strain fabric locally wraps around the more competent pyroxene porphyroclasts. Subordinate talc schist intervals are spatially associated with the metagabbro zones, and are characterized by strongly altered pale green and fine-grained foliated chlorite (Mg-chlorite?), which is associated with local coarse magnetite crystals.

GRANITE

The Coffee Creek granite underlies the southern third part of the map area and is characterized by an equigranular texture comprising approximately 30-50% plagioclase (5-10 mm in length), 20-30% K-feldspar (5-12 mm in length), 20-30% quartz (3-8 mm in diameter), 3-5% biotite (1-3 mm in diameter) and 3-5% hornblende (1-3 mm in length) (Fig. 3e). The contact between the granite and Paleozoic rocks was observed in drillhole CFD054 (at 54.5 m). Immediately along the contact zone, a 50 cm-wide andesite dyke has been emplaced in a pre-existing zone of weakness between the two adjacent lithologies. The foliated rocks are neither hornfelsed nor strongly altered in the drill core adjacent to the intrusion and no significant chilled margin textures have been observed within the granite.

DYKE SUITES

Andesite dykes are characterized by fine to coarse-grained plagioclase phenocrysts occurring within a dark aphanitic groundmass (Fig. 3f). The unit is largely unaltered and does not host gold mineralization. Although there is a spatial association between the andesite dykes and the gold-bearing structures, we interpret this suite to post-date the gold mineralizing event that occurs on the Coffee property.

Dacite porphyry dykes are unfoliated and are spatially associated with gold mineralization within several zones across the Coffee property (*e.g.,* Supremo, Latte, Kona). This suite of dykes is characterized by 10-30% feldspar phenocrysts (1-3 mm in length) and minor quartz (0-5%; <1 mm in diameter) that occur within an aphanitic light grey-green groundmass. Ferromagnesian mineral phases (hornblende, ± biotite) are the focus of macroscopic alteration, and where identified, have been pervasively replaced by pyrite.

STRUCTURAL GEOLOGY

Structural data measured from oriented drill core indicates that the transposed fabric of the augen gneiss in the Supremo zone (augen gneiss panel) strikes northwest and dips shallowly to the southwest (<20°; Fig. 4a), whereas foliation measurements from the Latte and Double Double zones indicate that the prevailing structural grain dips more steeply (40-50°; Figs. 4b,c), but maintains the same strike. Faults which are ubiquitous in drill core are both steeply dipping and foliation parallel, based on cross section interpretation of -50° and -70° paired drillholes (*i.e.,* shallow to moderate dip). Importantly, correlations between cross section interpretations and assay interval results indicate that gold-bearing structures are steeply dipping and crosscut all rock units throughout the Coffee property. Data from oriented drill core, such as vein orientations and breccia zone contacts, are less reliable due to the incohesive nature of drill core from the gold-rich zones.

The orientation of gold-bearing structures varies across the Coffee property. Within the Supremo zone, located in the northeast part of the property, the controlling structures are interpreted to strike north and cut the augen gneiss host. In contrast, within the Latte and Double Double zones (1.5 km south and 1.5 km southeast of Supremo, respectively), gold mineralization is associated
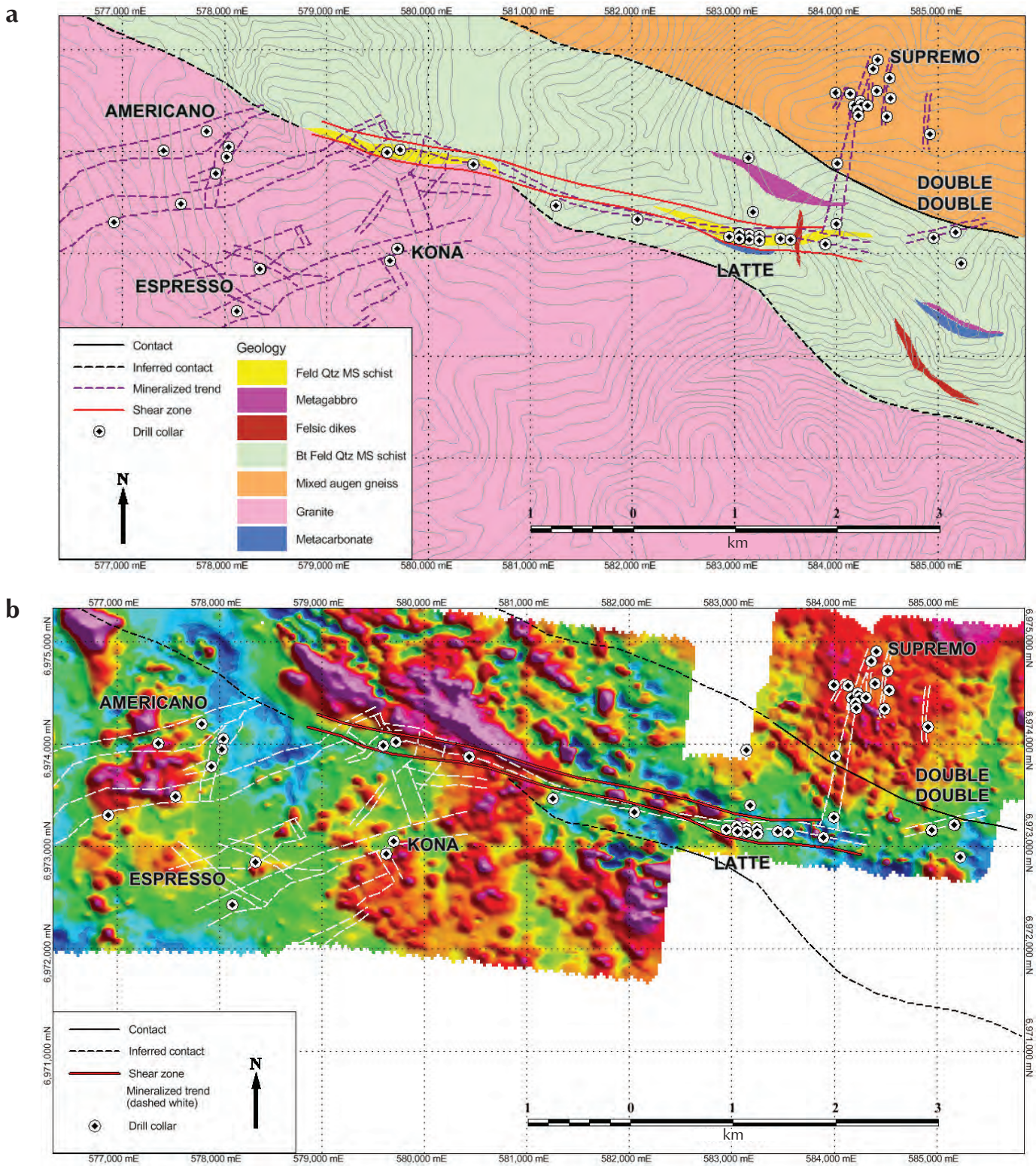
Figure 2. (a) *Simplified property geology map displaying lithologies, structures and drill collar locations, and* **(b)** *map of ground magnetic data and interpreted structures. Coordinate system is UTM NAD83 zone 7.*

Figure 3. Photographs of Coffee property area rock units: **(a)** augen gneiss (CFD033 – 167.3 m); **(b)** biotite-feldspar schist (CFD067 – 239 m); **(c)** feldspar-quartz mylonite (CFD038 – 188.3 m); **(d)** mylonitized gabbro (CFD060 – 145 m); **(e)** granite (outcrop; Kona area); and **(f)** andesite porphyry (sampled from trench in the Supremo area).
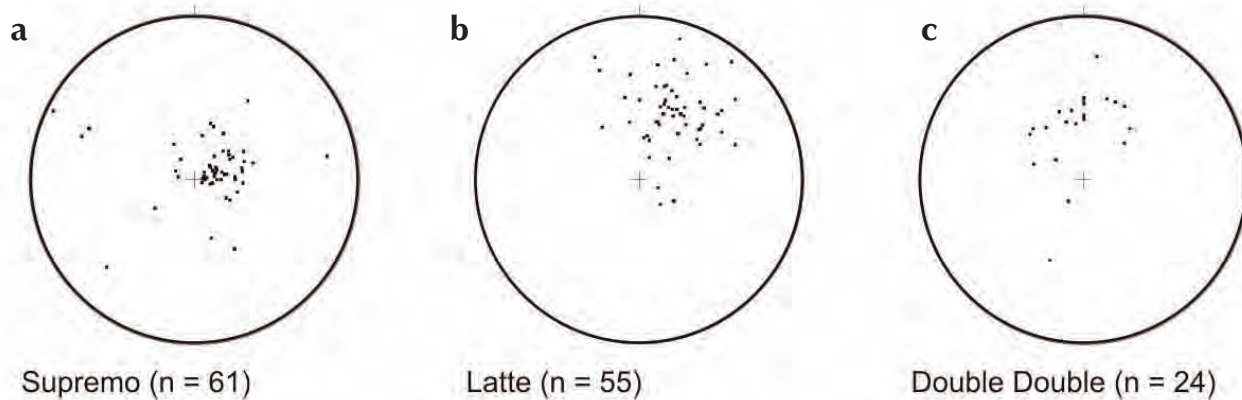
Figure 4. Lower hemisphere stereonet projections of poles to foliation: (a) Supremo; (b) Latte; and (c) Double Double.

with regionally significant, east-trending, south-dipping structures (Latte structure) and related splays (Fig. 2). The Latte structure comprises breccias that overprint older ductile strain fabrics occurring within the host biotite schist, consistent with a multiply reactivated shear zone environment. The Kona, Espresso and Americano gold zones which are located 3 to 8 km to the west-southwest of Supremo (Fig. 2) are hosted in steeply dipping fault zones that crosscut the Coffee Creek granite. The fault zones are characterized by brecciation, intense fracturing, sulphide veining and pervasive alteration of primary minerals. These structures correspond to a variety of orientations demarcated by linear gold-in-soil anomalies, and may represent an array of main faults connected by linking structures as interpreted in Figure 5.

OVERVIEW OF MINERALIZED ZONES

Gold mineralization throughout the Coffee property is characterized by extensive silica, sericite and clay alteration and is accompanied by variable As-Ag-Sb-Ba-Mo enrichment. Polyphase breccias (clast to matrix-supported) are commonly spatially associated with dacite dyke emplacement. The dominant sulphide species occurring within breccia zones is pyrite (arsenian and non-arsenian) with trace arsenopyrite, chalcopyrite and stibnite. Thin, microcrystalline silica veinlets are observed within gold zones, whereas opaque, white, foliation-parallel veins and vein fragments are common in the host rocks, and not commonly observed within the gold zones. Mineralization thus far encountered is strongly oxidized, with depths of oxidation ranging from 75 to 100 m. Sulphides are partially to completely replaced by Fe-oxides within gold-bearing zones. The lack of any recent glaciation in the region has helped preserve the oxidized zones, which often occur less than 2 m below the overburden and/or felsenmeer.

SUPREMO

Gold mineralization within the Supremo zone occurs within a 600 m-wide corridor and is hosted within several parallel, north-trending, steeply dipping fault structures that are spaced 50 to 100 m apart. Discrete mineralized zones associated with the faults have been outlined by linear gold-in-soil anomalies and subsequently defined by drilling. Although gold mineralization is hosted within steeply dipping north-northeast structures, assays from paired -50° and -70° drillholes along the same cross section line indicate that concentrations of gold may locally have a moderate to steep plunge down the plane of the steeply dipping structures. We interpret this on the basis of the distribution of alteration mineralogy and the presence of gold within the paired holes.

Gold mineralization is associated with silicified clast breccias (Fig. 6a) and dacite dykes (Fig. 6b). Furthermore, mineralized intervals are associated with intense clay and sericite alteration in addition to abundant oxidized pyrite. Secondary limonite, which replaces pyrite, occurs as clots, disseminations, and within fracture networks in all rock types including breccia clasts and the wallrock. Peripheral to mineralized zones, alteration consists of silica, chlorite, albite and epidote. The genetic association of this distal alteration assemblage to mineralization is not yet established.

Breccias are typically associated with higher gold grades within the Supremo zone. Matrix compositions range from incompetent limonite-clay material to indurated silicified cement (Fig. 6a). Angular to subrounded clasts range from 0.5 to 5 cm in diameter and consist predominantly of highly silicified fragments and subordinate altered wallrock and dacite porphyry fragments. Breccia textures range from mature matrix-dominant phases with rounded
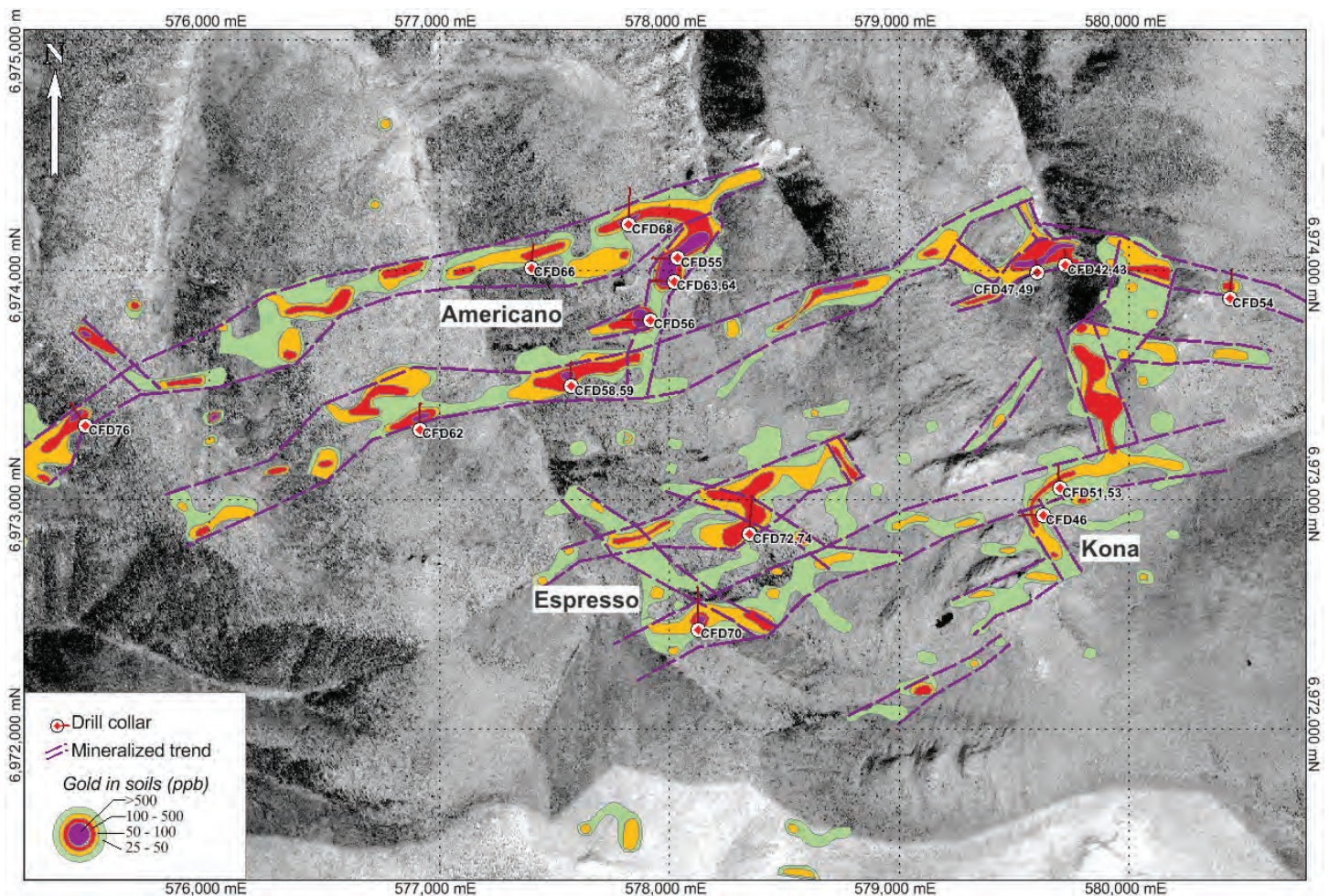
Figure 5. *Map of contoured gold-in-soil anomalies and drilled gold zones hosted in the Coffee Creek granite. Interpreted structures are indicated with dashed lines. Coordinate system is UTM NAD83 zone 7.*

fragments to wall-rock crackle breccias. Angular to subangular quartz microfragments (<1 mm) are locally observed in the matrix of all breccia subtypes observed.

Thin chalcedonic and porcelainic veins, as well as veins with open-space textures (*e.g.,* drusy and cockscomb), occur within some of the mineralized intervals. The silica veinlets cut both altered clasts and matrix material within the breccia units. Calcite veinlets are also noted, although these are not restricted to the gold-rich zones and may have formed during the loss of Ca from the alteration of plagioclase to albite in the host rocks.

LATTE

The Latte zone occurs within the biotite schist panel (Fig. 2a), and is characterized by moderately south-dipping ribbon quartz mylonite that prevails in what is termed 'Upper Latte' or the structurally higher part of the Latte

zone. Gold also occurs in deeper biotite-feldspar schist within 'Lower Latte', or the structurally lower interval of the Latte zone. Upper and Lower Latte are underlain by metagabbro intercalated with lenses of talc schist. Drilling in 2010 has defined a zone of west-trending and steeply south-dipping gold mineralization that extends for at least several hundred metres within the Latte zone. Upper and Lower Latte are defined on the basis of differences in the style of gold mineralization and the type of host rock.

Alteration associated with gold-bearing rocks within the Latte zone consists of silica, clay and sericite. Although strong limonite is noted in Upper Latte, the overall sulphide content (oxidized or unoxidized) appears to be higher in the mineralized intervals in Lower Latte.

Low to moderate gold grades over long intervals are associated with breccia and alteration zones that cut feldspar-muscovite schist, dacite dykes (Fig. 6b) and

ribbon-quartz mylonite (Fig. 6c), in the westernmost drillholes within the Upper Latte zone. In this part of the Latte zone, gold is typically not associated with biotite-feldspar schist. In contrast, higher-grade intervals of gold mineralization do occur in biotite-feldspar schist located in the easternmost part of the Latte zone. Mineralization is hosted in silicified-clast breccia with associated sulphide-rich matrix (Fig. 6d). Abundant pyrite (up to 12-15%) is strongly associated with breccia matrix and to a lesser extent located in fine sulphide veinlets that crosscut silicified host rock material.

DOUBLE DOUBLE

The Double Double zone is hosted in the biotite schist panel (Fig. 2a) in what we interpret as an east to northeast-trending splay off of the main west to northwest-trending Latte structure. Mineralization is accompanied by intense breccia development and strong quartz-sericite alteration and associated pyrite/limonite.

Mineralized breccia occurring within the Double Double zone ranges from polymictic to monomictic, and clast size varies from 1 to 4 cm. The clasts are hosted in either a clay-limonite or silica-pyrite matrix. Subangular clasts include silicified fragments of unknown origin, quartz vein fragments and dacite porphyry fragments (Fig. 6e). Sulphides are commonly oxidized to limonite and occur in clasts, matrix, as well as in networks and sub-parallel arrays of thin veinlets. Porcelainic to chalcedonic silica microveinlets are locally observed in the mineralized intervals.

KONA, ESPRESSO AND AMERICANO ZONES

The Kona, Espresso and Americano zones are hosted in the Cretaceous Coffee Creek granite and are located 3 to 8 km west of the Latte zone (Fig. 2a). Alteration typically consists of clay and limonite (Fig. 6f) with local relict zones of quartz-sericite-pyrite alteration. Pyrite commonly replaces ferromagnesian minerals (hornblende, ± biotite), and also occurs as veins/veinlets, fracture fill, and in the sulphide-rich matrix of fault breccias within these three zones. Andesitic to dacitic dykes are spatially associated with gold mineralization in the Kona area.

PRELIMINARY OBSERVATIONS ON LINKAGES BETWEEN GOLD, ALTERATION MINERALS AND SULPHIDES

A Portable Infrared Mineral Analyzer (PIMA) was used to determine alteration assemblages for samples from drillholes located both within mineralized corridors and unmineralized shoulders to establish linkages between gold zones and specific alteration minerals. We report preliminary results of PIMA analysis for diamond drillholes CFD016 and CFD017 (Supremo zone), which were paired drillholes from the same drill pad setup. CFD016 (-50° angle) contained a zone of significant Au concentration, whereas CFD017 (-70° angle) did not contain any significant zones of Au concentration. We also present data for mineralized and unmineralized sections of drillholes CFD029 (Supremo zone), CFD011 (Latte zone), CFD027 (Double Double zone) and CFD053 (Kona zone).

The preliminary PIMA data suggests that both the mineralized and unmineralized samples are characterized by specific white mica and clay mineralogy (Table 3). Within the gold bearing zone of CFD016, ammonium-bearing illite, illite and smectite are common, whereas in the unmineralized undercut hole CFD017, these minerals are absent to rare and the alteration assemblage is instead dominated by kaolinite. Similar results were obtained for Supremo hole CFD029, although high crystallinity illite was detected in the unmineralized section of drill core (not detected in the unmineralized section of hole CFD016 or in CFD017). Mineralized rocks in the Latte zone (CFD011) and Kona zone (CFD053) are characterized by ammonium-bearing illite, illite and smectite and unmineralized rocks are associated with kaolinite, high crystallinity illite and trace dickite. Gold-bearing rocks from the Double Double zone are characterized by illite alteration, whereas the unmineralized rocks in the drillhole are associated with smectite and kaolinite.

Aluminum-hydroxyl (Al-OH) responds on the PIMA at approximately 2200 nm, however shifts in the response can often be observed and have been correlated to, in the case of illite, changes in the crystallinity, Al content and Fe/Mg ratio of the illite (Hauff, 2005). These changes have also been linked to changes in the temperature at which the illite crystallized (Post and Noble, 1993; Hauff, 2005). Thus, higher wavelengths correspond to lower Al content and higher Mg/Fe ratios. These higher wavelengths also correlate to higher temperatures at which illite crystallized (Hauff, 2005). Within the zones examined to date, it
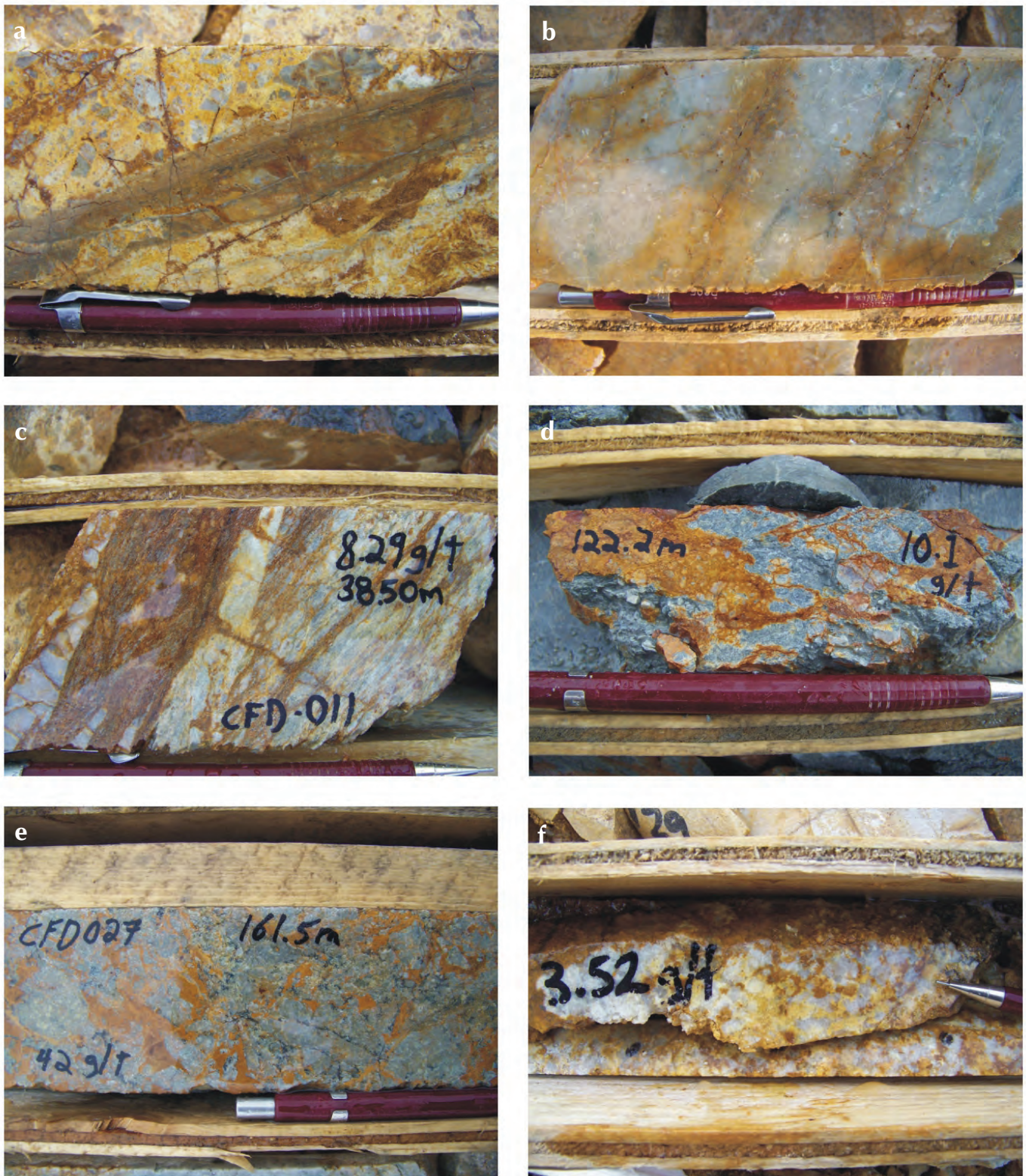
Figure 6. *Photographs of mineralized drill core from the Coffee property:* **(a)** *silicified-clast breccia cut by later chalcedonic (jasperoidal) silica veins (CFD001 – 28.60 m; Supremo zone);* **(b)** *quartz-sericite-altered dacite porphyry dyke (CFD006 – 68.75 m; Latte zone);* **(c)** *quartz-sericite-altered feldspathic schist (CFD011 – 38.50 m; Latte zone);* **(d)** *fine pyrite matrix, silicified-clast breccia (CFD010 – 122.2 m; Latte zone);* **(e)** *dacite porphyry clast breccia (CFD027 – 161.5 m; Double Double zone); and* **(f)** *clay limonite-altered granite (CFD051 – 30.1 m; Kona zone).*

Table 3. Alteration mineral species detected by PIMA; listed by zone and mineralized vs. non-mineralized.

	NH$_4$	HiXL_Ill	Illite	Smec	Kaol	Chl	Cb	Dik	Jar	Sil
Supremo Mineralized (>0.1g/t Au)										
CFD-16	**Tr-yes**	No	**Yes**	**Yes**	Tr	No	No	No	No-tr	?
CFD-17 (Hole not mineralized)	n/a	n/a	n/a	n/a	n/a	n/a	n/a	n/a	n/a	n/a
CFD-29	**Tr-yes**	No	**Yes**	**Yes**	Tr	Tr	No	No	No	?
Supremo Unmineralized (<0.1g/t Au)										
CFD-16	No	No	**Yes**	No-tr	**Yes**	**Yes**	**Yes**	No	No	?
CFD-17	No	No	Tr	No	**Yes**	Tr	No	No	No	?
CFD-29	No	**Yes**	Tr-yes	No	**Yes**	No	No	No	No	?
Latte Mineralized (>0.1g/t Au)										
CFD-11	**Tr**	No	**Yes**	**Yes**	Tr	Tr	No	No	No	?
Latte Unmineralized (<0.1g/t Au)										
CFD-11	No	**Yes**	No-tr	No	**Yes**	Tr	**Tr**	**Tr**	No	?
Double Double Mineralized (>0.1g/t Au)										
CFD-27	?	**Tr**	**Yes**	No	No	No	Tr	No	No	?
Double Double Unmineralized (<0.1g/t Au)										
CFD-27	No	No	Tr	**Yes**	**Yes**	**Yes**	**Tr-Yes**	No	No	No
Kona Mineralized (>0.1g/t Au)										
CFD-53	**Tr**	No	**Yes**	**Yes**	Tr	No	No	No	No	?
Kona Unmineralized (<0.1g/t Au)										
CFD-53	No	No	No	Tr-Yes	**Yes**	?	?	**Tr**	No	?

*CFD-17 had no samples above the 0.1 g/t threshold; above is a compilation of n=42 for CFD-16, n=42 for CFD-17, n=54 for CFD-29, n=66 for CFD-11, n=49 for CFD-27 and n=32 for CFD-53; NH$_4$=ammonium bearing illite, HiXL_Ill=high crystallinity illite, Smec=Smectite, Kaol=Kaolinite, Chl=Chlorite, Cb=Carbonate, Dik=Dickite, Jar=Jarosite, Sil=Silica, Tr=trace. Bold text indicates distinctive mineralogy for both mineralized and non-mineralized rocks.

appears that gold-bearing rocks are largely associated with wavelength responses between 2201 and 2212 nm (Fig. 7).

Preliminary scanning electron microscope (SEM) work has been completed on a limited number of mineralized samples from the Supremo and Latte areas. Thin section analysis of breccia samples from Supremo indicates that oxidized sulphide is fine grained to sub-microscopic. Backscatter electron images reveal micron-sized crystals of barite disseminated throughout breccia matrix. Gold grains occur within outer growth bands of pyrite, along oxidized margins of pyrite, and within fractures cutting the pyrite grains (Fig. 8). Gold mineralization at Latte is strongly associated with pyrite and linked with other secondary hydrothermal phases consisting of barite, monazite, apatite, zircon and rare arsenopyrite. Pyrite in the gold zones exhibits arsenic-rich domains and it occurs as fine-grained concentrations along pre-existing rock fabrics.

SUMMARY

GEOLOGY AND STRUCTURE

The Coffee property is underlain by intercalated Paleozoic schistose, mylonitic and gneissic rocks that are in contact with the younger mid-Cretaceous Coffee Creek granite to the south. The absence of a significant contact metamorphic aureole implies that the basement-granite contact may have been faulted. Other major structures that have been identified on the Coffee property include the Latte structure, which is spatially associated with gold mineralization, in addition to foliation-parallel shear zones associated with metagabbro and talc schist intervals in the structurally deep part of the Latte zone.

Soil sampling, detailed ground magnetic surveys, aerial photograph lineament analysis, trenching and subsequent drilling indicate that gold mineralization is structurally
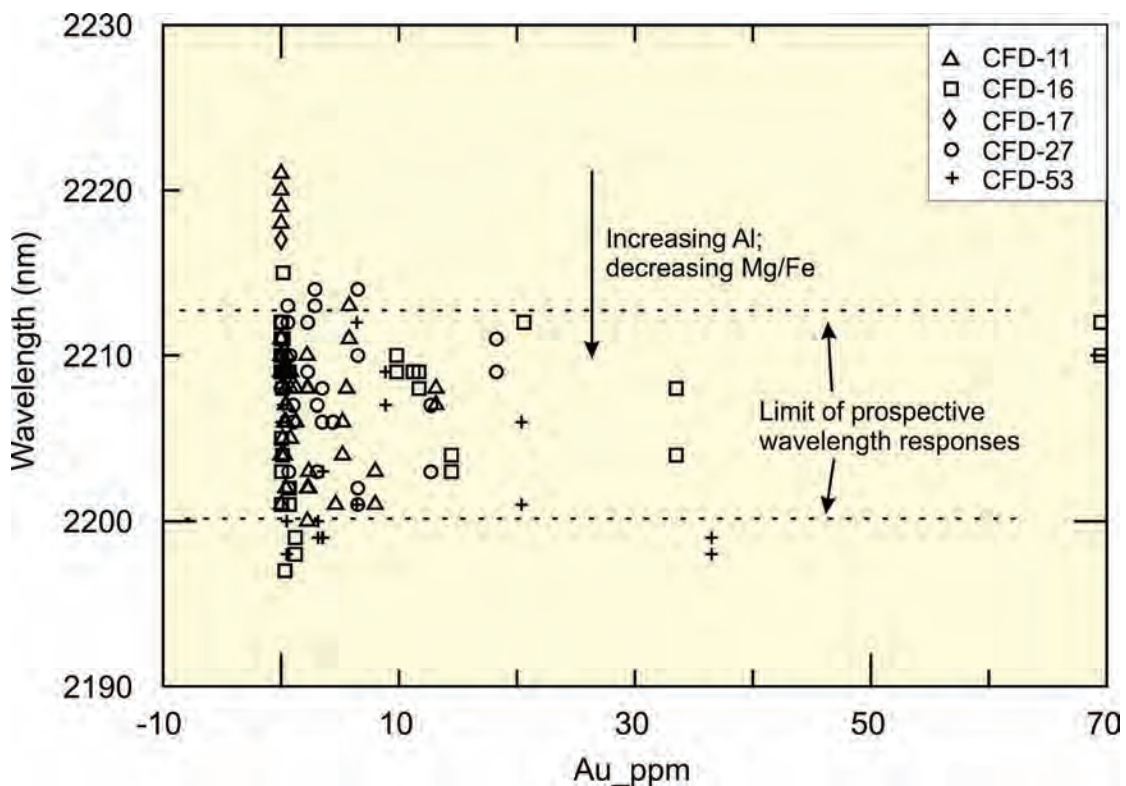
Figure 7. *Portable Infrared Mineral Analyzer (PIMA) data plot of gold (ppm) versus wavelength (nm).*
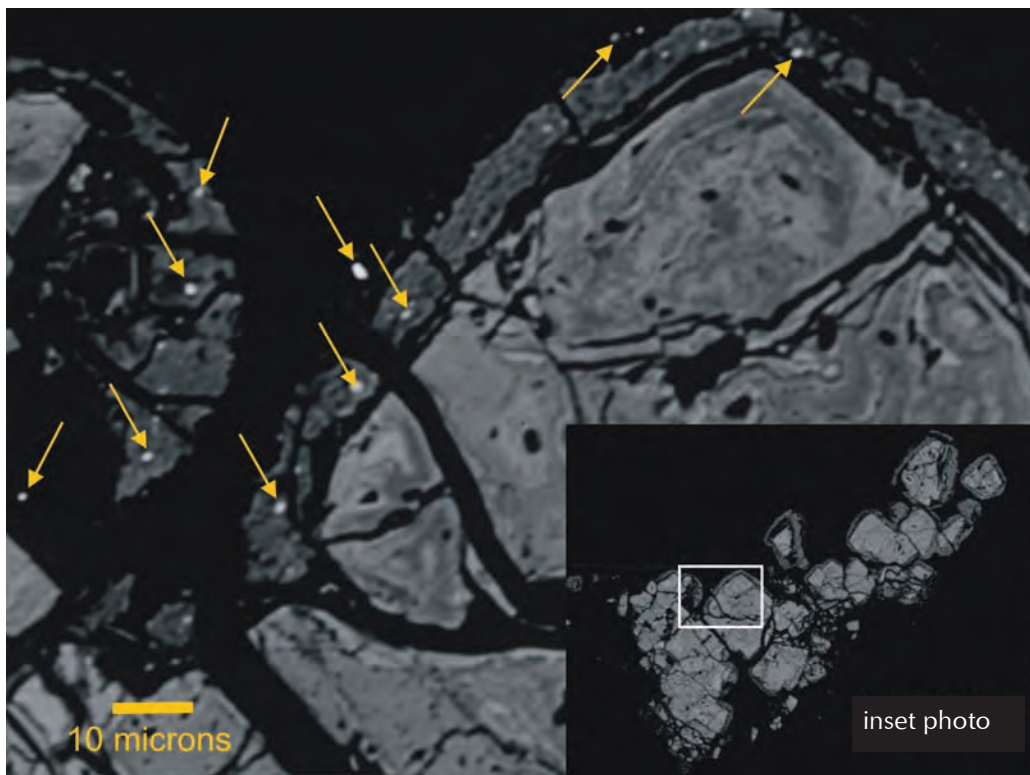

Figure 8. *Backscattered electron image of pyrite grain within Supremo breccia illustrating the linkage between gold (denoted with gold arrows) and pyrite. Note the occurrence of gold grains on the oxidized pyrite rim and near cracks in the grain. The grade over the one-metre interval in which this sample was taken was 34 g/t Au.*

controlled and cuts all lithologies on the property (Figs. 2b and 5). The metamorphic and intrusive host rocks are cut by dacite dykes that are spatially associated with gold and are interpreted as pre to syn-mineralization. A suite of andesite dykes appears to largely post-date the mineralization due to consistent lack of alteration and mineralization in these intrusive phases. The orientation and location of these dykes may have been influenced by pre-existing strain fabrics occurring in the Paleozoic metamorphic rocks. Fault zones occurring across the Coffee property have been multiply re-activated and exploited by the gold-bearing fluids, pre to post-mineralization dyke suites, in addition to relatively recent meteoric waters that contributed to the deep oxidation of the gold zones.

ALTERATION AND MINERALIZATION

Fragmental textures in each of the mineralized zones identified to date on the Coffee property record overprinting episodes of alteration, brecciation and veining. Breccia development may in part be due to fault propagation, but may also be due to the introduction of hydrothermal fluids. Breccia zones are generally strongly altered and well-mineralized, suggesting that they served as loci of high permeability for gold-bearing fluids.

Similar alteration assemblages, in addition to similar textures and styles of mineralization (*i.e.,* breccia, dacite dykes), as well as ubiquitous pyrite, implies that the mineralized zones at the Coffee property are genetically linked by the same protracted structural and hydrothermal event. The mineralized zones appear to be generally associated with illite alteration and PIMA analysis wavelengths of 2201 to 2212 nm, although the potential effects of supergene oxidation on the alteration assemblages have yet to be ascertained. Chalcedonic silica microveinlets, which are rarely found in unmineralized areas, are common in the gold zones, as are pyritic (or limonitic) veinlets, suggesting that these are related to fluid phases associated with the gold mineralizing event. Conversely, the opaque, white, typically foliation-parallel veins and vein fragments are interpreted to be pre-mineral and pre to syn-metamorphic.

The dominant sulphide phase occurring within all gold zones on the Coffee property is pyrite (arsenic-rich). Locally, subordinate amounts of arsenopyrite, stibnite and chalcopyrite are observed and gold is associated with increased As-Sb-Mo-Ba-Ag throughout the project area. Importantly, SEM imaging indicates a relationship between gold and pyrite growth bands, rims, as well as the fractures cutting pyrite grains, which suggests that gold may have

been introduced during multiple fluid pulses. Long, low to moderate-grade intervals of gold mineralization occurring within the Upper Latte zone appear to be preferentially hosted in ribbon-quartz mylonite, feldspar-muscovite schist and dacite dykes, as opposed to the shorter high-grade gold intervals at Lower Latte, hosted in biotite-feldspar schist. These contrasting host rocks imply some degree of lithological control on the style and tenor of gold mineralization within the overall Latte area.

CONCLUSIONS

The geology of the Coffee Creek area preserves a protracted history of Paleozoic metamorphism and ductile deformation, Cretaceous magmatism and subsequent faulting associated with the introduction of gold-bearing hydrothermal fluids. Gold mineralization occurs in a number of orientations and host rocks; however, we interpret the similarity of breccia textures and alteration/ sulphide mineralogy between gold zones to be the result of a common mineralization event.

At this time, we prefer not to classify the deposit style; however, we suggest that the gold system at the Coffee property is hosted in a structurally controlled, vein-poor, quartz-sericite-pyrite breccia environment. Mineralization within the Coffee property is similar to the Golden Saddle deposit where gold is associated with arsenic, pyrite, and sericite, and is controlled by vein-poor brittle structures and host rock-fluid interaction (Mackenzie *et al.*, 2010; Weiershäuser *et al.*, 2010). The dacitic dykes that occur throughout the mineralized zones, or possibly a buried pluton beneath the dykes at the Coffee property, may have served as a heat source for the superposed hydrothermal system. The highest-grade gold zones at the Coffee property occur in breccia zones within the main structures, locally related to very high sulphide content, which we interpret to reflect strong fragmentation and fluid flux zones within the multiply-reactivated fault structures.

ACKNOWLEDGEMENTS

REFERENCES

Bennett, V., Schulze, C., Ouellette, D. and Pollries, B., 2010. Deconstructing complex Au-Ag-Cu mineralization, Sonora Gulch project, Dawson Range: A Late Cretaceous evolu*tio*n to the epithermal environment. *In:* Yukon Exploration and Geology 2009, K.E. MacFarlane, L.H. Weston and L.R. Blackburn (eds.), Yukon Geological Survey, p. 23-45.

Berman, R.G., Ryan, J.J., Gordey, S.P. and Villeneuve, M., 2007. Permian to Cretaceous polymetamorphic evolution of the Stewart River region, Yukon-Tanana terrane, Yukon, Canada: P–T evolution linked with in situ SHRIMP monazite geochronology. Journal of Metamorphic Geology, vol. 25, p. 803-827.

Bineli Betsi, T. and Bennett, V., 2010. New U-Pb age constraints at Freegold Mountain: Evidence for multiple phases of polymetallic mid- to Late Cretaceous mineralization. *In:* Yukon Exploration and Geology 2009, K.E. MacFarlane, L.H. Weston and L.R. Blackburn (eds.), Yukon Geological Survey, p. 57-84.

Colpron, M., Nelson, J.L. and Murphy, D.C., 2006. A tectonostratigraphic framework for the pericratonic terranes of the northern Cordillera. *In:* Paleozoic Evolution and Metallogeny of Pericratonic Terranes at the Ancient Pacific Margin of North America, M. Colpron and J.L. Nelson (eds.), Geological Association of Canada, Special Paper 45, p. 1-23.

Hauff, P., 2005. Applied reflectance spectroscopy; with emphasis on data collection and data interpretation using field spectrometers. Spectral International Incorporated Version 4.1.

MacKenzie, D.J. and Craw, D., 2010. Structural controls on hydrothermal gold mineralization in the White River area, Yukon. *In:* Yukon Exploration and Geology 2009, K.E. MacFarlane, L.H. Weston and L.R. Blackburn (eds.), Yukon Geological Survey, p. 253-263.

MacKenzie, D., Craw, D., Cooley, M. and Fleming, A., 2010. Lithogeochemical localization of disseminated gold in the White River area, Yukon, Canada. Mineralium Deposita, vol. 45, p. 683–705.

MacKenzie, D.J., Craw, D. and Mortensen, J., 2008. Structural controls on orogenic gold mineralization in the Klondike goldfield, Canada. Mineralium Deposita, vol. 43, p. 435-448.

Mortensen, J.K., 1992. Pre-mid-Mesozoic tectonic evolution of the Yukon-Tanana Terrane, Yukon and Alaska. Tectonics, vol. 11, p.836–853.

Mortensen, J.K., 1996. Geological compilation maps of the northern Stewart River map area, Klondike and Sixtymile Districts (115 N/15, 16; 1150/13, 14; and parts of 1150/15, 16). Exploration and Geological Services Division, Yukon Region, Indian and Northern Affairs Canada, Open File 1996-1 (G), 43 p.

Mortensen, J.K. and Hart, J.R., 2010. Late and post-accretionary magmatism and metallogeny in the Northern Cordillera, Yukon and Eastern Alaska. Geological Society of America Abstracts with Programs, vol. 42, no. 5, p. 676.

Pavlis, T.L., Sisson, V.B., Foster, H.L., Nokleberg, W.J. and Plafker, G., 1993. Mid-Cretaceous extensional tectonics of the Yukon-Tanana terrane, Trans-Alaskan Crustal Transect (TACT), east central Alaska. Tectonics, vol. 12, p. 103-122.

Post, J.L. and Noble P.N., 1993. The near-infrared combination band frequencies of dioctahedral smecitites, micas, and illites. Clays and Clay Minerals, vol. 41, no. 6.

Ryan, J.J. and Gordey, S.P., 2004. Geology, Stewart River Area (Parts of 115 N/1,2,7,8 and 115–O/2-12), Yukon Territory. Geological Survey of Canada, Open File 4641, scale 1:100 000.

Weiershäuser, L., Nowak, M. and Barnett, W., 2010. White Gold Property Dawson Range, Yukon, Canada, 43-101 report prepared for Underworld Resources, 114 p.